# Georgia Institute of Technology

## School of Civil and Environmental Engineering

# Transfer and Development Length of High Strength Lightweight Concrete Precast Prestressed Bridge Girders

**Task 5 Report**

Prepared for

Office of Materials and Research
Georgia Department of Transportation

GDOT Research Project No. 2004

by

Karl F. Meyer, Lawrence F. Kahn
James S. Lai, and Kimberly E. Kurtis

June 2002

20020604 069

Contract Research
GDOT Research Project No. 2004


Behavior of High-Strength/High-Performance Lightweight Concrete
Prestressed Girders


Prepared for

Office of Materials and Research
Georgia Department of Transportation


by

Karl F. Meyer, Lawrence F. Kahn
James S. Lai, and Kimberly E. Kurtis

June 2002

# EXECUTIVE SUMMARY

This report presents the findings of a study that developed and tested high-strength lightweight concrete (HSLC) mixes having strengths from 8,000 psi to 12,000 psi made using slate lightweight aggregate. Based on optimized mix designs, 6 pretensioned AASHTO Type II girders were constructed using 8,000 psi and 10,000 psi slate HSLC and were prestressed using 0.6-inch diameter LOLAX strands tensioned to 75% of strand ultimate stress. The strands received no special preparation prior to girder casting.

After initial curing for approximately 24 hours, transfer length measurements were taken from time of release until the beams reached an age of 14 days. The current AASHTO and ACI code provisions conservatively predicted transfer length for slate HSLC; modification of the current code specifications for transfer length was not necessary for slate HSLC.

A direct pullout test was performed on both concrete design strengths to determine the bond between the slate lightweight concrete and the prestressing strand. A somewhat lower bond stress developed between the prestressing strand and the lightweight concrete when compared to similar strengths of normal-weight concrete. However, the average pullout strength for both series exceeded the minimum required value for 0.6-inch diameter strand of 43.2 kips.

Tests were conducted on each girder end to determine development length characteristics. The distance from the girder end to the load point was varied from

between 70 and 100 percent of the AASHTO specified development length. Strand slip was measured on each test. The current AASHTO and ACI code provisions conservatively predicted development length for slate HSLC; modification of the current code specifications for development length was not necessary for slate HSLC.

Tests were conducted on the center span of each girder to examine shear characteristics of HSLC. The combined center span and girder end shear results showed the current AASHTO Standard specification provided a conservative prediction of concrete and ultimate shear capacity when shear steel capacity was capped at a yield strength of 60 ksi. The alternate design procedure listed in ACI-318 Section 11.4.2.2 for predicting concrete shear strength produced some unconservative predictions for concrete compressive strengths over 10,000 psi. The current AASHTO LRFD specification provided a conservative prediction of ultimate shear capacity for slate HSLC.

An evaluation of girder flexural behavior showed the current prediction of cracking stress and cracking moment, when examined for slate HSLC, showed indications of becoming unconservative as concrete compressive strengths approached 11,000 psi. The use of a lambda factor ($\lambda$) of 0.85 for slate HSLC produced conservative results on average for compressive strengths below 11,000 psi. The modulus of rupture test, ASTM C 78, did not accurately predict the cracking stress of HSLC girders. The current AASHTO procedure for ultimate moment calculation was conservative for slate HSLC girders with normal weight concrete decks having a compressive strength under 6,000 psi.

# ACKNOWLEDGEMENTS

# TABLE OF CONTENTS

# LIST OF TABLES

xi

# LIST OF FIGURES

xv

# NOTATION

| Report | ACI 318-99 | AASHTO Standard | Description |
|---|---|---|---|
| $A_c$ | -- | -- | Cross sectional area of composite girder (combined area of girder and deck) |
| $A_{nc}$ | -- | -- | Cross sectional area of girder |
| AASHTO | -- | -- | American Association of State Highway and Transportation Officials |
| $A_{ps}$ | $A_{ps}$ | $A_s*$ | Cross sectional area of prestressing strand |
| $A_{pse}$ | -- | -- | Effective area of prestressed reinforcement adjusted inside the transfer or development length regions |
| BCL | -- | -- | Distance from bottom of girder to center line of bottom row of prestressing strands |
| CM | -- | -- | Cementitious Materials |
| CSS | -- | -- | Concrete Surface Strain |
| DAQ | -- | -- | Data Acquisition |
| $d_b$ | $d_b$ | D | Diameter of prestressing strand |
| DEMEC | -- | -- | Detachable Mechanical Strain Gage |
| $d_p$ | $d_p$ | d | Distance from compression fiber to centroid of prestressed reinforcement |
| $E_c$ | $E_c$ | $E_c$ | Modulus of elasticity of concrete based on 6 x 12 cylinder |
| $E_{ci}$ | -- | -- | Modulus of elasticity of concrete based on 6 x 12 cylinder at strand release |
| $f_c'$ | $f_c'$ | $f_c'$ | Concrete compressive strength at specified time |
| $f_{ci}'$ | $f_{ci}'$ | $f_{ci}'$ | Concrete compressive strength at strand release |
| $f_r$ | $f_r$ | $f_r$ | Modulus of rupture of concrete |
| $f_{pc}$ | $f_{pc}$ | $f_{pc}$ | Resultant compressive stress at the centroid of the composite section or at the junction of the web and flange when the centroid lies within the flange due to both prestress and moments resisted by the precast member acting alone. |
| $f_{ps}$ | $f_{ps}$ | $f_{su}*$ | Stress in prestressed reinforcement at nominal strength of member |
| $f_{pt}$ | -- | -- | Stress in prestressing strand just prior to strand release |
| $f_{pu}$ | $f_{pu}$ | $f_s'$ | Specified tensile strength of prestressed reinforcement |
| $f_{se}$ | $f_{se}$ | $f_{se}$ | Effective prestressing stress after losses |
| $f_{si}$ | -- | -- | Stress in prestressing strand just after strand release |
| $f_y$ | $f_y$ | $f_{sy}$ | Specified yield strength of non-prestressed reinforcement |

| Report | ACI 318-99 | AASHTO Standard | Description |
|---|---|---|---|
| h | h | h | Overall depth of the composite girder |
| $I_c$ | -- | -- | Moment of inertia of composite girder (girder and deck) |
| $I_{nc}$ | -- | -- | Moment of inertia of girder |
| $l_d$ | $l_d$ | -- | Development length of prestressing strand (In AASHTO Standard, $l_d$ refers to non-prestressed reinforcement development length) |
| $l_{fb}$ | -- | -- | Flexural bond length. Additional length over which the strand should be bonded so the stress $f_{ps}$ may develop in the strand at the nominal strength of the member. |
| $l_t$ | -- | -- | Transfer length of prestressing strand |
| LOLAX | -- | -- | Low relaxation loss prestressing strand |
| $M_{DL}$ | -- | -- | Moment due to Dead Load |
| n | n | -- | Modular Ratio |
| $S_{top-nc}$ | -- | -- | Top section modulus for non-composite girder |
| $S_{bot-nc}$ | -- | -- | Bottom section modulus of non-composite girder |
| $S_{top-c}$ | -- | -- | Top section modulus for composite girder |
| $S_{bot-c}$ | -- | -- | Bottom section modulus for composite girder |
| TCL | -- | -- | Distance from top of girder to center line of top row of prestressing strands |
| W/CM | -- | -- | Water to Cementitious Materials Ratio |
| $V_c$ | $V_c$ | $V_c$ | Nominal shear strength provided by concrete |
| $V_{ci}$ | $V_{ci}$ | $V_{ci}$ | Nominal shear strength provided by concrete when diagonal cracking results from combined shear and moment |
| $V_{cw}$ | $V_{cw}$ | $V_{cw}$ | Nominal shear strength provided by concrete when diagonal cracking results from excessive principal tensile stress in the web |
| $V_s$ | $V_s$ | $V_s$ | Nominal strength provided by shear reinforcing steel |
| VWSG | -- | -- | Vibrating Wire Strain Gage |

# CHAPTER I

# INTRODUCTION

Advances in concrete quality and engineering practices have enabled the design and construction of precast prestressed concrete bridge girders that approach 200 feet in length. Problems occur when trying to move and erect these long and heavy girders. In order to facilitate easier road movement and erection, high-strength lightweight concrete (HSLC) can be used to reduce member self-weight while still allowing a large load carrying capacity.

Previous research conducted relating to lightweight concrete (LWC) used in prestressed applications involved concrete with compressive strengths less than 7,500 psi. While this research is important and in most cases relevant, it does not verify current design procedures for use on higher strength lightweight concretes. There appears to have been little to no research conducted focusing on the use of HSLC for the construction of pretensioned bridge girders despite the fact that current articles indicate a belief that its use would be very beneficial.[1]

Additional research efforts are necessary in many areas before engineers can safely and confidently use HSLC in the design of pretensioned bridge girders.

## 1.1 Definitions

Transfer length is defined as the distance required to transfer the effective prestressing force from the strand to the surrounding concrete. Development length is defined as the sum of the "transfer length" and the "flexural bond length." The flexural bond length is the additional length of pretensioning strand beyond the transfer length over which bond is developed to allow the strand to reach the stress level $f_{ps}$ at the nominal flexural strength of the member. Development length can also be defined as the minimum distance from the end of the member beyond which the application of a point load will result in a flexural failure. Transfer length and development length are covered in detail in Chapters 9 and 13.

## 1.2 Research Objectives

The research objectives of this project were as follows:

1. To determine the transfer length, $l_t$, characteristics of 0.6-in prestressing strand used with slate HSLC.

2. To determine the development length, $l_d$, characteristics of 0.6-in prestressing strand used with slate HSLC.

3. To verify current code provisions for transfer and development length as appropriate for use with slate HSLC and to suggest more appropriate equations if necessary.

4. To determine the effect of shear reinforcement spacing on strand slip, development length, and shear capacity of pretensioned slate HSLC

5. To determine the shear strength, $V_c$, of pretensioned slate HSLC.

6. To verify current code provisions for shear strength of slate HSLC.

7. To verify the current code-specified reduction factor, $\lambda$, for sand lightweight concrete as related to concrete tensile strength, and suggest a more appropriate factor if necessary.

## 1.3 Need for Research

This research was necessary because girders constructed with slate HSLC with a strength approaching 12,000 psi and 0.6-in pretensioning strand had not been tested previously. The Georgia Department of Transportation wanted to use precast prestressed bridge girders with spans of 150 ft and with gross weights less than 150 kips. To achieve such designs, concrete with strengths of about 10,000 psi and unit weights less and 125 pcf would be required. Neither the concrete materials nor behavior of girders made with such material shad been investigated previously.

## 1.4 Analytical and Experimental Program

The analytical and experimental program involved the following six phases:

1. Analytically evaluate if HSLC bridge girders using 0.6-in diameter strand could achieve the 150 ft and 150 kip gross weight requirements.

2. Develop slate HSLC mix designs to meet objective strengths of 8,000, 10,000 and 12,000 psi under laboratory conditions.

3. Produce the laboratory-developed HSLC mix designs in a field environment at a commercial concrete plant.

4. Determine the mechanical properties of the slate HSLC.

3

5. Design, construct, and test six full-scale AASHTO Type II pretensioned girders using the slate HSLC to determine transfer and development length, shear, and flexural behavior characteristics.

6. Evaluate the girder behavior with respect to current design specifications.

**1.5 Organization of Report**

This report begins with a background review in Chapter II that covers the manufacture of slate lightweight aggregate, the use and field production of HSLC, HSLC short and long-term properties, the origins of transfer and development length, and shear behavior in pretensioned girders.

Chapters III through VII focus on HSLC as a material. Chapter III provides an analytical investigation to determine required HSLC properties to construct the objective pretensioned bridge girders. Chapter IV provides information on the components of HSLC, moisture control, mixing, and preparation and testing of specimens. Chapter V discusses the development of HSLC mix designs. Chapter VI discusses the field production of HSLC mix designs in a commercial concrete plant. Chapter VII covers the mechanical properties of HSLC as required for the evaluation. Chapters VIII through XIII focus on construction and testing of the six HSLC girders. Chapter VIII provides details on the design and construction of the AASHTO Type II girders. Chapter IX covers the determination of transfer length, evaluation of current code provisions, and the development of a new equation to predict transfer length. Chapter X addresses the procedures for test set-up and conduct of the test. Chapter XI provides flexural behavior results of the 18 girder

behavior results to include an evaluation of current code provisions. Chapter XIII covers development length test results, examines the effect of cracking in the transfer region, examines current code provisions, and suggests a new equation to predict development length.

Chapter XIV provides conclusions and recommendations based upon this research project.

# CHAPTER II

# BACKGROUND REVIEW

## 2.1 Introduction

Much research has been published on lightweight concrete, however, only a small portion of it focuses on high-strength lightweight concrete used for pretensioned bridge girders. In most cases the research involved concrete with compressive strengths less than 7,500 psi. While this research is important and in most cases relevant, it does not verify current code provisions for use on higher strength lightweight concretes (HSLC) commercially available today. In addition, since the properties of lightweight aggregate (LWA) vary based on the raw material from which it is made and the production technique, a direct comparison is not always possible.

This review provides information on both HSLC and normal weight concrete. Initially, the review covers terms and definitions related to lightweight concrete. The production of slate lightweight aggregate is described and a review of the use of HSLC in prestressed bridge applications is provided. Previously developed HSLC mix designs are described and comments about their production in a field environment are discussed. The development of equations to predict transfer length in normal weight concrete is reviewed and current research on transfer length is summarized. Information on shear relating to findings in this research is provided as well as a review of other ongoing research. The

review culminates with a summary of the development of equations to predict prestressing strand development length as well as a review of other related research.

## 2.2 Terms and Definitions Related to Lightweight Concrete

The following terms are used throughout this report:

**Lightweight Aggregate (LWA)** – Aggregate with a dry, loose unit weight of 70 lb/ft$^3$ or less.[2]

**Lightweight Concrete (LWC)** - A general term that includes "all-lightweight concrete" and "sand-lightweight concrete" defined below.[2]

**All-Lightweight Concrete (ALWC)** - Concrete containing all lightweight aggregate and does not exceed 115 lb/ft$^3$.[2]

**Sand-Lightweight Concrete (SLWC)** - Lightweight concrete in which all the all of the fine aggregate consists of normal weight sand.[2]

**Normal-Weight Concrete (NWC)** - Concrete having a unit weight of approximately 145 lb/ft$^3$.

**High-Performance Concrete (HPC)** – Concrete having a strength over 6,000 psi and/or having durability characteristics in excess of minimally accepted standards.

**High-Strength Lightweight Concrete (HSLC)** - Concrete meeting the conditions of lightweight concrete and having a compressive strength greater than 6,000 psi.

## 2.3 Production of Slate Lightweight Aggregate

The expanded slate LWA used in this research is produced from argillite slate found in the foothills region of North Carolina east of Charlotte. Found in a geologic

formation known as the "Tillery Formation," the slate is a thinly laminated, fine-grained siltstone composed of clastic (transported) rock fragments. The slate was from rock fragments of volcanic ash origin, which were deposited in a water environment and later solidified into solid rock. Subsequent burial and tectonic pressure changed the rock into argillite slate. Currently, the Tillery Formation is the only source of slate used to produce expanded slate LWA.[3]

Expanded slate LWA is produced using a rotary kiln approximately 11 feet in diameter and 160 feet in length. The rotary kiln is constructed on a slight incline on large bearings. The inside of the kiln is lined with insulation and a refractory material to protect the thick outer steel casing. Raw slate enters the kiln through pre-heaters that slowly heat the rock. Once in the kiln, the raw slate slowly tumbles within as it moves down the slight incline towards the "burn zone" where the raw material ultimately reaches temperatures in excess of 2200 degrees Fahrenheit. The kilns are normally heated by injecting coal dust or natural gas at the low end. In the "burn zone" the slate becomes sufficiently plastic for small gas pockets within the slate to expand forming masses of small, unconnected cells. As the expanded slate cools, the cells remain providing the material its low unit weight and absorption characteristics. The expanded material called clinker, exits the kiln and is either air or water cooled depending on the manufacturing process and is then crushed to the desired gradations.[3]

## 2.4 Use of LWC for Prestressed Bridge Applications

The following comments describe many of the known uses of LWC and in some cases HSLC in bridge applications. Many of the applications were not in pretensioned

bridge girders, but demonstrate the feasibility of LWC and HSLC in prestressed construction.

Raithby and Lydon[4] described the use of LWC for highway bridges in North America and various countries in Europe. Their overall summary of said bridges was that performance was satisfactory and durability was at least as good as NWC. In cases where performance was not satisfactory, improper detailing or quality control was at fault. They describe several advantageous aspects of LWC including weight savings and reduced superstructure requirements, reduced cost of foundations, and reduced handling costs.

Bender[5] made many of the same conclusions as Raithby and Lydon after performing a cost analysis on the construction of a prestressed concrete bridge. His main assertion was that the reduced weight of LWC allowed the casting of fewer larger pieces thus less total pieces were required to be moved during construction.

Brown and Davis[6] conducted a study on the long-term performance of a prestressed LWC used in a bridge in Fanning Springs, Florida. Initially built in the early 1960s with 121.5-ft AASHTO Type IV girders using 6,500-psi concrete weighing 120 pcf; the bridge underwent a comprehensive load test in 1968 and again in 1992. In comparing data from the two tests, the deflections were very close. Taking into account a margin of error, there was no change in the deflection values. Overall, Brown and Davis felt the bridge performed very well.

Janssen[7] wrote about the Shelby Creek Bridge in Pike County, Kentucky. The use of 7,000 psi HSLC reduced hauling and lifting weights and reduced dead loads on the

9

structure. The post-tensioned girders were 8.5 feet deep and were made with SLWC having a unit weight of 130 pcf.

Roberts[8] reported on the use of LWC for bridges in California again emphasizing the importance of reduced weight. He noted that successful use of LWC demanded accurate knowledge of shrinkage, creep and modulus coefficients.

Murillo, Thoman and Smith[1] described the use of LWC for design on the Benicia-Martinez Bridge across San Pablo Bay, California. In addition to being the least expensive alternative, the reduced weight of the structure was also more appealing from the standpoint of seismic design.

A publication from the Expanded Shale, Clay and Slate Institute (ESCSI)[9] provided a listing of the most significant uses of LWC for bridges worldwide. Of particular note were three bridges using pretensioned bridge girders including the Coronado Bay Bridge in California, the Lewiston Pump-Generating Plant Bridge in New York, and the Sebastian Inlet Bridge in Florida. All constructed in the 1960s, the bridge girders used LWC with a compressive strength between 5,000 and 6,000 psi. When the publication was issued in 1994, all the bridges were reported to be in excellent condition.

Melby, Jordet and Hansvold[10] described the use of HSLC for long-span bridges in Norway. The authors commented that LWC has been used for bridges in Norway since 1987. Their recommendations focused on testing mix designs thoroughly and ensuring excellent quality control to obtain consistent properties. They stated that the use of LWC was economical for long span bridges, but that bridge geometry would determine the

amount of savings. Compressive strengths up to 8,700 psi with a unit weight of 125 pcf were successfully used to construct the Raftsundet Bridge.

Holm and Bremner[11] noted that LWC was a very promising alternative for the replacement of functionally obsolete bridges throughout the United States. In many cases, the use of LWC for deck replacement would allow upgrading bridge capacity based on lower deck dead load. The authors cited as an example the Woodrow Wilson Memorial Bridge in Washington, D. C. By replacing the bridge deck with LWC, engineers reduced the dead load on the structure and were able to add an additional lane of traffic without exceeding the load carrying capacity of the structure.

## 2.5 HSLC Mix Designs

### 2.5.1 Coarse Aggregate

Coarse aggregate is a primary factor in developing a mix design that is lightweight, high-strength, and cost effective. Manufactured lightweight coarse aggregates include expanded clays, expanded shales, expanded slates, expanded perlite, exfoliated vermiculite, and sintered fly ash. Lightweight coarse aggregates also occur naturally in the form of pumice and tuff. Depending on the source of the aggregate, the particle shape and surface texture vary significantly impacting all other aspects of the mix design and the placement characteristics of the concrete.[11] Numerous authors commented on the need for specifications by particular aggregate manufacturer or source with respect to design characteristics.[12,13,14]

The raw material from which the LWA is produced determines the strength of the aggregate and thus the strength that can be achieved in the concrete. Expanded slate aggregates are normally recognized as being one of the LWA products able to produce the highest compressive strength and modulus of elasticity.

The porosity of the LWA determines the degree to which the aggregate will absorb and release water and varies significantly between LWA types. Based on an absorption test using ASTM C 127[15] and ASTM C 128[16], the absorption of LWA can vary from 5 percent to over 25 percent moisture by mass of dry aggregate as compared to less than 2 percent for normal weight aggregate.[11] Knowledge of the exact absorption characteristics of the chosen LWA is important in properly batching LWC. In addition, handling and quality control must be more exact when working with LWA. Bremner and Newman[17] found that the internal microstructure of each type of LWA was independent of the source.

A reduction in the maximum size of coarse aggregate can increase compressive strength without increasing the cement content or reducing the water-cement ratio.[18]

### 2.5.2 Fine Aggregate

The addition of fine LWA to a mix design further lowers the unit weight of the concrete; however, other characteristics are impacted. In a study by Pfeifer,[19] various amounts of the lightweight fine aggregate fraction were replaced with normal weight sand. The results showed that increasing the proportion of normal weight sand increased both compressive strength and modulus of elasticity.

### 2.5.3 Portland Cement

In HSLC mixes, the cement paste matrix must carry a higher portion of the load imposed on the concrete. As the strength limit of the cement paste matrix is reached, strength of the aggregate and interface between the aggregate and cement paste become the limiting factors.[3]

The type of cement used in the mix determined its curing characteristics. Use of a Type I/II cement results in lower initial strengths, but slightly higher strengths after 28 days. The use of Type III cement yields higher compressive strengths initially, which was desirable for prestressed construction, but results in slightly lower strengths at 28 days compared to Type I/II.

### 2.5.4 Silica Fume

The inclusion of silica fume in LWC mix designs was reported to significantly improve strength and other performance characteristics. Fujii et al.[20] reported results of a study where they showed a silica fume blended cement to provide superior strength results compared to a belite-rich cement. In a study including high-strength NWC and HSLC, Leming[21] reported that silica fume was particularly effective in increasing the compressive strength of any concrete. Mor[22] reported the dramatically improved bond strength between LWC and reinforcing steel based on the use of silica fume, an occurrence that was verified during this research.

## 2.5.5 Moisture Content

Control of moisture in HSLC is critical. In order to produce concrete having the water to cementitious materials ratio desired, the exact absorbed (moisture within the pore structure of the LWA) and adsorbed (moisture on the outside surface of the LWA – free moisture) moisture of the aggregate must be known. The amount of absorbed moisture directly impacts the specific gravity of the LWA as proportioned and mixed. Smeplass[23] made this point very clear by stating "The consequence of this observation may be that the mix water absorption of LWA must be determined in the actual initial moisture condition, as under concrete production, and as often as necessary to detect variation."

Based on the porosity of LWA, the determination of absorbed moisture content and specific gravity must be handled differently than with normal weight aggregate. Holm and Valsangkar[24] suggested a 1-day soak of LWA prior to determining specific gravity using a pycnometer. After soaking the aggregate for 24 hours, the additional water absorbed in the pycnometer during specific gravity testing is minimal. Based on the then determined absorbed moisture content, the dry specific gravity could be determined by dividing the 24-hour soak specific gravity by (1 + absorbed moisture content).

## 2.5.6 Mix Proportioning

Mix proportioning of LWC is covered in ACI 211.2-91.[18] The current guide does not cover mix designs for concrete in excess of 6,000 psi strength.

## 2.6 Field Production of HSLC

Comments on field production of HSLC were limited. Holm and Bremner[11] suggested four basic principles including well-proportioned, workable mixtures that use a minimum amount of water, equipment capable of expeditiously moving the concrete, proper consolidation in the forms, and quality workmanship in finishing. If the concrete is to be pumped, they suggested insuring the aggregate absorbed moisture content was maintained at a high level by presoaking. In the event of low absorbed moisture, pumping could force mix water into the LWA pores reducing the workability of the mix.

Valum and Nilsskog[25] reported on field production of HSLC having a compressive strength of 8,700 psi for the construction of the Raftsundet Bridge in Norway. Field production included steps to insure expanded slate aggregate absorption was maintained at between 7 and 9 percent to prevent mix water absorption. The time from batching until concrete placement could be as long as 2 hours. In addition, bulk density and surface moisture were determined prior to each concrete placement to insure proper mix proportioning. Prior to a concrete truck leaving the batch plant, concrete temperature, slump, air content and wet density were checked for compliance with design specifications. Any results out of specification resulted in the mix being discarded. While these standards would be common for the production of normal weight HPC, the more exacting control of aggregate moisture content was evident for HSLC. In addition, exact control of moisture also enabled better control of unit weight.

Hoff[26] described field production of HSLC for offshore platform construction. Many of the same steps were followed as mentioned by Valum and Nilsskog. Hoff

15

reiterated the importance of moisture control and the impact it could have on slump loss during placement and also commented that excessive moisture could result in unsuitable resistance to freezing and thawing damage.

## 2.7 HSLC Short and Long-Term Material Properties

The following sections address specific material properties and material related phenomenon where differences were noted between HSLC and NWC.

### 2.7.1 Modulus of Elasticity

An in-depth explanation of the determination of modulus of elasticity is covered in Chapter 3, Analytical Investigation on HSLC for Pretensioned Bridge Girders.

The current ACI[2] equation for modulus of elasticity is:

$$E_c = 33 w_c^{1.5} \sqrt{f_c'} \tag{2.1}$$

An equation by Morales[27] (Equation 2.2) was suggested for use with lightweight concrete.

$$E_c = (40,000\sqrt{f_c'} + 1,000,000)\left(\frac{w_c}{145}\right)^{1.5} \tag{2.2}$$

Table 2.1 lists compressive strengths, dry (equilibrium) unit weights and modulus values reported by various authors for slate HSLC mix designs having compressive strengths between 6,000 and 12,000 psi.

Table 2.1  Reported Strength, Weight and Elasticity Modulus Values for Slate HSLC

| Author(s) or Source | Compressive Strength $f_c'$ (psi) | Dry Unit Weight w (pcf) | Modulus of Elasticity $E_c$ (million psi) |
|---|---|---|---|
| Brown Davis[6] | 6,500 | 120 | 3.90 |
| Leming[28] | 7,180 | 116.4 | 3.58 |
| FIP Committee[29] | 7,500 | 118.6 | 3.55 |
| Harmon[3] | 8,170 | 111.7 | 3.27 |
| Bilodeau Chevrier Malhotra Hoff[30] | 9,090 | 119.2 | 4.06 |
| Valum Nilsskog[25] | 9,550 | 123.0 | 3.41 |
| Mor[22] | 9,650 | 130.0 | 3.91 |
| Holm Bremner[31] | 9,856 | 117.0 | 3.50 |
| Carolina Stalite Company[32] | 10,281 | 126.0 | 4.10 |
| Harmon[3] | 10,980 | 119.2 | 3.95 |
| Harmon[3] | 11,500 | 134.0 | 4.40 |
| Carolina Stalite Company[32] | 11,588 | 132.0 | 4.40 |
| Harmon[3] | 11,850 | 122.0 | 4.56 |

## 2.7.2  Strength Ceiling

Harmon[3] discussed a strength ceiling for HSLC being in the region of 12,000 to 13,000 psi based on the limiting strength of the slate LWA.  Holm[33] also discussed the strength ceiling with respect to smaller maximum size of aggregate.  As the maximum size of aggregate is reduced, strength increases to some upper limit determined by the

strength ceiling. Beyond the strength ceiling, additional binder does not increase the concrete's strength.

Bremner and Holm[34] addressed the elastic mismatch between LWA and the high-strength cement paste matrix. As the HSLC strength increases, the difference between the elasticity modulus values becomes more pronounced. Under load, the "elastic mismatch" results in fracture that begins as transverse splitting of the LWA. This splitting action is indirectly responsible for the strength ceiling of HSLC.

Holm[33] also reported a tensile strength ceiling for LWC. Since the LWA is approximately one half voids, its tensile strength will be reduced in comparison to NWA. Holm suggested the LWA tensile strength ceiling might also be responsible for compression strength limitations.

### 2.7.3 Internal Curing

Internal curing results when absorbed water in the LWA provides an internal reservoir to enhance cement hydration and extend the curing process. Several authors have commented on this phenomenon as related to LWC and HSLC.[21,33,35] Bremner, Holm and Ries[36] performed a study in which LWA was added to NWC mixes to provide additional internal cure water in mixes having strengths from 6,400 psi to 8,700 psi. The internal curing is reported to not only add in strength gain, but positively impacts durability characteristics by providing a higher quality and denser matrix.

18

## 2.8 Transfer Length

Transfer length is defined as the distance required to transfer the effective prestressing force from the strand to the surrounding concrete. The transfer length is developed when the pretensioning strands are released by flame cutting or other method from the restraining abutments. Numerous factors are thought to contribute to determining the transfer length including size and surface condition of the prestressing strand, concrete strength and modulus of elasticity at time of strand release, level of prestressing in the strand, and the amount of confining steel and concrete consolidation in the transfer length region. Many experimental programs have focused on the above factors in determining a relation to predict transfer length.

The Master's Thesis by Chris Reutlinger,[37] "Direct Pull-Out Capacity and Transfer Length of 0.6-Inch Diameter Prestressing Strand in High Performance Concrete" provides very thorough coverage of the history and development of equations to predict transfer length. The following is a summary of current code provisions and other proposed equations as determined for NWC. There are no known proposed equations specifically addressing transfer length for HSLC.

### 2.8.1 Janney, 1954

Initial transfer length testing by Janney[38] in 1954 concluded that transfer length and the general shape of the stress transfer distribution were attributable to diameter and surface condition of the prestressing wire and concrete strength. Janney did not suggest a relation for predicting transfer length.

## 2.8.2 Hanson and Kaar, 1959

Although the focus of Hanson and Kaar's[39] work was on flexural bond, an

appendix included comments on an assumed average transfer bond stress of 400 psi.

Equation 2.3 was proposed as a way to determine the transfer bond stress.

$$u_t = \frac{A_{ps} f_{se}}{\Sigma_0 l_t} \qquad (2.3)$$

$A_{ps}$ is the area of prestressing strand, $f_{se}$ is the effective prestressing stress at transfer, $\Sigma_0$

is the actual perimeter of the prestressing strand, $l_t$ is the transfer length and $u_t$ is the

transfer bond stress.

## 2.8.3 Kaar, LaFraugh and Mass, 1963

Kaar et al.[37] concluded that transfer length varied directly based on strand

diameter for ¼-inch and ½-inch strands but did not follow this same direct proportion for

0.6-inch strand. Kaar et al. found concrete strength did not impact transfer length, but

affected the shape of the stress distribution. Higher concrete strength allowed the

concrete to pick up stress more quickly when compared to lower strength specimens.

Kaar et al. also reported differences in transfer length between "dead" and "cut" ends.

## 2.8.4 Mattock, 1963

In 1963, Mattock[37] used Equation 2.3 with an assumed average transfer bond stress of 400 psi to derive the current ACI[2] equation for transfer length. The factors 0.725 and 4/3 were used to determine the actual area and perimeter respectively.

$$l_t = \frac{\left(0.725 \frac{\pi d_b^2}{4}\right) f_{se}}{\left(\frac{4}{3} \pi d_b\right) 0.4} = \frac{1}{2.94} f_{se} d_b \tag{2.4}$$

Equation 2.4 was simplified to Equation 2.5, which is the current ACI[122] expression.

$$l_t = \frac{f_{se} d_b}{3} \tag{2.5}$$

Mattock assumed the effective stress, $f_{se}$, for 250 ksi strand was 150 ksi and further simplified Equation 2.5 to Equation 2.6, which was adopted by ACI in 1963 and AASHTO[40] in 1973.

$$l_t = 50 d_b \tag{2.6}$$

Equation 2.6, currently maintained by AASHTO, is based on a limited number of tests where strand ultimate strengths were less than products available today.[37]

21

### 2.8.5 Martin and Scott, 1976

Martin and Scott[41] re-evaluated previous testing by Hanson and Kaar based on prestressing strand having an ultimate strength, $f_{pu}$, of 270 ksi, and commonly encountered strand surface conditions, and they recommended the implementation of Equation 2.7.

$$l_t = 80 d_b \qquad (2.7)$$

### 2.8.6 Zia and Mostafa, 1977

Based on an extensive review of transfer length testing, Zia and Mostafa[42] proposed Equation 2.8 to account for the effects of strand diameter, initial level of prestress, and concrete strength at transfer. Equation 2.9 was reported to be applicable for concrete strengths from 2,000 to 8,000 psi. This evaluation is reported in Chapter 9.

$$l_t = 1.5 \frac{f_{si}}{f'_{ci}} d_b - 4.6 \qquad (2.8)$$

### 2.8.7 FHWA Memorandum, 1988

Based on testing at the University of North Carolina in 1986 where poor transfer and development length results were recorded, the FHWA issued a memorandum specifying four interim restrictions, one of which was the restriction from using 0.6-inch

prestressing strand.[37] This restriction prevented the prestressed concrete industry from fully utilizing the benefits of higher strength concretes in larger members. Several research programs were initiated based on the FHWA restrictions.

### 2.8.8 Deatherage, Burdette and Chew, 1989

Deatherage et al.[43] conducted experimental testing on 20 AASHTO Type I girders with varying strand diameters and spacings. Their conclusions were that 0.6-inch diameter strand should be allowed and that strand spacing of 1.75 inches should be allowed for ½-inch diameter strand. Equation 2.10 was suggested for the calculation of transfer length for ½-inch, ½-inch special and $^9/_{16}$-inch diameter prestressing strand. Equation 2.9 was conservative and acceptable for use on 0.6-inch strand, but further research was recommended.

$$l_t = \frac{f_{si} d_b}{3}$$ (2.9)

### 2.8.9 Russell, 1992

Russell[44] performed an extensive series of testing of rectangular, scale model AASHTO-type and full-sized Texas Type C cross sections as part of a PhD Thesis under the supervision of Dr. Ned Burns. The specimens were all prestressed with ½-inch or 0.6-inch strand spaced at 2 inches, except for three rectangular sections that were prestressed with 0.6-inch strand spaced at 2.25 inches. In many of the specimens, strands were debonded to various distances from the girder ends. Russell concluded that larger

cross sections had shorter transfer lengths, larger strand diameters required longer

transfer lengths, strand spacing greater than 2 inches for 0.6-inch strand was not required,

debonded strands had transfer lengths similar to fully bonded, strands and confining

reinforcement did not affect transfer length. Russell suggested Equation 2.10 for

predicting transfer length.

$$l_t = \frac{f_{se}d_b}{2}$$ 
(2.10)

## 2.8.10 Mitchell, Cook, Khan and Tham, 1993

Mitchell et al.[45] based their research on determining the effect of concrete strength

on transfer length. They examined strand diameters of 3/8-inch, 1/2-inch and 0.6-inch

used to prestress rectangular sections made using normal weight concretes having

strengths from 4,500 to 12,900 psi at 28 days. The method of strand release was gradual

which was reported to provide a better comparison to the sudden strand release used in

most prestressing operations. Based on their results, Mitchell et al. proposed Equation

2.11.

$$l_t = 0.33 f_{si} d_b \sqrt{\frac{3}{f_{ci}'}}$$ 
(2.11)

## 2.8.11 Buckner, 1994

Buckner[46] noted that inconsistencies existed between the methods used by various researchers to determine transfer length. After an evaluation of results, Buckner concluded that the 95 Percent Average Mean Strain (AMS) Method provided the best overall prediction of transfer length. Furthermore, he recommended Equation 2.12 for predicting transfer length. Buckner noted that $1250/E_{ci}$ was about 3 for compressive strengths greater than 3,500 psi; thus, his findings endorsed Equation 2.9 as well.

$$l_t = \frac{1250 f_{si} d_b}{E_{ci}}$$

(2.12)

## 2.8.12 FHWA Study, 1996

In addition to the numerous studies aforementioned, the FHWA[47] also published findings from their own study addressing the bond of prestressing strand in NWC and HPC. The FHWA study addressed the following variables:

1. Concrete compressive strength at 28 days, $f_c'$

2. Square root of concrete compressive strength at 28 days, $f_c'$

3. Concrete compressive strength at transfer, $f_{ci}'$

4. Square root of concrete compressive strength at transfer, $f_{ci}'$

5. Concrete modulus of elasticity at 28 days, $E_c$

6. Concrete modulus of elasticity at transfer, $E_{ci}$

7. Prestressing strand diameter

8. Prestressing strand area

9. Stress in prestressing strand prior to transfer, $f_{si}$

10. Effective prestress, $f_{se}$

Based on FHWA results and their analysis of other research results, the restriction on the use of 0.6-inch strand was lifted. The FHWA proposed Equations 2.13 and 2.14 for "best-fit" and to provide a 95% confidence interval, respectively.

$$l_t = 4\frac{f_{pt} d_b}{f_c'} - 21 \tag{2.13}$$

$$l_t = 4\frac{f_{pt} d_b}{f_c'} - 5 \tag{2.14}$$

### 2.8.13  Summary of Transfer Length Review

Again, there are currently no equations specifically for predicting transfer length in girders made with LWC or HSLC. Chapter 9, Transfer Length, uses Equations 2.5 through 2.14 for an evaluation of transfer length results from this research program to determine which variables are most applicable for HSLC girders and to suggest a better equation for predicting transfer length.

### 2.9  Flexural Behavior

A review indicates that only limited research has been conducted on the flexural behavior of composite HSLC girders. Prior to the onset of flexural cracking and the

point at which flexural cracking occurs, the behavior of the HSLC is important. Beyond the cracking state, the behavior of the NWC deck is the governing concern. To the author's knowledge, no background information was available related to the findings and conclusions identified in this research for flexural behavior. The general flexural behavior of normal weight prestressed composite girders made with normal strength concrete is well understood and discussed in standard text books.[48,49,50]

## 2.10 Shear Behavior

Similar to flexural behavior, only a limited amount of research has been conducted on prestressed HSLC. Comments are provided for both HSLC and normal weight HPC as well as for LWC as applicable to this research.

### 2.10.1 Hanson, 1961

The origination of the lambda factor for use with LWC was based on work done by Hanson. Using the results of testing performed at PCA and at the University of Texas Hanson determined a good correlation between diagonal tensile strength in beams with the splitting tension test.[14] Hanson then determined that the ratio of splitting tension strength in lightweight concrete to that for normal weight concrete of the same compression strength was in general about 0.85 for concrete strengths below 5,000 psi. This relation was first reported in the 1963 ACI 318 Code. In the early 1970's, the reduction factor was formalized as lambda, $\lambda$, as 0.85 for sand LWC and 0.75 for all LWC. Based on the high degree of variability of LWA, concerns exist today that the lambda factors may become unconservative for concrete strengths over 5,000 psi.[51]

### 2.10.2 Johnson and Ramirez, 1989

Johnson and Ramirez[52] conducted research on non-prestressed beams, but made some observations that may be applicable for prestressed HSLC and normal weight HPC. One conclusion reached in their research was that in higher strength beams, shear reinforcement spacing was greater creating a deficiency in reserve shear strength. Once the upper limit of concrete shear capacity was exceeded, the shear force transferred to shear reinforcement would cause it to yield and rupture. They suggested applying either an upper limit to the term $(f_c')^{1/2}$ to limit the increase in $V_c$ due to increasing $f_c'$ or increasing the minimum shear reinforcement requirement as concrete strength increases. The 1989 ACI 318 code has included a specification reflecting this recommendation.[53]

### 2.10.3 Shahawy and Batchelor, 1996

Shahawy and Batchelor[54] conducted a research program examining the shear behavior of full-scale prestressed concrete girders made from 6,000 psi NWC. Of particular interest in their findings were comments that the AASHTO LRFD provisions for shear were very conservative and required modification to improve their reliability.

### 2.10.4 Barnes, Burns and Kreger, 1999

Barnes, Burns and Kreger[55] conducted an extensive research program at the University of Texas at Austin using 0.6-inch diameter prestressing strand in I-shaped prestressed girders made with normal weight HPC having strengths from 5,000 to 11,000 psi. The authors recommended limiting the principal tensile stress in the region from the composite section centroid to the extreme tensile fiber to $4(f_c')^{1/2}$. This recommendation

corresponds with ACI 318-99 Section 11.4.2.2[2] but extends the applicable area to include the section from the composite centroid to the extreme tension fiber.

### 2.10.5 Ma, Tadros and Baishya, 2000

Ma, Tadros, and Baishya[56] examined shear behavior in pretensioned I-girders made with 8,000 psi normal weight HPC. They concluded that both the AASHTO Standard and LRFD Specifications produced conservative predictions of girder shear capacity. When considering the results of their study, it must be recognized that prestressing strands were anchored in end diaphragms thus eliminating the possibility of slip and possibly increasing shear capacity at the girder ends.

### 2.10.6 Ramirez, Olek, Rolle, and Malone, 2000

Ramirez, Olek, Rolle, and Malone[57] conducted research on HSLC pretensioned girders made with ½-inch, and 0.6-inch diameter prestressing strands. The HSLC was made using expanded shale aggregate; the resulting concrete strengths ranged from 6,500 to 10,000 psi. The research at Purdue is thought to be the only other research conducted using 0.6-inch diameter prestressing strand in HSLC. As with Ma et al.,[56] an additional 1-meter anchorage was provided for the prestressing strand behind the center of bearing. Their conclusions related to shear were that the current AASHTO Standard and LRFD procedures were conservative for shear. Additionally they reported that the minimum amount of shear reinforcement for HSLC pretensioned girders must be further investigated based on a lower ratio of measured/calculated shear capacity with increased concrete strength.

### 2.10.7 ACI Committee 213, 2001

In a draft copy of Chapter 5, ACI 213,[58] shear and diagonal tension strength is covered in Section 5.8. Committee 213 reports that lightweight concrete members behave in fundamentally the same manner as normal weight concrete members. They recommend that the permissible shear capacity may be determined by substituting the splitting tensile strength, $f_{ct}/6.7$ for $(f_c')^{1/2}$ in the shear provisions of Chapter 11, ACI 318.[2]

### 2.11 Development Length

Development length of prestressing strands is the sum of the transfer length and the flexural bond length. Development length can be defined as the minimum distance from the end of the member beyond which the application of a point load will result in a flexural failure. As in transfer length, many factors are thought to affect development length. Many experimental programs have addressed development length resulting in suggested equations for its prediction.

The Master's Thesis by Chris Reutlinger,[37] "Direct Pull-Out Capacity and Transfer Length of 0.6-inch diameter Prestressing Strand in High Performance Concrete" provides very thorough coverage of the history and development of equations to predict development length. The following is a summary of current code provisions and other proposed equations as determined for NWC. The summary closely mirrors the development of transfer length equations. There are no known equations specifically addressing development length for HSLC.

### 2.11.1 Janney, 1954

Initial development length testing by Janney[38] in 1954 was based on the use of 5/16-inch wire having two different surface conditions prestressed to 0, 60, 120 and 165 ksi in beams made with NWC having strengths from 4,500 to 4,800 psi. Janney reported a "wave of flexural bond stress concentration" and noted that once general bond slip occurred, the beam failed shortly thereafter. Janney contributed bond in the transfer region predominantly to the Hoyer effect, which was the confining pressure applied to the wire by the concrete. Janney also reported improve bond characteristics for slightly rusted wire.

### 2.11.2 Hanson and Kaar, 1959

Hanson and Kaar[39] conducted a study involving 47 small-scale concrete beams reinforced with various sizes of Grade 250 stress-relieved strand. The tests focused on five factors including strand diameter, embedment length, concrete strength, percentage of reinforcement, and strand surface condition. All beams were loaded until failure. Hanson and Kaar reported observations similar to those of Janney.[38] The results of Hanson and Kaar's research were the basis for the current AASHTO development length expression shown in Equation 2.16 and developed by Mattock.[37] Equation 2.15 simplifies to Equation 2.16.

$$l_d = l_t + l_{fb} = \frac{f_{se}d_b}{3} + (f_{su}^* - f_{se})d_b \qquad (2.15)$$

$$l_d = (f_{su}^* - \frac{2}{3}f_{se})d_b \qquad\qquad (2.16)$$

Shortly after the development of Equation 2.16 concerns developed based on the

introduction and common use of Grade 270 prestressing strand.[37]

### 2.11.3 Martin and Scott, 1976

Martin and Scott[41] re-evaluated the currently suggested equation (Equation 2.16)

and determined that inconsistencies may have been responsible for the collapse of a 20-ft

span slab under construction loads. They suggested two new equations that did not

determine development length, but specified a maximum strand stress based on a given

embedment length. The two equations are shown below for the given location $l_x$.

For $l_x$ less than $80d_b$:

$$f_{su}^* \leq \frac{l_x}{80d_b}\left(\frac{135}{d_b^{\frac{1}{6}}}+31\right) \qquad\qquad (2.17)$$

For $l_x$ greater than $80d_b$:

$$f_{su}^* \leq \frac{135}{d_b^{\frac{1}{6}}}+\frac{0.39l_x}{d_b} \qquad\qquad (2.18)$$

32

Equation 2.18 was rewritten in terms of $l_x$ in Table 13.8 in order to determine its accuracy in predicting $l_d$.

### 2.11.4 Zia and Mostafa, 1977

Zia and Mostafa[42] also realizing the inconsistencies with Equation 2.16 suggested a new equation as well (Equation 2.19) which incorporated their suggested transfer length equation, Equation 2.8.

$$l_d = l_t + l_{fb} = \left(1.5\frac{f_{si}}{f'_{ci}}d_b - 4.6\right) + 1.25(f^*_{su} - f_{se})d_b \qquad (2.19)$$

### 2.11.5 FHWA Memorandum, 1988

Based on testing at the University of North Carolina in 1986 where poor transfer and development length results were recorded, the FHWA issued a memorandum specifying 4 interim restrictions as listed in Section 2.8.7.[37] Several research programs were initiated based on the FHWA restrictions.

### 2.11.6 Deatherage, Burdette and Chew, 1989

Deatherage et al.[43] conducted experimental testing on 20 AASHTO Type I girders with varying strand diameters and strand spacings and concrete design strengths of 5,000 psi. They suggested the flexural bond component suggested by AASHTO[40] should be increased by 50 percent as shown in Equation 2.20 below.

33

$$l_d = l_t + l_{fb} = \frac{f_{si}d_b}{3} + 1.50(f_{su}^* - f_{se})d_b \qquad (2.20)$$

### 2.11.7 Russell, 1992

Russell[44] performed an extensive series of testing of rectangular, scale model AASHTO-type and full-sized Texas Type C cross sections as part of a PhD Thesis under the supervision of Dr. Ned Burns. The specimens were all prestressed with ½-inch or 0.6-inch strand spaced at 2 inches except three rectangular sections that were prestressed with 0.6-inch strand spaced at 2.25 inches. In many of the specimens, strands were debonded to various distances from the girder ends. Russell concluded that "shear cracking through the transfer region will cause its bond to fail and that if cracks do not occur that the strand will develop is prestressing force plus any additional tension required by external loads."[44] To prevent cracking from occurring through the transfer region, Russell developed the criteria listed in Equation 2.21 where $l_t$ was calculated using Equation 2.10.

$$M_{cr} > l_t V_u \qquad (2.21)$$

In addition, Russell specified that if $V_u > V_{cw}$ that vertical and longitudinal mild steel shear reinforcement should be provided to prevent web shear cracking from passing through the transfer region.

### 2.11.8  Mitchell, Cook, Khan and Tham, 1993

Mitchell et al.[45] based their research on determining the effect of concrete strength
on develop length.  They examined strand diameters of $^3/_8$-inch, $^1\!/_2$-inch and 0.6-inch used
to prestress rectangular sections made using concretes having strengths from 3,000 to
7,310 psi at release and from 4,500 to 12,900 psi at 28 days.  Based on experimental
results, Equation 2.22 was suggested.

$$l_d = 0.33 f_{si} d_b \sqrt{\frac{3}{f'_{ci}}} + (f_{su} - f_{se}) d_b \sqrt{\frac{4.5}{f'_c}} \qquad (2.22)$$

### 2.11.9  Buckner, 1994

Buckner[46] noted that there was an interaction between transfer length, effective
prestress and design stress.  Buckner recommended using a procedure similar to that of
Hanson and Kaar.[39]  He also theorized that the development length expression should be
based also on ultimate strain and suggested Equations 2.23 and 2.24.

$$l_d = l_t + l_{fb} = \frac{f_{si} d_b}{3} + \lambda(f^*_{su} - f_{se}) d_b \qquad (2.23)$$

$$1.0 \le [\lambda = (0.6 + 40\varepsilon_{ps})] \le 2.0 \qquad (2.24)$$

In Equation 2.24, $\varepsilon_{ps}$ is the strain corresponding with $f_{su}$*.

## 2.11.10 FHWA Study, 1996

In addition to the numerous studies aforementioned, the FHWA[47] also published findings from their own study addressing the bond of prestressing strand in NWC and HPC. The FHWA study addressed variables as specified previously in 2.8.12. Based on FHWA results and the results of other research programs, the restriction on the use of 0.6-inch strand was lifted. The FHWA proposed Equations 2.25 and 2.26 for "best-fit" or "mean" and to provide a "95% confidence interval," respectively.

$$l_d = l_t + l_{fb} = \left( 4\frac{f_{pt}d_b}{f_c'} - 21 \right) + \left( \frac{6.4(f_{su} - f_{se})d_b}{f_c'} + 26 \right) \quad (2.25)$$

$$l_d = l_t + l_{fb} = \left( 4\frac{f_{pt}d_b}{f_c'} - 5 \right) + \left( \frac{6.4(f_{su} - f_{se})d_b}{f_c'} + 15 \right) \quad (2.26)$$

## 2.11.11 Barnes, Burns and Kreger, 1999

Barnes, Burns and Kreger[55] tested 36 AASHTO Type I normal weight HPC girders having release strengths from 4,000 to 7,000 psi and strengths at testing from 5,700 to 11,000 psi. All prestressing strand was 0.6-inch diameter Grade 270 ksi LOLAX strand in either a "bright" or "rusted" surface condition. Included in the test program were girders with fully bonded strands and debonded strands. One of the outcomes of the research program was Equation 2.27 for predicting development length.

$$l_d = \frac{5}{4}\left(\frac{f_{pt}}{\sqrt{f_{ci}'}} + (f_{ps} - f_{pe})\right)d_b \qquad (2.27)$$

### 2.11.12  Peterman, Ramirez, Olek, 2000

Peterman, Ramirez, and Olek[59,60] conducted research on HSLC bridge girders as referenced in Section 2.10.5.  Their research is the only other research known where HSLC girders using 0.6-inch diameter strands were tested.  Their report indicated that all multiple strand specimens were reinforced with sufficient stirrups to prevent web-shear cracking at the member ends.  The prevention of shear cracking in the transfer region has been shown to result in strand slip causing premature shear failure.

### 2.11.13  Kolozs, 2000

Kolozs,[61] under the supervision of Professors Ned Burns and John Breen, tested HSLC girders with strengths between 6,000 and 8,000 psi prestressed with ½-inch diameter Grade 270 LOLAX strand.  Kolozs found the current AASHTO[40] equation for development length was conservative.

### 2.11.14  Summary of Development Length Review

Again, there are currently no specific equations for predicting development length for girders made with HSLC.  Chapter 13, Development Length, uses Equations 2.16 through 2.20 and 2.22 through 2.27 for an evaluation of development length results from this research program to determine which variables are most applicable for HSLC girders and to suggest a better equation for predicting development length.

## 2.12 Elements of Bond

There are three mechanisms that allow the development of bond stress between the prestressing strand and the concrete to include adhesion, frictional bond due to Hoyer's effect, and mechanical interlock.[44] Slipping of the prestressing strand relative to the concrete is required to develop bond stress. In general, bond resistance of seven-wire prestressing strand remains constant or increases after initial slip.[62]

### 2.12.1 Adhesion

Adhesion occurs in a very thin layer at the interface between the concrete and prestressing strand. Acting like an "adhesive," adhesion exhibits rigid-brittle behavior preventing slip of the strand relative to the concrete up to a critical stress level. During the transfer of prestress or girder testing, adhesion is lost when the bond stress exceeds the critical stress level. Once the critical stress level is exceeded, the adhesion portion of bond is lost. In the case of seven-wire prestressing strand, the loss of adhesion is often replaced by other mechanisms of bond.[44] Because failure of the adhesive bond occurs at a very small displacement, the overall contribution of adhesion to bond is minor.[63]

### 2.12.2 Frictional Bond Due to Hoyer's Effect

Research by E. Hoyer in 1939 using small diameter smooth piano wire resulted in the identification of a mechanism of bond now known by his name.[44] When wire or prestressing strand is tensioned, Poisson effects cause the diameter to become smaller. After tensioning, concrete is cast around the strands and allowed to cure to some initial required strength. At strand release, the strand attempts to return elastically to its initial

length prior to tensioning. As the strand becomes shorter, Poisson effects cause an increase in strand diameter creating radial compression stress between the strand and concrete.[63] The resulting increase in strand diameter upon release is most pronounced at the free end of the strand and becomes less to a point where it becomes constant at a distance approximately equal to the transfer length from the end of the member. After initial end slip at strand release, the resulting frictional bond resistance and wedge action shown in Figure 2.1 restrain the strand and maintain tension in it.
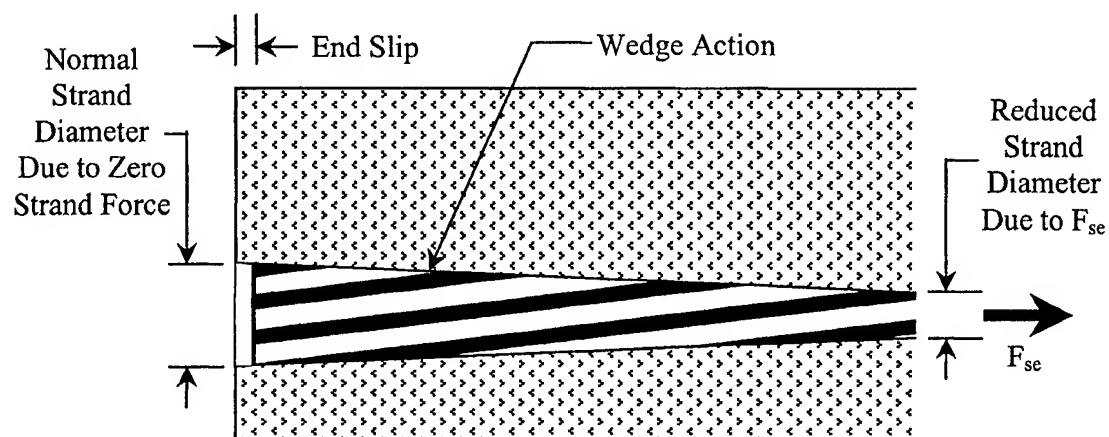


Figure 2.1 Wedge Action Resulting from Hoyer's Effect

During the application of load to a girder, the stress in the strand increases. At the point where the stress exceeds the stress in the strand at transfer in the transfer region, the wedge action begins to diminish.[44]

### 2.12.3 Mechanical Interlock

Standard seven-wire prestressing strand is manufactured by wrapping six wires around a seventh center wire in a helical pattern. Concrete placed around the strand fills the narrow spaces (interstices) between the individual wires completely encapsulating the strand. When the strand is prevented from twisting, the concrete ridges acting on the outside wires of the strand restrict movement by mechanical interlock. In order to prevent twisting, the wedge action created by Hoyer's effect must exist.[44] Mechanical interlock is reported to enhance the frictional bond component at strand release.[63]

# CHAPTER III

# ANALYTICAL INVESTIGATION OF HSLC FOR PRETENSIONED BRIDGE GIRDERS

## 3.1 Introduction

The potential advantages of using high strength HPC for precast prestressed bridge girders may be lost if those girders are too heavy to be transported. The advantages of using HPC for pretensioned girders presented by Kahn and Saber[64] included spans up to 40 percent longer than when normal strength (6 ksi) concrete was used, wider girder spacing and greater durability. Mr. Paul Liles, Georgia State Bridge Engineer, stated that the girders for spans over about 120 feet would weigh too much and that they would require a "super-load" permit for transportation. A gauge of the transportation problem is the necessity to obtain hauling permits or "super-load" permits.

In Georgia when the gross vehicle weight (GVW, weight of girder plus tractor-trailer rig) exceeds 150 kips, a "super permit" is required. This permit requires the hauler to obey certain additional restrictions that may include stopping before every bridge, proceeding over the bridge at a speed less than 5 miles per hour and that an escort vehicle lead and follow the truck. In addition, the state department of transportation must carefully review the route and evaluate the load capacity of each bridge. There may be no acceptable route. The slow rate over a bridge crossing can significantly disrupt traffic.

41

The established goal for this phase of the research was to achieve a 150 foot long pretensioned girder with a weight that when added to that of a tractor-trailer rig, was less than 150 kips; that is, create a 150-foot long girder that does not require a "super permit." A further goal was too have a minimum girder spacing of 7 feet for overall bridge efficiency. Use of either an all-lightweight or sand-lightweight concrete would be needed to achieve these goals. It was known from previous research[64] that AASHTO Type IV girders constructed with 15,000 psi NWC using 0.6-inch diameter prestressing strands and a girder spacing of 5 feet could achieve the span but with a GVW of about 185,000 lbs.

Therefore, the purpose of this analytical investigation was to determine if HSLC could be used to build pretensioned bridge girders with a length of 150 feet and girder spacing of 7 feet whose GVW did not exceed 150 kips. Standard AASHTO (American Association of State Highway and Transportation Officials) and AASHTO-PCI (Precast/Prestressed Concrete Institute) sections were considered. The range of girder strengths was 8, 10 and 12 ksi. The strength of the 7-inch thick, normal weight composite deck was 3,500 psi.

The scope of this study was limited to investigating AASHTO Type II-V and AASHTO-PCI Bulb-Tee 54, 63 and 72 sections (Standard and Modified) as shown in Figures 3.1, 3.2 and 3.3. For reference purposes, AASHTO-PCI Bulb-Tees were listed as "Bulb-Tees." A Modified AASHTO-PCI Bulb-Tee was listed as a "Modified Bulb-Tee."
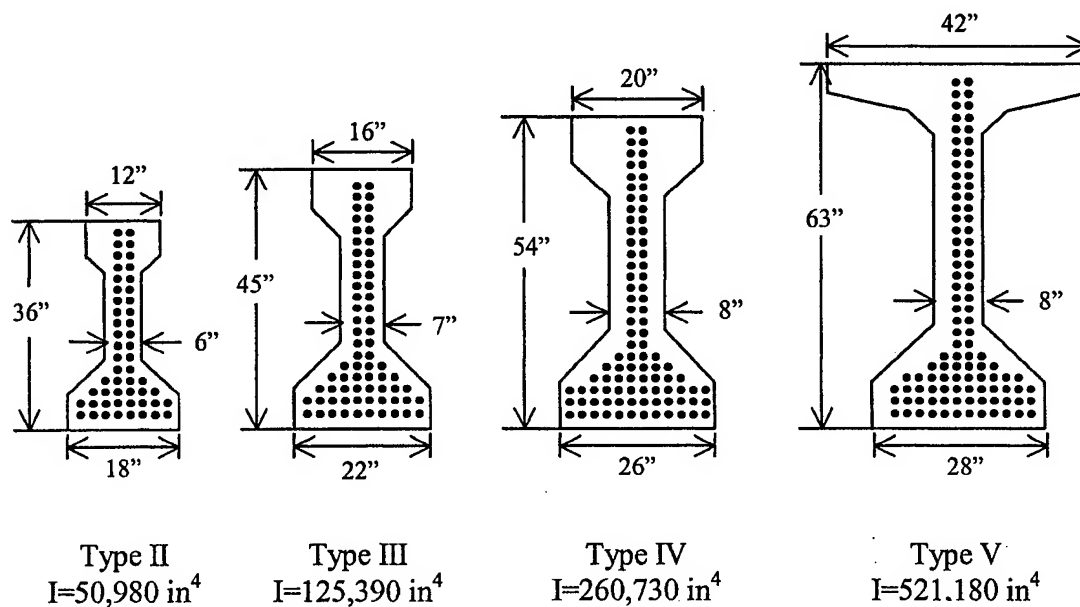
Figure 3.1  AASHTO Type II – V Sections

Type II
I=50,980 in$^4$

Type III
I=125,390 in$^4$

Type IV
I=260,730 in$^4$

Type V
I=521.180 in$^4$



BT-54
I=268,077 in$^4$

BT-63
I=392.638 in$^4$

BT-72
I=545,894 in$^4$
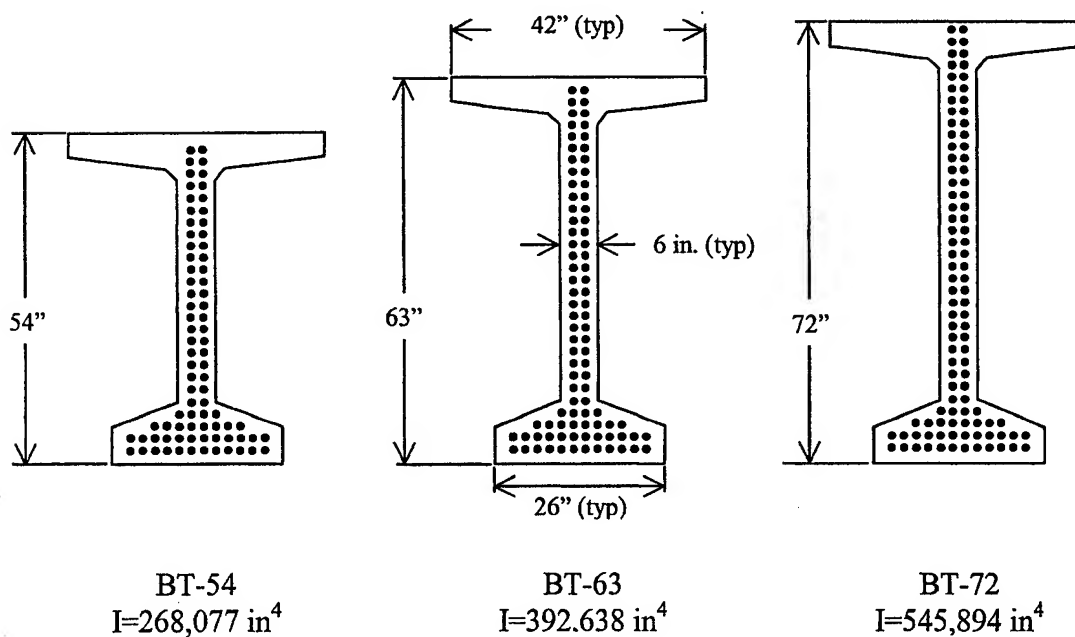
Figure 3.2  AASHTO-PCI Bulb Tee 54, 63 and 72 Shapes

43
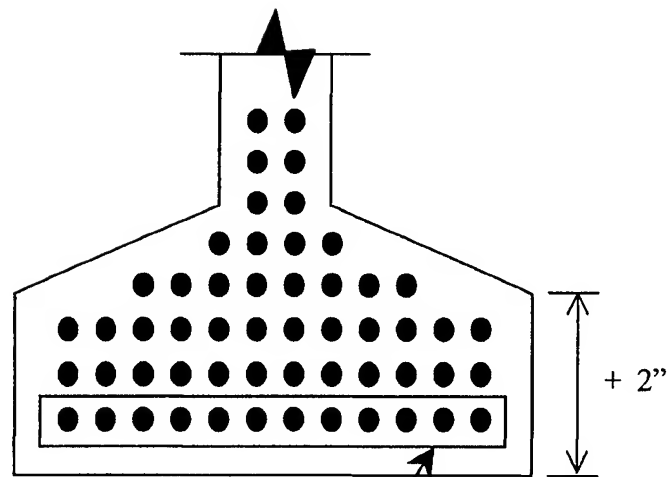
- One additional row of
  pre-tensioning strands
- 2 in (51 mm) deeper
  bottom flange

Moments of Inertia

54M – 308,318 in$^4$
63M – 446,700 in$^4$
72M – 616,067 in$^4$

Figure 3.3  Diagram of Bottom Flange of Modified Bulb Tee

The Modified Bulb-Tee sections consisted of a Standard Bulb-Tee with one additional row of 12 strands added to the bottom flange.  The additional row of 12 strands added 2 inches to the depth of the member, all in the bottom flange.  The inclusion of the Modified Bulb-Tee sections was precipitated by discussions with Georgia precast concrete producers who had previously constructed and recommended the section. Prestressing strands were 0.6-inch diameter, 270 ksi low relaxation strands spaced at 2 inches.

The HSLC in this study assumed the use of regionally available expanded slate LWA.  Based on the requirement to produce concrete compressive strengths up to 12 ksi, it was thought that the use of slate LWA would be necessary.  Furthermore, available

HSLC test data indicating strengths upwards of 12 ksi predominantly used slate LWA.[3,12,21,31]

It was possible that HSLC using other types of LWA (expanded shale or clay) could achieve upwards of 12 ksi strength, but available data were limited. An extensive literature search focusing on HSLC used for prestressed applications indicated that neither shale nor clay LWA had been used where concrete strengths approached 12 ksi.[65]

## 3.2 Parametric Study

All girder designs in this research were based on the 16th Edition of the AASHTO Standard Specification for Highway Bridges[40] and used the Georgia DOT bridge design program with modification by the authors to enable the use of HSLC. A spreadsheet to create input files for the bridge program is shown in Appendix A. Several steps were necessary prior to using the program to design HSLC bridge girders.

It was assumed that prestress losses would be the same for HSLC as for normal strength concrete. Other ongoing research by the author indicates that for normal weight and lightweight HPC, the creep and shrinkage losses were less than for normal strength concretes. Yet, consideration of deflection was a major concern.

The parameters that were varied were concrete strength, unit weight, and girder type. Other variables that remained constant are listed in Table 3.1.

Table 3.1 Critical Girder Design Variables That Remained Constant.

| | |
|---|---|
| Allowable top fiber tension stress at release | $3\sqrt{f_c'}$ |
| Allowable final bottom fiber tension stress | $6\sqrt{f_c'}$ |
| Release strength as percent of 28-day compressive strength | 75 percent |
| Composite deck thickness | 7 inches |
| Composite deck strength | 3500 psi |
| Pretensioning strand diameter | 0.6 inches |
| Pretensioning strand spacing | 2 inches |
| Pretensioning strand ultimate strength, $f_{pu}$ | 270 ksi |
| Type of pretensioning strand | LOLAX |
| Percent of strand ultimate strength allowed at time of pretensioning | 75 percent |
| Girder spacing | 7 feet |

## 3.3 Determination of Modulus of Elasticity

A critical requirement for design was to accurately predict the modulus of elasticity at both the time of release ($E_{ci}$) and at 28 days ($E_c$) for HSLC made using slate LWA. Accurate values of the modulus of elasticity were necessary to determine prestress losses and girder deflections. Experimental data from thirteen mixes using slate LWA were used to investigate the appropriate modulus values as shown in Table 2.1. The current ACI[2] and AASHTO[40] equation for $E_c$ is:

$$E_c = 33w_c^{1.5}\sqrt{f_c'} \qquad (2.1)$$

When used with HSLC, Equation 2.1 was found to overpredict the modulus values for strengths over 7,000 psi. The equation was specified for use on concretes having unit weights between 90 and 155 pcf. Morales[27] proposed Equation 2.2 for use with LWC:

46

$$E_c = (40{,}000\sqrt{f_c'} + 1{,}000{,}000)\left(\frac{w_c}{145}\right)^{1.5} \qquad (2.2)$$

Equation 2.2 more closely predicted modulus values; however, when used with HSLC

made using slate LWA, the predicted values were low for strengths below 10 ksi and high

for strengths over 10 ksi when compared to experimental data. In order to more

accurately predict modulus values, Equation 3.1 was developed similar in form to the

Morales equation, but based on a "best fit" analysis of the experimental data from the

thirteen slate mixes.

$$E_c = (33{,}000\sqrt{f_c'} + 4{,}000{,}000)(w_c/242)^{0.9} \qquad (3.1)$$

Figures 3.4 and 3.5 plot the experimental data and the three equations for modulus of

elasticity versus compressive strength and versus unit weight, respectively. Equation 2.3

was used for all further analyses.

### 3.4 Girder Design

The computer program was used to find the maximum span length for each girder

type in the study. The variable parameters were concrete strength and concrete unit

weight. Other critical variables were kept constant at AASHTO[40] specified or other

values as shown in Table 3.1.
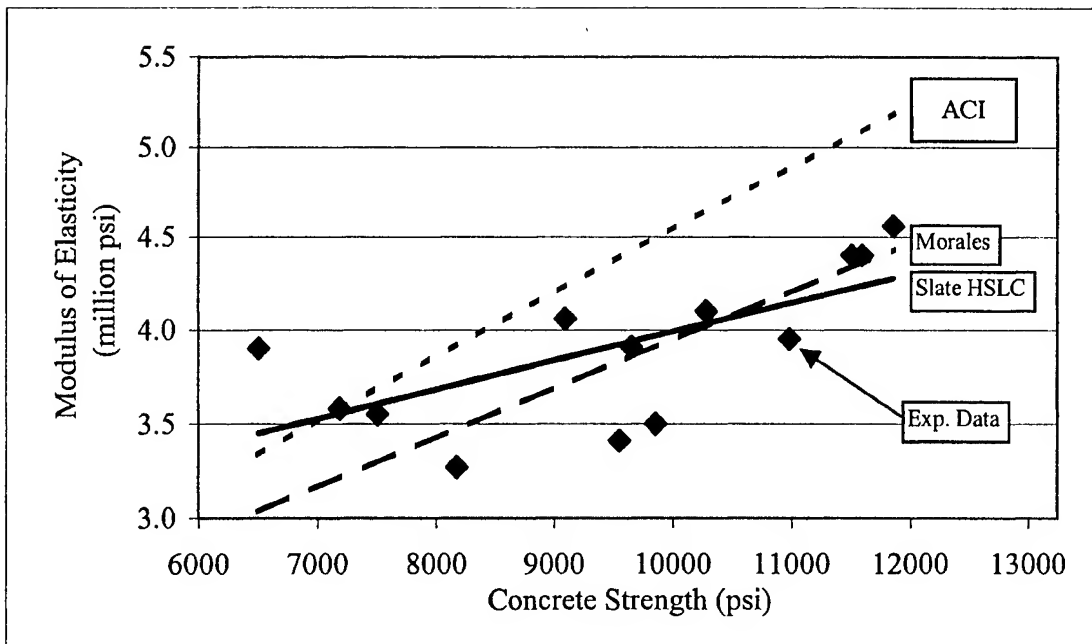
Figure 3.4  Modulus of Elasticity vs. Concrete Strength
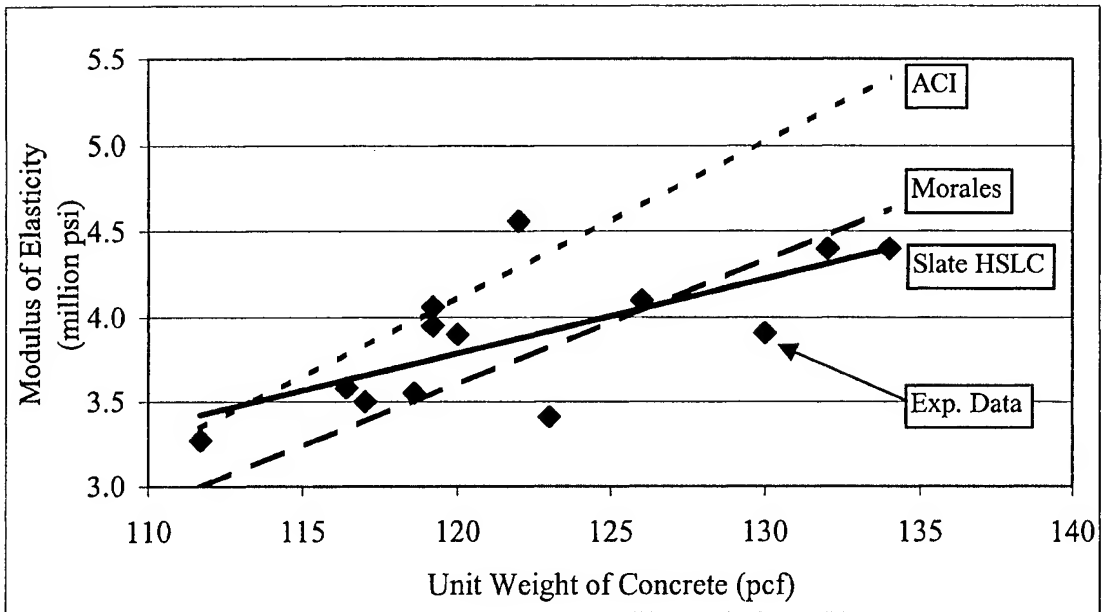


Figure 3.5  Modulus of Elasticity vs. Unit Weight of Concrete

48

The concrete strengths used were 8, 10 and 12 ksi.. When designing with high strength NWC, it was assumed the concrete weight was 150 pcf, and the modulus was determined with Equation 2.1 based upon previous high-strength NWC research in Georgia.[66] When using HSLC, Equation 2.3 was used with different unit weights.

Based on the study of the thirteen slate mixes, it was apparent that variations in unit weight existed for a given strength. A range of unit weights was established for each HSLC strength based on observed upper and lower limits. Table 3.2 shows the range of unit weights used in the study.

Table 3.2  Slate HSLC Unit Weight Values

| Concrete strength $f_c'$ (psi) | | Unit Weight | |
|---|---|---|---|
| | Low (pcf) | Average (pcf) | High (pcf) |
| 8,000 | 113 | 119 | 126 |
| 10,000 | 117 | 124 | 131 |
| 12,000 | 122 | 128 | 135 |

The variation in unit weights caused variations in modulus values as well as girder weights. Each bridge and girder design accounted for the differing modulus at release and final conditions. It is noted that of the strengths in Table 3.2, only the low unit weight 8,000 psi mix qualified as structural lightweight concrete according to the ACI definition.[2]

## 3.5 Analysis Results and Discussion

Figures 3.6 through 3.8 present the composite girder maximum simple-span length versus the girder's concrete compressive strength for AASHTO Type II through V sections, Bulb-Tee 54, 63 and 72 sections, and Modified Bulb-Tee 54, 63 and 72

49

sections.  Shown in the figures are girders of high strength NWC and HSLC.  The unit weights shown for HSLC are the "low" and "high" values listed in Table 3.2 to provide the range of results by concrete unit weight for each concrete strength.

### 3.5.1  Effect of Concrete Strength and Unit Weight on Girder Span Length

### 3.5.1.1  AASHTO Type II – V Sections

Girder span lengths using 8 ksi HSLC could be extended by up to about 4 percent (7 feet for 140-foot girders) as shown in Figure 3.6.  The most significant length increases resulted from the use of the lightest concrete unit weight.  The increase in length for Type II and III sections was less than for Type IV and V sections implying the use of HSLC provided the most significant benefit for girders with lengths over approximately 105 feet.   Figure 3.6 also indicates there is little benefit to using concrete over 10 ksi strength in Type V sections.  Length increase is proportional to the amount of reinforcement that can be located in the bottom flange.[64]  At maximum lengths for Type V sections, the total strands possible were used in the bottom flange with 10 ksi concrete.

HSLC girder maximum live load deflections resulting from HS 20-44 loading increased between 15 and 22 percent on average when compared to girders of high-strength NWC.  The lighter concrete unit weights experienced the greatest deflections; however, deflections were at most 85 percent of the AASHTO[40] maximum allowable L/800 requirement (where L is the span length) compared to 57 percent for high-strength NWC.  Further, the natural period of vibration increased by less than 19 percent when HSLC was used compared to high-strength NWC for the 10 ksi Type IV girders.

50
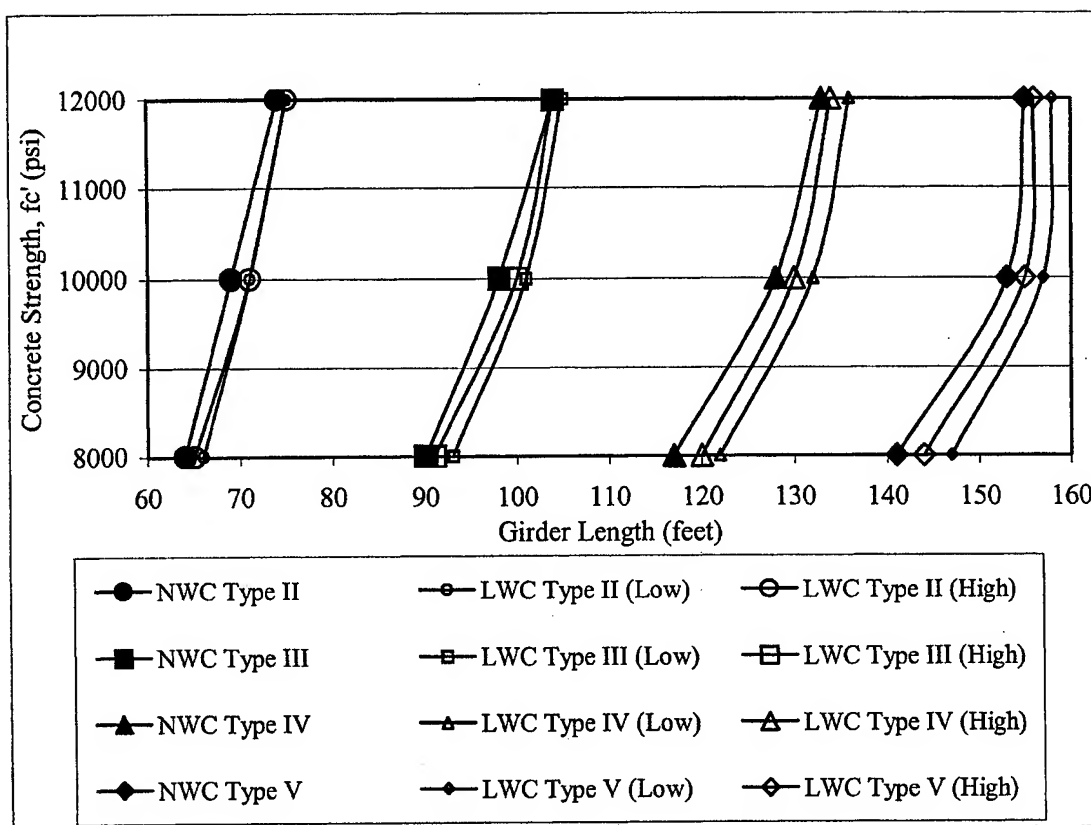
Figure 3.6 Concrete Strength vs. Maximum Length for AASHTO Girders

### 3.5.1.2 Bulb-Tee Sections

Figure 3.7 shows trends similar to those for AASHTO sections. HSLC with a strength of 8 ksi provided a length increase up to about 3 percent (3 feet for 110 foot girders). The major difference from AASHTO sections was that Bulb-Tee sections showed a consistent benefit from using concrete strengths up to 12 ksi. Based on the improved efficiency of the Bulb-Tee sections, there was not an observed plateau within the strength range investigated for the constant 7-foot girder spacing. Live load deflections of Bulb-Tee sections averaged at most 70 percent of the AASHTO maximum

allowable L/800. The natural period of vibration for a HSLC 135-foot, 63-inch deep

Bulb-Tee girder increased by less than 17 percent compared to that of a high-strength

NWC girder.
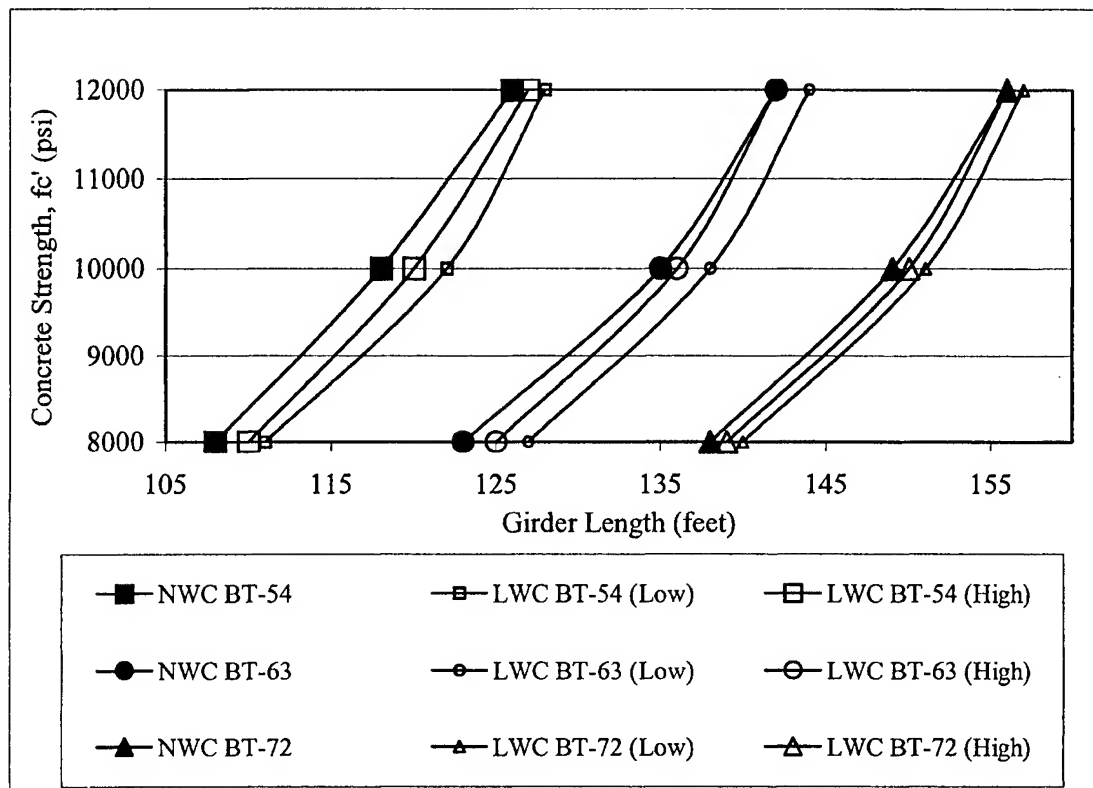


Figure 3.7 Concrete Strength vs. Maximum Length for Bulb-Tee Girders

### 3.5.1.3 Modified Bulb-Tee Sections

Figure 3.8 shows that Modified Bulb-Tee sections behaved in a similar manner to

the Standard Bulb-Tee sections. The greatest percent increase in length was gained with

8 ksi HSLC at about 3 percent (4 feet for 146-foot girders). The addition of a row of

pretensioning strands in the bottom flange allowed an increase in length of about 10 feet

52

at all strengths of concrete for all sections in comparison to Standard Bulb-Tee sections. Live load deflections were again well within the maximum allowable L/800 limit and averaged 64 percent of the allowable.

The additional strands and 2-inch increase in depth would allow designers to use a shallower section to reach lengths previously achievable only with the next larger size Bulb-Tee section. For the HSLC 156-foot, 65-inch deep Modified Bulb-Tee girders, the natural period of vibration increased by less than 15 percent compared to that of a high-strength NWC girder.

### 3.5.2 Weight Reduction Based on the Use of HSLC

The most significant advantage gained through the use of HSLC was overall girder weight reduction. Through the use of HSLC, it was possible to lower the GVW below the 150 kip threshold for the target 150-foot girder. The GVW was determined by adding the resulting girder weight to the estimated weight of an appropriate transport truck and trailer. Table 3.3 shows information related to Georgia permitting requirements for overweight cargo as provided by the Georgia DOT.
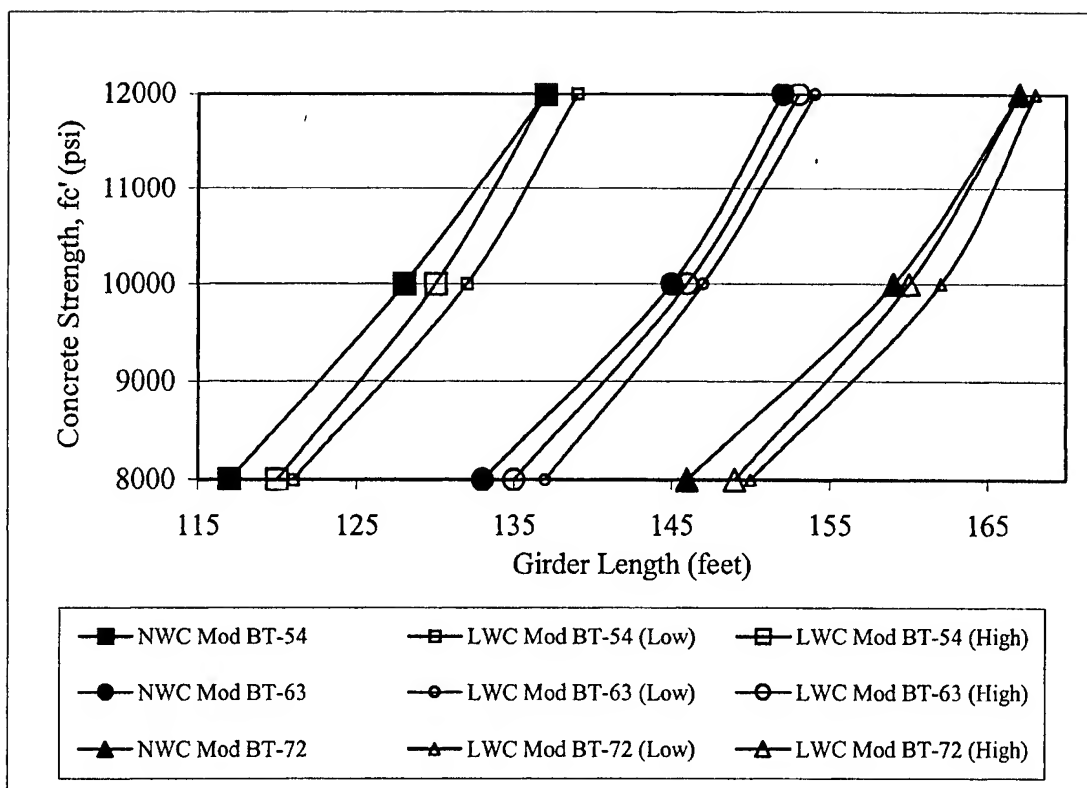
Figure 3.8 Concrete Strength vs. Maximum Length for Modified Bulb-Tee Girders

Table 3.3  Permitting Requirements for Overweight Cargo in Georgia.

| Load category | Gross vehicle weight range (kips) | Estimated vehicle weight (kips) | Maximum girder weight (kips) | Permit type | No. of axles required |
|---|---|---|---|---|---|
| 1 | 0 < GVW ≤ 80 | 40 | 40 | None | NA |
| 2 | 80 < GVW ≤ 125 | 40 | 85 | Regular | 6 |
| 3 | 125 < GVW ≤ 150 | 45 | 105 | Regular | 7 |
| 4 | 150 < GVW ≤ 160 | 50 | 110 | Superload | 8 |
| 5 | 160 < GVW ≤ 175 | 52.5 | 122.5 | Superload | 9 |
| 6 | 175 < GVW ≤ 180 | 55 | 125 | Superload | 10 |
| 7 | 180 < GVW | 55+ | 125+ | Superload | >10 |

**Note**: 1 kip = 454.5 kg.

It was difficult to provide exact data on weights and permitting requirements due to variations in tractor-trailer rig configurations and capabilities; however, Table 3.3 provides some average values that would be expected. Figure 3.9 illustrates the GVW for each of the maximum length girders for the ten sections using high-strength NWC at 8 ksi strength. Similar graphs were created for 10 and 12 ksi high-strength NWC and HSLC. The collective results of GVW, maximum girder length, and section type are shown in Figure 3.10. Since it was seen that AASHTO Type II and III girders showed little benefit from HSLC, they were not included in graph.
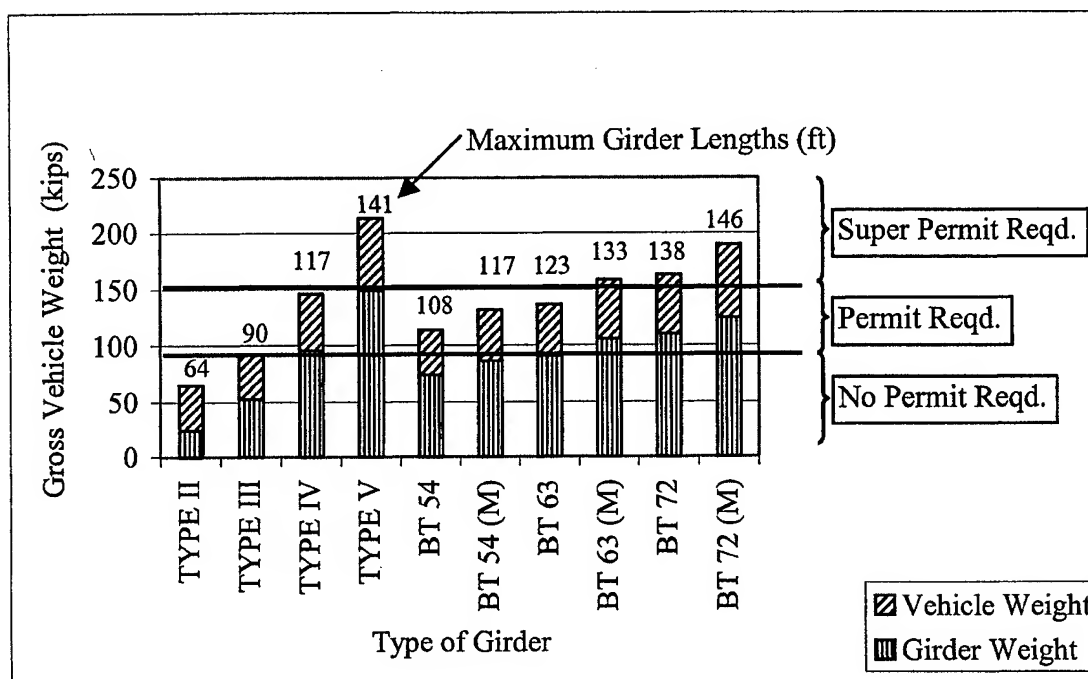


Figure 3.9 GVW by Girder Type, With Maximum Length Labeled, Based on 8 ksi NWC

Within Figure 3.10, there are three data points for each section listed. The three points correspond with the three strengths of concrete. In each case, the leftmost of the

three points represents 8 ksi. The center point represents 10 ksi, and the rightmost point

represents 12 ksi. The average unit weight given in Table 3.2 was used for the

lightweight (L) sections while a constant 150-pcf unit weight was used for the normal

weight (N) sections.
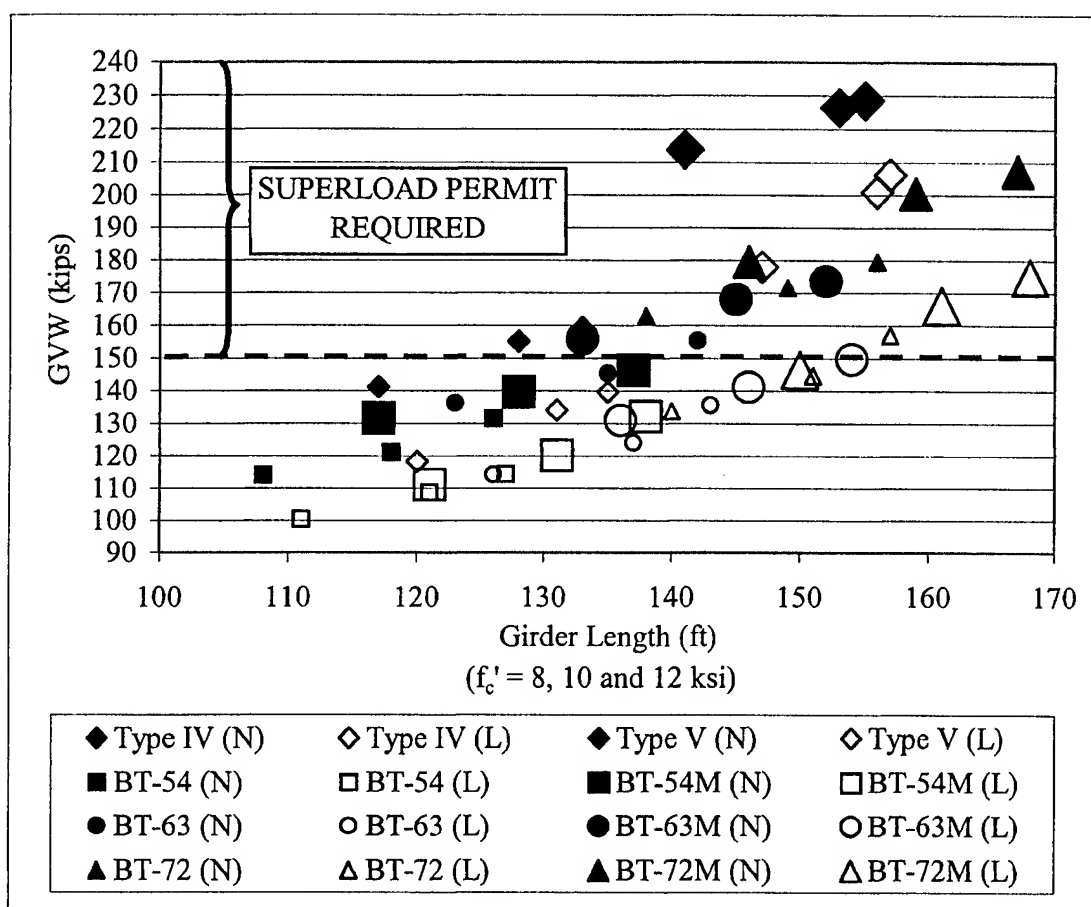


Figure 3.10 Gross Vehicle Weight vs. Maximum Girder Length

The most important finding was that it was possible to reach the target span of

150 feet without exceeding the 150 kip GVW limit through the use of HSLC. There were

three HSLC girders that satisfied the requirement: Modified BT-63 (12 ksi), BT-72 (10

ksi) and Modified BT-72 (8 ksi). Further economic analysis and a review of site constraints would be required to select the best possible alternative. For spans between 125 feet and 135 feet, Type IV lightweight girders were less than the 150 kip GVW while Type IV normal weight girders exceed the 150 kip GVW limit. Based on the parameters of this study, AASHTO Type IV and V sections were less efficient than similar height Bulb-Tee sections, both Standard and Modified.

If the AASHTO Type IV and V sections are removed from the chart, there are noticeable trendlines for the remaining normal weight and lightweight Bulb-Tee girders. The trendlines demonstrate the benefit in terms of GVW that result from the use of HSLC. The trendlines converge for girder lengths less than 105 ft (32 m) and diverge as girder lengths increase from that point.

## 3.6 Conclusions

Based on the results of this analytical investigation, the following conclusions were made:

The use of HSLC has the potential to increase the length of simple span AASHTO sections up to four percent and Bulb-Tee sections up to three percent.

For spans between 125 feet and 155 feet, the use of LWC can reduce the gross vehicle weight to less than 150 kips (68,200 kg) so that a superload permit is not required for transport of long span girders as compared to the need for a superload permit when normal weight concrete is used.

AASHTO Type II and III sections do not benefit appreciably from the use of HSLC. The Modified Bulb-Tee section extended the length of a Standard Bulb-Tee by 10 feet using 8, 10 and 12 ksi HSLC or high-strength NWC.

Bulb-Tee (Standard or Modified) sections provided longer spans at less weight for girders over 105 feet in length when compared to AASHTO sections.

# CHAPTER IV

# MATERIALS, MIXING AND TESTING OF HSLC

## 4.1 Introduction

The purpose of this chapter is to discuss the materials used, the methods of mixing, and the testing methods used in designing and then producing HSLC. Specific comments on mix design development, field production and material properties are addressed in Chapters 5, 6 and 7, respectively.

## 4.2 HSLC Components and Properties

### 4.2.1 Coarse Aggregate

The most important factor in creating a lightweight concrete that has high strength and high modulus of elasticity is the LWA. The coarse aggregate used during this project was a slate LWA provided by the Carolina Stalite Company, Salisbury, North Carolina. As described in Chapter 2, the Stalite LWA is a high-quality aggregate with a tight pore structure. Three different size gradations were used during this research including 3/8-inch, 1/2-inch and 3/4-inch. The 1/2-inch gradation was used predominantly during development and testing. The 3/8-inch aggregate was used in trying to exceed 12,000 psi strength. The 3/4-inch aggregate had a very limited use during this project because of its lower strength plateau.

When crushed, Stalite LWA takes on an angular appearance as shown in Figure 4.1. Figure 4.2 shows the LWA in clinker form, the way it appears upon exiting the rotary kiln. Note the voids in the LWA clinker that reduce its weight and specific gravity. Table 4.1 provides the specific gravity, weight, and gradation for the 3/8-inch and 1/2-inch aggregate used during this research.
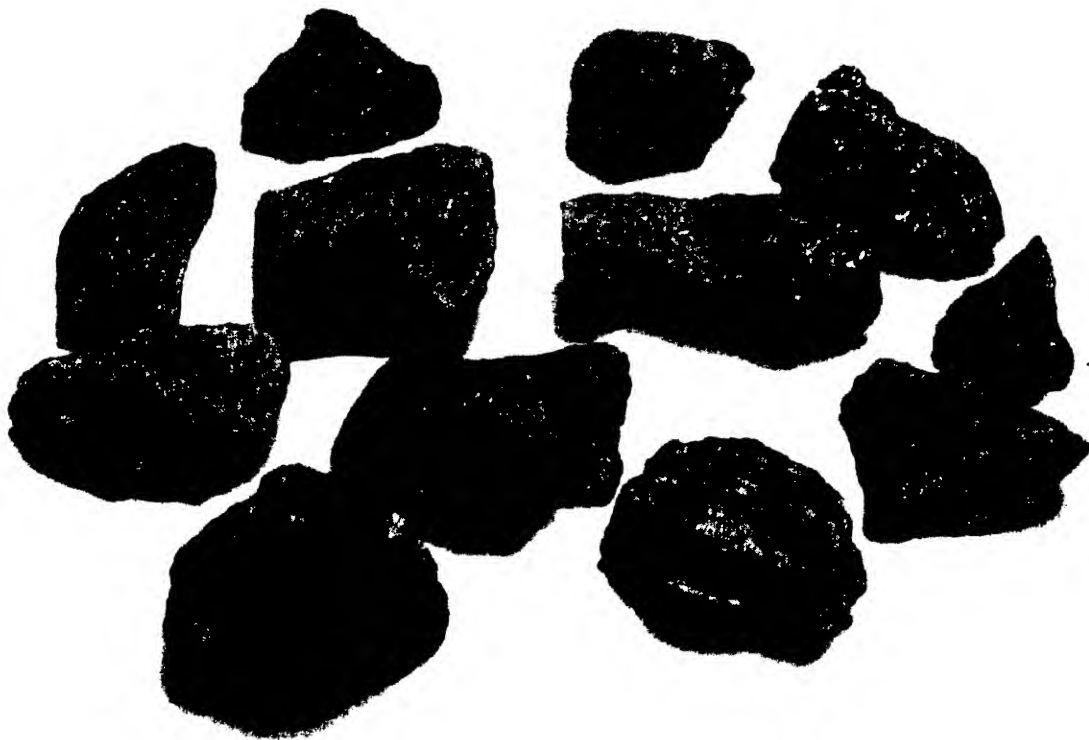


Figure 4.1  Crushed Slate LWA (3/4-inch Particles) From Carolina Stalite

Figure 4.2  Close-up of Slate LWA Clinker Showing Voids

Table 4.1  Stalite LWA Specifications

| Aggregate Size | 3/8-inch | | 1/2-inch | |
|---|---|---|---|---|
| Oven Dry Specific Gravity | 1.52 | | 1.44 | |
| Unit Weight Damp Loose (pcf) | 50 - 54 | | 48 – 52 | |
| Absorption 24-hr Soak After Oven Dry (Maximum Absorption) | 6 % (10 %) | | 6 % (10 %) | |
| Sieve Size | Percent Passing | ASTM[67] C 330 Specification | Percent Passing | ASTM[67] C 330 Specification |
| ¾-inch | 100 | 100 | 100 | 100 |
| ½-inch | 100 | 100 | 90 | 90-100 |
| ³/₈-inch | 100 | 75-100 | 53 | 40-80 |
| #4 | 33 | 20-45 | 12 | 0-20 |
| #8 | 3 | 0-15 | 5 | 0-10 |
| #100 | 2 | 0-10 | NA | NA |

61

LWA specific gravity values were checked on several occasions using a technique outlined by Holm as addressed in Section 2.5.5.[24] For comparison purposes, normal weight aggregate has a specific gravity in the range of 2.60-2.65 and a maximum absorption of about 2 percent.

## 4.2.2 Fine Aggregate

Initially, lightweight fines were used in mix development. Low strength values and the inability to control water absorption resulted in termination of lightweight fines. Locally available normal weight fine aggregate known as Brown Brothers (BB) natural concrete sand was used. BB sand was approved for structural concrete use by GDOT and resulted in better strength and mixes that were easier to control. The BB sand had a fineness modulus of 2.36, which is low for use in structural concrete. Table 4.2 lists the specifications of BB sand and shows how the sand meets DOT specifications but fails to meet ASTM specification C 33.[68]

Table 4.2  Brown Brothers Natural Concrete Sand Specifications

| Oven Dry Specific Gravity | 2.62 | | |
|---|---|---|---|
| Fineness Modulus | 2.36 | | |
| Percent Absorption | 0.5 % | | |
| Sieve Size | Percent Passing | ASTM C 33 Percent Passing | DOT 801.02D Percent Passing |
| # 4 | 100 | 95-100 | 95-100 |
| # 8 | 98.6 | 80-100 | |
| # 16 | 90.3 | 50-85 * | 45-95 |
| # 30 | 59.3 | 25-60 | |
| # 50 | 14.8 | 10-30 | 8-30 |
| # 100 | 1.3 | 2-10 * | 1-10 |
| Pass / Fail (*) | | Fail | Pass |

### 4.2.3  Overall Aggregate Gradation

Evaluations of the overall gradation of the coarse LWA and fine NWA combined indicated gaps in the grading for the # 8 and # 16 sieve sizes, but overages in the 3/8-inch, #4, and #50 sieve sizes.

### 4.2.4  Portland Cement

Type III cement supplied by Blue Circle Materials (now LaFarge) was used throughout mix design development based on the need to achieve early strength for prestressed girder construction.  Type III cement has a higher Blaine fineness modulus than Type I and has higher contents of $C_3S$ and $C_3A$ causing hydration to occur more rapidly.[69]

The field-mixing phase (Chapter 6) of the research project was conducted at Tindall Concrete in Jonesboro, Georgia.  Tindall used only Demopolis Type III Cement produced by CEMEX-Southdown Corporation.  It was discovered that the Demopolis Type III provided better early strength than the Blue Circle – LaFarge Type III. Demopolis Type III cement was also used for girder production.

Cement grind specifications were not available for either brand of cement.  Plant officials and quality control inspectors reported that the cements were ground in accordance with ASTM C 150.[70]

### 4.2.5  Mineral Admixtures

Silica fume and Class F fly ash were used in this research to improve concrete quality and durability, workability, and economy.  The silica fume used in this project

was provided by Grace Construction Products under the name of Force 10,000. The silica fume had a specific gravity of 2.2 and was included in mix designs in amounts of 2 to 10 percent of total cementitious materials by weight.

Boral Material Technologies provided the Class F fly ash used in this project under the name of "Bowen" ash. The fly ash was produced at the Georgia Power Generating Plant located in Bowen, Georgia. The Bowen fly ash had a specific gravity of 2.28 and was included in mix designs as 15 percent of cementitious materials by weight. The fly ash satisfied the requirements of ASTM C 618.[71]

### 4.2.6 Chemical Admixtures

The chemical admixtures, all provided by Grace Construction Products, included ADVA Flow, a high-range water reducer (HRWR), WRDA 35, a water reducer/set retarder, and Daravair 1000, an air-entraining admixture (AEA). ADVA Flow satisfied the requirements of ASTM C 494[72] Type F; the WRDA 35 satisfied the requirements of ASTM C 494[72] Type A and D; the Daravair 1000 satisfied the requirements of ASTM C 260.[73]

### 4.3 Moisture Control

Control of moisture and accurate determination of moisture content were two of the most important steps involved in making high quality HSLC. Low absorbed moisture in the LWA can result in mix water being absorbed thus reducing workability and changing the water cement ratio. Excess adsorbed water that is not properly accounted for in the mix design also impacts the mix by affecting the aggregate proportion and also

the water cement ratio. The following sections describe steps taken during the project to insure moisture was properly controlled in the lab. Moisture control in the field is addressed in Chapter 6.

### 4.3.1 Laboratory Material Storage

The LWA was initially stored in large sacs in the lab. Prior to using the aggregate, it was soaked in buckets overnight to insure the absorbed moisture content was adequate. The trouble with soaking aggregate in buckets was that the method was not something possible under plant conditions for the production of large amounts of HSLC. If a method did not transfer to plant operations, it was not used in the lab.

Aggregate storage hoppers were procured and installed outside the lab facility. A misting device was installed in the top of each hopper and run continuously until the aggregate had adequate absorbed moisture. Adequate absorbed moisture was 6 percent; anything below 6 percent was unacceptable.

The initial stages of mix development were conducted during the winter months when outside temperatures often dipped well below freezing at night. Often times, the water misted onto the LWA froze requiring that it be chipped from inside the hoppers. In the event this occurred, the aggregate was allowed to warm inside the lab prior to mixing concrete. Later in the development phase, hoppers were installed inside the lab where the temperature was above 55 degrees Fahrenheit at all times. Figures 4.3, 4.4, and 4.5 show the aggregate hoppers (outside and inside) and the misting devices as installed inside the lab facility. The misting devices were constructed with nozzles having an output of approximately 3 gallons per hour. The water flow through the aggregate was minimized

to prevent segregation of fine particles from occurring. To reduce the gradient of free

moisture inside the hoppers, the water was turned off 24 hours prior to concrete mixing.

The normal weight BB sand was also stored inside the lab in a hopper.
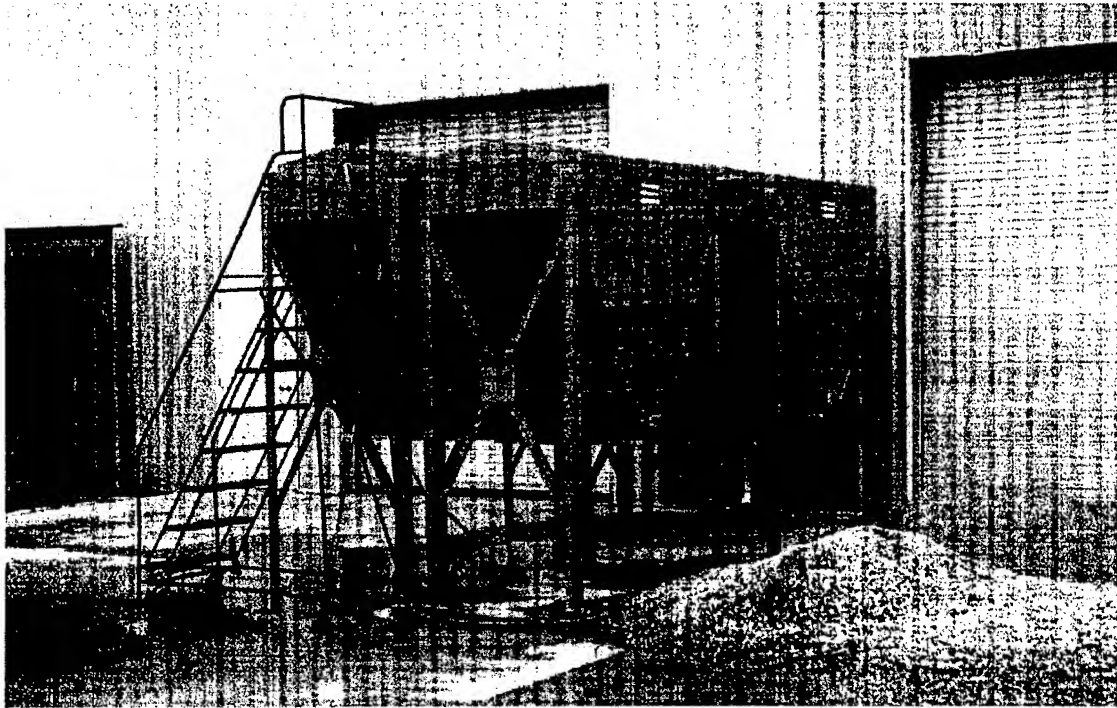


Figure 4.3  Exterior Aggregate Hoppers

Figure 4.4  Interior Aggregate Hoppers and Cement / Admixture Proportioning Station
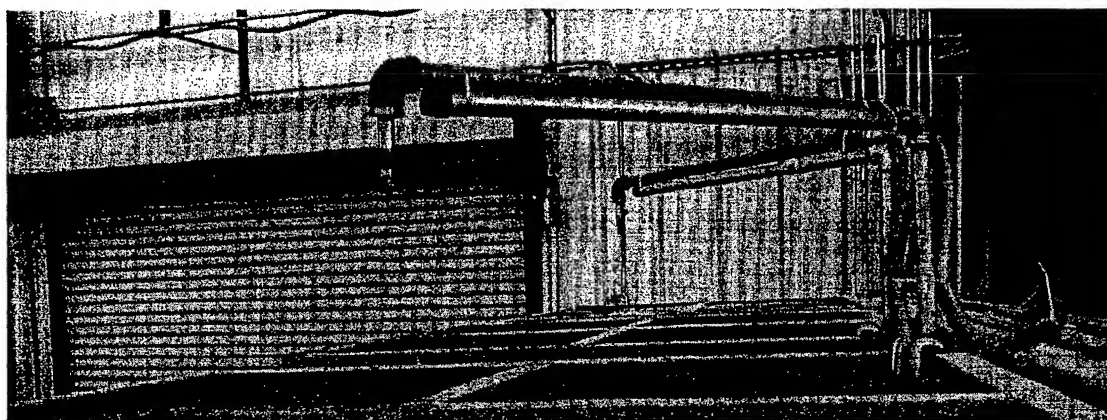


Figure 4.5  Misting Device Installed Over Interior Aggregate Hoppers

### 4.3.2 Determination of Moisture Content

Prior to mixing HSLC, a representative sample was taken from the aggregate hopper or stockpile. Moisture contents in the "as-is" and "saturated surface dry (SSD)" condition were determined from the representative sample by cooking the LWA over hotplates at a medium heat for approximately 1 hour or until all moisture had been removed. When LWA is heated, the internal pore water boils and explodes in a violent manner. To prevent flying aggregate particles from injuring people close by, screens were placed over top of the pan during cooking as shown in Figure 4.6.
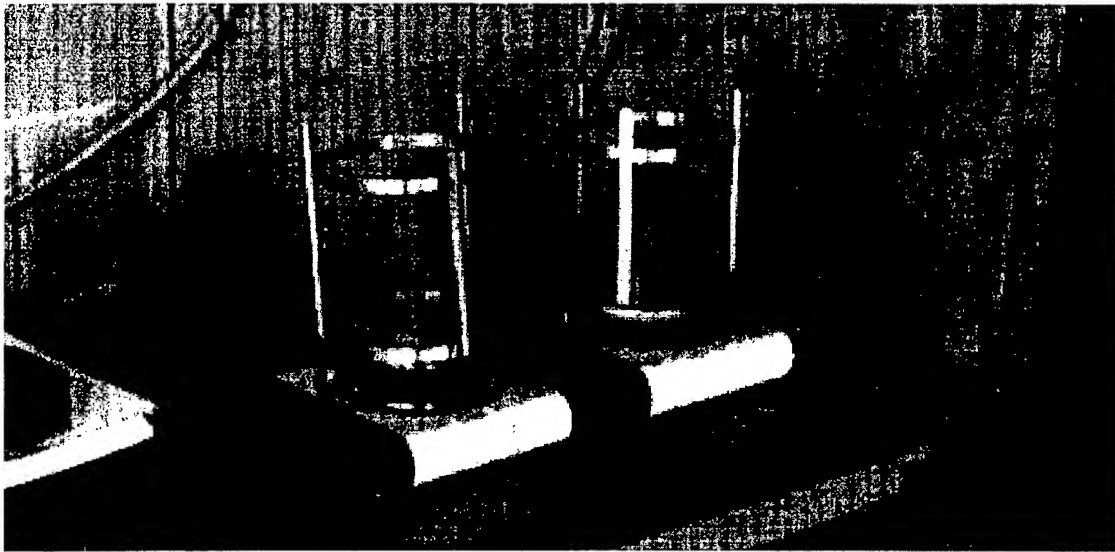


Figure 4.6 Screens Covering LWA During Moisture Test

When performing the "SSD" moisture check, the aggregate sample was placed on several layers of paper towels and patted dry prior to weighing. It was important to dry the aggregate sample to a point where there was no longer a shine on the surface.

Two methods were useful for determining when all moisture had been cooked from the aggregate. If no moisture accumulated on a piece of glass held over the cooking aggregate, it was dry. In addition, if the aggregate no longer "popped" it was considered dry.

Moisture content checks were also performed on the BB sand whenever a mix was made. Absorbed moisture was assumed to be 0.5 percent.

A material testing sheet was created as shown in Table 4.3 to simplify the testing procedure and reduce chances for error. The moisture content calculation procedure is explained on the sheet. Also covered in Table 4.3 is the determination of specific gravity using a pycnometer, which is covered in ACI 211.2-91.[18]

## 4.4 HSLC Mix Designs

As addressed in Chapter 2, there was no method available "off-the-shelf" for determining a mix design to achieve 12,000 psi HSLC. Previous mix designs and guidance from Stalite representatives provided the initial HSLC mix designs in this research. Based on suggestions from several sources, a mix design spreadsheet was developed to automate the numerous calculations required for a HSLC mix design. Appendix B provides an example of the spreadsheet and gives details on its use. The development of mix designs is covered in detail in Chapter 5, Development of HSLC Mix Designs.

Table 4.3 Material Testing Sheet

| Lightweight Concrete Material Testing Sheet |
|---|

Test Date / Location _____

Technician Name _____

| Aggregate Moisture Content Testing |
|---|

Time Test Started _____     Time Test Finished _____

Test Description                    _____ _____ _____ _____

A – Weight of Wet Aggregate and Pan     _____ _____ _____ _____

B – Weight of Pan                   _____ _____ _____ _____

C – Weight of Wet Aggregate  (A – B)    _____ _____ _____ _____

D – Weight of Dry Aggregate and Pan     _____ _____ _____ _____

E – Weight of Dry Aggregate  (D – B)    _____ _____ _____ _____

F – Weight of Water  (C – E)        _____ _____ _____ _____

**G – Percent Moisture  (F / E) x 100**   _____ _____ _____ _____

| Aggregate Specific Gravity Testing |
|---|

Time Test Started _____     Time Test Finished _____

Test Description                    _____ _____ _____ _____

A – Wt. of Pycnometer w/Agg. & Water    _____ _____ _____ _____

B – Wt. of Pycnometer w/ Water      _____ _____ _____ _____

C – Wt. of Aggregate                _____ _____ _____ _____

**SG = C / (C + B – A)**              _____ _____ _____ _____

## 4.5 Concrete Mixer

The concrete mixer used for all laboratory mixes was a pan mixer, model 30 DP, manufactured by Lancaster and shown in Figure 4.7.
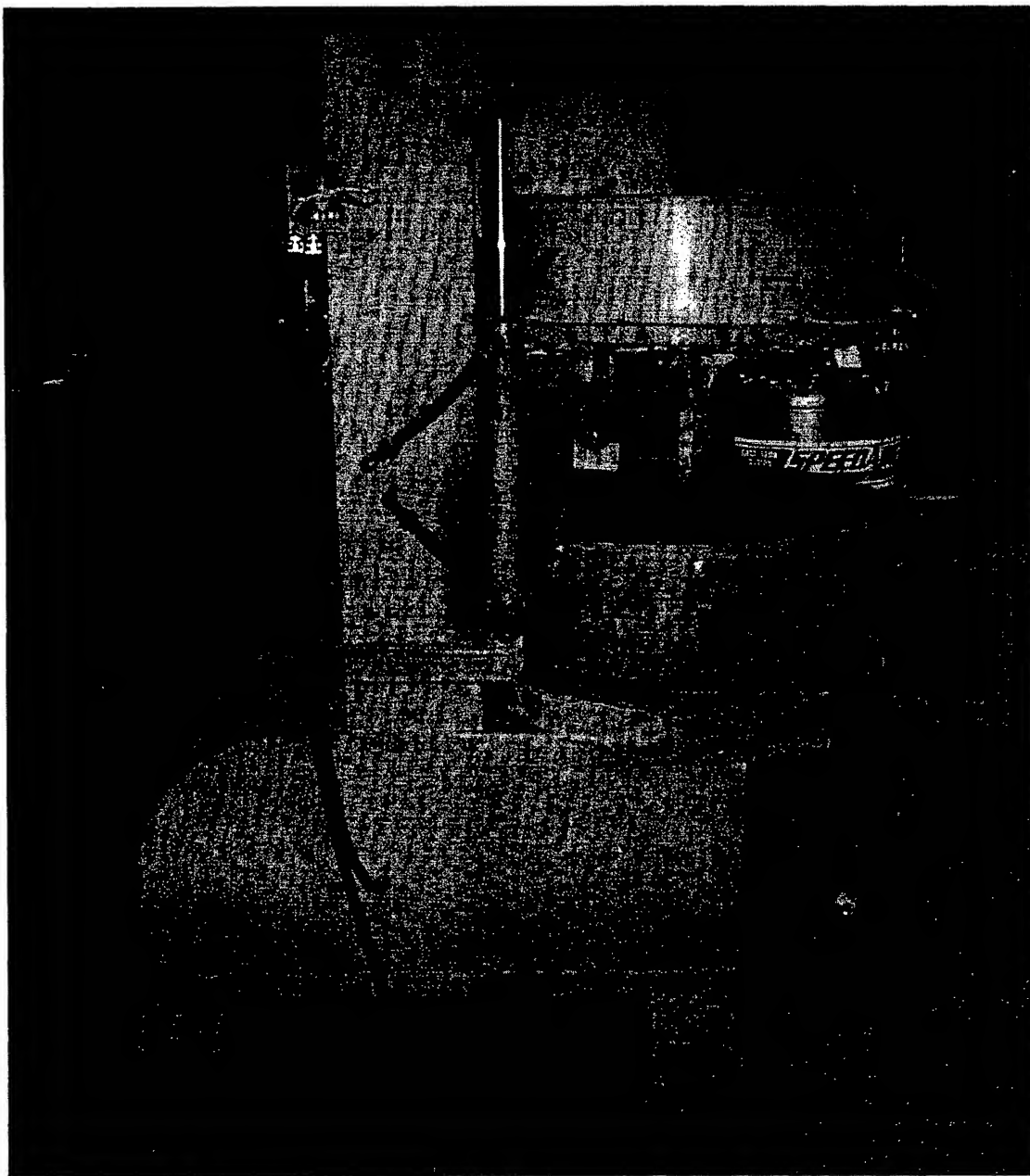


Figure 4.7  Lancaster Model 30 DP Pan Mixer

The Lancaster mixer operated with a shearing type action. The maximum amount of concrete that could be mixed in one batch was 1.75 cubic feet. Some trial mixes were made in a 4 cubic foot rotary mixer. The resulting mixes were poor; cylinder strengths were significantly lower than identical mixes made using the Lancaster mixer.

The concrete mixer used for field mixes is addressed in Chapter 6.

## 4.6 Order of Mixing

Components were added to the HSLC mixes in the following specific order. This order was developed over time and produced the best results.

1. Coarse Aggregate (Slate LWA)

2. Fine Aggregate (BB Natural Sand)

3. Approximately 2/3 of mix water combined with WRDA 35 (LRWR)

4. Daravair 1000 (AEA)

5. ADVA Flow (HRWR)

6. Type III Portland Cement

7. Class F Fly Ash

8. Remaining water / WRDA 35 mixture

9. Silica Fume

10. Additional ADVA Flow to achieve the desired workability

When mixing during the winter months, hot water (approximately 100 degrees F) was added to compensate for the cold aggregate to promote early strength gain. Steps 1-5

were performed immediately following each other. The components in the pan after step 5 were allowed to mix for one minute to insure consistent distribution of the AEA and water reducing admixtures. After the addition of the silica fume, the components were allowed to mix for approximately 2-3 minutes to insure thorough mixing. Additional ADVA (Step 10) was tracked on the mix design sheet for future reference. The same component addition sequence was used for lab and field mixing with good success.

## 4.7 HSLC Properties

After batching the HSLC, four properties of the concrete were tested. The slump was measured using a standard slump cone per ASTM C 143.[74] The unit weight was measured with a 1/4 cubic foot bucket per ASTM C 138.[75] The temperature of the concrete was measured using ASTM C 1064.[76] The air content was measured with a roll-a-meter per ASTM C 173.[77]

A common misconception is that air content can be determined for LWC with a pressure meter per ASTM C 231.[78] Since the LWA is a porous material, the pressure test can force water into the pore structure resulting in an incorrect (high) air content reading. Close examination of ASTM C 231 reveals that the test is not to be used for LWC.

## 4.8 Preparation of Specimens

Specimens were made per ASTM C 31.[79] Cylinders size 4 inches x 8 inches (4 x 8) were cast for determining compressive strength per ASTM C 39.[80] Cylinders size 6 inches x 12 inches (6 x 12) were cast for determining modulus of elasticity per ASTM C 469.[81] Beams size 4 inches x 4 inches x 14 inches (4 x 4 x 14) were cast to perform the

modulus of rupture test per ASTM C 78.[82] Cylinders size 4 inches in diameter x 15

inches with DEMEC gage inserts were cast in steel molds for creep testing per ASTM C

512.[83] Figures 4.8 and 4.9 show casting a beam and creep specimen molds, respectively.



Figure 4.8  Casting 4 x 4 x 14 Modulus of Rupture Specimens at Tindall Concrete Plant
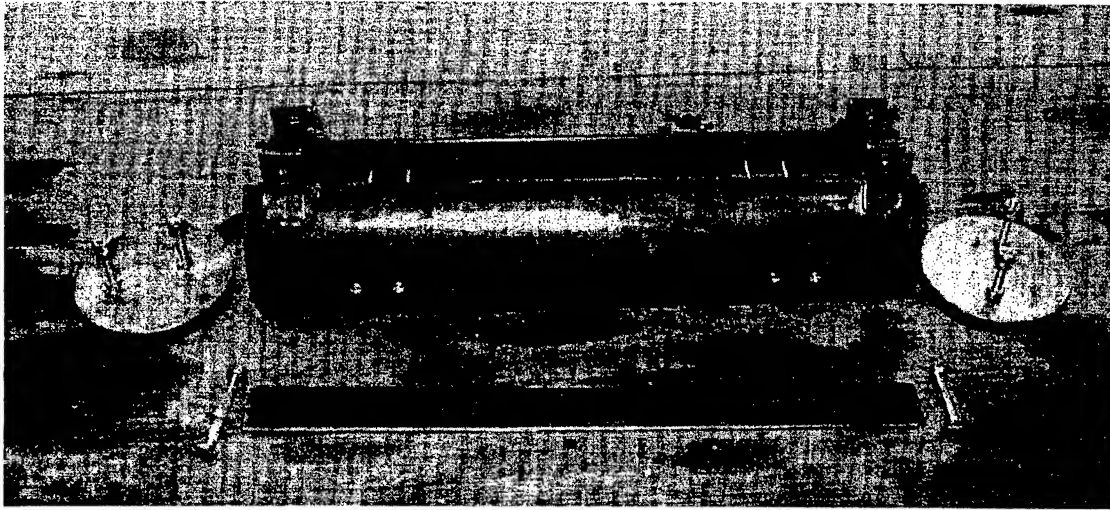
Figure 4.9  Specimen Mold for Creep and Shrinkage Testing

In addition to the standard specimen molds, a block measuring 24 inches x 12 inches x 36 inches was cast to allow coring cylinders for strength testing.  During girder construction, a similar block 24 inches deep was cast to perform the prestressing strand direct pullout test.  Figures 4.10 and 4.11 show construction of these two blocks.
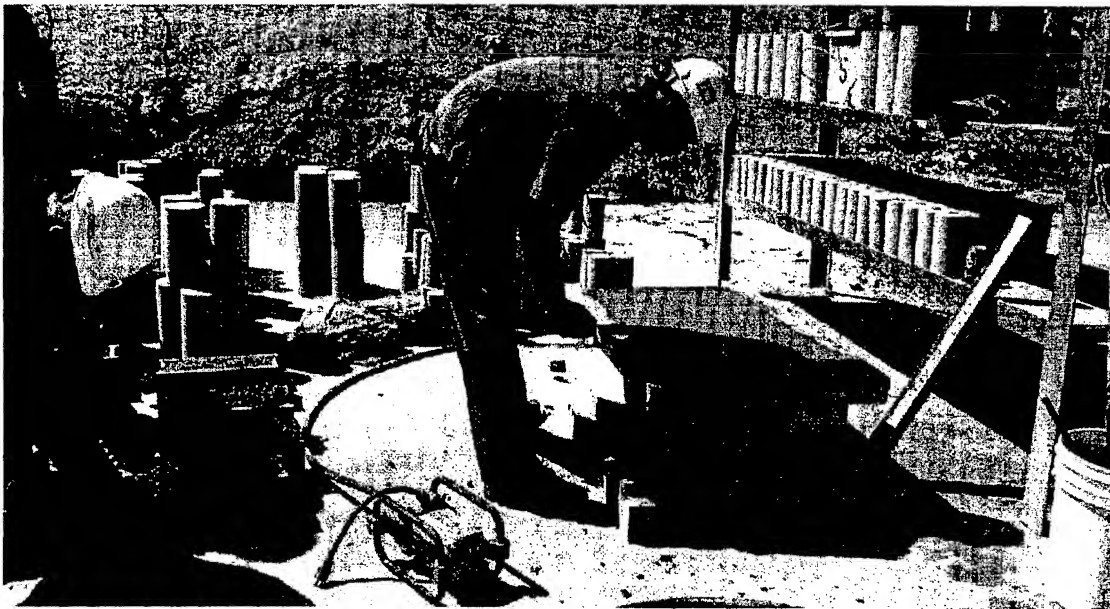


Figure 4.10  Construction of Block for Cored Cylinder Testing at Tindall Concrete Plant

Figure 4.11  Casting of Block for Direct Pullout Test at Tindall Concrete Plant

## 4.9 Specimen Curing

After casting specimens, the method of curing varied. Specimens were initially

cured either on site or in the lab as per ASTM C 31, or were placed in a curebox to retain

the heat of hydration. Accelerated curing using a curebox (Figure 4.12) was not covered

by any ASTM specification, but had been shown to closely replicate girder curing

conditions in previous research.[84] After 24 hours, all specimens (except cored cylinder

blocks and direct pullout test blocks which remained on site for 56 days) were removed

from molds and placed in a fog room for curing through the time of testing. The fog

room maintained 100 percent humidity and a temperature of approximately 73 degrees

Fahrenheit. Moduli of rupture specimens were cured in a lime bath in the fog room until

the time of testing.

76
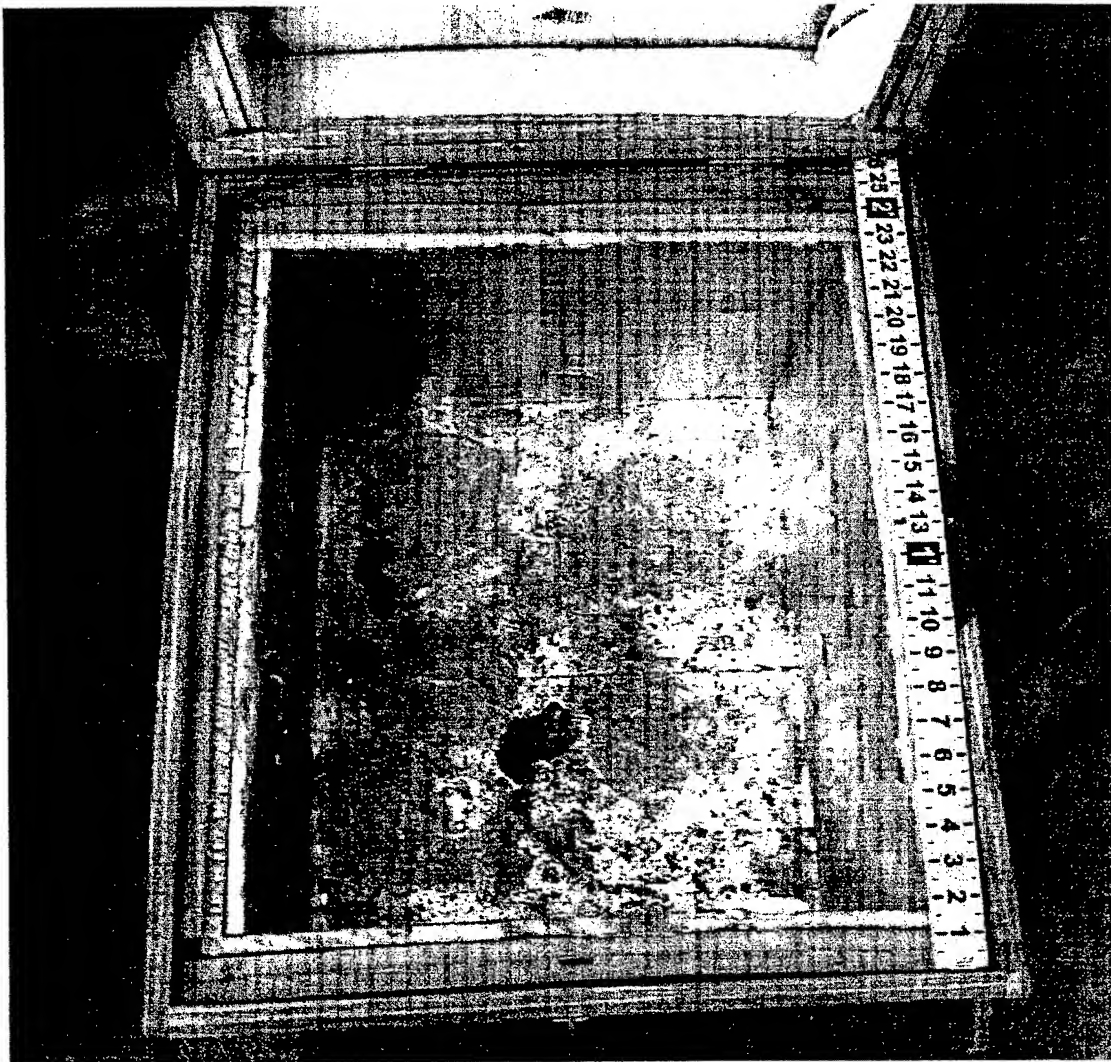
Figure 4.12  Insulated Curebox Used for Accelerated Curing

After placing specimens in the curebox, any remaining empty space around the specimens was filled with an insulating fabric.

## 4.10 Specimen Testing

Specimen testing was performed at specified times depending on the type of mix and phase of the research project. All tests were performed in accordance with the appropriate ASTM specification as follows.

### 4.10.1 Compressive Strength

Compressive strength testing was performed according to ASTM C 39[80] using hard rubber caps seated in steel end caps according to ASTM 1231.[85] The hard rubber caps were cut from 1/2-inch conveyor belt material and reused as long as the surface condition did not show signs of wear. Based on testing HSLC, a set of rubber caps could be used to test from 30 to 50 cylinders prior to replacement. Prior to testing, the cylinder ends were smoothed as necessary to remove ridges or bumps that could affect strength results.

### 4.10.2 Modulus of Elasticity

Modulus of elasticity testing was performed according to ASTM C 469[81] using 6 x 12 cylinders and hard rubber end caps as described in 4.10.1. Prior to performing the test, the average compressive strength of three 4 x 8 cylinders was determined. Based on the 4 x 8 strength, the predicted ultimate load was calculated for the 6 x 12 as well as 40 and 60 percent of the ultimate value. The modulus test frame (Figure 4.13) was installed on the 6 x 12 cylinder and the specimen placed in the 400-kip Baldwin load test machine. The specimen was initially loaded to 40 percent of ultimate to seat the cylinder and modulus test frame.

78
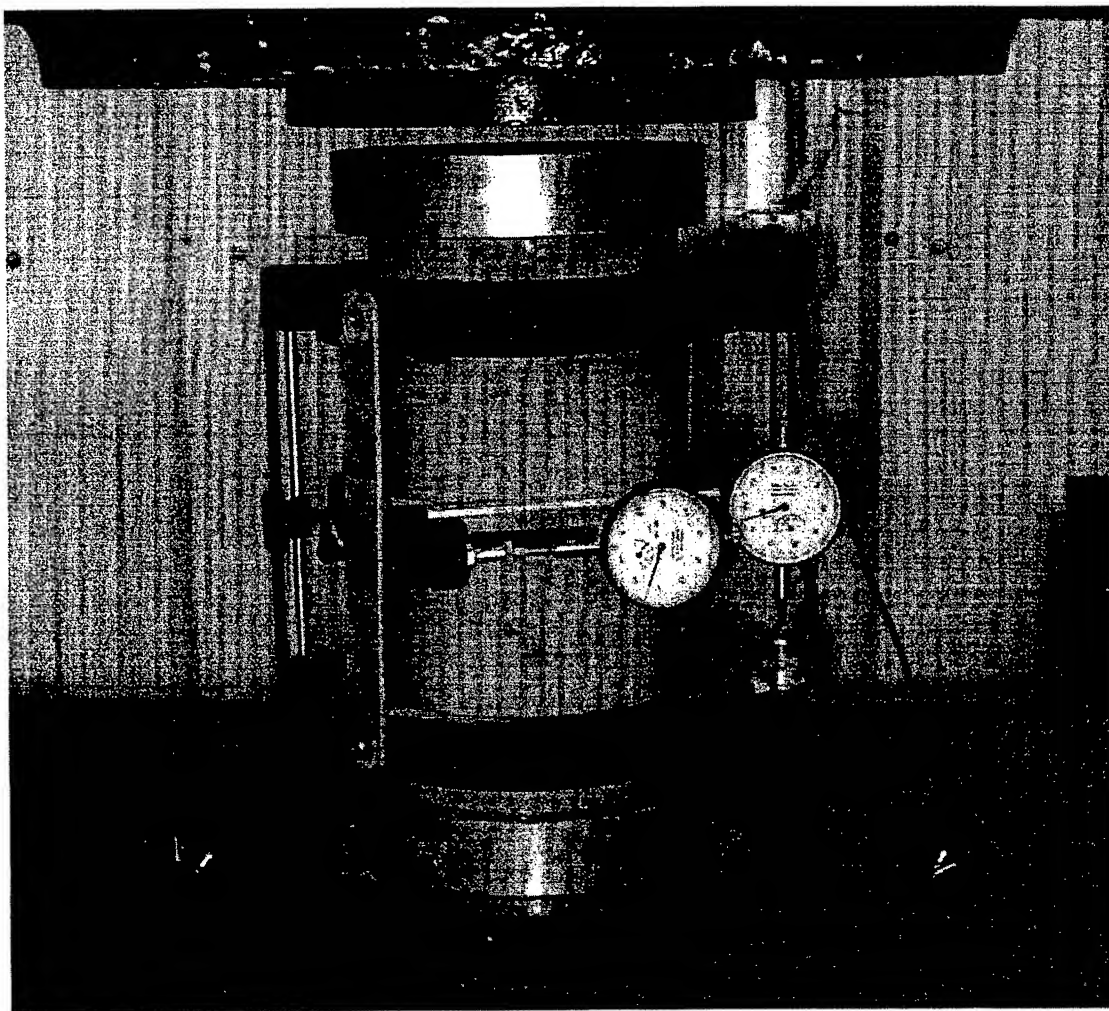
Figure 4.13  Modulus of Elasticity Testing Frame

After unloading the specimen, gages were zeroed and the specimen loaded to 60

percent of its ultimate strength.  A data-taking sheet (Table 4.4) was created to simplify

the test procedure.  Data from the sheet was entered into a spreadsheet, which then

determined the modulus of elasticity and Poisson's ratio.  Critical to properly calculating

the modulus of elasticity and Poisson's ratio values were determination of lengths and

gage ratios from the test frame as per ASTM C 469.[81]

Table 4.4  Elasticity Modulus and Poisson's Ratio Test Data Sheet

| **Elasticity Modulus and Poisson's Ratio Data Sheet** |
|---|

Spec. Number _____ Date / Time _____ Est. Ult. _____ kips (4x8)

40% Est. Ult. _____ kips   60% Est. Ult. _____ kips   Ult. Load _____ kips (6x12)

Initial load to 40% of estimated ultimate accomplished to seat cylinder - yes / no.

Load cylinder (Tests A,B) to 60% of estimated ultimate while recording data below.

| Longitudinal Gage Reading (inches) | Test A | | Test B | |
|---|---|---|---|---|
| | Load (kips) | Lateral Gage Reading (inches) | Load (kips) | Lateral Gage Reading (inches) |
| 0.00000 | | | | |
| 0.0008 | | | | |
| 0.001 | | | | |
| 0.002 | | | | |
| 0.003 | | | | |
| 0.004 | | | | |
| 0.005 | | | | |
| 0.006 | | | | |
| 0.007 | | | | |
| 0.008 | | | | |
| 0.009 | | | | |
| 0.010 | | | | |
| 0.011 | | | | |
| 0.012 | | | | |
| 0.013 | | | | |
| 0.014 | | | | |
| 0.015 | | | | |
| 0.016 | | | | |
| 0.017 | | | | |
| 0.018 | | | | |
| 0.019 | | | | |
| 0.020 | | | | |
| 0.021 | | | | |
| 0.022 | | | | |
| 0.023 | | | | |
| 0.024 | | | | |
| 0.025 | | | | |
| 0.026 | | | | |

### 4.10.3 Modulus of Rupture

The modulus of rupture was determined in accordance with ASTM C 78[82] using 4

x 4 x 14 beams tested using third-point loading. Figure 4.14 shows the modulus of

rupture test set-up.
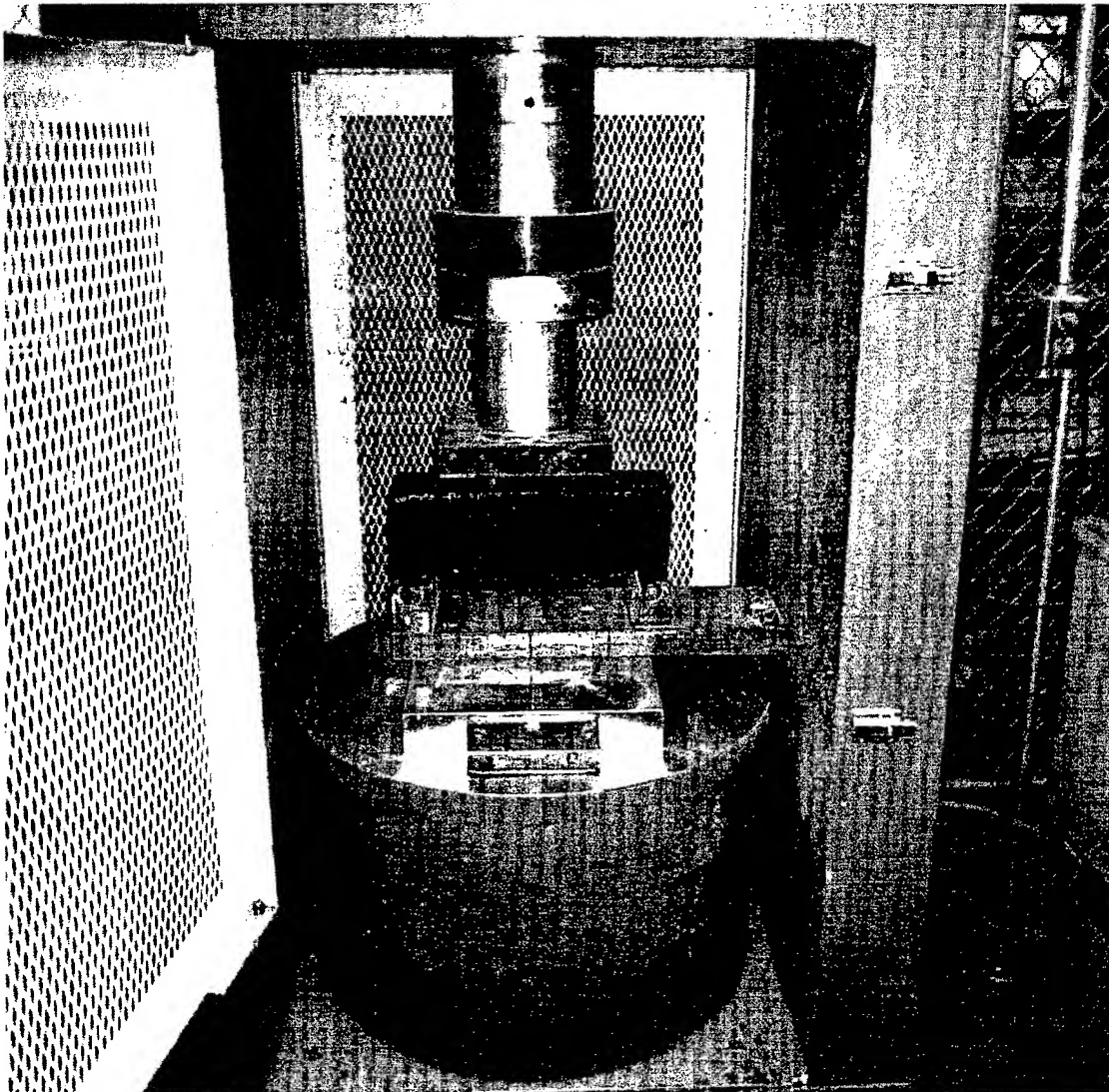


Figure 4.14  Modulus of Rupture Test Set-up

# CHAPTER V

# DEVELOPMENT OF HSLC MIX DESIGNS

## 5.1 Introduction

The purpose of this chapter is to discuss the laboratory development of the HSLC

mix designs that were later tested under field conditions and ultimately used to construct

pretensioned girders. The goal of this laboratory development phase was to configure

HSLC mix designs that would achieve 8, 10 and 12 ksi design compressive strengths at

28 days; the target mean compressive strengths were 1,400 psi greater than the design

strengths. In order to achieve those strengths, over 75 test mixes were batched and over

700 4 x 8 cylinders were tested.

## 5.2 Specimen and Curing Plan

The specimens cast during this phase predominantly 4 x 8 cylinders. The interest

initially was to configure mix designs to achieve the objective strengths. Thus, 9 each 4 x

8 cylinders were cast from each mix and cured initially in cureboxes. After 24 hours in

the curebox, 3 of the 9 cylinders were tested for compressive strength; the remaining 6

were placed in the fog room to continue curing for strength testing at 3 and 28 days.

82

## 5.3 Initial Mix Designs From Carolina Stalite

The starting points for the three objective HSLC mix design strengths were suggested mix designs received from experts at Carolina Stalite and shown in Table 5.1.

Table 5.1  Initial HSLC Mix Designs from Carolina Stalite

| Concrete Components to Produce 1 Cubic Yard of HSLC | | Concrete Strength (psi) | | |
|---|---|---|---|---|
| | | 8,000 | 10,000 | 12,000 |
| 1/2-inch Stalite LWA | (lbs) | 950 | 950 | 950 |
| Normal Weight Fine Aggregate | (lbs) | 1221 | 1063 | 905 |
| Class F Fly Ash | (lbs) | 200 | 200 | 200 |
| Silica Fume | (lbs) | 35 | 45 | 56 |
| Cement | (lbs) | 500 | 650 | 800 |
| Water | (gals) | 32 | 33 | 34 |
| Air Content | (percent) | 4 | 4 | 4 |
| Water / Cementitious Materials Ratio | (W/CM) | 0.36 | 0.31 | 0.27 |
| Theoretical Equilibrium Unit Weight | (pcf) | 117.5 | 117.9 | 118.3 |

The coarse aggregate used in all initial mixes was the 1/2-inch Stalite LWA. Dosing on chemical admixtures was not initially specified in the Stalite mixes. Literature from Grace Construction Products and guidance from the local sales representative served as starting points.

## 5.4 Plan for Mix Development

Below are listed the steps followed in determining the optimum HSLC mix designs to meet the objective strengths.

1. Holding all other parameters steady, vary the ratio of coarse LWA to fine NWA over a wide range from approximately 1 to 2. Determine if an optimum coarse to fine aggregate ratio exists in that range.

83

2. Using the result of Step 1 and holding all other parameters steady, vary the percent cement paste in the mix from approximately 33 percent to 45 percent. Cement paste was defined as all components in the mix design except the aggregate. Determine if an optimum percent cement paste exists in that range.

3. Using the result of Steps 1 and 2 and holding all other parameters steady, vary the percent of silica fume in the mix from approximately 4 to 12 percent of the total cementitious materials (CM). Determine if an optimum percent silica fume exists in that range.

4. Using the results of Steps 1 – 3 (if possible), test the apparent optimum mix design with different size aggregates to determine the effect.

Based on the objective strength of 12,000 psi, a water to cementitious materials (W/CM) ratio of 0.23 was selected for mix proportioning.

## 5.4.1 Initial Mixes and Entrained Air

During the execution of Step 1, manufacturer suggested dose rates were followed for chemical admixtures. The first major problem encountered involved excessive air content. It became apparent over time that the air-entraining agent (AEA) was enhanced by the use of high-range water reducing (HRWR) admixture. In some cases, the resulting air contents approached 10 percent.

In order to determine specific details about the source of the air, and whether it was entrapped or entrained air, a study was conducted that was not part of the original development plan. The study involved making three batches of concrete as described in

Table 5.2. The 8,000 psi suggested mix design from Carolina Stalite was used for the test mixes.

Table 5.2  Air Content Study

| Type of Coarse Aggregate | Admixtures Used | Resulting Percent Air Content |
|---|---|---|
| Normal Weight (Granite) | ADVA and WRDA 35 | 2.0 |
| 1/2-inch Stalite LWA | ADVA and WRDA 35 | 2.0 |
| 1/2-inch Stalite LWA | No Admixtures | 2.0 |

The resulting air contents shown in Table 5.2 indicated that neither the use of LWA or the use of ADVA and WRDA 35 had an impact on air content. Since the air content was the same for each mix, it was apparent that the mix most likely had 2 percent "entrapped" air. In order to achieve 4 percent air content total, only 2 additional percent were required. This was an indication that most likely a small dose of AEA would result in 4% total air content. Future mixes were dosed with only 0.75 to 1.0 fluid ounces of Daravair 1000 (AEA) per 100 weight of cementitious materials. Since the HRWR enhanced the effectiveness of the AEA, less AEA was required at higher HRWR dose rates. Based on manufacturer literature, 0.75 fluid ounces per 100 weight of CM was the lowest recommended AEA dose rate.

## 5.4.2 Variation of Coarse to Fine Aggregate Ratio – Step 1

The coarse to fine aggregate ratio was defined as the volume of coarse aggregate divided by the volume of fine aggregate. The parameters in Table 5.3 were held constant throughout all mixes in Step 1:

Table 5.3  Parameters Held Constant in Step 1

| Water / Cementitious Materials Ratio | 0.23 |
|---|---|
| Percent Cement Paste | 39 |
| Fly Ash as Percent of Total Cementitious Materials | 15 |
| Silica Fume as Percent of Total Cementitious Materials | 8 |
| Type III Cement as Percent of Total Cementitious Materials | 77 |

The results of Step 1 are shown in Table 5.4 and graphed in Figure 5.1.

Table 5.4  Results of Varying Coarse to Fine Aggregate Ratio – Step 1

| Coarse to Fine Aggregate Ratio By Volume | 1-Day Compressive Strength (psi) | 3-Day Compressive Strength (psi) | 28-Day Compressive Strength (psi) |
|---|---|---|---|
| 0.94 | 8,070 | 8,960 | 10,100 |
| 1.09 | 8,550 | 8,860 | 10,350 |
| 1.26 | 8,980 | 9,090 | 10,360 |
| 1.46 | 9,130 | 10,440 | 11,020 |
| 1.71 | 7,830 | 9,370 | 10,020 |
| 2.01 | 6,820 | 7,970 | 10,610 |

Figure 5.1 indicates that the optimum coarse to fine aggregate ratio using 1/2-inch Stalite LWA was approximately 1.46. The resulting strengths did not vary significantly, yet indicated a trend.

A similar study using 3/8-inch Stalite LWA showed the optimum ratio also to be approximately 1.5.
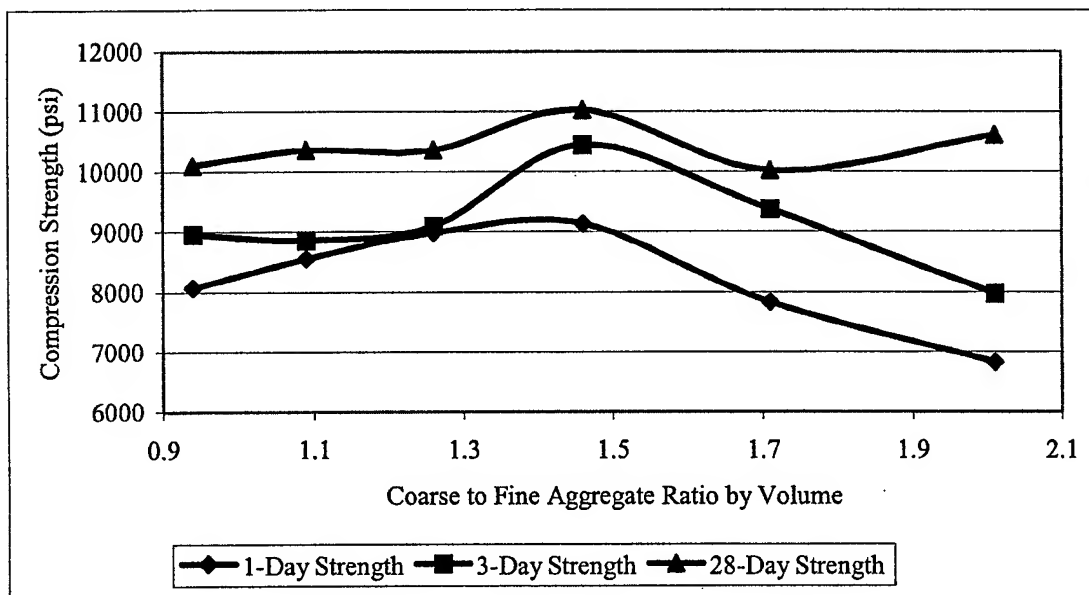
Figure 5.1  Results of Varying Coarse to Fine Aggregate Ratio

## 5.4.3  Variation of Percent Cement Paste – Step 2

Using the optimum coarse to fine ratio of 1.46 determined in Step 1, mixes were

configured for Step 2 where the percent cement paste was varied between 33 and 39

percent.  For a well-graded aggregate profile, 33 percent cement paste was considered

optimum.  The aggregate grading for this project contained gaps in the #8 and #16

particle sizes.  Thus, it was thought that by examining the range from 33 to 39 percent

that the additional paste would effectively fill the gaps in the smaller particle sizes.   The

parameters in Table 5.5 were held constant throughout all mixes in Step 2:

Table 5.5  Parameters Held Constant in Step 2

| Water / Cementitious Materials Ratio | 0.23 |
|---|---|
| Coarse to Fine Aggregate Ratio by Volume | 1.46 |
| Fly Ash as Percent of Total Cementitious Materials | 15 |
| Silica Fume as Percent of Total Cementitious Materials | 8 |
| Type III Cement as Percent of Total Cementitious Materials | 77 |

The results of Step 2 are shown in Table 5.6 and graphed in Figure 5.2.

Table 5.6  Results of Varying Percent Cement Paste – Step 2

| Percent Cement Paste | 1-Day Compressive Strength (psi) | 3-Day Compressive Strength (psi) | 28-Day Compressive Strength (psi) |
|---|---|---|---|
| 33 | 6,760 | 7,880 | 9,420 |
| 35 | 8,950 | 9,350 | 8,360 |
| 37 | 8,810 | 9,420 | 10,280 |
| 39 | 8,920 | 9,360 | 10,550 |
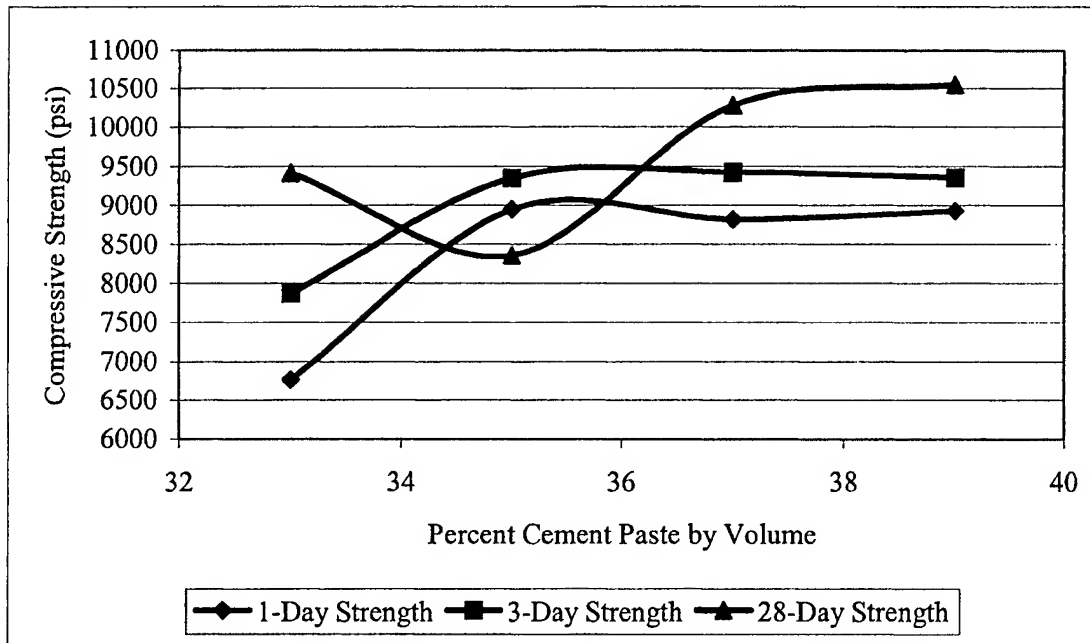


Figure 5.2  Results of Varying Percent Cement Paste

The results of Step 2 indicated the optimum percent cement paste was not at 33 percent based on the known gap grading in the aggregate profile. The need for additional cement paste appeared necessary. Figure 5.2 did not indicate an optimum value, but appeared to show a plateau that encompassed 39 percent based on 28-day strength. The drop in strength at 28 days for the 35 percent tests could not be explained. Thirty nine percent was chosen as the optimal percent cement paste value and was implemented in Step 3.

A similar study performed using 3/8-inch Stalite LWA and varying the percent cement paste from 35 to 45 percent also showed the optimum value to be around 39 percent. Based on gap grading in the overall aggregate profile considering 3/8-inch Stalite LWA and BB sand proportioned at a coarse to fine aggregate ratio of 1.5, this higher level of cement paste also was justifiable.

### 5.4.4 Variation of Percent Silica Fume– Step 3

Using the optimum coarse to fine ratio of 1.46 determined in Step 1, and the optimum percent cement paste of 39 percent determined in Step 2, mixes were configured for Step 3 where the percent silica fume was varied from 4 to 12 percent of total cementitious materials by weight. Based on the literature, it was thought that 8 percent silica fume was the upper limit for useful mix designs.[69] The parameters in Table 5.7 were held constant throughout all mixes in Step 3. Since the percent of silica fume varied during this step, the percent of cement had to vary as well in order to maintain a constant percent cement paste and W/CM ratio.

Table 5.7  Parameters Held Constant in Step 3

| Water / Cementitious Materials Ratio | 0.23 |
|---|---|
| Coarse to Fine Aggregate Ratio by Volume | 1.46 |
| Percent Cement Paste by Volume | 39 |
| Fly Ash as Percent of Total Cementitious Materials | 15 |

The results of Step 3 are shown in Table 5.8 and graphed in Figure 5.3.

Table 5.8  Results of Varying Percent Silica Fume – Step 3

| Percent Silica Fume | 1-Day Compressive Strength (psi) | 3-Day Compressive Strength (psi) | 28-Day Compressive Strength (psi) |
|---|---|---|---|
| 4 | 8,540 | 8,710 | 10,660 |
| 6 | 8,920 | 9,470 | 10,550 |
| 8 | 8,820 | 9,400 | 10,930 |
| 10 | 10,620 | 11,190 | 11,330 |
| 12 | 10,200 | 10,500 | 11,080 |
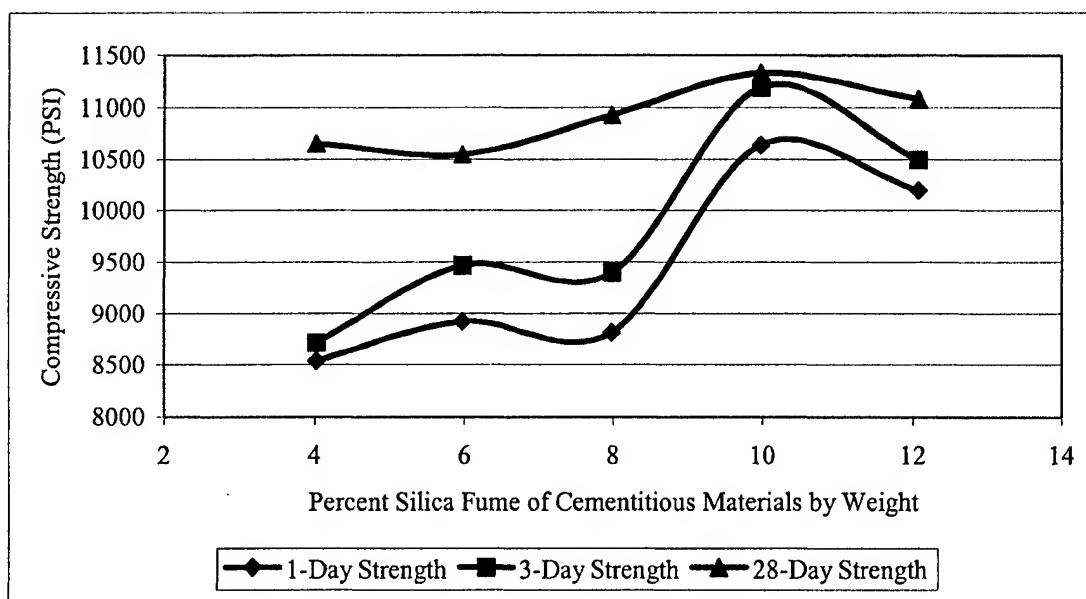


Figure 5.3  Results of Varying Percent Silica Fume

90

Figure 5.3 indicates that silica fume used as 10 percent of the total cementitious materials by weight provided the best strength results at 1, 3 and 28 days. The use of 10 percent silica fume required the use of additional HRWR to provide necessary workability.

### 5.4.5 Strength Ceiling

The concept of a strength ceiling was discussed in Section 2.7.2. During mix development, it was noticed that a reduction of the W/CM ratio below 0.23 did not result in higher strengths. The strength ceiling also appeared to be inversely related to LWA size. The use of smaller aggregate resulted in higher compressive strengths. In order to investigate this phenomenon, a series of mixes was conducted as specified in Table 5.9. The high-strength normal weight concrete (HSNWC) listed in Table 5.9 was used for two sets of specimens. The first set incorporated all components in the mix design as listed. The second set of specimens contained only the portion of the mix that would pass through a 3/8-inch screen. The mix was screeded through a 3/8-inch screen in an attempt to remove the larger size coarse aggregate for purposes of determining the strength of the paste. While there may have been some small particles of the granite remaining in the paste, the vast majority was removed during screeding. The volume of coarse aggregate was identical for both mixes; the weight difference between the LWA and NWA is an indication of the weight reduction achieved with HSLC.

Table 5.9  Mixes for "Strength Ceiling" Study

| Concrete Components to Produce 1 Cubic Yard | | HSLC | HSNWC |
|---|---|---|---|
| # 67 Crushed Granite | (lbs) | -- | 1,574 |
| ½-inch Stalite LWA | (lbs) | 948 | -- |
| BB Sand | (lbs) | 1100 | 1100 |
| Class F Fly Ash | (lbs) | 152 | 151 |
| Silica Fume | (lbs) | 101 | 101 |
| Type III Cement | (lbs) | 760 | 758 |
| WRDA 35 | (fl oz) | 61 | 61 |
| ADVA Flow | (fl oz) | 132 | 173 |
| Daravair 1000 | (fl oz) | 7.5 | 7.5 |
| Water | (gal) | 28.1 | 27.8 |

| Slump | (inches) | 4 | 5 |
|---|---|---|---|
| Plastic Unit Weight | (pcf) | 122.4 | 147.6 |
| Temperature | (def F) | 81 | 82 |

The results of the strength ceiling study are listed in Table 5.10.  The HSNWC paste had the highest strength followed by the HSNWC then the HSLC.  It would appear from the data that the strength ceiling for HSLC made with 1/2-inch Stalite LWA is around 11,400 psi.  This result is in keeping with values estimated by Harmon.[45]  Figure 5.4 shows a graph of the results in Table 5.10.

Table 5.10  Results of "Strength Ceiling" Study

| Concrete Type | 1-Day Strength (psi) | 3-Day Strength (psi) | 28-Day Strength (psi) |
|---|---|---|---|
| HSNWC Paste | 11,780 | 13,160 | 13,380 |
| HSNWC | 11,740 | 12,050 | 13,060 |
| HSLC | 10,800 | 11,190 | 11,390 |
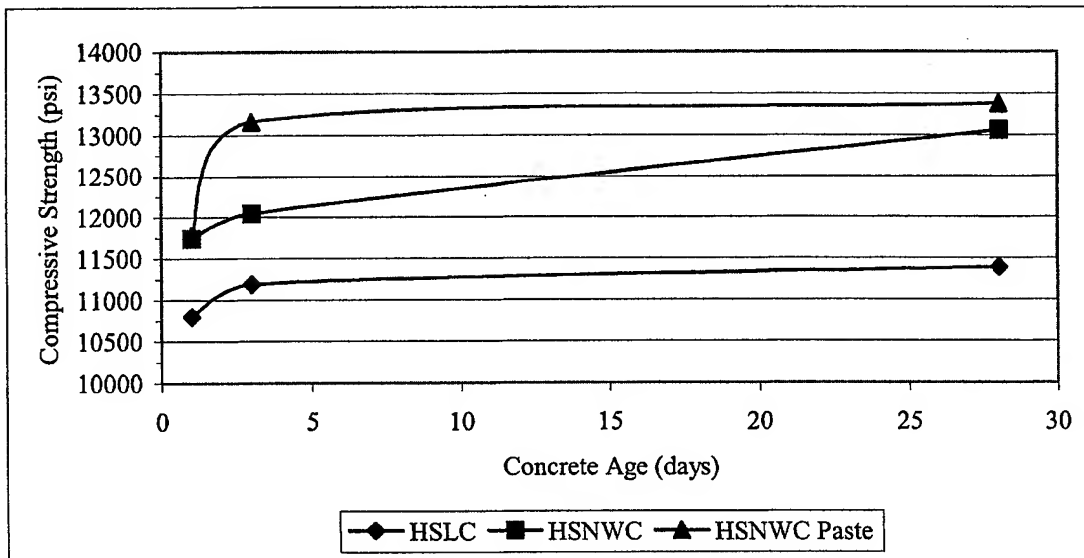
Figure 5.4  Results of "Strength Ceiling" Study

## 5.5  Final Mix Designs

Using the optimum values determined in Steps 1, 2 and 3 (1.46 coarse to fine

ratio, 39 percent cement paste, and 10 percent silica fume) and results of strength testing,

the mix designs shown in Table 5.11 were suggested for 8,000, 10,000, and 12,000-psi

strengths using 1/2-inch Stalite LWA.  It was thought that the use of 1/2-inch aggregate

would be more readily accepted in the precast industry than the smaller 3/8-inch

aggregate.  The mixes were configured by altering the content of CM based on W/CM

ratios deemed necessary for each concrete strength.

Strength results of laboratory mixes using the final mix designs are given in

Figure 5.5.  The 12 mix underwent a drop in strength between 1 and 7 days, but increased

in strength between 7 and 28 days.

93

Table 5.11  Objective 8,000, 10,000, and 12,000 psi Mix Designs for Field Testing

| Concrete Components to Produce 1 Cubic Yard of HSLC Aggregate Assumed to be at SSD | | Concrete Mix Designation Objective Strength (psi) | | |
|---|---|---|---|---|
| | | 8 Mix 8,000 | 10 Mix 10,000 | 12 Mix 12,000 |
| 1/2-inch Stalite LWA | (lbs) | 1022 | 1030 | 1030 |
| Normal Weight Fine Aggregate | (lbs) | 947 | 955 | 955 |
| Class F Fly Ash | (lbs) | 142 | 145 | 150 |
| Silica Fume | (lbs) | 19 | 50 | 100 |
| Type III Cement | (lbs) | 783 | 765 | 740 |
| WRDA 35 | (fl oz) | 57 | 58 | 59 |
| ADVA Flow | (fl oz) | 57 | 65 | 139 |
| Daravair 1000 | (fl oz) | 9.4 | 9.6 | 7.5 |
| Water | (gals) | 32.1 | 29.9 | 27.3 |
| Water / Cementitious Materials Ratio  (W/CM) | | 0.28 | 0.26 | 0.23 |
| Theoretical Equilibrium Unit Weight | (pcf) | 115.6 | 116.2 | 116.6 |



Figure 5.5  Strength Results of Laboratory Developed HSLC Mix Designs

94

# CHAPTER VI

# FIELD PRODUCTION OF HSLC

## 6.1 Introduction

The purpose of this chapter is to describe the field production of the HSLC mix

designs developed in the lab and discussed in Chapter 5. The goal of this phase of the

research project was to verify that the HSLC mix designs and procedures determined and

tested in the lab could be replicated under field conditions.

## 6.2 Concrete Plant Equipment Description

All field production testing was performed at the Tindall Concrete Plant in

Jonesboro, Georgia. The plant (Figure 6.1) specialized in the construction of bridge

girders for use on highway and rail applications and double-tee girders used for various

applications.



Figure 6.1 Tindall Concrete Plant, Jonesboro, Georgia

Aggregate storage was in large bins behind the mixing tower. Aggregate dropped

through control gates at the base of the bins to a conveyor belt, which transported the

material into hoppers atop the mixing tower. The bin into which the 1/2-inch Stalite

LWA was delivered (Figure 6.2) was equipped with a sprinkler to wet the aggregate prior

to use.



Figure 6.2  Tindall Aggregate Storage Bin With Sprinkler

At delivery, the Stalite LWA had an absorbed moisture content of over 6 percent.

In order to maintain and improve the level of absorbed moisture, the sprinkler was run

continuously until 24 hours prior to concrete placement. At the time of placement, tested

moistures indicated absorption levels of at least 7.5 percent, well above the minimum

allowable 6 percent standard established for producing HSLC. As in the lab, the reason for shutting off the sprinkler 24 hours prior to mixing was to reduce the moisture gradient throughout the stockpile. After 24 hours, the excess free water had drained leaving a fairly consistent level of free moisture on the aggregate.

The concrete mixer was a 3 cubic yard auger-style mixer as shown in Figure 6.3. The mixer was charged using conveyor belts for the aggregate and a chute for the cement. The mix tower was only equipped to dispense Portland cement; all silica fume and fly ash was added to the mixer manually as shown in Figure 6.4. After mixing, the concrete was dispensed through an opening in the side of the mixer to a chute that carried the concrete to the Tuckerbilt concrete transport vehicle shown in Figure 6.5.



Figure 6.3  Auger-Type Mixer at Tindall Concrete

Figure 6.4  Manual Addition of Fly Ash and Silica to Concrete Mixer at Tindall Concrete

## 6.3  Description of Materials Available at Tindall Concrete

The Tindall Plant used only Type III Cement manufactured by CEMEX-Southdown.  The particular brand of cement was "Demopolis" named for the city near which it was manufactured in Alabama.  The cement had a lower specific gravity (3.08) than the cement received from Blue Circle-LaFarge for mix development, which was about 3.15.  The "Demopolis" Type III was reputed for producing exceptional high-early strength gain.
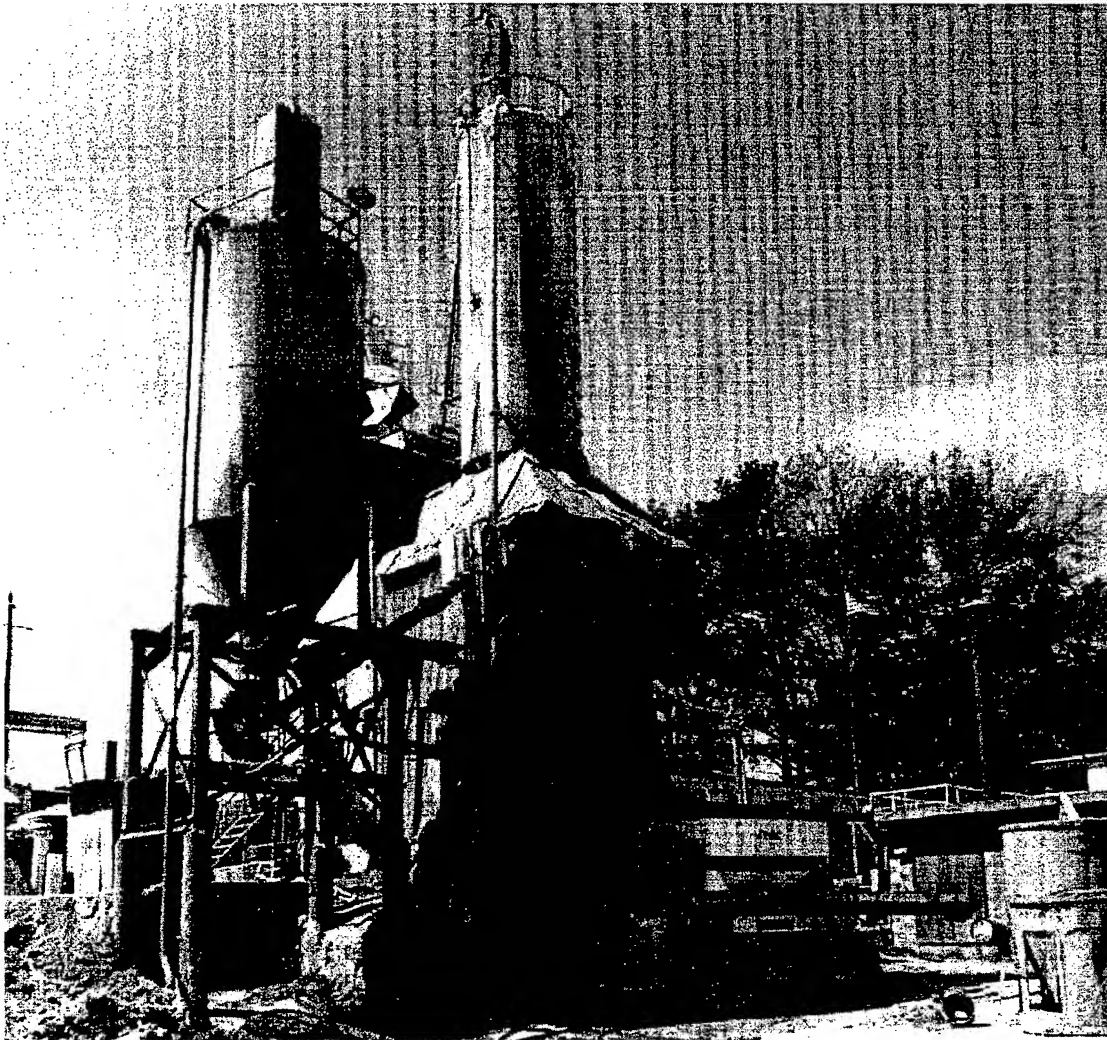
Figure 6.5  Mix Tower and Tuckerbilt Concrete Transport Vehicle

Tindall also used Brown Brothers sand, the same as used during HSLC mix development.  Quality control checks on the sand indicated it had a specific gravity of 2.5 and a fineness modulus of 2.38.

Chemical admixtures available were from Grace Construction Products and matched those used during HSLC mix development.  Chemical admixtures were dosed automatically from controls in the mix tower.

## 6.4 Area for Casting Specimens

The Tindall Plant Superintendent, Mr. Todd Davidson, was very accommodating during the field production testing phase. A large, flat area was provided for casting specimens and access was provided to quality control equipment. Figure 6.6 shows casting specimens outside the Tindall quality control shop.
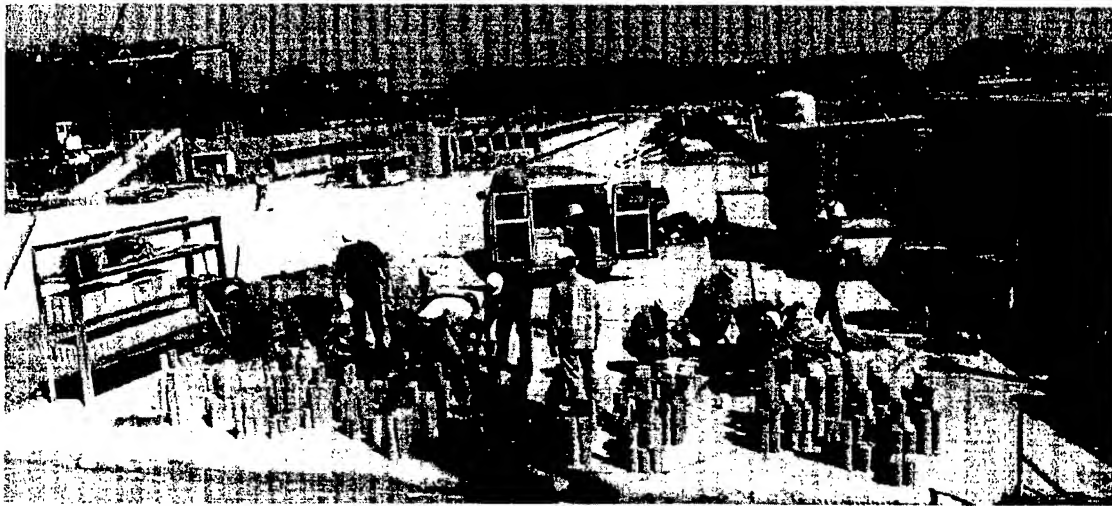


Figure 6.6  Casting Specimens at Tindall Concrete

## 6.5 Field Production of HSLC Mixes

The following sections address the field placements of the 8,000, 10,000 and 12,000 psi HSLC mixes identified as 8F, 10F and 12F, respectively. Several common actions occurred prior to mixing concrete to include positioning all molds and equipment in the casting area, performing quality control checks (moisture contents on LWA and NW sand), coordination with the plant manager, mix proportioning, and a briefing for student assistants on safety and the correct technique for casting specimens. The

100

specimens cast during each field-mixing test are specified in Table 6.1. Resulting

material properties are covered in Section 6.6.

Table 6.1  Number of Specimens Cast During Each Field Mixing Test

| Specimen Type Curing Method Type of Test | Time of Testing After Placement (H=Hours, D=Days) | | | | | | |
|---|---|---|---|---|---|---|---|
| | 16H | 20H | 24H | 7D | 28D | 56D | 365D |
| 4 x 8 Cylinder Curebox Compressive Strength | 3 | 3 | 3 | 3 | 3 | 3 | 3 |
| 4 x 8 Cylinder ASTM Compressive Strength | | | 3 | | 3 | 3 | 3 |
| 6 x 12 Cylinder Curebox Modulus of Elasticity | 3 | | 3 | | 3 | 3 | |
| 6 x 12 Cylinder ASTM Modulus of Elasticity | | | | | | 3 | |
| 4 x 4 x 14 Beam Curebox Modulus of Rupture | | | 3 | | | 3 | |
| 4 x 8 Cylinder Curebox Chloride Permeability | | | | | | 3 | 3 |
| 20 x 36 x 12 Block ASTM Cored Cylinder Compressive Strength (3 Cores Tested) | | | | | | 1 | |

The 20 x 36 x 12 (W x L x H) block was cast to replicate curing conditions in the

bottom flange of a girder. In addition to the specimens listed above, extra specimens

were cast to the greatest extent possible based on space in cureboxes and availability of

molds. Extra specimens provided flexibility in the event a specimen was dropped, testing

was improperly conducted, or test results were irregular.

101

After casting, the specimens were covered with plastic lids or other suitable material to provide protection, and placed on a level surface. Thermocouples were inserted into select specimens to monitor the heat of hydration for each type of specimen. After reaching initial set (about 2-3 hours), those specimens identified as curebox specimens were placed into an insulated curebox as pictured in Figure 4.12. The cureboxes had been prepositioned in the back of a van prior to casting. ASTM specimens were placed in open containers and allowed to cure exposed to the ambient temperature. Approximately 12-14 hours after placement (after final set of the concrete), the specimens were transported back to the Georgia Tech Structures Lab and prepared for testing as necessary. The specimens were not removed from the curebox until their specified time of testing or until 24 hours had passed, whichever occurred first. Upon removal from the curebox, the specimen was demolded, labeled with its mix number, date and researchers initials, then either tested or placed in the fog room for additional curing through its time of testing.

### 6.5.1 Field Production Test # 1 – 8,000 PSI HSLC (Designation = 8F)

The first field production test was conducted on March 27, 2001. The weather was ideal for concrete placement with a temperature of $50^\circ$ F, dry conditions, and no wind. Quality control tests on the aggregate resulted in "absorbed" and "as-is" moistures of 7.83 and 11.00 percent, respectively, for the Stalite LWA. The "as-is" moisture for the NW sand was 4.1 percent. The 8,000 psi mix "as batched" is listed in Table 6.2.

Mixing was initiated using a "buttering mix" to prepare the concrete mixer for future batches. The purpose of the buttering mix was to coat the mixer with cement paste

and prevent mix water from being pulled out of mixes to follow. The buttering mix was 1/4-cubic yard in size and had the same proportions as the mix planned for casting specimens. After buttering the mixer, the buttering mix was discarded.

Table 6.2  8,000 PSI (8F) Field Production Mix

| Concrete Components to Produce 1 Cubic Yard | | |
|---|---|---|
| 1/2-inch Stalite LWA | (lbs) | 978 |
| Brown Brothers Sand | (lbs) | 1062 |
| Class F Fly Ash | (lbs) | 142 |
| Silica Fume | (lbs) | 19 |
| Type III Cement | (lbs) | 785 |
| WRDA 35 | (fl oz) | 57 |
| ADVA Flow | (fl oz) | 47+10 |
| Daravair 1000 | (fl oz) | 9.5 |
| Water | (gal) | 23.9+0.5 |

| | | |
|---|---|---|
| Slump | (inches) | 4 |
| Planned Wet Unit Weight | (pcf) | 118.1 |
| Actual Wet Unit Weight | (pcf) | 118.6 |
| Temperature | (def F) | 67.5 |
| Air Content | (Percent) | 3.5 |
| Curing Start Time | | 3:00 pm |

Mixing proceeded without any major problems. The components of the mix were added in the same order determined during laboratory mix development and listed in Section 4.6. An additional 10 fluid ounces of ADVA was added to provide the required workability. The additional water resulted from a valve that could not be closed completely. It was estimated that 1/2-gallon leaked into the mixer; however it was impossible to determine an exact value.

103

After mixing, the HSLC was dispensed into the Tuckerbilt and taken to the specimen casting area for quality control checks and then casting. Results of the quality control checks are listed at the bottom of Table 6.2. The resulting mix was within standard for all tests performed.

Several lessons were learned and noted for future placements. The most important issue of note was the valve that allowed water to leak into the concrete mixer. This leak made it impossible to determine the exact amount of water in the batch.

### 6.5.2 Field Production Test # 2 – 10,000 PSI HSLC (Designation = 10F)

The second field production test was conducted on April 3, 2001. The temperature was 62° F, but the weather was not ideal for concrete placement. Immediately after beginning to batch the concrete, heavy rain began to fall. The wind picked up to the point where it was raining almost horizontally. In anticipation of the rain, the molds had been moved under cover next to the casting area. Heavy rain continued through the conclusion of casting.

Earlier quality control tests on the aggregate resulted in "absorbed" and "as-is" moistures of 7.88 and 11.19 percent respectively for the Stalite LWA. The "as-is" moisture for the NW sand was 2.98 percent. The 10,000 psi mix as batched is listed in Table 6.3.

Mixing was again initiated using a 1/4-cubic yard "buttering mix.

During this mix, only 15 gallons of the planned 23.4 gallons were added. It appeared that the moisture content of the sand was much higher than determined earlier, which would have reduced the amount of required mix water. Since the aggregate

104

hoppers in the mix tower were covered, the rain was not the cause of the higher moisture contents.

Table 6.3  10,000 PSI (10F) Field Production Mix

| Concrete Components to Produce 1 Cubic Yard | | |
|---|---|---|
| 1/2-inch Stalite LWA | (lbs) | 984 |
| Brown Brothers Sand | (lbs) | 1055 |
| Class F Fly Ash | (lbs) | 146 |
| Silica Fume | (lbs) | 49 |
| Type III Cement | (lbs) | 765 |
| WRDA 35 | (fl oz) | 57 |
| ADVA Flow | (fl oz) | 62+2 |
| Daravair 1000 | (fl oz) | 9 |
| Water | (gal) | 23.4 (15) |

| | | |
|---|---|---|
| Slump | (inches) | 7.5 |
| Planned Wet Unit Weight | (pcf) | 118.7 |
| Actual Wet Unit Weight | (pcf) | 121.0 |
| Temperature | (def F) | 62 |
| Air Content | (Percent) | 3.8 |
| Curing Start Time | | 2:00 pm |

The components of the mix were added in the same order determined during laboratory mix development and listed in Section 4.6. An additional 2 fluid ounces of ADVA was added to provide the required workability.

Results of the quality control checks are listed at the bottom of Table 6.3. The resulting mix had a slump and unit weight that were higher than planned, but still acceptable.

Despite the rain and moisture control problems, the mix produced good results.

### 6.5.3 Field Production Test # 3 – 12,000 PSI HSLC (Designation = 12F)

The third and final field production test was conducted on April 10, 2001. The temperature was 90° F in the shade. Conditions were dry with no wind.

Quality control tests on the aggregate resulted in "absorbed" and "as-is" moistures of 7.69 and 11.12 percent respectively for the Stalite LWA. The "as-is" moisture content of the NW sand was 6.12 percent. The 12,000-psi mix "as batched" is listed in Table 6.4.

Mixing was again initiated using a 1/4-cubic yard "buttering mix.

During this mix, only 14 gallons of the planned 16.7 gallons were added. It appeared that the moisture content of the sand was slightly higher than tested earlier.

Table 6.4  12,000 PSI (12F) Field Production Mix

| Concrete Components to Produce 1 Cubic Yard | | |
|---|---|---|
| 1/2-inch Stalite LWA | (lbs) | 985 |
| Brown Brothers Sand | (lbs) | 1088 |
| Class F Fly Ash | (lbs) | 150 |
| Silica Fume | (lbs) | 100 |
| Type III Cement | (lbs) | 740 |
| WRDA 35 | (fl oz) | 59 |
| ADVA Flow | (fl oz) | 129+8 |
| Daravair 1000 | (fl oz) | 7 |
| Water | (gal) | 16.7 (14) |

| | | |
|---|---|---|
| Slump | (inches) | 4.5 |
| Planned Wet Unit Weight | (pcf) | 119.1 |
| Actual Wet Unit Weight | (pcf) | 124.2 |
| Temperature | (def F) | 86 |
| Air Content | (Percent) | 2.5 |
| Curing Start Time | | 4:00 pm |

The components of the mix were added in the same order determined during laboratory mix development and listed in Section 4.6. An additional 8 fluid ounces of ADVA was added to provide the required workability.

Results of the quality control checks are listed at the bottom of Table 6.4. The resulting mix had a low air content that was cause in part for the mix having a higher unit weight than anticipated. The 4.5-inch slump enabled easily casting the specimens. Despite the heat, the casting went well.

## 6.6 Results of Field Mixing

The combined results of field mixing are shown in Table 6.5 by specimen type, mix designation, and age of specimen. Each strength or modulus result shown is the average of three tests. The Masters Thesis by Brandon Buchberg,[86] "Investigation of Mix Design and Properties of High-Strength/High-Performance Lightweight Concrete" addresses chloride permeability, creep and shrinkage, coefficient of thermal expansion, and provides extensive detail on the results of each mix in this research project. Chapter 7 of this report compares the results of the field testing program (8F, 10F and 12F) with results achieved during a similar laboratory testing program using the same specified 8,000, 10,000, and 12,000 psi mixes (8L, 10L, and 12L) and with the 8,000 and 10,000 mixes (G1 and G2) used in girder construction.

There are several trends seen in Table 6.5 that are addressed further in the following sections.

Table 6.5 Results of Field Mixing

| Specimen Curing Test | Units | Mix | Mean Strength or Modulus at Time of Testing (H=Hours, D=Days) | | | | | | |
| --- | --- | --- | --- | --- | --- | --- | --- | --- | --- |
| | | | 16H | 20H | 24H | 7D | 28D | 56D | 365D |
| 4 x 8 Cyl Curebox Comp. Str. | psi | 8F | 7,920 | 8,470 | 8,870 | 9,570 | 9,830 | 10,600 | 10,830 |
| | | 10F | 7,710 | 9,070 | 9,750 | 10,010 | 10,430 | 11,170 | 11,520 |
| | | 12F | 10,990 | 10,500 | 11,490 | 11,250 | 11,460 | 11,550 | 12,140 |
| 4 x 8 Cyl ASTM Comp. Str. | psi | 8F | | | 6,760 | | 10,250 | 11,090 | 11,800 |
| | | 10F | | | 6,200 | | 11,140 | 11,300 | 11,680 |
| | | 12F | | | 9,330 | | 11,550 | 11,620 | 12,280 |
| 6 x 12 Cyl Curebox Elast. Mod. | $10^6$ psi | 8F | 3.49 | | 3.67 | | 3.85 | 3.86 | |
| | | 10F | 3.48 | | 3.75 | | 4.22 | 4.08 | |
| | | 12F | 3.92 | | 4.12 | | 4.30 | 4.26 | |
| 6 x 12 Cyl ASTM Elast. Mod. | $10^6$ psi | 8F | | | | | | 4.13 | |
| | | 10F | | | | | | 4.26 | |
| | | 12F | | | | | | 4.40 | |
| 4 x 4 x 14 Curebox Rupt. Mod. | psi | 8F | | | 788 | | | 1,089 | |
| | | 10F | | | 641 | | | 998 | |
| | | 12F | | | 761 | | | 1,014 | |
| Block ASTM Comp. Str. | psi | 8F | | | | | | 9,550 | |
| | | 10F | | | | | | 10,270 | |
| | | 12F | | | | | | 11,470 | |

## 6.6.1 Strength Gain of 4 x 8 Cylinders

For all three mixes, the 1-day curebox strengths showed remarkable early strength gain. The 8F mix continued to gain strength through 365 days ultimately achieving 10,830 psi and 11,800 psi for curebox and ASTM specimens, respectively. The 10F mix also showed remarkable early strength gain and continued to gain strength through 365 days. The 12F mix reached within 650 psi of its ultimate strength after 24 hours based on curebox specimen results. From that point through 365 days, the mix initially lost strength then rose again to reach 12,140 psi and 12,280 psi for curebox and ASTM specimens, respectively. The effect of the silica fume can be seen in mix 12F. After 24

hours, it had achieved a compressive strength 1,700 psi greater than the 10F mix and 2,600 psi greater than the 8F mix. The main differences between the mixes were the silica fume content and W/C ratio. Figures 6.7 and 6.8 show plots of strength gain for the three mixes through 56 and 365 days, respectively.
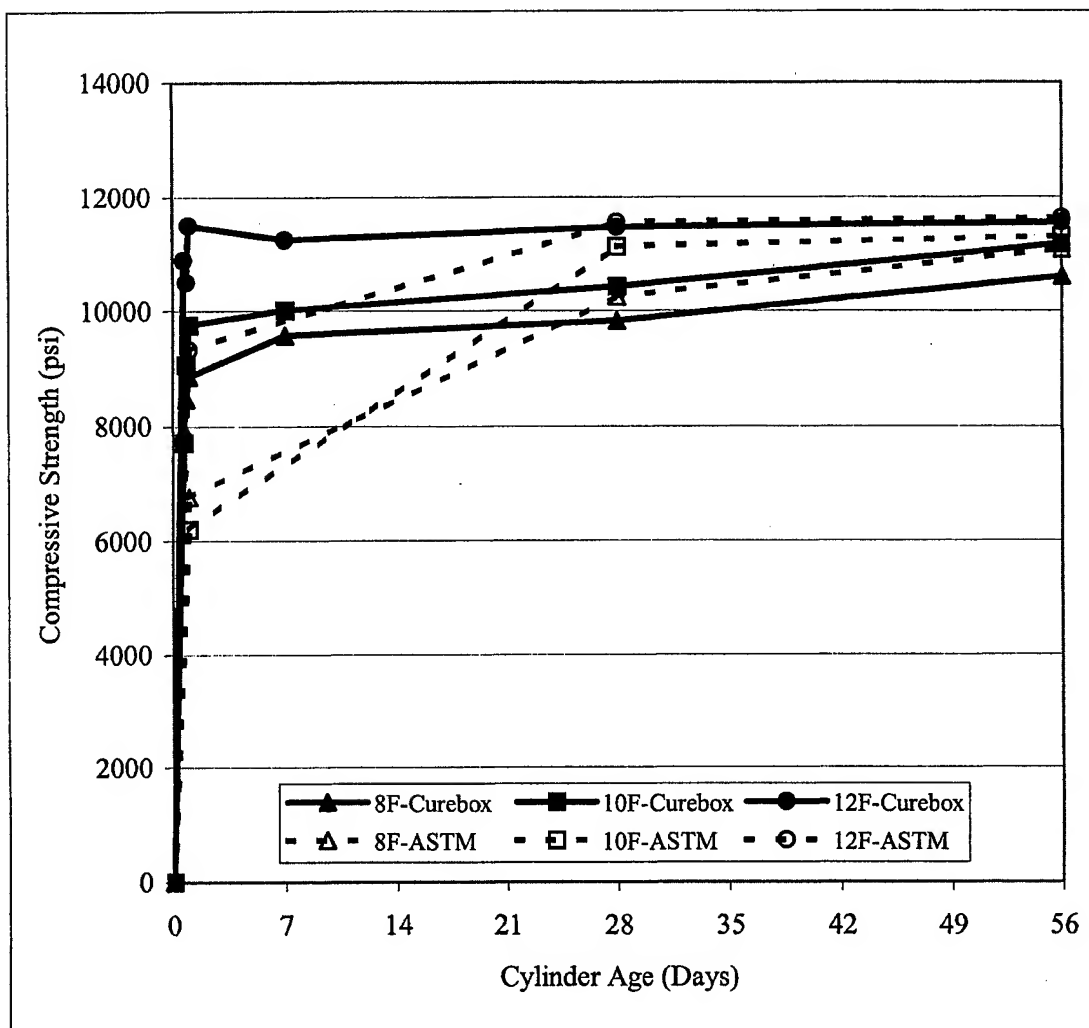


Figure 6.7  Strength Gain for 4 x 8 Curebox and ASTM Cylinders Through 56 Days
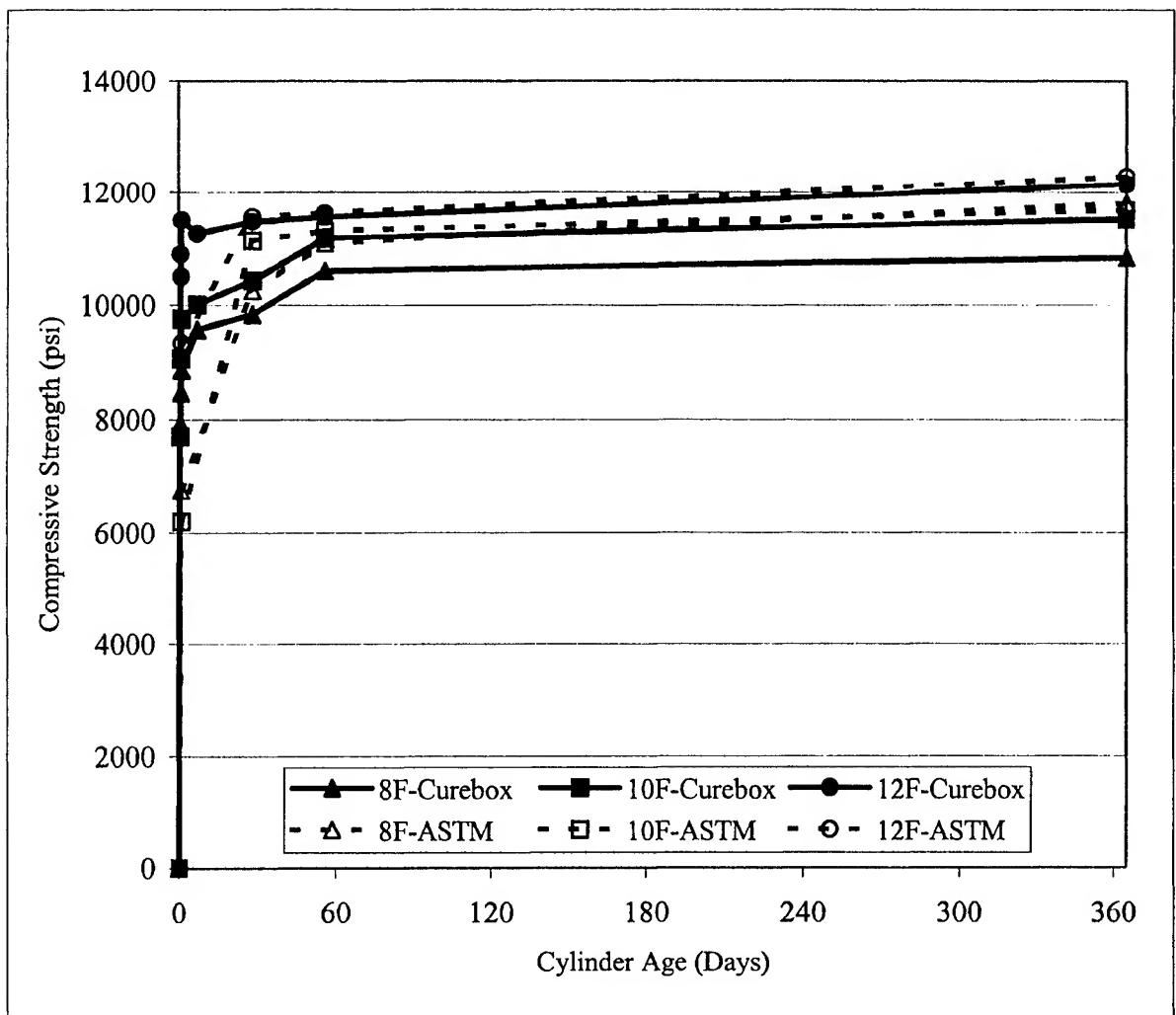
Figure 6.8 Strength Gain for 4 x 8 Curebox and ASTM Cylinders Through 365 Days

### 6.6.2 Curebox vs. ASTM 4 x 8 Cylinders

After 24 hours of curing, the curebox cylinders had reached a strength between

2,000 and 2,500 psi greater than the ASTM cured cylinders. The insulated cureboxes

held in the heat of hydration causing the curebox cylinders to hydrate more quickly and

achiever higher early strengths. After 56 days, the ASTM strengths were about 2 percent

greater than the curebox strengths for each mix. After 365 days, the 8F ASTM strengths

110

were about 9 percent greater than curebox strengths; the 10F and 12F ASTM strengths were less than 1 percent greater. Figures 6.7 and 6.8 show how the ASTM and curebox strength gains differed.

### 6.6.3 Strength Ceiling

The concept of a strength ceiling was discussed in Sections 2.7.2 and 5.4.5. Examination of Figure 6.8 reveals that an apparent strength ceiling exists at just above 12,000 psi, slightly higher than it was thought to be during the laboratory development phase. The 12F mix provides the best indication of a strength ceiling. After 24 hours, the 12F cylinders had practically reached their maximum strength at 11,490 psi. At 56 days, the 12F cylinders had effectively gained 60 psi strength. 60 psi could be considered as normal variation in testing between the two sets of cylinders. The 12F ASTM cylinders showed a similar trend gaining only 70 psi from 28 through 56 days. After 365 days, the curebox and ASTM cylinders had gained an additional 590 psi and 660 psi, respectively.

### 6.6.4 Modulus of Elasticity

The modulus of elasticity results showed a slight drop at 56 days for the 10F and 12F cylinders. The ASTM cylinders achieved about 5 percent higher modulus values on average at 56 days in comparison to the curebox cylinders. Further analysis of modulus of elasticity values is covered in Chapter 7, Short and Long-Term Properties.

### 6.6.5 Modulus of Rupture

Table 6.5 shows how the moduli of rupture results were unpredictable. As the compressive strength increased, the modulus of rupture was expected to have increased.

The 8F mix produced the highest modulus of rupture results of the three tests, but it had the lowest compressive strength. Based on these results it is hypothesized that there is an upper limit for $f_r$ in HSLC. Chapter 7 compares these results with laboratory specimens and specimens created during girder construction.

### 6.6.6 Target Strengths

According to ACI 318, Section 5.3.2.2,[2] the required average compressive strength when data are not available to establish a standard deviation is the design strength + 1,400 psi for strengths over 5,000 psi. Table 6.6 outlines the test results for each mix and the allowable design strength based on 56-day results.

Table 6.6  Resulting Strengths and Allowable Design Strengths

| Mix Designation | Average Curebox Strength (psi) | Average ASTM Strength (psi) | Maximum Specifiable Design Strength (psi) |
|---|---|---|---|
| 8F | 10,600 | 11,090 | 9,690 |
| 10F | 11,170 | 11,300 | 9,900 |
| 12F | 11,550 | 11,620 | 10,220 |

Based on ACI requirements, the maximum design strength achievable from the three mixes was 10,220 psi. The maximum specifiable design strength was based on the average ASTM strength results since they were greater. These results indicate that the existence of a strength ceiling at about 11,500 psi limits the specifiable design strength to just over 10,000 psi.

During girder construction, a series of cylinders was cast such that a statistical study could be performed. ACI 318[2] allows the use of statistical results to reduce the code specified 1,400-psi strength reduction. Chapter 7 includes discussion of the statistical study conducted for HSLC.

## 6.7 Conclusions

Mixing HSLC in a commercial plant can be accomplished with good success. The strength results in Table 6.5 indicate that with proper quality control that the same strengths can be achieved in the field as in the laboratory.

Moisture content in slate LWA can be adequately controlled in a field environment by sprinkling the aggregate continuously until just prior to mixing.

Curebox cured specimens achieved greater early strengths at 24 hours, but ultimately did not achieve the strengths reached by ASTM specimens at 56 days.

Moduli of elasticity values for ASTM cured specimens were greater than for curebox-cured specimens.

# CHAPTER VII

# MECHANICAL PROPERTIES OF HSLC

## 7.1 Introduction

The purpose of this chapter is to report and compare the mechanical properties from all HSLC mixes determined and tested during this research project and to discuss the aspects that relate directly to girder performance characteristics examined. Specific batch information and test results including compression strength, modulus of elasticity, and modulus of rupture are reported. The results of a statistical study are discussed. The Masters Thesis by Brandon Buchberg[86] "Mix Design Performance of High Strength – High Performance Lightweight Concrete" provides a more in-depth analysis of all material property related data.

## 7.2 Overview of HSLC Material Testing Program

The mixing and testing of HSLC was accomplished in four phases with specimens designated as shown in Table 7.1.

Table 7.1  HSLC Material Testing Program Specimen Designation

| Objective Mix Design Strength (psi) | Phase 1 Mix Development In Laboratory | Phase 2 Field Production | Phase 3 Laboratory Verification | Phase 4 Girder Construction |
|---|---|---|---|---|
| 8,000 | 8 Mix | 8F | 8L | G1 |
| 10,000 | 10 Mix | 10F | 10L | |
| 12,000 | 12 Mix | 12F | 12L | G2 |

In Phase 1, mix designs labeled "8 Mix," "10 Mix," and "12 Mix" were developed in order to meet objective design strengths of 8,000, 10,000, and 12,000 psi as described in Chapter 5. A strength ceiling of approximately 12,200 psi prevented the 12,000 psi objective design strength from being reached; the designation was maintained for consistency of reference.

In Phase 2, the mix designs developed during Phase 1 underwent a field production test as described in Chapter 6; the Phase 2 mix designs and specimens were designated 8F, 10F, and 12F to signify the objective design strength of the mix and that it was field-produced at Tindall Concrete.

In Phase 3, the same mix designs developed in Phase 1 and field-produced in Phase 2 were more fully evaluated in the laboratory. The Phase 3 mix designs and specimens were designated 8L, 10L, and 12L to signify the objective strength of the mix and that they were produced in the laboratory. Many individual batches of concrete were required during Phase 3. Every attempt was made to maintain consistency between the batches.

In Phase 4, the same mix designs developed in Phase 1 and field-produced in Phase 2 were used to construct girders; only the 8,000 and 12,000 psi objective strength mixes were used for girder construction. During girder construction, the 8,000 psi mix design and specimens were labeled G1 indicating a Grade 1 concrete. The 12,000 psi objective strength mix design and specimens were labeled G2 indicating a Grade 2 concrete

## 7.3 Specimen Casting Plan

Table 6.1 listed the specimen casting plan used during each field-production test. Table 7.2 shows the specimen casting plan during laboratory evaluation (Phase 3). The number in parenthesis indicates the individual batch from which the specimens were cast. The 10L series of batches had only three matches (1-3) as explained in Section 7.5.3.

Table 7.2  Specimens Cast During Laboratory Verification Batches (Phase 3)

| Specimen Type Curing Method Type of Test | Time of Testing After Placement (H=Hours, D=Days) | | | | | | |
|---|---|---|---|---|---|---|---|
| | 16H | 20H | 24H | 7D | 28D | 56D | 365D |
| 4 x 8 Cylinder Curebox Compression Strength | 3(4) | 3(4) | 3(4) | 3(1) | 3(1) | 3(1) | 3(1) |
| 4 x 8 Cylinder ASTM Compression Strength | | | 3(1) | | 3(1) | 3(1) | 3(1) |
| 6 x 12 Cylinder Curebox Modulus of Elasticity | 3(4) | | 3(4) | | | 3(2) | |
| 6 x 12 Cylinder ASTM Modulus of Elasticity | | | | | | 3(2) | |
| 4 x 4 x 14 Beam Curebox Modulus of Rupture | | | 3(3) | | | 3(3) | |
| 4 x 4 x 14 Beam ASTM Modulus of Rupture | | | 3(3) | | | 3(3) | |
| 4 x 8 Cylinder Curebox Chloride Permeability | | | | | | 2(2) | 2(2) |
| 4 x 15 Cylinder Curebox Creep / Shrinkage | 5(5) | | 5(5) | | | | |

Table 7.3 shows the specimen casting plan for girder construction (Phase 4). The first number listed is the number of specimens cast from the initial batch of concrete

116

(G1A1, G1B1, G2A1, G2B1) on each day girders were cast.  The number in parenthesis

is the number of specimens cast from all subsequent batches of concrete (G1A2-4, G1B2

3, G2A2-5, G2B2-4) on each day girders were cast.  The direct pullout test block was

only cast during placements G1A and G2A.  Extra specimens were cast when possible.

Table 7.3  Specimens Cast During Girder Construction Batches (Phase 4)

| Specimen Type Curing Method Type of Test | Time of Testing After Placement (D=Days) | | | | |
|---|---|---|---|---|---|
| | 1D | 7D | 28D | 56D | Time Of Girder Testing |
| 4 x 8 Cylinder Curebox Compression Strength | 3(3) | 3 | 3 | 3 | 3(3) |
| 4 x 8 Cylinder ASTM Compression Strength | 3 | 3 | 3 | 3(3) | 3 |
| 6 x 12 Cylinder Curebox Modulus of Elasticity | 3 | | | 3 | |
| 6 x 12 Cylinder ASTM Modulus of Elasticity | | | | 1(1) | |
| 4 x 4 x 14 Beam Curebox Modulus of Rupture | | | | 3 | |
| 4 x 4 x 14 Beam ASTM Modulus of Rupture | | | | 1(1) | |
| 4 x 15 Cylinder Curebox Creep / Shrinkage | 6 | | | | |
| 20 x 36 x 24 Block ASTM Direct Pullout Test | | | | 1 | |

## 7.4 Mix Designs as Determined in Phase 1

For reference, Table 7.4 lists the resulting mix designs from Phase 1.

117

Table 7.4  Objective 8,000, 10,000, and 12,000 psi Mix Designs from Phase 1

| Concrete Components to Produce 1 Cubic Yard of HSLC Aggregate Assumed to be at SSD | | Concrete Mix Designation Objective Strength (psi) | | |
|---|---|---|---|---|
| | | 8 Mix 8,000 | 10 Mix 10,000 | 12 Mix 12,000 |
| 1/2-inch Stalite LWA | (lbs) | 1,022 | 1,030 | 1,030 |
| Normal Weight Fine Aggregate | (lbs) | 947 | 955 | 955 |
| Class F Fly Ash | (lbs) | 142 | 145 | 150 |
| Silica Fume | (lbs) | 19 | 50 | 100 |
| Type III Cement | (lbs) | 783 | 765 | 740 |
| WRDA 35 Low-Range Water Reducer (LRWR) | (fl oz) | 57 | 58 | 59 |
| ADVA Flow High-Range Water Reducer (HRWR) | (fl oz) | 57 | 65 | 139 |
| Daravair 1000 Air Entraining Agent (AEA) | (fl oz) | 9.4 | 9.6 | 7.5 |
| Water | (gals) | 32.1 | 29.9 | 27.3 |
| Water / Cementitious Materials Ratio | (W/CM) | 0.28 | 0.26 | 0.23 |
| Theoretical Wet Unit Weight | (pcf) | 118.1 | 118.7 | 119.1 |
| Theoretical Equilibrium Unit Weight | (pcf) | 115.6 | 116.2 | 116.6 |

## 7.5  Mixes as Batched and Wet Concrete Properties

The following sections provide the "as batched" component listings for each batch of concrete produced in Phases 2, 3 and 4.  The components listed are based on aggregate at the saturated surface dry (SSD) condition.

### 7.5.1  Girder Placement Dates, Times and Ambient Temperatures

Table 7.5  Girder Construction Batch Information

| Girders | Batch Series | Date/Time | Ambient Temp. $^0$ F | Weather |
|---|---|---|---|---|
| G1A, G1B | G1A | 9 July 01, 1800 | 87 | Dry, Clear |
| G2A, G2B | G2A | 12 July 01, 1000 | 88 | Dry, Clear |
| G1C | G1B | 17 July 01, 1700 | 90 | Dry, Clear |
| G2C | G2B | 17 July 01, 1600 | 92 | Dry, Clear |

### 7.5.2  8,000 psi HSLC Design Strength

Tables 7.6 and 7.7 show batching results for the 8,000 psi design strength mixes.

118

Table 7.6  8,000 psi HSLC Mixes (8F and 8L)

| Concrete Components to Produce 1 Cubic Yard | | | | | | | |
|---|---|---|---|---|---|---|---|
| Component | Unit | 8F | 8L1 | 8L2 | 8L3 | 8L4 | 8L5 |
| 1/2-in LWA | Lbs | 947 | 954 | 954 | 954 | 954 | 954 |
| NW Sand | Lbs | 1,022 | 1,029 | 1,029 | 1,029 | 1,029 | 1,029 |
| Class F Fly Ash | Lbs | 141 | 140 | 140 | 140 | 140 | 140 |
| Silica Fume | Lbs | 19 | 19 | 19 | 19 | 19 | 19 |
| Type III Cement | Lbs | 780 | 774 | 774 | 774 | 774 | 774 |
| LRWR | fl oz | 56 | 56 | 56 | 56 | 56 | 56 |
| HRWR | fl oz | 57 | 81 | 78 | 85 | 90 | 104 |
| AEA | fl oz | 9.4 | 9.3 | 9.3 | 9.3 | 9.3 | 9.3 |
| Water | Gal | 32.0 | 31.7 | 31.7 | 31.7 | 31.7 | 31.7 |

| Slump | in | 4.00 | 4.25 | 4.5 | 4.5 | 4.5 | 7 |
|---|---|---|---|---|---|---|---|
| Wet Unit Wt | pcf | 118.6 | 118.6 | 119.4 | 120.3 | 122.0 | 123.8 |
| Batch Temp | $^0$F | 68 | 90 | 89 | 90 | 88 | 89 |
| Air Content | % | 3.50 | 4.00 | 3.75 | 4.00 | -- | -- |

Table 7.7  8,000 psi HSLC Mixes (G1)

| Concrete Components to Produce 1 Cubic Yard | | | | | | | | |
|---|---|---|---|---|---|---|---|---|
| Component | unit | G1A1 | G1A2 | G1A3 | G1A4 | G1A5 | G1B1 | G1B2 | G1B3 |
| 1/2-in LWA | lbs | 944 | 937 | 925 | 925 | 925 | 941 | 960 | 941 |
| NW Sand | lbs | 1,018 | 1,011 | 999 | 999 | 999 | 1,029 | 1,050 | 1,030 |
| Class F Fly Ash | lbs | 141 | 140 | 138 | 138 | 138 | 143 | 146 | 143 |
| Silica Fume | lbs | 19 | 19 | 19 | 19 | 19 | 19 | 19 | 19 |
| Type III Cement | lbs | 780 | 774 | 765 | 765 | 765 | 788 | 804 | 788 |
| LRWR | fl oz | 56 | 56 | 55 | 55 | 55 | 57 | 58 | 57 |
| HRWR | fl oz | 64 | 64 | 63 | 63 | 63 | 58 | 53 | 58 |
| AEA | fl oz | 9.4 | 9.3 | 9.2 | 9.2 | 9.2 | 9.5 | 9.7 | 9.5 |
| Water | gal | 34.1 | 35.3 | 37.3 | 37.3 | 37.3 | 32.3 | 28.8 | 32.3 |

| Slump | in | 8.00 | -- | -- | -- | -- | 7.00 | -- | -- |
|---|---|---|---|---|---|---|---|---|---|
| Wet Unit Wt | pcf | 118.6 | -- | -- | -- | -- | 120.8 | -- | -- |
| Batch Temp | $^0$F | 85 | -- | -- | -- | -- | 86 | -- | -- |
| Air Content | % | 4.5 | 3.2 | -- | -- | -- | -- | -- | -- |

### 7.5.3 10,000 psi HSLC Design Strength

Table 7.8 shows batching results for the 10,000 psi design strength mixes. This mix design was only batched during the field production test (Phase 1) and the laboratory verification (Phase 3). No girders were cast with this mix design; thus only three batches of this mix design were made during the laboratory evaluation phase.

Table 7.8  10,000 psi HSLC Mixes (10F and 10L)

| Concrete Components to Produce 1 Cubic Yard | | | | | |
|---|---|---|---|---|---|
| Component | unit | 10F | 10L1 | 10L2 | 10L3 |
| 1/2-inch LWA | lbs | 955 | 952 | 952 | 952 |
| NW Sand | lbs | 1,030 | 1,027 | 1,027 | 1,027 |
| Class F Fly Ash | lbs | 146 | 146 | 146 | 146 |
| Silica Fume | lbs | 49 | 49 | 49 | 49 |
| Type III Cement | lbs | 765 | 762 | 764 | 764 |
| LRWR | fl oz | 58 | 57 | 58 | 58 |
| HRWR | fl oz | 64 | 88 | 88 | 88 |
| AEA | fl oz | 9.6 | 9.6 | 9.6 | 9.6 |
| Water | gal | 29.9 | 31.8 | 31.4 | 31.4 |

| | | | | | |
|---|---|---|---|---|---|
| Slump | in | 7.50 | 3.50 | 4.25 | 4.25 |
| Wet Unit Weight | pcf | 121.0 | 122.7 | 122.4 | 122.3 |
| Temperature | $^0$F | 62 | 92 | 91 | 92 |
| Air Content | % | 3.80 | 3.00 | 3.00 | 3.00 |

### 7.5.4 12,000 psi HSLC Design Strength

Tables 7.9 to 7.11 show batching results for the 12,000 psi objective mix design.

Table 7.9  12,000 psi HSLC Mixes (12F and 12L)

| Concrete Components to Produce 1 Cubic Yard | | | | | | | |
|---|---|---|---|---|---|---|---|
| Component | Unit | 12F | 12L1 | 12L2 | 12L3 | 12L4 | 12L5 |
| 1/2-in LWA | Lbs | 955 | 947 | 947 | 947 | 956 | 955 |
| NW Sand | Lbs | 1,029 | 1,021 | 1,021 | 1,021 | 1,026 | 1,024 |
| Class F Fly Ash | Lbs | 150 | 149 | 149 | 149 | 149 | 149 |
| Silica Fume | Lbs | 100 | 99 | 99 | 99 | 100 | 100 |
| Type III Cement | Lbs | 740 | 734 | 734 | 735 | 740 | 740 |
| LRWR | fl oz | 59 | 59 | 59 | 59 | 59 | 59 |
| HRWR | fl oz | 131 | 135 | 135 | 135 | 185 | 222 |
| AEA | fl oz | 9.9 | 7.4 | 7.4 | 7.4 | 9.9 | 9.9 |
| Water | Gal | 27.2 | 27.2 | 27.2 | 28.6 | 27.7 | 27.6 |

| | | | | | | | |
|---|---|---|---|---|---|---|---|
| Slump | In | 4.50 | 3.50 | 3.00 | 3.50 | 4.00 | 6.00 |
| Wet Unit Wt | Pcf | 124.0 | 121.2 | 121.7 | 120.9 | 122.8 | 123.2 |
| Batch Temp | $^0$F | 86 | 90 | 91 | 89 | 93 | 95 |
| Air Content | % | 2.50 | 3.50 | 3.00 | 3.50 | -- | -- |

Table 7.10  12,000 psi HSLC Mixes (G2A)

| Concrete Components to Produce 1 Cubic Yard | | | | | | |
|---|---|---|---|---|---|---|
| Component | Unit | G2A1 | G2A2 | G2A3 | G2A4 | G2A5 |
| ½-in LWA | lbs | 968 | 949 | 940 | 939 | 945 |
| NW Sand | lbs | 1,039 | 1,018 | 1,009 | 1,007 | 1,014 |
| Class F Fly Ash | lbs | 151 | 148 | 147 | 147 | 148 |
| Silica Fume | lbs | 101 | 99 | 98 | 98 | 98 |
| Type III Cement | lbs | 746 | 732 | 725 | 724 | 728 |
| LRWR | fl oz | 60 | 59 | 58 | 58 | 58 |
| HRWR | fl oz | 148 | 150 | 146 | 144 | 144 |
| AEA | fl oz | 7.5 | 7.3 | 7.3 | 7.3 | 7.3 |
| Water | gal | 25.8 | 29.2 | 30.9 | 31.1 | 30.0 |

| | | | | | | |
|---|---|---|---|---|---|---|
| Slump | in | 5.75 | -- | -- | -- | -- |
| Wet Unit Wt | pcf | 120.0 | -- | -- | -- | -- |
| Batch Temp | $^0$F | 86 | -- | -- | -- | -- |
| Air Content | % | 5.40 | 3.50 | -- | -- | -- |

Table 7.11  12,000 psi HSLC Mixes (G2B)

| Concrete Components to Produce 1 Cubic Yard | | | | | |
|---|---|---|---|---|---|
| Component | Unit | G2B1 | G2B2 | G2B3 | G2B4 |
| ½-in LWA | lbs | 956 | 933 | 933 | 945 |
| NW Sand | lbs | 1,025 | 1,001 | 1,001 | 1,014 |
| Class F Fly Ash | lbs | 149 | 146 | 146 | 148 |
| Silica Fume | lbs | 100 | 97 | 97 | 98 |
| Type III Cement | lbs | 737 | 719 | 719 | 729 |
| LRWR | fl oz | 59 | 58 | 58 | 59 |
| HRWR | fl oz | 147 | 145 | 145 | 146 |
| AEA | fl oz | 7.4 | 7.3 | 7.3 | 7.3 |
| Water | gal | 28.1 | 32.1 | 32.1 | 31.7 |

| | | | | | |
|---|---|---|---|---|---|
| Slump | in | 4.5 | -- | -- | -- |
| Wet Unit Wt | pcf | 114.0 | -- | -- | -- |
| Batch Temp | $^0$F | 86 | -- | -- | -- |
| Air Content | % | 3.00 | 3.20 | 3.60 | -- |

## 7.6  Compression Strength Results

Compression strength results are shown according to cylinder size, type of curing, and age of cylinder.  The 6 x 12 compression strength results were determined when performing modulus of elasticity tests.  A comparison between the 4 x 8 and 6 x 12 results is provided as are the results of a statistical study performed on specimens cast during batch series G2B.

## 7.6.1  4 x 8 Cylinder Compression Strength Results

The results of compression strength testing for all 4 x 8 cylinders are shown in Table 7.12.  For field production and laboratory evaluation, the resulting strengths shown are the average of three compression strength tests.  For girder construction batches, the values are the average of all cylinders made from the four or five batches in the batch

122

series. The number after the "Time of Test" strength is the average specimen age in Days. Figures 7.1, 7.2 and 7.3 graph the strength vs. age of the 8,000, 10,000 and 12,000 psi concretes, respectively. The 1-day strength was not available for the 10L ASTM specimen.

Table 7.12  Results of 4 x 8 Cylinder Compression Strength Testing

| Objective Strength Curing | Batch # | Mean Cylinder Strength (psi) (H=Hours, D=Days, Y=Year) | | | | | | | |
|---|---|---|---|---|---|---|---|---|---|
| | | 16H | 20H | 24H | 7D | 28D | 56D | Time Of Test | 1Y |
| 8,000 Curebox | 8F | 7,920 | 8,470 | 8,870 | 9,570 | 9,830 | 10,600 | | 10,830 |
| | 8L | 7,320 | 7,630 | 7,730 | 9,300 | 9,630 | 10,430 | | |
| | G1A | | | 7,470 | 7,810 | 8,710 | 9,080 | 9,418 | 103D |
| | G1B | | | 6,320 | 6,300 | 7,480 | 7,750 | 8,792 | 110D |
| 8,000 ASTM | 8F | | | 6,760 | | 10,250 | 11,090 | | 11,802 |
| | 8L | | | 6,300 | | 9,830 | 10,520 | | |
| | G1A | | | 5,740 | 7,320 | 8,840 | 9,350 | 10,229 | 103D |
| | G1B | | | 5,400 | 5,890 | 7,600 | 8,460 | 9,118 | 110D |
| 10,000 Curebox | 10F | 7,710 | 9,070 | 9,750 | 10,010 | 10,430 | 11,170 | | 11,516 |
| | 10L | | | | 9,260 | 9,410 | 9,920 | | |
| 10,000 ASTM | 10F | | | 6,200 | | 11,140 | 11,300 | | 11,675 |
| | 10L | | | 6,950 | | 10,360 | 11,040 | | |
| 12,000 Curebox | 12F | 10,990 | 10,500 | 11,490 | 11,250 | 11,460 | 11,550 | | 12,138 |
| | 12L | 9,840 | 9,760 | 11,101 | 10,230 | 10,590 | 10,860 | | |
| | G2A | | | 9,640 | 9,460 | 10,170 | 10,420 | 10,965 | 123D |
| | G2B | | | 8,260 | 9,150 | 9,340 | 10,250 | 10,454 | 144D |
| 12,000 ASTM | 12F | | | 9,330 | | 11,550 | 11,620 | | 12,278 |
| | 12L | | | 6,890 | | 10,600 | 11,480 | | |
| | G2A | | | 9,290 | 9,460 | 10,120 | 10,820 | 11,012 | 123D |
| | G2B | | | 6,550 | 8,070 | 9,810 | 10,510 | 10,868 | 144D |
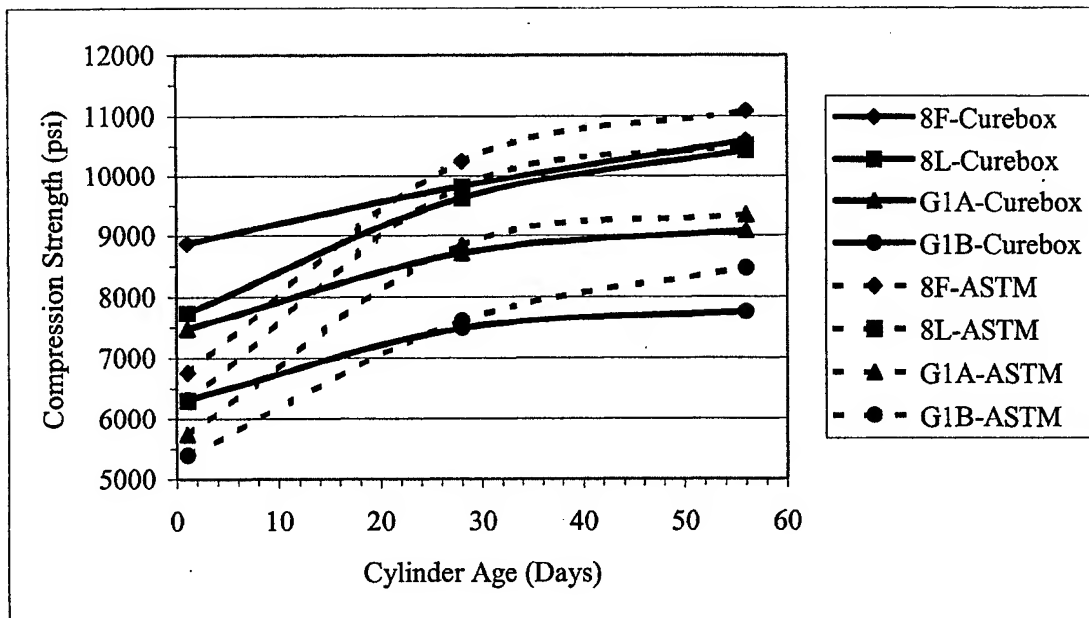
Figure 7.1  Compression Strength vs. Cylinder Age for 8,000 psi Mixes to 56 Days
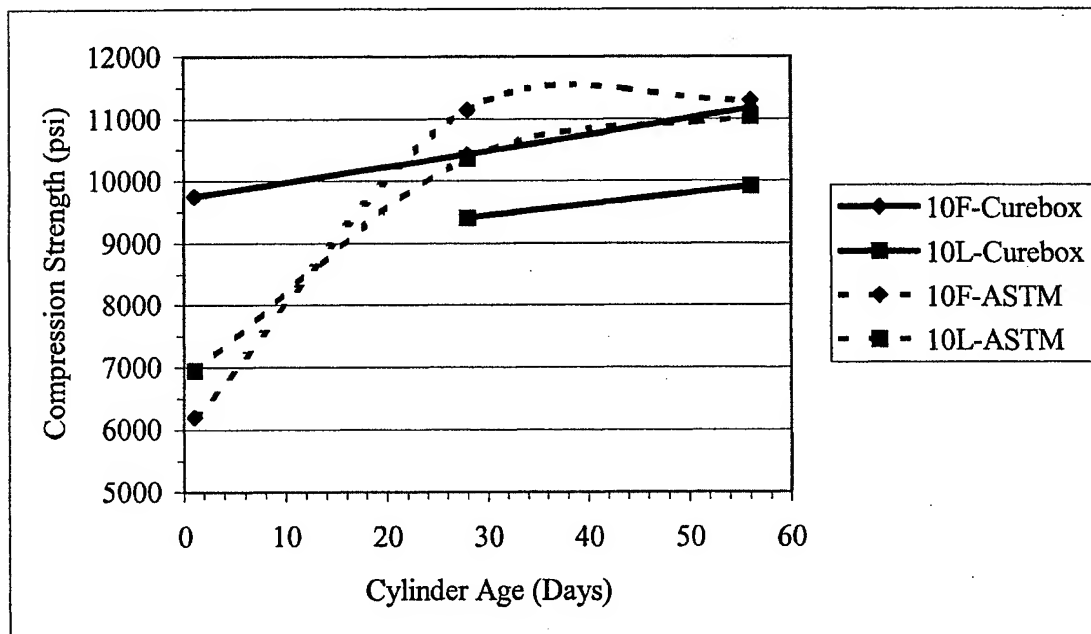


Figure 7.2  Compression Strength vs. Cylinder Age for 10,000 psi Mixes to 56 Days
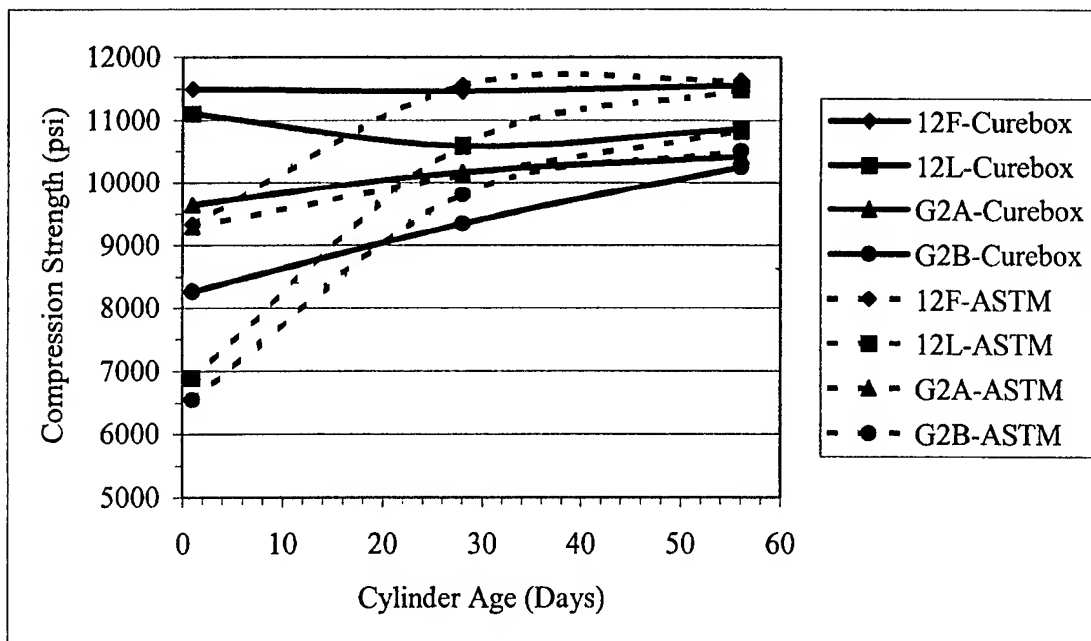
Figure 7.3 Compression Strength vs. Cylinder Age for 12,000 psi Mixes to 56 Days

Examination of Table 7.12 and Figures 7.1 through 7.3 show the difference between ASTM cylinder strengths and curebox strengths is significant at early ages and after 100 days. After 103 days, the G1A batch series ASTM specimens had about 800 psi greater strength than the curebox specimens. On average at the time of testing, ASTM specimens had about 4 percent greater strength than curebox specimens compared to 8 percent for the G1A batch series specimens.

Examination of results at the time of testing showed that strength gain continued from 56 days through the time of testing. The strength gain for the 8,000-psi batches was 729 psi on average, a gain of about 8.5 percent. The strength gain for the 12,000-psi batches was 324 psi on average, a gain of about 3 percent.

Examination of results after 365 days for the 8F, 10F and 12F showed that strength gain continued through 365 days. The 8F ASTM specimens had about 9 percent greater strength than the curebox specimens, but that ASTM specimens for the 10F and 12F mixes had less than 1 percent greater strength in comparison to the curebox specimens.

Comparison of the laboratory evaluation mixes with field-production test mixes shows that the field-production mixes had an average strength 3 percent greater than the corresponding laboratory mixes. When making the laboratory mixes, the same type of cement was used as during the field-production batches. The difference could be attributed to mix effort, age of cement, or the slightly different proportioning between the field and laboratory mixes.

The strength of girder mixes made on different days (G1A vs. G1B, G2A vs. G2B) were normally within 7%. In the case of batch series G1A vs. G1B, the difference was about 12 percent. The difference was most likely attributed to the water leak in the concrete mixer.

### 7.6.2  6 x 12 Cylinder Compression Strength Results

The results of 6 x 12 cylinder compression strength tests are shown in Table 7.13. All strengths are based on an average of three cylinder tests, except the ASTM values for batches G1A, G1B, G2A, and G2B were based on the average of tests of one cylinder from each of the four or five batches in the batch series.

126

Table 7.13  Results of 6 x 12 Cylinder Compression Strength Testing

| Objective Strength Curing | Batch # | Mean Cylinder Strength (psi) (H=Hours, D=Days) | | | |
|---|---|---|---|---|---|
| | | 16H | 24H | 28D | 56D |
| 8,000 Curebox | 8F | 7,910 | 8,460 | 9,940 | 10,450 |
| | 8L | 8,110 | 8,520 | | 10,330 |
| | G1A | | 7,890 | | 9,420 |
| | G1B | | 6,650 | | 7,480 |
| 8,000 ASTM | 8F | | | | 10,740 |
| | 8L | | | | 10,520 |
| | G1A | | | | 9,350 |
| | G1B | | | | 8,580 |
| 10,000 Curebox | 10F | 7,940 | 9,060 | 10,410 | 10,510 |
| | 10L | | | | 9,770 |
| 10,000 ASTM | 10F | | | | 11,720 |
| | 10L | | | | 10,150 |
| 12,000 Curebox | 12F | 10,880 | 10,870 | 10,990 | 11,460 |
| | 12L | 10,290 | 10,750 | | 10,550 |
| | G2A | | 9,270 | | 10,240 |
| | G2B | | 9,280 | | 10,710 |
| 12,000 ASTM | 12F | | | | 11,520 |
| | 12L | | | | 10,690 |
| | G2A | | | | 10,660 |
| | G2B | | | | 10,840 |

## 7.6.3  Comparison of 4 x 8 and 6 x 12 Cylinder Compression Strength Results

In cases where a comparison was possible, 4 x 8 compression strength results were compared to 6 x 12 compression strength results.  Table 7.14 provides the percentage differences for the Phases 2, 3 and 4.  The percent difference was calculated by subtracting the 6 x 12 value from the 4 x 8 value, dividing the result by the 6 x 12 value, and multiplying by 100.  A negative value indicates the 4 x 8 compression strength was less than the 6 x 12 compression strength.

Table 7.14 Comparison of 4 x 8 to 6 x 12 Cylinder Compression Strengths

| Objective Strength Curing | Batch # | Percent Difference (H=Hours, D=Days) | | | |
|---|---|---|---|---|---|
| | | 16H | 24H | 28D | 56D |
| 8,000 Curebox | 8F | 0% | 5% | -1% | 1% |
| | 8L | -10% | -9% | | 1% |
| | G1A | | -10% | | -5% |
| | G1B | | -11% | | 4% |
| 8,000 ASTM | 8F | | | | 3% |
| | 8L | | | | 0% |
| | G1A | | | | 0% |
| | G1B | | | | -6% |
| 10,000 Curebox | 10F | -3% | 8% | 0% | 6% |
| | 10L | | | | 1% |
| 10,000 ASTM | 10F | | | | -4% |
| | 10L | | | | 9% |
| 12,000 Curebox | 12F | 1% | 6% | 4% | 1% |
| | 12L | -4% | -3% | | 3% |
| | G2A | | 6% | | 2% |
| | G2B | | -10% | | -4% |
| 12,000 ASTM | 12F | | | | 1% |
| | 12L | | | | 7% |
| | G2A | | | | 1% |
| | G2B | | | | -6% |

Examination of Table 7.14 shows great variation from one strength group to another. For the 8,000 psi batches, early strength data (16H and 24H) indicate that 6 x 12 cylinders had greater strength than 4 x 8 cylinders on average. However, after 56 days, the resulting strengths were about the same on average. For the 10,000 psi batches, there is limited data on which to base a conclusion. For the 12,000 psi batches, results indicate 4 x 8 and 6 x 12 early strengths to be about the same on average. After 56 days, 4 x 8 cylinders had about 1.4% greater strength on average.

### 7.6.4 Statistical Study

A statistical study was conducted using 30 each 4 x 8 and 30 each 6 x 12 cylinders cast from batch series G2B.[86] Ten each 4 x 8 cylinders and 10 each 6 x 12 cylinders were taken from the three different batches of batch series G2B. The cylinders were allowed to cure under ASTM conditions for 56 days and tested for compression strength.

According to Chapter 5, ACI 318-99,[2] the testing of 100 or more specimens is desirable. However, based on the inherent uncertainty that like conditions will exist at the time test specimens are created and the time concrete is produced, a sample size of 30 is deemed adequate. The average required compressive strength, $f_{cr}'$, was determined as the minimum of Equations 7.1 and 7.2 (ACI[2] Equations 5-1 and 5-2, respectively) below where "s" is the standard deviation.

$$f_{cr}' = f_c' + 1.34s \qquad (7.1)$$

$$f_{cr}' = f_c' + 2.33s - 500 \qquad (7.2)$$

Table 7.15 provides the results of the study.

Table 7.15  Results of Statistical Study

| Batch # | 4 x 8 | | | 6 x 12 | | |
|---|---|---|---|---|---|---|
| | Mean | Required Mean | Standard Deviation | Mean | Required Mean | Standard Deviation |
| G2B-1 | 10,717 | 10,730 | 528 | 10,930 | 10,300 | 224 |
| G2B-2 | 10,464 | 10,740 | 532 | 10,349 | 10,428 | 319 |
| G2B-3 | 10,703 | 10,214 | 160 | 10,106 | 10,557 | 416 |
| G2B Overall | 10,628 | 10,533 | 443 | 10,462 | 10,635 | 474 |

The results in Table 7.15 indicate that the three different batches were not statistically different and that based on 4 x 8 compression strength results the G2B batch series satisfied the requirements for being considered a 10,000 psi design strength mix. Based on 6 x 12 results, the batch series did not satisfy the requirements for being considered a 10,000 psi design strength mix, rather the design strength would be 9,988 psi.

In this research, 4 x 8 cylinders have been used to determine compression strength. Based on this statistical study, an average break strength for the G2 series batches over 10,533 psi indicates the batch series has a 10,000 psi design strength.

## 7.7 Modulus of Elasticity Results

Modulus of elasticity specimens were cast as specified in Tables 6.1, 7.2 and 7.3. Table 7.16 shows the combined results of all modulus of elasticity testing.  Each value represents the average of 3 tests except the ASTM values for batches G1A, G1B, G2A, and G2B that are based on the average of tests on one cylinder from each of the four or five batches in the batch series.

130

Table 7.16  Modulus of Elasticity Results

| Objective Strength Curing | Batch # | Mean Modulus of Elasticity (10^6 psi) (H=Hours, D=Days) | | | |
|---|---|---|---|---|---|
| | | 16H | 24H | 28D | 56D |
| 8,000 Curebox | 8F | 3.49 | 3.67 | 3.85 | 3.86 |
| | 8L | 3.53 | 3.67 | | 4.02 |
| | G1A | | 3.57 | | 3.86 |
| | G1B | | 3.00 | | 3.28 |
| 8,000 ASTM | 8F | | | | 4.13 |
| | 8L | | | | 4.39 |
| | G1A | | | | 3.83 |
| | G1B | | | | 3.56 |
| 10,000 Curebox | 10F | 3.48 | 3.75 | 4.22 | 4.08 |
| | 10L | | | | 4.08 |
| 10,000 ASTM | 10F | | | | 4.26 |
| | 10L | | | | 4.33 |
| 12,000 Curebox | 12F | 3.92 | 4.12 | 4.30 | 4.26 |
| | 12L | 4.08 | 4.25 | | 4.24 |
| | G2A | | 3.55 | | 3.93 |
| | G2B | | 3.91 | | 4.10 |
| 12,000 ASTM | 12F | | | | 4.40 |
| | 12L | | | | 4.33 |
| | G2A | | | | 4.06 |
| | G2B | | | | 4.05 |

Examination of Table 7.16 shows that the modulus of elasticity increased with age. In two cases (10F and 12F curebox) the modulus dropped somewhat between 28 and 56 days. In general, it would not appear that significant gain in modulus of elasticity occurs after 28 days.

ASTM specimens produced higher modulus of elasticity results. On average, ASTM results were 5.6 percent higher for the 8,000 psi design strength batches and 1.9 percent higher for the 12,000 psi design strength batches. Percent difference was

calculated by subtracting the ASTM modulus value from the curebox value, dividing the result by the ASTM modulus value and multiplying the result by 100.

The 56-day results from girder construction tests (G1A, G1B, G2A, G2B) were on average 8.9 percent less than the corresponding field production and laboratory evaluation results. This same trend was evident in Table 7.12 with compression strength results. The suspected cause of the lower results for both strength and modulus was the water leak in the concrete mixer. Despite every effort to control moisture, the water leak allowed more water into the mixes than designed.

The results indicate good consistency between the field production (Phase 2) and laboratory evaluation (Phase 3) modulus of elasticity values.

The results from batch G1B indicate a very low modulus value. The cause of the low results could be poorly compacted cylinders or a higher W/CM ratio than anticipated. Cross-referencing the modulus of elasticity results with strength results in Table 7.12 indicates that a higher W/CM ratio was probably the cause.

Figures 7.4 and 7.5 plot the results of modulus of elasticity vs. equilibrium unit weight and modulus of elasticity vs. compression strength, respectively, from this research and from the data presented in Chapter 2 (Table 2.1). Linear trendlines representing the experimental data and the proposed equation (Equation 3.1) are plotted on each graph. The results from this research are based on 56-day tests; the exact age of data presented in Table 2.1 is unknown. Appendix C lists all modulus of elasticity values. Overall, Equation 3.1 conservatively predicted modulus of elasticity by 4.4 percent with a standard deviation of 6.2 percent.
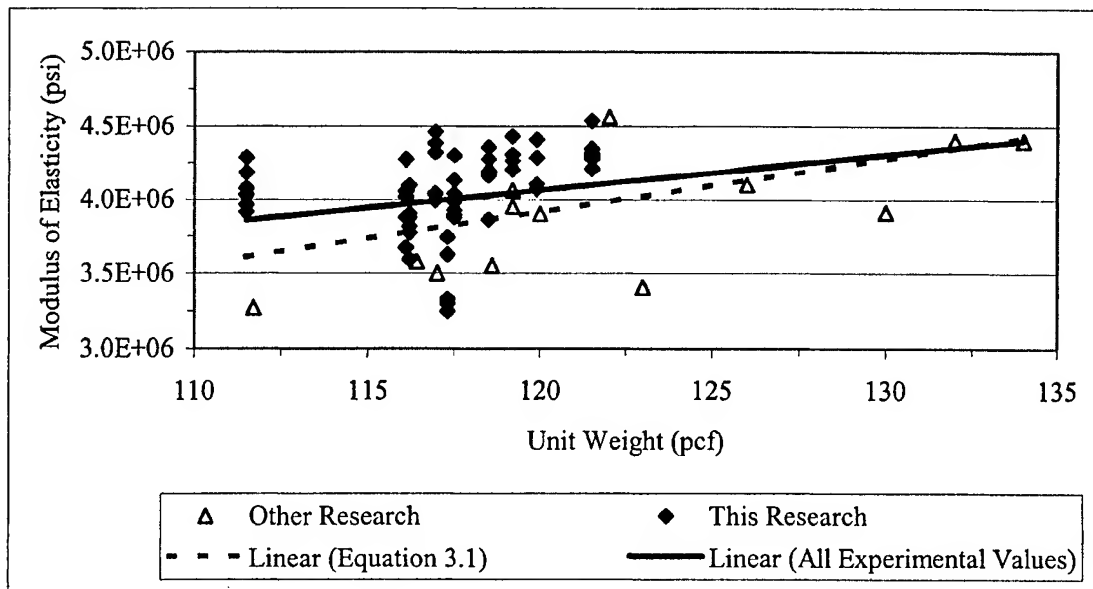
Figure 7.4 Modulus of Elasticity vs. Equilibrium Unit Weight
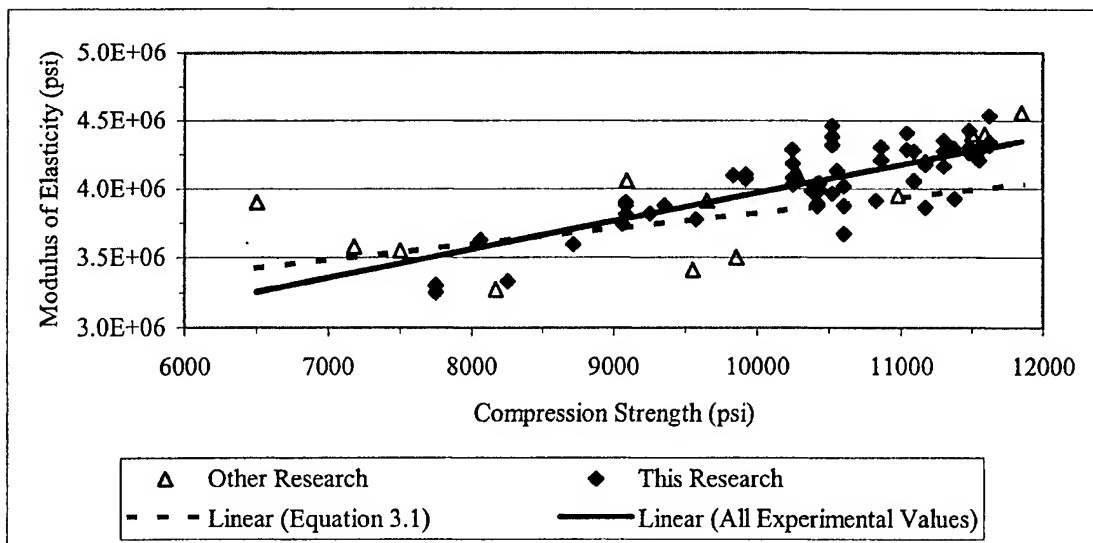


Figure 7.5 Modulus of Elasticity vs. Compression Strength

133

$$E_c = (33,000\sqrt{f_c'} + 4,000,000)(w_c/242)^{0.9} \qquad (3.1)$$

For comparison, the same modulus of elasticity values used previously to evaluate Equation 3.1 were used to evaluate the current equations (Equations 7.3 and 2.1) for modulus of elasticity suggested in ACI 363[87] and by ACI 318[2], respectively.

$$E_c = (40,000\sqrt{f_c'} + 1,000,000)(w_c/145)^{1.5} \qquad (7.3)$$

$$E_c = 33w_c^{1.5}\sqrt{f_c'} \qquad (2.1)$$

On average, Equation 7.3 conservatively predicted the modulus of slate HSLC by about 9.5 percent with a standard deviation of 5.5 percent. On average, Equation 2.1 predicted the modulus of slate HSLC by about 5.3 percent greater than that found experimentally with a standard deviation of 4.6 percent.

In an attempt to better align the predicted modulus of elasticity values with the experimental values, and to determine a simpler equation than Equation 3.1, a similar investigation was done as detailed in Section 3.3 and shown in Figures 3.4 and 3.5.

The experimental modulus of elasticity values were normalized separately by dividing by $(f_c')^{0.5}$, $(w_c)^{0.5}$, and $(w_c)^{1.5}$. The resulting plot normalized by $(f_c')^{0.5}$ is shown in Figure 7.6.
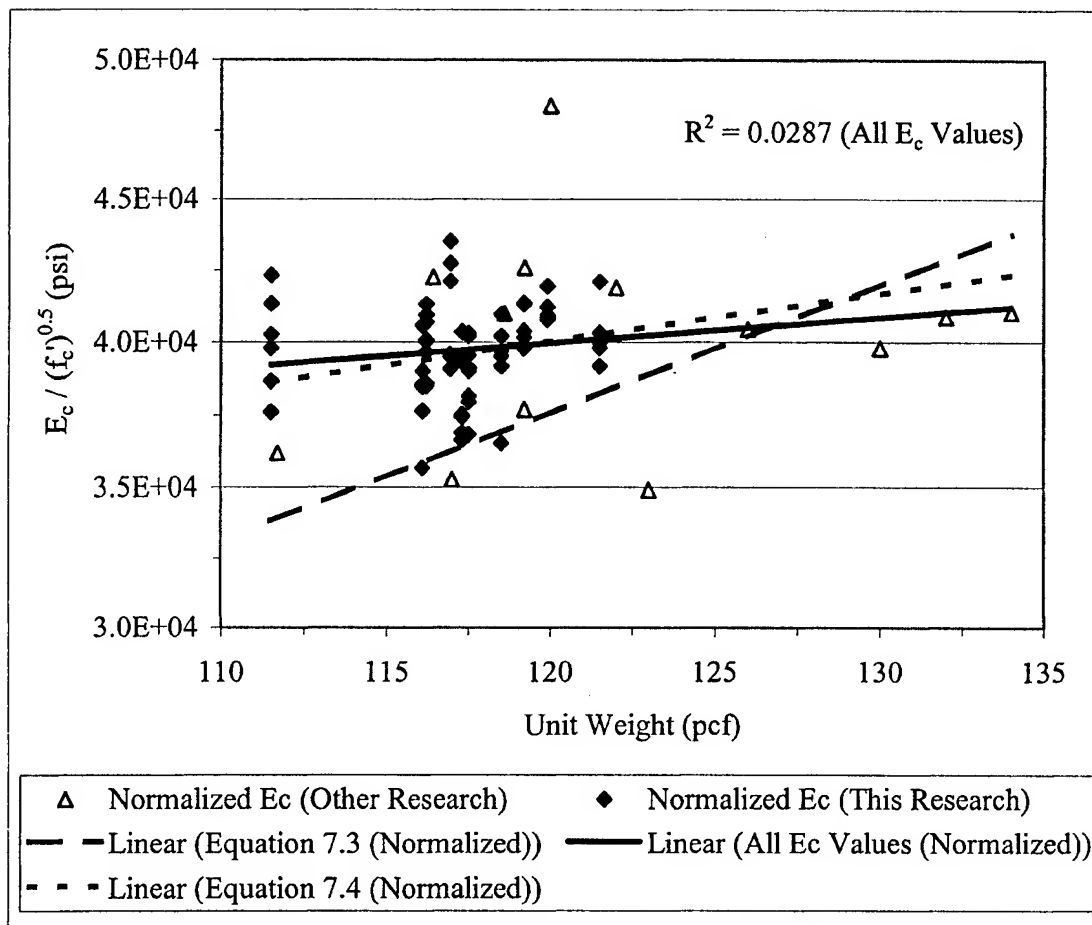
Figure 7.6  Experimental Modulus of Elasticity Values Normalized by $(f_c')^{0.5}$

An evaluation of the best-fit relation for "All $E_c$ Values" (all experimental $E_c$

values from this research and other research) showed that a linear trend line was as good

or better than other possible curves.  The $R^2$ value for the linear relation was 0.0287 for

"All $E_c$ Values."  The indication in Figure 7.6 was that the roll of unit weight in

determining modulus of elasticity was highly variable resulting in wide scatter and a low

$R^2$ value.  In other words, modulus of elasticity for slate HSLC showed little relation to

$w_c$.

The linear trend resulting from Equation 7.3 used to predict modulus of elasticity, normalized by $(f_c')^{0.5}$, is also plotted in Figure 7.6. Equation 7.3 contains the term $w_c^{1.5}$, which emphasizes the effect of unit weight. The resulting linear trend does not compare favorably with the trend indicated by experimental values (all $E_c$ values).

Similar evaluations with other variable forms indicated that $(f_c')^{0.5}$ was the variable that appeared most appropriate in predicting modulus of elasticity.

After examining several equation forms, Equation 7.4 was determined to be the equation that best predicted the modulus of elasticity of slate HSLC.

$$E_c = 44,000\sqrt{f_c' \frac{w_c}{145}} \qquad (7.4)$$

Overall, Equation 7.4 provided a better prediction of modulus of elasticity for slate HSLC than the previously suggested Equation 3.1. Equation 7.4 conservatively predicted modulus of elasticity values by 0.2 percent on average with a standard deviation of 5.1 percent. The linear trend resulting from Equation 7.4 used to predict $E_c$ values is also plotted in Figure 7.6. Since Equation 7.4 contains the term $w_c^{0.5}$, which de-emphasizes unit weight, the resulting linear trend compares more favorably with the trend indicated by the experimental values (all $E_c$ values).

Low, mean, and high unit weight values of 111.5 pcf, 118.2 pcf, and 134 pcf, respectively, were determined from the 56-day experimental modulus of elasticity values from this research project and modulus of elasticity values from other research as listed in

136

Table 2.1. Figure 7.7 shows a plot of the above-mentioned values vs. compression

strength and also shows lines plotting the predicted modulus of elasticity using Equation

7.4 based on the low, mean and high unit weight values. Figure 7.7 shows that at a given

compressive strength, the variation in modulus of elasticity can be substantial. At a

compressive strength of approximately 10,600 psi, the modulus of elasticity varied from

approximately 3.65 million psi to 4.45 million psi.

Figures 7.8 and 7.9 show Equation 2.1 and Equation 7.3, respectively, evaluated

using the low, mean, and high unit weight values plotted over the same modulus of

elasticity values shown in Figure 7.7. Equation 2.1 unconservatively predicted modulus

of elasticity for slate HSLC; Equation 7.3 conservatively predicted modulus of elasticity

for slate HSLC.
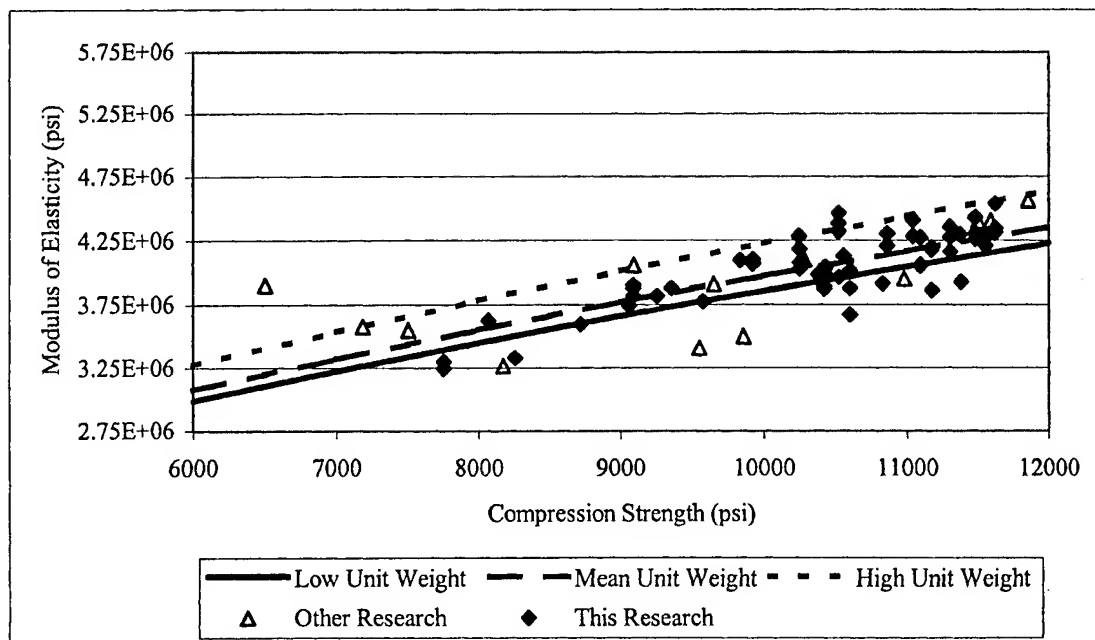
Figure 7.7  Low, Mean, and High Unit Weight Values Plotted Using Equation 7.4
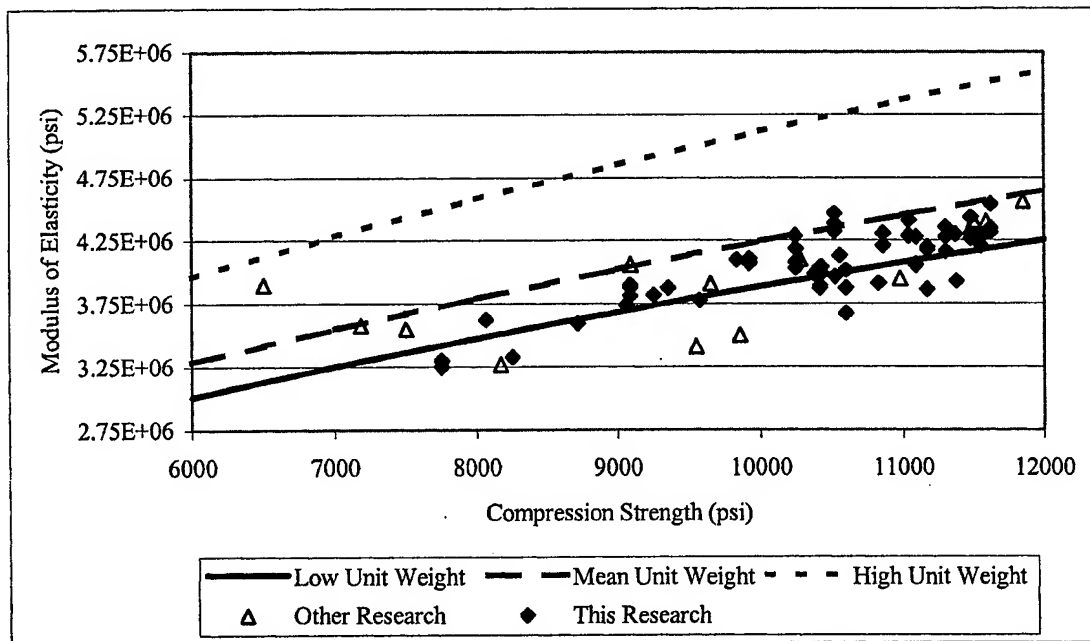
Figure 7.8  Low, Mean, and High Unit Weight Values Plotted Using Equation 2.1
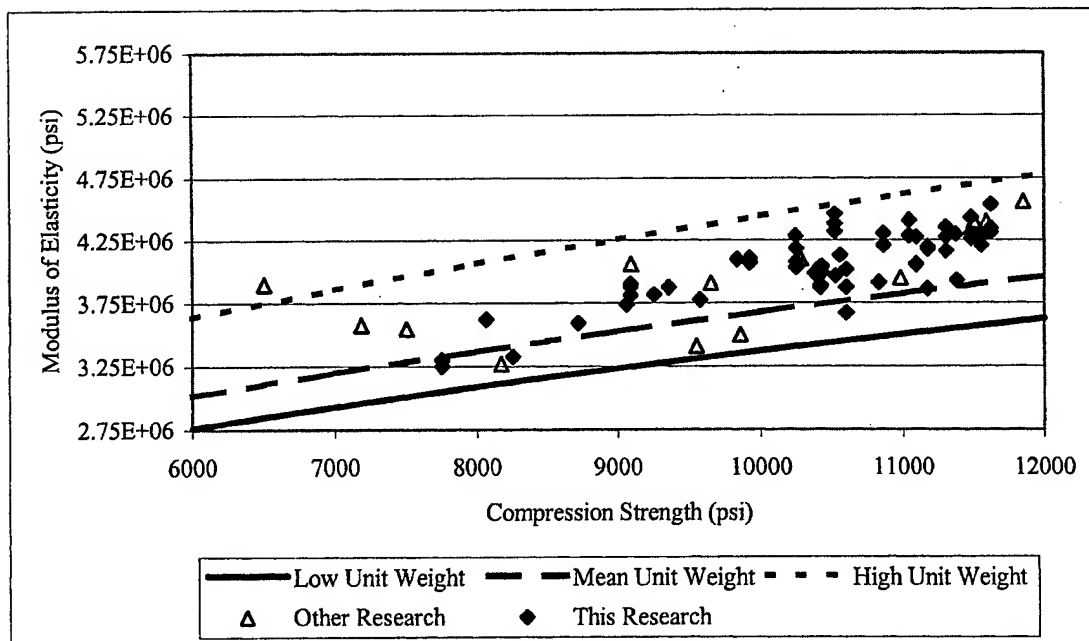


Figure 7.9  Low, Mean, and High Unit Weight Values Plotted Using Equation 7.3

138

## 7.8 Modulus of Rupture Results

Modulus of rupture specimens were cast as specified in Tables 6.1, 7.2 and 7.3. Table 7.17 shows the combined results of all modulus of rupture testing. Each value represents the average of 3 tests except the ASTM values for batches G1A, G1B, G2A, and G2B that are based on the average of tests on one specimen from each batch in the batch series. The 56-day normalized modulus of rupture value was calculated by dividing the 56-day modulus of rupture by $\lambda$ and $(f_c')^{\frac{1}{2}}$.

Table 7.17  Modulus of Rupture ($f_r$) Results

| Objective Strength Curing | Batch Series # | Mean Modulus of Rupture (H=Hours, D=Days) (psi) | | $\dfrac{f_r}{\lambda\sqrt{f_c'}}$ | Concrete Compressive Strength (psi) | Mean Normalized Values |
|---|---|---|---|---|---|---|
| | | 24H | 56D | 56D | 56D | 56D |
| 8,000 Curebox | 8F | 788 | 1,089 | 12.43 | 10,160 | 12.20 |
| | 8L | 649 | 1,077 | 12.40 | 10,430 | |
| | G1A | | 1,042 | 12.86 | 9,080 | |
| | G1B | | 830 | 11.09 | 7,750 | |
| 8,000 ASTM | 8F | | | | | 10.84 |
| | 8L | 761 | 1,030 | 11.81 | 10,520 | |
| | G1A | | 992 | 11.21 | 9,350 | |
| | G1B | | 743 | 9.50 | 8,460 | |
| 10,000 Curebox | 10F | 641 | 998 | 11.10 | 11,170 | 12.42 |
| | 10L | 670 | 1,164 | 13.74 | 9,920 | |
| 10,000 ASTM | 10F | | | | | 11.26 |
| | 10L | 678 | 1,006 | 11.26 | 11,040 | |
| 12,000 Curebox | 12F | 761 | 1,014 | 11.10 | 11,550 | 12.10 |
| | 12L | 645 | 926 | 10.45 | 10,860 | |
| | G2A | | 1,283 | 14.79 | 10,420 | |
| | G2B | | 1,038 | 12.06 | 10,250 | |
| 12,000 ASTM | 12F | | | | | 10.79 |
| | 12L | 678 | 918 | 10.07 | 11,480 | |
| | G2A | | 1,156 | 13.07 | 10,820 | |
| | G2B | | 805 | 9.23 | 10,510 | |

139

The modulus of rupture results shown in Table 7.17 are difficult to interpret. Based on 56-day strengths, the specimens cured in insulated cureboxes produced higher rupture strengths than ASTM cured specimens. This trend is opposite of that seen for all other specimens where ASTM cured specimens resulted in higher strengths.

In examining specimens cast during field production, the specimens coming from batches with the highest compression strength produced the lowest modulus of rupture values on average for both 24-hour and 56-day data. In examining specimens cast during girder construction, the specimens coming from batches with the highest compression strength produced the highest modulus of rupture values on average.

ACI 318-99[2] specifies that rupture modulus, $f_r$, can be predicted using ACI Equation (9-9) shown in Equation 7.5 below.

$$f_r = 7.5\lambda\sqrt{f_c'}$$
(7.5)

The normalized values shown in Table 7.17 indicate good consistency between curebox and ASTM values. The average normalized curebox values are consistently higher than the average ASTM values. It would appear these values indicate a consistency of specimen casting and curing throughout all strengths and types of curing.

Other researchers[11,12,14] have commented on difficulties encountered in using modulus of rupture test results for predicting the cracking strength of concrete beams. They indicated the test is significantly impacted by the level of moisture during curing and indicated the splitting tension test per ASTM C 496[88] provided a better indication of

140

beam cracking strength. Nevertheless, the normalized values indicate that the "7.5" value used in Equation 7.5 is conservative.

## 7.9 Conclusions

Batching concrete in a mixer having a water leak will most likely produce more widely scattered test results.

For 4 x 8 cylinders cast during girder construction, substantial strength gain occurred between 56 days and the time of testing. For 4 x 8 cylinders cast as part of field production testing (8F, 10F, and 12F) strength gain continued through 365 days. It is likely that internal curing contributed to these gains.

As a general rule, for strength testing after 56 days, 4 x 8 cylinders provided on average about 1 percent higher strength values than 6 x 12 cylinders.

ASTM cylinders on average had about 4 percent higher strength than curebox cylinders at 56 days of age or later.

Modulus of elasticity tests on ASTM cylinders produced higher values than corresponding tests on curebox cylinders.

Equation 3.1 conservatively predicted modulus of elasticity results for slate HSLC. Equation 7.4 provided a better overall prediction that was still conservative. Equation 2.1 provided an unconservative prediction of modulus of elasticity. The modulus of elasticity for slate HSLC showed little relation to $w_c$.

The modulus of rupture test results indicated great variability and that the current ACI equation (Equation 7.5) conservatively predicts $f_r$.

# CHAPTER VIII

# DESIGN AND CONSTRUCTION OF HSLC PRETENSIONED BRIDGE GIRDERS

## 8.1 Introduction

The following objectives were established to serve as guidelines to prioritize and focus the experimental design and procedure.

1. To determine the transfer length, $l_t$, for 0.6-inch diameter prestressing strand used with slate HSLC.

2. To determine the development length, $l_d$, for 0.6-inch diameter prestressing strand used with slate HSLC.

3. To verify current code equations for $l_t$ and $l_d$ as appropriate for use with slate HSLC and suggest better equations if necessary.

4. To determine the effect of shear reinforcement spacing on strand slip, development length, and shear capacity of pretensioned slate HSLC girders.

5. To determine the shear strength, $V_c$, of prestressed slate HSLC.

6. To verify current code equations for shear strength of slate HSLC.

7. To verify the current code-specified reduction factor, $\lambda$, for SLWC as related to concrete tensile strength, and, suggest a more appropriate factor if necessary.

In order to achieve the seven experimental objectives, the following variables were altered in order to observe the results.

**Concrete Compressive Strength, $f_c'$.** Concrete design strengths of 8,500 and 10,000 psi were used for girder construction.

**Shear Span to Depth Ratio, a/d.** The "a" distance was varied from approximately 63 to 100 percent of the current code-specified $l_d$ value.

**Yield Strength of Shear Reinforcement Steel, $f_y$.** Only Grade 60 # 4 bar stirrups were used. Values of $f_y$ of 60 ksi (414 MPa) and the actual $f_y$ value were used to determine whether an upper limit was appropriate for use with HSLC.

**Spacing of Shear Reinforcement Steel, "s."** The "s" distance was varied to determine the impact of $A_v/s$ on $l_d$, strand slip, and shear strength.

**Span Length of Tested Section, $L_1$.** In order to achieve three tests per girder, the span length was varied to focus on specific sections of the girder for each test.

## 8.2 Design of Experiment

### 8.2.1 Type of Girders and Prestressing Strands

AASHTO Type II cross-sections were chosen for testing for several reasons. First, other recent experimental research on transfer and development length was done at Georgia Tech[84] and at the University of Texas at Austin[44] using AASHTO Type II girders. The ability to compare results was desirable. Second, Type II girders were more easily fabricated, transported and handled in the lab and were more economical to produce than larger sections. Third, the section was sufficiently deep to yield the

prestressing strands, which was required to investigate development length. By properly configuring the girder cross-section, it was possible to achieve applicable testing results and data.

The prestressing reinforcement chosen was 0.6-inch diameter, 270-ksi, 7-wire, low relaxation (LOLAX) strand provided by Insteel.

In order to produce the worst-case bond situation, the girders were configured with 8 each 0.6-inch diameter strands in the bottom row. In an AASHTO Type II girder, 8 strands constituted a full layer in the bottom flange. In the event of a severe bond failure, a horizontal crack would be induced across the full layer of prestressed reinforcement. The bottom strands were positioned at a distance 3 inches from the bottom of the girder as per GDOT standards and designed for prestressing to $0.75*f_{pu}$ or 203 ksi creating the worst-case bond situation.

In addition to the 8 bottom strands, 2 each 0.6-inch strands were placed 2.5 inches from the top of the girder. The purpose of these strands was to control tension stress at the top of the girder at time of strand release, and as a means to space and secure shear reinforcement. The top strands were also stressed to a level of $0.75*f_{pu}$ or 203 ksi.

## 8.2.2 Configuration of Girders for Testing

In previous work,[44,84] pretensioned girders were configured such that two tests per girder were possible; one test at each girder-end. In some cases, the center portion of the girder was left predominantly undamaged in the testing process. It was thought that a third test might be possible at the center of the girder with careful planning and proper design. There were two important reasons for wanting to test the center of the girder.

144

First, since girder cost was a major portion of the research budget, it was thought that by lengthening the girders it would be possible to achieve a third test at relatively little additional cost. Second, and more importantly, by testing the center portion of the girder, it would be possible to insure a fully developed strand and to more clearly focus on the shear characteristics of HSLC. When testing at the girder's ends, the data related to shear could possibly be skewed by less than fully developed pretensioning strands. Each of the six girders in this research project was configured to allow three tests per girder. This reduced the cost per test and provided substantially more data related to the shear strength of HSLC.

### 8.2.3 Prestressed Girder Design Spreadsheet

In order to facilitate the design of each girder, an EXCEL spreadsheet was developed to perform repetitive calculations related to the design of prestressed slate HSLC girders. The spreadsheet was very comprehensive and allowed the user to input numerous variables related to pretensioned girder design. Calculations within the spreadsheet were based on the 1996 AASHTO[40] Standard Specification. A complete description of the spreadsheet along with an example of the design of girder test G1C-West is presented in Appendix D.

### 8.2.4 Composite Girder Cross Section

It was desirable to construct the deck with a width as close to the width of the top flange of the girder as possible for ease of forming and testing. In addition, based on

previous research,[55,84] it was desirable to achieve a greater depth of composite girder to increase the strain at the level of the bottom strands.

The goal of the testing was to simulate the conditions seen in composite girders found in actual bridges. As such, it was desirable to replicate the moment arm "jd" in testing, as it would be encountered in actual bridge structures. An analysis was conducted assuming AASHTO Type II girders and deck thicknesses as specified by a standard GDOT deck design guide.[89] For girder spacings from 42" to 120", the minimum deck thickness varied from about 6.5 inches to 8.6 inches and jd varied from 31.65 to 34.74 inches with a jd of 33.75 inches for a 7-foot girder spacing

A deck thickness of 11.5 inches and width of 19 inches was selected. This combination produced a predicted internal moment arm of 33.61 inches, which closely matched the desired 7-foot girder spacing. In addition, a deck width of 19 inches meant simplified formwork for deck placement. Thus, by increasing the deck thickness to 11.5 inches, it was possible to increase the depth of the composite girder to increase strain demand on the bottom strands, simplify the formwork for casting of the deck, and closely replicate the moment arm "jd" encountered in standard bridge design.

### 8.2.5 Composite Girder Design

Having determined the configuration of the composite girder cross-section, it was possible to determine the layout of the girders for testing. In designing three tests per girder, it was important to insure that one test did not overly damage other future test areas on the girder.

146

### 8.2.5.1 Concept of Testing Sequence

Portion of Girder Damaged During Test # 1

Test # 1 on Composite Girder

Portion of Girder Damaged During Test # 2

Test # 2 on Composite Girder

Center
Of
Bearing

Center
Of
Bearing

a

L₂

L₁

L
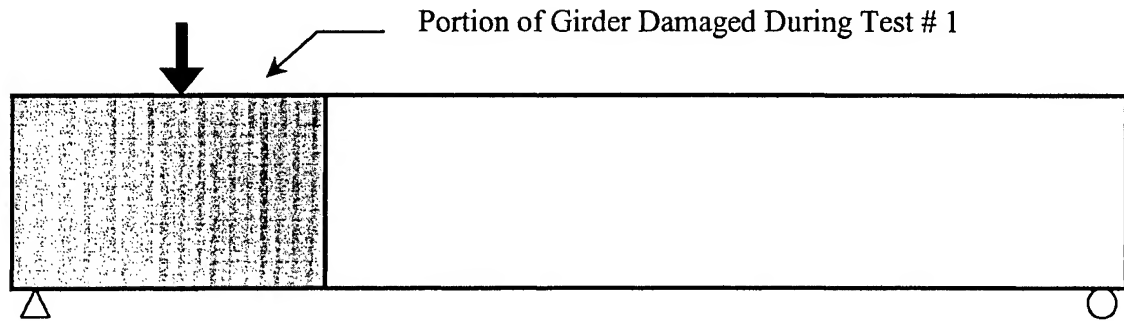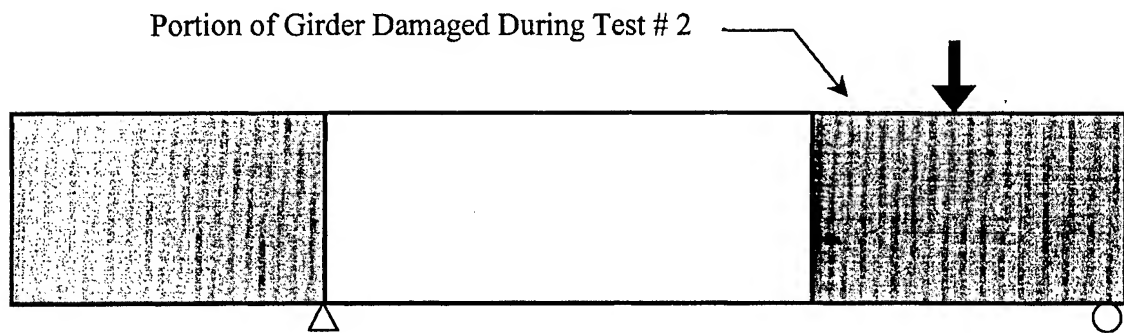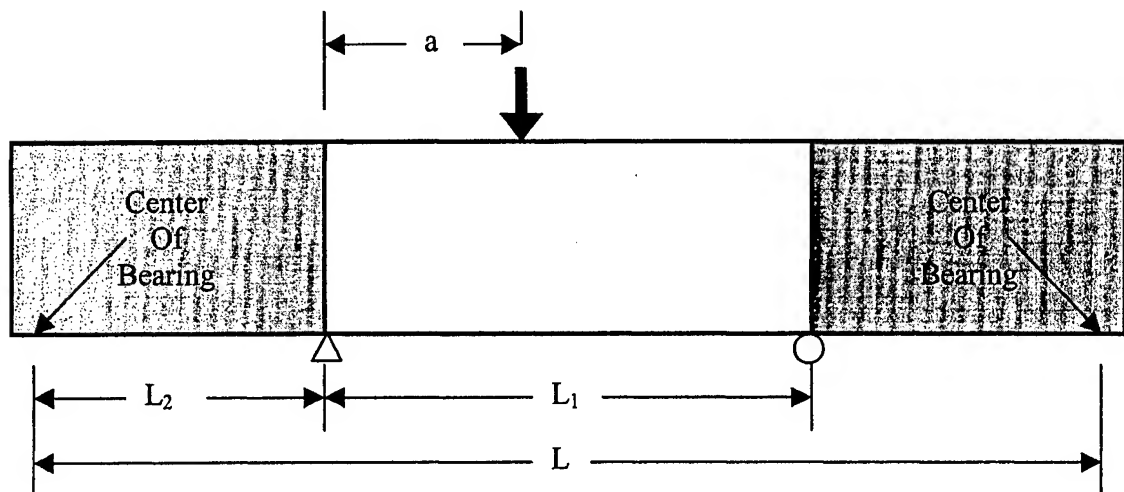
Test # 3 on Composite Girder

Figure 8.1  Concept of Girder Testing Sequence

147

The first test entailed supporting the girder over its entire length and testing one end. The second test involved moving the left support to a point inside any significant damage resulting from the first test, and testing the opposite end of the girder. The third test involved moving the right support to a point inside any significant damage resulting from the second test and testing the center portion of the girder. By using this sequence, it was possible to achieve three tests from one girder.

### 8.2.5.2 Experimental Objectives vs. Girder Design

The following guidelines were established for girder design to accomplish the objectives set in Section 8.2.

1. Install DEMEC gage points on the girder at the ends on both sides of the top flange (from girder-end to a distance of 30 inches) and bottom flange (from girder-end to a distance of 48 inches) to facilitate measurement of concrete surface strains and allow calculation of the transfer length, $l_t$. This action allowed achievement of research objective 1.

2. Install DEMEC gage points on the girder on both sides of the top and bottom flange at midspan over a distance of 24". This action allowed determination of the effective prestressing force at midspan which was essential information for the achievement of all objectives.

3. Apply a point load to the composite girder at approximately 70 percent, 85 percent, 95 percent and 100 percent of $l_d$ where $l_d$ was determined by the 1996 AASHTO[40] Standard Specification. The point at which the failure transitioned from a "shear-type" failure to a "flexural-type" failure was the point at which the

148

strand was considered fully developed. Shear reinforcement in these tests was in accordance with the 1996 AASHTO[40] Standard Specification. This action allowed achievement of research objectives 2 and 3 and partial achievement of objective 4.

4. Using double the amount of shear reinforcement required according to the 1996 AASHTO[40] Standard Specification together with applying a point load at approximately 70 percent and 85 percent of $l_d$ allowed achievement of research objective 4, and partial achievement of objectives 5, 6 and 7.

5. Using varying amounts of shear reinforcement and loading the girder with varying a/d ratios allowed achievement of research objectives 5, 6 and 7.

### 8.2.5.3 Composite Girder Design Procedure

Three each Series G1 girders and three each Series G2 girders were designed with concrete design strengths, $f_c'$, of 8,500 psi and 10,000 psi, respectively. Based on previous experiences, it was assumed the girder lengths would be in the range of 35-45 feet. Final design lengths were revised to accommodate the tests as needed. Three tests were planned for each of the six girders indicating 18 total tests. Since two concrete strengths were being investigated, there were 9 different test configurations that were performed on each series of girders. The prestressed girder design spreadsheet was used to iteratively design the tests to fit on the girders. The resulting tests were detailed in Table 8.1. The a/d ratio listed under "Point Load Placement Criteria" is the shear span to depth ratio where "d" is the total height of the composite girder.

Table 8.1 – Girder Test Configurations

| Test Configuration | Stirrup Density | Point Load Placement Criteria | Shear Span "a" (inches) | Distance "$L_1$" (inches) | Distance "$L_2$" (inches) | Distance "L" (inches) |
|---|---|---|---|---|---|---|
| 1 | Single | $l_d$ | 90 | 456 | 0 | 456 |
| 2 | Double | $0.70*l_d$ | 61 | 316 | 0 | 456 |
| 3 | Double | $0.85*l_d$ | 75 | 456 | 0 | 456 |
| 4 | Single | $0.95*l_d$ | 85 | 504 | 0 | 504 |
| 5 | Single | $0.70*l_d$ | 61 | 321 | 0 | 456 |
| 6 | Single | $0.85*l_d$ | 75 | 369 | 0 | 504 |
| 7 | Minimum | a/d=2.28 | 82 | 185 | 140 | 456 |
| 8 | Minimum | a/d=2.67 | 96 | 210 | 135 | 456 |
| 9 | Minimum | a/d=3.33 | 120 | 244 | 135 | 504 |

d = 47.5 inches

The dimension "a" was the shear span. The dimension $L_1$ was the distance from the left support to the right support. The dimension $L_2$ was the distance from the left COB to the left support. The COB was the point a distance of 6 inches in from each girder-end that was assumed to be the girder's support point for curing. $L_2$ was used to signify a cantilever on the left girder-end. The dimension L was the distance from COB to COB. The dimensions "a," $L_1$, $L_2$ and L are shown in Figure 8.1.

Diagrams of the test configurations are depicted in Figures 8.2 through 8.10. Diagrams of the resulting three girders, configuration "A", "B" and "C", in each series, G1 and G2, are depicted in Figures 8.11 through 8.13. The testing sequence was alike for each girder with the left end tested first, the right end next, and the center section last.
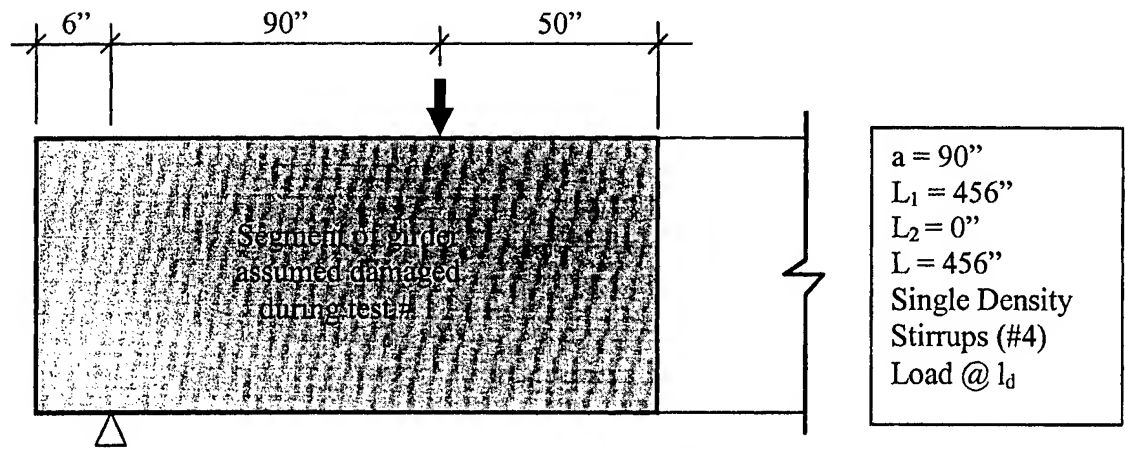
Figure 8.2 Test Configuration 1

a = 90"
$L_1$ = 456"
$L_2$ = 0"
L = 456"
Single Density
Stirrups (#4)
Load @ $l_d$
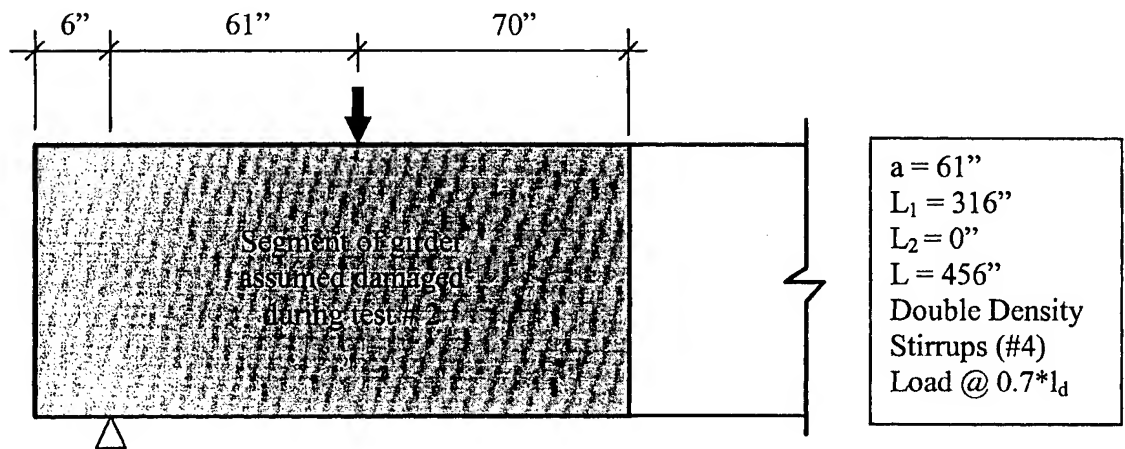


Figure 8.3 Test Configuration 2

a = 61"
$L_1$ = 316"
$L_2$ = 0"
L = 456"
Double Density
Stirrups (#4)
Load @ 0.7*$l_d$
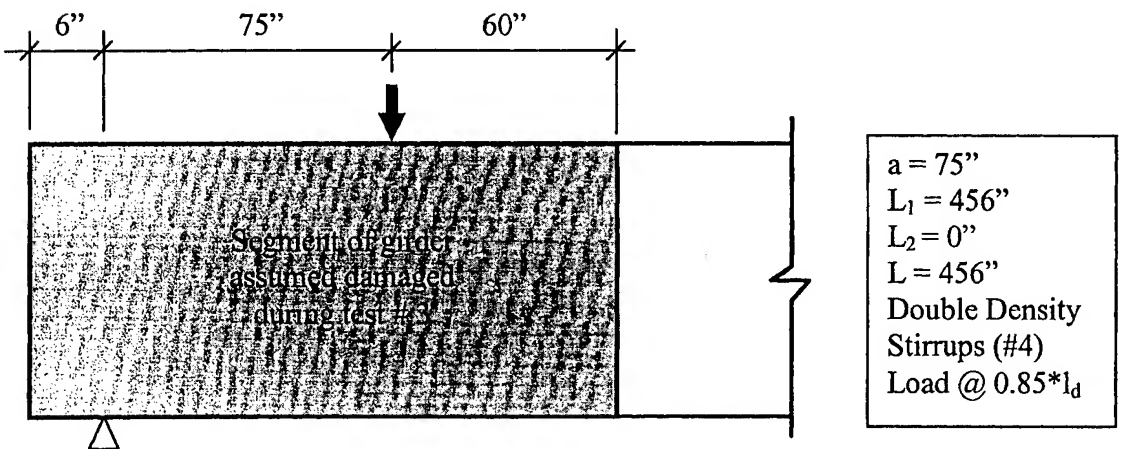


Figure 8.4 Test Configuration 3

a = 75"
$L_1$ = 456"
$L_2$ = 0"
L = 456"
Double Density
Stirrups (#4)
Load @ 0.85*$l_d$

151
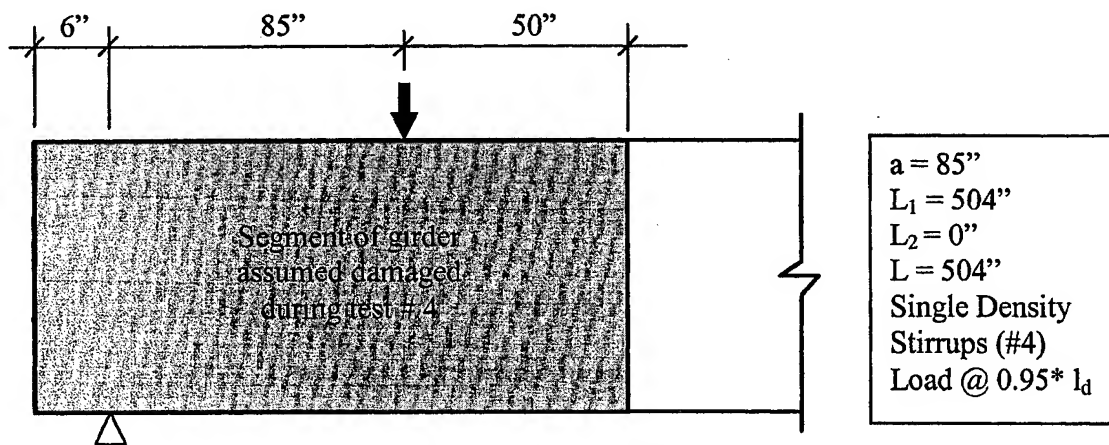
Figure 8.5  Test Configuration 4

a = 85"
$L_1$ = 504"
$L_2$ = 0"
L = 504"
Single Density
Stirrups (#4)
Load @ 0.95* $l_d$
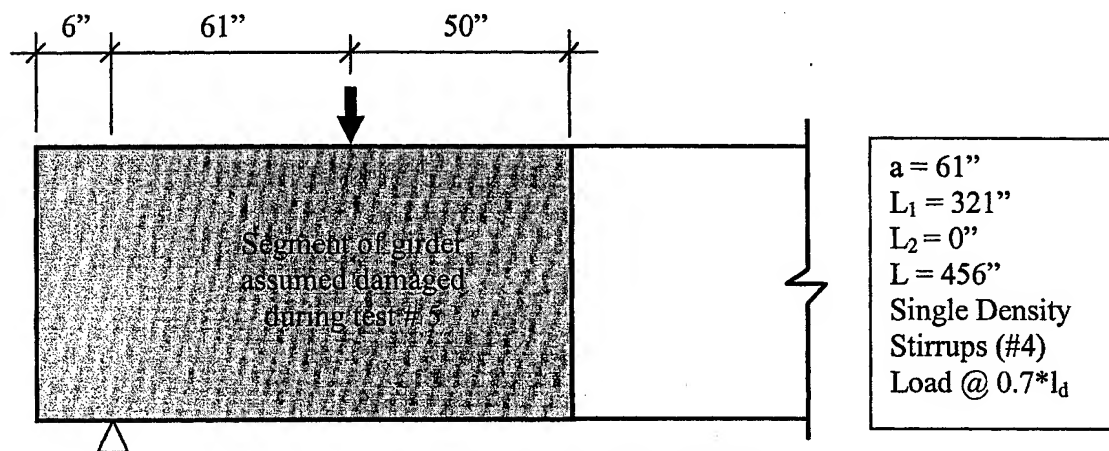


Figure 8.6  Test Configuration 5

a = 61"
$L_1$ = 321"
$L_2$ = 0"
L = 456"
Single Density
Stirrups (#4)
Load @ 0.7*$l_d$
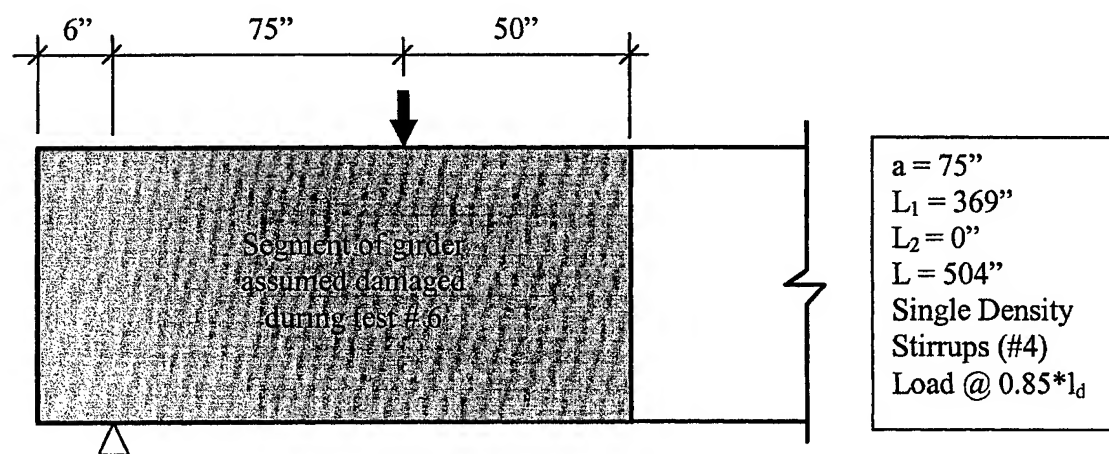


Figure 8.7  Test Configuration 6

a = 75"
$L_1$ = 369"
$L_2$ = 0"
L = 504"
Single Density
Stirrups (#4)
Load @ 0.85*$l_d$

152
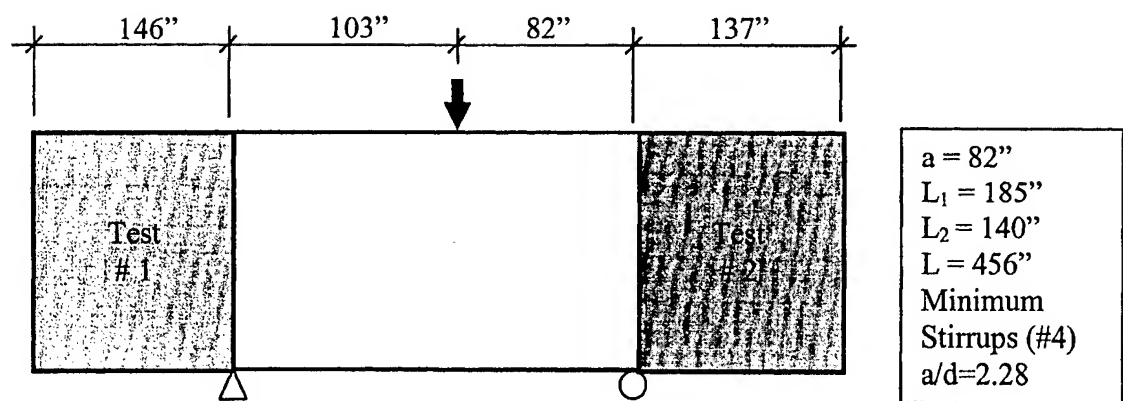
Figure 8.8  Test Configuration 7
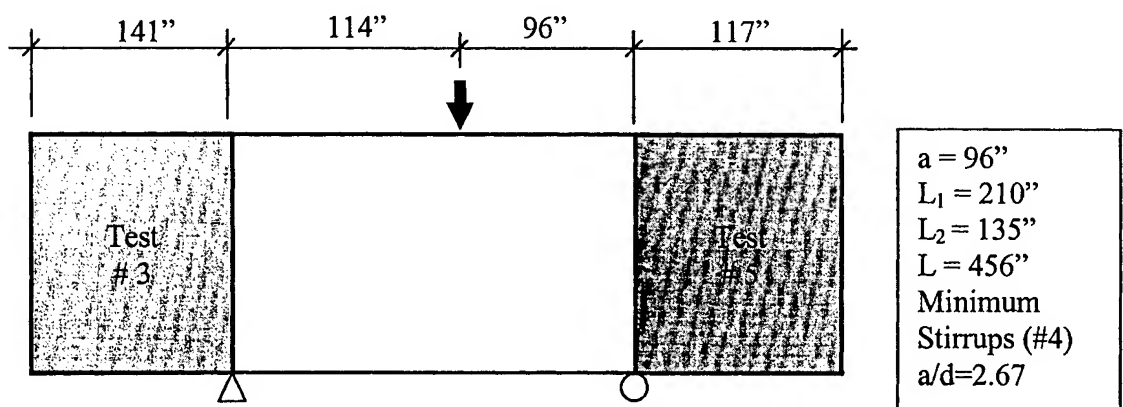


Figure 8.9  Test Configuration 8
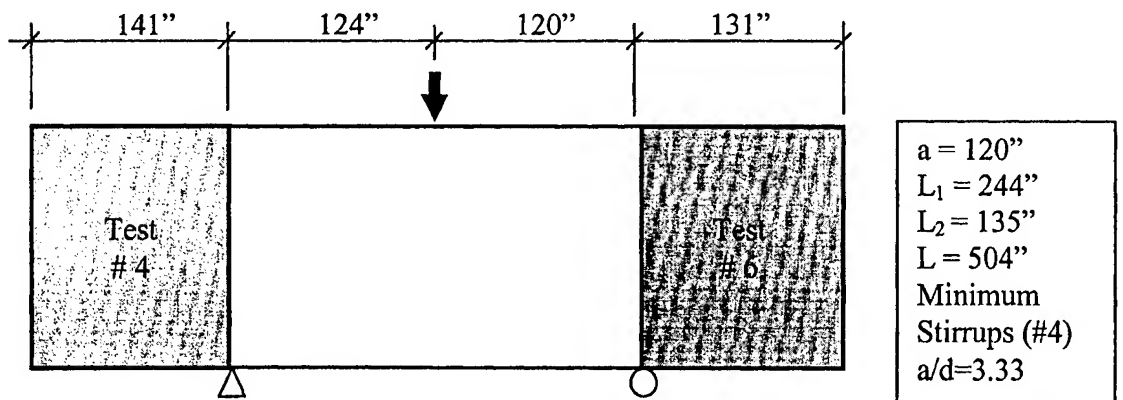


Figure 8.10  Test Configuration 9

153

|  146" | 89" | 96" | 137" |

Stirrups @ 24" Spacing

Test #1 | Test #7 | Test #2
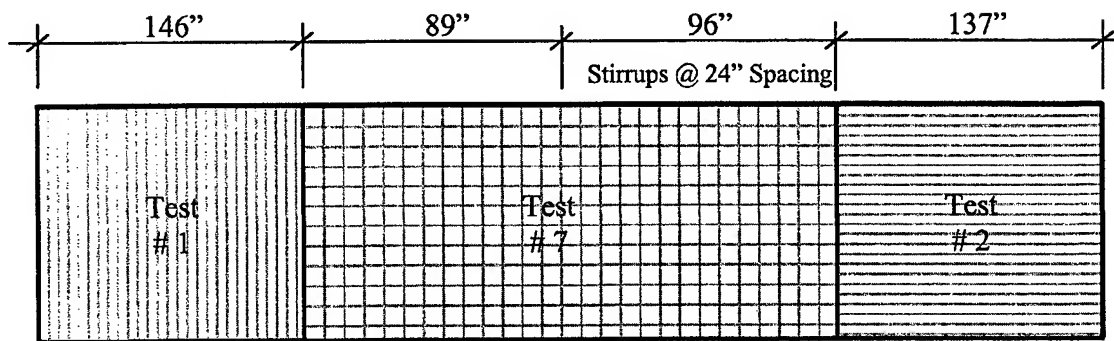
Figure 8.11  Girder Layout A



| 141" | 114" | 96" | 117" |

Stirrups @ 24" Spacing

Test #3 | Test #8 | Test #5
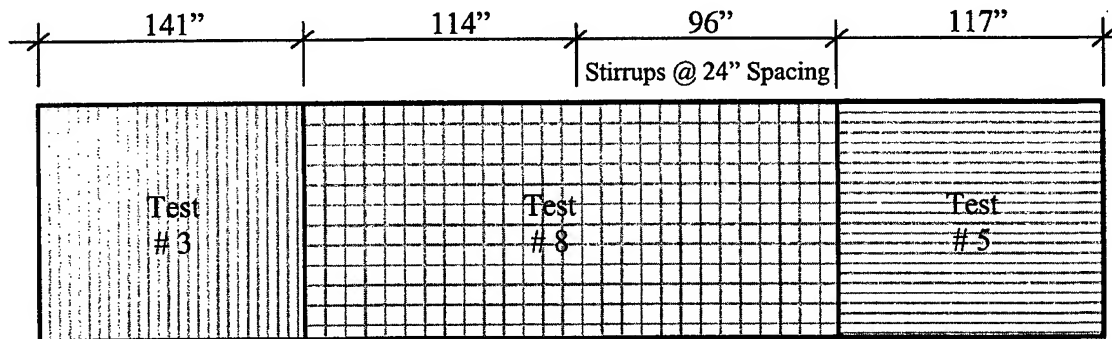
Figure 8.12  Girder Layout B



| 141" | 124" | 120" | 131" |

Stirrups @ 24" Spacing

Test #4 | Test #9 | Test #6
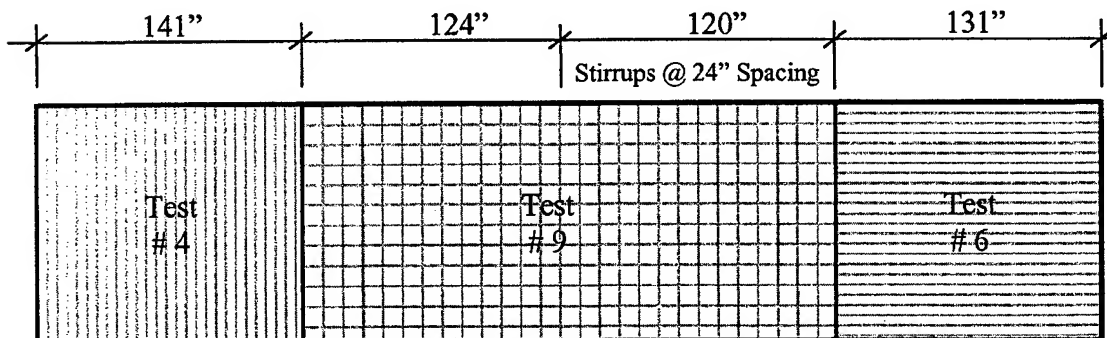
Figure 8.13  Girder Layout C

154

### 8.2.5.4 Design Considerations

In designing the test girders, it was necessary to assume a damaged area resulting from each test. In the case of tests 1 through 6, it was assumed that a distance equal to at least "d" away from the point of load application towards the center of the girder would be damaged in addition to the specific area of interest. In the case of girders having double the AASHTO specified amount of shear reinforcing steel, additional area was added for damage as a precaution.

Another consideration in configuring tests 2, 5 and 6 was the fact that a portion of the center of each girder was reinforced with only the minimum-specified 24" steel spacing as seen in Figures 8.8 through 8.10. This 24" spacing area would be used during tests 7 through 9 to specifically examine the shear capacity of the girders. In order to ensure that this area would not undergo significant damage other than minor flexural cracking, girder-bottom stresses were examined for tests 2, 5 and 6 in the area of 24" stirrup spacing. Tests 2, 5 and 6 were critical since the distance between supports would be less allowing a greater point load and thus a greater shear to develop. As long as the resulting bottom stresses were less than $12(f_c')^{1/2}$, it was assumed that resulting damage would not be a significant factor for center-girder tests. In all cases, the bottom stresses were below the critical level.

### 8.2.5.5 Final Girder Designs

In order to arrive at the final girder designs, tests 1-9 were configured into three girders such that consistent lengths could be achieved to the greatest extent possible. For each series, two each 39-foot girders and one 43-foot girder were configured. Based on

155

the closeness of the Series 1 and Series 2 concrete design strengths, the shear design varied only slightly. Based on this closeness of design, it was decided to construct both series of girders with the same shear reinforcement spacing.

As part of the final design, additional # 4 stirrups were positioned in the initial d/4 of the girder at both ends to control bursting forces as per AASHTO[40] Section 9.22.1. Five # 3 "doghouse bars" were spaced at 12 inches on center in the bottom flange at both ends of each girder to enclose the prestressing steel as per AASHTO[40] Section 9.22.2.

Figures 8.14 through 8.16 provide sketches of girders "A", "B", and "C." The final designs were the same for both series of girders. These final designs were provided to the fabricator for production of the girders.

**Stirrup Detail**

43-3/4"

7"

# 4

8-1/2"

5 each # 3 "doghouse" bars spaced at 12" (Typ both ends)

10' – 7"
37 spaces
(3-1/2" max spacing)

8' – 0"
4 spaces
(24" max spacing)

18' – 9"
33 spaces
(7" max spacing)

2" End Cover (Typ both ends)
4 Spaces @ 2" (Typ both ends)

39' – 0"

**AASHTO Type II**

$f_c'$ = 8,500 psi (10,000 psi) (75% of $f_c'$ at Release)

Strand = 0.6" 270 ksi LOLAX pulled to 75% of $f_{pu}$

Strand Spacing = 2"

Distance From Bottom to 1st Row of Strands = 3.0"

Distance From Bottom to TOP Row of Strands = 33.5"

Stirrup (# 4 Bars) Spacing Shown Above

Total Stirrups = 186 (2 at each location)

Total Doghouse Bars = 10

Beam top surface to be intentionally roughened (raked)

Drawn by: KFM  Phone (404) 385-1429

Figure 8.14  Girder Layout A

157

5 each # 3 "doghouse" bars spaced at 12" (Typ both ends)

8' – 11"
16 spaces
(7" max spacing)

8' – 0"
4 spaces
(24" max spacing)

9' – 6"
17 spaces
(7" max spacing)

39' – 0"

10' – 11"
38 spaces
(3.5 " max spacing)

2" End Cover (Typ both ends)

4 Spaces @ 2" (Typ both ends)

**Stirrup Detail**

43-3/4"

7"

# 4

8-1/2"

**AASHTO Type II**

$f_c'$ = 8,500 psi (10,000 psi) (75% of $f_c'$ at Release)

Strand = 0.6" 270 ksi LOLAX pulled to 75% of $f_{pu}$

Strand Spacing = 2"

Distance From Bottom to 1$^{st}$ Row of Strands = 3.0"

Distance From Bottom to TOP Row of Strands = 33.5"

Stirrup (# 4 Bars) Spacing Shown Above

Total Stirrups = 186 (2 at each location)

Total Doghouse Bars = 10

Beam top surface to be intentionally roughened (raked)

Drawn by KFM   Phone: (404) 385-1429

Figure 8.15  Girder Layout B

158

5 each # 3 "doghouse" bars spaced at 12" (Typ both ends)

2" End Cover (Typ both ends)

4 Spaces @ 2" (Typ both ends)

21' – 3"
37 spaces
(7" max spacing)

10' – 0"
5 spaces
(24" max spacing)

10' – 1"
18 spaces
(7" max spacing)

43' –

**AASHTO Type II**

$f_c'$ = 8,500 psi (10,000 psi) (75% of $f_c'$ at Release)

Strand = 0.6" 270 ksi LOLAX pulled to 75% of $f_{pu}$

Strand Spacing = 2"

Distance From Bottom to 1st Row of Strands = 3.0"

Distance From Bottom to TOP Row of Strands = 33.5"

Stirrup (# 4 Bars) Spacing Shown Above

Total Stirrups = 138 (2 at each location)

Total Doghouse Bars = 10

Beam top surface to be intentionally roughened (raked)

Drawn by KFM   Phone: (404) 385-1429

**Stirrup Detail**

43-3/4"

7

# 4

8-1/2"

Figure 8.16  Girder Layout C

159

## 8.3 Girder Instrumentation

During construction, instrumentation points were installed in each girder to allow measurement of concrete surface strains and deflections. The following sections describe the construction of devices to allow installation of the measurement points.

Concrete surface strain data were obtained using DEMEC gage points. The gage points were cast into each girder by attaching the points to steel strips, which were bolted to the steel girder forms. Figure 8.17 shows a diagram of the DEMEC inserts and the method used for embedding them in the girders. The embedment strips were constructed from steel bar 1½ inches wide by 1/4 inch thick. The DEMEC embedments were installed at a distance of 2 inches on center. The mounting screws were placed at a distance of approximately 10 to 12 inches apart to adequately affix the strips to the girder formwork. Distances greater than 12 inches resulted in the strips bowing away from the formwork. The wing nuts pictured in CUT A were the DEMEC embedments.

Mounting the strips to the formwork was accomplished as pictured in CUT B of Figure 8.17. The strips were placed as shown in Figure 8.18.
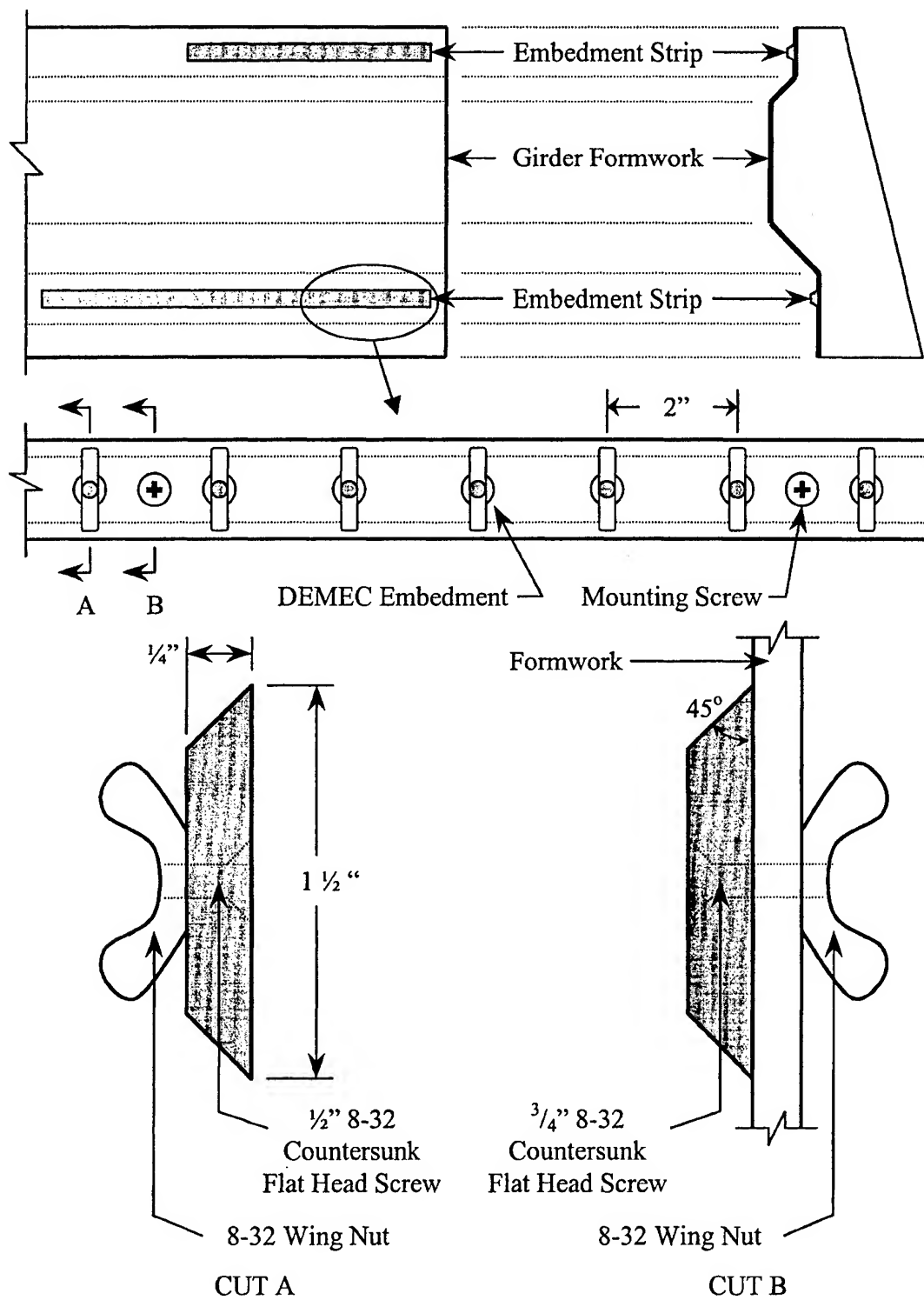
Figure 8.17 Diagram of DEMEC Embedment Strip Construction and Installation

161

30" Strip

$C_L$

48" Strip

24" Strip

1"
typical
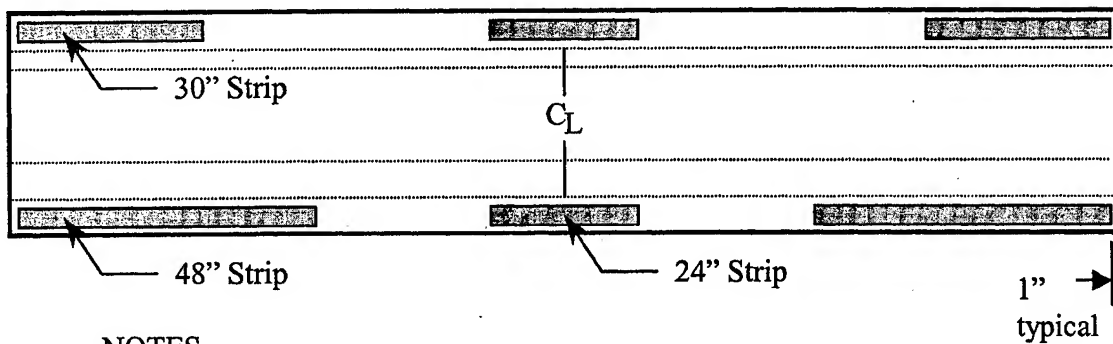
NOTES
1. Place embedment strips as close to end of girder as possible.
2. Place embedment strips such that embedments are at the same level as the prestressing strands.

Figure 8.18  DEMEC Embedment Strip Placement on Girder



$C_L$

2"

Dead End

Pulley End

6"

Pulley

¼" x 1¼" Bolt

¼" Nut

¼" Coupling Nut

¼" Washer

Cast into
Girder

¼" x ½" Bolt

¼" x 1¼" Bolt

¼" Nut
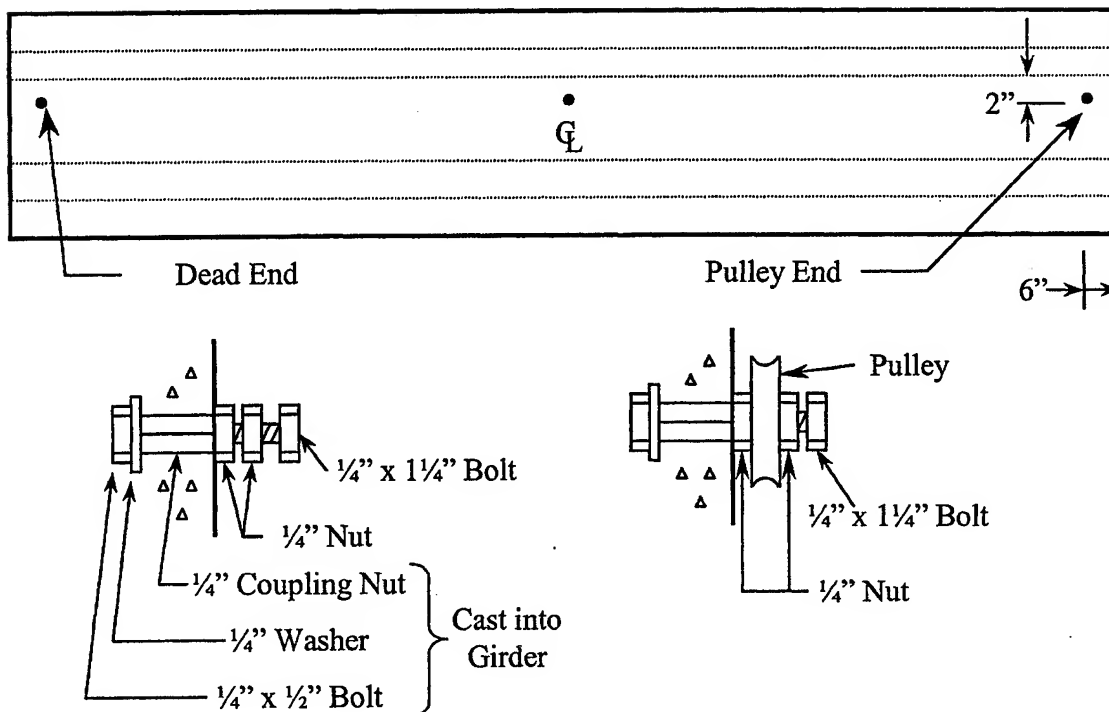
Figure 8.19  Attachment Points for Taut Wire

162

Deflection at midspan was measured using a piano wire stretched between a mounting post at one end and a pulley at the other as shown in Figure 8.19 A 10-pound weight was attached to the wire to keep it taut. At midspan, a metal ruler and mirror were affixed to the girder with epoxy. (Figure 8.20) The ruler enabled deflection measurement and the mirror prevented error due to parallax.



Figure 8.20 Use of Taut Wire for Deflection Measurement at Midspan

Vibrating wire strain gages (VWSG) with a 6-inch gage length were installed at midspan at the level of the bottom strands. (Figure 8.21)
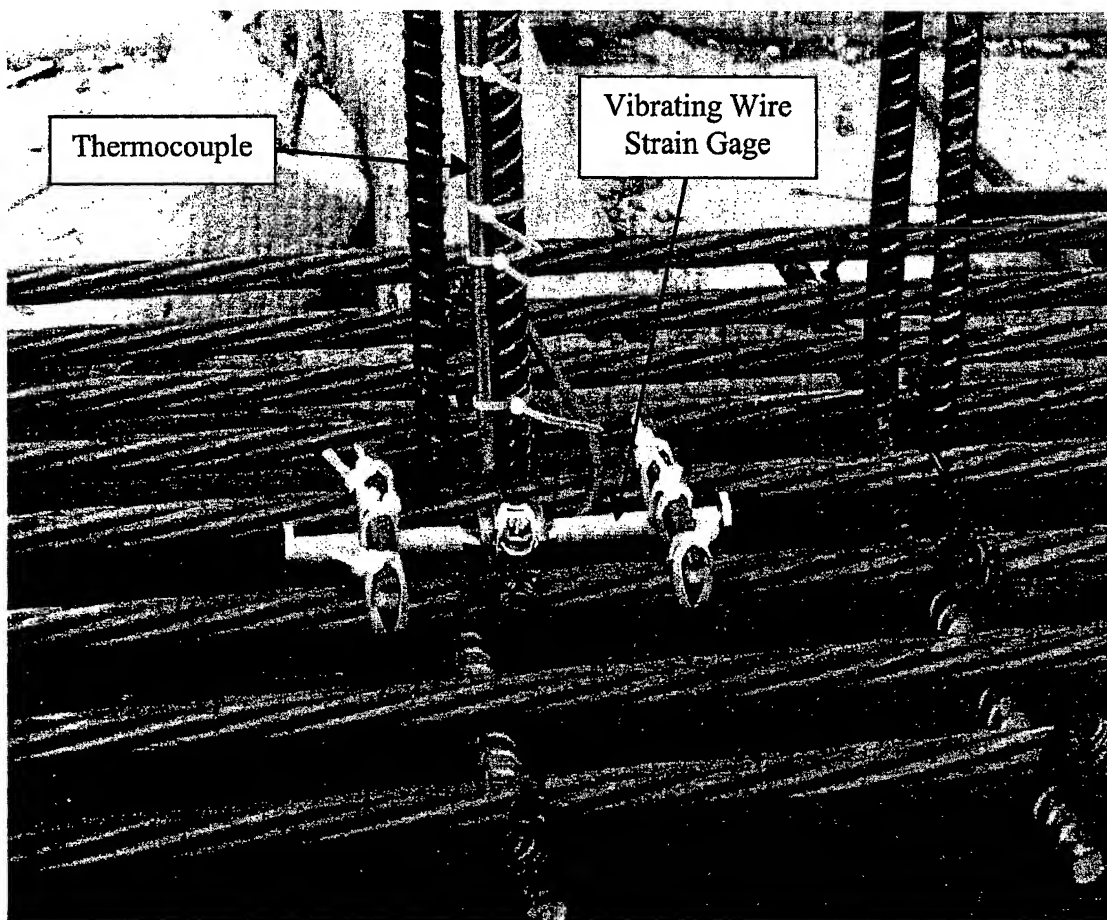
Figure 8.21 VWSG and Thermocouple Prior to Concrete Placement

Thermocouples were installed in each girder to measure heat of hydration during the curing process. The thermocouples were 6 inches long, ¼ inch in diameter, type K with 1-meter lead wires. The thermocouples were placed in the vicinity of the VWSGs as shown in Figure 8.21.

## 8.4 Girder Construction

The six girders were constructed at Tindall Corporation precast plant in Jonesboro, Georgia using plant personnel and standard precast plant procedures. The author together with Georgia Tech students and faculty installed and measured all instrumentation and fabricated all material test specimens. The girders were constructed in three identical sequences. During each sequence, two girders were constructed. During the first sequence, girders G1A and G1B were constructed. During the second sequence, girders G2A and G2B were constructed. During the third and final sequence, girders G1C and G2C were constructed.

### 8.4.1 DEMEC Gage Embedment and Taut Wire Insert Installation

Installation of the DEMEC gages was accomplished a few days in advance of the actual start of construction. Careful coordination with the concrete plant manager was essential to insure formwork was positioned to allow drilling holes and installation of the DEMEC gage embedment strips. Cordless drills with backup batteries and chargers, a good supply of back-up drill bits, cutting oil, grease pencils and measuring tapes were the keys to success.

Before the strips were attached, a layer of grease was spread across the back of the strip to fill the screw heads of the screws holding the wing nuts (embedments) in place on the strip. The backside of the strip was placed against the formwork. Once in place, any gap between the edge of the strip and the formwork was filled with grease to prevent concrete from getting behind the strip. In addition, the exposed portion of the

165

strip was coated with grease to prevent the strip from sticking to the girder. Grease was kept from the wing nuts because their firm bond to the concrete was essential.

Connection points were also attached to the inside of the formwork to allow installation of connections for the taut wire.

Prior to the formwork being moved into place for girder placement, it was sprayed with form release oil. It was necessary to wipe any excess oil from the wing nuts before the forms were lowered into position.

### 8.4.2 Strand Tensioning

After the prestressing strands were threaded through the bulkheads, load cells were installed on the passive end to monitor the prestressing force. The load cells were calibrated in advance of tensioning. Results of the calibration can be found in Appendix E. Figure 8.22 shows the load cells in place.
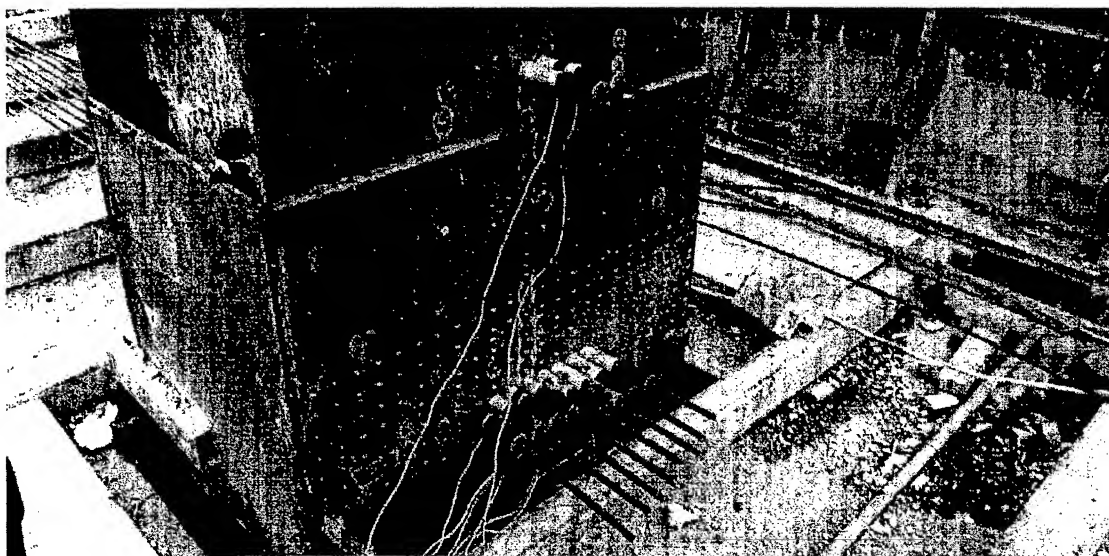


Figure 8.22 Strand Load Cells Installed at Passive End of Girder Line

166

The load cells were wired to a BLH 1225 Portable 10 Channel Switch and Balance Unit, which was then connected to a BLH 1200B Portable Digital Strain Indicator. The same units used during construction were also used during load cell calibration. Figure 8.22 shows the BLH 1225 and BLH 1200B.
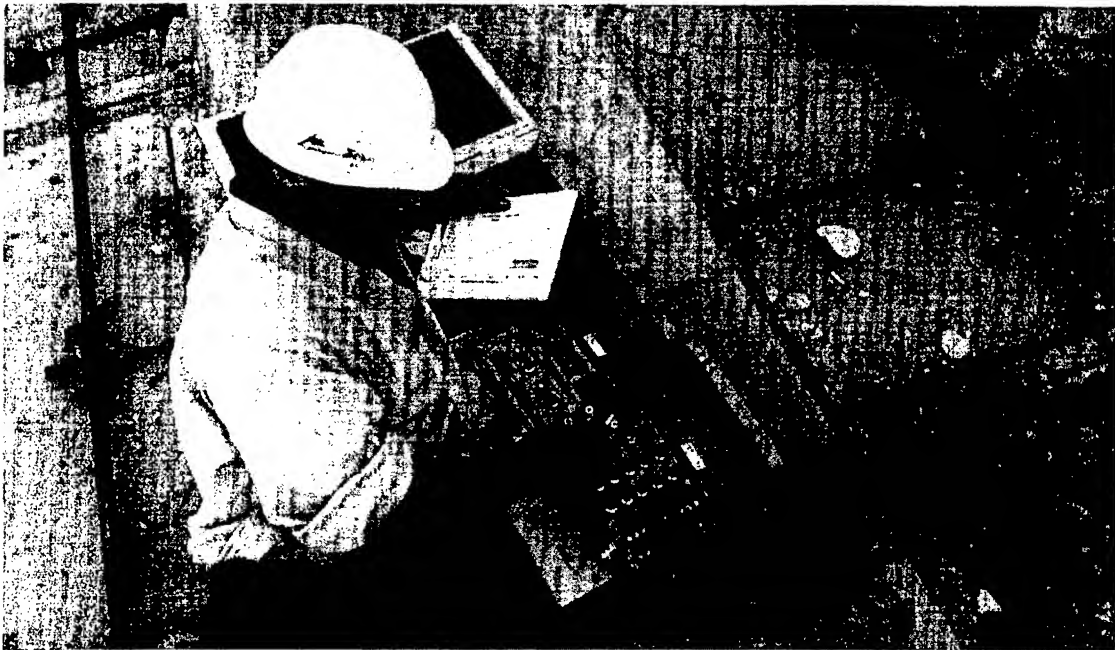


Figure 8.23 Strand Load Cell Monitoring Equipment

With the load cells connected and zeroed, plant personnel tensioned the strands using a Hercules hydraulic jack. Tensioning the 0.6-inch strands to 75 percent of $f_{pu}$ or 203 ksi required a tension force of approximately 44.5 kips. All tensioning and strand elongation data can be found in Appendix H. For purposes of tensioning and tracking strand force, strands were numbered as shown in Figure 8.24. Figure 8.24 also provides the order in which the strands were released.
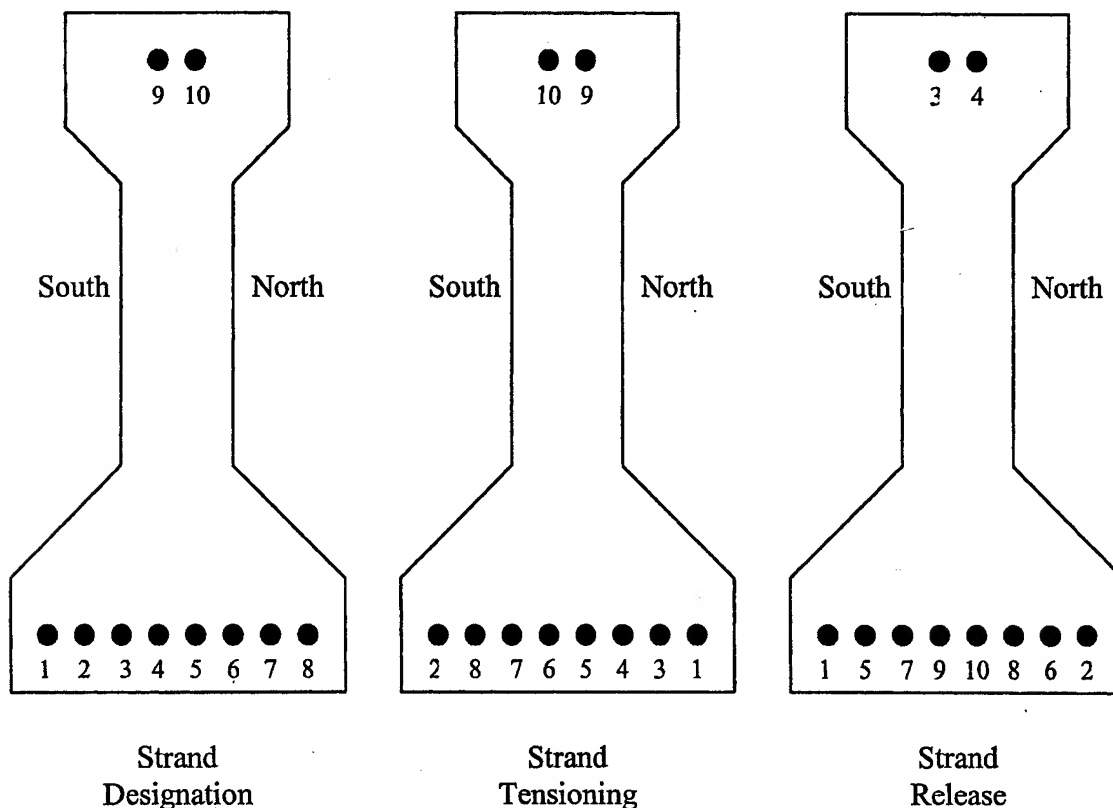
Figure 8.24 Strand Designation, Tensioning Order, and Release Order

The plant had trouble with their tensioning machine while tensioning the third

sequence of girders and had to replace the hydraulic ram. The Hercules tensioning

machine was designed for use on 0.5-inch strand and struggled to tension the 0.6-inch

strand. In comparing the reported strand tension values with the values recorded using

the strand load cells, the strand load cells reported tension values up to 20 percent less

than that reported by the hydraulic pump. Appendix F includes determination of

prestress force from the strand load cell reported strains and a comparison with plant

reported tension values. Load cell data were used for all subsequent analyses. Figures

8.25 and 8.26 show Tindall personnel tensioning the strands.

Figure 8.25  Tindall Personnel Operating Tensioning Machine



Figure 8.26  Jacking of Prestressing Strand

### 8.4.3 Installation of Shear Reinforcing Steel

Following the tensioning of prestressing strands, the shear reinforcing steel was

installed per the sketches shown in Figures 8.14, 8.15 and 8.16. Georgia Tech personnel

carefully checked stirrup locations to insure they were in accordance with the plans.

Figure 8.27 shows the installation of shear reinforcing steel.



Figure 8.27  Installation of Shear Reinforcing Steel Near Girder End

### 8.4.4 Installation of VWSG and Thermocouples

The last step taken prior to installing the formwork was to attach the VWSG and

thermocouple at midspan. As seen in Figure 8.21, the VWSG was firmly attached to the

prestressing strand at the level of the bottom strands. The thermocouple was securely

attached in the same vicinity as the VWSG.

### 8.4.5 Place Formwork

Prior to lifting the formwork into place, the forms were coated with a form release agent (form oil). It was necessary to recheck the DEMEC embedments and wipe any excess oil from the wing nuts prior to form installation. In a few cases, wing nuts had been knocked off the embedment strips and required replacement. Once properly aligned, the forms were locked into place by large threaded rods beneath the formwork and wishbone struts on top. Figures 8.28 and 8.29 show installation of the formwork.
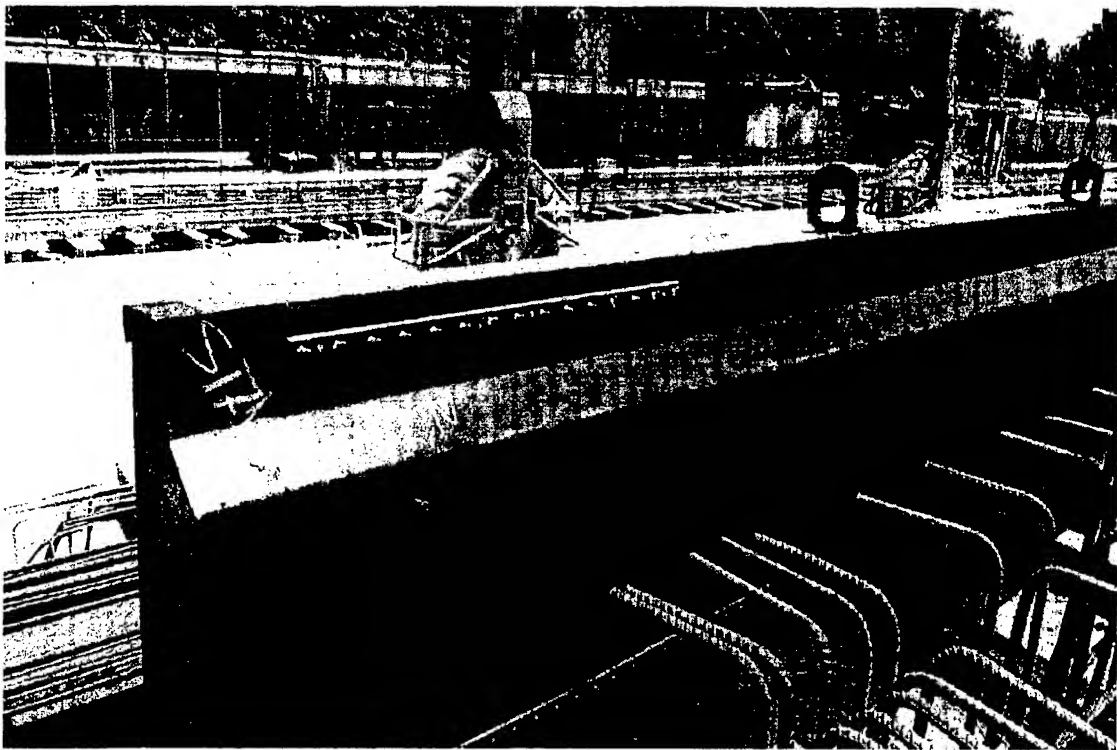


Figure 8.28 Formwork with DEMEC Embedment Strips Being Lifted Into Place

Figure 8.29  Tindall Supervisor Directing Placement of Formwork.

### 8.4.6  Batch and Place Concrete

Prior to batching the HSLC, moisture tests were conducted on the lightweight

aggregate and sand to determine the exact mix design.  The moisture tests were started at

least two hours prior to placement to allow time to correctly dry the aggregate and

configure the mix design.

### 8.4.6.1 Mix Designs

Table 8.5 provides an overview of the mix design for each girder placement. The mix designs below were based on making 2 cubic yard batches. Each girder required approximately 3.5 cubic yards.

Table 8.2 Mix Designs for Girder Placements (2 cubic yard mix)

| Girder # | | G1A, G1B | G2A, G2B | G1C | G2C |
|---|---|---|---|---|---|
| Date of Placement | | 9 July 01 | 12 July 01 | 17 July | 17 July 01 |
| Lightweight Aggregate | (lbs) | 1977 | 1958 | 1947 | 1995 |
| Normal Weight Sand | (lbs) | 2195 | 2173 | 2155 | 2165 |
| Class F Fly Ash | (lbs) | 284 | 300 | 284 | 300 |
| Silica Fume | (lbs) | 38 | 200 | 38 | 200 |
| Type III Portland Cement | (lbs) | 1570 | 1480 | 1570 | 1480 |
| WRDA 35 (LRWR) | (fl oz) | 114 | 119 | 114 | 119 |
| Daravair 1000 (AEA) | (fl oz) | 24 | 20 | 24 | 20 |
| ADVA Flow (HRWR) | (fl oz) | 95 | 258 | 95 | 258 |
| Water | (gal) | 39.5 | 36.7 | 44.8 | 33.1 |

### 8.4.6.2 Concrete Mixing

The concrete was mixed in a rotary auger-type mixer located in an elevated mix station approximately 200 feet from the prestressing bed. The mix station did not have a silo for fly ash or silica fume, thus those two components had to be added manually. The concrete components were added in a specific sequence for each batch of concrete. The lightweight and normal weight aggregates were added first with all the low range water reducer (LRWR), air entraining agent (AEA), high range water reducer (HRWR), and approximately half the mix water. Water was held out of the mix because Tindall's mixer had a water leak making exact determination of water added impossible. The initial components were allowed to mix for approximately 1 minute to insure thorough

173

dispersion of the chemical admixtures. Next, the Type III cement was added. Additional water was added as necessary to allow proper mixing of the cement. Next the Class F fly ash was added with additional water as required. Last, the silica fume was added. Any remaining water up to the specified mix design amount was added and the result observed. If the mix was still stiff, additional HRWR was added to bring the mix to a workable state.

When working with low water cement ratio mixes, water content is crucial. Noted variations in aggregate moisture content made a relatively large difference in the amount of added mix water required. During the batching process, water beyond the specified mix amount was added based on aggregate observed to be drier than measured during testing. While this may seem imprecise, experience with a particular mix design allows the person supervising the batch process to make adjustments and still achieve excellent results. In each batch process, water was added beyond the specified mix design with resulting strengths being in line with that expected. Without exact moisture control, such changes "on the fly" were unavoidable.

Figure 8.30 shows the elevated mix platform at Tindall Concrete. Concrete transport vehicles (Tuckerbilt) transport the concrete from the base of the platform to the girder line.

### 8.4.6.3 Material Testing

Upon batching of concrete, it was loaded into the transport vehicle and brought to the quality control station. Tindall personnel performed a slump test according to ASTM C231,[74] a unit weight test according to ASTM C138,[75] and recorded the temperature

174

according to ASTM C1064.[76] Georgia Tech personnel performed an air content test using a roll-a-meter according to ASTM C173.[77] To the greatest extent possible, these tests were performed on each batch of concrete.
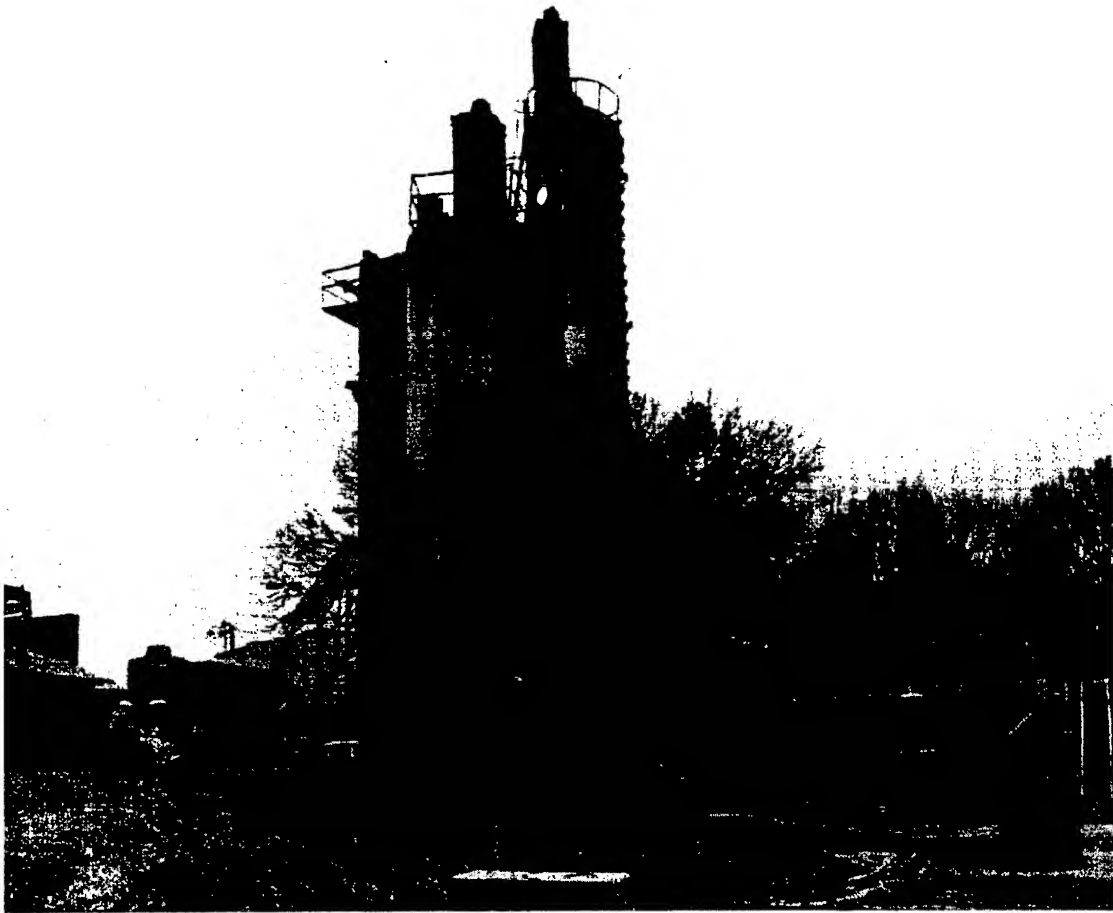


Figure 8.30  Elevated Mix Platform

A significant number of quality control specimens were cast during each girder placement; many of the specimens were cured in insulated boxes. Based on previous research at Georgia Tech,[84] cylinders cured in insulated boxes more closely matched

actual girder strengths for full-sized girders for the first 7 days. Temperature plots for cylinders cured in insulated boxes compared well to actual girder curing curves during this project.

During the third girder placement, cylinders were cast for a statistical study to determine the actual variation in placing HSLC.

### 8.4.6.4 Concrete Placement in Girders

After delivering concrete to the quality control station, the remaining concrete was transported to the girder line where it was placed into the forms. The Tindall concrete workers placed the concrete in lifts vibrating each lift with a spud vibrator. One Georgia Tech researcher was present on the girder line at all times during concrete placement to insure the concrete workers did not damage any instrumentation or DEMEC inserts. After all lifts of concrete were in place, the top of the girder was screeded and raked to give it the required 1/4-inch variation for good bond between the deck and girder. The girders were then covered with heavy plastic to protect them from rain and hold in heat during the curing process.

### 8.4.6.5 Comments on Placement Conditions

The girders in this project were placed during July when the ambient temperature reached well above 90 degrees Fahrenheit at mid-day. During the third concrete placement, events occurred at the plant that forced the placement time to be at about 3:00 pm, the hottest part of the day. The following key conditions existed that created placement problems.

1. The formwork had been exposed to direct sunlight throughout the day and was extremely hot to the touch.

2. The concrete transport vehicle had been sitting in the sun as well, and the metal hopper was hot.

3. The aggregate had been sitting in the silo above the elevated mix platform all day. In addition to being warm, the moisture content was probably not as high as that recorded from earlier testing.

The first batch of concrete mixed was for girder G2C. The water to cementitious materials ratio was 0.23. The batch was mixed as previous ones had been mixed. The consistency in the mixer appeared to have a slump of approximately 5-6 inches. When the concrete was released from the mixer into the transport vehicle, a flash set initiated when the concrete touched the hot metal in the hopper. Although not initially noticed, the problem became apparent when concrete was released for quality control checks. The slump was about 3 inches, the air content was about 3 percent and the unit weight was low at 114 pcf. It was decided to use the concrete because it still appeared workable enough to use in the girder. When the delivery vehicle began placing concrete into the girder, it was discovered that better than half the concrete in the vehicle had set in the hopper and could not be discharged into the formwork. In retrospect, the decision to use this initial batch of concrete was an error. At that point, Tindall personnel and volunteers worked quickly to remove the setting concrete from the hopper of the delivery vehicle. After about 30 minutes of effort, all the concrete had been removed.

In the mean time, the small amount of concrete placed in the girder was setting. Before another batch of concrete was mixed, the delivery vehicle was sprayed with cold water to lower the temperature of the hopper and coated with a lubricant to prevent the concrete from becoming bonded to the metal surface. The resulting girder, G2C was acceptable. There was no honeycombing and the cold joint did not appear to be a significant problem. As it turned out during testing, the particular girder end, G2C-West, performed acceptably.

The lessons learned in this event were numerous and related mostly to temperature. The formwork and equipment should have been kept cool prior to the placement. The aggregate should be kept cool to the greatest extent possible.

### 8.4.7 Concrete Curing

The girders were allowed to cure overnight. Temperature was monitored on each girder using the embedded thermocouple and a printing thermometer. A typical temperature curing curve for girder G1A is shown in Figure 8.31 together with the temperature in the curing box for test cylinders.

Tindall quality control personnel performed compressive strength tests on ASTM cured cylinders approximately 16 hours after casting. For comparison, curebox cylinders were also tested. The curebox cylinders always broke at a much higher strength than the ASTM cylinders. Table 8.3 provides times from concrete placement to form removal and release of prestress. The drop in the ambient temperature at 20 hours resulted from moving the cureboxes from outside into the laboratory.

178
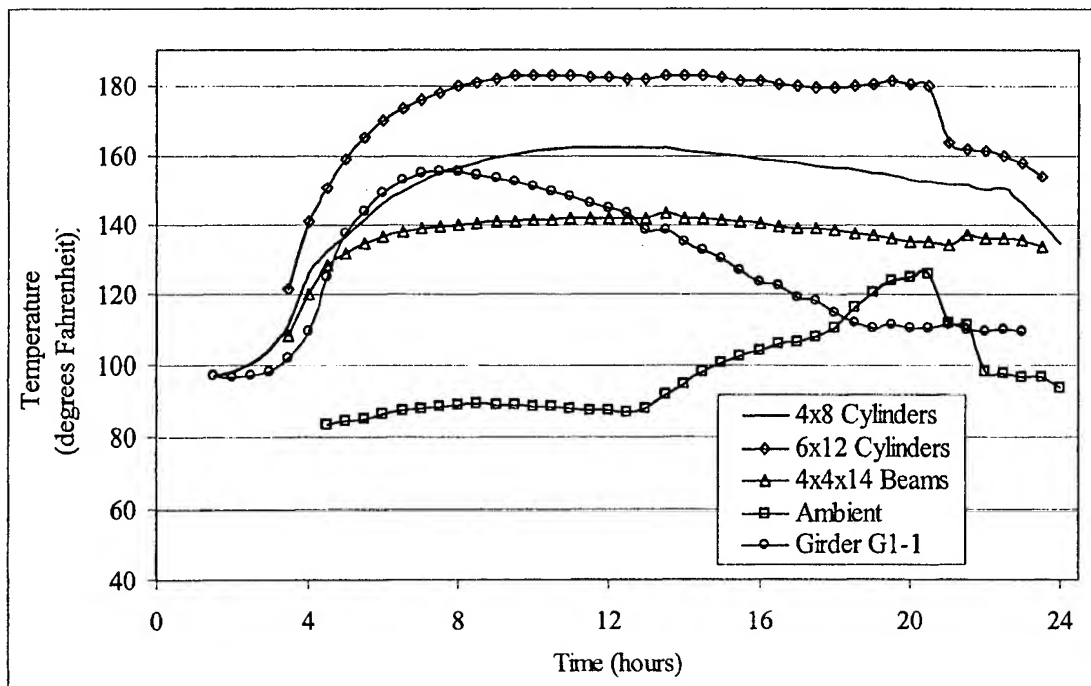
Figure 8.31  Typical Temperature Curing Curve for Girder G1A

Table 8.3  Concrete Placement Time; Hours Until Form Removal, Release of Prestress

| Girder | Time/Date of Placement | Hours Until Form Removal | Hours Until Prestress Release |
|--------|------------------------|--------------------------|-------------------------------|
| G1A | 9 July 01, 1800 | 17.5 | 21.5 |
| G1B | 9 July 01, 1800 | 17.5 | 21.5 |
| G1C | 17 July 01, 1700 | 18 | 22 |
| G2A | 12 July 01, 1000 | 24 | 29 |
| G2B | 12 July 01, 1000 | 24 | 29 |
| G2C | 17 July 01, 1600 | 20.5 | 23 |

## 8.4.8  Formwork Removal, Embedment Preparation and Initial Readings

After the metal forms were removed, the DEMEC steel embedment strips were

unscrewed and stripped out (Figure 8.32).  Once the embedments (wing nuts) were

exposed, "initial" DEMEC readings were taken as described in detail in Section 9.6.2.

179

Figure 8.32 Removal of Screws from DEMEC Embedment Strips

The taut wire was also installed at this time. The mounting hardware as pictured in Figure 8.19 was installed, the wire stretched and the weight hung. The metal ruler was attached using 90-second epoxy at midspan such that two inches was exposed above the wire and 4 inches was exposed below the wire. The mirror was attached also using 90-second epoxy to the side of the ruler following the same spacing guidelines. After two sets of "initial" readings were taken using the DEMEC gage reader and the "initial" deflection was taken, the girder was ready for release of prestress.

### 8.4.9  Release of Prestress and "Release" Readings

Three Tindall workers using oxy-acetylene welding torches simultaneously flame cut the strands following the pattern identified in Figure 8.24 and shown in Figure 8.33. After all strands were cut, the "release" concrete surface strain, VWSG, and deflection readings and subsequent readings were recorded as outlined in Section 9.6.2.



Figure 8.33  Flame Cutting of Prestressing Strands with Oxy-Acetylene Welding Torch

### 8.4.10  Movement From Prestressing Bed to Temporary Storage Location

After prestress release, the girders were moved to a storage area and placed on wooden dunnage located at the centers of bearing (6 inches from each end).  While in storage, Georgia Tech researchers took readings as outlined in Chapter 9 to examine

transfer length. Figure 8.34 shows the movement of a girder to the storage location using an overhead crane.
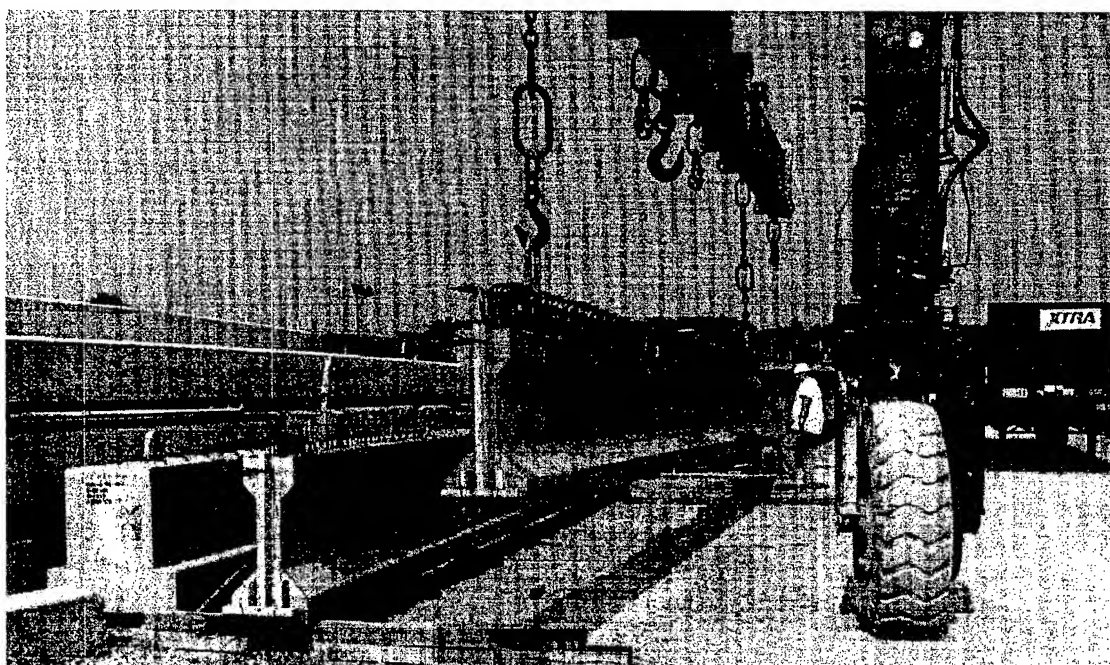


Figure 8.34  Movement of Girder to Storage Location Using Overhead Crane

### 8.4.11  Movement of Girders to Georgia Tech Structures Lab

After curing for approximately 3-4 weeks at the Tindall Plant, the girders were transported on flatbed trucks to the Georgia Tech Structures Lab. In the lab, the girders were stored as they had been at the concrete plant. One final set of surface strain, VWSG, and deflection readings were taken upon arrival and prior to beginning deck construction. Figure 8.35 shows girder delivery to the Georgia Tech Structures Lab.

Figure 8.35  Delivery of Girders to Georgia Tech Structures Lab

## 8.5 Composite Deck Construction

Two weeks after the girders were delivered to the Georgia Tech Structures Lab, composite decks were cast on each girder. The concept for deck placement was to cast the entire deck on all six girders in one placement.

### 8.5.1 Formwork Construction

Figure 8.36 shows a cross section of the formwork used to place the composite decks.



Figure 8.36 Formwork for Composite Deck

By placing the girders close together, it was possible to share formwork between two girders. Based on the selection of 19 inches for the deck width, a 2 x 4 (nominal 1.5 inches by 3.5 inches) was used to form the bottom underneath side of the deck. The side

of the deck was formed with ¾ inch plywood ripped into 13-inch widths and attached to the 2 x 4 boards with screws. The two "L" shaped pieces were then attached with screws to 2 x 4 uprights that ran to the floor for support. The upright lengths were adjusted as necessary to account for camber in the girders. The dead weight of the girders held the formwork in place nicely during deck placement.

Formwork for the outside of edge girders was held in place by ¼-inch threaded rods. Holes were drilled through the formwork through which the threaded rods were run. The rods were then bent around shear stirrups and secured with tie wire. Washers and nuts were installed on the threaded rod on the outside and tightened until the formwork was pulled snugly against the edge of the girder. The upright 2 x 4 boards of the outside edge formwork were held in place by a 2 x 4 that was bolted to the floor cover plates. The plates covered the tie-down locations and were conveniently placed at 4 feet on center. This detail can be seen in Figure 8.38.

## 8.5.2 Temperature and Shrinkage Steel

Temperature and shrinkage steel reinforcement consisting of two #4 bars was fastened to the shear stirrups at a distance of 3½ inches from the edge of the deck and approximately 2 inches down from the top surface. The bars came in 20-foot lengths and were overlapped by 18 inches as necessary. Figure 8.37 shows the temperature and shrinkage steel in place.
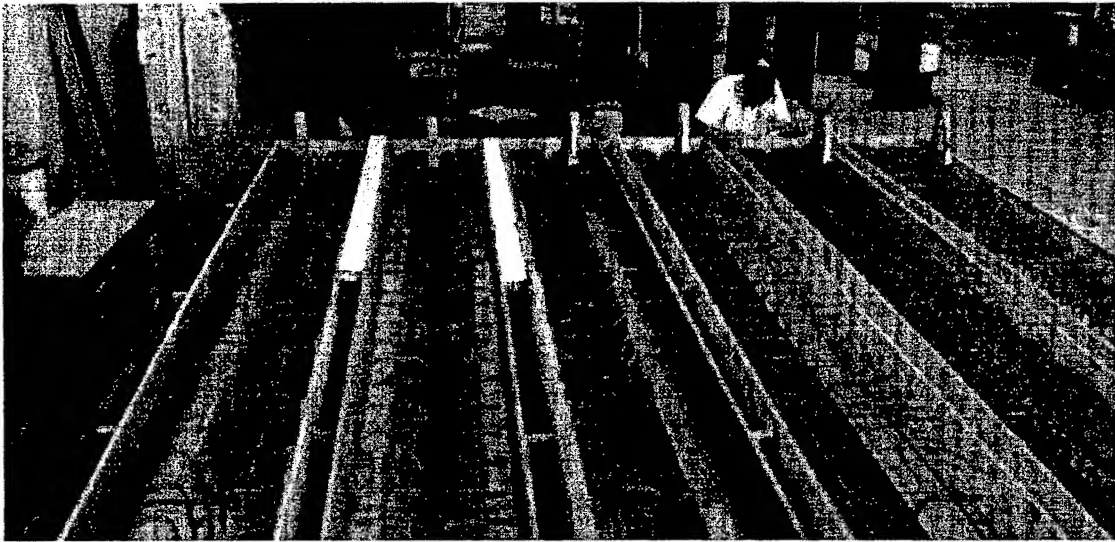
Figure 8.37  Formwork in Place with Temperature and Shrinkage Steel Installed
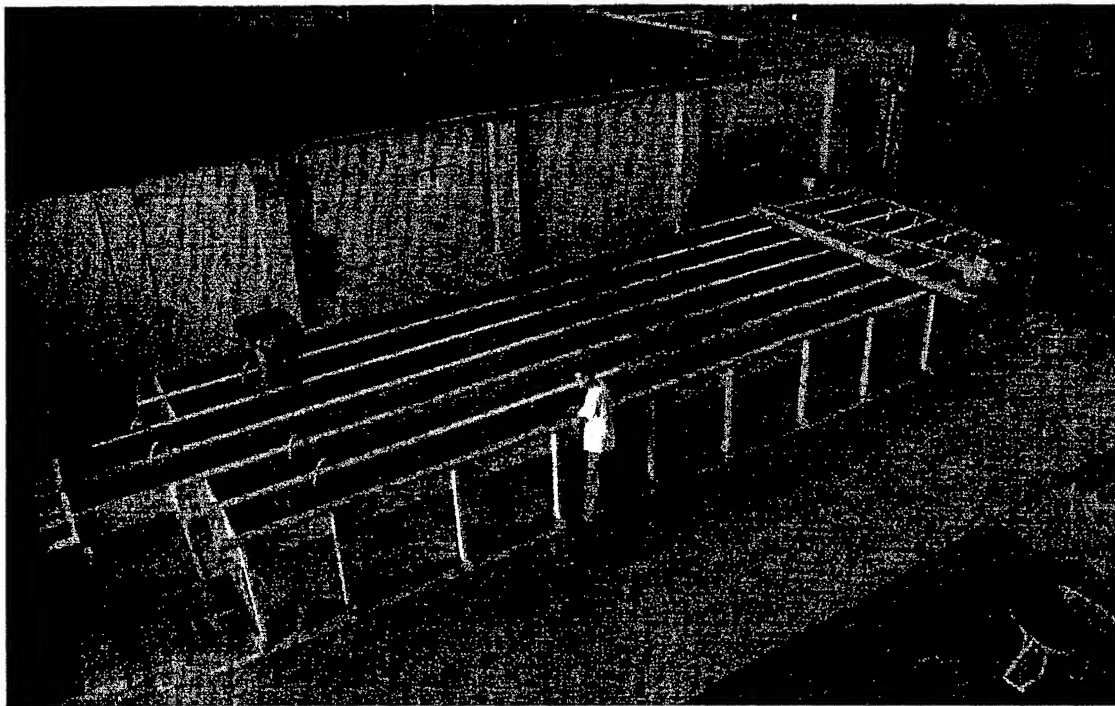


Figure 8.38  Formwork Ready for Concrete Placement

### 8.5.3 Concrete Placement

### 8.5.3.1 Type of Concrete

The type of concrete used for the composite deck was the standard Georgia Department of Transportation 3,500 psi normal weight bridge deck mix. Thomas Concrete, of Atlanta, Georgia delivered the concrete to the Structures Lab in readymix trucks.

### 8.5.3.2 Concrete Placement and Finishing

The readymix trucks were equipped with a concrete conveyor assembly as pictured in Figure 8.39.

Several Georgia Tech researchers assisted in the deck placement. One person operated the spud vibrator to insure good consolidation of the concrete into the forms and around the steel. Two other researchers used a large screed beam to smooth the top surface of the concrete. Two persons insured concrete from the chute was placed into the correct location.

In total, three readymix truckloads were required for completion of the deck. The first truckload was somewhat dry. Water was added on site to increase the slump to 6 inches. The second and third truckloads required no additional water; the measured slump was adequate upon arrival.

After the concrete began to set, the surface was finished with a trowel and then a broom surface was applied. The deck concrete was covered with plastic after initial set was reached. The deck was watered as necessary to keep it moist under the plastic.

After 7 days, the deck was uncovered and formwork removed. The formwork was completely disassembled, cleaned and stored for future use. Girder testing began approximately 52 days after the deck was cast.
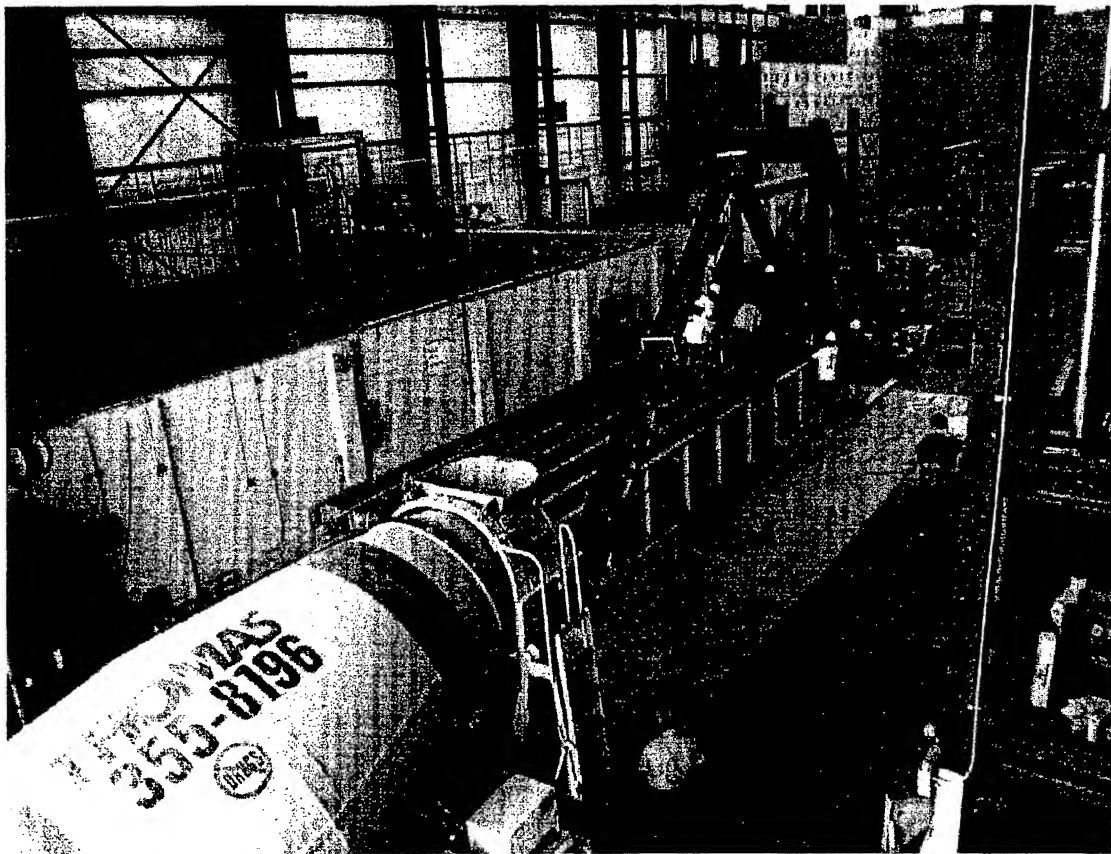


Figure 8.39 Readymix Truck with Conveyor Attachment

### 8.5.3.3 Materials Testing

Both 4 x 8 and 6 x 12 cylinders were cast for compressive strength and modulus of elasticity tests, respectively. The cylinders were cured under ASTM conditions for the first 24 hours then moved to the fog room for curing through the time at which the girders

were tested. The average strength of the deck concrete was 5,385 psi and the modulus of elasticity, E, was 3.37 million psi.

## 8.6 Direct Pull-Out Test

During girder placement, 24-inch x 36-inch x 24-inch specimen blocks were cast from the G1 and G2 series mixes for the "Mostafa", prestressing strand the direct pull-out test as shown in Figure 8.40.[90]
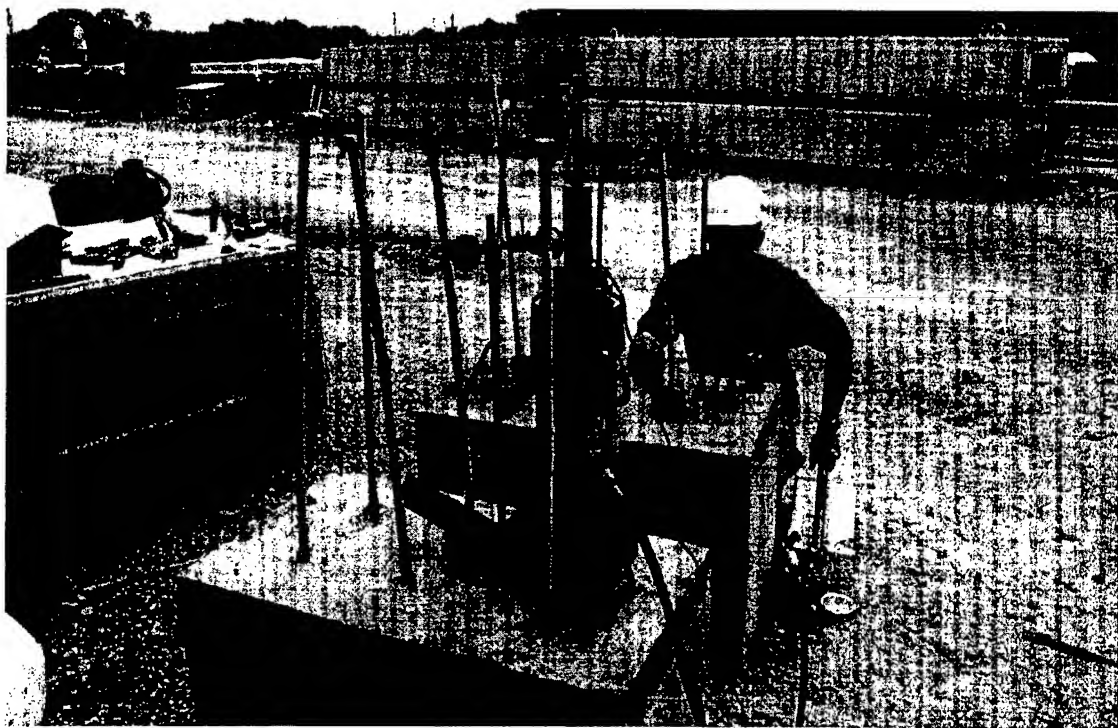


Figure 8.40  Mostafa Prestressing Strand Direct Pull-out Test

Each block had six, 48-inch segments of strand that were taken from the same reel used for girder construction. The segments were embedded 20 inches into the block with the top 2 inches being encased by PVC pipe as a bond breaker. The total embedded length

was 18 inches. The dimensions of the block were such that each strand had a free radius of at least 8 inches in all directions. Nominal reinforcing and lifting hooks made with #4 bars were placed in the block. Table 8.4 provides an overview of pull-out test results. The listed value is the load at which the strand underwent initial significant slip. Figures 8.41 and 8.42 provide plots of force vs. strand pull-out.

Table 8.4  Direct Pull-Out Test Results

| Strand Test # | G1 Series (kips) | G2 Series (kips) |
|---|---|---|
| 1 | 47.43 | 43.82 |
| 2 | 48.22 | 49.52 |
| 3 | 50.75 | 42.81 |
| 4 | 51.47 | 54.36 |
| Average | 49.47 | 47.63 |
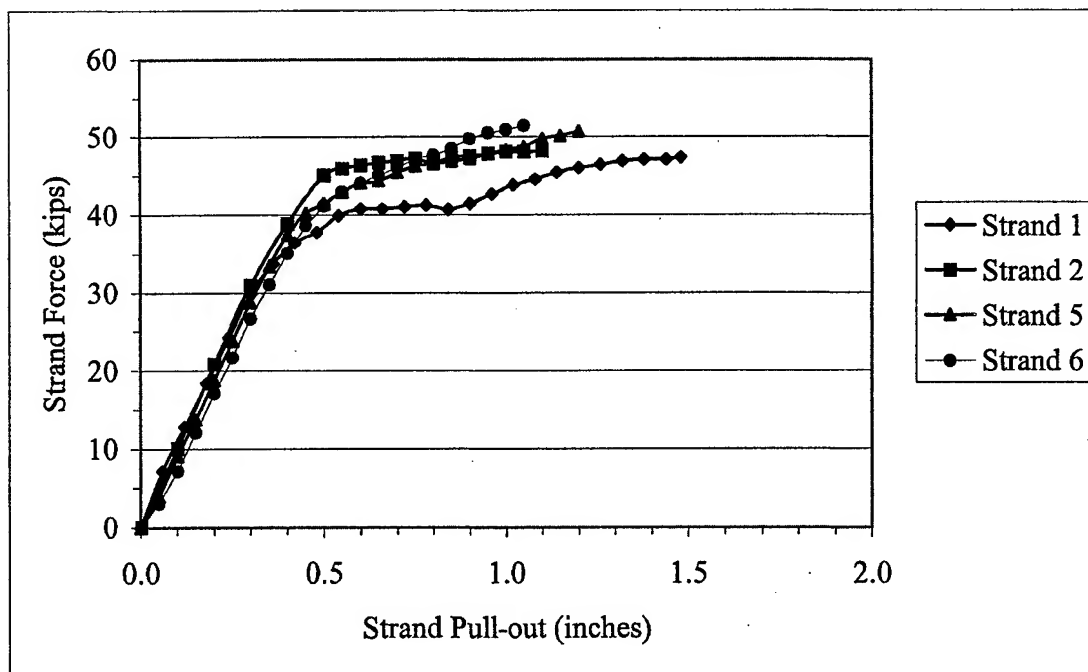


Figure 8.41  Direct Pull-Out Results for G1 Series HSLC

190
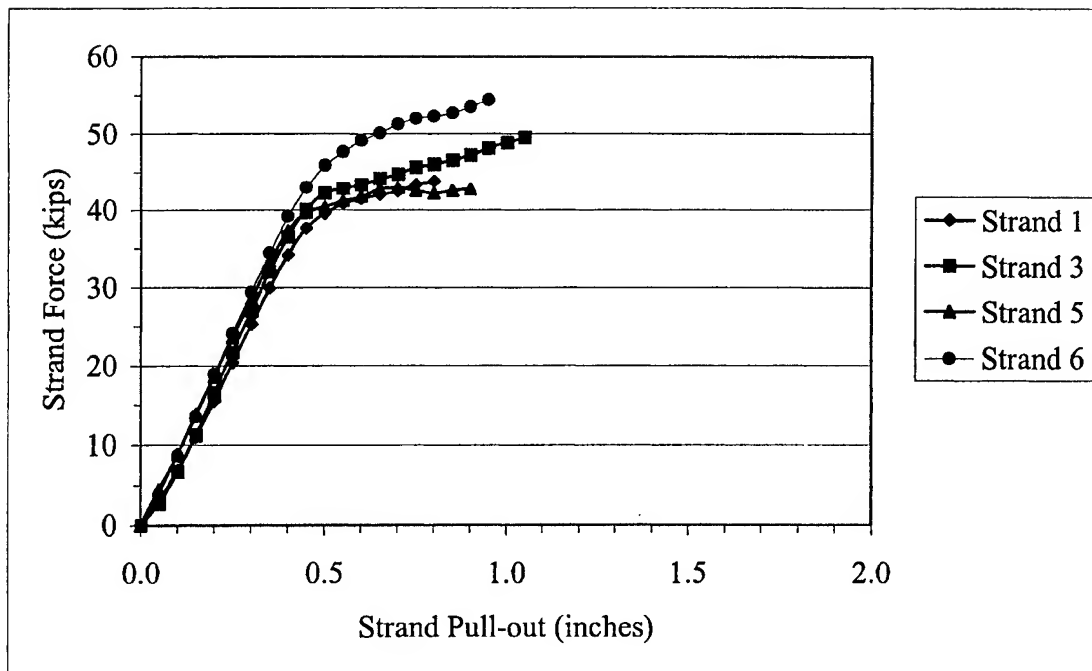
Figure 8.42  Direct Pull-Out results for G2 Series HSLC

Measurement of the load was accomplished using a strand load cell connected to

the BLH 1200B.  The same procedure was used as during girder construction.  Load cell

# 1 was used for this test.  Force was calculated from the strain data using a direct

relationship determined during the calibration process.  Consult Appendix E for load cell

calibration data.

The determination of pull-out capacity was based on the point at which the strand

experienced increased slip with little or no increase in load or the point at which the

strand underwent a sudden increase in slip and drop in load.  This "popping" occurrence

was common for all 8 tests performed.  In Figures 8.41 and 8.42, the last data point

shown was the point at which popping occurred.

Based on Logan's work, the minimum direct pull-out capacity for 0.6-inch diameter strand was 43.2 kips.[90] The average pull-out strength for both series exceeded the minimum value. One G2 test was slightly below the 43.2 kip minimum.

## 8.7 Material Properties

In order to evaluate the flexural performance of the girders, it was necessary to determine various material properties. The following sections provide material properties of the girders at the time of testing. Appendix C provides information on the reinforcing steel used for the shear stirrups and "doghouse" bars. Variations in concrete strength for the composite deck were the result of three different concrete deliveries during deck placement.

### 8.7.1 Girder Concrete Properties

Specimens were cast at the time of girder placement to allow determination of compressive strength, modulus of elasticity, and modulus of rupture strength at specific times. Table 8.5 lists the results of specimen testing with the range of test values listed.

The initial compressive strength values, $f_{ci}'$, and modulus of elasticity values, $E_{ci}$, were based solely on curebox cured specimens and were tested at 24 hours, the approximate time of strand release. The compressive strength values, $f_c'$, are based on an average of curebox and ASTM cured specimens tested just prior to girder testing approximately 3-4 months after casting. The moduli of elasticity values, $E_c$, are based on an estimate using the HSLC modulus equation. When compared with 56-day test values, the estimated values were in agreement. The $E_c$ values listed for the G2C girders are the

56-day test values. Suspected inconsistencies in wet unit weight measurement at the time

of placement produced predicted values from the HSLC modulus equation that were less

than the known 56-day values. The modulus of rupture values, $f_r$, are based on an

average of curebox and ASTM cured specimens tested at 56 days.

Table 8.5 Girder Concrete Properties

| Test # | $f_{ci}'$ 24-hour Curebox (psi) | $f_c'$ Time of Test Curebox & ASTM[79] (psi) | $E_{ci}$ 24-hour Curebox (psi) | $E_c$ Time of Test Estimated (psi) | $f_r$ 56-day Curebox & ASTM[79] (psi) |
|---|---|---|---|---|---|
| G1A-E | | | | | |
| G1A-W | | | | | |
| G1A-C | 7,465 | 9,580 | 3.47E+06 | 3.72E+06 | 1,010 |
| G1B-E | | | | | |
| G1B-W | | | | | |
| G1B-C | | | | | |
| Range | 6,753-8,689 | 8,702-10,640 | 3.39E+06-3.52E+06 | NA | 861-1,101 |
| | | | | | |
| G1C-E | | | | | |
| G1C-W | 6,315 | 8,911 | 3.00E+06 | 3.69E+06 | 796 |
| G1C-C | | | | | |
| Range | 5,444-7,666 | 8,001-9,450 | 2.98E+06-3.03E+06 | NA | 729-908 |
| | | | | | |
| G2A-E | | | | | |
| G2A-W | | | | | |
| G2A-C | 9,640 | 10,975 | 3.55E+06 | 3.88E+06 | 1,204 |
| G2B-E | | | | | |
| G2B-W | | | | | |
| G2B-C | | | | | |
| Range | 8,459-10,307 | 10,499-11,455 | 3.11E+06-3.79E+06 | NA | 1,024-1,352 |
| | | | | | |
| G2C-E | | | | | |
| G2C-W | 8,261 | 10,523 | 3.91E+06 | 4.08E+06 | 905 |
| G2C-C | | | | | |
| Range | 7,737-8,738 | 9,900-11,485 | 3.87E+06-3.96E+06 | NA | 744-1,086 |

## 8.7.2 Deck Concrete Properties

Specimens were cast during deck placement to allow determination of compressive strength and modulus of elasticity. Table 8.6 lists the results of testing with the range of test values listed.

Table 8.6  Deck Concrete Properties

| Test # | $f_c'$ Time of Test ASTM[79] (psi) | $E_c$ Time of Test ASTM[79] (psi) |
|---|---|---|
| G1A-East | | |
| G1A-West | | |
| G1A-Center | | |
| G1B-East | | |
| G1B-West | 5,384 | 3.35E+06 |
| G1B-Center | | |
| G1C-East | | |
| G1C-West | | |
| G1C-Center | | |
| Range | 4,848-5,929 | 3.24E+06-3.45E+06 |
| | | |
| G2A-East | | |
| G2B-East | 5278 | 3.45E+06 |
| G2C-West | | |
| Range | 5,047-5,560 | 3.28E+06-3.55E+06 |
| | | |
| G2A-West | | |
| G2A-Center | | |
| G2B-West | | |
| G2B-Center | 5440 | 3.36E+06 |
| G2C-East | | |
| G2C-Center | | |
| Range | 4,975-6,109 | 3.32E+06-3.42E+06 |

Three batches of concrete were delivered to place the deck. The first batch encompassed all G1 series girders. The second batch encompassed all the G2 series

girder sections except G2A-East, G2B-East, and G2C-West, which were covered by the third and final batch delivered. The concrete compressive strength, $f_c'$, and modulus of elasticity, $E_c$, values were determined by averaging the test results of specimens from each batch of concrete delivered for the deck. Although the girder tests encompassing a particular batch of deck concrete took place over a range of a few weeks, the strengths and moduli values recorded were in a tight range.

### 8.7.3 Prestressing Strand Properties

Manufacturer test results were received at the time of girder construction. Table 8.7 lists pertinent properties of the prestressing strand.

Table 8.7 Prestressing Strand Properties

| 0.6-inch Diameter Grade 270 ksi Low-Relaxation Strand | | |
|---|---|---|
| Property | Value | Units |
| Strand Diameter, $d_b$ | 0.6 | inches |
| Cross Sectional Area, $A_{ps}$ | 0.2183 | inches$^2$ |
| Modulus of Elasticity, $E_{ps}$ | 29,000 | ksi |
| Yield Strain, $\varepsilon_y$ | 0.01 | inch/inch |
| Yield Stress, $f_y$ | 259.6 | ksi |
| Ultimate Strain, $\varepsilon_{su}$ | 0.065 | inch/inch |
| Ultimate Stress, $f_{su}$ | 283.2 | ksi |

### 8.8 Effective Prestressing Stress and Losses

It was necessary to determine the strand effective prestressing stress, $f_{se}$, at the time transfer length was determined and at the time of testing. Two methods were used to determine $f_{se}$ and the results compared. The first method made use of vibrating wire strain gages cast into the girders at midspan at the level of the bottom strands. The second method made use of concrete surface strain (CSS) data. One inherent difference

in these two methods was that the VWSG method read strain internal to the girder and the CSS method read surface strains. A second difference between the two methods was the gage length over which strain was determined. The VWSG had a 6-inch gage length; the CSS measurements were made over a 24-inch distance at midspan. The measurements made over a greater distance should have been more accurate.

Prior to release of prestress, the stress in the strands was known based on load cell readings. Refer to Appendix F for details on the determination of prestressing stress. At release, the known force was transferred to the girders. The elastic shortening of the girder reduced the effective stress in the prestressing strand. At the initial release of prestress, the VWSG and CSS values differed by almost 40 percent. At the time of testing, the measured strains differed by only about 7-9 percent indicating stabilization had occurred across the section.

When the initial prestressing stress was adjusted by the effect of the change in strain in the strand over time, the resulting effective stress values were within about 3 ksi. Force in the strand at a given strain was determined using Figure 8.43. Figure 8.43 was created using a manufacturer provided strand force vs. strand strain test plot.

**Force - Strain Curve for 0.6-inch Diameter 270 ksi LOLAX Strand**

$y = 0.8063x + 56.5921$
$R^2 = 1.0000$

$y = 95.9317x^3 - 348.9161x^2 + 423.6514x - 114.2059$
$R^2 = 0.9985$

$y = 63.7701x + 0.0000$
$R^2 = 1.0000$

Load (Kips)

Strain (Percent)

◆ Elastic ■ Transition ▲ Plastic ━━ Linear (Elastic) ━━ Linear (Plastic) ━━ Poly. (Transition)
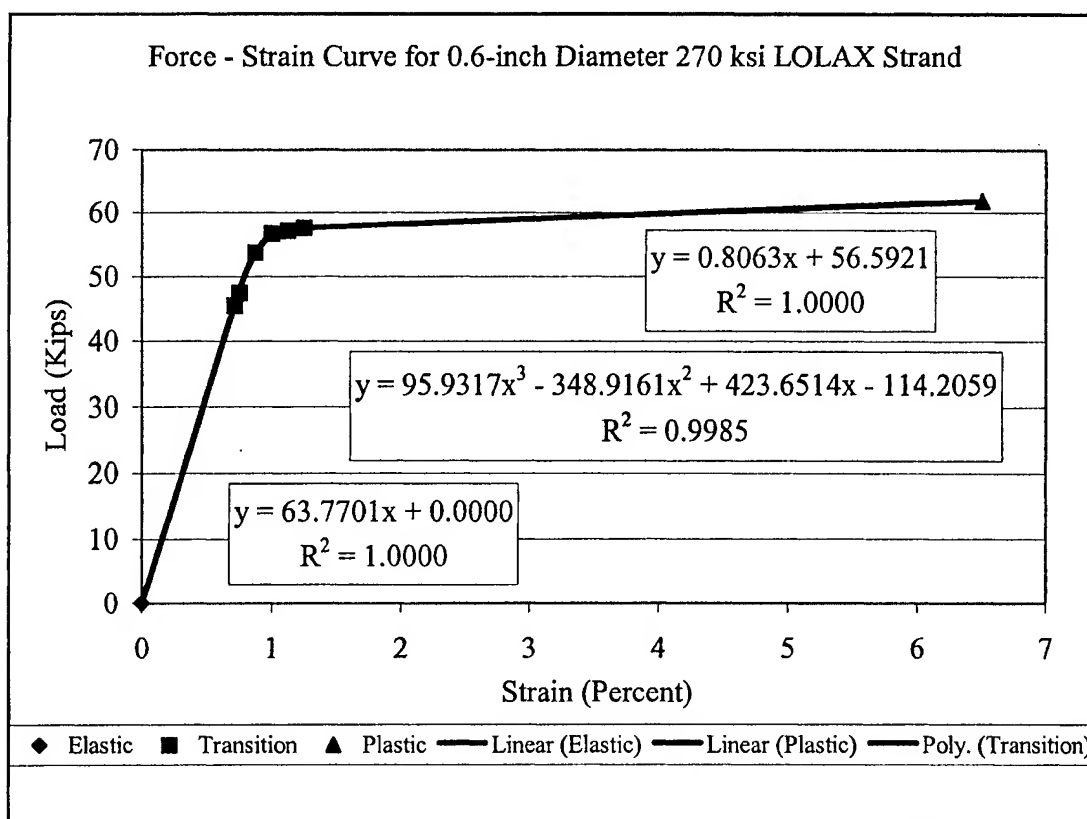
Figure 8.43 Force-Strain Curve for Prestressing Strand

Based on previous research that used VWSGs successfully, it was decided to use the VWSG indicated strain values to determine the effective prestressing stress. Table 8.8 provides details on the effective prestressing stress and losses determined experimentally and estimated using the AASHTO[40] procedure.

Although not a specific focus of this research, it is interesting to note the differences between AASHTO[40] estimated losses and experimentally measured losses. Table 8.9 lists the percent differences between the two values by batch number.

Table 8.8 Effective Prestressing Stress and Losses

| Test # | Effective Prestressing Stress at Time of Test $f_{se}$ (ksi) | Girder Age at Time of Test (days) | Batch # | AASHTO[40] Predicted Losses (ES,R,CR,SH) (ksi) | Experimentally Determined Losses (ES,R,CR,SH) (ksi) |
|---|---|---|---|---|---|
| G1A-East | 153.7 | 111 | 1T1 | 34.6 | 25.4 |
| G1A-West | 152.3 | 106 | 1T1 | 34.6 | 26.8 |
| G1A-Center | 151.5 | 113 | 1T1 | 34.6 | 27.5 |
| G1B-East | 151.2 | 94 | 1T1 | 34.6 | 27.8 |
| G1B-West | 149.7 | 99 | 1T1 | 34.6 | 29.3 |
| G1B-Center | 149.4 | 101 | 1T1 | 34.6 | 29.7 |
| G1C-East | 149.0 | 110 | 1T2 | 35.7 | 30.2 |
| G1C-West | 147.6 | 107 | 1T2 | 35.7 | 31.5 |
| G1C-Center | 147.7 | 112 | 1T2 | 35.7 | 31.4 |
| G2A-East | 175.8 | 122 | 2T1 | 36.1 | 15.5 |
| G2A-West | 175.7 | 119 | 2T1 | 36.1 | 15.6 |
| G2A-Center | 175.0 | 124 | 2T1 | 36.1 | 16.3 |
| G2B-East | 176.2 | 131 | 2T1 | 36.1 | 15.1 |
| G2B-West | 175.6 | 126 | 2T1 | 36.1 | 15.8 |
| G2B-Center | 175.6 | 136 | 2T1 | 36.1 | 15.7 |
| G2C-East | 159.3 | 140 | 2T2 | 33.3 | 19.8 |
| G2C-West | 158.8 | 133 | 2T2 | 33.3 | 20.3 |
| G2C-Center | 157.7 | 142 | 2T2 | 33.3 | 21.5 |

Table 8.9 Comparison of AASHTO[40] Predicted Losses to Experimental Losses

| Batch # | AASHTO Predicted Losses (ksi) | Experimental Losses (Average) (ksi) | Percent Difference By Batch | Percent Difference By Series |
|---|---|---|---|---|
| 1T1 | 34.6 | 27.8 | -19.8% | -17.6% |
| 1T2 | 35.7 | 31.0 | -13.1% | |
| 2T1 | 36.4 | 15.7 | -56.6% | -50.5% |
| 2T2 | 33.3 | 20.5 | -38.3% | |

Batch 1T1 was the G1 series mix made during the "first" G1 series girder

placement session. Batch 1T2 was the G1 series mix made during the "second" G1 series

girder placement. The numbering for batches 2T1 and 2T2 follows the same rule. Although the mix designs were the same for both sessions, exact determination of water content was not possible due to a malfunctioning valve. The batches during both second sessions produced greater losses. The percent difference by series indicates the overall difference for all girders made from a particular mix design. The resulting losses for the G2 series girders differed significantly from the AASHTO[40] estimated values.

Further details on determination of the effective prestressing stress were included in Appendix F.

## 8.9 Girder Section Properties

The AASHTO Type II girders had section properties as listed in Table 8.10.

Table 8.10  AASHTO Type II Girder Section Properties (Non-Composite Girder)

| Property | Non-Composite Value | Units |
|---|---|---|
| Moment of Inertia, $I_{nc}$ | 50,979 | $in^4$ |
| Cross Sectional Area, $A_{nc}$ | 369 | $in^2$ |
| Height, $h_{nc}$ | 36 | in |
| Centroid to Girder Top, $y_{top-nc}$ | 20.17 | in |
| Centroid to Girder Bottom, $y_{bot-nc}$ | 15.83 | in |
| Top of Girder to Top Strands, TCL | 2.5 | in |
| Bot of Girder to Bot Strands, BCL | 3 | in |

The resulting girder dimensions deviated slightly from the designed dimensions. Table 8.11 lists the resulting composite section dimensions and properties for each test.

199

Table 8.11 Composite Section Properties

| Test # | Mod. Ratio $\eta$ | Girder Height $h_c$ (inches) | Moment Of Inertia $I_c$ (inches) | Cross Section Area $A_c$ (inches) | Centroid to Top $y_{top-c}$ (inches) | Centroid to Bottom $y_{bot-c}$ (inches) |
|---|---|---|---|---|---|---|
| G1A-East | 0.900 | 48.00 | 145736 | 581 | 10.62 | 25.38 |
| G1A-West | 0.900 | 47.88 | 142657 | 572 | 10.90 | 25.10 |
| G1A-Center | 0.900 | 48.00 | 143768 | 574 | 10.82 | 25.18 |
| G1B-East | 0.900 | 48.00 | 144954 | 578 | 10.70 | 25.30 |
| G1B-West | 0.900 | 47.50 | 140492 | 570 | 11.04 | 24.96 |
| G1B-Center | 0.900 | 47.50 | 139730 | 567 | 11.12 | 24.88 |
| G1C-East | 0.907 | 47.75 | 143550 | 577 | 10.79 | 25.21 |
| G1C-West | 0.907 | 47.88 | 144285 | 578 | 10.74 | 25.26 |
| G1C-Center | 0.907 | 48.19 | 147106 | 583 | 10.52 | 25.48 |
| G2A-East | 0.890 | 47.75 | 140863 | 568 | 11.06 | 24.94 |
| G2A-West | 0.867 | 47.88 | 141167 | 567 | 11.05 | 24.95 |
| G2A-Center | 0.867 | 47.88 | 140391 | 565 | 11.13 | 24.87 |
| G2B-East | 0.890 | 48.00 | 143464 | 573 | 10.85 | 25.15 |
| G2B-West | 0.867 | 47.75 | 138916 | 561 | 11.25 | 24.75 |
| G2B-Center | 0.867 | 48.19 | 143919 | 572 | 10.84 | 25.16 |
| G2C-East | 0.824 | 48.00 | 137292 | 553 | 11.46 | 25.54 |
| G2C-West | 0.846 | 47.63 | 135266 | 551 | 11.59 | 24.41 |
| G2C-Center | 0.824 | 48.13 | 138744 | 556 | 11.34 | 24.66 |

# CHAPTER IX

# TRANSFER LENGTH TEST RESULTS AND DISCUSSION

## 9.1 Introduction

This chapter discusses transfer length in pretensioned girders. Definitions are provided, the importance and use of transfer length is discussed, current code provisions are presented and explained, and the results of the experimental program are presented. Based on experimentally measured transfer length values from this experimental program and others, current code provisions and equations previously suggested for predicting transfer length are evaluated. New equations for predicting transfer length are suggested based on experimental data.

## 9.2 Definition

Transfer length is the distance required to transfer the effective prestressing force from the strand to the surrounding concrete. Transfer length is developed when the pretensioning strands are released by flame cutting or other method from the restraining abutments. In order for the force transfer to take place, there must be sufficient bond between the pretensioning strand and the concrete. The transfer of force from the strand to the concrete is represented in Figure 9.1.[40]

201
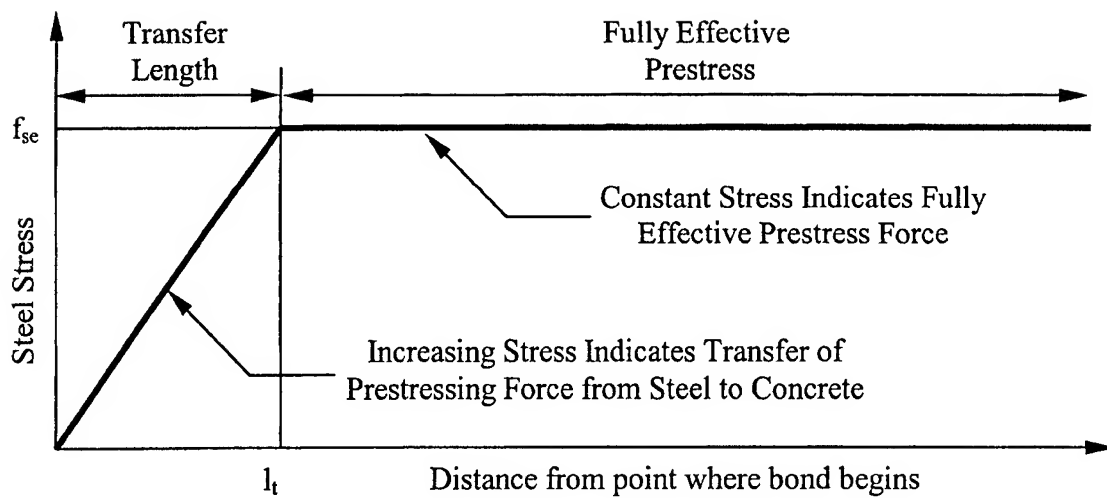
Figure 9.1 Diagram of $f_{se}$ vs Distance From Girder End

The initial sloped portion of the diagram begins at a stress level of zero where bond

begins and is assumed to increase linearly over a distance equal to the transfer length.

The second horizontal portion of the diagram is the region where the strand has fully

transferred the effective prestress. The stress in the strand is assumed to remain constant

in this region.

## 9.3 Importance of Transfer Length

While in most cases, transfer length is not the governing design consideration in a

pretensioned bridge girder, its importance and implications must be understood. Of

greatest importance with regard to transfer length is the design of adequate confinement,

transverse steel to enclose the prestressing strands at the ends of the girder where initial

stress transfer occurs. The 1996 AASHTO[40] Standard Specification for Highway Bridges

Section 9.22.2 identifies the requirement to detail "nominal reinforcement" in the bottom

flange of the beam to enclose the strands over at least a distance "d" from the beam end. Without adequate steel present in the transfer region, cracking can occur around pretensioning strands effectively increasing the transfer length.

The elastic behavior of the beam also is affected by transfer length. As the stress in the strand increases from zero at the free-end of the beam to the level of effective prestress, $f_{se}$, at a distance equal to the transfer length from the girder end, the flexural stress required to cause cracking on the bottom surface of the beam also increases. Close to the end of the beam, the required cracking moment is less than that at a distance greater than the transfer length from the end of the girder. This change in cracking moment is important not only as a flexural design consideration but also for shear design, which is discussed in Chapter 11. Shear design within the transfer region must consider the reduced effective prestressing force.

## 9.4 Current Code Provisions

Current code provisions differ on the way transfer length is determined. Both the AASHTO and ACI techniques are conservative and produce similar results; but the two approach the phenomenon differently. AASHTO[40] Section 9.20.2.4 states the transfer length for prestressing strand shall be taken as 50 diameters (50*$d_b$) for strand and 100 diameters for single wire. Section R12.9 of the ACI 318[2] Commentary specifies that transfer length shall be determined using the equation 2.5.

$$l_t = \frac{f_{se}d_b}{3} \tag{2.5}$$

The value $f_{se}$ is the effective stress in the prestressed reinforcement in ksi after allowance for all losses and $d_b$ is the strand diameter in inches. The derivation of the ACI equation was covered in detail in Section 2.8. The current research program examined only 0.6-inch diameter, seven-wire, 270 ksi, low-relaxation pretensioning strand.

## 9.5 Test Specimens

Six full-scale AASHTO Type II girders were constructed for this research program. The cross section of each girder was identical; each used eight 0.6-inch Grade 270 low-relaxation strands in the bottom flange and two strands in the top flange. Both bottom and top strands were stressed to 75 percent of the strand ultimate strength, $f_{pu}$. The 28-day concrete design strengths, $f_c'$, were 8,000 psi for the G1 series girders and 10,000 psi for the G2 series girders.

Transfer length data were taken on each girder end producing 12 sets of data. The girders were designated as described in Chapter 8 with a girder number (G1A, G1B, G1C, G2A, G2B and G2C) and end (East or West). Girder numbers were based on concrete design strength, girder length and reinforcement layout. Girder ends were designated based on their orientation in the precast plant at time of construction; i.e. west would indicate the beam end pointed in the westerly direction. For example, transfer length data are reported as G1A-West indicating information about the West end of girder G1A.

## 9.6 Measurement of Transfer Length Data

Transfer length data for the bottom prestressing strands were measured using the Concrete Surface Strain (CSS) method. As the prestressing strands transferred stress to the concrete, compressive stress and thus strain was induced in the concrete. Based on compatibility, the strain profile in the concrete should mirror the strain in the prestressing strand. Thus, the concrete strain profile should appear the same as the prestressing strand strain profile shown in Figure 9.1. The point at which the concrete strain reaches a maximum value and stabilizes at a constant strain level is the transfer length.

### 9.6.1 CSS Method

The CSS method of measuring strain in the concrete was accomplished through the use of a detachable mechanical strain gage known as a DEMEC gage. The DEMEC gage measured the distance between two points through the use of two conical points that were inserted into embedments on the surface of the concrete. A DEMEC gage is pictured in Figure 9.2; use of the DEMEC gage is pictured in Figure 9.3.
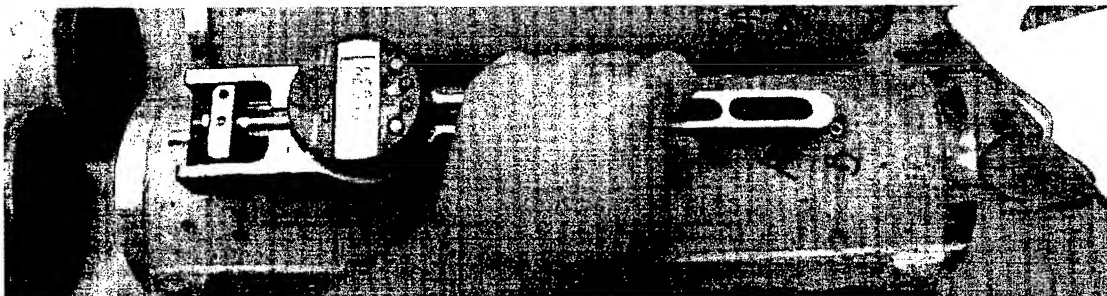


Figure 9.2  DEMEC Gage

Figure 9.3 DEMEC Gage in Use

The DEMEC gage was used to collect CSS data for determination of the transfer length, development length, and level of prestressing in the strands. A thorough description of construction and installation of the DEMEC gage embedments was covered in Chapter 8.

In order to collect transfer length data on the bottom strands, DEMEC gage embedments were installed at the level of the bottom strands over a 48-inch distance from each girder end on each side of the girder. Spacing on the embedments was set at two inches to produce a well-defined strain profile over the transfer length region. The distance between the conical inserts on the DEMEC gage was approximately 8 inches; this distance varied slightly based on small variations in hole placement on the

embedment strips. On average, the 8-inch gage length coupled with the 0.0001-inch accuracy of the gage produced a sensitivity of 12.5 microstrains in the measurements.

### 9.6.2 Measurement of Surface Strains and Other Data

It is important to note that the DEMEC gage did not directly measure concrete strains. The readings from the DEMEC gage were distances between the embedments from which the strains could be calculated. The DEMEC gage readings were referred to as "CSS readings" throughout this report; calculations were necessary to determine the strain. The DEMEC gage measured distance over an 8-inch distance. Within that 8-inch distance were located four 2-inch segments. The reading over the 8-inch gage distance inherently averaged the strains over the four included segments.

CSS measurements were made at specified times in the life of each girder. A CSS data-recording sheet shown in Appendix G, Figure G.1 was created to facilitate organized and consistent collection of the thousands of CSS readings and other data. The following readings were taken on each of the six girders prior to strand release, just after strand release and 1, 2, 3, 7, and 14 days after strand release.

- Transfer length CSS readings

- Girder internal temperature and ambient temperature

- Vibrating Wire Strain Gage reading at level of bottom strands at midspan

- CSS readings at midspan used for prestress loss (not used for transfer length calculations)

- Girder midspan deflection (not used for transfer length calculations)

There were several important rules that were followed when making the CSS and other readings. First, the readings before strand release served as "initial" readings and were the basis for all strain calculations. If the initial readings were in error, all subsequent strain calculations would be flawed. Previous research showed that taking two sets of initial CSS readings and averaging the results provided a good indication of the initial distance between embedments.[37] Since some variation in the readings might occur based on operator inconsistency or environmental conditions, two initial readings helped to remove some of the inherent error. On subsequent readings, inconsistencies on data measurement would tend to average out and produce acceptable results.

Second, except for the "initial" and "just after release" readings, the time at which the CSS readings were taken was just prior to sunrise. Based on experience from previous research, it was found that temperature and solar radiation had a tremendous effect on surface strain.[37] In order to alleviate these effects to the greatest extent possible, CSS readings were made early in the morning before the girders were exposed to direct sunlight. Also based on previous research, transfer length CSS readings were only taken up through 14 days. After 14 days, the transfer length stabilized. Results in this research indicated stabilization of results occurred as soon as 7 days after release.

Third, when taking the CSS readings, it was essential to use the same DEMEC gage to make the readings each time. It was found that slight differences existed between the two gages that could impact the consistency of the readings. Two DEMEC gages were available; they were labeled #1 and #2. Likewise, the beam sides were labeled with #1 and #2, respectively, to insure the DEMEC gages were used on the same side for each

reading. In addition, two people were required to make the CSS readings. One person took readings while the other person recorded data. To the greatest extent possible, the same people were used to take CSS readings each time. Prior to using a DEMEC gage, it was zeroed to 8 inches between the conical points using a length "standard" bar.

VWSG readings at midspan, temperature readings, and other CSS readings at midspan and at other locations on the beam also were taken. The VWSG and CSS readings at midspan at the level of the bottom strands were used to determine the stress in the prestressing strand. Accurate knowledge of prestressing stress was necessary when evaluating existing transfer length equations and suggesting new ones. Differences occurred between strain readings using the VWSG and CSS methods. Just after release, there were significant differences in the strains that resulted between the two methods. As time progressed, the difference became less, but remained between 5 and 10 percent. Appendix F addresses the determination of prestressing force.

### 9.6.3 Reduction of Transfer Length Data

Determination of the transfer length was a several step process. An EXCEL spreadsheet was created such that raw transfer length data could be entered with the outcome being a smoothed strain profile for each girder end. The analysis process was broken into steps as listed below. A complete listing of the various worksheets in the spreadsheet to evaluate Girder G1C is provided in Appendix G and referenced below in STEPS 1-8.

**STEP 1**: Girder data with respect to strand tensioning, temperatures, VWSG readings, midspan deflections and times at which measurements were taken was entered into the "Data" worksheet (Table G.2).

**STEP 2**: Dimensions describing the location of embedment strips were entered into two worksheets titled "Gages-North" (Table G.3) and "Gages-South" (Table G.4). These dimensions allowed the calculation of exact strain measurement locations with respect to the girder ends. The figures indicate the location of each embedment strip on the particular side of the girder. For transfer length calculations, only data from the embedment strips at the bottom of the girder at each end were used.

**STEP 3**: CSS readings for each individual embedment strip were entered on the next series of 12 worksheets. Tables G.5 through G.16 show worksheets for each embedment strip on the girder. The location of the embedment strip is indicated by a shaded rectangle in the box below the header line. For example, a reading of -0156 on this sheet would indicate the distance between the measured embedments was 8"- 0.0156" or 7.9844". The "Initial" readings on this series of worksheets were averaged and used to determine the initial gage lengths on "Gages-North" and "Gages-South."

**STEP 4**: Tables G.17 and G.18 show worksheets "Raw-North" and "Raw-South" which subtracted initial CSS readings from subsequent readings and divided the result by the initial gage length. The resulting values were raw strains for both sides of the girder.

**STEP 5**: In order to smooth the CSS plots, values were averaged using a 3-point floating average as specified in equation 9.1.

$$\varepsilon_x = \frac{\varepsilon_{x-2} + \varepsilon_x + \varepsilon_{x+2}}{3} \qquad (9.1)$$

The values $\varepsilon_{x-2}$ and $\varepsilon_{x+2}$ are the strains at 2 inches before and after the strain at "x" inches from the end of the girder. This floating 3-point average smoothed out the peaks and valleys in the CSS data to produce a strain plot that better facilitated determination of the transfer length. Tables G.19 and G.20 show worksheets "Smooth-North" and "Smooth-South." A comparison of the "smooth" and "raw" data demonstrates the smoothing effect. As with the "raw" data, this operation was performed for data from both sides of the girder.

**STEP 6**: Strains from the left and right sides were averaged and smoothed in Tables G.21 and G.22 respectively.

**STEP 7**: From the "Average Raw" and "Average Smooth" worksheets were plotted the CSS profiles just after release, and 1, 3, 7 and 14 days after release for both ends of the girder. Figure 9.4 shows a typical "raw" CSS plot for the East end of girder G1C. Figure 9.5 shows a typical "smooth" CSS plot for the same girder end. It was very useful to plot both average raw and average smooth data for error checking.
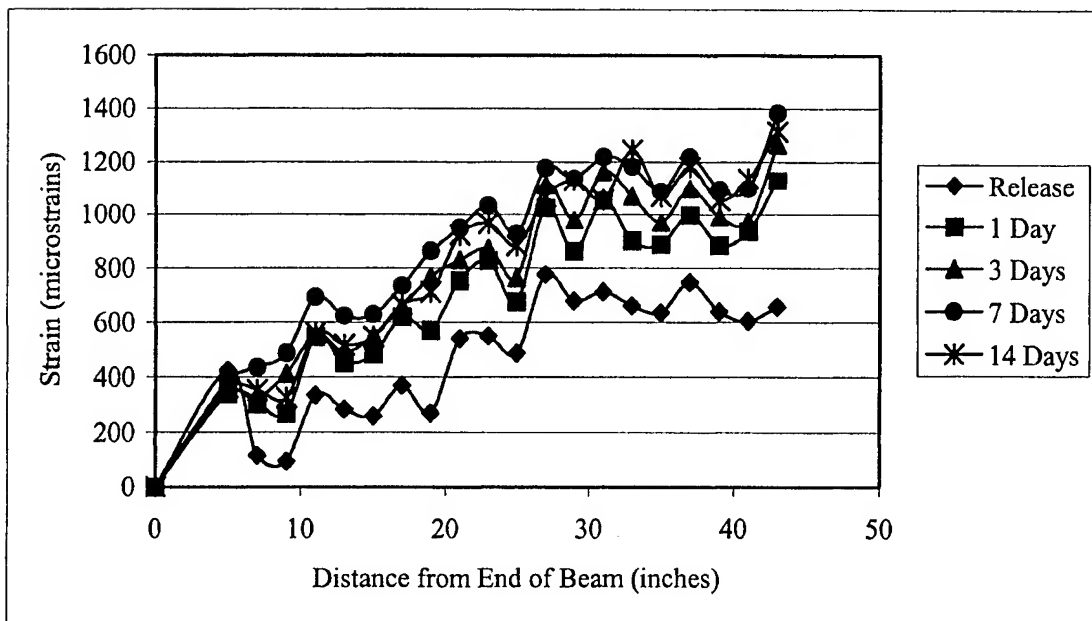
Figure 9.4 Raw CSS Plot for East End of Girder G1C
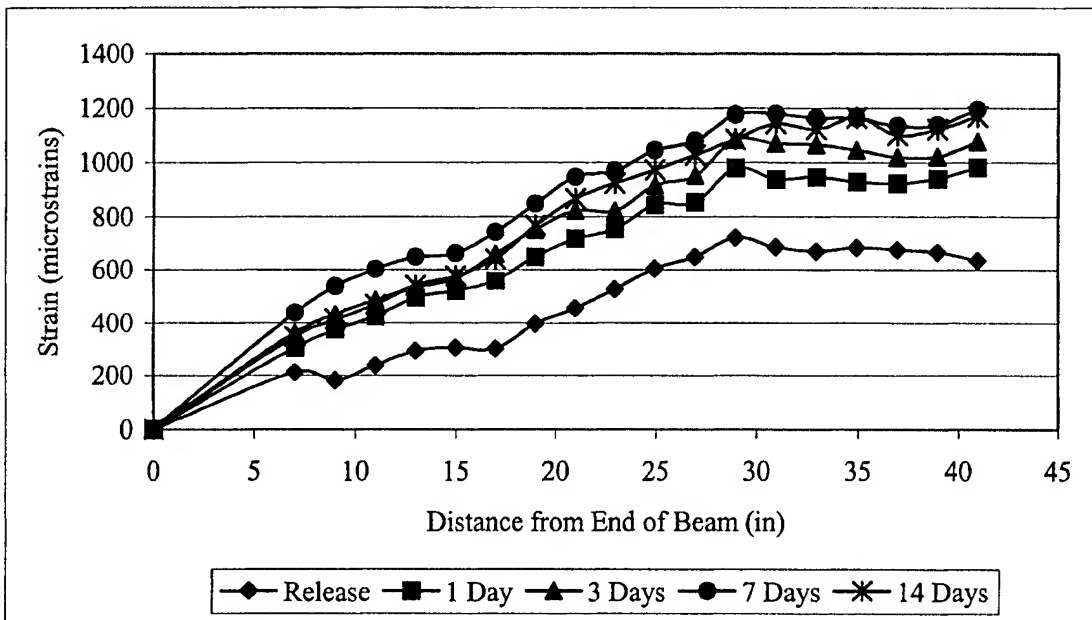


Figure 9.5 Smoothed CSS Plot for East End of Girder G1C

212

**STEP 8**: Examination of CSS profiles for each of the 12 girder ends and experience

from previous research showed that 14-day data provided an excellent prediction of

transfer length.[37] Based on this observation, two final plots were constructed, one for

each end of the girder. Figure 9.4 shows a typical 14-day smooth CSS plot for the East

end of girder G1C. The process for determining transfer length from the CSS plot is

covered in Section 9.6.4.
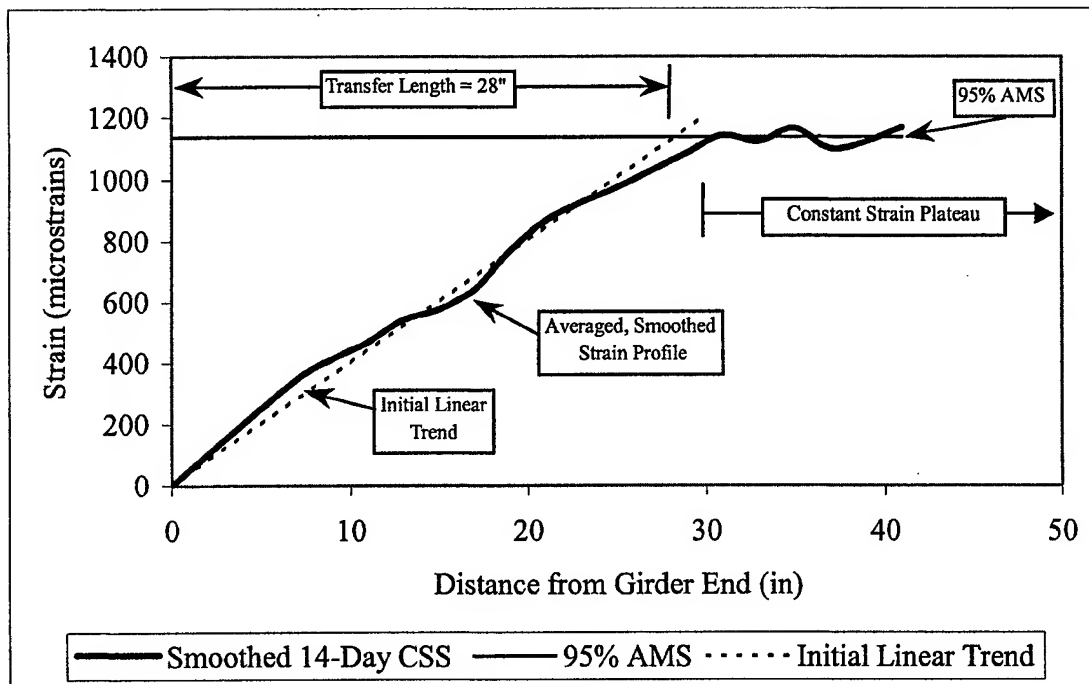


Figure 9.6 Transfer Length Determined Using 95 Percent AMS Method for G1C-East

### 9.6.4 Determination of Transfer Length

Transfer length was determined using the 95% Average Maximum Strain Method (95% AMS). Both Buckner[46] and Russell[44] recommended this method as a conservative and objective technique for determining transfer length.

### 9.6.4.1 95% Average Maximum Strain Line

Recalling Figure 9.1, which provided the idealized profile of stress in the prestressing strand, the second portion of the curve identifying the region of constant strand stress is analogous with the "Constant Strain Plateau." Determination of this region required identifying the point on the 14-day CSS plot where the transition to constant strain occurred. After evaluating the 12 girder-end CSS plots, it was determined that the constant strain plateau began at a point approximately 30 inches from the girder end in each case. The 30-inch distance was chosen for consistency and provided an excellent prediction overall of the strain plateau for all specimens. Referring to Table G.22, there is a column labeled 95%. The values in this column were calculated by taking 95% of the average of the strain values measured at greater than 30 inches from the girder end.

### 9.6.4.2 Initial Linear Trend Line

The "Initial Linear Trend" line shown in Figure 9.6 was determined in a much more subjective manner. Previous researchers took the intersection of the CSS plot with the constant strain plateau as the defined transfer length.[44] In many of the CSS plots in this project, the initial sloped portion of the plot was highly non-linear and undependable

for an accurate prediction of transfer length. It was decided to use a technique where a best-fit line was determined by visual inspection for the initial sloped portion of the CSS plot. After determining the approximate location of the line, the CSS data point marking the x-coordinate of the top end of the line was identified. Using the "trend line" option in EXCEL, the best-fit trend line passing through the origin was plotted. The intersection of the initial linear trend line with the 95% AMS line was identified as the transfer length.

### 9.6.5 CSS Transfer Length Results

Table 9.1 provides transfer length results after 14 days for the 12 girder-ends.

Table 9.1 – CSS Transfer Length Results (inches)

| G1A | | G1B | | G1C | | G2A | | G2B | | G2C | |
|------|------|------|------|------|------|------|------|------|------|------|------|
| East | West | East | West | East | West | East | West | East | West | East | West |
| 19.5 | 18.75 | 25.00 | 18.75 | 28.00 | 21.50 | 17.50 | 13.25 | 13.00 | 13.00 | 19.00 | 18.00 |
| | | FREE | | FREE | | FREE | | | | | |

### 9.6.6 Potential Sources of Error in CSS Transfer Length Results

As presented by Reutlinger[37], past work by Buckner and Deatherage pointed out that potential differences existed between transfer lengths of top and bottom strands. Buckner noted a study at the University of Illinois which reported a 25% decrease in bond strength for strands having 10 inches or more of concrete cast beneath them as compared to strands with only 2 inches of concrete below them. A study conducted by Deatherage on fully pretensioned top strands found that end slip for top strands was 1.5 to 5.2 times that for bottom strands. These results suggest that the transfer length of top

strands may be significantly longer than for bottom strands based on accumulation of excess water and air below the top strands.

Reutlinger[37] performed a parametric study to determine the potential effect of differences between the top and bottom strand transfer length on bottom strand transfer length calculations. Assuming that top-strand transfer lengths were between 1 and 5.5 times the bottom-strand transfer lengths, he determined that 95% AMS transfer lengths for the bottom strands could be unconservative by as much as 37%.

Transfer lengths were not determined for top strands in this research project. However, the concrete used had very little mix water and was dosed heavily with superplasticizers; no excess bleed water was observed at any time. It is very unlikely there was a difference between the top and bottom strand transfer lengths.

## 9.7 Discussion of Results

### 9.7.1 Effect of Girder Orientation

Chapter 8 provided details concerning girder construction. The girders were constructed in pairs: G1A and G1B, G2A and G2B and G1C and G2C. The pairs of girders had a combined length in each case at least 35 feet less than the length of the prestressing bed. This 35-foot difference meant there was 35 feet of free prestressing strand between the end of the second girder and the dead end of the prestressing bed. In Table 9.1, girder ends labeled "FREE" were the ends exposed to the excess strand. In each case, the transfer length was substantially longer than similar ends in the girder pairs. Other researchers also have reported this phenomenon.[44]

## 9.7.2 Effect of Concrete Grade

A single variable statistical analysis produced the results shown in Table 9.2 for the two grades of concrete:

Table 9.2 Statistical Analysis of Transfer Length Data

| Girder Series | $f_c'$ Design Strength (psi) | Average $f_{ci}'$ Actual Strength at 24 Hours (psi) | Average Transfer Length (in) | Standard Deviation (in) |
|---|---|---|---|---|
| G1 | 8,000 | 7,082 | 21.92 | 3.81 |
| G2 | 10,000 | 9,180 | 15.63 | 2.83 |

The average transfer length for the G1 series girders was 6.29 inches longer than that of the G2 series girders indicating a clear relation between concrete strength and transfer length. The standard deviation was also significantly less for the G2 series girders compared to the G1 series potentially indicating more consistent transfer lengths overall for higher strength concrete.

In examining the relation between concrete strength and transfer length, it was recognized that concrete strength affected material properties and the amount of change in prestress from release until all losses had occurred. For the purpose of examining transfer length, this study focused on concrete strength and modulus of elasticity. Indirectly, however, the strength of concrete impacted the resulting initial level and effective level of prestress. Initial elastic shortening was determined by the modulus of elasticity of the concrete at release. Creep shortening over the period of time from release until the transfer length was measured was directly related to the concrete grade; a higher strength of concrete, in general, underwent less creep.

217

## 9.8 Comparison of Results with Code Provisions and Proposed Equations

This section compares the transfer length results from this research with transfer lengths predicted by code specified provisions and techniques proposed by other researchers. The goal of this comparison was to determine which variables provided the best prediction of transfer length. For comparison purposes, 12 transfer length values from this HSLC research were evaluated along with 8 values from a previous normal weight HPC study by Reutlinger[37] to determine what differences if any existed between HSLC and HPC. The transfer length tests in the HPC study were labeled in a manner similar to those in this research project. A transfer length test label of G4A-N indicated "grade 4" concrete, girder reinforcement pattern "A," and the "North" end of the girder. The 8 sets of normal weight HPC data were listed as the last 8 values in the tables. All the transfer length tests used 0.6-in diameter prestressing strand.

### 9.8.1 Material Properties

To evaluate current equations, a material property listing was composed. Table 9.3 shows concrete strengths at times from release through 56 days. The curing method was either accelerated using a curebox for the first 24 hours or by the ASTM[79] procedure

Table 9.3  Concrete Strength Data

| Test # | $l_t$ (in) | $f_{ci}'$ 24-hour Curebox (psi) | $f_{ci}'$ 24-hour ASTM (psi) | $f_c'$ 28-Day Curebox (pse) | $f_c'$ 28-Day ASTM (psi) | $f_c'$ 56-Day Curebox (psi) | $f_c'$ 56-Day ASTM (psi) |
|---|---|---|---|---|---|---|---|
| G1A-E | 19.50 | 7465 | 5735 | 8711 | 8835 | 9084 | 9346 |
| G1A-W | 18.75 | 7465 | 5735 | 8711 | 8835 | 9084 | 9346 |
| G1B-E | 25.00 | 7465 | 5735 | 8711 | 8835 | 9084 | 9346 |
| G1B-W | 18.75 | 7465 | 5735 | 8711 | 8835 | 9084 | 9346 |
| G1C-E | 28.00 | 6315 | 5400 | 7478 | 7595 | 7750 | 8457 |
| G1C-W | 21.50 | 6315 | 5400 | 7478 | 7595 | 7750 | 8457 |
| G2A-E | 17.50 | 9640 | 9294 | 10166 | 10116 | 10418 | 10816 |
| G2A-W | 13.25 | 9640 | 9294 | 10166 | 10116 | 10418 | 10816 |
| G2B-E | 13.00 | 9640 | 9294 | 10166 | 10116 | 10418 | 10816 |
| G2B-W | 13.00 | 9640 | 9294 | 10166 | 10116 | 10418 | 10816 |
| G2C-E | 19.00 | 8261 | 6553 | 9344 | 9807 | 10249 | 10512 |
| G2C-W | 18.00 | 8261 | 6553 | 9344 | 9807 | 10249 | 10512 |
| G2A-S | 15.40 | 14989 | 10078 | 16513 | 17058 | 16770 | 18714 |
| G2A-N | 17.00 | 12379 | 7590 | 12939 | 14139 | 13430 | 15456 |
| G2B-S | 17.90 | 12379 | 7590 | 12939 | 14139 | 13430 | 15456 |
| G2B-N | 17.80 | 11721 | 7186 | 12251 | 13387 | 12716 | 14634 |
| G4A-S | 16.70 | 14675 | 9866 | 16166 | 16700 | 16418 | 18321 |
| G4A-N | 13.80 | 14395 | 9678 | 15858 | 16382 | 16105 | 17972 |
| G4B-S | 13.50 | 14395 | 9678 | 15858 | 16382 | 16105 | 17972 |
| G4B-N | 13.40 | 14610 | 9822 | 16094 | 16626 | 16345 | 18240 |

Table 9.4 lists modulus of elasticity values at release (24 hours) and after 56 days

Methods of curing were the same as for the concrete strength specimens.

219

Table 9.4 Modulus of Elasticity Data

| Test # | $l_t$ (in) | $E_{ci}$ 24-hour Curebox (psi) | $E_c$ 56-Day Curebox (psi) | $E_c$ 56-Day ASTM (psi) |
|---|---|---|---|---|
| G1A-E | 19.50 | 3.47E+06 | 3.86E+06 | 3.83E+06 |
| G1A-W | 18.75 | 3.47E+06 | 3.86E+06 | 3.83E+06 |
| G1B-E | 25.00 | 3.47E+06 | 3.86E+06 | 3.83E+06 |
| G1B-W | 18.75 | 3.47E+06 | 3.86E+06 | 3.83E+06 |
| G1C-E | 28.00 | 3.00E+06 | 3.28E+06 | 3.56E+06 |
| G1C-W | 21.50 | 3.00E+06 | 3.28E+06 | 3.56E+06 |
| G2A-E | 17.50 | 3.55E+06 | 3.93E+06 | 4.06E+06 |
| G2A-W | 13.25 | 3.55E+06 | 3.93E+06 | 4.06E+06 |
| G2B-E | 13.00 | 3.55E+06 | 3.93E+06 | 4.06E+06 |
| G2B-W | 13.00 | 3.55E+06 | 3.93E+06 | 4.06E+06 |
| G2C-E | 19.00 | 3.91E+06 | 4.10E+06 | 4.05E+06 |
| G2C-W | 18.00 | 3.91E+06 | 4.10E+06 | 4.05E+06 |
| G2A-S | 15.40 | 6.16E+06 | 5.58E+06 | 6.12E+06 |
| G2A-N | 17.00 | 5.78E+06 | 5.71E+06 | 5.61E+06 |
| G2B-S | 17.90 | 5.78E+06 | 5.71E+06 | 5.61E+06 |
| G2B-N | 17.80 | 5.78E+06 | 5.71E+06 | 5.61E+06 |
| G4A-S | 16.70 | 6.16E+06 | 5.58E+06 | 6.12E+06 |
| G4A-N | 13.80 | 6.16E+06 | 5.58E+06 | 6.12E+06 |
| G4B-S | 13.50 | 6.16E+06 | 5.58E+06 | 6.12E+06 |
| G4B-N | 13.40 | 6.16E+06 | 5.58E+06 | 6.12E+06 |

### 9.8.2 Prestressing Strand Stresses

Table 9.5 lists average prestressing strand stresses prior to release ($f_{pt}$), just after release ($f_{si}$), and after all losses ($f_{se}$). The strand tensioning stress, $f_{pt}$, was determined using strand load cells as described in Chapter 8. Both a CSS technique and VWSG output were used to determine stress in the strands. When strand stresses were required to predict transfer length, values from both techniques were used and the results

220

compared to measured values. CSS determined prestressing stress values were not

determined on the four normal weight HPC girders.

Table 9.5  Prestressing Levels

| Test # | $l_t$ (in) | $f_{pt}$ (ksi) | $f_{si}$ VWSG (ksi) | $f_{si}$ CSS (ksi) | $f_{se}$ VWSG 14-Days (ksi) | $f_{se}$ CSS 14-Days (ksi) |
|---|---|---|---|---|---|---|
| G1A-E | 19.50 | 179.06 | 161.73 | 167.40 | 154.74 | 152.20 |
| G1A-W | 18.75 | 179.06 | 161.73 | 167.40 | 154.74 | 152.20 |
| G1B-E | 25.00 | 179.06 | 160.90 | 167.94 | 153.34 | 153.04 |
| G1B-W | 18.75 | 179.06 | 160.90 | 167.94 | 153.34 | 153.04 |
| G1C-E | 28.00 | 179.11 | 162.11 | 159.52 | 153.65 | 146.76 |
| G1C-W | 21.50 | 179.11 | 162.11 | 159.52 | 153.65 | 149.76 |
| G2A-E | 17.50 | 191.30 | 178.66 | 181.52 | 176.52 | 171.14 |
| G2A-W | 13.25 | 191.30 | 178.66 | 181.52 | 176.52 | 171.14 |
| G2B-E | 13.00 | 191.30 | 178.94 | 181.28 | 176.52 | 169.92 |
| G2B-W | 13.00 | 191.30 | 178.94 | 181.28 | 176.52 | 169.92 |
| G2C-E | 19.00 | 179.11 | 164.64 | 161.87 | 159.82 | 161.87 |
| G2C-W | 18.00 | 179.11 | 164.64 | 161.87 | 159.82 | 156.14 |
| G2A-S | 15.40 | 190.86 | 178.13 | | 169.75 | |
| G2A-N | 17.00 | 190.86 | 178.13 | | 169.75 | |
| G2B-S | 17.90 | 190.86 | 177.24 | | 168.72 | |
| G2B-N | 17.80 | 190.86 | 177.24 | | 168.72 | |
| G4A-S | 16.70 | 190.86 | 179.31 | | 170.62 | |
| G4A-N | 13.80 | 190.86 | 179.31 | | 170.62 | |
| G4B-S | 13.50 | 190.86 | 179.14 | | 169.90 | |
| G4B-N | 13.40 | 190.86 | 179.14 | | 169.90 | |

## 9.8.3  Code and Suggested Transfer Length Equations

Transfer lengths were predicted using 20 equation variations.  Included were

code-specified equations and equations suggested by researchers.  Table 9.6 provides an

221

overview of the equations examined. The equation number listed refers to the discussion

of the equation in Chapter 2, Background Review.

Table 9.6  Summary of Transfer Length Equations

| Source / Author of Equation | Transfer Length, $l_t$ | Equation Number |
|---|---|---|
| AASHTO[40] | $50d_b$ | 2.6 |
| ACI[2] | $\dfrac{f_{se}d_b}{3}$ | 2.5 |
| Zia and Mostafa[42] | $1.5\dfrac{f_{si}}{f'_{ci}}d_b - 4.6$ | 2.8 |
| Martin and Scott[41] | $80d_b$ | 2.7 |
| Deatherage et al.[43] | $\dfrac{f_{si}d_b}{3}$ | 2.9 |
| Russell[44] | $\dfrac{f_{se}d_b}{2}$ | 2.10 |
| Mitchell et al.[45] | $0.33f_{si}d_b\sqrt{\dfrac{3}{f'_{ci}}}$ | 2.11 |
| Buckner[46] | $\dfrac{1250f_{si}d_b}{E_{ci}}$ | 2.12 |
| Lane (Mean)[47] | $4\dfrac{f_{pt}d_b}{f'_c} - 21$ | 2.13 |
| Lane (95% Confidence)[47] | $4\dfrac{f_{pt}d_b}{f'_c} - 5$ | 2.14 |

$d_b$      Prestressing strand diameter

$l_t$       Transfer length

$f_{pt}$     Stress in prestressing strand prior to release

$f_{si}$     Stress in prestressing strand immediately after release ($f_{pt}$-ES)

$f_{se}$     Stress in prestressing strand after all losses ($f_{pt}$-ES-CR-SH)

ES      Prestress losses due to elastic shortening

CR      Prestress losses due to creep

SH     Prestress losses due to shrinkage

$f'_{ci}$     Concrete compressive strength at release

$f'_c$     Concrete compressive strength at 28 or 56 days

$E_{ci}$     Concrete modulus of elasticity at release

In order to compare the experimentally measured transfer length values with code and suggested equation results, the following relationship was used to determine the average difference between equation and experimental results:

$$\frac{l_{t(Equation)} - l_{t(Experimental)}}{l_{t(Equation)}} \tag{9.2}$$

By performing the difference comparison in this manner, the code or suggested equation served as the accepted value.

### 9.8.4 Results of Comparison

Table 9.7 provides an overview of the results of a comparison of experimentally measured to predicted transfer lengths. The curing method and time of curing specified describe whether an accelerated (curebox) or ASTM curing procedure was used and the age of the specimen. The prestress stress measurement technique describes whether CSS readings or vibrating wire strain gage (VWSG) output was used. The "Max Over" column lists the predicted transfer length value with the largest percentage greater than the experimentally measured value. The "Max Under" column lists the predicted transfer length value with the largest percentage less than the experimentally measured value.

Table 9.7 Overview of Results Sorted by Equation Source

| Equation Source & Designation | Equation Predicting $l_t$ | Curing Method & Age | Prestress Stress Msmt. Technique | Overall Results | | |
|---|---|---|---|---|---|---|
| | | | | Avg Diff (%) | Max Over (%) | Max Under (%) |
| AASHTO | $50d_b$ | NA | NA | 42% | 57% | 7% |
| ACI-a | $\dfrac{f_{se}d_b}{3}$ | NA | VWSG | 46% | 63% | 9% |
| ACI-b | $\dfrac{f_{se}d_b}{3}$ | NA | CSS | 40% | 62% | 5% |
| Buckner - a | $\dfrac{1250\ f_{si}d_b}{E_{ci}}$ | Curebox-24 | VWSG | 41% | 66% | 22% |
| Buckner - b | $\dfrac{1250\ f_{si}d_b}{E_{ci}}$ | Curebox-24 | CSS | 49% | 66% | 30% |
| Deatherage et al. - a | $\dfrac{f_{si}d_b}{3}$ | NA | VWSG | 49% | 64% | 14% |
| Deatherage et al. - b | $\dfrac{f_{si}d_b}{3}$ | NA | CSS | 44% | 64% | 12% |
| Lane - 95 - a | $4\dfrac{f_{pt}d_b}{f'_c}-5$ | Curebox-28 | NA | 50% | 68% | 28% |
| Lane - 95 - b | $4\dfrac{f_{pt}d_b}{f'_c}-5$ | ASTM-28 | NA | 48% | 68% | 26% |
| Lane - a | $4\dfrac{f_{pt}d_b}{f'_c}-21$ | Curebox-28 | NA | -7% | 46% | -129% |
| Lane - b | $4\dfrac{f_{pt}d_b}{f'_c}-21$ | ASTM-28 | NA | -20% | 47% | -163% |
| Martin, Scott | $80d_b$ | NA | NA | 63% | 73% | 42% |
| Mitchell et al. - a | $0.33\ f_{si}d_b\sqrt{\dfrac{3}{f'_{ci}}}$ | Curebox-24 | VWSG | 7% | 34% | -27% |
| Mitchell et al. - b | $0.33\ f_{si}d_b\sqrt{\dfrac{3}{f'_{ci}}}$ | ASTM-24 | VWSG | 19% | 35% | -17% |
| Russell, Burns - a | $\dfrac{f_{se}d_b}{2}$ | NA | VWSG | 64% | 75% | 39% |
| Russell, Burns - b | $\dfrac{f_{se}d_b}{2}$ | NA | CSS | 60% | 74% | 36% |
| Zia, Mostafa - a | $1.5\dfrac{f_{si}}{f'_{ci}}d_b-4.6$ | Curebox-24 | VWSG | -66% | -7% | -161% |
| Zia, Mostafa - b | $1.5\dfrac{f_{si}}{f'_{ci}}d_b-4.6$ | ASTM-24 | VWSG | -10% | 10% | -42% |
| Zia, Mostafa - c | $1.5\dfrac{f_{si}}{f'_{ci}}d_b-4.6$ | Curebox-24 | CSS | -28% | -5% | -60% |
| Zia, Mostafa - d | $1.5\dfrac{f_{si}}{f'_{ci}}d_b-4.6$ | ASTM-24 | CSS | -4% | 14% | -35% |

224

### 9.8.4.1 Results of Analysis Based on Average Difference

Analysis of Table 9.7 showed that Mitchell et al.–a produced the best overall estimate of transfer length. The Mitchell et al.-a equation would be considered a "best-fit" equation where a "best-fit" equation was defined as the equation having the lowest average difference between experimental and predicted values.

The use of initial concrete compressive strengths, $f'_{ci}$, based on curebox data produced better results overall than ASTM strengths. This occurrence was logical. A comparison of heat of hydration curves between girders and curebox specimens showed a close correlation.

The use of prestressing stresses based on CSS data seemed to produce slightly better results than VWSG data. However, the differences were small and results from Buckner's equation showed the opposite trend. Data from Reutlinger's[37] tests were based on VWSG data making it desirable to also base this current analysis on VWSG predicted prestress values. Based on the above, VWSG predicted prestress values were used for future analyses.

Although Mitchell et al.-a and Mitchell et al.-b were the best overall equations, there were cases where transfer lengths were underestimated by as much as 27%. Equations by Buckner, Deatherage, ACI and AASHTO always provided a conservative estimate of transfer length.

### 9.8.4.2 Results of Analysis Based on Maximum Underestimate

Analysis of Table 9.7 based on maximum underestimate showed equation ACI-b to provide a good overall estimate of transfer length without being overconservative.

ACI-b would be the best choice as a "design equation." A "design" equation was defined as the equation having the lowest positive maximum underestimate value without being overly conservative. Determination of the amount an equation was overconservative was based on the maximum overestimate value. The most favorable combination of these two values indicated the best "design" equation.

Table 9.7 also showed the AASHTO equation and the equation by Deatherage provided good conservative estimates without being overconservative. An interesting note concerning these five equations was that they did not include a term describing the properties of the concrete.

### 9.8.4.3 Evaluation of Top Five "Best-Fit" and "Design" Equations

In order to determine a strategy for improving current transfer length equations, Table 9.8 was created to show a listing of the top five equations in both the "best-fit" and "design" categories. From this table, it was possible to summarize which factors appeared to be important when predicting transfer length. It was obvious that strand diameter, $d_b$ was a necessary equation variable. It appeared that $f_{si}$ was a better variable for describing the impact of the level of prestress. The variable that appeared to best describe the concrete was $f'_{ci}$; Since the Mitchell et al. equations ranked highest with respect to "best-fit," $f'_{ci}$ was considered an important variable. However, based on the use of HSLC and the effect reducing concrete unit weight has on modulus of elasticity, the consideration of $E_{ci}$ was not discarded from further analysis.

Table 9.8  Review of Top Five "Best-Fit" and "Design" Equations

| Best-Fit Equations | | | | | | | | |
|---|---|---|---|---|---|---|---|---|
| Rank | Equation Source & Designation | Equation | Curing Method & Age | Equation Variables | | | | |
| | | | | $d_b$ | $f'_{ci}$ | $E_{ci}$ | $f_{si}$ | $f_{se}$ |
| 1 | Mitchell et al. - a | $0.33\, f_{si} d_b \sqrt{\dfrac{3}{f'_{ci}}}$ | Curebox-24 | X | X | | X | |
| 2 | Mitchell et al. - b | $0.33\, f_{si} d_b \sqrt{\dfrac{3}{f'_{ci}}}$ | ASTM-24 | X | X | | X | |
| 3 | ACI-b | $\dfrac{f_{se} d_b}{3}$ | NA | X | | | | X |
| 4 | Buckner - a | $\dfrac{1250\, f_{si} d_b}{E_{ci}}$ | Curebox-24 | X | | X | X | |
| 5 | AASHTO | $50 d_b$ | NA | X | | | | |

| Design Equations | | | | | | | | |
|---|---|---|---|---|---|---|---|---|
| Rank | Equation Source & Designation | Equation | Curing Method & Age | Equation Variables | | | | |
| | | | | $d_b$ | $f'_{ci}$ | $E_{ci}$ | $f_{si}$ | $f_{se}$ |
| 1 | ACI-b | $\dfrac{f_{se} d_b}{3}$ | NA | X | | | | X |
| 2 | AASHTO | $50 d_b$ | NA | X | | | | |
| 3 | ACI-a | $\dfrac{f_{se} d_b}{3}$ | NA | X | | | | X |
| 4 | Deatherage et al. - b | $\dfrac{f_{si} d_b}{3}$ | NA | X | | | X | |
| 5 | Deatherage et al. - a | $\dfrac{f_{si} d_b}{3}$ | NA | X | | | X | |

## 9.9  Development of an Improved Transfer Length Equation

Table 9.8 helped focus efforts in determining an improved transfer length

equation.  Using the base equations specified by AASHTO and ACI and the equations

suggested by Buckner, Deatherage et al., and Mitchell et al., numerous different equation

configurations were developed and evaluated. In evaluating the equation forms, the following values were used:

$f'_{ci}$    Curebox (accelerated) 24-hour concrete compressive strength

$E_{ci}$    Curebox (accelerated) 24-hour modulus of elasticity

$f_{si}$    Initial prestressing force based on vibrating wire strain gage output

$f_{se}$    Effective prestressing force based on vibrating wire strain gage output

For initial equation development, only the 20 sets of transfer length data (12 HSLC and 8 HPC) were used. For later development, more data from several other researchers was considered.

When determining the percent difference, a different method was used. During the evaluation of existing equations, the "accepted" value was taken as the "equation" value. While developing a new equation, the "accepted" value was the "measured" value. The percent difference was calculated using the following relation:

$$\frac{l_{t(Equation)} - l_{t(Experimental)}}{l_{t(Experimental)}} \qquad (9.3)$$

### 9.9.1 Determination of Equation Variables

The first step taken in developing an improved equation was to identify the variable or variables that would best predict transfer length. Plots were created which singled out one variable and compared it to measured transfer length values. Figures 9.7 through 9.10 show plots involving $f'_{ci}$ and $E_{ci}$.
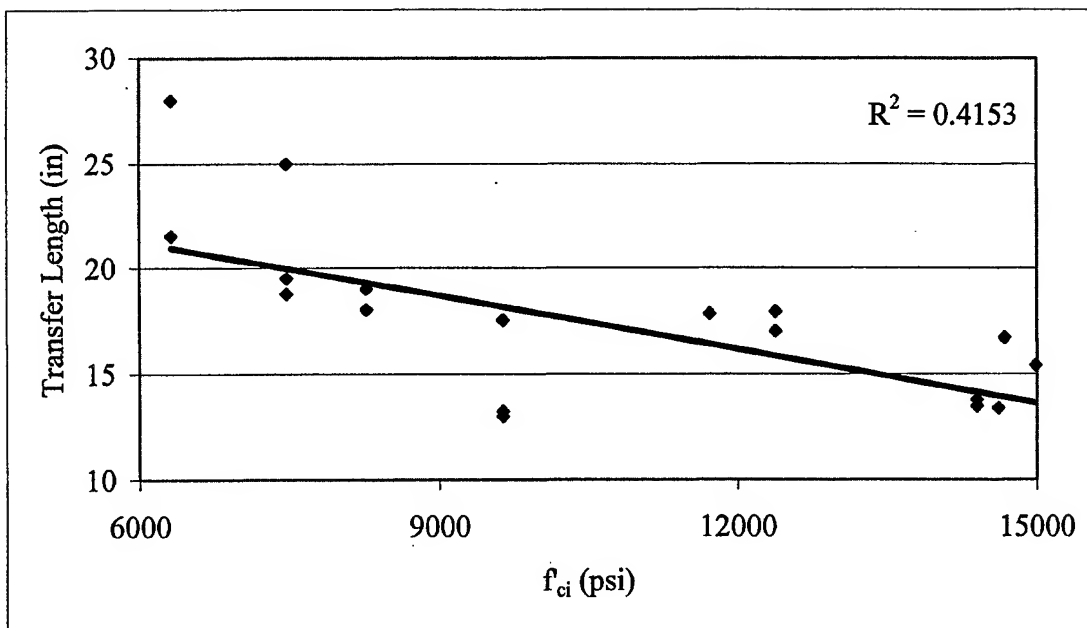
Figure 9.7  Transfer Length vs. f'$_{ci}$
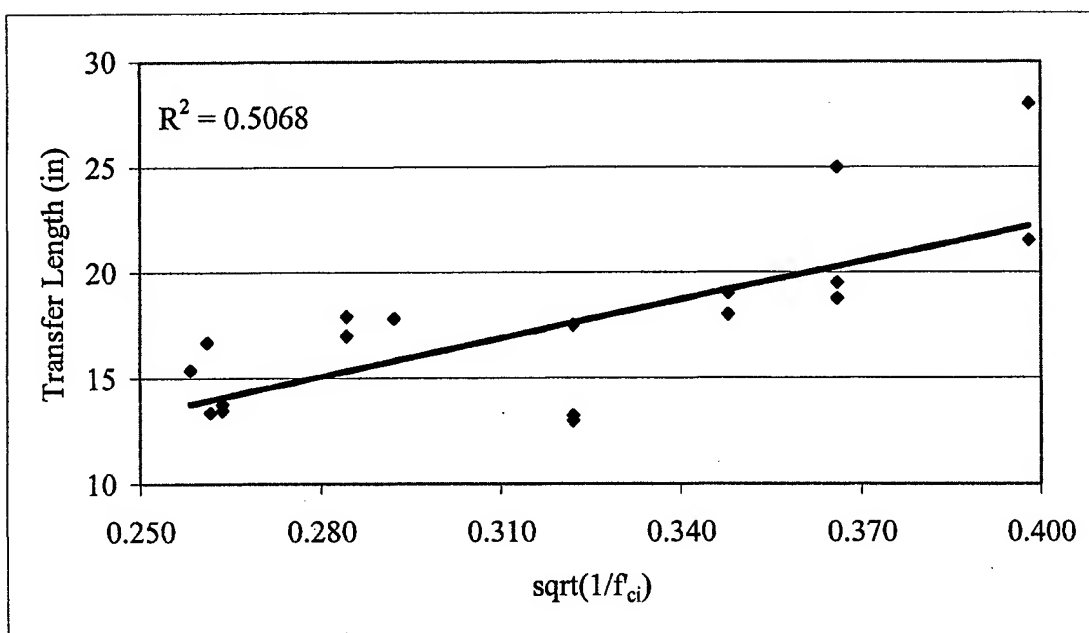


Figure 9.8  Transfer Length vs. $(1/f'_{ci})^{0.5}$

229
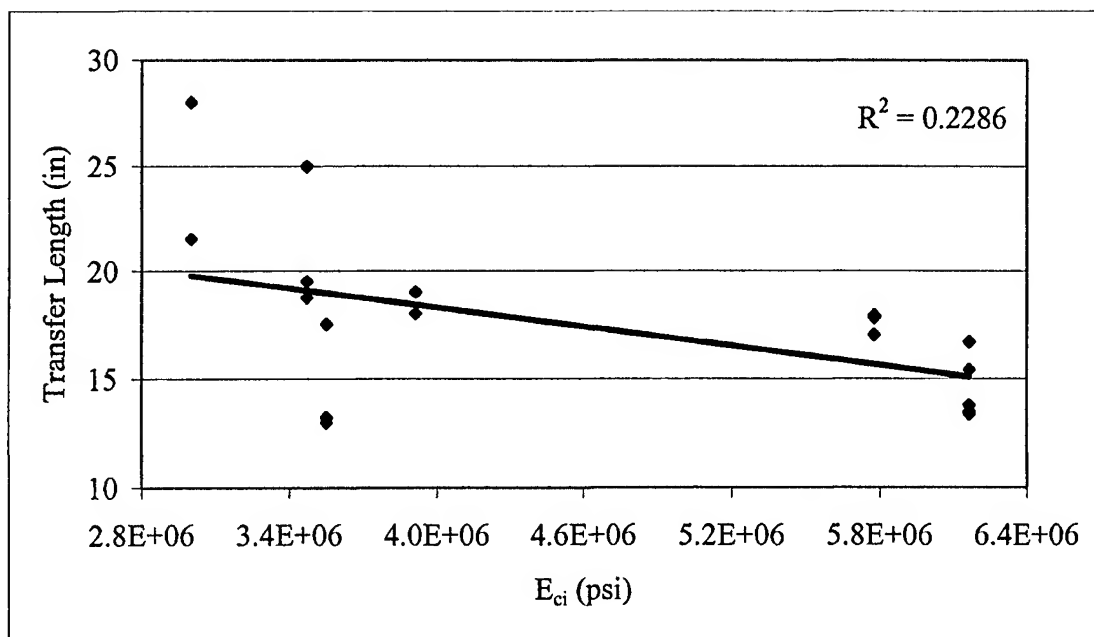
Figure 9.9  Transfer Length vs. $E_{ci}$
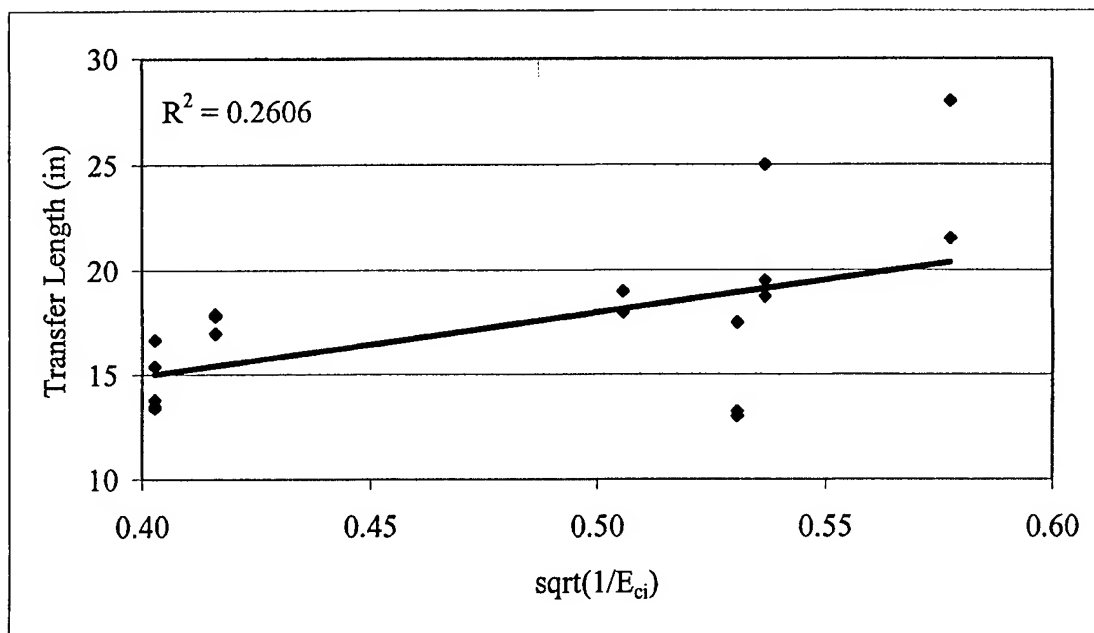


Figure 9.10  Transfer Length vs. $(1/E_{ci})^{0.5}$

In Figures 9.7 through 9.10, the data points are not separated by lightweight or normal weight concrete. Each point describes one of the 20 tests. In a few cases, two data points are at the same location. A trendline and $R^2$ values were plotted in each figure to provide an idea of which variable form might best fit the transfer length data.

The results of Figures 9.7 through 9.10 indicated the variable $f'_{ci}$ was most likely a better predictor of transfer length than $E_{ci}$. The $R^2$ values for comparison of $f'_{ci}$ related variables with transfer length were greater indicating better correlation than those for $E_{ci}$. As a note, the $R^2$ value provided an indication of the degree of fit of a series of data points to a line. In comparisons to $f_c'$, a straight line was the best-fit line. In the comparisons involving $E_{ci}$, other curve forms provided only a very slight improvement in correlation. Overall, the straight line provided a good common basis of comparison.

### 9.9.2 Determination of Equation Forms

Figures 9.7 through 9.10 showed that $f'_{ci}$ was most likely the material-related variable to predict transfer length. Based on the use of HSLC in this research, it was decided to consider both $f'_{ci}$ and $E_{ci}$. Using these variables, existing code specified equations and equations seen in Table 9.8, 27 different equation forms were configured and evaluated using the 12 sets of HSLC transfer length data and the 8 sets of normal weight HPC transfer length data from Reutlinger.[37] The value $f_{ci}'$ was based on 24-hour curebox specimens and prestress levels were based on measurements using VWSG data.

### 9.9.3 Results of Equation Analysis

The results of the equation analysis showed that the same equation form provided both the "best fit" and "design" equation. The definitions for "best fit" and "design" were defined previously in Sections 9.8.4.1 and 9.8.4.2. The only difference between the two equations was a constant value under the radical. Concrete strength values at release, $f_{ci}'$, are in psi; transfer lengths are in inches.

The equation that provided the best fit was:

$$50 \, d_b \sqrt{\frac{3170}{f'_{ci}}} \qquad\qquad (9.4)$$

The best equation for design was:

$$50 \, d_b \sqrt{\frac{5500}{f'_{ci}}} \qquad\qquad (9.5)$$

Equation 9.4 was similar to one suggested by Mitchell for conservatively checking stress in concrete at the time of transfer. Mitchell's equation used 3000 as the constant in lieu of 3170. Mitchell did not recommend using the equation to calculate the transfer length portion of development length.[45]

### 9.9.4 Equation Verification with Transfer Length Data from other Researchers

To verify the applicability equations 9.4 and 9.5, transfer length data from several other researchers were compiled into a database and evaluated. The data were based only on 0.6-in diameter prestressing strand. In most cases, the tests involved I-shaped girders; however, tests by Mitchell[45] and Russell[44] used rectangular cross sections. Table J.1 lists data used in the verification.

Each set of transfer length datum was plotted on a graph with f'$_{ci}$ on the X-axis and transfer length on the Y-axis. Plotting the "best fit" and "design" equations specified in Section 9.9.3 on the overall data plot was successful. However, by slightly increasing the constant values under the radical as seen in equations 9.6 (best fit) and 9.7 (design) below, the predicted plot line better fit the scatter of data points.

$$50\, d_b \sqrt{\frac{4000}{f'_{ci}}} \qquad\qquad (9.6)$$

$$50\, d_b \sqrt{\frac{6000}{f'_{ci}}} \qquad\qquad (9.7)$$

Figures 9.11 and 9.12 show equations 9.6 and 9.7 plotted respectively against the experimental data points listed in Appendix J.

233

It is important to comment that the rectangular shapes tested by Russell[44] were released simultaneously by flame cutting. Specimens by Mitchell[45] were released gradually which was reported to more closely match transfer lengths recorded under similar conditions in I-shaped girders. When finally configuring the equations, the rectangular shapes from Russell's testing were not included.
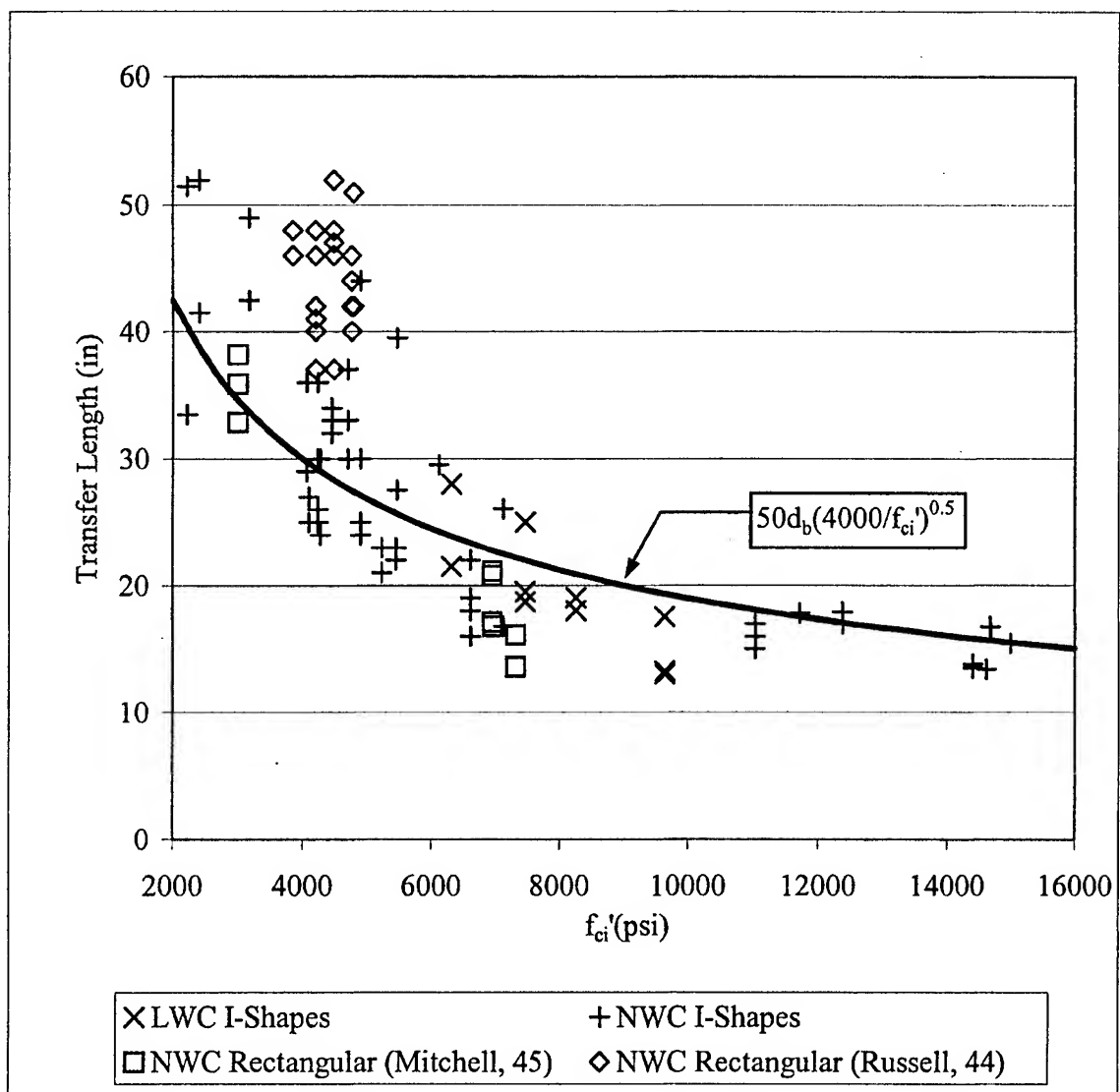


Figure 9.11  Proposed Best Fit Equation Plotted on Transfer Length Data
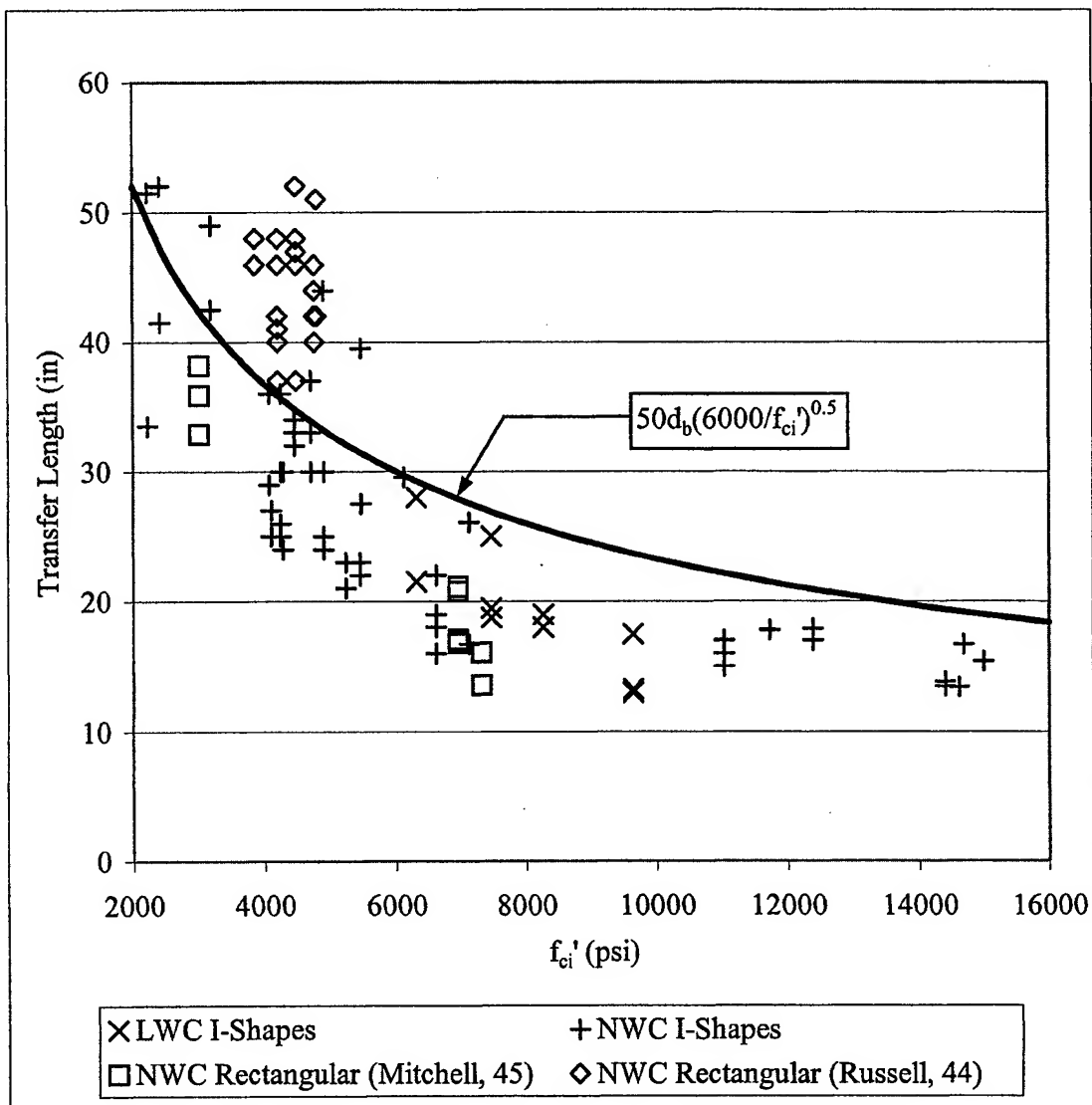
Figure 9.12  Proposed Design Equation Plotted on Transfer Length Data

Evaluation of the proposed equation for both "best fit" and "design" is shown in

Table 9.9 where $f_{ci}'$ is in psi units.  In the "Overall I Shape" category, comparison of both

the "Best Fit" and "Design" equations with the current AASHTO equation showed

favorable results.

Table 9.9  Results of Evaluation of the Proposed Equations

| Basis Of Comparison | AASHTO CODE[40] | Proposed Design Equation | Proposed Best Fit Equation |
|---|---|---|---|
| | $50\,d_b$ | $50\,d_b\sqrt{\dfrac{6000}{f'_{ci}}}$ | $50\,d_b\sqrt{\dfrac{4000}{f'_{ci}}}$ |
| Avg Diff (Overall I Shape) | 33% | 25% | 2% |
| Max Over (Overall I Shape) | 131% | 82% | 49% |
| Max Under (Overall I Shape) | -42% | -25% | -38% |
| | | | |
| Avg Diff (LWC I-Shape) | 69% | 44% | 18% |
| Max Over (LWC I-Shape) | 131% | 82% | 49% |
| Max Under (LWC I-Shape) | 7% | 4% | -15% |
| | | | |
| Avg Diff (NWC I-Shape) | 27% | 22% | 0% |
| Max Over (NWC I-Shape) | 124% | 79% | 46% |
| Max Under (NWC I-Shape) | -42% | -25% | -38% |
| | | | |
| Avg Diff (NWC Rect) | -10% | -1% | -19% |
| Max Over (NWC Rect) | 121% | 100% | 63% |
| Max Under (NWC Rect) | -42% | -34% | -46% |
| | | | |
| Avg Diff (Overall) | 21% | 18% | -3% |
| Max Over (Overall) | 131% | 100% | 63% |
| Max Under (Overall) | -42% | -34% | -46% |

The reason the proposed equations provided a better estimate was found in the strength range below 6,000 psi. Examination of the equations shows that the constant term under the radical determines the point at which the equation begins to increase the predicted transfer length above the AASHTO suggested $50d_b$. In the case of the "best fit" form of the equation, strengths below 4,000 psi underwent an increase in predicted transfer length above $50d_b$. Examination of Figure 9.11 demonstrates this condition. In the case of the "design" form of the equation, strengths below 6,000 psi underwent an

increase in predicted transfer length above 50$d_b$. Examination of Figure 9.12 demonstrates this condition.

In examining the results of 32 different equation forms, it was observed that equation forms based on the AASHTO 50$d_b$ prediction of transfer length in all cases showed better accuracy than the same equation form based on the ACI prediction $f_{se}d_b/3$. For 0.6-inch strand, 50$d_b$ is 30 inches. On average, $f_{se}$ is about 165 ksi meaning $f_{se}/3$ would equal about 55. Heuristically speaking, it makes sense to include a term addressing the level of prestress; however, the results of this evaluation did not indicate it produced the most accurate prediction.

Further examination of Table 9.18 showed insignificant difference between transfer length results for HSLC and normal weight HPC. Figures 9.11 and 9.12 show how transfer lengths for HSLC plotted consistently with the normal weight HPC values. To the author's knowledge, there is no other transfer length data available for 0.6-inch prestressing strand used in lightweight concrete in this strength and unit weight range.

## 9.10 Conclusions

An evaluation of current code provisions using the 12 HSLC transfer lengths in this research and 8 normal weight HPC transfer lengths from Reutlinger[37] showed the current AASHTO[40] and ACI[2] equations to be conservative. The AASHTO equation overestimated transfer lengths by 42% on average and never underestimated transfer lengths. The ACI equation using VWSG data also overestimated transfer lengths by 46% and never underestimated transfer lengths. Use of either the AASHTO or ACI equations to predict transfer length for slate HSLC was conservative. Based on the concrete

237

strength range addressed in this research project, modification of the current code specifications for transfer lengths was not necessary for HSLC.

An evaluation of other suggested equations for predicting transfer length showed an equation by Mitchell et al.[45] to provide the best overall prediction of transfer length. Equations by Buckner[46] and Deatherage et al.[43] also produced good overall predictions. The above equations were applicable to both HSLC and normal weight HPC with good results.

An evaluation of the applicability of initial concrete compressive strength, $f_{ci}$', and initial modulus of elasticity, $E_{ci}$, and 32 possible equation forms showed that $d_b$ and $f_{ci}$' were the best parameters for predicting transfer length. New equations for predicting transfer length based on "Best Fit" and "Design" produced more accurate results than current code equations.

There was no indication throughout this analysis that a need existed to differentiate between slate HSLC and normal weight HPC with regard to transfer length. For initial concrete strengths, $f_{ci}$', over 6,000 psi, the prediction of transfer length was the same for both lightweight and normal weight concrete.

# CHAPTER X

# GIRDER TEST SET-UP AND PROCEDURE

## 10.1 Introduction

This chapter provides a description of the set-up and procedure used to test the composite HSLC girders. Detail is provided on the site layout, data acquisition system, and conduct of the test.

## 10.2 Test Set-up

Figure 10.1 illustrates the overall test set-up. Figure 10.2 shows the test frame with the hydraulic ram attached. Details on pieces of the set-up were included in Figure 10.1.

## 10.3 Instrumentation

The load cell used to monitor the applied load was a Strainsert 700 kip load cell. The model number was (CLC-FB) Q14928. The voltage rating was 2.00-mv/V (Nom.). The load cell was a full-bridge configuration that required an excitation voltage of 10 volts direct current (DC).

The wire potentiometer used to measure deflection at the point of load application was a Rayelco Position Transducer, model P5-A, 10 volts DC excitation. In addition to the wire pot covered in Section 10.2.3, a dial gage was positioned at the point of load

239

application to verify wire pot output. The dial gage readings matched wire pot output during each girder test.
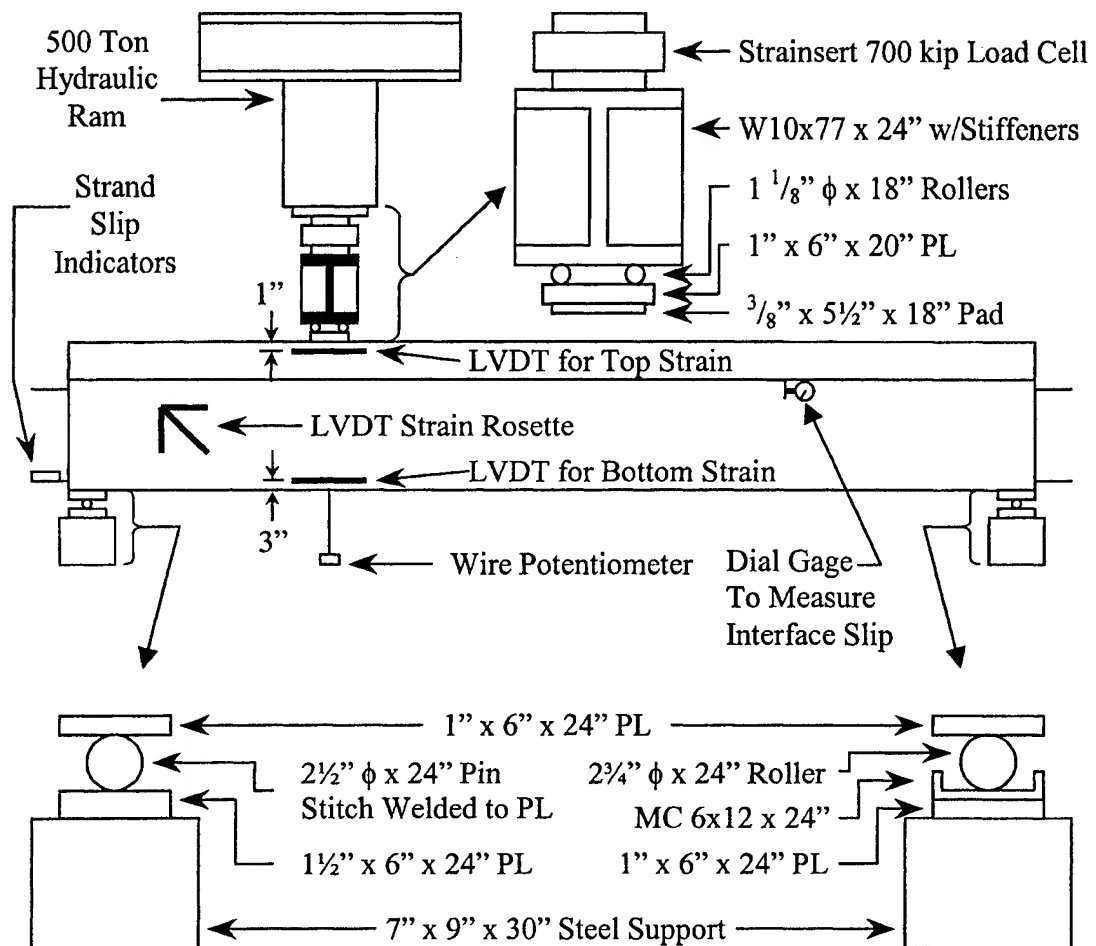


Figure 10.1 Experimental Test Set-up
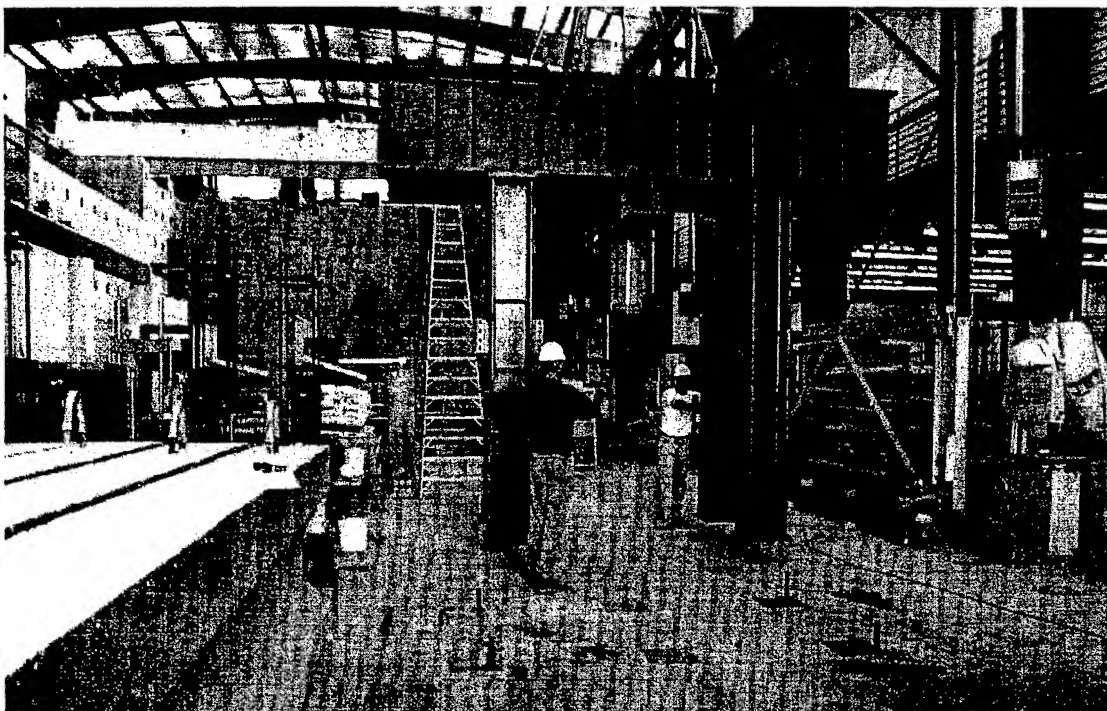
Figure 10.2  Load Frame

The linear variable displacement transducers (LVDT) were manufactured by the Lucas Schaevitz Company. The 3-inch LVDTs were model number HCD 1000. The 6-inch LVDTs were the HCD 2000. The LVDT measuring strain at the top of the girder was a 3-inch LVDT; the gage length was 24 inches. The LVDT measuring strain at the bottom of the girder was a 6-inch LVDT; the gage length was 24 inches. The 0 and 45 degree LVDTs in the rosette were 6-inch LVDTs. The 90 degree LVDT was a 3-inch LVDT. The 0 and 90 degree LVDTs had 10.5-inch gage lengths; the 45 degree LVDT had a 16.25 inch gage length. All LVDTs required a minimum of 12 volts ± up to a maximum of 15 volts ±. This voltage requirement is known as a "bi-polar" voltage. It was required to connect two power supplies in tandem to provide this voltage.

241
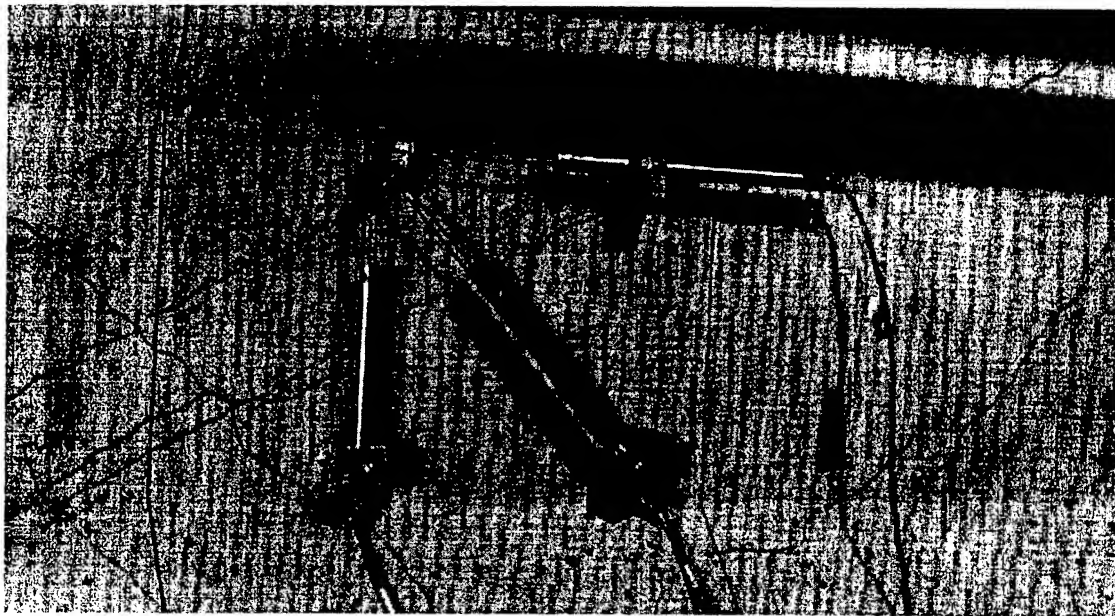
Figure 10.3  LVDTs Configured in Strain Rosette

The devices used to measure strand slip were linear potentiometers having a 2-inch maximum range.  The devices had an excitation voltage requirement of 10 volts DC. The devices were calibrated prior to use to verify factory values.  Figure 10.4 shows the strand slip indicators attached to the exposed strand segments.

To measure slip between the interface of the deck and the girder, a dial gage was installed halfway between the load point and a support.  There was never any indication of slip seen in any of the tests.  The only reading on the dial gage was related to the strain gradient between the gage connection points on the girder and the bottom surface of the deck.  Figure 10.5 shows the dial gage positioned to record interface slip.
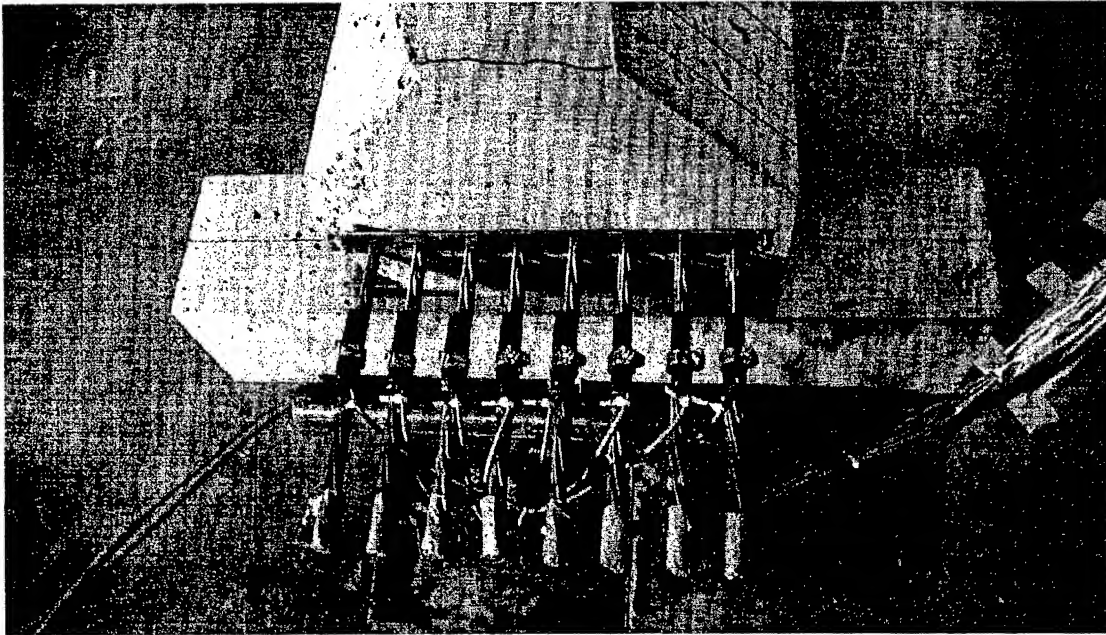
Figure 10.4  Strand Slip Indicators
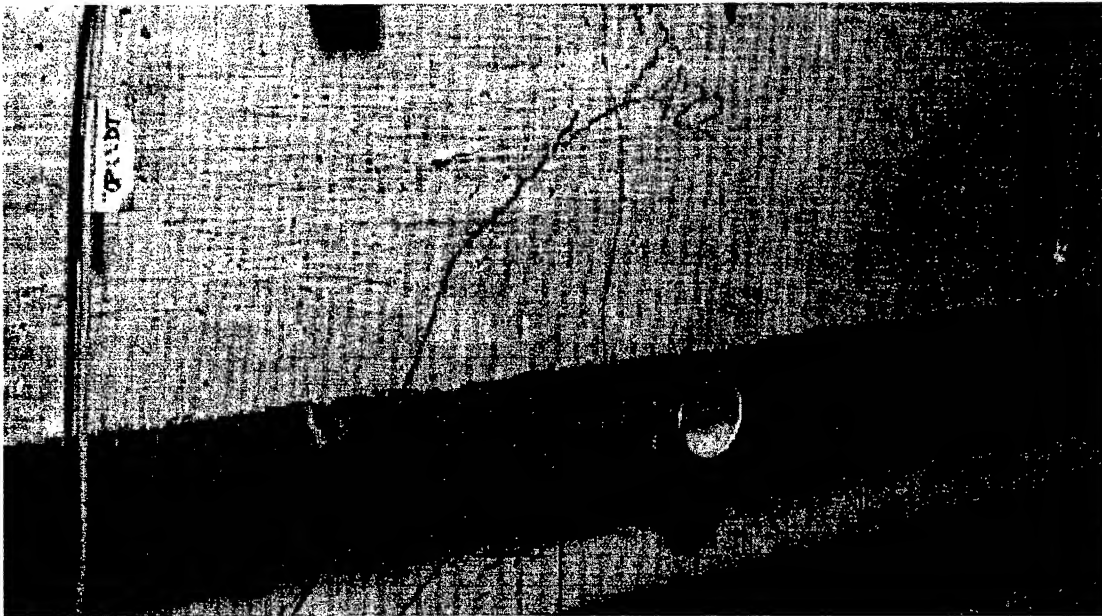


Figure 10.5  Dial Gage to Measure Interface Slip

243

## 10.4 Data Acquisition System

All instrumentation discussed in Section 10.3 was connected to a data acquisition (DAQ) system. A National Instruments DAQ system was used for all tests. Table 10.1 identifies the DAQ system components and uses.

Table 10.1 DAQ System Components and Functions

| DAQ Component | Component Description | Component Function(s) | DAQ Channel Assignments |
|---|---|---|---|
| SCXI-1000 | 4 Slot Chassis | Support DAQ Cards | NA |
| SCXI-1520 | 8 Channel Strain Card | Provided 8 Multi-Use Channels Which Supported all DAQ Requirements | 0 – Load Cell<br>1 – Top LVDT<br>2 – Bottom LVDT<br>3 – Wire Pot<br>4 – 0 Deg LVDT<br>5 – 45 Deg LVDT<br>6 – 90 Deg LVDT |
| SCXI-1127 | Multiplexer Capable of<br>64 ¼-Bridge Outputs<br>32 ½-Bridge Outputs<br>16 Full-Bridge Outputs | Multiplexed Output from 8 Strand Slip Indicators into Channel 7 of the SCXI-1520 | 7,0 – Strand 1 Slip<br>7,1 – Strand 2 Slip<br>7,2 – Strand 3 Slip<br>7,3 – Strand 4 Slip<br>7,4 – Strand 5 Slip<br>7,5 – Strand 6 Slip<br>7,6 – Strand 7 Slip<br>7,7 – Strand 8 Slip |

Figure 10.6 shows a photo of the DAQ system connected to a laptop PC. The power supplies providing the bipolar power for the LVDTs are also pictured. The DAQ system was driven by LABVIEW, the proprietary software of National Instruments. A LABVIEW program was written to support the girder testing.
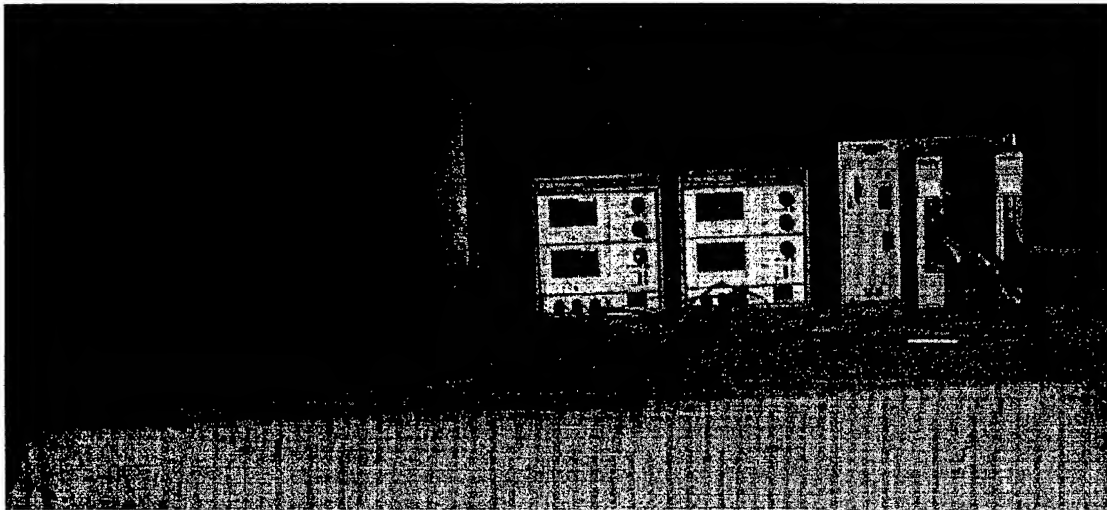
Figure 10.6  Data Acquisition System with Power Supplies and Laptop Computer

## 10.5  Conduct of Girder Test

Several steps were involved with the conduct of a girder test.  A checklist was created as seen in Figure 10.7, which covered all aspects of test set-up and conduct.  The checklist was followed for each test and prevented oversights during tests.  Data recording sheets were also created and used to collect CSS readings, deflection measurements and other miscellaneous readings during the test.

| Testing Checklist for Girder # | Test Configuration # | Date |
|---|---|---|

**TEST PREPARATION PERIOD**

- ☐ Position beam on supports – confirm measurements with testing plan
- ☐ Identify all cylinders for breaking and modulus testing. Record numbers on this sheet
- ☐ Ensure beam is restrained laterally with chain for end tests. Not required for middle test
- ☐ Install all instrumentation to include slip gage between beam and deck
- ☐ Hook-up and test instrumentation
- ☐ Confirm volunteers to assist during test

**ON DAY OF TESTING**

- ☐ Test strength and modulus cylinders and record values on this sheet
- ☐ Install surge protector at wall for electronics power cord, Connect VWSG reader at midspan
- ☐ Set-up camera and check for operability. Check tape. Position lights.
- ☐ Label data sheets, place on clipboard and place on beam with crack marking pen of correct color
- ☐ Check for free travel of linear pots on prestressing strand
- ☐ Zero dial gage under point of load application and at beam / slab interface
- ☐ Check for free travel of wire potentiometer at point of load application
- ☐ Start EXCEL and bring up strength prediction sheet for test – check max predicted loading, $M_{cr}$
- ☐ Start MAX (Never run MAX and LABVIEW concurrently)
  - o Check for operability of all instrumentation and zero all LVDTs close to below values
  - o LVDT Top (-0.2), LVDT Bot (+0.4), LVDT 0 (0), LVDT 45 (+0.2), LVDT 90 (+0.2)
  - o Close MAX
- ☐ Start LABVIEW and open Beam Testing VI dated 9 Oct 01. Check for proper operation then close.
- ☐ Brief assistants and visitors on safety and test procedure
- ☐ Take initial DEMEC and VWSG readings and record on data sheet
- ☐ Start LABVIEW and open Beam Testing VI dated 9 Oct 01
  - o Click on WHITE ARROW to START program
  - o At SET-UP tab do the following
    - ▪ Data acquisition rate = 1 reading every 5 seconds
    - ▪ Set Linear POT upper and lower levels (–0.1" – 0.2")
    - ▪ Set SAVE TO FILE to YES
    - ▪ Set LVDT Lengths (Top,Bot = 24", 0,90 = 12", 45 = 16.97")
  - o At NULL COMPENSATION tab do the following
    - ▪ Null all channels EXCEPT the WIRE POT.
    - ▪ Run null on Linear POTs 5 times.
  - o At SET-UP tab do the following
    - ▪ Click on START button – this will kick over to the display screens
    - ▪ Set deflection limits on Wire POT at first tab of display screens (~2.4", 1")
    - ▪ Set deflection limits on LOAD-DEFLECTION display (~2.4", 1")
    - ▪ Check all screens for initial readings and to ensure lines are plotting correctly
    - ▪ Record all initial values in table below.

| Load Cell | Top LVDT | Bot LVDT | Wire POT | 0 LVDT | 45 LVDT | 90 LVDT | |
|---|---|---|---|---|---|---|---|
| | | | | | | | |
| Strand 0 | Strand 1 | Strand 2 | Strand 3 | Strand 4 | Strand 5 | Strand 6 | Strand 7 |
| | | | | | | | |

  - o Start applying load

- ☐ At conclusion of test, save data to hard-drive, back-up data on floppy disk and record any notes.

Figure 10.7 Girder Testing Checklist

246

## 10.5.1 Loading Sequence

Each girder was loaded monotonically until failure at a load of approximately 400 kips. Loading proceeded in increments of approximately 30 kips or in deflection increments of about 0.25 inches. After each load or deflection increment, CSS readings, deflection readings, crack spacings, and VWSG readings were recorded. Readings were also taken at special occurrences such as first flexural or shear crack observation or initial strand slip.

The decision to terminate loading was based on observed failure characteristics. If crushing in the deck was occurring and total strain in the bottom strands was over 2 percent, the failure was judged a flexural failure and loading was terminated. If shear cracking was extensive and indicative of impending failure, loading was sometimes terminated to prevent further extensive damage. If strand slip over 0.1 inches occurred, the girder was watched closely. Strand slip would allow shear cracks to open and sudden violent shear failures to occur. If the test became a potential safety issue, loading was terminated as well. In a few cases, sudden violent failures occurred.

## 10.5.2 Concrete Surface Strain Readings

Before loading commenced, CSS readings were taken from the DEMEC gage inserts on the girder-end being tested and at midspan. The girder end readings provided an initial value on which to base CSS readings during the test. The midspan readings were useful in verifying the level of effective prestress before load was applied.

After each load increment, CSS readings were taken on the 48-inch strips located on the bottom flange of the girder end being tested. No CSS readings were taken during center span tests because development length was not considered a problem.

### 10.5.3 Marking Cracks

After each load increment, any newly formed cracks were marked. At the end of the marked crack, the load at which the crack occurred was marked as well. Close examination of the girder surface was necessary to note all the cracks formed. Figure 10.8 shows the marking of cracks.

### 10.5.4 Visual and Audio Recording of Test

Each girder test was recorded on video in its entirety and photographed with a digital camera. The video footage allowed review of the test to determine the initiation point of failures. In several instances, violent failures were captured on video. Digital photos allowed easy review of important points of the test.

### 10.5.5 Conclusion of Test

After load was removed, the girder was repositioned for the next test. If all three tests had been conducted on the girder, it was removed from the frame, photographed and placed back in storage.

Figure 10.8  Marking of Cracks During Girder Test

# CHAPTER XI

# FLEXURAL BEHAVIOR RESULTS AND DISCUSSION

## 11.1 Introduction

This chapter discusses flexural behavior in HSLC pretensioned girders. Girder

material and section properties are provided. Based on experimentally measured values

during the 18 girder tests, current code provisions are evaluated.

## 11.2 Experimental Results

Table 11.1 provides an overview of experimental results listing failure types,

ultimate strain values and moments at cracking and ultimate conditions. The failure types

were classified using the definitions below:

**FL** - The girder failed by "BOTH" crushing of the deck and yielding of the strands.

**SH** - The girder failed purely in shear. It did not meet the criteria for a flexural failure.

**SH/FL** - The girder failed predominantly in shear, but still yielded the strands and

crushed the deck. The two failure states occurred almost simultaneously.

**SH-SL** - The girder underwent a shear failure initiated by the strands slipping.

**FL/SH-SL or SH-SL/FL** - The girder underwent both failure modes with one occurring

more predominantly than the other. Both failures would result in yielding of the strands

and crushing of the deck.

Table 11.1 Overview of Experimental Results

| Test # | Failure Type | Crushing Status of Deck | Cracking Moment $M_{cr}$ (ft-kips) | Ultimate Moment $M_{ult}$ (ft-kips) | Max Deck Strain $\varepsilon_{cu}$ (in/in) | Max Strand Strain $\varepsilon_{ps}$ (in/in) |
|---|---|---|---|---|---|---|
| G1A-E | FL/SH-SL | Crushed | 1224 | 1836 | 0.0038 | 0.0158 |
| G1A-W | FL | Crushed | 1109 | 1844 | 0.0042 | 0.0168 |
| G1A-C | SH | Not Crushed | 1064 | 1671 | 0.0029 | 0.0086 |
| G1B-E | SH-SL | Not Crushed | 1133 | 1578 | 0.0033 | 0.0078 |
| G1B-W | FL | Crushed | 1109 | 1840 | 0.0032 | 0.0190 |
| G1B-C | SH/FL | Crushed | 1188 | 1774 | 0.0039 | 0.0107 |
| G1C-E | SH-SL/FL | Crushed | 1155 | 1796 | 0.0032 | 0.0113 |
| G1C-W | FL | Crushed | 1145 | 1828 | 0.0036 | 0.0140 |
| G1C-C | FL | Crushed | 1142 | 1898 | 0.0049 | 0.0146 |
| G2A-E | FL | Crushed | 1220 | 1855 | 0.0036 | 0.0190 |
| G2A-W | FL | Crushed | 1176 | 1855 | 0.0072 | 0.0204 |
| G2A-C | SH | Crushed | 1124 | 1657 | 0.0086 | 0.0084 |
| G2B-E | FL | Crushed | 1110 | 1799 | 0.0082 | 0.0155 |
| G2B-W | FL | Crushed | 1124 | 1840 | 0.0064 | 0.0199 |
| G2B-C | SH/FL | Crushed | 1210 | 1869 | 0.0035 | 0.0122 |
| G2C-E | FL | Crushed | 1079 | 1870 | 0.0045 | 0.0228 |
| G2C-W | FL | Crushed | 1094 | 1793 | 0.0049 | 0.0198 |
| G2C-C | FL | Crushed | 1219 | 1885 | 0.0089 | 0.0215 |

| G1 Avg | | | 1141 | 1785 | 0.0037 | 0.0132 |
| G2 Avg | | | 1151 | 1824 | 0.0062 | 0.0177 |

Although there are five failure types listed in Table 11.1, the failures fell into two major categories; flexural failures and shear failures. Sections 11.2.1 and 11.2.2 provide photos of the failures, typical moment-curvature diagrams, and typical load-displacement diagrams for the two main failure categories.

### 11.2.1 Flexural Failures

Figure 11.1 shows a photo of girder test G1-B West, a typical flexural failure. The vertical lines indicate the location of shear reinforcement. Flexural failures were ductile in nature. A typical flexural failure showed flexural cracks extending from the bottom of the girder up into the deck and evenly spaced shear cracks less than 0.02 inches in width between the support and point of load application.

Spalling of concrete from the top surface was evidence of crushing in the deck. Figure 11.2 provides a picture of deck crushing from test G1B-West. In Figure 11.2, the loading hardware was removed and the crushed concrete chipped from the deck to show the extent of crushing.

Some flexural failures resulted in longitudinal cracking in the deck as shown in Figure 11.3. Since there was only temperature and shrinkage steel running longitudinally in the deck, the occurrence of this cracking was understandable.
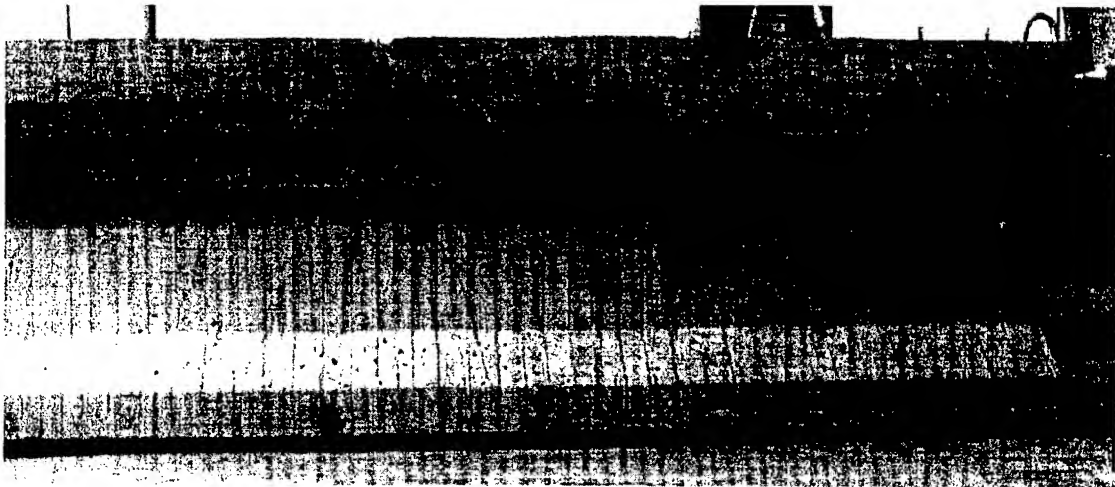


Figure 11.1 Typical Flexural Failure Shown in Girder Test G1B-West

252
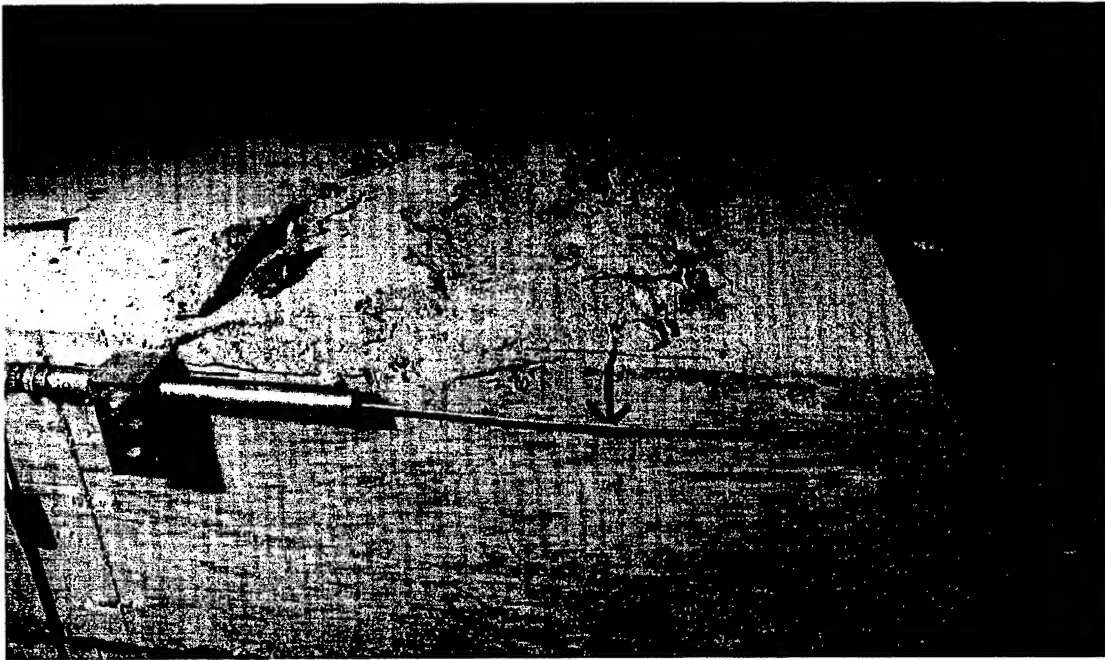
Figure 11.2  Details of Deck Crushing in Girder Test G1B-West
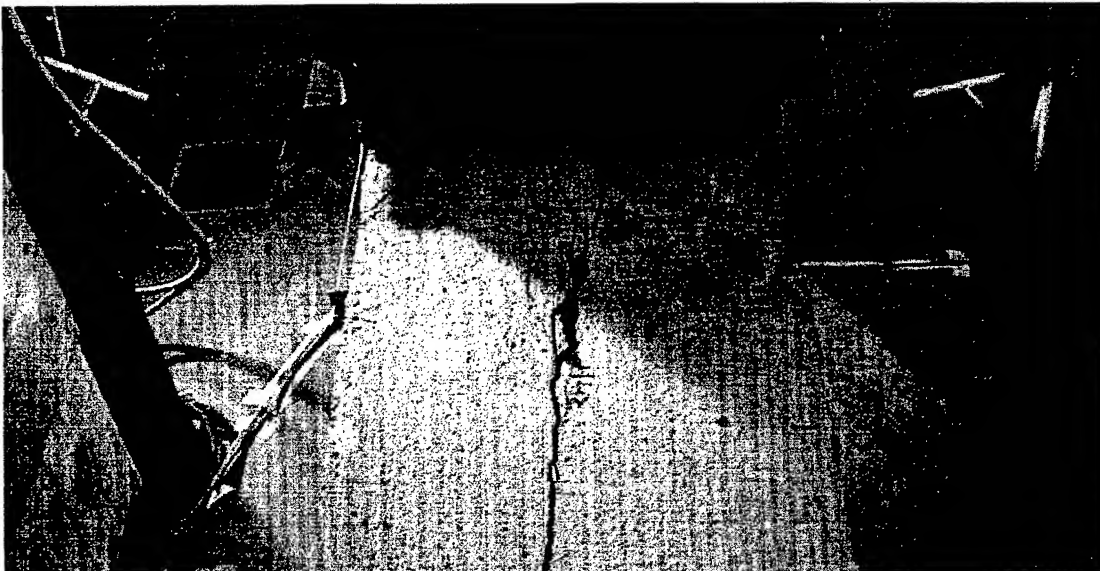


Figure 11.3  Example of Longitudinal Deck Cracking in Girder Test G1A-East

Figure 11.4 provides a typical moment-curvature plot from a flexural failure. This moment-curvature plot from girder test G1B-West shows the theoretical and experimental behavior. The theoretical behavior is slightly offset from the experimental behavior because the girder was assumed to have zero curvature at the initiation of testing. The theoretical curvature value accounted for initial negative curvature due to prestressing where the experimental value did not. Both the theoretical and experimental plots begin at a moment value greater than zero reflecting the initial dead load moment being carried by the girder. The theoretical curve was determined with values at zero applied load, decompression of concrete at the level of the bottom strands, flexural cracking, yielding of the strand, and deck surface strains of 0.001, 0.002 and 0.003. The Construction of the theoretical moment-curvature curve is described in Appendix L.
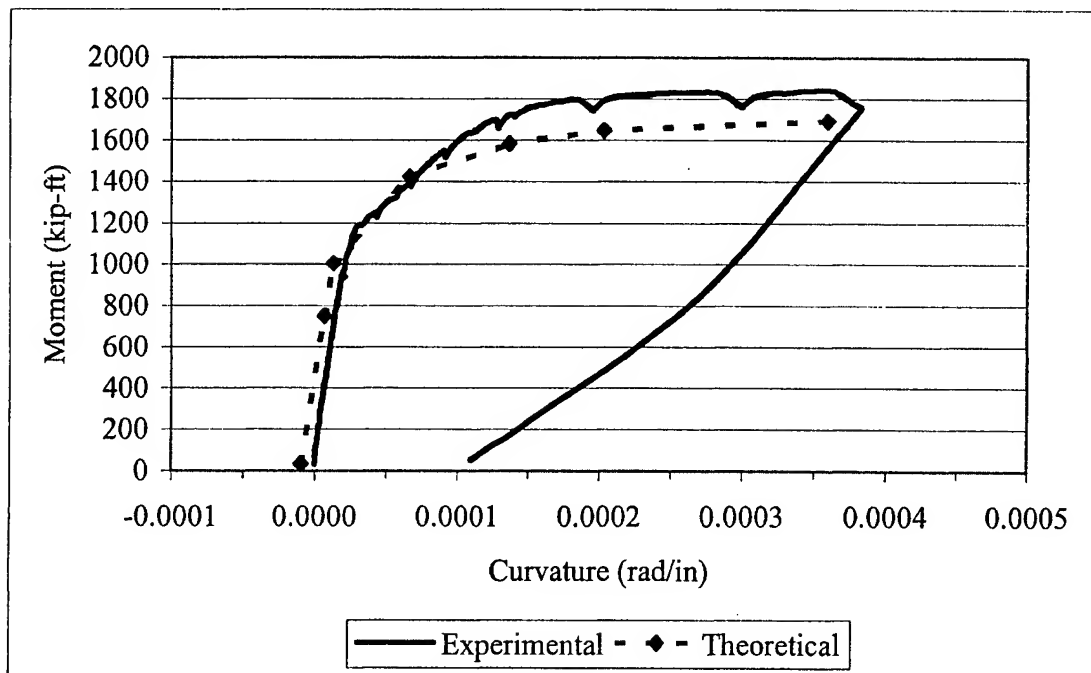


Figure 11.4 Moment-Curvature Plot from Girder Test G1B-West

254

Figure 11.5 shows the load-displacement curve from girder test G1B-W, a typical flexural failure. The two points used to describe the predicted curve were based on deflection at cracking and ultimate. A description of the calculation of predicted deflection values is also included in Appendix L.
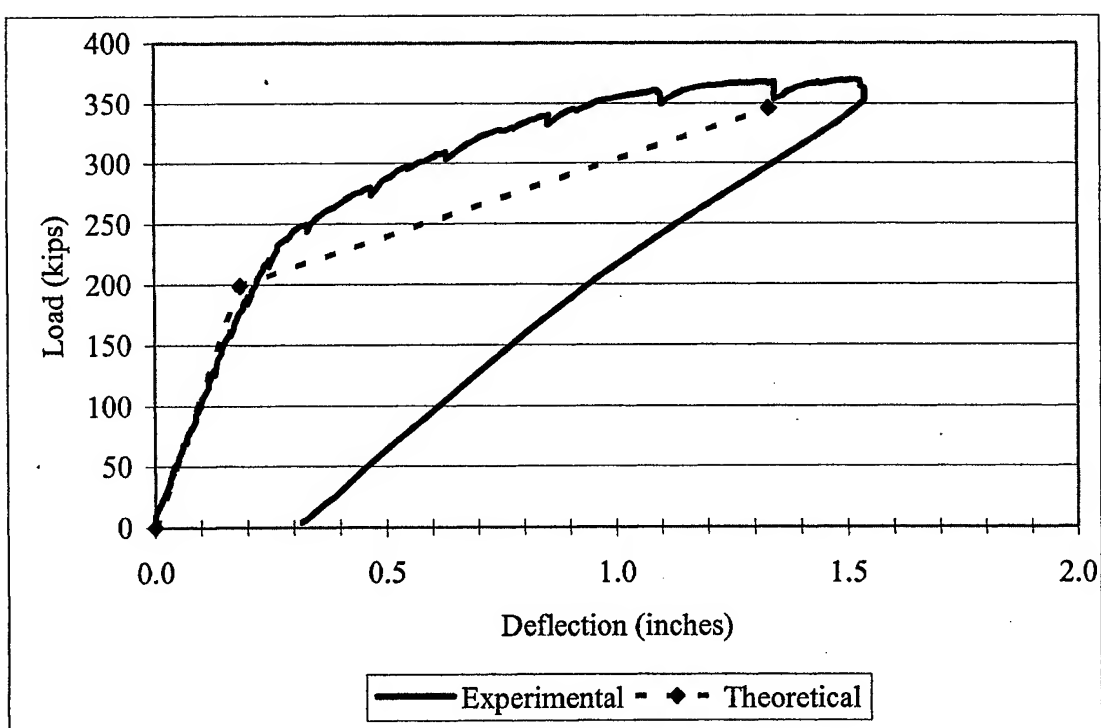


Figure 11.5  Load-Deflection Plot from Girder Test G1B-West

The load-displacement curves for flexural failures normally returned to within a small deflection from zero reflecting any strand yielding or deck crushing that may have occurred.

Figures 11.6 and 11.7 show a dramatic flexural failure where a large section of the deck and top flange separated from the girder. Note the exposed prestressing strand.

255

Figure 11.6  Flexural Failure During Girder Test G2B-East.



Figure 11.7  Close-up of Girder-Deck Interface in Girder Test G2B-East Flexural Failure

### 11.2.2 Shear Failures

Within the category of shear failures were included girder tests that failed purely in shear and those that underwent a shear failure initiated by strand slip. In general, the resulting moment-curvature and load-displacement curves were similar. For explanation purposes, the categories were handled separately. A much more in-depth explanation of shear failures is provided in Chapter 12, Shear Behavior Results and Discussion; this section is provided for better understanding of Table 11.1.

### 11.2.2.1 Pure Shear Failures
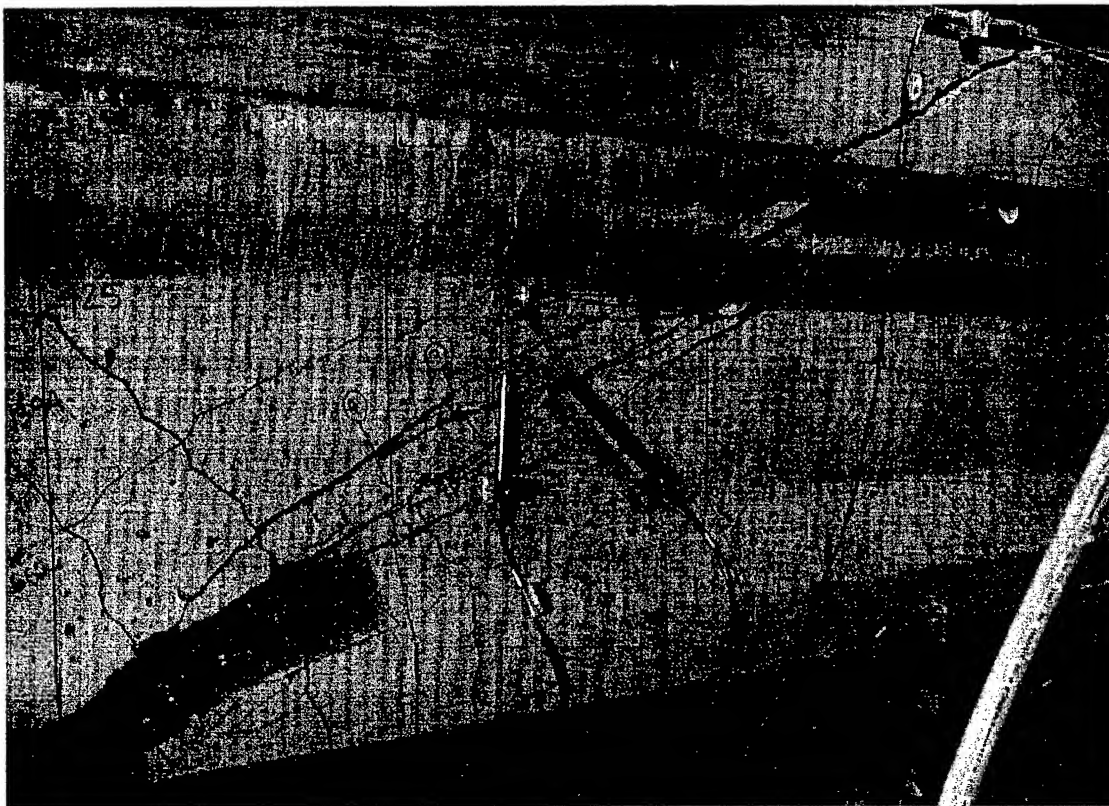


Figure 11.8 Girder Test G2A-Center Showing Pure Shear Failure

257

Girder test G2A-Center seen in Figure 11.6 involved a center span where the

shear reinforcement was spaced at 24 inches. The objective of this test was to examine

the shear strength of concrete. The shear crack running from bottom to top occurred very

suddenly and violently and was indicative of a pure shear failure. Girders undergoing

shear failures precipitated by strand slip showed different failure modes. Figure 11.9

shows a typical moment-curvature diagram for a pure shear failure.
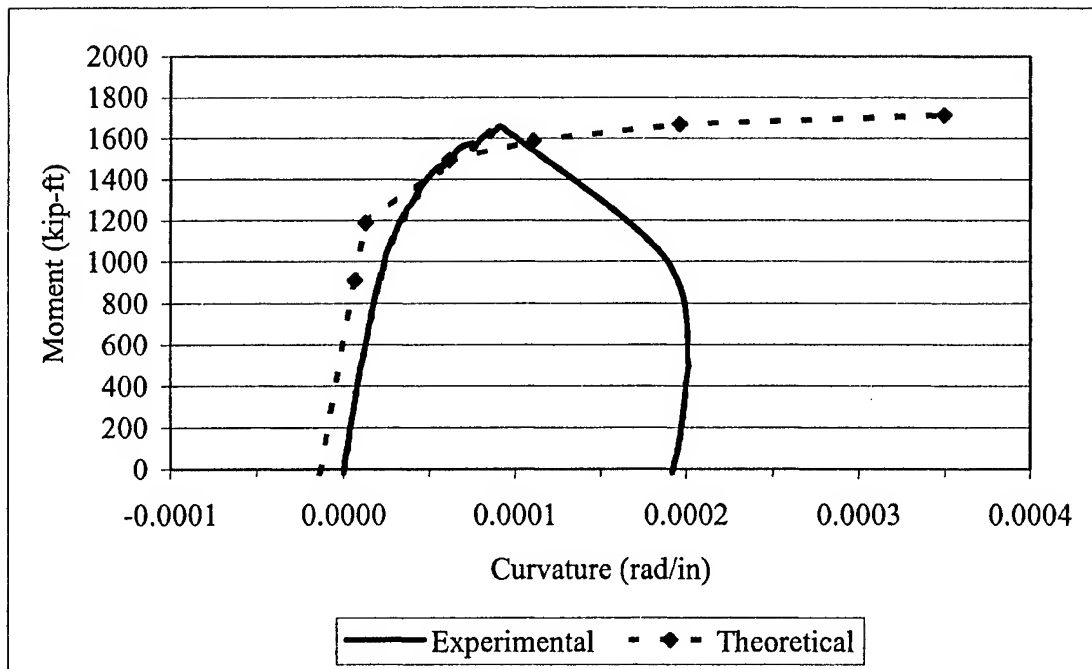


Figure 11.9  Moment-Curvature Plot for Girder Test G2A-Center, a Pure Shear Failure

The sudden shear failure is indicated in Figure 11.9 by the sudden drop on the

moment-curvature diagram. Figure 11.10 shows the load-deflection plot for girder test

G2A-Center. The same sudden drop in load and increase in deflection is seen.
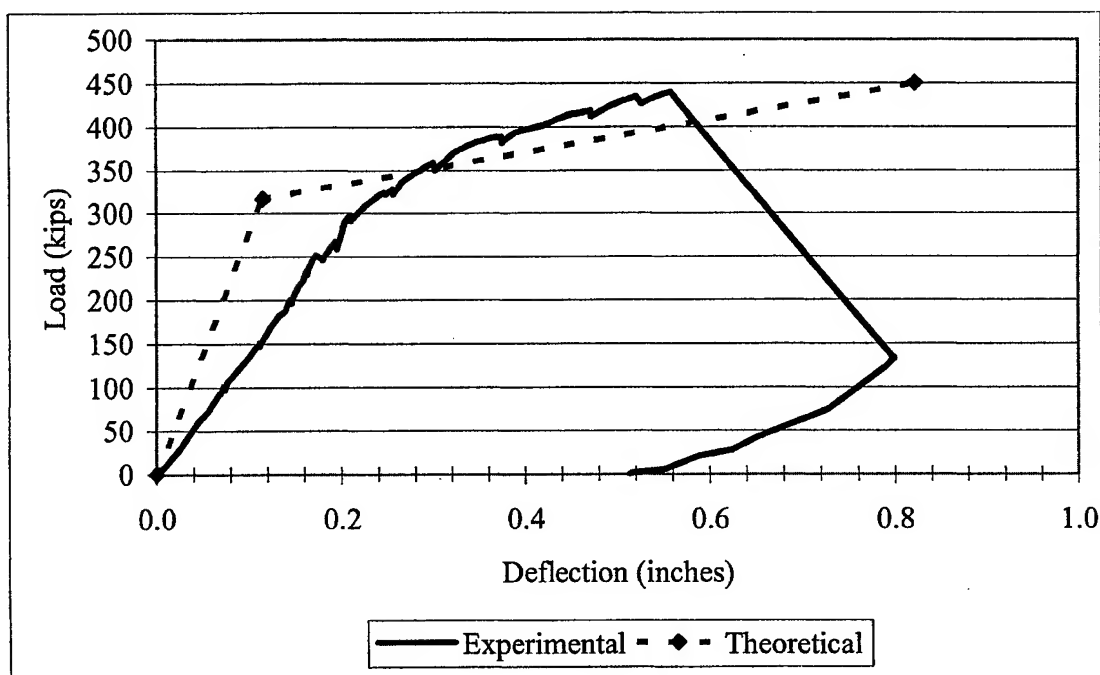
Figure 11.10  Load-Deflection Plot for Girder Test G2A-Center

## 11.2.2.2  Shear Failures Initiated by Strand Slip

Girders that underwent excessive strand slip experienced shear failures as well.
However, the mode of failure appeared somewhat different.  Figure 11.11 shows a photo
of girder test G1C-East, a test where excessive strand slip resulted in a predominantly
shear-based failure.  Although the deck crushed and the strand yielded, the failure was
dominated by shear.  The shear cracking did not extend from bottom to top as in Figure
11.6, but ended prior to entering the deck.  Figure 11.12 shows a photo of shear cracking
at the bottom of the girder vicinity the support.  The shear cracks were approximately 0.2
inches wide at the widest.  Figures 11.13 and 11.14 show moment-curvature and load-
deflection curves for girder test G1C-East.

259
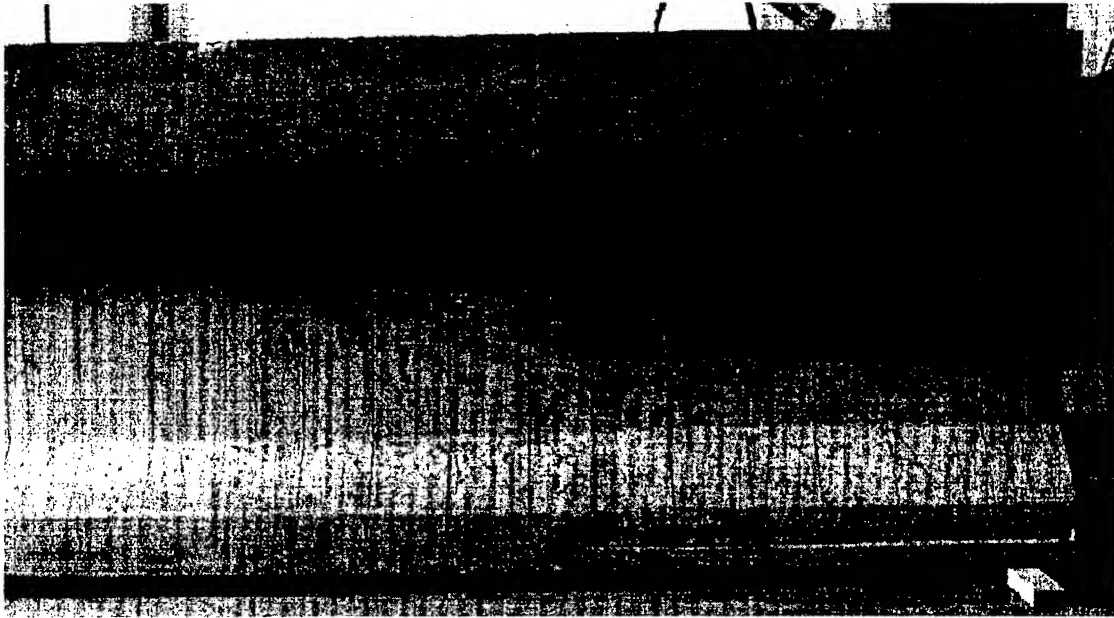
Figure 11.11  Girder Test G1C-East After Strand Slip Induced Shear Failure



Figure 11.12  Girder Test G1C-E Showing 0.2-inch Wide Shear Cracks
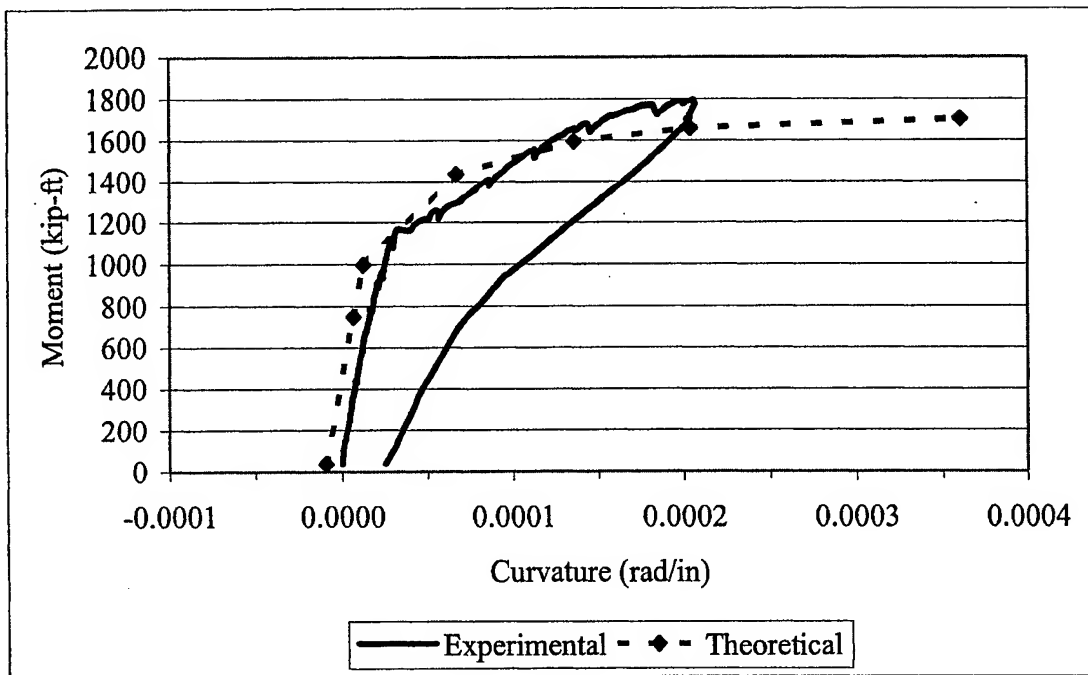
Figure 11.13  Moment-Curvature Plot for Girder Test G1C-East
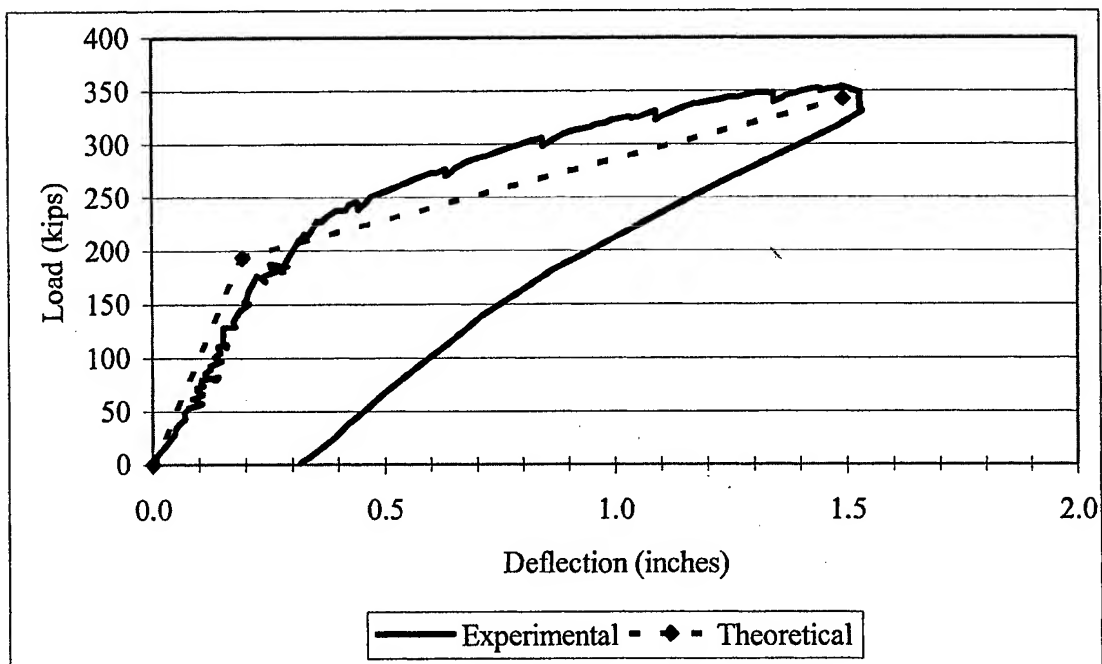


Figure 11.14  Load-Deflection Plot for Girder Test G1C-East

261

Examination of Figures 11.13 and 11.14 show the different behavior of this type

of shear failure compared to the pure shear failure. The shear failure precipitated by

strand slip was a gradual shear failure and not the sudden violent failure seen in pure

shear failures. Figure 11.13 indicates the girder was unable to reach its predicted

curvature value due to strand slip. Figure 11.14 shows that ultimate deflection was close

to predicted, however, it was more the result of shear deformation due to strand slip than

flexural deformation due to strand yielding as predicted. The girder's response to

unloading showed that it experienced some permanent deformation due to strand slip,

strand yielding and deck crushing. Its behavior on unloading more resembled a flexural

failure and did not resemble a pure shear failure.

### 11.2.3 Comments on Experimental Results

Specific discussion of experimental results was addressed at the cracking and

ultimate conditions in Sections 11.3 and 11.4 respectively. Appendix L provides a

complete listing of all moment-curvature and load-deflection diagrams for each test.

Photos of girder all end-span tests can be seen in Appendix Q. Photos of all center-span

tests can be seen in Appendix M. A spreadsheet encompassing the calculations to

evaluate the girders' flexural performance can be seen in Appendix K. All percent

difference calculations in the following sections are based on equation 11.1 below.

$$Percent\ Difference = \left( \frac{Value_{Exp} - Value_{Pred}}{Value_{Pred}} \right) 100 \qquad (11.1)$$

## 11.3 Results at Cracking

Table 11.2 provides an overview of the predicted and experimental cracking

moment for each girder test. Percent difference was calculated using equation 11.1.

Table 11.2 Cracking Moment Results

| Test # | Predicted $M_{cr}$ (ft-kips) | Experimental $M_{cr}$ (ft-kips) | Percent Difference |
|---|---|---|---|
| G1A-East | 1052 | 1224 | 16.4% |
| G1A-West | 1005 | 1109 | 10.4% |
| G1A-Center | 1065 | 1064 | -0.2% |
| G1B-East | 1019 | 1133 | 11.2% |
| G1B-West | 1004 | 1109 | 10.4% |
| G1B-Center | 1029 | 1188 | 15.5% |
| G1C-East | 999 | 1155 | 15.6% |
| G1C-West | 971 | 1145 | 17.9% |
| G1C-Center | 1035 | 1142 | 10.4% |
| G2A-East | 1165 | 1220 | 4.7% |
| G2A-West | 1136 | 1176 | 3.5% |
| G2A-Center | 1189 | 1124 | -5.5% |
| G2B-East | 1177 | 1110 | -5.6% |
| G2B-West | 1133 | 1124 | -0.9% |
| G2B-Center | 1200 | 1210 | 0.8% |
| G2C-East | 1059 | 1079 | 1.9% |
| G2C-West | 1025 | 1094 | 6.8% |
| G2C-Center | 1082 | 1219 | 12.6% |

| | | | |
|---|---|---|---|
| G1 Average | 1020 | 1141 | 12.0% |
| G2 Average | 1130 | 1151 | 2.0% |
| G1 Std Dev | | | 5.4% |
| G2 Std Dev | | | 5.8% |

The experimental cracking moment was determined by examining the

experimental load vs. deflection plot identifying the point at which a slope change

occurred. In every case, the cracking load indicated on the load vs. deflection plot matched the load recorded where visible flexural cracking first occurred.

Based on the use of equation 11.2, the predicted cracking moment for the G2 series girders was 10.8 percent greater than for G1 girders.

$$f_{cr-Pred} = 7.5\lambda\sqrt{f_c'} \qquad (11.2)$$

Since G2 girders had a higher concrete compressive strength than G1 girders, this was logical. Experimentally, the G1 and G2 series average cracking moments were about identical. It is important to note that the predicted cracking moments appeared to become less conservative as compressive strength increased.

Table 11.3 provides an overview of the predicted cracking stress, $f_{cr-Pred}$, based on equation 11.2, the rupture stress, $f_r$, recorded during testing of beam specimens per ASTM C-78[82] at an age of 56 days, and the experimental cracking stress, $f_{cr-Exp}$.

The trend seen in Table 11.3 is the same seen in 11.2 for the cracking moment, except more dramatic. The experimental cracking stress, $f_{cr-Exp}$, was calculated using equation 11.3 below.

$$f_{cr-Exp} = \frac{M_{cr} - M_{DL}}{S_{bot-c}} + \frac{M_{DL}}{S_{bot-nc}} - \frac{F_{se}}{A_{nc}} + \frac{F_{se}e}{S_{bot-nc}} \qquad (11.3)$$

Table 11.3  Cracking Stress Results

| Test # | Predicted $f_{cr-Pred}$ (psi) | ASTM C-78 $f_r$ (psi) | Experimental $f_{cr-Exp}$ (psi) | Percent Difference Exp. Vs. Pred. | Percent Difference Exp. vs. ASTM | Normalized Cracking Stress Factor, $\xi_{cr}$ |
|---|---|---|---|---|---|---|
| G1A-East | 624 | 1010 | 985 | 57.8% | -2.5% | 11.83 |
| G1A-West | 624 | 1010 | 844 | 35.3% | -16.4% | 10.14 |
| G1A-Center | 624 | 1010 | 621 | -0.5% | -38.6% | 7.46 |
| G1B-East | 624 | 1010 | 863 | 38.3% | -14.6% | 10.37 |
| G1B-West | 624 | 1010 | 846 | 35.6% | -16.2% | 10.17 |
| G1B-Center | 624 | 1010 | 964 | 54.5% | -4.5% | 11.59 |
| G1C-East | 602 | 796 | 930 | 54.5% | 16.8% | 11.58 |
| G1C-West | 602 | 796 | 968 | 60.8% | 21.6% | 12.06 |
| G1C-Center | 602 | 796 | 825 | 37.1% | 3.6% | 10.28 |
| G2A-East | 668 | 1204 | 785 | 17.5% | -34.8% | 8.81 |
| G2A-West | 668 | 1204 | 752 | 12.6% | -37.6% | 8.44 |
| G2A-Center | 668 | 1204 | 999 | 49.6% | -17.0% | 11.22 |
| G2B-East | 668 | 1204 | 528 | -20.9% | -56.1% | 5.93 |
| G2B-West | 668 | 1204 | 647 | -3.1% | -46.3% | 7.27 |
| G2B-Center | 668 | 1204 | 687 | 2.9% | -42.9% | 7.72 |
| G2C-East | 654 | 905 | 697 | 6.6% | -22.9% | 8.00 |
| G2C-West | 654 | 905 | 804 | 22.9% | -11.2% | 9.22 |
| G2C-Center | 654 | 905 | 946 | 44.6% | 4.5% | 10.84 |

| | Predicted | ASTM C-78 | Experimental | Exp. Vs. Pred. | Exp. vs. ASTM | Factor, $\xi_{cr}$ |
|---|---|---|---|---|---|---|
| G1 Average | 617 | 939 | 872 | 41.5% | -5.6% | 10.61 |
| G2 Average | 663 | 1104 | 761 | 14.7% | -29.4% | 8.61 |
| G1 Std Dev | | | | | | 1.42 |
| G2 Std Dev | | | | | | 1.67 |

Since all the girders were of approximately the same dimension, the only factors that affected the cracking stress were the experimental cracking moment and the effective prestressing force, $F_{se}$.  In the G2 series girders, the modulus of elasticity was higher at release in comparison to the G1 series girders meaning less initial losses (ES).  In addition, the denser matrix of the G2 mix design allowed less time dependent losses (CR and SH).  Both factors meant a higher effective prestressing force at time of testing.  A

265

higher prestressing force meant more of the cracking moment was required to overcome the effect of prestress thus the cracking stress was less. On average, the experimental cracking stress values for the G1 and G2 series tests were greater than the predicted values. The trend indicates that predicted cracking strengths become less conservative as the compressive strength increases.

The normalized rupture stress factor, $\xi_{cr}$, was calculated as below where $\lambda$ was the lightweight concrete factor equal to 0.85 for SLWC:

$$\xi_{cr} = \frac{f_{cr-Exp}}{\lambda\sqrt{f_c'}} \tag{11.4}$$

As long as the factor $\xi_{cr}$ was greater than 6, the predicted value was conservative. On average, both the G1 and G2 series were conservative. However, girder test G2B-East had a normalized value less than 6. There were no common trends between the girders that explained the lower cracking stress values. Figure 11.15 provides a plot of the normalized cracking stress factor, $\xi_{cr}$, vs. concrete compressive strength, $f_c'$, showing the downward trend as compressive strength increased. Also plotted on Figure 11.15 for comparison were the normalized values based on modulus of rupture test results again showing the modulus of rupture, $f_r$, to be a poor predictor of cracking stress.

Comparison of the experimental cracking strengths with modulus of rupture strengths, $f_r$, determined with the ASTM[82] beam test showed it to be an unconservative

predictor of cracking strength. This finding also was reported by Dill for high-strength

normal weight concrete.[84]
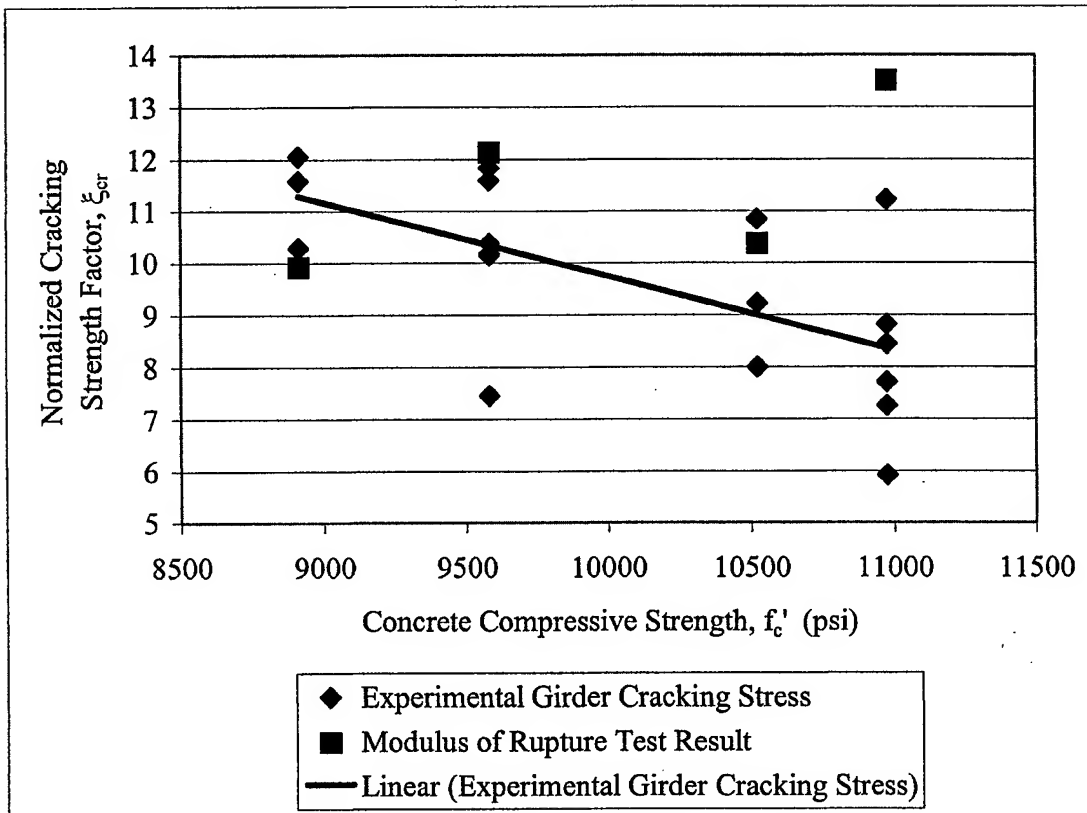


Figure 11.15 Normalized Rupture Strength Factor, $\xi_{cr}$ vs. Compressive Strength, $f_c'$

Table 11.4 provides an overview of predicted and experimental deflections at

cracking. The experimental deflections at cracking were from 16 to 145 percent greater

for the G1 series girders and 17 to 96 percent greater for the G2 series girders. Some of

this error was due to material properties of the girders. Despite having made numerous

specimens, localized variations in the concrete could impact the cracking deflection. In

addition, minor errors in identifying the cracking deflection may have occurred. While

267

exact visual determination of initial flexural cracking was sometimes difficult, close examination of data acquisition system output allowed its identification with good accuracy. Since the gage length of the LVDTs measuring strain at the bottom of the girder spanned 24 inches, initial flexural cracking almost always occurred somewhere in that region. When flexural cracking was first visually noted, the load at which it occurred was noted. In all cases but one, the visually noted cracking load matched the cracking load identified from the test output.

Table 11.4 Deflection Results at Cracking

| Test # | Predicted Deflection $\delta_{cr}$ (inches) | Experimental Deflection $\delta_{cr}$ (inches) | Percent Difference Predicted vs. Exp. |
|---|---|---|---|
| G1A-East | 0.154 | 0.270 | 75.3% |
| G1A-West | 0.267 | 0.330 | 23.6% |
| G1A-Center | 0.106 | 0.260 | 145.3% |
| G1B-East | 0.208 | 0.312 | 50.0% |
| G1B-West | 0.185 | 0.250 | 35.1% |
| G1B-Center | 0.123 | 0.230 | 87.0% |
| G1C-East | 0.194 | 0.352 | 81.4% |
| G1C-West | 0.273 | 0.441 | 61.5% |
| G1C-Center | 0.149 | 0.173 | 16.1% |
| G2A-East | 0.168 | 0.303 | 80.4% |
| G2A-West | 0.294 | 0.344 | 17.0% |
| G2A-Center | 0.115 | 0.220 | 91.3% |
| G2B-East | 0.170 | 0.216 | 27.1% |
| G2B-West | 0.265 | 0.312 | 17.7% |
| G2B-Center | 0.134 | 0.210 | 56.7% |
| G2C-East | 0.194 | 0.255 | 31.4% |
| G2C-West | 0.279 | 0.357 | 28.0% |
| G2C-Center | 0.148 | 0.290 | 95.9% |

| | |
|---|---|
| G1 Average | 63.9% |
| G2 Average | 49.5% |
| G1 Std Dev | 39.6% |
| G2 Std Dev | 32.1% |

## 11.4 Results at Ultimate

Table 11.5 provides an overview of the ultimate moment predicted by the AASHTO[40] technique utilizing the rectangular stress block, the ultimate moment predicted by a cracked section analysis using a Todeschini[91] stress block, and the experimental ultimate moment.

Table 11.5  Moment Results at Ultimate

| Test # | Predicted $M_{ult}$ AASHTO[40] (ft-kips) | Predicted $M_{ult}$ Todeschini[91] (ft-kips) | Exp. $M_{ult}$ (ft-kips) | Percent Difference Exp. vs. AASHTO[40] | Percent Difference Exp. vs. Todeschini[91] |
|---|---|---|---|---|---|
| G1A-East | 1719 | 1721 | 1836 | 6.8% | 6.7% |
| G1A-West | 1704 | 1707 | 1844 | 8.2% | 8.0% |
| G1A-Center * | 1711 | 1713 | 1671 | -2.3% | -2.5% |
| G1B-East * | 1716 | 1717 | 1578 | -8.0% | -8.1% |
| G1B-West | 1691 | 1692 | 1840 | 8.9% | 8.8% |
| G1B-Center * | 1687 | 1689 | 1774 | 5.2% | 5.1% |
| G1C-East * | 1705 | 1705 | 1796 | 5.3% | 5.3% |
| G1C-West | 1710 | 1710 | 1828 | 6.9% | 6.9% |
| G1C-Center | 1726 | 1726 | 1898 | 10.0% | 10.0% |
| G2A-East | 1693 | 1705 | 1855 | 9.6% | 8.8% |
| G2A-West | 1711 | 1717 | 1855 | 8.4% | 8.0% |
| G2A-Center * | 1707 | 1714 | 1657 | -3.0% | -3.4% |
| G2B-East | 1707 | 1718 | 1799 | 5.4% | 4.7% |
| G2B-West | 1699 | 1707 | 1840 | 8.3% | 7.8% |
| G2B-Center * | 1727 | 1733 | 1869 | 8.2% | 7.8% |
| G2C-East | 1708 | 1713 | 1870 | 9.5% | 9.2% |
| G2C-West | 1679 | 1688 | 1793 | 6.8% | 6.2% |
| G2C-Center | 1716 | 1720 | 1885 | 9.8% | 9.6% |

| | | |
|---|---|---|
| G1 Average | 8.16 | 8.06 |
| G2 Average | 8.25 | 7.75 |
| G1 Std Dev | 1.35 | 1.37 |
| G2 Std Dev | 1.63 | 1.75 |

* Failed predominantly in shear.  Not included in average or standard deviation.

As noted in Table 11.5, ultimate moment results for girders failing predominantly in shear were not included in the statistical values. On average, the two techniques produced very similar results. The Todeschini[91] stress block provided very slightly closer results. Both techniques produced conservative predictions of ultimate moment.

Table 11.6 provides an overview of deflection at ultimate.

Table 11.6 Deflections at Ultimate

| Test # | Predicted Deflection $\delta_{ult}$ (inches) | Experimental Deflection $\delta_{ult}$ (inches) | Percent Difference Exp. vs. Predicted |
|---|---|---|---|
| G1A-East | 1.394 | 1.245 | -10.7% |
| G1A-West | 2.067 | 2.416 | 16.9% |
| G1A-Center | 0.900 | 0.625 | -30.6% |
| G1B-East | 1.508 | 1.350 | -10.5% |
| G1B-West | 1.331 | 1.539 | 15.6% |
| G1B-Center | 1.067 | 1.122 | 5.2% |
| G1C-East | 1.492 | 1.534 | 2.8% |
| G1C-West | 2.332 | 2.270 | -2.7% |
| G1C-Center | 1.472 | 1.550 | 5.3% |
| G2A-East | 1.262 | 1.428 | 13.2% |
| G2A-West | 1.902 | 2.566 | 34.9% |
| G2A-Center | 0.821 | 0.799 | -2.7% |
| G2B-East | 1.283 | 1.205 | -6.1% |
| G2B-West | 1.584 | 2.060 | 30.1% |
| G2B-Center | 0.954 | 0.982 | 2.9% |
| G2C-East | 1.330 | 1.891 | 42.2% |
| G2C-West | 2.065 | 2.208 | 6.9% |
| G2C-Center | 1.373 | 2.170 | 58.0% |

| | |
|---|---|
| G1 Average | -1.0% |
| G2 Average | 19.9% |
| G1 Std Dev | 14.7% |
| G2 Std Dev | 22.3% |

On average, the G1 series girders deflected 1 percent less than predicted. The G2 girders deflected 19.9 percent more than predicted on average. The reason for this variation was how far the girders were pushed during testing. The G1 girders were tested first and were not pushed to as high of strain levels as the G2 girders. As the test program proceeded, there was an increasing effort to push the girders such that the total strain in the prestressing strands approached or exceeded 2 percent. Overall, the ultimate deflection predictions matched experimental values well.

## 11.5 Conclusions

The current prediction for cracking strength when examined for HSLC showed indications of becoming unconservative as concrete compressive strengths approached 11,000 psi. In some cases, the predicted cracking strengths exceeded the experimental values. The use of a lambda factor of 0.85 for HSLC made with slate aggregate produced conservative results on average for compressive strengths below 11,000 psi. More research is required to examine a potential tension strength ceiling for HSLC and to examine the lambda factor for use with HSLC over 10,000 psi compressive strength.

The modulus of rupture test, ASTM C-78, did not accurately predict cracking strength of HSLC girders.

The current AASHTO procedure for ultimate moment calculation was conservative for HSLC girders with normal weight concrete decks having a compressive strength under 6,000 psi.

271

# CHAPTER XII

# SHEAR BEHAVIOR RESULTS AND DISCUSSION

## 12.1 Introduction

This chapter discusses shear behavior in the HSLC pretensioned girders. Based on experimentally measured values during testing, current code provisions were evaluated.

## 12.2 AASHTO 1996 Standard Shear Design Approach

The following sections outline the process for calculating the strength of the concrete, $V_c$, and strength of the steel reinforcement, $V_s$, based on the 1996 AASHTO Standard Specification for Highway Bridges.[40]

### 12.2.1 Concrete Strength, $V_c$

The concrete strength, $V_c$, is the lesser of the flexure shear strength, $V_{ci}$, and the web shear strength, $V_{cw}$. Based on the shear spans and characteristics of the girders in this research, the web shear strength, $V_{cw}$, was always the governing value. The calculation of both values is explained further in the following sections.

#### 12.2.1.1 Flexure Shear Strength, $V_{ci}$

The flexure shear strength was calculated using AASHTO[40] equation (9-27):

$$V_{ci} = 0.6\lambda\frac{\sqrt{f_c'}}{1000}b'd + V_d + \frac{V_i M_{cr}}{M_{max}} \geq 1.7\lambda\frac{\sqrt{f_c'}}{1000}b'd \qquad (12.1)$$

The value b' was taken as the minimum web thickness of the girder which was 6 inches

for an AASHTO Type II. The code specifies that d, the distance from the topmost

compression fiber to the centroid of the prestressing strands need not be less than 0.8*h.

The value of d normally exceeded the minimum 0.8*h. $V_i$ and $M_{max}$ were the maximum

moment and shear at the section in question. The lightweight concrete factor, $\lambda$, having a

value of 0.85 was included in the equation based on the use of HSLC. The concrete

strength $f_c'$ was listed in psi. Calculation of the cracking moment was accomplished with

AASHTO equation (9-28):

$$M_{cr} = \frac{I}{Y_t}(6\lambda\frac{\sqrt{f_c'}}{1000} + f_{pe} - f_d) \qquad (12.2)$$

The composite section properties were used in calculating $M_{cr}$. The concrete strength, $f_c'$,

was based on cylinder tests at the time of girder testing.

### 12.2.1.2 Web Shear Strength, $V_{cw}$

The web shear strength was calculated using AASHTO[40] equation (9-29):

$$V_{cw} = (3.5\lambda\frac{\sqrt{f_c'}}{1000} + 0.3f_{pc})b'd + V_p \qquad (12.3)$$

273

In the girders tested, there were no draped strands thus $V_p$ was zero. The value $f_{pc}$ accounted for the effect of prestress and the dead load of the girder alone at the centroid of the composite section. It was calculated as shown in equation 12.4 below:

$$f_{pc} = \frac{F_{se}}{A_{nc}} - \frac{F_{se}e(y_{bot-c} - y_{bot-nc})}{I_{nc}} - \frac{M_{DL}(y_{bot-c} - y_{bot-nc})}{I_{nc}} \tag{12.4}$$

The effective prestressing force was reduced when the section being examined was inside a distance equal to the transfer length from the end of the girder. The procedure also accounted for the reduced effective prestressing force in calculating $f_{pc}$. The $\lambda$ factor equal to 0.85 was included to account for the use of HSLC.

## 12.2.2 Transverse Steel Shear Strength, $V_s$

The transverse steel shear strength was calculated using AASHTO[40] equation (9-30):

$$V_s = \frac{A_v f_y d}{s} \leq 8\frac{\sqrt{f_c'}}{1000}b'd \tag{12.5}$$

For the girders tested, the shear area, $A_v$, was 0.4 in$^2$ for double # 4 bar stirrups. The value "s" was the spacing of the stirrups, which was 3.5 inches for the double density stirrups, 7" for single density stirrups and 24" for minimum stirrup spacing. The yield

strength of the stirrups was 62 ksi as determined experimentally. Refer to Appendix C for more information on the material properties of the shear reinforcement.

### 12.2.3 Nominal Shear Strength, $V_n$

The nominal shear strength was calculated as:

$$V_n = V_c + V_s \tag{12.6}$$

## 12.3 ACI Alternate Approach for Calculating $V_{cw}$

ACI 11.4.2.2 provides an alternate technique for calculating $V_{cw}$ that was investigated in this evaluation.[2] The ACI Code states that $V_{cw}$ shall be computed as the shear force corresponding to dead load plus live load that results in a principal tension stress of $4\lambda(f_c')^{1/2}$ at the centroidal axis of the member. In composite members, the principal tensile stress is computed using the cross section that resists live load. Lin and Burns[50] addressed this alternate technique and provided the following equations which come directly from the application of Mohr's circle:

$$V_{cw-Pred} = f_{t-Pred}'' \sqrt{1 + \frac{f_{pc}}{f_{t-Pred}''}} \, bd_p \tag{12.7}$$

The predicted diagonal tensile strength, $f_{t-Pred}''$ was calculated using equation 12.8:

275

$$f''_{t-Pred} = 4\lambda\sqrt{f'_c} \qquad (12.8)$$

The value of $f_{pc}$ was calculated using equation 12.4 based on conditions at the midpoint of the shear span.

The experimental cracking load, $V_{cw-Exp}$ was recorded when the first shear cracking occurred during the girder test. Based on $V_{cw-Exp}$, the experimental diagonal tensile strength, $f''_{t}$-Exp was calculated using equation 12.9.

$$f''_{t-Exp} = \sqrt{\left(\frac{V_{cw-Exp}}{bd_p}\right)^2 + \left(\frac{f_{pc}}{2}\right)^2} - \frac{f_{pc}}{2} \qquad (12.9)$$

The $f''_{t}$-EXP value was then normalized using equation 12.10.

$$\xi_t = \frac{f''_{t-Exp}}{\lambda\sqrt{f'_c}} \qquad (12.10)$$

A normalized value, $\xi_t$, less than 4 was an indication that equation 12.8 provided an unconservative prediction of the tensile stress at which initial web shear cracking occurred.

## 12.4 1998 AASHTO LRFD Shear Design Approach

The following sections outline the process for calculating the shear strength using the 1998 AASHTO LRFD Specification for Highway Bridges.[92]

### 12.4.1 Concrete Strength, $V_c$

The LRFD approach for strength calculation is much different than the Standard procedure. The first step was to calculate the effective shear depth, $d_v$, using equation 12.11.

$$d_v = d_p - \frac{a}{2} \qquad (12.11)$$

The value "a" was the depth of the rectangular stress block required to balance the prestress force at the particular section of interest.

The effective web width, $b_v$, was taken as the web width of the AASHTO Type II girder, 6 inches.

The effective area of prestress, $A_{pse}$, was calculated by determining the effective number of strands on the flexural tension side of the member. The flexural tension side of the member indicated the bottom half of the composite member. If the distance "x" from the free end of the member to the girder section being evaluated was less than the experimental development length, the total number of bottom strands, 8, was multiplied by $x/l_d$. If the section being evaluated was greater than $l_d$ from the free end of the member, the effective number of strands was the total number, 8. The effective number

of strands was then multiplied by the area of a prestressing strand, 0.2183 in$^2$, to

determine $A_{pse}$.

The shear stress on the concrete was calculated using AASHTO equation

(5.8.3.4.2-1):

$$v = \frac{V_u - \phi V_p}{\phi b_v d_v} \tag{12.12}$$

Since there were no draped strands in these girders, $V_p$ was zero. The resistance factor

for shear, $\phi$, was taken as 1.0 since the nominal stress was desired. The value $v/f_c$' was

then calculated.

In order to use the modified compression field theory from the AASHTO[92] LRFD

Specification, the angle of inclination of diagonal compressive stress, $\theta$, was required.

To determine $\theta$, crack angles were measured at the mid-point of the shear span as listed

in Table 12.1.

The strain in the tensile reinforcement on the flexural tension side, $\varepsilon_x$, was then

calculated using AASHTO equation (5.8.3.4.2-2):

$$\varepsilon_x = \frac{\dfrac{M_u}{d_v} + 0.5 N_u + 0.5 V_u \cot\theta - A_{ps} f_{po}}{E_s A_s + E_p A_{ps}} \le 0.002 \tag{12.13}$$

Table 12.1 Measured Crack Angles

| Test # | Measured Crack Angle (degrees CCW from Horizontal) |
|---|---|
| G1A-East | 31.0 |
| G1A-West | 25.0 |
| G1A-Center | 25.0 |
| G1B-East | 32.0 |
| G1B-West | 38.0 |
| G1B-Center | 25.0 |
| G1C-East | 30.0 |
| G1C-West | 30.0 |
| G1C-Center | 25.0 |
| G2A-East | 38.0 |
| G2A-West | 34.0 |
| G2A-Center | 33.0 |
| G2B-East | 35.0 |
| G2B-West | 33.0 |
| G2B-Center | 26.0 |
| G2C-East | 27.0 |
| G2C-West | 30.0 |
| G2C-Center | 33.0 |

Since there was no non-prestressed flexural reinforcement in the test girders and no axial

load, equation 12.13 simplified to equation 12.14 as below:

$$\varepsilon_x = \frac{\dfrac{M_u}{d_v} + 0.5V_u \cot\theta - A_{ps}f_{po}}{E_p A_{ps}} \le 0.002 \qquad (12.14)$$

The value $f_{po}$, the stress in the prestressing strand when the stress in the surrounding

concrete is zero was conservatively taken as the effective prestress, $f_{se}$. A correction

factor specified by AASHTO equation (5.8.3.4.2-3) was included in the event $\varepsilon_x$ was

279

calculated as a negative number. Since the strain in the strand at effective prestress was

0.005 in/in at a minimum outside the transfer length region, the only point along the

strand $\varepsilon_x$ could ever approach a value less than 0.002 would be within approximately 12

inches from the free end of the girder.

Using the value $v/f_c'$ and $\varepsilon_x$, a $\beta$ value was determined from AASHTO Figure

5.8.3.4.2-1. The concrete shear strength, $V_c$ was calculated using AASHTO equation

(5.8.3.3-3) below. The equation was modified to reflect the inclusion of the lightweight

concrete factor, $\lambda$.

$$V_c = 0.0316\lambda\beta\sqrt{f_c'}b_v d_v \tag{12.15}$$

### 12.4.2 Transverse Steel Shear Strength, $V_s$

The strength of the shear reinforcing steel was calculated with AASHTO equation

(C5.8.3.3-1):

$$V_s = \frac{A_v f_y d_v \cot\theta}{s} \tag{12.16}$$

The abbreviated version of the equation for $V_s$ was used because the shear stirrups were

placed vertically.

### 12.4.3  Nominal Shear Strength, $V_n$

The nominal shear strength of the girder was then calculated using AASHTO

equations (5.8.3.3-1) and (5.8.3.3-2) combined below:

$$V_n = V_c + V_s \leq 0.25 f_c' b_v d_v \qquad (12.17)$$

### 12.5  Variable Angle Truss Model

The variable angle truss model (VATM) was used as an analysis tool for two

reasons.  First, on the girder end tests where strand slip occurred, it was desired to

determine the force in the bottom strands near the girder end.  Knowing the force in the

bottom strands, the bond stress could be estimated and compared to values calculated at

transfer, and to values calculated for girders not experiencing strand slip.

The VATM assumes that the girder experiences shear and flexural failure

simultaneously.  The stirrups resist the entire shear force and are assumed to be at yield.

The concrete is assumed to resist zero shear force.  The model is addressed in *Prestressed*

*Concrete Structures*, Michael P. Collins and Denis Mitchell.[48]

## 12.5.1 Shear Force

$V_{ult}$ was equal to the support reaction at the support closest to the applied load.
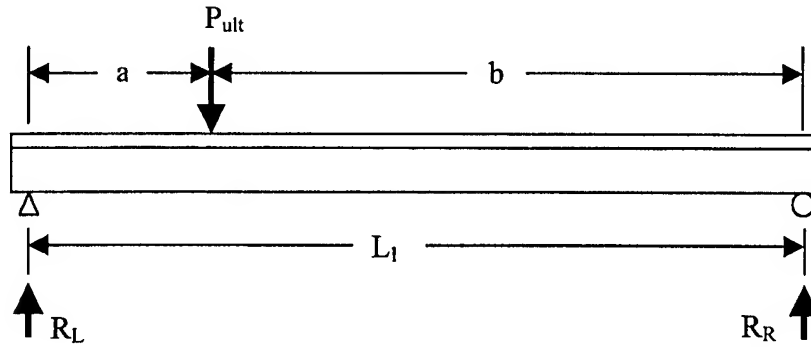


Figure 12.1  Figure for Calculation of $V_{ult}$

$V_{ult}$ was calculated based on Figure 12.1 and equation 12.18.

$$V_{ult} = R_L = R_{L-self\,wt} + P_{ult}\frac{b}{L_1}$$
(12.18)

## 12.5.2 Stirrup Force

The force in the shear stirrups, $F_{stirrup}$, was calculated using equation 12.19.

$$F_{stirrup} = A_v f_y$$
(12.19)

### 12.5.3 Stirrups Required to Carry $V_{ult}$

The number of stirrups required, $\#_{stirrups}$, to carry $V_{ult}$ was calculated with equation 12.18.

$$\#_{Stirrups} = \frac{V_{ult}}{F_{stirrup}} \qquad (12.20)$$

The number of stirrups calculated determined the number of compression struts beginning at the applied load and carrying force to the intersection of stirrups with the centroid of the prestressing strands. In addition, the number of stirrups required indirectly determined the angle of the compression field. In general, the more stirrups required to carry $V_{ult}$, the shallower the compression field angle was to the horizontal. The same number of compression struts initiating at the applied load would also end at the support. The connecting pieces between the compression struts are the shear stirrups.

When configuring the VATM, the maximum angle a strut could make with the horizontal was 70 degrees and the minimum was 25 degrees. This limited the number of struts and stirrups that could carry shear force in the truss. It was possible that insufficient stirrups were available in the angle range from 25 to 70 degrees to carry $V_{ult}$. In this case, the predicted shear capacity of the girder could be limited by the VATM to a level well below that reached during testing. Girder test G1C-West was an example of this type of test. The VATM predicted a much lower shear capacity than the girder achieved. Figure 12.2 provides a diagram of the VATM for girder test G1C-West. The

critical point on the VATM was at a distance equal to the transfer length, $l_t$, from the girder free end as labeled in Figure 12.2.

Stirrup Spacing = 7"

85" 6"

θ_max = 70°  Compression Field Crack Angle  θ_min = 25°  Prestress Force Centroid

Critical Region within $l_t$ from girder end
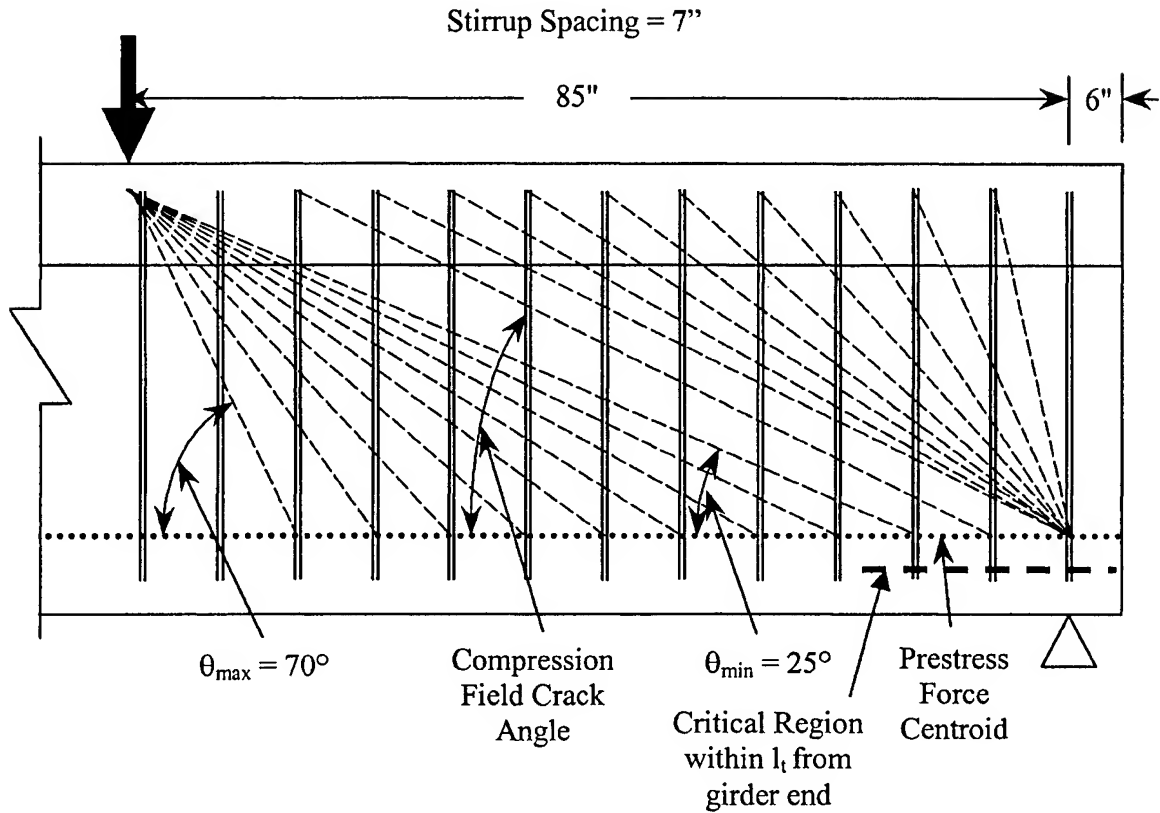
Figure 12.2  Variable Angle Truss Model for Girder Test G1C-West

## 12.5.4 Internal Moment Arm

The internal moment arm, jd, was calculated using equation 12.21.

$$jd = d_p - \frac{a}{2}$$

(12.21)

### 12.5.5  Force in Strands at Point of Loading

Since the VATM assumes the girder to be at flexural and shear failure simultaneously, the strands must be near failure. The values $f_{su}^*$ and $f_{se}$ were assumed as the stress in the bottom and top strands respectively. The total strand force at the point of loading was be $(f_{su}^* * 8 \text{ strands} + f_{se} * 2 \text{ strands}) * 0.2183 \text{ in}^2$. This strand force was assumed to act at the prestress force centroid labeled in Figure 12.2.

### 12.5.6  Strand Force Reduction

At each intersection of the strand force centroid with a stirrup, some of the strand force was removed and carried by truss action to the support. Equation 12.22 was used to determine the strand force reduction.

$$F_{Reduction} = \frac{x}{jd} F_{stirrup} \qquad (12.22)$$

The value x indicated the distance the stirrup was from the point of loading. As the distance x increases, the amount of reduction in the strands increases also. Figure 12.3 provides a typical plot of the strand force reduction from the point of loading to the support.
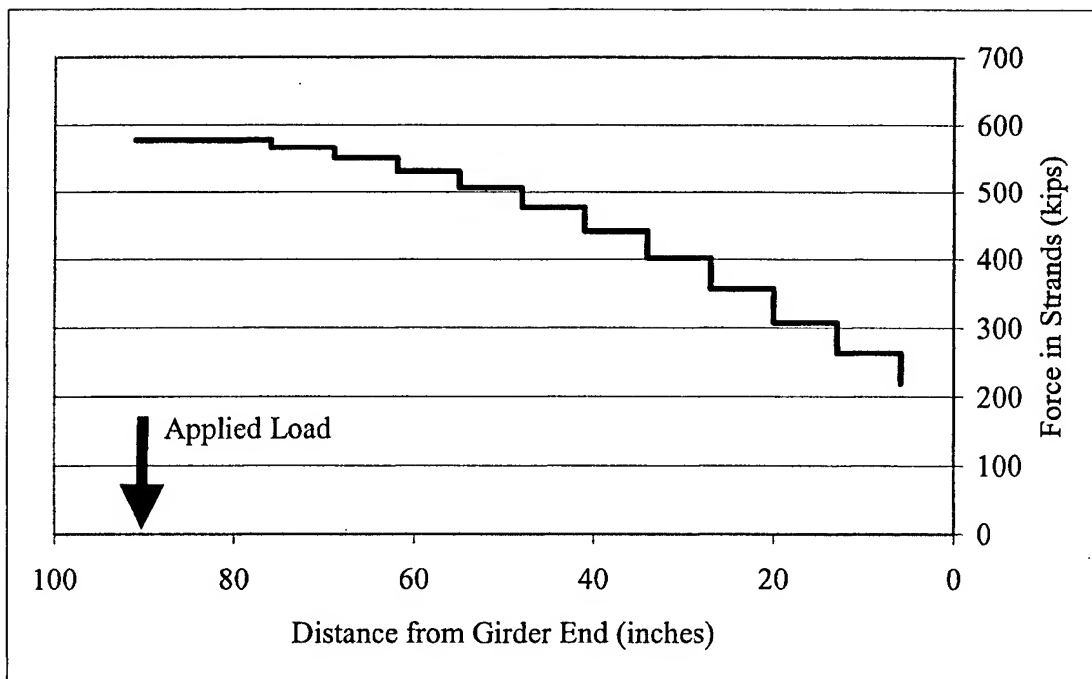
Figure 12.3 VATM Strand Force Reduction Plot for Girder Test G1C-West

### 12.5.7 Compression Field Crack Angle

The compression field crack angle is labeled in Figure 12.2. In the case of girder test G1C-West, the compression field crack angle was based on the angle of a "carryover strut." A carryover strut is one that neither begins at the point of loading nor ends at the support. If there is no carryover strut, the compression field crack angle will be the angle of the strut originating from the point of loading with smallest angle to the horizontal.

### 12.5.8 Strand Bond Stress

Strand bond stress was calculated based on the force remaining in the strand, $F_{strand}$, the length of embedment at the point, $l_e$, and the nominal circumference, $\pi d_b$, of the strand using equation 12.23 below.

286

$$f_{bond} = \frac{F_{strand}}{l_e \pi d_b}$$  (12.23)

A plot of bond stress from the point of loading to the support shows how the bond stress dramatically increases near the support. In the VATM, it was assumed that within one stirrup spacing of the support that only the bottom strands carried the strand force. A plot of bond stress can be seen in Figure 12.4. The bond stress over the transfer length due to the effective prestress was also plotted on the diagram for comparison purposes.

### 12.5.9 Stress in Compression Strut

Stress in the compression strut, $f_{strut}$, was calculated with equation 12.24 using $V_{ult}$.

$$f_{strut} = \frac{V_{ult}}{jd \cos\theta\, b_w \sin\theta} \le 0.85\beta_1 \lambda\, f_c'$$  (12.24)

The value $\beta_1$ was 0.6 based on the use of HSLC with a compressive strength over 6,000 psi. Compliance with this requirement as specified by ACI 318[91] (2002) ensured a level of stress in the strut below which shear crushing would not occur.
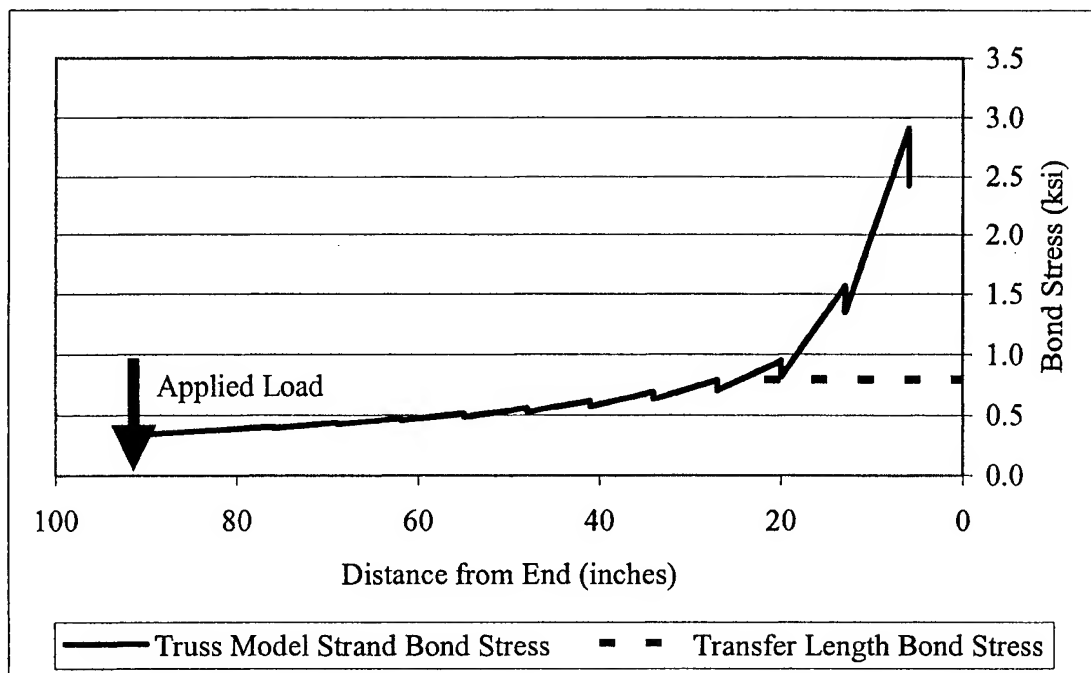
Figure 12.4  Bond Stress Plot for Girder Test G1C-West

## 12.6 Experimental Measurement of Shear Behavior

In order to monitor and measure girder shear behavior, a large strain rosette made with LVDTs was placed on the web of each girder at the mid point of the shear span as pictured in Figure 12.5.
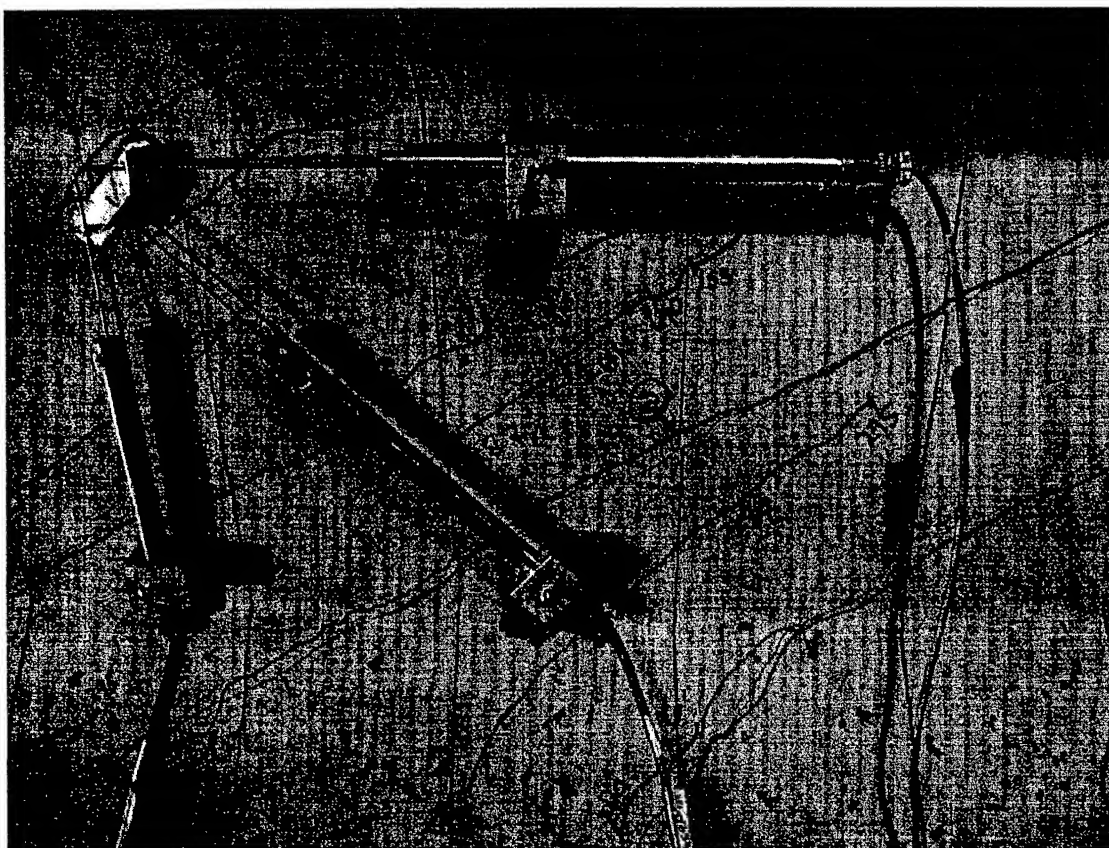


Figure 12.5  Strain Rosette Made with LVDTs on Girder Test G1C-West

The LVDTs oriented in the horizontal and vertical positions had gage lengths of approximately 10.5 inches.  The LVDT at a 45-degree angle had a gage length of approximately 16.5 inches.  To calculate strains in the three directions, the displacement of the LVDT was divided by its gage length.  The gage lengths were carefully measured

for each girder test to ensure proper strain calculation. Having strain information for

three distinct directions, and knowledge of the initial prestressing strain along the

longitudinal axis of the girder, it was possible to calculate principal strains and directions

using a simple strain transformation. Figure 12.6 below shows a typical plot of applied

shear vs. principal strains.
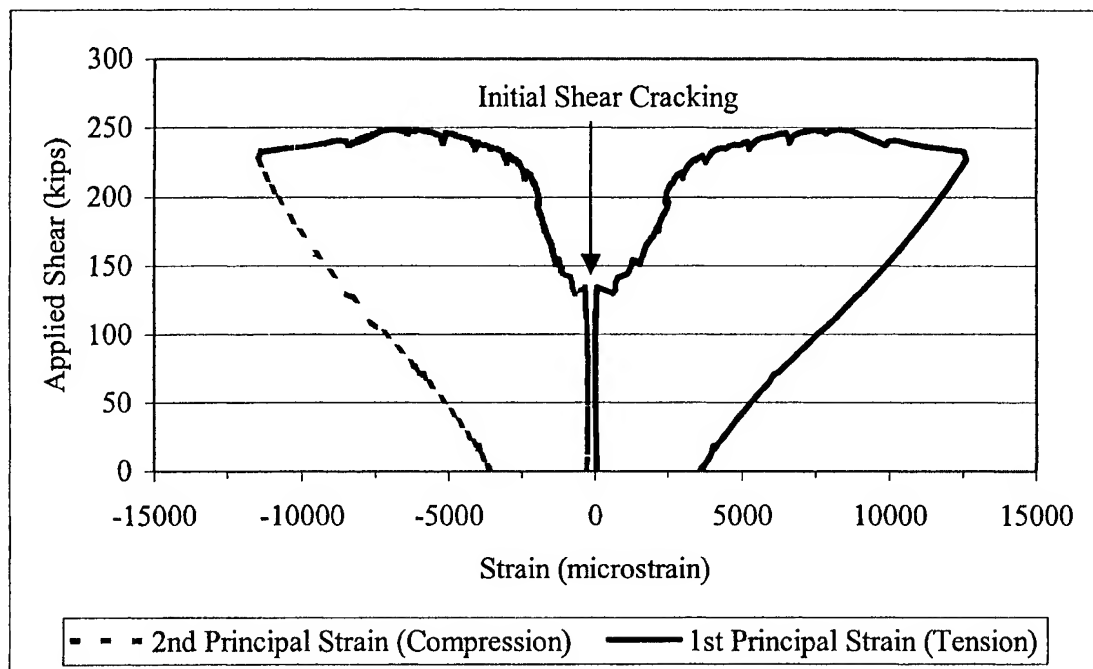


Figure 12.6 Plot of Applied Shear vs. Principal Strains for Girder Test G1C-West

The point at which initial shear cracking occurred was where the two principal strain

plots separated. This value matched very closely the value at which initial shear cracking

was visually and audibly detected during the test. The plot shows initial shear cracking at

an applied shear of 134.2 kips. The latter agreed with the applied load of 155 kips at

which a shear crack occurred. In order for the LVDTs to measure the onset of shear

cracking, the initial crack had to pass through the rosette. Initial cracking did not pass

through the rosette on one girder test.

Another useful aspect of the principal strain information was a plot of how the

principal angles varied during the test. Figure 12.7 below provides a typical plot of the

second principal strain (compression strain) angle, which indicated the angle of shear

cracking through the LVDT rosette.
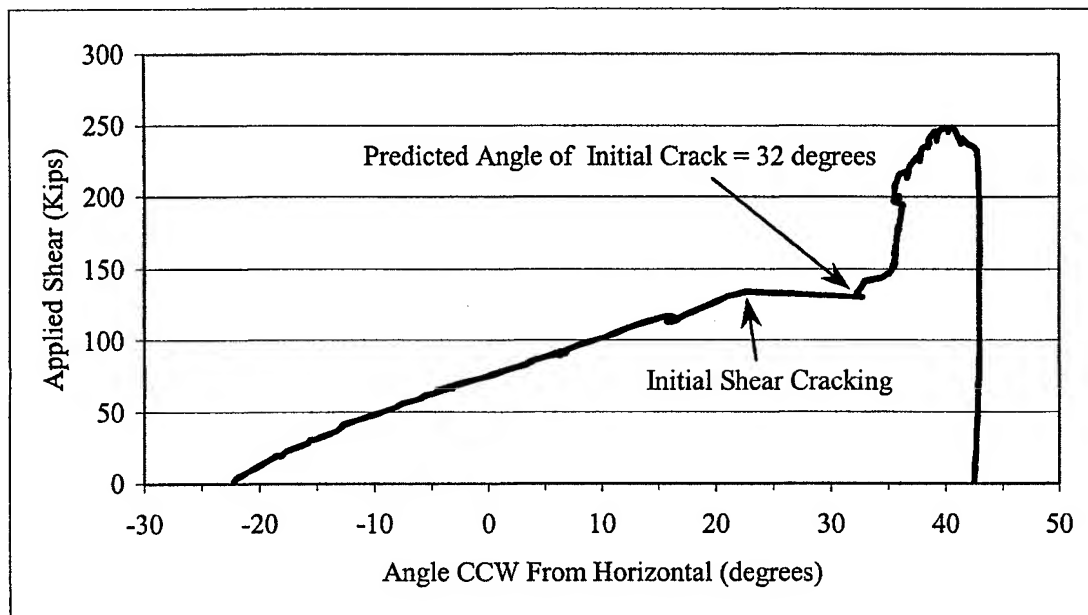


Figure 12.7 Second Principal Strain Direction (Cracking Angle) for Test G1C-West

The horizontal plateau from the point labeled "initial shear cracking" also was an

indication of the applied shear at which cracking occurred. The angle indicated at the end

of the plateau was most representative of the actual cracking angle on the girder;

protractor measurements of the crack angle normally agreed within ± 5 degrees with this

plateau angle.

Figure 12.7 shows an increase in crack angle with increased applied load. As applied shear increased, the stirrups were required to pick-up more shear increasing the vertical force component and causing the angle of cracking to become greater. This trend was observed during testing. As the applied shear increased, new shear cracks formed at greater angles than those seen at initial cracking. In Figure 12.7, the indicated crack angle appeared to increase from about 32 degrees to 40 degrees as the applied shear increased.

## 12.7 Experimental Results

Discussion of experimental results was divided into the discussion of the initial shear cracking, ultimate shear capacity, and the variable angle truss model (VATM). Percent difference was calculated using equation 11.1.

### 12.7.1 Initial Shear Cracking

Table 12.2 provides an overview of initial shear cracking. The predicted values were calculated at the midpoint of the shear span. The experimental value was the applied shear at which cracking was first recorded visually or electronically.

Examination of Table 12.2 showed that the AASHTO[40] Standard method of calculating concrete shear strength was conservative overall. In the case of girder tests G1C-Center and G2C-Center, the prediction was less than 3 percent unconservative. The AASHTO[92] LRFD technique provided predictions of concrete strength that far underestimated their capacity. The ACI[2] alternate approach provided the closest prediction for $V_c$ where the cracking shear was equated to the shear strength provided by

the concrete. Overall, the predicted $V_c$ values were within about 6 percent of experimental values for both the G1 and G2 girder tests. Girder tests G1C-Center and G2C-Center showed the greatest difference from the ACI alternate predicted values, about 18 percent unconservative overall. Both the tests involved the minimum stirrup spacing of 24 inches.

Table 12.2  Overview of Initial Cracking Shears

| Test # | $V_{c\text{-EXP}}$ Exp. (kips) | $V_{cw}$ AASHTO Standard (kips) | $V_{cw}$ ACI Alternate (kips) | $V_c$ AASHTO LRFD (kips) | Percent Diff. Exp. vs. Standard | Percent Diff. Exp. vs. ACI Alt | Percent Diff. Exp. vs. LRFD |
|---|---|---|---|---|---|---|---|
| G1A-E * | 145.0 | 104.1 | 124.0 | 24.7 | 39.4% | 16.9% | 488% |
| G1A-W | 120.0 | 107.1 | 127.5 | 26.3 | 12.1% | -5.9% | 356% |
| G1A-C * | 134.0 | 98.5 | 118.0 | 23.5 | 36.1% | 13.6% | 470% |
| G1B-E * | 140.0 | 105.5 | 125.5 | 24.7 | 32.7% | 11.6% | 466% |
| G1B-W | 141.2 | 103.9 | 123.6 | 24.3 | 35.9% | 14.2% | 482% |
| G1B-C * | 136.1 | 98.9 | 118.4 | 25.0 | 37.6% | 14.9% | 445% |
| G1C-E * | 123.5 | 101.5 | 120.7 | 23.6 | 21.7% | 2.3% | 423% |
| G1C-W | 134.2 | 104.0 | 123.3 | 23.6 | 29.0% | 8.8% | 468% |
| G1C-C | 94.0 | 96.7 | 115.8 | 24.6 | -2.8% | -18.8% | 282% |
| G2A-E | 178.6 | 114.4 | 135.7 | 26.0 | 56.1% | 31.6% | 588% |
| G2A-W | 157.3 | 118.1 | 139.5 | 28.8 | 33.2% | 12.8% | 447% |
| G2A-C * | 140.0 | 109.4 | 130.6 | 25.0 | 27.9% | 7.2% | 460% |
| G2B-E | 163.1 | 114.6 | 136.1 | 25.2 | 42.3% | 19.8% | 549% |
| G2B-W | 148.0 | 117.4 | 138.7 | 25.8 | 26.1% | 6.7% | 473% |
| G2B-C * | 120.4 | 110.5 | 131.9 | 25.2 | 9.0% | -8.7% | 377% |
| G2C-E | 143.4 | 112.0 | 133.0 | 25.6 | 28.1% | 7.8% | 461% |
| G2C-W | 122.4 | 113.4 | 134.2 | 27.1 | 8.0% | -8.8% | 352% |
| G2C-C | 107.0 | 107.3 | 128.1 | 31.3 | -0.2% | -16.5% | 241% |

| | | | | | | | |
|---|---|---|---|---|---|---|---|
| G1 Avg | 129.8 | 102.2 | 121.9 | 24.5 | 26.8% | 6.4% | 431% |
| G2 Avg | 142.2 | 113.0 | 134.2 | 26.7 | 25.6% | 5.8% | 439% |
| G1 Std Dev | | | | | 14.1% | 11.9% | 68.9% |
| G2 Std Dev | | | | | 17.8% | 15.2% | 104.1% |

* Girder failed in shear at ultimate as primary or secondary failure mode

## 12.7.2 Initial Shear Cracking Considering Stirrup Spacing

Figure 12.8, plots the concrete shear strength, $V_{c-Exp}$, vs. shear stirrup spacing.

The trend lines indicated that $V_{c-Exp}$ appeared to increase with smaller stirrup spacing.

Since the stirrups carried some load prior to concrete cracking, it was understandable that

the apparent $V_{c-Exp}$ value would be higher with closer stirrup spacing. A very interesting

aspect of Figure 12.8 was the convergence of the G1 and G2 trendlines at a stirrup

spacing of 24 inches. The indication here was that little difference existed between $V_c$

for the G1 and G2 girders. Based on the use of minimum stirrup spacing in these 6

center-span tests, it was likely that these data most truly reflected the $V_c$ value of the

girders.
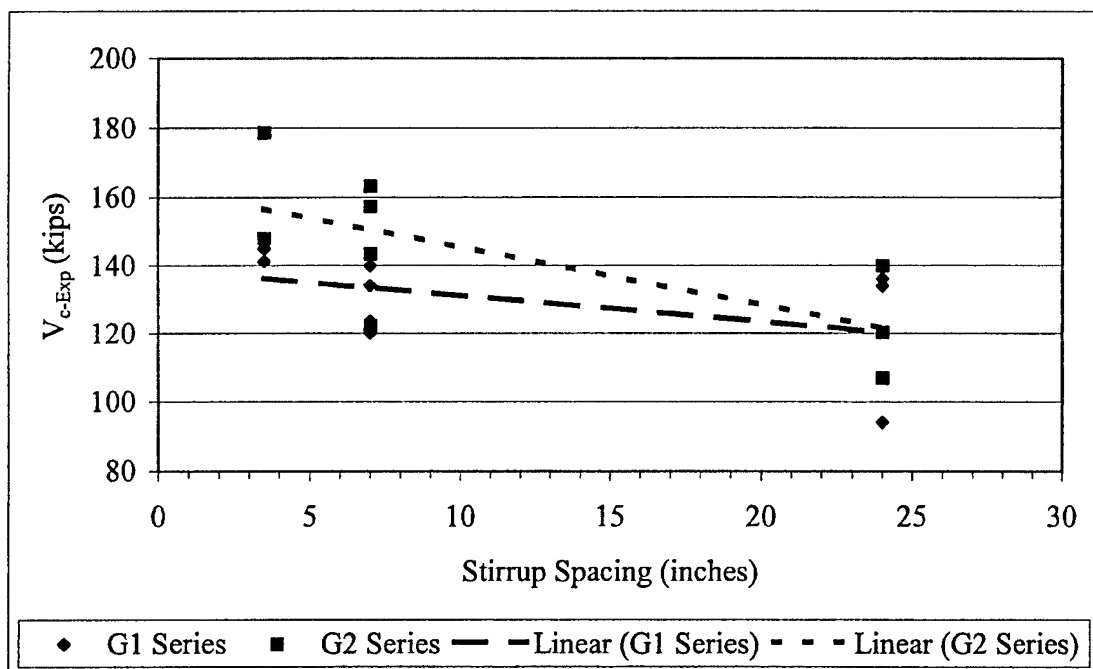


Figure 12.8 Concrete Shear Strength, $V_c$ vs. Stirrup Spacing

The implication of this finding was that an apparent ceiling exists which limits the tension strength of concrete. In order to investigate this possibility, a similar normalization was conducted on the shear results as was done on the cracking strength results at flexural cracking.

### 12.7.3 Normalized Diagonal Tension Strength Factor, $\xi_t$

Table 12.3 provides an overview of predicted diagonal tension strengths using the ACI[2] alternate approach, experimental diagonal tension strengths and the normalized diagonal tension factor, $\xi_t$.

Table 12.3 shows that $\xi_t$ becomes unconservative at 3.70 (less than 4) on average for the G2 series girders with 24-inch stirrup spacing. Figure 12.9 depicts graphically the data from Table 12.3 and shows how the ACI alternate prediction technique for diagonal tensile strength produced some unconservative predictions. Any data points below the 4.0 line were unconservative.

Table 12.3 Normalized Diagonal Tension Strength Factors, $\xi_t$

| Test # | Stirrup Spacing (inches) | ACI Alternate Predicted Diagonal Tension Strength (Equation 12.8) $f_{t\text{-Pred}}$" (psi) | Experimental Diagonal Tension Strength $f_{t\text{-Exp}}$" (psi) | Normalized Diagonal Tension Strength Factor $\xi_t$ |
|---|---|---|---|---|
| G1A-East | 3.5 | 333 | 415 | 4.99 |
| G1A-West | 7 | 333 | 304 | 3.66 |
| G1A-Center | 24 | 333 | 396 | 4.76 |
| G1B-East | 7 | 333 | 389 | 4.67 |
| G1B-West | 3.5 | 333 | 402 | 4.83 |
| G1B-Center | 24 | 333 | 404 | 4.85 |
| G1C-East | 7 | 321 | 332 | 4.14 |
| G1C-West | 7 | 321 | 363 | 4.52 |
| G1C-Center | 24 | 321 | 238 | 2.96 |
| G2A-East | 3.5 | 356 | 525 | 5.89 |
| G2A-West | 7 | 356 | 424 | 4.77 |
| G2A-Center | 24 | 356 | 393 | 4.41 |
| G2B-East | 7 | 356 | 461 | 5.18 |
| G2B-West | 3.5 | 356 | 392 | 4.40 |
| G2B-Center | 24 | 356 | 312 | 3.51 |
| G2C-East | 7 | 349 | 389 | 4.46 |
| G2C-West | 7 | 349 | 304 | 3.49 |
| G2C-Center | 24 | 349 | 268 | 3.17 |

| | | | |
|---|---|---|---|
| G1 Average | 3.5 | 409 | 4.91 |
| G2 Average | 3.5 | 459 | 5.15 |
| G1 Average | 7 | 347 | 4.25 |
| G2 Average | 7 | 395 | 4.48 |
| G1 Average | 24 | 346 | 4.19 |
| G2 Average | 24 | 324 | 3.70 |

296
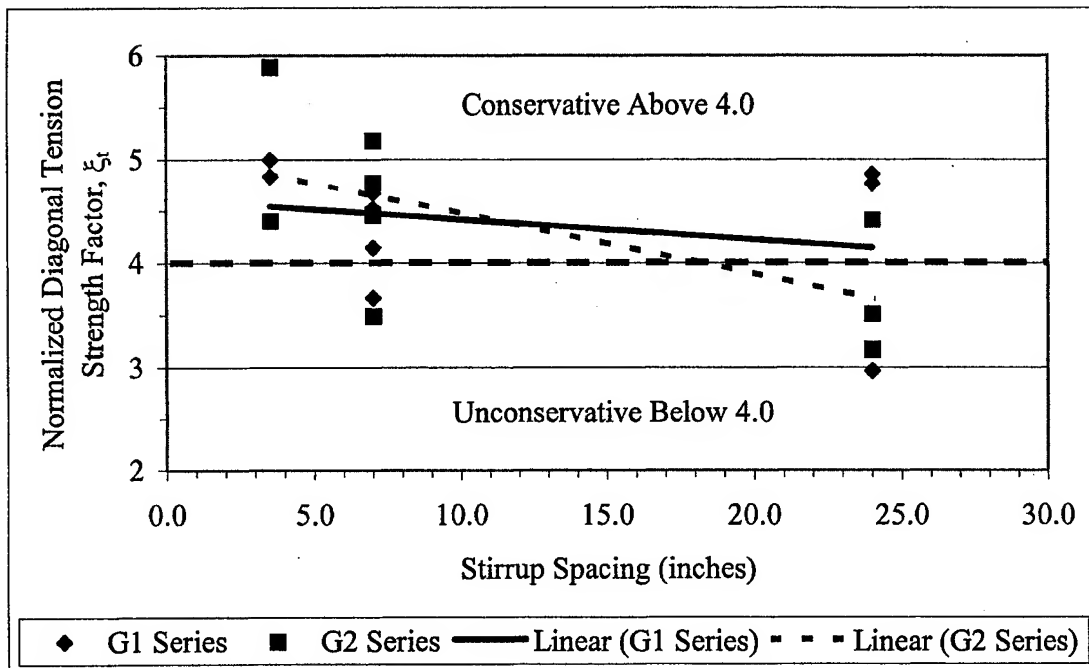
Figure 12.9 Normalized Diagonal Tension Strength Factor, $\xi_t$, vs. Stirrup Spacing

### 12.7.4 Ultimate Shear Capacity, $V_u$

Table 12.4 provides an overview of predicted ultimate shear capacity calculated by the AASHTO Standard method and the AASHTO LRFD method with the strength reduction factor, $\phi_s$, of 1 and compares them to the experimental maximum shear values. Using the AASHTO Standard method, the stirrup yield strength was capped at 60 ksi as required by the code, and the results also recorded. Since the value of $f_y$ was 62 ksi, there was an insignificant difference in predicted values.

Table 12.4 lists the results of all tests; Table 12.5 lists only the tests that exhibited a shear, shear-slip or shear-flexure failure. Both tables show the AASHTO[40] Standard technique produced conservative results overall. Limiting the yield strength to 60 ksi

caused the prediction to be slightly more conservative. The AASHTO[92] LRFD technique

produced more conservative results overall because the girders with 24-inch spacing were

predicted to carry much less shear. The AASHTO LRFD penalized those girders with a

very low concrete strength relative to the AASHTO Standard procedure.

Table 12.4 Predicted vs. Experimental $V_u$ Values

| Test # | AASHTO Standard $f_y = 62$ ksi $V_u$ (kips) | AASHTO Standard $f_y = 60$ ksi $V_u$ (kips) | AASHTO LRFD $f_y = 62$ ksi $V_u$ (kips) | Exp. $V_u$ (kips) | Percent Diff. Exp vs Std 62 | Percent Diff. Exp vs Std 60 | Percent Diff. Exp vs LRFD |
|---|---|---|---|---|---|---|---|
| G1A-East * | 379.7 | 370.8 | 473.5 | 362.8 | -4.5% | -2.2% | -23.4% |
| G1A-West * | 244.9 | 240.4 | 312.8 | 248.9 | 1.6% | 3.5% | -20.4% |
| G1A-Center | 138.7 | 137.4 | 103.8 | 258.0 | 86.0% | 87.8% | 148.5% |
| G1B-East | 243.3 | 238.9 | 241.1 | 312.2 | 28.3% | 30.7% | 29.5% |
| G1B-West * | 376.0 | 367.2 | 363.5 | 296.3 | -21.2% | -19.3% | -18.5% |
| G1B-Center | 138.6 | 137.3 | 104.3 | 234.1 | 68.9% | 70.5% | 124.5% |
| G1C-East | 238.4 | 234.0 | 255.5 | 289.2 | 21.3% | 23.6% | 13.2% |
| G1C-West * | 241.4 | 237.0 | 255.6 | 260.3 | 7.8% | 9.8% | 1.8% |
| G1C-Center * | 137.1 | 135.8 | 105.5 | 202.2 | 47.5% | 48.9% | 91.6% |
| G2A-East * | 388.3 | 379.4 | 365.4 | 366.5 | -5.6% | -3.4% | 0.3% |
| G2A-West * | 255.4 | 251.0 | 223.8 | 249.7 | -2.3% | -0.5% | 11.6% |
| G2A-Center | 149.5 | 148.2 | 82.3 | 255.9 | 71.2% | 72.7% | 211.0% |
| G2B-East * | 252.5 | 248.0 | 215.8 | 355.4 | 40.8% | 43.3% | 64.7% |
| G2B-West * | 391.3 | 382.4 | 432.0 | 296.3 | -24.3% | -22.5% | -31.4% |
| G2B-Center | 150.9 | 149.6 | 102.7 | 246.3 | 63.2% | 64.6% | 139.9% |
| G2C-East * | 249.8 | 245.3 | 268.9 | 301.0 | 20.5% | 22.7% | 11.9% |
| G2C-West * | 249.9 | 245.5 | 254.2 | 255.2 | 2.1% | 4.0% | 0.4% |
| G2C-Center * | 147.6 | 144.1 | 89.2 | 200.3 | 35.7% | 39.0% | 124.7% |

| G1 Average | | | | | 26.2% | 28.1% | 38.5% |
| G2 Average | | | | | 22.4% | 24.4% | 59.2% |

* Tests which exhibited a flexural failure as the primary failure mode

Table 12.5 Predicted vs. Experimental $V_u$ Values for Tests Failing in Shear

| Test # | AASHTO Standard $f_y = 62$ ksi $V_u$ (kips) | AASHTO Standard $f_y = 60$ ksi $V_u$ (kips) | AASHTO LRFD $f_y = 62$ ksi $V_u$ (kips) | Exp. $V_u$ (kips) | Percent Diff. Exp vs Std 62 | Percent Diff. Exp vs Std 60 | Percent Diff. Exp vs LRFD |
|---|---|---|---|---|---|---|---|
| G1A-Center | 138.7 | 137.4 | 103.8 | 258.0 | 86.0% | 87.8% | 148.5% |
| G1B-East | 243.3 | 238.9 | 241.1 | 312.2 | 28.3% | 30.7% | 29.5% |
| G1B-Center | 138.6 | 137.3 | 104.3 | 234.1 | 68.9% | 70.5% | 124.5% |
| G1C-East | 238.4 | 234.0 | 255.5 | 289.2 | 21.3% | 23.6% | 13.2% |
| G2A-Center | 149.5 | 148.2 | 82.3 | 255.9 | 71.2% | 72.7% | 211.0% |
| G2B-Center | 150.9 | 149.6 | 102.7 | 246.3 | 63.2% | 64.6% | 139.9% |

| | | | |
|---|---|---|---|
| G1 Average | 51.1% | 53.2% | 78.9% |
| G2 Average | 67.2% | 68.7% | 175.5% |
| G1 Std Dev | 31.3% | 31.0% | 67.5% |
| G2 Std Dev | 5.7% | 5.7% | 50.3% |

Figure 12.10 provides a plot of the data from Table 12.6 normalized by dividing the ultimate shear capacity, $V_u$, by the lightweight concrete factor, $\lambda$, and the square root of the compressive strength. Trendlines are depicted in Figure 12.9 for the AASHTO Standard[40] and LRFD[92] Specifications. The figure shows how the AASHTO[92] LRFD Specification becomes overly conservative at larger stirrup spacings where the contribution of $V_s$ is low. At closer stirrup spacings, the figure shows how the results from the Standard and LRFD specifications provide very similar results.
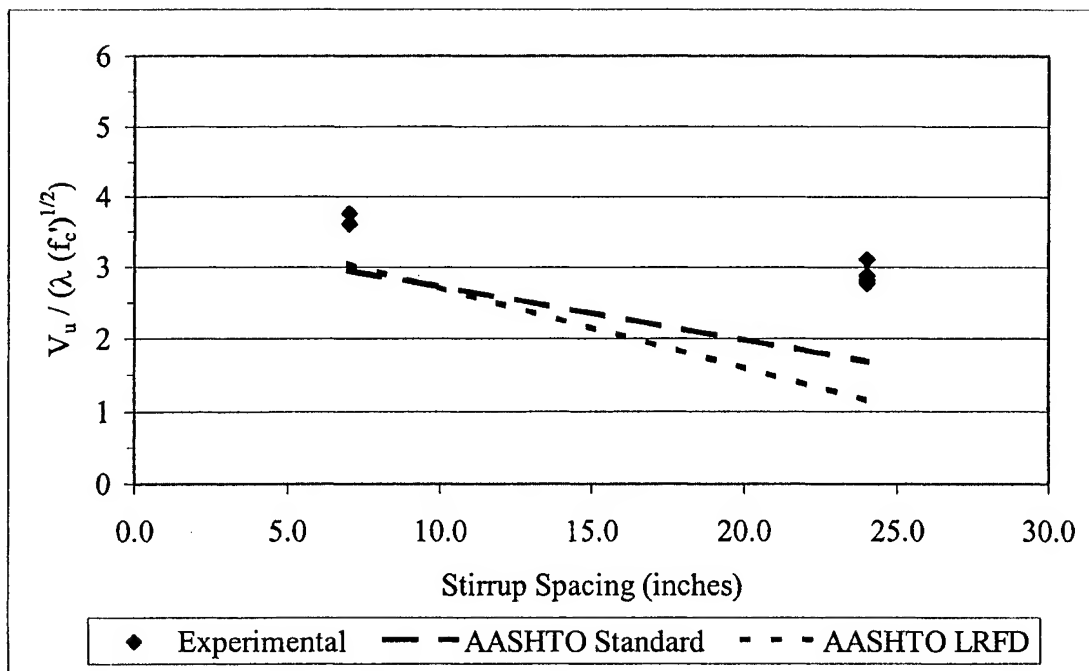
Figure 12.10 Normalized Ultimate Shear Capacity, $V_u$, vs. Stirrup Spacing

## 12.7.5 Variable Angle Truss Model

The variable angle truss model was considered as a technique for estimating the shear capacity of HSLC girders. Table 12.6 provides an overview of the results for girders failing in shear. On average for all G1 and G2 girders failing in shear, the VATM under predicted shear capacity by a significant amount. Discounting the girders having 24-inch stirrup spacing, the predictions were about 35 percent conservative on average for the G1 girders. The girders with 24-inch stirrup spacing were penalized because the VATM does not consider concrete strength in determining shear capacity.

300

Table 12.6 Variable Angle Truss Model Results

| Test # | VATM $V_n$ (kips) | Experimental $V_n$ (kips) | Percent Difference Experimental vs. VATM |
|--------|-------|---------------|------------------------------------------|
| G1A-Center | 49.6 | 258.0 | 420.1% |
| G1B-East | 223.2 | 312.2 | 39.9% |
| G1B-Center | 49.6 | 234.1 | 372.0% |
| G1C-East | 223.2 | 289.2 | 29.6% |
| G2A-Center | 49.6 | 255.9 | 416.0% |
| G2B-Center | 49.6 | 246.3 | 396.6% |

| G1 Average | | 215.4% |
|------------|--|--------|
| G2 Average | | 406.3% |

## 12.7.6 Interface Shear

There was no recorded interface shear slip during any test.

## 12.8 Conclusions

The current AASHTO Standard specification provides a conservative prediction of concrete and ultimate shear capacity when shear steel capacity is capped at a yield strength of 60 ksi. The alternate design procedure listed in ACI-318 Section 11.4.2.2 for predicting shear strength produced some unconservative predictions for concrete compressive strengths over 10,000 psi. The method for predicting interface shear strength is conservative for HSLC.

The current AASHTO LRFD specification provides a conservative prediction of ultimate strength.

The VATM provides an overconservative prediction of shear capacity in HSLC girders.

301

# CHAPTER XIII

# DEVELOPMENT LENGTH RESULTS AND DISCUSSION

## 13.1 Introduction

This chapter presents the results of the development length tests, discusses the findings and compares the behavior to predicted values and that observed by others. Based on experimentally measured transfer length values from this experimental program and others, current code provisions and equations previously suggested for predicting development length are evaluated. New equations for predicting development length are suggested based on these findings.

## 13.2 Definition

The development length is the sum of the "transfer length" and the "flexural bond length." The flexural bond length is the additional length of pretensioning strand beyond the transfer length over which bond is developed to allow the strand to reach the stress level $f_{ps}$ at the nominal flexural strength of the member. Development length can also be defined as the minimum distance from the end of the member beyond which the application of a point load will result in a flexural failure. The transfer of force from the strand to the concrete that occurs along the development length is represented in Figure 13.1.
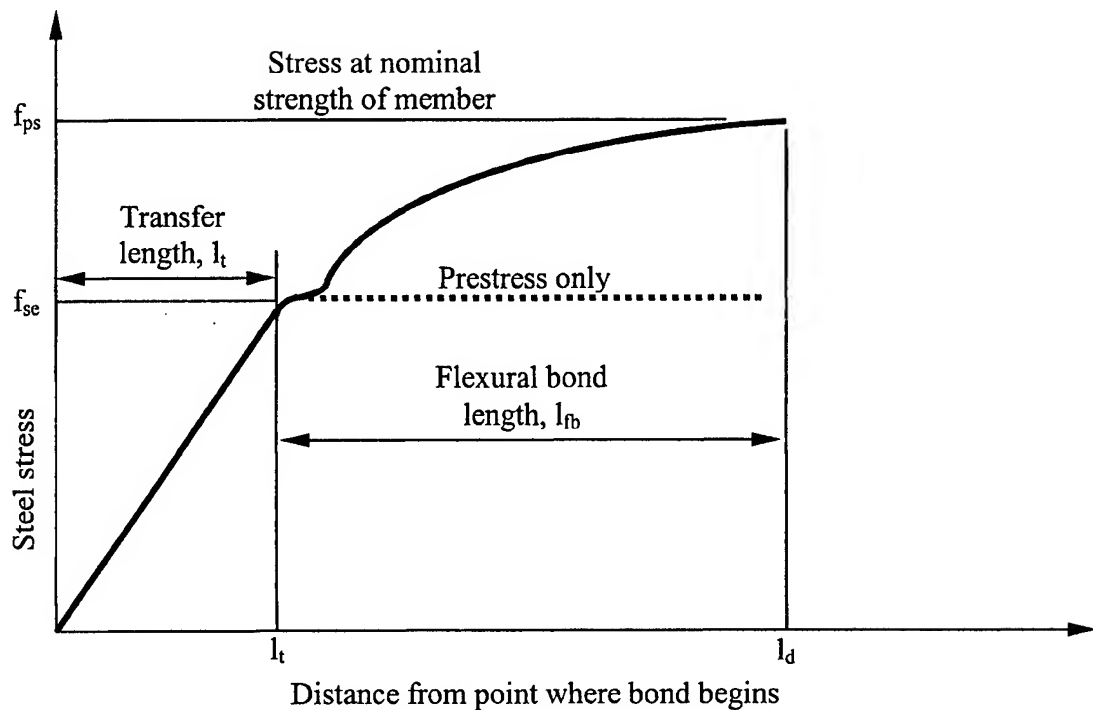
Figure 13.1  Diagram of Components of Development Length, $l_d$ [2]

The initial sloped portion of the diagram begins at a stress level of zero where

bond begins and is assumed to increase linearly over a distance equal to the transfer

length.  The dashed line indicates the effective stress level due to prestressing only ($f_{se}$).

The sloped portion of the diagram beyond the transfer length where the stress level

increases gradually to the level $f_{ps}$ is the flexural bond length.  The shape of this diagram

is codified in the AASHTO[40] and ACI[2] design specifications.   For the purpose of this

research, embedment length was defined as the distance from the girder end to the point

load.

## 13.3  Importance of Development Length

Similar to transfer length, development length will not likely be the governing design criteria on a pretensioned bridge girder. However, the development length extends three to four times farther than transfer length from the end of the member and thus impacts the girder design over a longer region. At a distance less than the development length from the end of the member, the required cracking moment is less than that at a distance greater than the development length. This change in cracking moment is important not only as a flexural design consideration, but for shear capacity as well. Shear design within the development length region must consider the variation of prestressing force.

## 13.4  Current Code Provisions

Current code provisions for determining development length are similar in form. AASHTO[40] Section 9.28.1 specifies the development length shall be determined using the Equation 13.1.

$$l_d = (f_{su}^* - \tfrac{2}{3} f_{se}) D \qquad\qquad (13.1)$$

where $f_{su}^*$ is the average stress in the prestressing steel at ultimate load in ksi, $f_{se}$ is the effective steel prestress after losses in ksi, and D is the nominal diameter of the prestressing steel in inches. Section 12.9.1 of the ACI 318 Code[2] specifies the development length shall be determined using the Equation 13.2.

$$l_d = (f_{ps} - \tfrac{2}{3}f_{se})d_b \qquad\qquad (13.2)$$

where $f_{ps}$ is the stress in the prestressed reinforcement at nominal strength in ksi, $f_{se}$ is the effective stress in the prestressed reinforcement after allowance for all prestress losses in ksi, and $d_b$ is the strand diameter in inches. Both equations produce the same prediction for development length.

## 13.5 Measurement of Development Length

Each girder end of the six Type II girders was tested for development length producing 12 sets of data. Girder end designations were the same as used in transfer length testing. In order to determine development length, the position of the point load must be varied from girder to girder. The precise development length would be where the point load resulted in concurrent flexural, shear and bond failure. If the failure mode is purely flexural, the tested embedment length is greater than the development length. If the failure mode is shear and bond failure, the tested embedment length is less than the development length. Load positioning in several locations is necessary to bracket the actual development length.

For this research, the girder ends were designed to allow the application of point loads at embedment lengths calculated as varying percentages of the current code-specified development length. The original girder design assumed $f_{ps}$ and $f_{su}{}^*$ to be 270 ksi. The values of $f_{se}$ were calculated using the standard AASHTO[40] technique as 165.02 ksi and 165.65 ksi for the G1 and G2 girders, respectively. Using these values and a strand diameter of 0.6 inches, the predicted development lengths were 96 inches and 95.7

305

inches for the G1 and G2 girders respectively. Table 13.1 shows the embedment lengths

tested as a percentage of the estimated development length values and also shows the

embedment lengths tested as a percentage of the development length calculated based on

experimentally determined values of $f_{ps}$, $f_{su}^*$, and $f_{se}$, which are listed for each girder.

Table 13.1  Embedment Lengths Tested as Percentages of AASHTO[40] Predicted Values

| Girder # | Stirrup Density 1X 2X | Embed. Length (in) | Percent of $l_d$ based on estimated values of $f_{ps}$, $f_{su}^*$, and $f_{se}$ | Experimental Values | | $l_d$ based on exp. values (in) | Percent of $l_d$ based on experimental values of $f_{ps}$, $f_{su}^*$ and $f_{se}$ |
|---|---|---|---|---|---|---|---|
| | | | | $f_{ps}$, $f_{su}^*$ (ksi) | $f_{se}$ (ksi) | | |
| G1A-E | 2X | 67 | 70 % | 265.1 | 153.7 | 97.6 | 69 % |
| G1A-W | 1X | 96 | 100 % | 265.4 | 152.3 | 105.9 | 91 % |
| G1B-E | 1X | 67 | 70 % | 227.6 | 151.2 | 106.3 | 63 % |
| G1B-W | 2X | 81 | 84 % | 266.3 | 149.8 | 106.9 | 76 % |
| G1C-E | 1X | 81 | 84 % | 263.0 | 149.0 | 107.2 | 76 % |
| G1C-W | 1X | 91 | 95 % | 264.4 | 147.6 | 107.8 | 84 % |
| G2A-E | 2X | 67 | 70 % | 266.3 | 175.8 | 96.5 | 70 % |
| G2A-W | 1X | 96 | 100 % | 266.8 | 175.7 | 96.5 | 100 % |
| G2B-E | 1X | 67 | 70 % | 265.0 | 176.2 | 96.3 | 70 % |
| G2B-W | 2X | 81 | 85 % | 266.6 | 175.6 | 96.6 | 84 % |
| G2C-E | 1X | 81 | 85 % | 267.7 | 159.3 | 103.1 | 79 % |
| G2C-W | 1X | 91 | 95 % | 266.6 | 158.8 | 103.3 | 88 % |

The value listed in the "Stirrups" column of Table 13.1 describes the amount of

shear stirrups used in the girder end. A "1X" indicates the AASHTO specified stirrup

spacing was used. A "2X" indicates that one half the AASHTO specified stirrup spacing

was used or stated otherwise, twice the amount of stirrups. The amount of stirrups is

referred to as the stirrup density. The AASHTO specified stirrup spacing is "Single

Density." One half the AASHTO specified spacing is "Double Density." As explained in Chapter 8, varying the stirrup density was designed to determine its effect on strand slip.

By determining the type of failure on each of the girder end tests, the actual development length can be bracketed into a tight range of values.

### 13.6 Development Length Test Results

One failure criteria for development length testing focused on end slip of the prestressing strands. Slip for each of the eight bottom strands was measured continually throughout girder loading as described in Chapter 10. For each data acquisition reading, an average of the eight values was calculated. If the average value exceeded 0.01 inches during the test, this was assumed to be a "bond" or "slip" type of failure. Russell[44] and Dill[82] also used this 0.01-inch slip to define a slip condition. This type of failure was often termed "shear-slip" because it was believed that the formation of a shear crack was the trigger for strand slip to begin. As discussed in Chapter 12, shear failure was always associated with slip at the girder ends. If the value did not exceed 0.01 inches, and girder end failed in flexure. For a failure to be considered a flexural failure, yielding of the prestressing strands and crushing of the deck had to occur.

CSS data were also collected after each load step. The CSS data were used to track the level of stress in the cross section and the location of cracks occurring in the first 48 inches of the girder. Perfect bond between the strand and concrete was assumed so that the concrete surface strains were equated to added strain in the strands. Table 13.2 provides the results of development length testing.

Table 13.2  Development Length Test Results

| Test #<br>E=East<br>W=West | Stirrup<br>Density<br>1X<br>2X | Strand<br>Embedment<br><br><br>(inches) | Average<br>Strand<br>Slip<br>at $P_{max}$<br>(inches) | Maximum<br>Strand<br>Strain<br>$\varepsilon_{ps}$<br>(in/in) | Maximum<br>Deck<br>Strain<br>$\varepsilon_{cu}$<br>(in/in) | Failure Mode<br>FL-Flexure<br>SH-Shear<br>SL-Strand Slip |
|---|---|---|---|---|---|---|
| G1A-E | 2X | 67 | 0.0102 | 0.0158 | 0.0038 | FL/SH-SL |
| G1A-W | 1X | 96 | 0.0000 | 0.0168 | 0.0042 | FL |
| G1B-E | 1X | 67 | 0.7350 | 0.0078 | 0.0030 | SH-SL |
| G1B-W | 2X | 81 | 0.0007 | 0.0190 | 0.0032 | FL |
| G1C-E | 1X | 81 | 0.1988 | 0.0113 | 0.0032 | SH-SL/FL |
| G1C-W | 1X | 91 | 0.0000 | 0.0140 | 0.0036 | FL |
| G2A-E | 2X | 67 | 0.0033 | 0.0190 | 0.0036 | FL |
| G2A-W | 1X | 96 | 0.0000 | 0.0204 | 0.0072 | FL |
| G2B-E | 1X | 67 | 0.0065 | 0.0155 | 0.0045 | FL |
| G2B-W | 2X | 81 | 0.0000 | 0.0199 | 0.0064 | FL |
| G2C-E | 1X | 81 | 0.0041 | 0.0228 | 0.0045 | FL |
| G2C-W | 1X | 91 | 0.0000 | 0.0198 | 0.0049 | FL |

### 13.6.1  Notes on Development Length Test Results

In girder tests G1A-East, G2A-East and G2B-East the flexural failure was accompanied by the deck splitting longitudinally down the middle as shown in Figure 13.2. The failure mode of Girder G1A-E is listed as FL/SH-SL. This indicates that the girder exhibited both flexural and shear-slip modes with the flexural mode occurring most predominantly. The failure mode of Girder G1C-E is listed as SH-SL/FL. This also indicates the girder exhibited both flexural and shear-slip modes, but the shear-slip mode was predominant. Girders listing just FL exhibited only flexural failure characteristics. Shear cracking occurred in all tests.

Figure 13.2  Longitudinal Cracking in Deck of Girder G1A-East

### 13.6.2  Development Length for G1 Girders

In order to evaluate the development length test results, strand end slip was

graphed against embedment length.  Since only selected embedment lengths were tested,

it was not possible to exactly pinpoint the development length.  It was possible, however,

to identify points at which the failure transitioned from flexure to shear-slip.  Figure 13.3

shows a bar graph for all G1 girders.  The G1 1X bar graphs for the 67 and 81-inch

embedment length strand slip results were limited to 0.02 inches to better show the 2X

bar graph results. The table below the bar graph shows the actual strand slip values.



| | 67 | 81 | 91 | 96 |
|---|---|---|---|---|
| ■ G1 1X Stirrups | 0.7350 | 0.1988 | 0.0000 | 0.0000 |
| ▨ G1 2X Stirrups | 0.0102 | 0.0007 | | |

Strand Embedment Length (in)
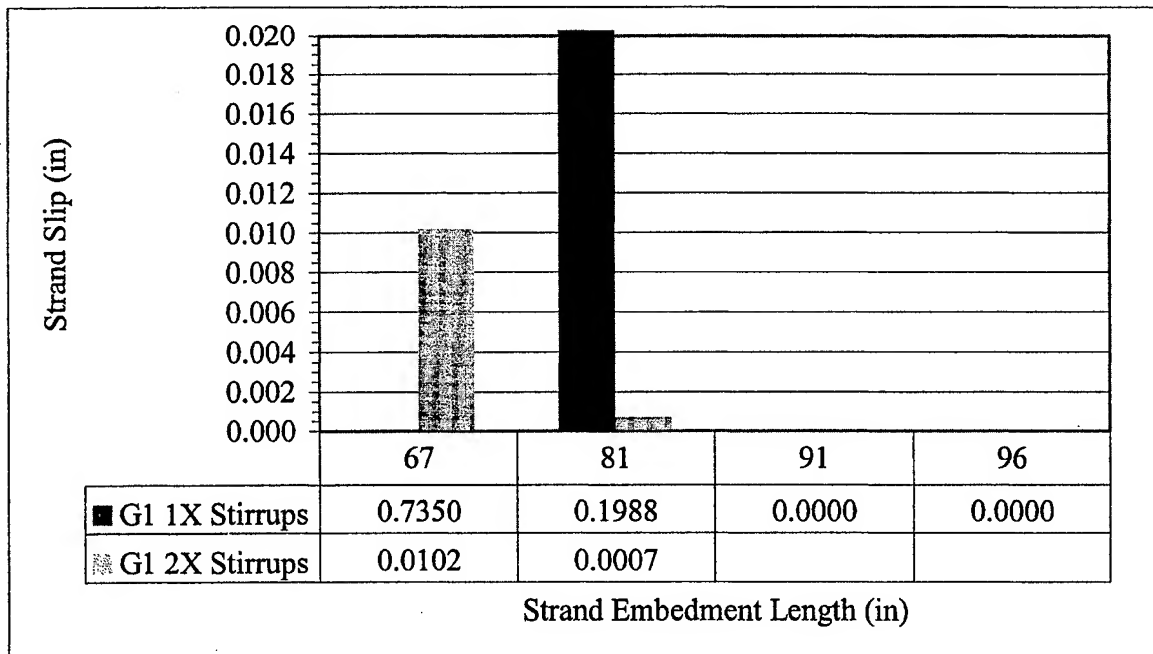
Figure 13.3  G1 Series Girder Average Strand End Slip vs Embedment Length Values

Figure 13.3 shows the development length for G1 series girders with single

density stirrups to be greater than 81 inches, but less than 91 inches. Since at an

embedment length of 81 inches, the level of average end slip exceeds the 0.01-inch limit,

the actual development length must be greater than 81 inches. At an embedment length

of 91 inches, the level of average slip is less than 0.01 inches; thus the actual

development length must be less than 91 inches. Without test data to fill the void

between 81 and 91 inches, the conservative conclusion is that the development length for

G1 series girders with single density stirrups was 91 inches.

A similar analysis for G1 series girders with double density stirrups indicates a development length greater than 67 inches but less than 81 inches. Again, without other data, a conservative conclusion is that the development length was 81 inches.

### 13.6.3 Development Length for G2 Girders

Figure 13.4 shows a bar graph for all G2 girder tests that compares average strand end slip with embedment length.

| | 67 | 81 | 91 | 96 |
|---|---|---|---|---|
| ■ G2 1X Stirrups | 0.0065 | 0.0041 | 0.0000 | 0.0000 |
| G2 2X Stirrups | 0.0033 | 0.0000 | | |

Strand Embedment Length (in)
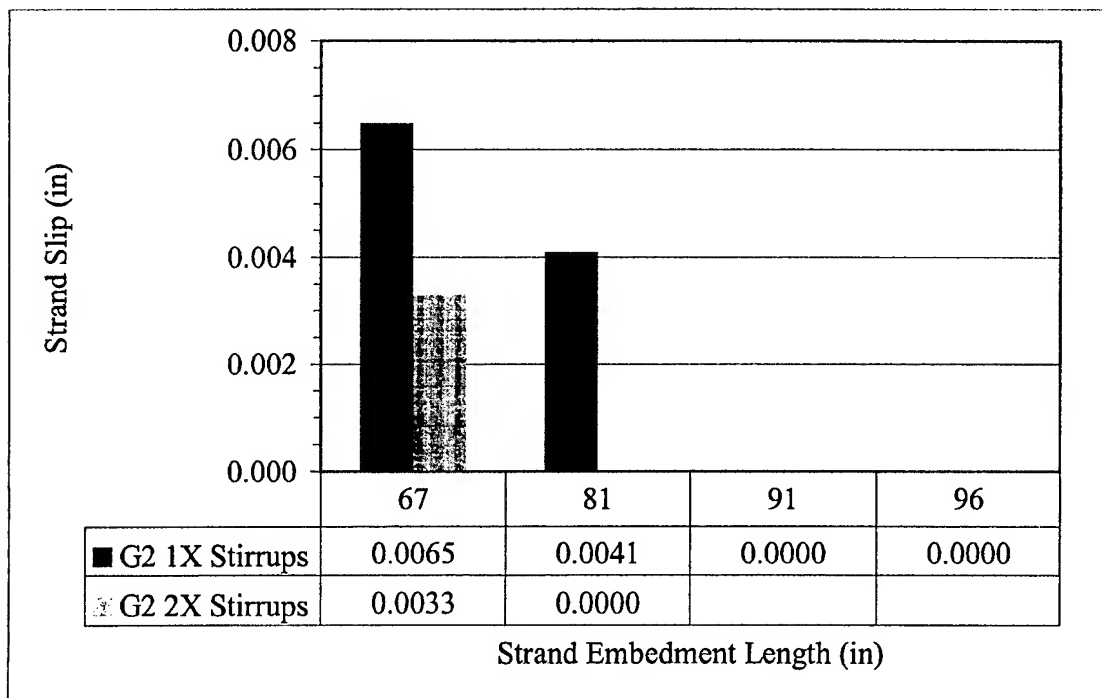
Figure 13.4 G2 Series Girder Average Strand End Slip vs Embedment Length Values

No G2 series girder test exceeded the end slip limit of 0.01 inches. Again, without additional test data to provide conclusive results for embedment lengths less than 67 inches, the conservative conclusion is that the development length for G2 series girders was 67 inches for both single and double density stirrups.

Table 13.3 provides a consolidated listing of development lengths.

Table 13.3  Experimentally Determined Development Lengths (inches)

| Girder Series | Single Stirrup Density (1X) | Double Stirrup Density (2X) |
|---|---|---|
| G1 | 91 | 81 |
| G2 | 67 | 67 |

## 13.7  Discussion of Results

### 13.7.1  Strand Stress Plots

This section addresses the level of strand stress determined based on CSS data. Each strand stress plot provides a depiction of the effective level of prestress over the entire embedment length, a plot of the strand stress over the first 48 inches of the girder when the strand was at its yield stress at the point of loading, and a plot of strand stress over the first 48 inches of the girder when the strand was at its maximum stress at the point of loading. A complete listing of photographs and strand stress graphs for each development length test is found in Appendix Q.

### 13.7.1.1  Strand Stress Plots When End Slip Occurred

If significant strand end slip over occurred during the test, it was impossible to accurately estimate what the level of stress was at a point along the strand based on CSS data. Strand end slip indicates there is a lack of adequate bond between the strand and concrete; near perfect bond is necessary for CSS to be a meaningful predictor of an increase in strand stress. A telling depiction of the effect of strand end slip can be seen in Figure 13.5 for test G1B-East, which shows the stress level in the strand to be 260 ksi

near the end of the girder and only 227 ksi at the point of load application. Extensive

shear cracking in the transfer length region during test G1B-East initiated a strand slip

failure resulting in strand end slip of 0.75 inches. The slip allowed the shear cracks to

expand causing CSS values in that region to become extremely large. When used to

predict strand strain, the values were found to be erroneous.
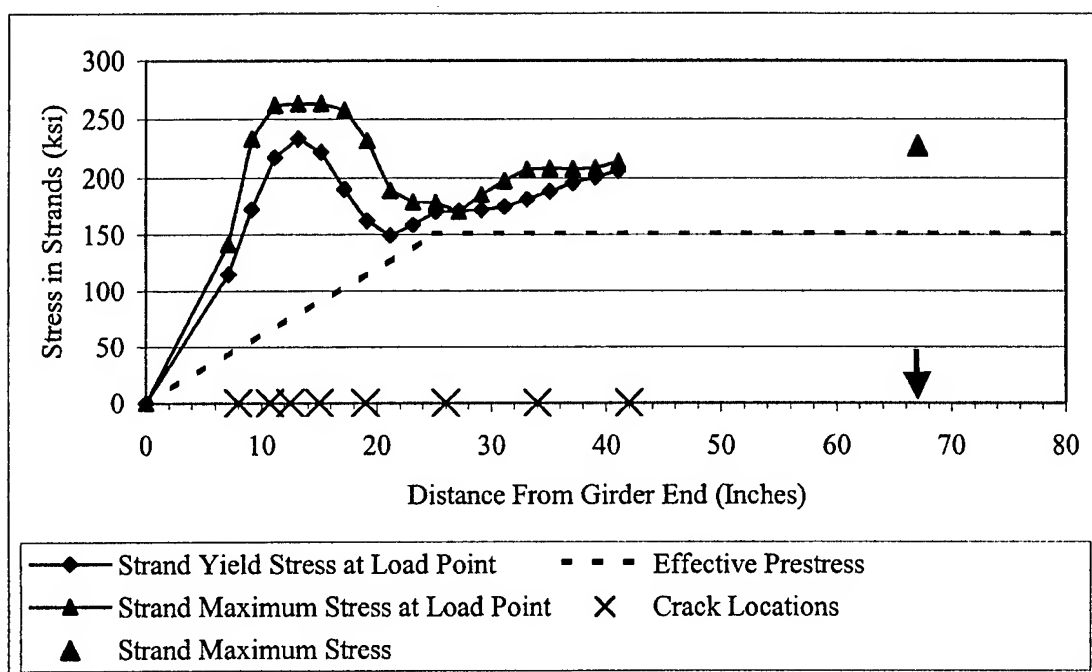


Figure 13.5  G1B-East Strand Stress vs. Distance from Girder end

## 13.7.1.2 Strand Stress Plots Where End Slip Was Less Than 0.01 Inches

In tests where strand slip was less than 0.01 inches, the CSS data appeared

consistent and was used to determine the strain and the stress in the prestressing strand.

Two trends became evident in examining these plots. First, in every case where strand

slip was under 0.01 inches, there was an observed increase in strand stress in the transfer

length region above the level of effective prestress. The effect was far more pronounced

313

with shorter embedment lengths. Second, in some cases, the length over which the largest amount of prestressing force was transferred appeared to be a distance somewhat less than the original transfer length discussed in Chapter 9. Figure 13.6 shows test G1A-East as an example of the strand stress increase in the transfer length region as well as the apparent reduction in transfer length. The embedment length on this test was only 67 inches. The "lone" triangle plots the maximum stress in the strand at the point of loading at the girder's ultimate load. This actual plot of strand stress differs significantly from the theoretical diagram shown in Figure 13.1.
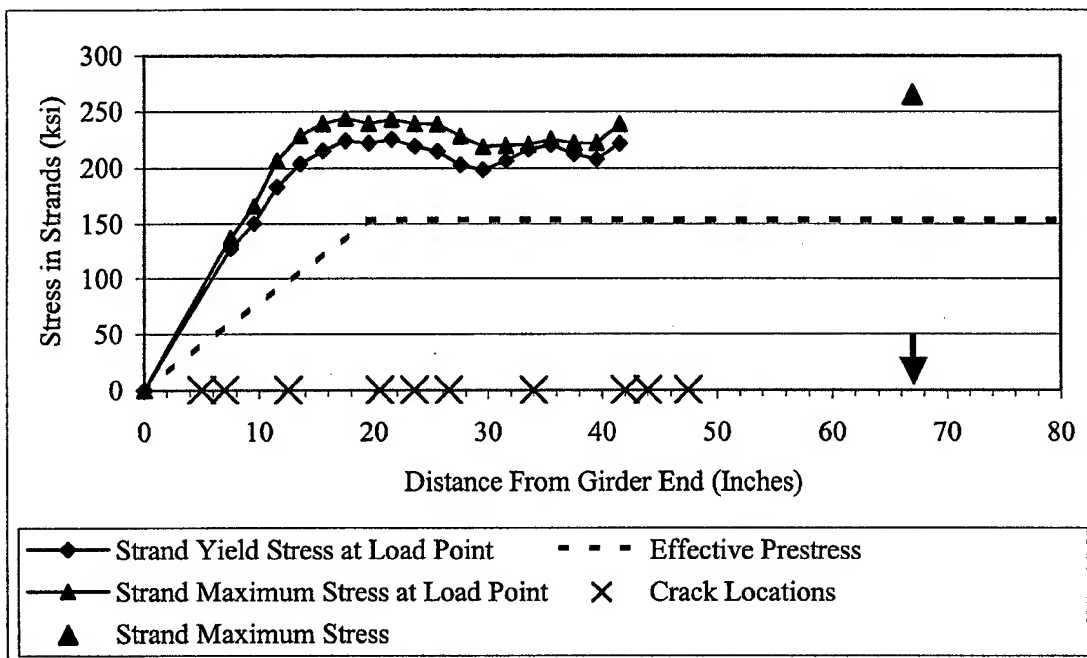


Figure 13.6 G1A-East Strand Stress vs. Distance from Girder End

The variable angle truss model concept discussed in Chapter 12, Shear Behavior Results and Discussion, required a high strand force at the end of the girders with low shear span-to-depth ratios or low values of embedment length. The high stress values

314

developed in the transfer length zone for the girders with embedment lengths of 67 and 81 inches correspond to the compression strut requirement.

Figure 13.7 shows test G2C-West, which resulted in a much less pronounced example of stress increase in the transfer length region. In this example, the embedment length was 91 inches. The strand stress increased above the level of effective prestress, but not to the extent seen in Figure 13.6. The apparent transfer length remained about the same. The dip in the stress plot in Figure 13.7 was based on a lack of cracking in the region of the girder between 12 and 40 inches from the girder end. Cracking across the DEMEC embedment line caused large increases in the CSS values read.
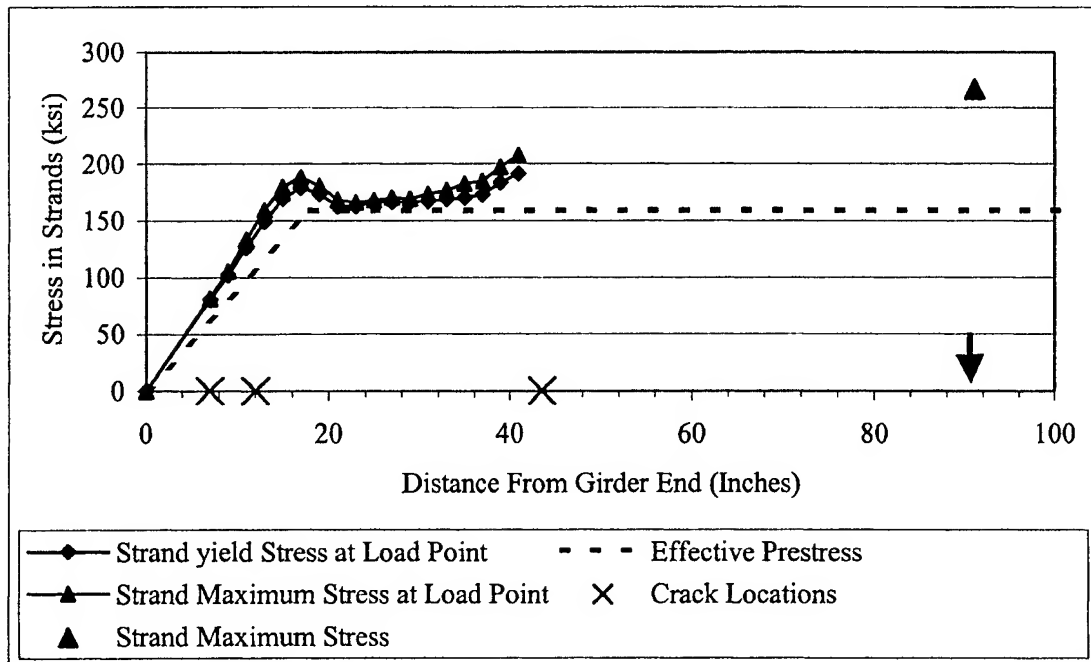


Figure 13.7  G2C-West Strand Stress vs. Distance from Girder End

### 13.7.2  Strand Slip vs. Shear Cracking

A comparison was made between the onset of shear cracking and strand slip. The comparison was accomplished by examining the plot of applied shear vs. average end slip to determine the applied shear at which slip initiated and comparing that shear value to cracks on the girder. This comparison was made for all tests where the initiation of end slip could be determined. Figure 13.8 shows an applied shear vs. average strand end slip for test G1A-East; diagram has a well-defined slip initiation point. Several tests produced slip diagrams as in Figure 13.9 where it was not possible to determine an end slip initiation point. Based on this level of scatter in the data, any average slip value less than 0.0006 inches was considered zero slip. Figure 13.8 also shows an increase in strand end slip as the girder was unloaded. This phenomenon was seen in several tests and appeared to relate to a clamping effect on the prestressing strand. With the ultimate load on the girder, the end reactions were at a maximum and tended to clamp the strand. As the girder was unloaded, this clamping action was reduced. As the reaction decreased, additional slip occurred. This phenomenon only occurred in tests where slip was greater than 0.0006 inches. This unloading end slip was not included in the average maximum slip values recorded. Appendix R presents all applied shear vs. average strand slip diagrams.
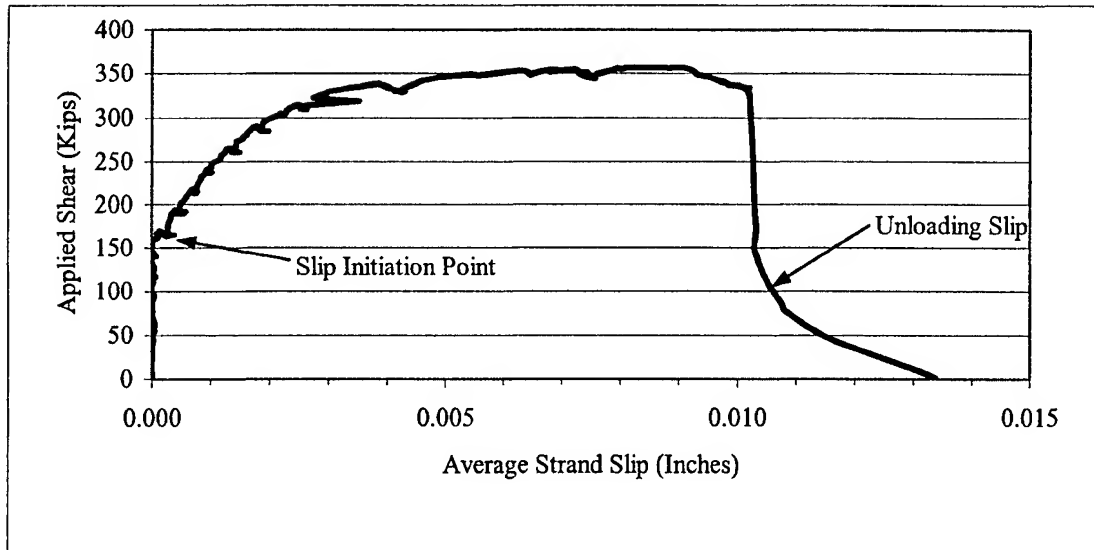
Figure 13.8 Applied Shear vs. Strand Slip (G1A-East) Showing Slip Initiation Point
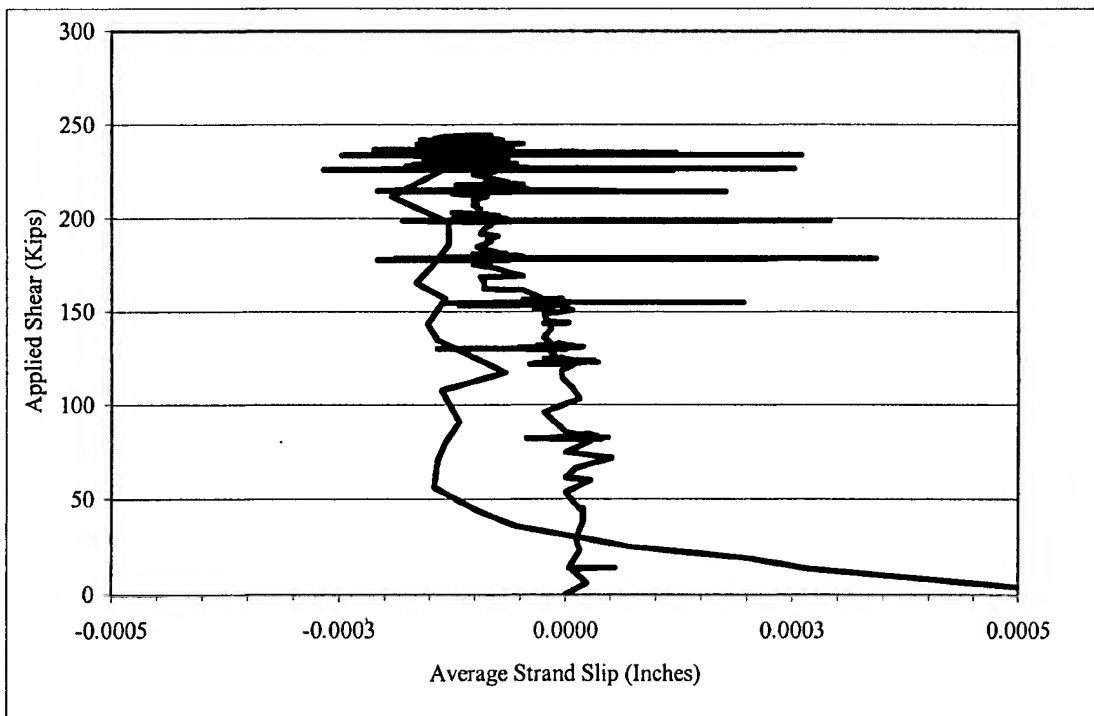


Figure 13.9 Applied Shear vs. Strand End Slip (G2C-West) Showing NO Slip Initiation

317

Figure 13.10 shows typical CSS data corresponding with applied shear levels, the location of shear cracks crossing the bottom strands, and the transfer length region. CSS data was plotted because it provided a measure of crack growth and allowed identification of the cracks that were increasing most significantly in size. Comparing crack locations with the resulting end slip allowed determination of the region where shear cracking most significantly impacted strand slip. Based on crack location, a comparison was made between strand slip in girders with single and double density shear reinforcement. Similar graphs for each girder test are listed in Appendix R.
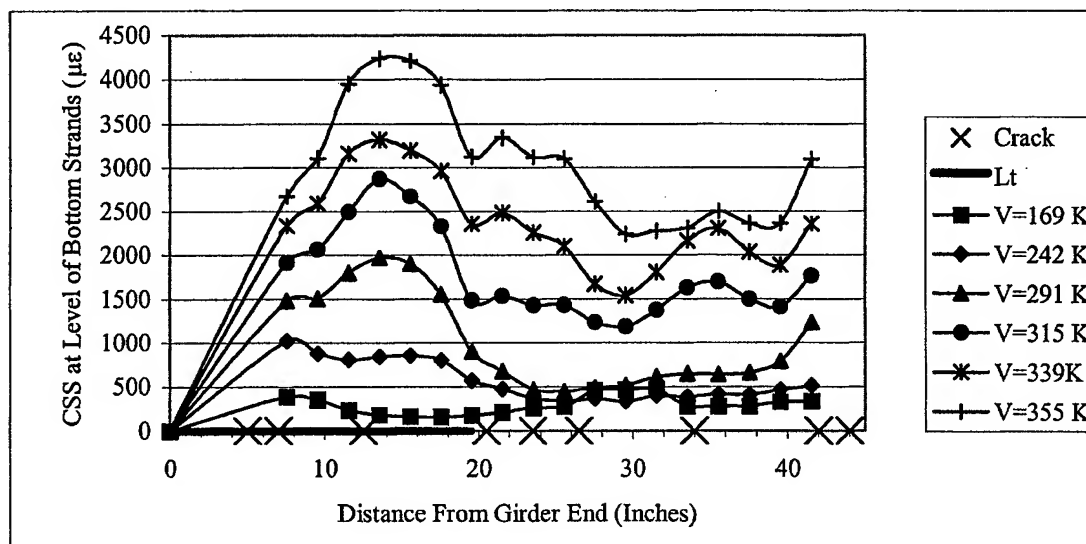


| Shear Crack Data | | | | | | | | | |
|---|---|---|---|---|---|---|---|---|---|
| Distance From End (Inches) | 5.0 | 7.0 | 12.5 | 20.5 | 23.5 | 26.5 | 34.0 | 42.0 | 44.0 | 47.5 |
| Applied Shear at Cracking (Kips) | 169 | 315 | 242 | 339 | 315 | 355 | 339 | 339 | 291 | 355 |

Figure 13.10 G1A-East CSS and Shear Cracking vs. Distance from Girder End

### 13.7.2.1 Results for Single Stirrup Density (1X)

Table 13.4 Applied Shear vs. Strand Slip Results for Single Stirrup Density

| Test # | Strand Embedment $l_e$ ($l_t$) (Inches) | Applied Shear At Crack Formation (Max Applied Shear) (Kips) | Shear Crack Distance From Girder End (Inches) | Average Strand Slip at Applied Shear (Maximum Average Slip Recorded) (Inches) |
|---|---|---|---|---|
| G1B-East | 67 (25) | 156 191 208 277 295 (302) | 8 10.75 12.5 42 15, 19, 26, 34 | No Slip 0.0006 0.0009 0.0138 0.0441 0.2133 (0.7350) |
| G1C-East | 81 (28) | 147 243 261 277 (282) | 9 17 14, 20, 30 39 | No Slip 0.0034 0.0126 0.0431 0.0944 (0.1988) |
| G2B-East | 67 (13) | 177 225 299 322 344 (349) | 4 10 37, 43.5 13.5 30 | No Slip 0.0008 0.0020 0.0034 0.0053 0.0060 (0.0065) |
| G2C-East | 81 (19) | 143 215 281 (294) | 7 15 27.5, 34, 42 | No Slip No Slip No Slip 0.0022 (0.0041) |

Table 13.4 shows the results of examining the onset of strand slip in the development length tests with single stirrup density. The "Applied Shear at Crack Formation" column specifies the level of applied shear at which a specific crack formed across the bottom layer of strands. In the same column is also listed the maximum

319

applied shear reached during the test. The "Shear Crack Distance From Girder End" column specifies the distance the crack across the lower strands is from the end of the girder. The "Average Strand Slip at Applied Shear" column lists the strand end slip at the listed applied shear value. Also listed in the column is the value of the maximum average strand slip recorded.

Table 13.4 shows that in every case, a shear crack passing through the level of the bottom strands within the transfer length region initiated or dramatically increased strand end slip. When examining the result of a crack, one must look to the resulting end slip on the following line. For example, during test G1B-East, the recorded slip at an applied shear of 208 kips was 0.0009 inches. The next recorded slip value was 0.0138 inches at an applied shear of 277 kips. This was a fifteen-fold increase in end slip initiated by the formation of the crack at 12.5 inches from the girder end. Similar results were evident when cracks formed at 15, 19, 26, and 34 inches from the girder end at an applied shear of 295 kips. The resulting slip of 0.2133 measured at the maximum applied shear of 302 kips showed a five-fold increase in end slip. Test G1C-East showed a four-fold increase in end slip after the formation of a crack at 17 inches from the girder end, and a three-fold increase after the formation of cracks at 14, 20 and 30 inches from the girder end. Tests G2B-East and G2C-East also showed similar increases in end slip after cracking occurred in or near the transfer length region. Although neither test resulted in a shear-slip failure, the impact of transfer length region cracking is evident.

### 13.7.2.2 Results for Double Stirrup Density (2X)

Table 13.5  Applied Shear vs. Strand Slip Results for Double Stirrup Density

| Test # | Strand Embedment $l_e$ $(l_t)$ (Inches) | Applied Shear At Crack Formation (Max Applied Shear) (Kips) | Shear Crack Distance From Girder End (Inches) | Average Strand Slip at Applied Shear (Maximum Average Slip Recorded) (Inches) |
|---|---|---|---|---|
| G1A-East | 67 (19.5) | 169 242 291 315 339 355 (357) | 5 12.5 44 7, 23.5 20.5, 34, 42 26.5, 47.5 | No Slip 0.0010 0.0018 0.0025 0.0039 0.0072 0.0082 (0.0102) |
| G1B-West | 81 (18.75) | 243 266 286 (289) | 5 7.5, 12 29, 39.5, 42.5 | No Slip No Slip No Slip No Slip (No Slip) |
| G2A-East | 67 (17.5) | 245 318 343 355 (361) | 7.5 34, 39.5 14.5, 23 11, 46 | No Slip No Slip 0.0007 0.0017 0.0030 (0.0033) |
| G2B-West | 81 (13) | 201 226 251 279 (286) | 6 8 10, 14, 45 18.5, 32, 41.5 | No Slip No Slip No Slip No Slip (No Slip) |

Table 13.5 provides the results for girder ends having double stirrup density.  The order of listing in Table 13.5 compares directly with the order in Table 13.4:  the concrete grade and embedment lengths match.  Direct comparison shows that the resulting slips were much less than the single density stirrups.  The only double density stirrup test that

underwent a shear-slip greater than 0.01 inches was G1A-East with a slip of 0.0134

inches. For the G1 series girders, doubling the stirrup density dramatically reduced end

slip values. For the G2 series girders, the effect was much less pronounced; however, the

increased density did reduce end slip.

### 13.7.2.3 Results for Other Single Stirrup Density Tests

It was not possible to perform an analysis of shear cracking vs. strand slip for

girder tests G1A-West, G1C-West, G2A-West and G2C-West since no strand slip

occurred.

### 13.7.3 Shear Crack Location

Shear cracking across the bottom strands within the transfer length region

initiated large increases in strand end slip. Other researchers have reported this

phenomenon.[44] Despite several shear cracks in the transfer length region, tests G1B-

West and G2B-West showed no slip because of the double stirrup density. Tests G1A-

East and G2A-East showed slip, but at very small or almost acceptable levels. Russell[44]

reported that additional bond stresses can be developed beyond initial strand slip and that

small slips are not always followed by complete anchorage failure. Russell[44] also

reported that closely spaced cracks were an indication of good bond and wide crack

spacing indicated poor bond. Both of Russell's observations were confirmed in the

present tests.

### 13.7.4 Effect of Concrete Grade

Concrete grade also played a significant role in determining development length. Table 13.3 clearly demonstrates a reduction in development length based on concrete grade alone. The G1 series girders had compressive strengths on average approximately 1500 psi less than the G2 series girders. The water cement ratios were approximately 0.29 for the G1 series girders and 0.23 for the G2 series girders. A significant difference between the two mix designs was the amount of silica fume. The G1 series girders had 2 percent silica fume by weight of the total cementitious materials, and the G2 series girders had 10 percent. Past researchers have stated that the addition of silica fume will significantly improve the tensile strength and bond of lightweight concrete to prestressing strand.[21,94,95] The results of the present research confirm this observation.

### 13.7.5 Bond Stress Examined with the Variable Angle Truss Model

The VATM was discussed in Chapter 12 as a technique for predicting girder shear capacity. Another use for the VATM was the evaluation of bond stress at the girder end, the calculation of which was addressed in Section 12.5.8. Figure 13.11 shows a typical plot of bond stress from girder test G1C-East, a shear failure. Table 13.6 provides an overview of bond stress predictions using the VATM for all girder end tests and compares them to strand slip that occurred during development length testing. The "Bond Stress at Ultimate-VATM" value was taken as the maximum bond stress value within the transfer length region as labeled in Figure 13.11. Appendix N provides strand force and bond stress plots for girder tests G1A-East, G1B-East, and G1C-East, those tests that resulted in development length failures due to excessive strand slip.

323
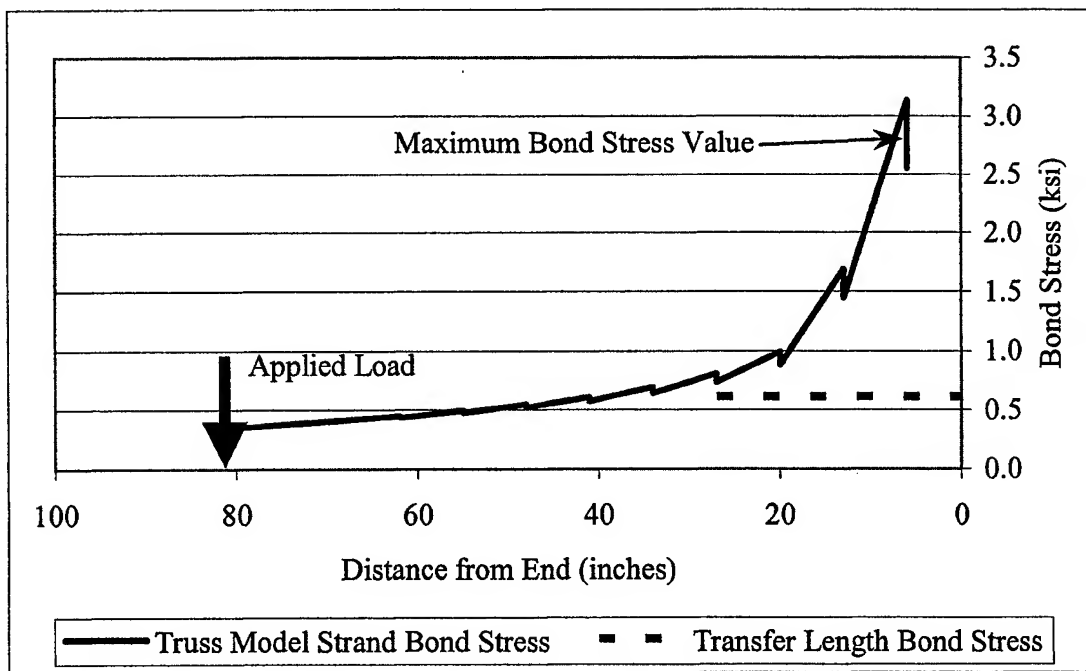
Figure 13.11  Bond Stress Plot Using VATM for Girder G1C-East

Only data from the girder-end tests was provided since strand slip and bond stress were not a problem in center-span tests. Table 13.6 shows that the VATM predicted higher bond stresses for those girder ends that underwent strand slip failures. Examining average VATM bond stress values, it was evident that the model was predicting higher bond stress values for the girder ends undergoing strand slip failures. For the G1 girders, the average bond stress from all tests was 2.55 ksi; the average bond stress for G1 girders not undergoing strand slip was 1.88 ksi. For the G2 girders, there was a wide scatter of bond stress predictions. Since no G2 girder failed due to strand slip, it was not possible to determine a bond stress above which slip would occur. It appeared the VATM was useful for verifying trends, but not for making predictions.

Table 13.6 VATM Bond Stress Prediction vs. Strand Slip Results

| Test # | Bond Stress At Transfer (ksi) | Bond Stress At Ultimate VATM (ksi) | Average Maximum Strand Slip (inches) | Status of Development Length Test |
|---|---|---|---|---|
| G1A-East * | 0.91 | 1.98 | 0.0102 | FAIL |
| G1A-West | 0.94 | 1.77 | 0.0000 | PASS |
| G1B-East | 0.70 | 3.92 | 0.7350 | FAIL |
| G1B-West * | 0.92 | 0.77 | 0.0007 | PASS |
| G1C-East | 0.62 | 2.84 | 0.1988 | FAIL |
| G1C-West | 0.80 | 2.10 | 0.0000 | PASS |
| G2A-East * | 1.16 | 2.02 | 0.0033 | PASS |
| G2A-West | 1.54 | 1.89 | 0.0000 | PASS |
| G2B-East | 1.57 | 4.02 | 0.0065 | PASS |
| G2B-West * | 1.56 | 0.92 | 0.0000 | PASS |
| G2C-East | 0.97 | 2.89 | 0.0041 | PASS |
| G2C-West | 1.02 | 2.28 | 0.0000 | PASS |

| | | |
|---|---|---|
| G1 Average All Tests | 0.82 | 2.23 |
| G2 Average All Tests | 1.30 | 2.34 |
| G1 Average Passing Tests | | 1.55 |
| G2 Average Passing Tests | | 2.34 |

* Indicates Double Stirrup Density

## 13.8 Comparison of Results with Code Provisions and Proposed Equations

This section compares the development length results from this research with development lengths predicted by code specified provisions and with predictive equations proposed by other researchers. The goal of these comparisons was to determine if the code equations were adequate for design of slate HSLC girders and which variables provided the best prediction of development length. For comparison purposes, the twelve

325

development length values found from this HSLC research were evaluated along with

eight values from a previous normal weight HPC study by Dill[84] to determine what

differences, if any, existed between HSLC and HPC. All development length tests used

0.6-inch diameter prestressing strand.

### 13.8.1 Material Properties and Prestressing Strand Stresses

Table 13.7 lists material properties and prestressing strand stresses for the twenty

development length tests. Included are concrete strengths at release, $f_{ci}'$, and at time of

testing, $f_c'$; strand stress values at time of prestressing, $f_{pt}$, just after strand release, $f_{si}$, just

prior to girder testing, $f_{se}$, and at ultimate load, $f_{ps}$. Accelerated cure strengths were used

for $f_{ci}'$ (24-hour) and for $f_c'$ (time of testing). Based on the evaluation of transfer length

data, the accelerated cure strengths provided more consistent data. Strand load cells were

used to measure strand stresses at the time of tensioning. Strand strain measurements

after release and prior to testing were done with a VWSG. Strand strain at ultimate load

was determined by measuring CSS with an LVDT, adding that strain to the strain due to

effective prestress, and converting the total strand strain to a stress using the strand's

stress-strain curve. Again, based on the evaluation of transfer length data, it was found

that VWSG data provided a good estimate of strand stress values. Work by Reutlinger[37]

used VWSG data for strand stress calculation; the use of VWSG data from this research

helped maintain consistency for this evaluation.

Table 13.7 Concrete Strengths and Prestressing Levels

| Girder # | Develop-ment Length (Inches) | $f_{ci}'$ (psi) | $f_c'$ Prior to Testing (psi) | $f_{pt}$ Before Release (ksi) | $f_{si}$ After Release VWSG (ksi) | $f_{se}$ Prior To Testing VWSG (ksi) | $f_{ps}$ at Ultimate Load CSS (ksi) |
|---|---|---|---|---|---|---|---|
| G1A-E | 81 | 7465 | 9580 | 179 | 162 | 154 | 266 |
| G1A-W | 91 | 7465 | 9580 | 179 | 162 | 152 | 266 |
| G1B-E | 91 | 7465 | 9580 | 179 | 161 | 151 | 266 |
| G1B-W | 81 | 7465 | 9580 | 179 | 161 | 150 | 266 |
| G1C-E | 91 | 6315 | 8911 | 179 | 162 | 149 | 266 |
| G1C-W | 91 | 6315 | 8911 | 179 | 162 | 148 | 266 |
| G2A-E | 67 | 9640 | 10975 | 191 | 179 | 176 | 266 |
| G2A-W | 67 | 9640 | 10975 | 191 | 179 | 176 | 266 |
| G2B-E | 67 | 9640 | 10975 | 191 | 179 | 176 | 266 |
| G2B-W | 67 | 9640 | 10975 | 191 | 179 | 176 | 266 |
| G2C-E | 67 | 8261 | 10523 | 179 | 165 | 159 | 266 |
| G2C-W | 67 | 8261 | 10523 | 179 | 165 | 159 | 266 |
| G2A-S* | 80 | 14989 | 16770 | 191 | 178 | 170 | 275 |
| G2A-N* | 80 | 12379 | 13430 | 191 | 178 | 170 | 275 |
| G2B-S* | 80 | 12379 | 13430 | 191 | 177 | 169 | 275 |
| G2B-N* | 80 | 11721 | 12716 | 191 | 177 | 169 | 275 |
| G4A-S* | 80 | 14675 | 16418 | 191 | 179 | 171 | 275 |
| G4A-N* | 80 | 14395 | 16105 | 191 | 179 | 171 | 275 |
| G4B-S* | 80 | 14395 | 16105 | 191 | 179 | 170 | 275 |
| G4B-N* | 80 | 14610 | 16345 | 191 | 179 | 170 | 275 |

* Tests done by Reutlilnger[37]

## 13.8.2 Code and Suggested Development Length Equations

Development lengths were predicted using 12 different techniques. Table 13.8 provides an overview of the equations examined. The equation number listed refers to the discussion of the equation in Chapter 2, Background Review.

Table 13.8  Summary of Development Length Equations

| Source / Author of Equation | Development Length, $l_d$ | Equation Number |
|---|---|---|
| AASHTO[40] / ACI[2] | $(f_{ps} - \frac{2}{3}f_{se})d_b$ | 2.16 |
| Barnes, Burns and Kreger[55] | $1.25\left(\dfrac{f_{pt}}{\sqrt{f_{ci}'}} + (f_{ps} - f_{pe})\right)d_b$ | 2.27 |
| Buckner[46] | $f_{si}\dfrac{d_b}{3} + \lambda\,(f_{su} - f_{se})d_b$ | 2.23 |
| Deatherage et al.[43] | $f_{si}\dfrac{d_b}{3} + 1.5(f_{su} - f_{se})d_b$ | 2.20 |
| Lane 95%[47] | $\left(\dfrac{4f_{pt}d_b}{f_c'} - 5\right) + \left(\dfrac{6.4(f_{su} - f_{se})d_b}{f_c'} + 15\right)$ | 2.26 |
| Lane 95%[47] (10 ksi limit on $f_c'$) | $\left(\dfrac{4f_{pt}d_b}{f_c'} - 5\right) + \left(\dfrac{6.4(f_{su} - f_{se})d_b}{f_c'} + 15\right)$ | 2.26 |
| Lane Mean[47] | $\left(\dfrac{4f_{pt}d_b}{f_c'} - 21\right) + \left(\dfrac{6.4(f_{su} - f_{se})d_b}{f_c'} + 26\right)$ | 2.25 |
| Lane Mean[47] (10 ksi limit on $f_c'$) | $\left(\dfrac{4f_{pt}d_b}{f_c'} - 21\right) + \left(\dfrac{6.4(f_{su} - f_{se})d_b}{f_c'} + 26\right)$ | 2.25 |
| Martin and Scott[41] | $\left(f_{ps} - \dfrac{135}{d_b^{1/6}}\right)\dfrac{d_b}{0.39}$ | 2.18 |
| Mitchell et al.[45] | $0.33 f_{si}\,d_b\sqrt{\dfrac{3}{f_{ci}'}} + (f_{su} - f_{se})d_b\sqrt{\dfrac{4.5}{f_c'}}$ | 2.22 |
| Zia and Mostafa[42] | $\left(1.5\dfrac{f_{si}}{f_{ci}'}d_b - 4.6\right) + 1.25(f_{su} - f_{se})d_b$ | 2.19 |

$d_b$      Prestressing strand diameter

$f_{pt}$      Stress in prestressing strand prior to release

$f_{si}$      Stress in prestressing strand immediately after release ($f_{pt}$-ES)

$f_{se}$      Stress in prestressing strand after all losses ($f_{pt}$-ES-CR-SH)

$f_{pe}$      Same as $f_{se}$

$f_{ps}$      Stress in prestressing strand at member nominal strength

$f_{su}$      Ultimate stress of prestressing strand

| ES | Prestress losses due to elastic shortening |
|---|---|

ES    Prestress losses due to elastic shortening

CR    Prestress losses due to creep

SH    Prestress losses due to shrinkage

$f_{ci}'$    Concrete compressive strength at release

$f_c'$    Concrete compressive strength at time of testing

$M_n$    Nominal moment capacity of a member

$M_{cr}$    Cracking moment capacity of a member

$I_t$    Transformed moment of inertia of a member

$\lambda$    $1.0 \le [\lambda = (0.6 + 40\varepsilon_{ps})] \le 2.0$

In order to compare the experimentally measured development length values with code and suggested equation results, the following relationship was used to determine the average difference between equation and experimental results:

$$Average\ Difference = \frac{l_{d(Equation)} - l_{d(Experimental)}}{l_{d(Equation)}} \qquad (13.3)$$

By performing the difference comparison in this manner, the code or suggested equation served as the accepted value. If the experimental development length is less than that predicted, the ratio is positive, indicating a conservative prediction.

### 13.8.3 Results of Experimental and Predicted Results

Table 13.9 compares predicted and experimental development lengths.

Table 13.9 Overview of Development Length Prediction Results for HSLC

| Equation Source | Equation | Overall Results | | |
|---|---|---|---|---|
| | | Avg Diff (%) | Max Over (%) | Max Under (%) |
| AASHTO[40] / ACI[2] | $(f_{ps} - \tfrac{2}{3}f_{se})d_b$ | 19% | 30% | 8% |
| Barnes, Burns, Kreger[55] | $1.25\left(\dfrac{f_{pt}}{\sqrt{f_{ci}'}} + (f_{ps} - f_{pe})\right)d_b$ | 37% | 47% | 31% |
| Buckner[46] | $f_{si}\dfrac{d_b}{3} + \lambda\,(f_{su} - f_{se})d_b$ | 42% | 54% | 18% |
| Deatherage et al.[43] | $f_{si}\dfrac{d_b}{3} + 1.5(f_{su} - f_{se})d_b$ | 44% | 54% | 39% |
| Lane 95%[47] | $\left(\dfrac{4f_{pt}d_b}{f_c'} - 5\right) + \left(\dfrac{6.4(f_{su} - f_{se})d_b}{f_c'} + 15\right)$ | 7% | 30% | -28% |
| Lane 95%[47] (10 ksi limit on $f_c'$) | $\left(\dfrac{4f_{pt}d_b}{f_c'} - 5\right) + \left(\dfrac{6.4(f_{su} - f_{se})d_b}{f_c'} + 15\right)$ | 17% | 32% | 1% |
| Lane Mean[47] | $\left(\dfrac{4f_{pt}d_b}{f_c'} - 21\right) + \left(\dfrac{6.4(f_{su} - f_{se})d_b}{f_c'} + 26\right)$ | 1% | 27% | -39% |
| Lane Mean[47] (10 ksi limit on $f_c'$) | $\left(\dfrac{4f_{pt}d_b}{f_c'} - 21\right) + \left(\dfrac{6.4(f_{su} - f_{se})d_b}{f_c'} + 26\right)$ | 12% | 28% | -5% |
| Martin and Scott[41] | $(f_{ps} - \dfrac{135}{d_b^{1/6}})\dfrac{d_b}{0.39}$ | 58% | 63% | 50% |
| Mitchell et al.[45] | $0.33 f_{si}\, d_b\sqrt{\dfrac{3}{f_{ci}'}} + (f_{su} - f_{se})d_b\sqrt{\dfrac{4.5}{f_c'}}$ | -27% | 2% | -60% |
| Zia and Mostafa[42] | $(1.5\dfrac{f_{si}}{f_{ci}'}d_b - 4.6) + 1.25(f_{su} - f_{se})d_b$ | 6% | 24% | -3% |

The average difference was calculated using equation 13.3 for the twelve lightweight girder tests and the eight normal weight HPC girder tests and is listed in the "Avg Diff" column. The "Max Over" column lists greatest positive percent difference between the

predicted and experimental value. The "Max Under" column lists the greatest negative percent difference between the predicted and experimental value.

### 13.8.3.1 Results of Analysis Based on Average Difference

Analysis of Table 13.9 showed that the equation by Zia and Mostafa produced the best overall prediction of development length. The Zia and Mostafa equation would be considered a "best-fit" equation where a "best-fit" equation was defined as the equation having the lowest average difference between experimental and predicted values as well as not having excessive overestimates or underestimates. Lane's Mean equation was within 1 percent on average, but had a maximum underestimate of –39 percent. Lane's 95 percent confidence equation was within 7 percent on average, but had a maximum underestimate of –28 percent. The AASHTO/ACI equation and equations by Lane (95 percent confidence with 10 ksi cap on $f_c'$), Barnes, Burns and Kreger, Buckner, Deatherage et al., and Martin and Scott did not provide as accurate a prediction, but always provided a conservative estimate of development length. Martin and Scott's equation as well as the equation by Deatherage et al. were overly conservative.

### 13.8.3.2 Results of Analysis Based on Maximum Underestimate

Analysis of Table 13.9 based on maximum underestimate showed that Lane's 95 percent confidence equation having a 10 ksi cap on $f_c'$ to provide a good overall estimate of development length without being overconservative. This equation would be the best choice as a "design" equation. A "design" equation was defined as the equation having the lowest positive maximum underestimate value without being overly conservative.

331

The most favorable combination of these two values indicated the best "design" equation. Lane's 95 percent confidence equation having a 10 ksi cap on $f_c'$ had a maximum underestimate value of 1 percent, which indicates the equation did not under predict any value, and had an average difference of 17 percent. The AASHTO/ACI equation produced a maximum underestimate of 8 percent again indicating the equation did not under predict any value, and had an average difference of 19 percent. The equation by Zia and Mostafa produced a maximum underestimate of −3 percent and had an average difference of 6 percent. Equations by Barnes, Burns and Kreger, Buckner, Martin and Scott, and Deatherage et al. never underestimated development lengths, but all had average differences in excess of 35 percent.

### 13.8.3.3 Evaluation of Top Five "Best-Fit" and "Design" Equations

Tables 13.10 and 13.11 show a listing of the top five equations in both the "best-fit" and "design" categories. From these tables it was possible to identify which variables used in the flexural bond portion of the equations were the best predictors. The variables $d_b$, $f_{se}$, $f_{ps}$, $f_{su}$ and $f_c'$ appeared to be the most important in predicting development length.

Table 13.10  Review of Top Five "Best-Fit" Equations

| Best-Fit Equations | | | | | | |
|---|---|---|---|---|---|---|
| Rank | Equation Source | Equation | Equation Variables | | | |
| | | | $d_b$ | $f_{se}$ | $f_{su}$ | $f_c{}'$ |
| 1 | Zia and Mostafa[42] | $(1.5\frac{f_{si}}{f'_{ci}}d_b-4.6)+1.25(f_{su}-f_{se})d_b$ | X | X | X | |
| 2 | Lane Mean[47] (10 ksi limit on $f_c{}'$) | $\left(\frac{4f_{pt}d_b}{f'_c}-21\right)+\left(\frac{6.4(f_{su}-f_{se})d_b}{f'_c}+26\right)$ | X | X | X | X |
| 3 | Lane Mean[47] | $\left(\frac{4f_{pt}d_b}{f'_c}-21\right)+\left(\frac{6.4(f_{su}-f_{se})d_b}{f'_c}+26\right)$ | X | X | X | X |
| 4 | Lane 95%[47] | $\left(\frac{4f_{pt}d_b}{f'_c}-5\right)+\left(\frac{6.4(f_{su}-f_{se})d_b}{f'_c}+15\right)$ | X | X | X | X |
| 5 | Lane 95%[47] (10 ksi limit on $f_c{}'$) | $\left(\frac{4f_{pt}d_b}{f'_c}-5\right)+\left(\frac{6.4(f_{su}-f_{se})d_b}{f'_c}+15\right)$ | X | X | X | X |

Table 13.11  Review of Top Five "Design" Equations

| Design Equations | | | | | | | |
|---|---|---|---|---|---|---|---|
| Rank | Equation Source | Equation | Equation Variables | | | | |
| | | | $d_b$ | $f_{se}$ | $f_{ps}$ | $f_{su}$ | $f_c{}'$ |
| 1 | Lane 95%[47] (10 ksi limit on $f_c{}'$) | $\left(\frac{4f_{pt}d_b}{f'_c}-5\right)+\left(\frac{6.4(f_{su}-f_{se})d_b}{f'_c}+15\right)$ | X | X | | X | X |
| 2 | Zia and Mostafa[42] | $(1.5\frac{f_{si}}{f'_{ci}}d_b-4.6)+1.25(f_{su}-f_{se})d_b$ | X | X | | X | |
| 3 | Lane Mean[47] (10 ksi limit on $f_c{}'$) | $\left(\frac{4f_{pt}d_b}{f'_c}-21\right)+\left(\frac{6.4(f_{su}-f_{se})d_b}{f'_c}+26\right)$ | X | X | | X | X |
| 4 | AASHTO[40] / ACI[2] | $(f_{ps}-\tfrac{2}{3}f_{se})d_b$ | X | X | X | | |
| 5 | Barnes, Burns, Kreger[55] | $1.25\left(\frac{f_{pt}}{\sqrt{f'_{ci}}}+(f_{ps}-f_{pe})\right)d_b$ | X | X | X | | |

333

## 13.9 Development of an Improved Development Length Equation

### 13.9.1 Determination of Equation Forms

Two equations were presented in Chapter 9 for predicting transfer length. One

goal in determining a new development length equation was to incorporate the suggested

transfer length relations. The two transfer length equations suggested were:

Best Fit Equation:

$$l_t = 50 d_b \sqrt{\frac{4000}{f_{ci}'}} \tag{9.6}$$

Design Equation:

$$l_t = 50 d_b \sqrt{\frac{6000}{f_{ci}'}} \tag{9.7}$$

Based on equations suggested by other researchers in Tables 13.10 and 13.11, the

following equation characteristics were thought to show promise:

- Equations including $d_b$

- Equations incorporating $(f_{su} - f_{se})$

- Equations incorporating $(f_{ps} - f_{se})$

- Equations incorporating $f_c'$

- Equations based on current ACI or AASHTO forms

- Equations incorporating the transfer length equation suggested in this research

334

Using these guidelines, numerous equation forms were evaluated using data from the 20 development length tests from this research and that by Dill.[84] Percent difference was calculated using the following expression as articulated in Chapter 9.

$$Average\ Difference = \frac{l_{d(Equation)} - l_{d(Experimental)}}{l_{d(Experimental)}}$$

(9.3)

### 13.9.2 Results of Equation Analysis

Sixteen equation forms were investigated which incorporated the basic form of the suggested transfer length equations. Current code equation forms were modified to provide more accurate results. Concrete compressive strengths were based on accelerated curing during the first 24 hours. All strand stress values were based on VWSG data. Two equation forms emerged from the process that met the "best fit" and "design" equation criteria. The most promising "best fit" equation was:

$$\left( 50\sqrt{\frac{2500}{f'_{ci}}} + f_{ps} - f_{se} \right) d_b$$

(13.3)

The most promising "design" equation was:

$$\left( 50\sqrt{\frac{5000}{f'_{ci}}} + f_{ps} - f_{se} \right) d_b$$

(13.4)

335

The "best-fit" equation has the smallest average difference and the most promising "design" equation has the smallest positive maximum under length prediction. The initial term of each equation is very similar to the equations for transfer length. Close comparison and evaluation indicates that the transfer length portion of the equation is apparently reduced in the development length equation. This further indicates the trends seen in the strand stress plots in Appendix Q and discussed in Section 13.7.1.2. As the girder was loaded, the strands tended to transfer more force in a region somewhat shorter than the specified transfer length. Tables 13.12 and 13.13 provide a comparison of the above equations with the top ranked "best fit" and "design" equations and current code equations. The comparison shows that the proposed equations provide better predictions of development, especially the design equation.

Table 13.12  Comparison of Proposed Best Fit Equation With Other Equations

| Equation Source | Best Fit Equation | Overall Results | | |
|---|---|---|---|---|
| | | Avg Diff (%) | Max Over (%) | Max Under (%) |
| Proposed Equation | $\left(50\sqrt{\dfrac{2500}{f_{ci}'}} + f_{ps} - f_{se}\right)d_b$ | 1% | 21% | -6% |
| Zia and Mostafa[42] | $\left(1.5\dfrac{f_{si}}{f_{ci}'}d_b - 4.6\right) + 1.25(f_{su} - f_{se})d_b$ | 6% | 24% | -3% |
| AASHTO[40] / ACI[2] | $(f_{ps} - \tfrac{2}{3}f_{se})d_b$ | 19% | 30% | 8% |

336

Table 13.13 Comparison of Proposed Design Equation With Other Equations

| Equation Source | Design Equation | Overall Results | | |
|---|---|---|---|---|
| | | Avg Diff (%) | Max Over (%) | Max Under (%) |
| Proposed Equation | $\left(50\sqrt{\dfrac{5000}{f'_{ci}}}+f_{ps}-f_{se}\right)d_b$ | 9% | 31% | 0% |
| Lane 95% [47] (10 ksi limit on $f_c'$) | $\left(\dfrac{4f_{pt}d_b}{f'_c}-5\right)+\left(\dfrac{6.4(f_{su}-f_{se})d_b}{f'_c}+15\right)$ | 17% | 32% | 1% |
| AASHTO[40] / ACI[2] | $(f_{ps}-\tfrac{2}{3}f_{se})d_b$ | 19% | 30% | 8% |

## 13.9.3 Proposed Equation Evaluation for use on HSLC

Table 13.14 provides a comparison of results for the proposed equation for HSLC and high strength normal weight concrete.

Table 13.14 Proposed Equation Evaluation for use on HSLC

| Basis of Comparison | AASHTO[40] ACI[2] Code $(f_{ps}-\tfrac{2}{3}f_{se})d_b$ | Proposed Equation For Design $\left(50\sqrt{\dfrac{5000}{f'_{ci}}}+f_{ps}-f_{se}\right)d_b$ | Proposed Equation For Best Fit $\left(50\sqrt{\dfrac{2500}{f'_{ci}}}+f_{ps}-f_{se}\right)d_b$ |
|---|---|---|---|
| Avg Diff (HSLC) | 19% | 13% | 4% |
| Max Over (HSLC) | 30% | 31% | 21% |
| Max Under (HSLC) | 8% | 2% | -6% |
| | | | |
| Avg Diff (NWC) | 18% | 2% | -5% |
| Max Over (NWC) | 18% | 4% | -3% |
| Max Under (NWC) | 17% | 0% | -6% |
| | | | |
| Avg Diff (Overall) | 19% | 9% | 1% |
| Max Over (Overall) | 30% | 31% | 21% |
| Max Under (Overall) | 8% | 0% | -6% |

Table 13.14 showed the AASHTO/ACI equation gave consistent and conservative values for both HSLC and NWC. There appears to be more scatter in the values for HSLC than for NWC. The proposed equation for design produced more conservative results for HSLC than for NWC. Since the proposed equation incorporates a term addressing initial concrete compressive strength, this could indicate the equation becomes less conservative as initial compressive strength increases. The initial compressive strengths for the NWC were about 5,000 psi higher than the HSLC strengths on average. Similar trends are seen for the proposed best-fit equation. Figure 13.12 provides a plot of the results in Table 13.14.
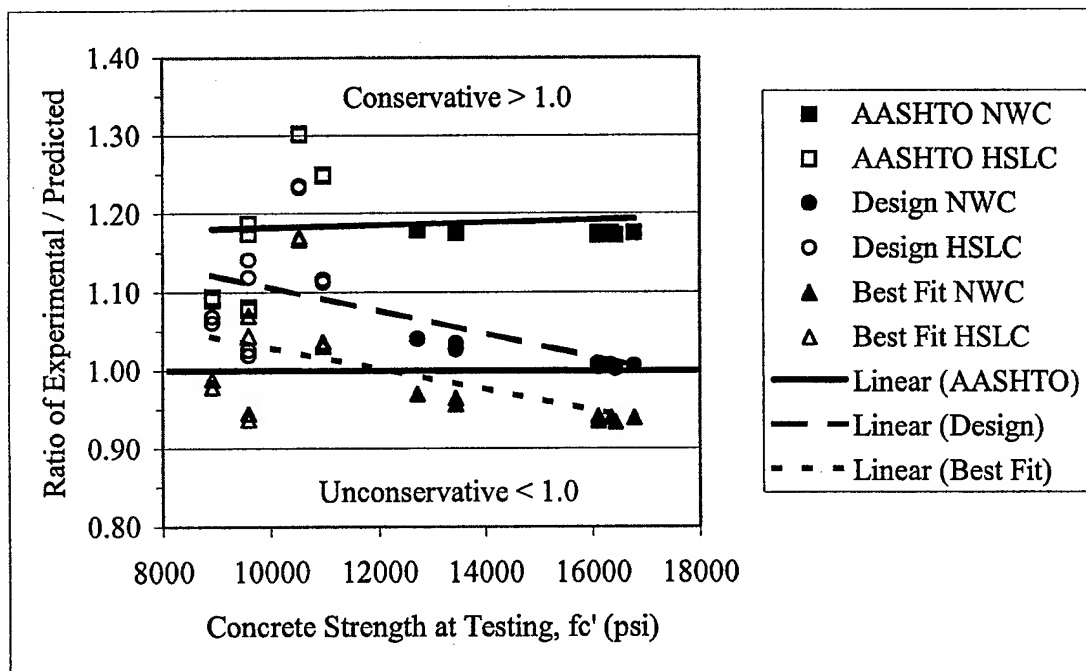


Figure 13.12 Comparison of Design and Best-Fit Equations to AASHTO Equation

To further verify the proposed equations, data from other researchers on HSLC would be useful. Yet no other development length data has been published for 0.6-inch prestressing strand used in lightweight concrete. Evaluation using data from other NWC and sand lightweight concrete tests would prove useful for comparison and further verification.

## 13.10   Conclusions

An evaluation of current code provisions using the twelve slate HSLC girder development length tests in this study and eight normal weight HPC girder tests from Dill[82] showed the current AASHTO[40] and ACI[2] provisions to be conservative. The code equations overestimated development lengths by 19 percent for both slate HSLC and normal weight HPC and never underestimated them. Use of the current code provisions for design of development length for slate HSLC and 0.6-inch diameter strand was conservative. Based on the concrete strength range addressed in this research project, modification of the current code specifications for development length was not necessary for HSLC or for 0.6-inch diameter strands.

An evaluation of other suggested equations for predicting development length showed an equation by Zia and Mostafa[42] to provide the best overall prediction of development length. Equations by Lane as identified in Table 13.10 also produced good overall predictions. The above equations were applicable to both slate HSLC and normal weight HPC with good results.

Based on an evaluation of 16 different equation forms, two new equations were suggested. The new equations for predicting development length based on "best-fit" and

339

"design" produced more accurate results than current code specifications and showed slight improvements over other suggested equation forms.

Test results showed conclusively that shear cracking in the transfer length region across the bottom strands did not induce significant strand slip if stirrup density was doubled over the current AASHTO[40] specified density in the region.

The addition of silica fume into the mix design at a 10% replacement rate by weight of cementitious materials substantially reduced development length. Although the silica fume increased compressive strength and early strength, the apparent major impact was the creation a much better bond between the prestressing strand and the concrete matrix.

There was no indication throughout this analysis that need existed to differentiate between slate HSLC and normal weight HPC. With regard to development length, for concrete compressive strengths over 8,000 psi, the prediction of development length was the same for both lightweight and normal weight concrete.

# CHAPTER XIV

# CONCLUSIONS AND RECOMMENDATIONS

## 14.1 Conclusions

Conclusions are presented in the following sections by topic.

### 14.1.1 Analytical Investigation

The use of HSLC has the potential to increase the length of simple span AASHTO

Type IV and V sections up to four percent and Bulb-Tee sections up to three percent.

However, AASHTO Type II and III sections do not benefit appreciably from the use of

HSLC. The Modified Bulb-Tee section extended the length of a Standard Bulb-Tee by

10 feet using 8, 10 and 12 ksi HSLC or high-strength NWC. Bulb-Tee (Standard or

Modified) sections provided longer spans at less weight for girders over 105 feet in

length when compared to AASHTO sections. For spans between 125 feet and 155 feet,

the use of HSLC can reduce the gross vehicle weight to less than 150 kips so that a super-

load permit is not required for transport of long span girders.

### 14.1.2 HSLC Mixes and Properties

HSLC mixes were developed in the laboratory for 8,000 psi and 10,000 psi using

slate lightweight ½-in coarse aggregate and normal weight, natural sand. The dry unit

weight of the concretes was approximately 117 and 119 pcf, respectively. A 12,000 psi

design strength mix could not be developed. The strengths of mixes using lightweight fine aggregate could not be controlled, therefore no recommended mix used lightweight fines.

The laboratory mixes were verified during field production. The field mixes yielded slightly higher strengths than found in the laboratory. Close monitoring of LWA moisture was required.

The HSLC, both 8,000 psi and 10,000 psi design strength continued to gain strength over the 100-day test period. Accelerated cured cylinders, which matched curing conditions of precast beams showed about 25 percent higher one-day strength than ASTM cured cylinders; at 56 days, the ASTM cured cylinders were about 4% stronger than the accelerated cured cylinders. Equation 7.4 was developed and provides a better estimate of the modulus of elasticity for slate HSLC than previous relations for normal strength concretes.

### 14.1.3 Transfer Length

An evaluation of current code provisions using the 12 HSLC transfer lengths in this research and 8 normal weight HPC transfer lengths from Reutlinger[84] showed the current AASHTO[40] and ACI[2] equations to be conservative. The AASHTO equation overestimated transfer lengths by 42% on average and never underestimated transfer lengths. The ACI equation using VWSG data to determine prestressing strand stress also overestimated transfer lengths by 46% and never underestimated transfer lengths. Use of either the AASHTO or ACI equations to predict transfer length for slate HSLC was conservative. Based on the concrete strength range addressed in this research project,

342

modification of the current code specifications for transfer lengths was not necessary for slate HSLC.

An evaluation of other suggested equations for predicting transfer length showed an equation by Mitchell et al.[45] to provide the best overall prediction of transfer length. Equations by Buckner[46] and Deatherage et al.[43] also produced good overall predictions. The above equations were applicable to both slate HSLC and normal weight HPC with good results.

An evaluation of the applicability of initial concrete compressive strength, $f_{ci}'$, and initial modulus of elasticity, $E_{ci}$, and 32 possible equation forms showed that $d_b$ and $f_{ci}'$ were the best parameters for predicting transfer length.

There was no indication throughout this analysis that a need existed to differentiate between slate HSLC and normal weight HPC with regard to transfer length. For initial concrete strengths, $f_{ci}'$, over 6,000 psi, the prediction of transfer length was the same for both slate lightweight and normal weight concrete.

### 14.1.4 Flexural Behavior

The current prediction of cracking stress and cracking moment, when examined for slate HSLC, showed indications of becoming unconservative as concrete compressive strengths approached 11,000 psi. In some cases, the predicted cracking moments exceeded the experimental values. The use of a lambda factor ($\lambda$) of 0.85 for HSLC made with slate LWA produced conservative results on average for compressive strengths below 11,000 psi. More research is required to examine a potential tension

343

strength ceiling for HSLC and adjustments to lambda for concrete compressive strengths over 10,000 psi.

The modulus of rupture test, ASTM C 78[82], did not accurately predict the cracking stress of HSLC girders.

The current AASHTO procedure for ultimate moment calculation was conservative for slate HSLC girders with normal weight concrete decks having a compressive strength under 6,000 psi.

## 14.1.5  Shear Behavior

The current AASHTO[40] Standard specification provided a conservative prediction of concrete and ultimate shear capacity when shear steel capacity was capped at a yield strength of 60 ksi. The alternate design procedure listed in ACI-318[2] Section 11.4.2.2 for predicting shear strength produced some unconservative predictions for concrete compression strengths over 10,000 psi. The method for predicting interface shear strength was conservative for slate HSLC.

The current AASHTO LRFD[92] specification provided a conservative prediction of ultimate shear strength for slate HSLC.

The variable angle truss model provided an overconservative prediction of shear capacity in HSLC girders.

## 14.1.6  Development Length

An evaluation of current code provisions using the twelve HSLC girder development length tests in this study and eight normal weight HPC girder tests from

Dill[84] showed the current AASHTO[40] and ACI[2] provisions to be conservative. The code equations overestimated development lengths by 19 percent for both HSLC and normal weight HPC and never underestimated them. Use of the current code provisions for design of development length for slate HSLC and 0.6-inch diameter strand was conservative. Based on the concrete strength range addressed in this research project, modification of the current code specifications for development length was not necessary for HSLC or for 0.6-inch diameter strands.

An evaluation of other suggested equations for predicting development length showed an equation by Zia and Mostafa[42] to provide the best overall prediction of development length. Equations by Lane[47] as identified in Table 13.10 also produced good overall predictions. The above equations were applicable to both slate HSLC and normal weight HPC with good results.

Test results showed conclusively that shear cracking in the transfer length region across the bottom strands did not induce significant strand slip if stirrup density was doubled over the current AASHTO[40] specified density in the region.

The addition of silica fume into the mix design at a 10% replacement rate by weight of cementitious materials gave indications of reducing development length.

There was no indication throughout this analysis that need existed to differentiate between slate HSLC and normal weight HPC. With regard to development length, for concrete compressive strengths over 8,000 psi, the prediction of development length was the same for both slate lightweight and normal weight concrete.

## 14.2 Recommendations

Recommendations are presented in the following sections by topic.

### 14.2.1 Analytical Investigation

When designing girders in excess of 105 feet, use Bulb-Tee sections (Standard or Modified). Use the Modified Bulb-Tee (one additional layer of strands in a 2-in deeper bottom flange) to gain an additional 10 feet in span length instead of designing for the next larger size Bulb-Tee section. Use slate HSLC to reduce both girder and gross vehicle weight.

### 14.2.2 HSLC Mixes and Properties

Accurately control the absorbed water in the LWA. Determine the percentage of absorbed moisture above which mix water will not be absorbed during concrete batching. Apply water by sprinkling or other method to the LWA stockpile for a sufficient length of time prior to batching such that the absorbed moisture is in excess of the minimum required amount. Test the LWA as often as is necessary during batching to insure that moisture contents are within the tolerance of the given mix design.

Use match curing of cylinders to predict initial strength of the concrete for precast prestressed concrete girder production. For later age testing (28-days and after) ASTM cured specimens are adequate. The 4 x 8 cylinders provide a reliable measure of compressive strength and may be used in place of 6 x 12 cylinders.

Use Equation 7.4 to predict the modulus of elasticity for slate HSLC.

$$E_c = 44,000\sqrt{f_c' \frac{w_c}{145}}$$ (7.4)

### 14.2.3 Transfer Length

Use the current AASHTO[40] and ACI[2] equations to conservatively predict transfer length in pretensioned girders constructed with slate HSLC and 0.6-in pretensioning strands. For a more accurate prediction that is still conservative, use equation 9.7.

$$50 \, d_b \sqrt{\frac{6000}{f'_{ci}}}$$ (9.7)

### 14.2.4 Flexural Behavior

Do not use the modulus of rupture test, ASTM C 78,[82] for determining the cracking stress and cracking moment for pretensioned slate HSLC girders.

More research is required to examine a potential tension strength ceiling for HSLC, as related to flexural cracking, and adjustments to lambda for concrete compressive strengths over 10,000 psi.

Use the current AASHTO procedure for ultimate moment calculation for slate HSLC girders with normal weight concrete decks having a compressive strength under 6,000 psi.

### 14.2.5 Shear Behavior

Use the current AASHTO Standard specification to provide a conservative prediction of concrete and ultimate shear capacity in slate HSLC pretensioned girders when shear steel capacity is capped at a yield strength of 60 ksi.

More research is required to examine a potential tension strength ceiling for HSLC, as related to diagonal tension cracking, and adjustments to lambda for concrete compressive strengths over 10,000 psi. Examination of the alternate design procedure listed in ACI-318 Section 11.4.2.2 for predicting shear strength, $V_c$, is necessary for concrete compressive strengths over 10,000 psi.

The AASHTO Standard Specification can be used to conservatively predict interface shear strength between slate HSLC and normal weight concrete.

The AASHTO LRFD Specification can be used to conservatively predict ultimate shear strength in slate HSLC pretensioned girders.

### 14.2.6 Development Length

The current AASHTO[40] and ACI[2] provisions can be used to conservatively predict development length in pretensioned girders constructed with slate HSLC and 0.6-in diameter pretensioning strands. For a more accurate prediction that is still conservative, use equation 13.4.

$$\left( 50\sqrt{\frac{5000}{f_{ci}'}} + f_{ps} - f_{se} \right) d_b \qquad (13.4)$$

In the transfer length region, use two times the stirrup density currently specified by the AASHTO[40] Standard Specification to limit strand slip in the event of shear cracking.

Use silica fume at up to a 10% replacement rate by weight of cementitious materials to reduce development length.

### 14.2.7 Future Research

As a result of this research project, some areas requiring additional research became apparent.

First, the tension strength ceiling of HSLC and its effect on diagonal tension cracking strength and flexural cracking strength is unknown. The overall relation between concrete strength and the LWC reduction factor, $\lambda$, requires examination, especially for concrete compressive strengths over 10,000 psi.

Second, a spectrum of testing using the same concrete strengths with varying amounts of silica fume is required to determine its exact impact on development length.

Third, based on the tremendous property variation between different types of LWA, there is a need to thoroughly investigate the use of various light weight aggregates in like test configurations to determine material specific factors for each category of design.

# REFERENCES

1. Murillo, J. A., Thoman S., Smith, D., "Lightweight Concrete for a Segmental Bridge," *Civil Engineering*, Vol. 64, No. 5, May 1994, pp. 68-70.

2. *Building Code Requirements for Reinforced Concrete*, ACI 318-99, *and Commentary*, ACI 318R-99, American Concrete Institute, Detroit, 1999.

3. Harmon, K., "Physical Characteristics of Rotary Kiln Expanded Slate Lightweight Aggregate," *Proceedings, Second International Symposium on Structural Lightweight Aggregate Concrete*, Kristiansand, Norway, June 2000, 11 pp.

4. Raithby, K. D., Lydon, F. D., "Lightweight Concrete in Highway Bridges," *The International Journal of Cement Composites and Lightweight Concrete*, Vol. 2, No. 3, May 1981, pp. 133-146.

5. Bender, B. F., "Economics and Use of Lightweight Concrete in Prestressed Structures," *PCI Journal*, Vol. 35, No. 6, November-December 1980, pp. 62-67.

6. Brown, W. R., Davis, C. R., *A Load Response Investigation of Long Term Performance of a Prestressed Lightweight Concrete Bridge at Fanning Springs, Florida,* Final Report, No. FL/DOT/SMO-93-401, Florida Department of Transportation, April 1993, 66 pp.

7. Hansen, H. H., "Shelby Creek Bridge," *Portland Cement Association Engineered Concrete Structures*, Vol. 5, No. 2, August 1992, p. 3.

8. Roberts, J. E., "Lightweight Concrete Bridges for California Highway System," *ACI SP 136*, American Concrete Institute, Detroit, 1992, pp. 254-271.

9. Expanded Shale, Clay and Slate Institute, "Back-up Statistics to Building Bridges," Information Sheet # 470.4, Salt Lake City, June 1994, 15 pp.

10. Melby, K., Jordet, E. A., Hansvold, C., "Long-span Bridges in Norway Constructed in High-Strength LWA Concrete," *Engineering Structures*, Vol. 18, No. 11, November 1996, pp. 845-849.

11. Holm, T. A., Bremner, T. W., *State-of-the-Art Report on High-Strength, High-Durability Structural Low-Density Concrete for Applications in Severe Marine Environments*, U. S. Army Corps of Engineers Engineer Research and Development Center No. ERDC/SL TR-00-3, August 2000, 103 pp.

12. Shideler, J. J., "Lightweight-Aggregate Concrete for Structural Use," *Journal of the American Concrete Institute*, Vol. 54, No. 10, October 1957, pp. 299-328.

13. Wang, P. T., Shah, S. P., Naaman A. E., "Stress-Strain Curves of Normal and Lightweight Concrete in Compression," *ACI Journal*, Vol. 75, No. 11, November 1978, pp. 603-611.

14. Hanson, J. A., "Tensile Strength and Diagonal Tension Resistance of Structural Lightweight Concrete," *Journal of the American Concrete Institute*, Vol. 58, No. 1, July 1961, pp. 1-37.

15. ASTM C 127, *Standard Test Method for Specific Gravity and Absorption of Coarse Aggregate*, American Society for Testing and Materials, West Conshohocken, PA, 1993, 5 pp.

16. ASTM C 128, *Standard Test Method for Specific Gravity and Absorption of Fine Aggregate*, American Society for Testing and Materials, West Conshohocken, PA, 1997, 5 pp.

17. Bremner, T. W., Newman, "Microstructure of Low Density Concrete Aggregate," *Proceedings of the Ninth Congress of the Federation Internationale de la Precontrainte*, Volume 3, Commission Reports, Stockholm, June 1982.

18. *ACI Manual of Concrete Practice*, "Standard Practice for Selecting Proportions for Structural Lightweight Concrete (ACI 211.2-91), American Concrete Institute, Detroit, 1996.

19. Pfeiffer, D. W., "Sand Replacement in Structural Lightweight Concrete," *ACI Journal*, Vol. 64, No. 7, July 1967, pp. 384-392.

20. Fujji, K., Kakizaki, M., Edahiro, H., Unisuga, Y., Yamamoto, Y., "Properties of High-Strength and High-Fluidity Lightweight Concrete," *ACI SP 179*, American Concrete Institute, Detroit, pp. 254-271.

21. Leming, M. L., *Properties of High Strength Concrete – An Investigation of High Strength Concrete Characteristics using Materials in North Carolina*, Final Report, No. 23241-86-3, North Carolina Department of Transportation, July 1988 186 pp.

22. Mor, A., "Steel-Concrete Bond in High Strength Lightweight Concrete," *ACI Materials Journal*, Vol. 89, No. 1, January-February 1992, pp. 76-82.

23. Smeplass, S., "Moisture in Light Weight Aggregates – Practical Consequences for the Production Properties of Light Weight Aggregate Concrete", *Proceedings, Second International Symposium on Structural Lightweight Aggregate Concrete*, Kristiansand, Norway, June, 2000.

24. Holm, T. A., Valsangkar, A. J., "Lightweight Aggregate Soil Mechanics: Properties and Applications," *Transportation Research Record 1422; Soils, Geology, and Foundations; Lightweight Artificial and Waste Materials for Embankments Over Soft Soils*, Transportation Research Board, January 1993, pp. 7-13.

25. Valum, R., Nilsskog, J. E., "Production and Quality Control of High Performance Lightweight Concrete for the Raftsundet Bridge," *Proceedings of the Fifth International Symposium on Utilization of High Strength / High Performance Concrete, Sandefjord, Norway*, June 2000, pp. 909-918.

26. Hoff, G. C., "High Strength Lightweight Aggregate Concrete for Arctic Applications," *ACI SP 136*, American Concrete Institute, Detroit, 1992, pp. 1-65.

27. Morales, J., *Short-Term Mechanical Properties of High Strength Lightweight Concrete*, Report 82-9 on NSF Grant No. ENG78-05124, Ithaca, August 1982.

28. Leming, M. L., *Creep and Shrinkage of Lightweight Concrete*, North Carolina State University Publication, 1990, 4 pp.

29. FIP Committee, "Chapter 7, Design of Prestressed Lightweight Concrete Structures," *Federation Internationale de la Precontrainte Manual of Lightweight Aggregate Concrete, 2nd Edition*, 1983, pp. 168-206.

30. Bilodeau, A., Chevrier, R., Malhotra, M., Hoff, G. C., "Mechanical Properties, Durability and Fire Resistance of High-Strength Lightweight Concrete," *Proceedings of the International Symposium on Structural Lightweight Aggregate Concrete*, Sandefjord, Norway, June 1995, pp. 432-443.

31. Holm, T. A., Bremner, T. W., "Chapter 10, High Strength Lightweight Aggregate Concrete," *High Performance Concretes and Applications*, S. P. Shah and S. H. Ahmad, ed., Edward Arnold, London, pp. 341-374.

32. Carolina Stalite, Information from Carolina Stalite Company, Salisbury, NC, 2000, 6 pp.

33. Holm, T. A., Bremner, T. W., "70 Year Performance record for High-Strength Structural Lightweight Concrete," *Proceedings of the First Materials Engineering Congress, Serviceability & Durability of Construction Materials*, Denver, August 2000, pp. 884-893.

34. Bremner, T. W., Holm, T. A., "Elastic Compatibility and the Behavior of Concrete," *ACI Journal*, Vol. 83, No. 2, March-April 1986, pp. 244-250.

35. Kohno, K., Okamoto, T., Isikawa, Y., Sibata, T., Mori, H., "Effects of Artificial Lightweight Aggregate on Autogenous Shrinkage of Concrete," *Cement and Concrete Research*, Vol. 29, 1999, pp. 611-614.

36. Bremner, T. W., Holm, T. A., Ries, J. P., "Enhanced Hydration and Properties of Specified Density Concrete," Expanded Shale, Clay and Slate Institute Information Sheet 4284.1, February 2001, 8 pp.

37. Reutlinger, C., "Direct Pull-Out Capacity and transfer Length of 0.6-inch Diameter Prestressing Strand in High-Performance Concrete," Masters Thesis, Georgia Institute of Technology, Atlanta, GA, May 1999, 352 pp.

38. Janney, J. R., "Nature of Bond in Pre-Tensioned Prestressed Concrete," *Journal of the American Concrete Institute*, Vol. 50, No. 9, May 1954, pp. 717-736.

39. Hanson, N. W., Karr, P. H., "Flexural Bond Tests of Pretensioned Prestressed Beams," *Journal of the American Concrete Institute*, Vol. 55, No. 7, January 1959, pp. 783-802.

40. *Standard Specifications for Highway Bridges*, 16th ed., American Association of State Highway and Transportation Officials, Washington, D. C., 1996.

41. Martin, L. D., Scott, N. L., "Development of Prestressing Strand in Pretensioned Members," *ACI Journal*, Vol. 73, No. 8, August 1976, pp. 453-456.

42. Zia, P., Mostafa, T., "Development Length of Prestressing Strands," *PCI Journal*, Vol. 22, No. 5, September/October 1977, pp. 54-65.

43. Deatherage, J. H., Burdette, E. G., and Chew, C. K., "Development Length and Lateral Spacing Requirements of Prestressing Strand for Prestressed Concrete Bridge Girders," *PCI Journal*, Vol. 39, No. 1, January/February 1994, pp. 70-83.

44. Russell, B. W., "Design Guidelines for Transfer, Development and Debonding of Large Diameter Seven Wire Strands in Pretensioned Concrete Girders," Doctoral Thesis, The University of Texas at Austin, 1992, 464 pp.

45. Mitchell, D., Cook, W. D., Khan, A. A., Tham, T., "Influence of High Strength Concrete on Transfer and Development Length of Pretensioning Strand," *PCI Journal*, Vol. 38, No. 3, May/June 1993, pp. 52-56.

46. Buckner, C. D., "A Review of Strand Development Length for Pretensioned Concrete Members," *PCI Journal*, Vol. 40, No. 2, March/April 1995, pp. 84-105.

47. Lane, S. N., *A New Development Length Equation for Pretensioned Strands in Bridge Beams and Piles, Final Report*, No. FHWA-RD-98-116, Federal Highway Administration, December 1998, 131 pp.

48. Collins, M. P., Mitchell, D., *Prestressed Concrete Structures*, Prentice Hall, Englewood Cliffs, New Jersey, 1991.

49. Nawy, E. G., *Prestressed Concrete A Fundamental Approach*, Third Edition, Prentice Hall, Upper Saddle River, New Jersey, 2000,

50. Lin, T. Y., Burns, N. H., *Design of Prestressed Concrete Structures*, Third Edition, John Wiley and Sons, New York, New York, 1981.

51. Holm, T. A., Personal telephone conversation on March 25, 2002 concerning the origination of the lightweight concrete factor, $\lambda$.

52. Johnson, M. K., Ramirez, J. A., "Minimum Shear Reinforcement in Beams with Higher Strength Concrete," *ACI Structural Journal*, Vol. 86, No. 4, July-August 1989, pp. 376-382.

53. *Building Code Requirements for Reinforced Concrete*, ACI 318-89, *and Commentary*, ACI 318R-89, American Concrete Institute, Detroit, 1989.

54. Shahawy, M. A., Batchelor, B., "Shear Behavior of Full-Scale Prestressed Concrete Girders: Comparison Between AASHTO Specifications and LRFD Code," *PCI Journal*, Vol. 41, No. 3, May-June 1996, pp. 48-62.

55. Barnes, R. W., Burns, N. H., Kreger, M. E., "Development Length of 0.6-inch Prestressing Strand in Standard I-Shaped Pretensioned Concrete Beams," Research Report 1388-1, Center for Transportation Research, Bureau of Engineering Research, The University of Texas at Austin, December 1999, 318 pp.

56. Ma, J., Tadros, M. H., Baishya, M, "Shear Behavior of Pretensioned High-Strength Concrete Bridge I-Girders," *ACI Structural Journal*, Vol. 97, No. 1, January-February 2000, pp. 185-192.

57. Ramirez, J., Olek, J., Rolle, E., Malone, B., "Performance of Bridge Decks and Girders with Lightweight Aggregate Concrete, Final Report," Report FHWA/IN/JTRP-98/17, Purdue University, October 2000, 616 pp.

58. *Guide for Structural Lightweight Aggregate Concrete*, ACI 213, (Draft Copy for Voting by Committee 213), American Concrete Institute, Detroit, 2002.

59. Peterman, R. J., Ramirez, J. A., Olek, J., "Design of Semi-lightweight Bridge girders, Development Length Considerations," Transportation Research Board Record 1696, Paper No. 5B0063, Transportation Research Board, 2000.

60. Peterman, R. J., Ramirez, J. A., Olek, J., "Evaluation of Strand Transfer and Development Lengths in Pretensioned Girders with Semi-Lightweight Concrete," Final Report," Report FHWA/IN/JTRP-99/3, Purdue University, July 1999, 89 pp.

61. Kolozs, R. T., "Transfer and Development Lengths of Fully Bonded 1/2-Inch Prestressing Strand in Standard AASHTO Type I Pretensioned High Performance Lightweight Concrete (HPLC) Beams," Masters Thesis, The University of Texas at Austin, May 2000, 155 pp.

62. *Bond of Reinforcement in Concrete*, International Federation for Structural Concrete (fib) State-of-Art Report, Bulletin 10, Lausanne, Switzerland, 2000, 427 pp.

63. den Uijl, J. A., "Bond Modeling of Prestressing Strand," *ACI SP 180*, ed. Roberto Leon, American Concrete Institute, Farmington Hills, pp. 145-169.

64. Kahn, L. F., Saber, A., "Analysis and Structural Benefits of High Performance Concrete for Pretensioned Bridge Girders," *PCI Journal*, Vol. 45, No. 4, July/August 2000, pp. 100-107.

65. Meyer, K. F., Kahn, L. F., "Annotated Bibliography for High-Strength, Lightweight Prestressed Concrete Bridge Girders," Task 1 Report, Georgia Department of Transportation Project No. 2004, Georgia Institute of Technology, January 2001, 14 pp.

66. Shams, M., "Time-Dependent Behavior of High-Performance Concrete," Doctoral Thesis, Georgia Institute of Technology, May 2000, 572 pp.

67. ASTM C 330, *Standard Specification for Lightweight Aggregates for Structural Concrete*, American Society for Testing and Materials, West Conshohocken, PA, 1999, 4 pp.

68. ASTM C 33, *Standard Specification for Concrete Aggregates*, American Society for Testing and Materials, West Conshohocken, PA, 1999, 8 pp.

69. Mehta, P. K., Monteiro, P. J. M., *Concrete Microstructure, Properties, and Materials*, Second Edition, McGraw Hill, New York, New York, 1993.

70. ASTM C 150, *Standard Specification for Portland Cement*, American Society for Testing and Materials, West Conshohocken, PA, 2000.

71. ASTM C 618, *Standard Specification for Coal Fly Ash and Raw or Calcined Natural Pozzolan for Use as a Mineral Admixture in Concrete*, American Society for Testing and Materials, West Conshohocken, PA, 1999, 4pp.

72. ASTM C 494, *Standard Specification for Chemical Admixtures for Concrete*, American Society for Testing and Materials, West Conshohocken, PA, 1999, 9 pp.

73. ASTM C 260, *Standard Specification for Air Entraining Admixtures for Concrete* American Society for Testing and Materials, West Conshohocken, PA, 2000, 3 pp.

74. ASTM C 143, *Standard Test Method for Slump of Hydraulic-Cement Concrete*, American Society for Testing and Materials, West Conshohocken, PA, 1998, 3 pp.

75. ASTM C 138, *Standard Test Method for Unit Weight, Yield, and air Content (Gravimetric) of Concrete*, American Society for Testing and Materials, West Conshohocken, PA, 2000, 3 pp.

76. ASTM C 1064, *Standard Test Method for Temperature of Freshly Mixed Portland Cement Concrete*, American Society for Testing and Materials, West Conshohocken, PA, 1999, 2 pp.

77. ASTM C 173, *Standard Test Method for Air Content of Freshly Mixed Concrete by the Volumetric Method*, American Society for Testing and Materials, West Conshohocken, PA, 1994, 3 pp.

78. ASTM C 231, *Standard Test Method for Air Content of Freshly Mixed Concrete by the Pressure Method*, American Society for Testing and Materials, West Conshohocken, PA, 1994, 3 pp.

79. ASTM C 31, *Standard Practice for Making and Curing Concrete Test Specimens in the Field*, American Society for Testing and Materials, West Conshohocken, PA, 1998, 5 pp.

80. ASTM C 39, *Standard Test Method for Compressive Strength of Cylindrical Concrete Specimens*, American Society for Testing and Materials, West Conshohocken, PA, 1999, 5 pp.

81. ASTM C 469, *Standard Test Method for Static Modulus of Elasticity and Poisson's Ratio of Concrete in Compression*, American Society for Testing and Materials, West Conshohocken, PA, 1994, 4 pp.

82. ASTM C 78, *Standard Test Method for Flexural Strength of Concrete (Using Simple Beam with Third-Point Loading)*, American Society for Testing and Materials, West Conshohocken, PA, 1994, 3 pp.

83. ASTM C 512, *Standard Test Method for Creep of Concrete in Compression*, American Society for Testing and Materials, West Conshohocken, PA, 1992, 4 pp.

84. Dill, J. C., "Development Length of 0.6-inch Diameter Prestressing Strand in High-Performance Concrete," Masters Thesis, Georgia Institute of Technology, May 2000, 322 pp.

85. ASTM C 1231, *Standard Practice for Use of Unbonded Caps in Determination of Compressive Strength of Hardened Concrete Cylinders*, American Society for Testing and Materials, West Conshohocken, PA, 2000, 4 pp.

86. Buchberg, B. S., "Investigation of Mix Design and Properties of High-Strength/High-Performance Lightweight Concrete," Masters Thesis, Georgia Institute of Technology, January 2002, 453 pp.

87. *Guide for High-Strength Concrete*, ACI 363, American Concrete Institute, Detroit, 2000.

88. ASTM C 496, *Standard Test Method for Splitting Tensile Strength of Cylindrical Concrete Specimens*, American Society for Testing and Materials, West Conshohocken, PA, 1996, 4 pp.

89. Sikes, G. H., Strougal, E. J., Meisner, J. L., "Computer Manual for Service Load Design of Concrete Bridge Slabs," Georgia Department of Transportation, January 1999, 18 pp.

90. Logan, D. R., "Acceptance Criteria for Bond Quality of Strand for Pretensioned Prestressed Concrete Applications," PCI Journal, Vol. 42, No. 2, March/April 1997. pp. 52-90.

91. MacGregor, J. G., *Reinforced Concrete*, Second Edition, Prentice Hall, Englewood Cliffs, New Jersey, 1992, 848 pp.

92. *LRFD Specifications for Highway Bridges*, American Association of State Highway and Transportation Officials, Washington, D. C., 1998.

93. Cagley, J. R., "Changing from ACI 318-99 to ACI 318-02, What's New?," *Concrete International*, Vol. 23, No. 6, June 2001, pp. 69-182.

94. Vaysburg, A., "Durability of Lightweight Concrete Bridges in Severe Environments," *Concrete International*, Vol. 18, No. 7, July 1996, pp. 33-38.

95. Yeginobali, A., Sobolev, K. G., Soboleva, S. V., Tokyay, M., "High Strength Natural Lightweight Aggregate Concrete with Silica Fume," *ACI SP 178*, American Concrete Institute, Detroit, May 1998, pp. 739-758.

# Georgia Institute of Technology

**School of Civil and Environmental Engineering**

Structural Engineering, Mechanics and Materials
Research Report No. 02-5

# Appendices for
# Transfer and Development Length of High Strength Lightweight Concrete Precast Prestressed Bridge Girders

**Task 5 Report**

Prepared for

Office of Materials and Research
Georgia Department of Transportation

GDOT Research Project No. 2004

by

Karl F. Meyer, Lawrence F. Kahn
James S. Lai, and Kimberly E. Kurtis

June 2002

# APPENDIX A

## INPUT FILE CREATOR FOR GDOT COMPUTER PROGRAM

This Appendix contains an example of the spreadsheet used to create input files

for use with the Georgia Department of Transportation prestressed girder design program

The worksheet shown in Table A.1 shows the input variables. Most of the

variables were held constant; the shaded variables were changed for the parametric study.

The worksheet shown in Table A.2 lists values calculated based on the variables

entered in Table A.1. For determination of diaphragm locations, it was assumed that

diaphragm spacing would be at a maximum of 35 feet.

The worksheet shown in Table A.3 provides the values to be entered for rows 1

through 8 in the program input file. The shaded values were entered as listed except for

the decimal points that are shown for clarity. The initial row of the input file providing

information is not listed in Table A.3.

Table A.1 Input Values for Girder Design

# INPUT VALUES FOR GDOT PRESTRESSED GIRDER PROGRAM IN DESIGN MODE

## DECK VARIABLES

| | | | |
|---|---|---|---|
| MINIMUM DECK THICKNESS | $t_d$ | 7.000 | INCHES |
| AVERAGE COPING DEPTH | | 3.00 | INCHES |
| FUTURE PAVING ALLOWANCE | | 0.015 | KSF |
| LIGHTWEIGHT CONCRETE | | NO | YES/NO |
| CONCRETE STRENGTH | $f'_c$ | 3500 | PSI |
| CONCRETE WEIGHT | $W_c$ | 145 | PCF |
| ALLOWANCE FOR GRINDING | | 0.00 | INCHES |
| WEIGHT OF SIDEWALK | | 0.00 | K/FT |
| DISTANCE FROM DECK TO GIRDER | DF | 0.00 | INCHES |
| DECK PANELS USED | | NO | YES/NO |
| **MISCELLANEOUS VARIABLES THAT ARE NORMALLY CONSTANT VALUES** | | | |
| WEIGHT OF BARRIERS | | 820 | LB/FT |
| DISTRIBUTION FOR DEFLECTION | DFD | 1.000 | NO UNITS |
| WEIGHT OF FORMWORK | | 16 | PSF |
| FACTOR INITIAL BM TOP STRESS | SIT | -3.0 | NO UNITS |
| FACTOR FINAL BM BOTTOM STRESS | SFB | -6.0 | NO UNITS |
| ALLOW FINAL BEAM END TOP STRESS | SFT | -200 | PSF |
| AASHTO CODE VERSION | | 1996 | |
| CONCRETE WEIGHT FOR DIAPHRAGMS | | 150 | PCF |
| THICKNESS OF DIAPHRAGMS | | 10 | INCHES |
| TOP OF BEAM TO TOP STRANDS | TCL | 2.50 | INCHES |
| BOTTOM OF BEAM TO BOTTOM STRANDS | BCL | 3.00 | INCHES |
| STRAND SPACING | SPAC | 2.00 | INCHES |
| NUMBER OF TOP STRANDS | NST | 2 | EACH |
| MAXIMUM DRAPED STRANDS PER ROW | | 2 | NO UNITS |

## GIRDER VARIABLES

| | | | |
|---|---|---|---|
| GIRDER TYPE (AASHTO,BT) | | BT72 | 1-6,BT |
| NUMBER OF GIRDERS | | 13 | EACH |
| GIRDER SPACING | s | 84.00 | INCHES |
| GIRDER LENGTH | L | 166.00 | FEET |
| LIGHTWEIGHT CONCRETE | | YES | YES/NO |
| LIGHTWEIGHT CONCRETE REDUCTION FACTOR | $\lambda$ | 0.75 | NO UNITS |
| CONCRETE STRENGTH | $f'_c$ | 10000 | PSI |
| % CONCRETE STRENGTH AT RELEASE | | 90% | PERCENT |
| CONCRETE WEIGHT (WHOLE NUMBERS ONLY) | $W_c$ | 118 | PCF |
| STRAND DIAMETER | D | 0.6 | INCHES |
| TOP STRAND C/S AREA | $A_{st}$ | 0.217 | INCH^2 |
| BOTTOM STRAND C/S AREA | $A_{sb}$ | 0.217 | INCH^2 |
| STRAND ULTIMATE STRENGTH | $f_{pu}$ | 270 | KSI |
| STIRRUP SIZE | | 5 | # |
| STIRRUP ULTIMATE STRENGTH | $f_u$ | 60 | KSI |
| DISTANCE END TO SUPPORT | XDIST | 8.00 | INCHES |
| BOTTOM STRAND REDUCTION FACTOR | RBFPU | 0.75 | NO UNITS |
| TOP STRAND REDUCTION FACTOR | RTFPU | 0.75 | NO UNITS |
| LOLAX STRANDS USED | LL | YES | YES/NO |
| DRAPED STRANDS | | YES | YES/NO |
| NUMBER OF DIAPHRAMS ON GIRDER | NPL | 4 | EACH |

USER INPUT VALUES ————>  OPEN

USER INPUT VALUES ————>  TMP LOCK

USER INPUT VALUES (CONSTANTS) ————>

Table A.2  Calculated Values

| NON-COMPOSITE DEAD LOAD | | | |
|---|---|---|---|
| WEIGHT OF SLAB | | 0.592 | KIP/FT |
| WEIGHT OF COPINGS | | 0.127 | KIP/FT |
| WEIGHT OF FORMWORK | | 0.056 | KIP/FT |
| TOTAL NON-COMPOSITE DEAD LOAD | WDL$_{nc}$ | 0.775 | KIP/FT |
| **COMPOSITE DEAD LOAD** | | | |
| FUTURE WEARING SURFACE | | 0.105 | KIP/FT |
| BARRIERS | | 0.063 | KIP/FT |
| TOTAL COMPOSITE DEAD LOAD | WDL$_c$ | 0.168 | KIP/FT |
| **MISCELLANEOUS CALCULATED VALUES** | | | |
| WIDTH OF GIRDER TOP FLANGE | | 42 | INCHES |
| GIRDER MODULUS OF ELASTICITY | E$_c$ | 3.82 | 1E6 PSI |
| GIRDER MODULUS AT RELEASE | E$_{ci}$ | 3.74 | 1E6 PSI |
| DISTRIBUTION FOR MOMENT | DFM | 1.273 | NO UNITS |
| DISTRIBUTION FOR SHEAR (INT) | DFV | 1.571 | NO UNITS |
| APPROXIMATE GIRDER WEIGHT | | 104.33 | KIPS |
| DECK MODULUS OF ELASTICITY | E$_c$ | 3.41 | 1E6 PSI |
| DIAPHRAGM WEIGHT PER FOOT | | 0.667 | KIPS |
| **POINT LOADS ON GIRDER** | | | |
| POINT LOAD # 1 | -> | 4.001 | KIPS |
| LOCATION # 1 FROM END | | 33.200 | FEET |
| POINT LOAD # 2 | -> | 4.001 | KIPS |
| LOCATION # 2 FROM END | | 66.400 | FEET |
| POINT LOAD # 3 | -> | 4.001 | KIPS |
| LOCATION # 3 FROM END | | 99.600 | FEET |
| POINT LOAD # 4 | -> | 4.001 | KIPS |
| LOCATION # 4 FROM END | | 132.800 | FEET |
| POINT LOAD # 5 | | | KIPS |
| LOCATION # 5 FROM END | | | FEET |
| **PROGRAM CALCULATED VALUES ———>** | | | |

Table A.3 Input File for GDOT Prestressed Girder Computer Program

| ROW | DS/AN | LOADS | T,L,M | LENGTH | DFM | DFV | DFD | WDFD | WDLnc | WDLc | Wsw | Wf | fc' | fci' | SKIP | NPL | SIT | SFB | SFT | CODE |
|---|---|---|---|---|---|---|---|---|---|---|---|---|---|---|---|---|---|---|---|---|
| 1 | D | HS20 | XXX | 166.000 | .1273 | .1571 | 1.000 | 0.775 | 0.168 | 0.000 | 10.000 | 09.000 | XXXX | 04 | .285 | .000 | .200 | 6 | | |

| ROW | Wtc | Ht | Ft | Ws | Hb | Fb | Wb | Db | Tf | Df | EBM | fcs | SKIP | STIR | SKIP | IFL | FuST | R1 | R3 | RF |
|---|---|---|---|---|---|---|---|---|---|---|---|---|---|---|---|---|---|---|---|---|
| 2 | 042.00 | 0350 | 02.50 | 06.00 | 0630 | 04.50 | 026.00 | 072.00 | 02.000 | 10.000 | 3.82 | 13.50 | X | S | X | 40 | XX | XX | 0.75 | |

TYPE  NST  XDIST

———————————————— MAXIMUM NUMBER OF STRANDS PER ROW ————————————————

| ROW | | | 1 | 2 | 3 | 4 | 5 | 6 | 7 | 8 | 9 | 10 | 11 | 12 | 13 | 14 | 15 | 16 | 17 | 18 | 19 |
|---|---|---|---|---|---|---|---|---|---|---|---|---|---|---|---|---|---|---|---|---|---|
| 3 | XX | 11 | 0.667 | 12 | 08 | 04 | 02 | 02 | 02 | 02 | 02 | 02 | 02 | 02 | 02 | 02 | 01 | 02 | 02 | 02 | 02 |

ROW ———>

ROW (CONTINUED)

| | ASB | AST | DIAM | TCL | BCL | SPAC |
|---|---|---|---|---|---|---|
| 3 | 02 | 2170 | 0.600 | 2.50 | 3.00 | 1.00 |
| | 20 | | | | | |

| ROW | RBFPU | BFPU | IBLOSS | FBLOSS | RTFPU | TFPU | ITLOSS | FTLOSS | WTC | LOLAX | ITLG | FTLG | DLG |
|---|---|---|---|---|---|---|---|---|---|---|---|---|---|
| 4 | 0.75 | 270.00 | XXXX | XXXX | 0.75 | 270.00 | XXXX | XXXX | 0.118 | X | XXXX | XXXX | XXXX |

| ROW | DBOND |
|---|---|
| 5 | 0 |

| ROW |
|---|
| 6 |

——————————————— MAXIMUM DRAPED STRANDS PER ROW ———————————————

| ROW | DRAPE | RS HT | HOLD | 1 | 2 | 3 | 4 | 5 | 6 | 7 | 8 | 9 | 10 | 11 | 12 | 13 | 14 | 15 | 16 | 17 | 18 | 19 |
|---|---|---|---|---|---|---|---|---|---|---|---|---|---|---|---|---|---|---|---|---|---|---|
| 7 | T | XXX | XX | 02 | 02 | 02 | 02 | 02 | 02 | 02 | 02 | 02 | 02 | 02 | 02 | 02 | 02 | 02 | 02 | 02 | 02 |

ROW ———>

ROW (CONTINUED)

| | 02 |
|---|---|
| 7 | 20 |

| ROW | XP1 | P1 | XP2 | P2 | XP3 | P3 | XP4 | P4 | XP5 | P5 |
|---|---|---|---|---|---|---|---|---|---|---|
| 8 | 033.200 | 04.001 | 066.400 | 04.001 | 099.600 | 04.001 | 132.800 | 04.001 | | |

X = SPACE

362

# APPENDIX B

## MIX DESIGN SPREADSHEET

This Appendix contains an example of the LWC Mix Design Spreadsheet. Table B.1 shows the spreadsheet with an example mix design.

The user does the following:

1. Enter values for SG (Specific Gravity) and Cost for each component to set the material parameters. Enter the desired air content and batch size.

2. Enters the weight of each particular component per cubic yard at SSD, except chemical admixtures, in the "Theoretical Mix Design at SSD" Section.

3. Enter the dose of chemical admixtures in fl oz / 100 weight of cementitious materials.

4. Adjust the components until the W/CM ratio is as desired. The percent cement paste and ratio of coarse to fine aggregate are listed at the bottom of the page.

5. While batching, if additional chemical admixtures or water are added, enter the values in the spreadsheet in ml for chemical admixtures and pounds for water.

6. The final mix design reflecting added amounts during batching, if any, is reflected in the "Final Mix Design at SSD" section. If nothing additional was added, this will be the same as the "Theoretical Mix Design at SSD."

363

Table B.1 Mix Design Spreadsheet

## LIGHTWEIGHT CONCRETE MIX DESIGN | ID # | XXXX | $f_c'$ | X | ksi | Date

| Material Data | | | Moisture Data | | | | Theoretical Mix Design at SSD | | $H_2O$ Adjusted Batch | | Final Mix Design at SSD | |
|---|---|---|---|---|---|---|---|---|---|---|---|---|
| Description | SG | Cost Per | % SSD | SGF | % As Is | % Free | Per Cubic Yard | Per Batch | EDV(cf) | Amount | Per Cubic Yard | |
| 3/4" - NWA | 2.649 | $ 0.0046 | 0.60 | 2.665 | 0.60 | 0.00 | 0 | 0.00 | 0.00 | 0.00 | 0 | $  - |
| 1/2" - NWA | 2.665 | $ 0.0048 lb | 0.60 | 2.681 | 0.60 | 0.00 | 0 lb | 0.00 lb | 0.00 | 0.00 lb | 0 lb | $  - |
| 3/8" - NWA | 2.665 | $ 0.0050 | 0.60 | 2.681 | 0.60 | 0.00 | 0 | 0.00 | 0.00 | 0.00 | 0 | $  - |
| NW Sand | 2.608 | $ 0.0054 | 0.50 | 2.621 | 0.00 | -0.50 | 1215 | 45.00 | 0.27 | 44.78 | 1205 | $ 6.48 |
| 3/4" - LWA | 1.415 | $ 0.0276 | 6.00 | 1.500 | 6.00 | 0.00 | 0 | 0.00 | 0.00 | 0.00 | 0 | $  - |
| 1/2" - LWA | 1.440 | $ 0.0276 lb | 7.67 | 1.550 | 9.27 | 1.60 | 945 lb | 35.00 lb | 0.37 | 35.55 lb | 937 lb | $ 25.86 |
| 3/8" - LWA | 1.570 | $ 0.0300 | 6.00 | 1.664 | 6.00 | 0.00 | 0 | 0.00 | 0.00 | 0.00 | 0 | $  - |
| LW Fines | 1.710 | $ 0.0275 | 5.00 | 1.796 | 5.00 | 0.00 | 0 | 0.00 | 0.00 | 0.00 | 0 | $  - |
| Tot Aggregate > | | | | | | | 2160 lb / 17.20 cf | 80.00 lb | 0.64 | 80.30 lb | 2141.7 lb | $ 32.34 |

| % by Wt | | | | W/CM | 0.358 | | Per Cubic Yard | Per Batch | EDV(cf) | Amount | Per Cubic Yard | |
|---|---|---|---|---|---|---|---|---|---|---|---|---|
| FA - Class C | 2.250 | $ 0.0300 | 0.0 | | | | 0 | 0.00 | 0.00 | 0.00 | 0 | $  - |
| FA - Class F | 2.250 | $ 0.0300 lb | 19.4 | $/CY | 75.48 | | 150 | 5.56 | 0.04 | 5.56 | 149 | $ 4.46 |
| GGBFS | 2.900 | $ 0.0300 | 0.0 | | | | 0 | 0.00 | 0.00 | 0.00 | 0 | $  - |
| Metakaolin | 2.500 | $ 0.0500 | 0.0 | LB/FT³ | 118.3 | | 0 | 0.00 | 0.00 | 0.00 | 0 | $  - |
| SF - (F 10,000) | 2.200 | $ 0.0500 | 7.1 | | | | 55 | 2.04 | 0.01 | 2.04 | 55 | $ 2.73 |
| Type III Cement | 3.150 | $ 0.0440 lb | 73.5 | | | | 570 lb | 21.11 lb | 0.11 | 21.11 lb | 565 lb | $ 24.87 |
| Tot Cementitious > | | | | | | | 775 lb / 4.37 cf | 28.70 lb | 0.16 | 28.70 lb | 768.4 lb | $ 32.06 |

| | | | fl oz / 100 wt | | ml added during mixing | | Per Cubic Yard | Per Batch | EDV(cf) | Amount | Per Cubic Yard | |
|---|---|---|---|---|---|---|---|---|---|---|---|---|
| WRDA 35 | 1.199 | $ 0.0500 fl | 2 - 8 | 7.00 | 10 | | 54.3 ml | 2.01 fl oz | 0.002 | | 8.18 fluid oz | $ 3.14 |
| Daracem 65 | 1.139 | $ 0.0500 oz | 3 - 9 | 0.00 | | | 0.0 | 0.00 | 0.000 | 0.00 | 0.00 per 100 wt | $  - |
| ADVA Flow | 1.043 | $ 0.1197 | 3 - 10 | 8.00 | 5 | | 62.0 | 2.30 | 0.002 | | 8.59 | $ 7.90 |
| Daravair 1000 | 1.000 | $ 0.0500 | 1/4 - 3 | 0.00 | | | 0.0 | 0.00 | 0.000 | 0.00 | 0.00 | $  - |
| Tot Admixtures > | | | | | | | 116.3 | 4.31 | 0.004 | 0.31 | 9.40 | $ 11.04 |

Total additional volume added > 0.0085 cf

| Water | 1.000 | $ 0.0013 gal | Pounds water added => | 0.50 | 264.2 lb / 4.23 cf | 9.78 | 0.152 | 9.49 gal | 275.3 lb | $ 0.04 |
|---|---|---|---|---|---|---|---|---|---|---|

Design Air => 4.00 %
Design Slump => 3-5 Inches

| Batch Size => | 1.00 cf | 1.08 cf | 0.04 cf | 3.97 % Air |

Percent Cement Paste > 36

Coarse / Fine Aggregate Ratio 1.31

Direct any questions about this spreadsheet to LTC Fred Meyer, Georgia Institute of Technology, Atlanta, GA (404) 385-1429 – Version 4, 7 Feb 2001

The following calculations verify the values listed in Table B.1.

## Assumed Values

**Brown Brothers Sand (NW Sand)** : Theoretical Mix Design at SSD = 1215 pcy
Specific gravity (SG) = 2.608
SSD moisture = 0.5%
As-Is moisture = 0%

**1/2" Stalite LWA (1/2" - LWA)** : Theoretical Mix Design = 945 pcy,
SG = 1.44
SSD moisture = 7.67%
As-is moisture = 9.27%

**Class "F" flyash (FA - Class F)** : Theoretical Mix Design = 150 pcy
SG = 2.25

**Silica Fume (SF - F 10,000)** : Theoretical Mix Design = 55 pcy
SG = 2.2

**Type III Cmt (Type III Cement)** : Theoretical Mix Design = 570 pcy
SG = 3.15

**Water Reducer (WRDA 35)** : Theoretical Mix Design = 7 oz/100 weight
of cementitious material
SG = 1.199

**Superplasticizer (ADVA Flow)** : Theoretical Mix Design = 8 oz/100 weight
of cementitious material
SG = 1.043

**AEA (Daravair 1000)** : Theoretical Mix Design = 1 oz/100 weight
of cementitious material
SG = 1.0

**Air - 4%**

**During batching the following were added:** WRDA 35 = 10 ml = .00003531 cf
ADVA Flow = 5 ml = .00001766 cf
water = 0.5 lbs = .008013 cf

**Batch Size = 1 cubic foot**

## Calculated Values

**NW Sand :**

Specific gravity factor (SGF) = (2.608) x (1+0.005) = 2.621

percent free moisture = 0 % - 0.05 % = -0.5 %

volume of material per cy = (1215 pcy) x (1 / ((62.4pcf) x ( 2.621)) = 7.428 cf

weight of material per cf of batch = (1215 pcy) / (27 cf/cy) = 45 lbs

Water adjusted weight of material per cf of batch =
  (45 lbs) x (1/(1+(.5 / 100))) x (1+0.0 / 100) = 44.776 lbs

Water adjusted volume of material per cf of batch =
  ((45 lb) / ((2.621) x (62.4 pcf)))+((44.776 lbs) - (45 lbs)) / 62.4 pcf = 0.2716 cf


**1/2" - LWA:**

Specific gravity factor (SGF) = (1.44) x (1+0.0767) = 1.550

percent free moisture = 9.27 % - 7.67 % = 1.60 %

volume of material per cy = (945 pcy) x (1 / ((62.4pcf) x ( 1.55)) = 9.77 cf

weight of material per cf of batch = (945 pcy) / (27 cf/cy) = 35 lbs

Water adjusted weight of material per cf of batch =
  (35 lbs) x (1 / (1+(7.67 / 100))) x (1+9.27 / 100) = 35.52 lbs

Water adjusted volume of material per cf of batch =
  ((35 lb) / ((1.55) x (62.4 pcf)))+((35.52 lbs) - (35 lbs)) / 62.4 pcf = 0.3702 cf


**Total Aggregate:**

weight = 1215 lbs (NW Sand) + 945 lbs (1/2" - LWA) = 2,160 lbs

volume = 7.43 cf (NW Sand) + 9.77 (1/2" - LWA) = 17.20 cf

# Calculated Values (cont'd)

**FA - Class F:**

volume per cy = (150 lbs) / ((2.25) x (62.4 pcf)) = <u>1.0683</u> cf

weight = (150 pcy)) / (27cuf/cuy) x (1 cf/batch) = <u>5.555</u> lbs/batch

volume = (5.555 lbs/batch) / ((2.25) x (62.4 pcf)) = <u>0.0395</u> cf/batch

**SF - F 10,000:**

volume per cy = (55 lbs) / ((2.2) x (62.4 pcf)) = <u>0.4006</u> cf

weight = (55 pcy)) / (27cf/cy) x (1 cf/batch) = <u>2.037</u> lbs/batch

volume = (2.037 lbs/batch) / ((2.5) x (62.4 pcf)) = <u>0.01484</u> cf/batch

**Type III Cement:**

volume = (570 lbs/cy) / ((3.15) x (62.4 pcf)) = <u>2.8998</u> cf/cy

weight = (570 pcy)) / (27cuf/cuy) x (1 cf/batch) = <u>21.11</u> lbs/batch

volume = (21.11 lbs/batch) / ((3.15) x (62.4 pcf)) = <u>0.1074</u> cf/batch

**Total Cementitious:**

weight = 150 lbs (FA -Class F) + 55 lbs (SF - F 10,000) + 570 lbs (Type III Cement) = <u>775</u> lbs

volume = 1.0683 cf (FA - Class F) + 0.4006 cf (SF - F 10,000) + 2.8998 cf (Type III Cement) = <u>4.37</u> cf

## Calculated Values (cont'd)

**WRDA 35:**

volume = (7 fl oz/100 wt) x ((775 / 100) 100 wt/cy) = <u>54.25</u> fl oz/cy

volume = (54.25 fl oz/cy) x (1 cf/batch) / (27 cf/cy) = <u>2.009</u> fl oz/batch

volume = (54.25 fl oz/cy) / (957.5065 fl oz/cf) = <u>0.05666</u> cf/cy

volume = (.05666 cf/cy) x (1 cf/batch) / (27 cf/cy) = <u>0.00210</u> cf/batch

volume = (.00210 cf/batch) x (28316.8466 ml/cf) = <u>59.42</u> ml/batch


**ADVA Flow:**

volume = (8 fl oz/100 wt) x ((775 / 100) 100 wt/cy) = <u>62</u> fl oz/cy

volume = (62 fl oz/cy) x (1 cf/batch) / (27 cf/cy) = <u>2.296</u> fl oz/batch

volume = (62 fl oz/cy) / (957.5065 fl oz/cf) = <u>0.06475</u> cf/cy

volume = (.06475 cf/cy) x (1 cf/batch) / (27 cf/cy) = <u>0.00239</u> cf/batch

volume = (.00239 cf/batch) x (28316.8466 ml/cf) = <u>67.909</u> ml/batch


**Total Admixtures:** By using the milliliters of admixtures and the specific gravities, a weight of equivalent water can be found.

equivalent water mass = 59.42 ml (WRDA 35) x (1.199) = <u>71.2446</u> g

equivalent water mass = 67.909 ml (ADVA Flow) x (1.043) = <u>70.8291</u> g

total equivalent water mass = 71.2466 g (WRDA 35) + 70.8291 g (ADVA Flow) = <u>142.0757</u> g

weight = (142.0757 g) x (1 oz / 28.3498 g) x (1 lb / 16 oz) =
= <u>0.3132</u> lb

volume = .05666 cf (WRDA 35) + .06475 cf (ADVA Flow) = <u>0.121</u> cf

## Calculated Values (cont'd)

**Water:**

volume of water per cy = 27 cf - $vol_{aggregate}$ - $vol_{cement}$ - $vol_{admixture}$ - $vol_{air}$

volume of air (4 %) = (.04) x (27 cf/cy) = 1.08 cf/cy

volume of water = 27 cf - 17.20 cf - 4.37 cf - 0.121 cf - 1.08 cf = <u>4.233</u> cf/cy

volume of water = 1.0 cf - 0.64 cf - 0.16 cf - 0.004 cf - 0.04 = <u>0.152</u> cf/batch

weight = (4.233 cf/cy) x (62.4 pcf) = <u>264.1392</u> pcy

weight = (264.1392 pcy) x (1 cf/batch) x (1 cy / 27 cf) = <u>9.783</u> lbs/batch

**Final Mix Design:** The additions of WRDA 35, ADVA Flow and water need to be accounted for when reporting the final mix design

volume added = .00003531 cf (WRDA 35) + .00001766 cf (ADVA FLOW) + .008013 cf = .008066 cf

new volume of mix = (1 cy) + (.008066 cf) = <u>1.008066</u> cf

Final NW Sand weight = (1215 lbs) / (1.008066) = <u>1205.28</u> lbs

Final 1/2" - LWA weight = (945 lbs) / (1.008066) = <u>937.44</u> lbs

Final FA - Class F weight = (150 lbs) / (1.008066) = <u>148.80</u> lbs

Final SF - F 10,000 weight = (55 lbs) / (1.008066) = <u>54.55</u> lbs

Final Type III Cement weight = (570 lbs) / (1.008066) = <u>565.44</u> lbs

Final WRDA 35 volume = (7 fl oz/100 wt) + (10 ml/cf) x (27 cf/cy) x (1 fl oz / 29.5735 ml) x (1 cy / 775 lb) x (100 lb / per 100 wt) = = <u>8.178</u> fl oz/100 wt

Final WRDA 35 volume = (8 fl oz/100 wt) + (5 ml/cf) x (27 cf/cy) x (1 fl oz / 29.5735 ml) x (1 cy / 775 lb) x (100 lb / per 100 wt) = = <u>8.589</u> fl oz/100 wt

Final admixture water equivalent weight = (8.178 fl oz) x (1.199) + (8.589 fl oz) x (1.043) = 18.76719 fl oz of water

369

## Calculated Values (cont'd)

Final admixture weight = (18.76719 fl oz) x (768 lbs / 100 lbs) x (29.5735 ml/fl oz) x (.002205 lb/ml) = 9.397 lbs

Final Water weight = ((267.1 lbs) + (.5 lb) x (1 / 1cf) x (27 cf/cy)) x (1 / (1 + .0085) = 275.3 lbs

Final Air Content = 4 % x (1 / (1+.0085)) = 3.97 %

**Cost:**

| | | | |
|---|---|---|---|
| NW Sand | = (1205.28 lbs) x ($0.0054/lbs) | = | $ 6.48 |
| 1/2" - LWA | = (937.44 lbs) x ($0.0276/lbs) | = | $ 25.86 |
| FA - Class F | = (148.80lbs) x ($0.03/lbs) | = | $ 4.46 |
| SF - F 10,000 | = (54.55 lbs) x ($0.05/lbs) | = | $ 2.73 |
| Type III Cement | = (565.44 lbs) x ($0.044/lbs) | = | $ 24.87 |
| WRDA 35 | = (8.18 fl oz/100 wt) x (7.6879**) x ($0.05) | = | $ 3.14 |
| ADVA Flow | = (8.59 fl oz/100 wt) x (7.6879**) x ($0.1197/fl oz) = | | $ 7.90 |
| Water | = (275.3 lb) x ($0.0013/gal) / (8.34 lbs/gal) | = | $ 0.04 |
| Total | | | $ 75.48 |

**Water/Cementitious Ratio** = (275.3 lbs) / (768.79) = 0.358

**Unit Weight** = (aggregate wt + cement wt + admixture wt + water wt)/ 27
= ((2142.7 lbs) + (768.4 lbs) + (9.40 lbs) + (275.3 lbs)) / 27 = 3195.8
= 118.3 lbs/cf

** The number of 100 weight of cement in the cubic yard

# APPENDIX C

# MATERIAL PROPERTIES

This Appendix contains material property data in the sections listed below.

C.1  HSLC material properties used in evaluating modulus of elasticity equations in

   Chapter 7.

C.2  Tension test results of #4 bar reinforcing steel used for all shear stirrups.

C.3  Tension test results of #3 bar reinforcing steel used for "doghouse" bars in the

   transfer region.

## C.1 Material Properties for Modulus of Elasticity Specimens

Table C.1  16-Hour Curebox Cured Specimens

| Specimen Identification | Wet Unit Weight (pcf) | As-Tested Unit Weight (pcf) | Compression Strength (4 x 8) (psi) | Modulus of Elasticity (psi) |
|---|---|---|---|---|
| 8F-1 | 118.6 | 117.9 | 7,920 | 3,407,479 |
| 8F-2 | 118.6 | 117.9 | 7,920 | 3,530,161 |
| 8F-3 | 118.6 | 117.9 | 7,920 | 3,515,616 |
| 10F-1 | 121.0 | 120.3 | 7,710 | 3,427,358 |
| 10F-2 | 121.0 | 120.3 | 7,710 | 3,430,741 |
| 10F-3 | 121.0 | 120.3 | 7,710 | 3,572,510 |
| 12F-1 | 124.0 | 123.3 | 10,990 | 3,998,394 |
| 12F-2 | 124.0 | 123.3 | 10,990 | 3,592,513 |
| 12F-3 | 124.0 | 123.3 | 10,990 | 4,161,776 |
| 8L-1 | 122.0 | 121.3 | 7,320 | 3,458,627 |
| 8L-2 | 122.0 | 121.3 | 7,320 | 3,658,242 |
| 8L-3 | 122.0 | 121.3 | 7,320 | 3,467,933 |
| 12L-1 | 122.8 | 122.1 | 9,840 | 4,058,913 |
| 12L-2 | 122.8 | 122.1 | 9,840 | 4,019,955 |
| 12L-3 | 122.8 | 122.1 | 9,840 | 4,167,468 |

Table C.2  24-Hour Curebox Cured Specimens

| Specimen Identification | Wet Unit Weight (pcf) | As-Tested Unit Weight (pcf) | Compression Strength (4 x 8) (psi) | Modulus of Elasticity (psi) |
|---|---|---|---|---|
| G1A-1-24 | 118.7 | 117.7 | 7,093 | 3,386,729 |
| G1A-2-24 | 118.7 | 117.7 | 7,093 | 3,524,518 |
| G1A-3-24 | 118.7 | 117.7 | 7,093 | 3,508,675 |
| G1B-1-24 | 119.8 | 118.8 | 5,915 | 2,975,988 |
| G1B-2-24 | 119.8 | 118.8 | 5,915 | 3,005,111 |
| G1B-3-24 | 119.8 | 118.8 | 5,915 | 3,032,753 |
| G2A-1-24 | 120.0 | 119.0 | 9,807 | 3,789,901 |
| G2A-2-24 | 120.0 | 119.0 | 9,807 | 3,745,692 |
| G2A-3-24 | 120.0 | 119.0 | 9,807 | 3,109,247 |
| G2B-1-24 | 114.0 | 113.0 | 8,313 | 3,963,880 |
| G2B-2-24 | 114.0 | 113.0 | 8,313 | 3,865,080 |
| G2B-3-24 | 114.0 | 113.0 | 8,313 | 3,888,308 |
| 8F-4 | 118.6 | 117.6 | 8,870 | 3,577,737 |
| 8F-5 | 118.6 | 117.6 | 8,870 | 3,673,648 |
| 8F-6 | 118.6 | 117.6 | 8,870 | 3,747,778 |
| 10F-4 | 121.0 | 120.0 | 9,750 | 3,744,977 |
| 10F-5 | 121.0 | 120.0 | 9,750 | 3,686,261 |
| 10F-6 | 121.0 | 120.0 | 9,750 | 3,801,950 |
| 12F-4 | 124.0 | 123.0 | 11,490 | 4,139,841 |
| 12F-5 | 124.0 | 123.0 | 11,490 | 4,188,613 |
| 12F-6 | 124.0 | 123.0 | 11,490 | 4,031,863 |
| 8L-4 | 122.0 | 121.0 | 7,730 | 3,748,723 |
| 8L-5 | 122.0 | 121.0 | 7,730 | 3,688,108 |
| 8L-6 | 122.0 | 121.0 | 7,730 | 3,558,556 |
| 12L-4 | 122.8 | 121.8 | 11,101 | 4,224,670 |
| 12L-5 | 122.8 | 121.8 | 11,101 | 4,262,995 |
| 12L-6 | 122.8 | 121.8 | 11,101 | 4,262,688 |

Table C.3  28-Day Curebox Cured Specimens

| Specimen Identification | Wet Unit Weight (pcf) | As-Tested Unit Weight (pcf) | Compression Strength (4 x 8) (psi) | Modulus of Elasticity (psi) |
|---|---|---|---|---|
| 8F-7 | 118.6 | 116.6 | 9,830 | 3,890,477 |
| 8F-8 | 118.6 | 116.6 | 9,830 | 3,849,350 |
| 8F-9 | 118.6 | 116.6 | 9,830 | 3,806,191 |
| 10F-7 | 121.0 | 119.0 | 10,430 | 4,016,648 |
| 10F-8 | 121.0 | 119.0 | 10,430 | 4,684,482 |
| 10F-9 | 121.0 | 119.0 | 10,430 | 4,043,618 |
| 10F-10 | 121.0 | 119.0 | 10,430 | 4,120,260 |
| 12F-7 | 124.0 | 122.0 | 11,460 | 4,361,462 |
| 12F-8 | 124.0 | 122.0 | 11,460 | 4,331,051 |
| 12F-9 | 124.0 | 122.0 | 11,460 | 4,207,477 |

Table C.4  56-Day Curebox Cured Specimens

| Specimen Identification | Wet Unit Weight (pcf) | As-Tested Unit Weight (pcf) | Compression Strength (4 x 8) (psi) | Modulus of Elasticity (psi) |
|---|---|---|---|---|
| G1A-1-56 | 118.7 | 116.2 | 9,084 | 3,814,994 |
| G1A-2-56 | 118.7 | 116.2 | 9,084 | 3,901,364 |
| G1A-3-56 | 118.7 | 116.2 | 9,084 | 3,877,308 |
| G1B-1-56 | 119.8 | 117.3 | 7,750 | 3,302,301 |
| G1B-2-56 | 119.8 | 117.3 | 7,750 | 3,247,403 |
| G1B-3-56 | 119.8 | 117.3 | 7,750 | 3,295,650 |
| G2A-1-56 | 120.0 | 117.5 | 10,418 | 4,036,274 |
| G2A-2-56 | 120.0 | 117.5 | 10,418 | 3,874,421 |
| G2A-3-56 | 120.0 | 117.5 | 10,418 | 3,891,948 |
| G2B-1-56 | 114.0 | 111.5 | 10,249 | 4,076,345 |
| G2B-2-56 | 114.0 | 111.5 | 10,249 | 4,184,515 |
| G2B-3-56 | 114.0 | 111.5 | 10,249 | 4,029,685 |
| 8F-10 | 118.6 | 116.1 | 10,600 | 3,875,411 |
| 8F-11 | 118.6 | 116.1 | 10,600 | 3,671,790 |
| 8F-12 | 118.6 | 116.1 | 10,600 | 4,016,215 |
| 10F-11 | 121.0 | 118.5 | 11,170 | 4,195,290 |
| 10F-12 | 121.0 | 118.5 | 11,170 | 4,176,745 |
| 10F-13 | 121.0 | 118.5 | 11,170 | 3,861,762 |
| 12F-10 | 124.0 | 121.5 | 11,550 | 4,209,773 |
| 12F-11 | 124.0 | 121.5 | 11,550 | 4,276,240 |
| 12F-12 | 124.0 | 121.5 | 11,550 | 4,295,494 |
| 8L-7 | 119.4 | 116.9 | 10,430 | 4,034,355 |
| 8L-8 | 119.4 | 116.9 | 10,430 | 4,040,931 |
| 8L-9 | 119.4 | 116.9 | 10,430 | 3,990,007 |
| 10L-1 | 122.4 | 119.9 | 9,920 | 4,104,663 |
| 10L-2 | 122.4 | 119.9 | 9,920 | 4,067,865 |
| 10L-3 | 122.4 | 119.9 | 9,920 | 4,075,294 |
| 12L-7 | 121.7 | 119.2 | 10,860 | 4,207,700 |
| 12L-8 | 121.7 | 119.2 | 10,860 | 4,207,945 |
| 12L-9 | 121.7 | 119.2 | 10,860 | 4,304,298 |

375

Table C.5  56-Day ASTM Cured Specimens

| Specimen Identification | Wet Unit Weight (pcf) | As-Tested Unit Weight (pcf) | Compression Strength (4 x 8) (psi) | Modulus of Elasticity (psi) |
|---|---|---|---|---|
| G1A-1-ASTM-56 | 118.7 | 116.2 | 9,352 | 3,875,746 |
| G1A-2-ASTM-56 | 118.7 | 116.2 | 9,575 | 3,774,216 |
| G1A-3-ASTM-56 | 118.7 | 116.2 | 9,834 | 4,096,713 |
| G1A-4-ASTM-56 | 118.7 | 116.2 | 8,715 | 3,593,701 |
| G1A-5-ASTM-56 | 118.7 | 116.2 | 9,252 | 3,816,347 |
| G1B-1-ASTM-56 | 119.8 | 117.3 | 8,063 | 3,623,900 |
| G1B-2-ASTM-56 | 119.8 | 117.3 | 8,252 | 3,328,719 |
| G1B-3-ASTM-56 | 119.8 | 117.3 | 9,056 | 3,740,114 |
| G2A-1-ASTM-56 | 120.0 | 117.5 | 10,377 | 3,984,773 |
| G2A-2-ASTM-56 | 120.0 | 117.5 | 11,377 | 3,927,559 |
| G2A-3-ASTM-56 | 120.0 | 117.5 | 11,369 | 4,297,258 |
| G2A-4-ASTM-56 | 120.0 | 117.5 | 10,555 | 4,131,074 |
| G2A-5-ASTM-56 | 120.0 | 117.5 | 10,405 | 3,979,495 |
| G2B-1-ASTM-56 | 114.0 | 111.5 | 10,244 | 4,283,444 |
| G2B-2-ASTM-56 | 114.0 | 111.5 | 10,826 | 3,912,993 |
| G2B-3-ASTM-56 | 114.0 | 111.5 | 10,523 | 3,964,648 |
| 8F-13 | 118.6 | 116.1 | 11,090 | 4,059,005 |
| 8F-14 | 118.6 | 116.1 | 11,090 | 4,272,725 |
| 8F-15 | 118.6 | 116.1 | 11,090 | 4,051,198 |
| 10F-14 | 121.0 | 118.5 | 11,300 | 4,273,372 |
| 10F-15 | 121.0 | 118.5 | 11,300 | 4,353,486 |
| 10F-16 | 121.0 | 118.5 | 11,300 | 4,163,007 |
| 12F-13 | 124.0 | 121.5 | 11,620 | 4,344,719 |
| 12F-14 | 124.0 | 121.5 | 11,620 | 4,535,964 |
| 12F-15 | 124.0 | 121.5 | 11,620 | 4,313,065 |
| 8L-10 | 119.4 | 116.9 | 10,520 | 4,382,289 |
| 8L-11 | 119.4 | 116.9 | 10,520 | 4,461,557 |
| 8L-12 | 119.4 | 116.9 | 10,520 | 4,318,485 |
| 10L-4 | 122.4 | 119.9 | 11,040 | 4,406,935 |
| 10L-5 | 122.4 | 119.9 | 11,040 | 4,285,072 |
| 10L-6 | 122.4 | 119.9 | 11,040 | 4,283,424 |
| 12L-10 | 121.7 | 119.2 | 11,480 | 4,429,366 |
| 12L-11 | 121.7 | 119.2 | 11,480 | 4,304,119 |
| 12L-12 | 121.7 | 119.2 | 11,480 | 4,262,217 |

## C.2 Tension Test Results of Steel Used for Shear Stirrups
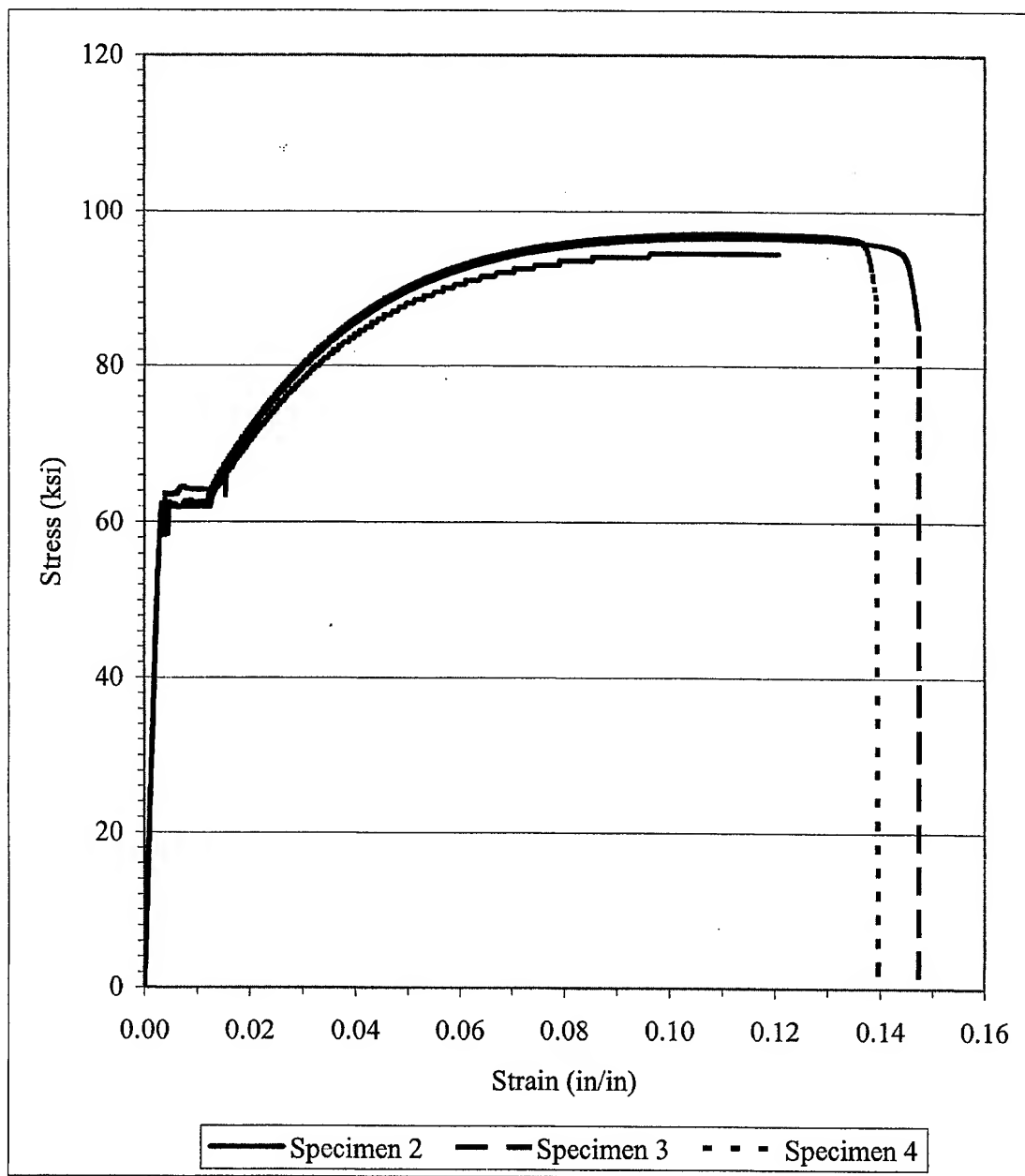


Figure C.1  Stress vs. Strain Plot for Shear Reinforcement Steel

## C.3 Tension Test Results of Steel Used for "Doghouse Bars"
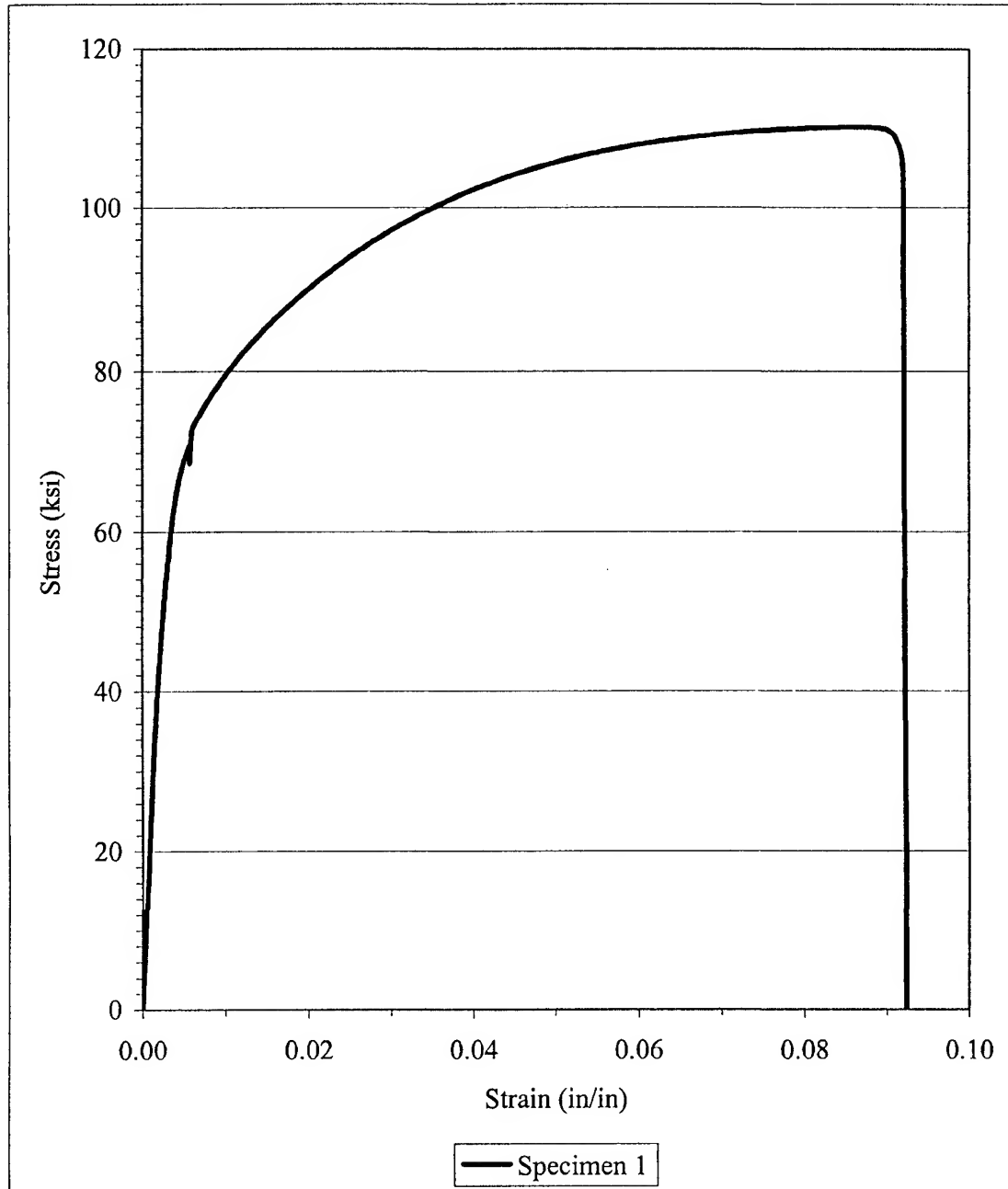


Figure C.2  Stress vs. Strain Plot for "Doghouse Bar" Reinforcement Steel

# APPENDIX D

## GIRDER DESIGN SPREADSHEET

Appendix D contains the individual pages from the Girder Design Spreadsheet. The entire set of worksheet pages is provided from the design of girder test G1C-West. The pages are listed in the order the calculations occur. All calculations are based on the 1996 AASHTO[40] Standard Specification for Highway Bridges. A similar series of worksheets was prepared for each girder test to determine girder test design characteristics. Listed below are the individual worksheets within the overall spreadsheet and a brief description of the worksheet's function. The Tables are all placed at the end of this Appendix.

**Table D.1 – Section and Material Properties for Girder Design**

**Table D.2 – Support Conditions, Calculation of $M_f$ and $P_u$** – Worksheet used to specify support conditions and determine predicted ultimate load.

**Table D.3 – Predicted Loss**

**Table D.4 – Non-Composite Girder Stress Calculations**

**Table D.5 – Composite Girder Stress Calculations**

**Tables D.6 and D.7 – Shear Design Calculations**

**Table D.8 – Deck / Girder Interface Shear Calculations**

Below is a description of each page of the spreadsheet. The general concept of the spreadsheet was to determine the flexural capacity based on the selected girder and strand pattern, then design the shear reinforcement to allow reaching the flexural capacity. Interface shear was checked as a precaution to insure no problems would occur during testing.

## D.1 Assumptions for Using Spreadsheet

This spreadsheet assumed the prestressed girder had straight prestressing strand. The strand could be set at any height, but was assumed to be straight. It was not possible to drape the strands within this spreadsheet. A possible modification to provide better flexibility in the spreadsheet would be to include this option.

## D.2 Worksheet 1 - Section and Material Properties for Girder Design

Worksheet 1 seen in Table D.1 allowed the user to enter variable data describing the girder's section and material properties. Following user-entered variables, the spreadsheet calculated values as follows.

The modulus of elasticity was based on the entered unit weight value. A unit weight greater than 135 pcf triggered the use of equation 3.1. A unit weight less than or equal to 135 pcf triggered the use of equation 3.3.

The modular ratio, $\eta$, was calculated using equation D.1.

$$\eta = \frac{E_{c-Deck}}{E_{c-Girder}} \qquad (D.1)$$

The non-composite girder properties (girder only) were hard-wired into the spreadsheet and triggered by user entry of the AASHTO or PCI Bulb Tee Type. The weight per foot of the girder was calculated based on the girder cross sectional area times the estimated equilibrium weight of the concrete. An allowance was incorporated into the worksheet where the user could enter a value for the added weight of steel (prestressed and non-prestressed) per cubic foot of concrete. This value was assumed to be 3 pcf for each girder design.

Composite girder properties were calculated as follows assuming full composite action between the girder and deck. The composite moment of inertia, $I_c$, was calculated using equations D.2 and D.3.

$$I_c = I_{nc} + A_{nc}(y_{bot-c} - y_{bot-nc})^2 + \frac{1}{12}\eta W_f t_d^3 + (\eta W_f t_d)(\frac{t_d}{2} + h_{g-nc} - y_{bot-c})^2 \qquad (D.2)$$

$$y_{bot-c} = \frac{A_{g-nc}y_{bot-nc} + \eta W_f t_d (h_{g-nc} + \frac{t_d}{2})}{A_{g-nc} + \eta W_f t_d} \qquad (D.3)$$

The remaining composite girder properties were calculated using equations D.4 through D.8.

$$y_{top-c} = h_{g-nc} - y_{bot-c} \qquad (D.4)$$

$$S_{bot-c} = \frac{I_c}{y_{bot-c}} \qquad (D.5)$$

$$A_{g-c} = A_{g-nc} + \eta\, W_f t_d \qquad (D.6)$$

$$Q_d = (\eta W_f t_d)(\frac{t_d}{2} + y_{top-c}) \qquad (D.7)$$

$$h_{g-c} = h_{g-nc} + t_d \qquad (D.8)$$

The composite girder weight per foot was the combined weight of the non-composite girder, the deck and the specified steel allowance.

The depth to prestressing steel, $d_p$, was calculated using equations D.9 and D.10.

$$d_p = MAX\left(h_{g-nc} + t_d - (y_{bot-nc} + e), 0.8 h_{g-c}\right) \qquad (D.9)$$

$$e = \frac{\sum F_{ps} d}{\sum F_{ps}} - y_{bot-nc} \qquad (D.10)$$

The variable "e" described the location of the centroid of the prestressing force in reference to the non-composite girder centroid. A negative value of "e" indicated the prestressing force centroid was below the non-composite centroid.

382

The predicted strand development length, $l_d$, was calculated using AASHTO[40] equation (9-32) shown in equation D.11 below.

$$l_d = (f_{ps} - \frac{2}{3}f_{se})d_b \qquad (D.11)$$

The predicted strand transfer length, $l_t$, was calculated using the AASHTO[40] specified $50*d_b$.

## D.3 Worksheet 2 – Supports, Applied Load and Moment Furnished

Worksheet 2 shown in Table D.2 provided the user a visual image of the girder with support locations and location of point load application. This page allowed the user to input values describing the location of the left and right support and the location at which the point load was applied. Based on this input, the spreadsheet adjusted the support locations, determined the moment furnished at all points along the girder based on the number of prestressing strands developed, then determined the maximum point load, based on flexural capacity, that could be applied at the location specified. The spreadsheet accounted for the self-weight of the girder and deck in determining the maximum point load and also calculated the support reactions.

At the lower right portion of the page were values required to calculate the maximum furnished moment. This section of Worksheet 2 determined, based on user input on the girder and deck characteristics, whether the girder was "under" or "over" reinforced and whether "a" was within the deck. The spreadsheet provided calculations

383

for all combinations except "over" reinforced and "a" being greater than the deck thickness. The desired condition for this research was to be under-reinforced and to have "a" within the deck. Equations D.12 through D.18 were used to determine the moment furnished.

$$f_{ps} = f_{pu}\left(1 - \frac{\gamma_p \rho_p f_{pu}}{\beta_1 f_c^{'}}\right)$$ (D.12)

$$\gamma_p = 0.55 \; for \frac{f_{py}}{f_{pu}} \geq 0.80, \; 0.40 \; for \frac{f_{py}}{f_{pu}} \geq 0.85, \; 0.28 \; for \frac{f_{py}}{f_{pu}} \geq 0.90$$ (D.13)

$$\rho_p = \frac{A_{ps}}{bd_p}$$ (D.14)

$$\beta_1 = 0.85 - (f_c^{'} - 4,000)0.05 \geq 0.65$$ (D.15)

$$\varpi_p = \frac{\rho_p f_{ps}}{f_{c-Deck}^{'}}$$ (D.16)

If $\omega_p$ was less than $0.36\beta_1$, the girder was considered under-reinforced. The rectangular stress block depth, "a" was determined based on the composite girder characteristics. If "a" was less than the deck thickness, the girder was considered a rectangular section and the moment furnished (nominal moment) was calculated using equation D.17.

$$M_n = A_{ps} f_{ps} (d_p - \frac{a}{2})$$ (D.17)

If "a" was greater than the deck thickness, the moment furnished (nominal moment) was calculated using equation D.18.

$$M_n = 0.85 f'_{c-Dk} t_d W_f (d_p - \frac{a}{2}) + 0.85 f'_{c-Girder} \left( W_{f-Girder} (a - t_d) \left( d_p - t_d - \frac{(a - t_d)}{2} \right) \right)$$ (D.18)

## D.4 Worksheet 3 – Loss Calculations

Worksheet 3 as shown in Table D.3 provided loss calculations based on procedures specified in the 1996 AASHTO[40] Specification. The losses were divided into three groups. The first group included elastic shortening (ES) and initial steel relaxation (R) losses experienced at the time prestressing strands were released. The second group included creep (CR), shrinkage (S) and additional steel relaxation (R) experienced from the time of strand release until the time of deck placement. The third and final group included additional steel relaxation (R) and creep (CR) that occurred in the time between deck placement and testing. The user had only limited input on this page. It was necessary for the user to input an assumption for the percent of losses due to elastic shortening (ES) which occurred at the time the prestressing strand was cut. It was necessary for the user to iterate this guess until the assumed amount and the actual amount were within 0.1 percent of each other. A good initial assumption was around six

percent. It was also necessary for the user to input percentages of steel relaxation that occurred during the different stages. If the user-entered percentages did not total 100, the spreadsheet automatically indicated an error was made. At the bottom of the sheet, a consolidated listing was provided showing the effective levels of prestress at the different stages of the girder's construction sequence. Losses were calculated using equations D.19 through D.22.

$$ES = \frac{E_{ps}}{E_{ci-g}}\left(\frac{P_i}{A_{g-nc}}\left(1+\frac{e^2}{r_{nc}^2}\right)-\frac{M_D e}{I_{nc}}\right) \qquad (D.19)$$

$$CR = 12\left(\frac{P_i}{A_{g-nc}}\left(1+\frac{e^2}{r_{nc}^2}\right)-\frac{M_D e}{I_{nc}}\right)+7f_{cds} \qquad (D.20)$$

In the case of the test girders, $f_{cds}$, the stress at the centroid of the prestressing strand was zero at the time of deck placement. At testing, $f_{cds}$ was no longer zero based on the addition of the deck. An additional creep component, although small, was added at that stage.

$$SH = (17,000-150RH) \qquad (D.21)$$

$$R = 5000-0.10ES-0.05(SH+CR) \qquad (D.22)$$

Steel relaxation losses were broken into three pieces including "initial", "at deck placement" and "at testing." Percentages were assigned to each particular component as deemed appropriate.

## D.5 Worksheet 4 - Non-Composite Stress Calculations (Stages 1 and 2)

Worksheet 4 as shown in Table D.4 provided stresses at the TOP and BOTTOM of the girder at the 20$^{th}$ points at stages 1 (Strand Release) and 2 (Deck Placement). Shown on the girder were the values of girder self-weight and deck self-weight. Included in the self-weight values was a small component due to the weight of the reinforcing and prestressing steel. This value was entered on Worksheet 1 as the Steel Weight Allowance per Cubic Foot. The stresses were broken down by axial component, strand eccentricity (F*e) component, and dead load (DL) component. The stress level used at stage 1 was the effective prestress after elastic shortening (ES) and initial strand relaxation (R) losses occurred. The stress level used at stage 2 was the effective prestress after all losses occurred except final strand relaxation and final creep losses. The stress levels at the various stages can be seen on Worksheet 3, Table D.3 at the bottom left corner. In order to calculate the stress level at a given 20$^{th}$ point, the spreadsheet calculated the transfer length on Worksheet 1 then determined the number of strands developed. Throughout the sheet, negative (-) values indicate compression stress and positive (+) values indicate tension stress. Equations D.23 and D.24 were used to calculate stresses at the top and bottom of the non-composite girder at stages 1 and 2.

$$f_{top} = -\frac{F_{se}}{A_{g-nc}} - \frac{F_{se}e}{S_{top-nc}} - \frac{M_{DL}}{S_{top-nc}} \qquad (D.23)$$

$$f_{bot} = -\frac{F_{se}}{A_{g-nc}} + \frac{F_{se}e}{S_{bot-nc}} + \frac{M_{DL}}{S_{bot-nc}} \qquad (D.24)$$

The values of $F_{se}$ and $M_{DL}$ were different between the two stages. Fse became less over time. $M_{DL}$ was the weight of the girder only for stage 1. For stage 2, it was the weight of the girder and the deck.

## D.6  Worksheet 5 - Composite Stress Calculations (Stage 3)

Worksheet 5 shown in Table D.5 provided calculations of composite stresses at the top and bottom of the girder and slab at time of testing. The stresses were broken down by axial component, strand eccentricity (F*e) component, dead load (DL) component, and live load (LL) component. The stress level used at stage 3 was the effective prestress after all losses occurred. The live load component reflected stresses resulting from the point load application. Determination of the number of strands developed was based on the strand development length specified in Worksheet 1. Moment values shown were listed in ft-kips. The support condition number indicated the position of the supports. A support condition number "1" indicated the supports were located at the ends of the girder offset by the X-DIST. A support condition "2" indicated the right-side support was moved in from the end forming a cantilever. A support condition "3" indicated both the left and right side supports were moved in from their

respective ends forming a double-cantilevered girder. The spreadsheet referred to these support condition numbers when determining the dead load moment values. As a note, these support condition numbers were not shown on the non-composite stress calculations page since at stages 1 and 2 the girder was supported at its centers of bearing (COB). Only during testing would the supports be moved to other than the end center of bearing locations. Equations D.25 and D.26 were used to calculate stresses at top and bottom of the girder at stage 3.

$$f_{top} = -\frac{F_{se}}{A_{g-nc}} - \frac{F_{se}e}{S_{top-nc}} - \frac{M_{DL}}{S_{top-nc}} - \frac{M_{LL}}{S_{top-c}} \qquad (D.25)$$

$$f_{bot} = -\frac{F_{se}}{A_{g-nc}} + \frac{F_{se}e}{S_{bot-nc}} + \frac{M_{DL}}{S_{bot-nc}} + \frac{M_{LL}}{S_{bot-c}} \qquad (D.26)$$

The stresses at the top and bottom of the deck were calculated based on the live load moment only using equations D.27 and D.28.

$$f_{top} = -\frac{M_{LL}(y_{top-c} + t_d)}{I_c} \qquad (D.27)$$

$$f_{bot-Deck} = -\frac{M_{LL}y_{top-c}}{I_c} \qquad (D.28)$$

## D.7 Worksheet 6 – Girder Shear Design (Left of Load)

Worksheet 6 shown in Table D.6 performed shear design calculations for the section of the girder at $10^{th}$ points from the left support to the point load based on the 1996 AASHTO[40] Specification. The distance from the left support to the point load was "a." Values of $M_u$ and $V_u$ were calculated at each point based on all dead and live loads. The value of $M_u$ at the point load location was the same as the maximum furnished moment if all strands were developed at that point. $V_{ci}$ (flexure shear strength) and $V_{cw}$ (web shear strength) were calculated to determine the concrete strength component $V_c$ using equations D.29 through D.32. $V_c$ was the minimum of the $V_{ci}$ and $V_{cw}$ values.

$$V_{ci} = 0.6\lambda \frac{\sqrt{f_c'}}{1000} bd_p + V_d + \frac{V_i M_{cr}}{M_{max}} \geq 1.7\lambda \frac{\sqrt{f_c'}}{1000} bd_p \qquad (D.29)$$

$$M_{cr} = \frac{I}{Y_t}(6\lambda \frac{\sqrt{f_c'}}{1000} + f_{pe} - f_d) \qquad (D.30)$$

$$V_{cw} = (3.5\lambda \frac{\sqrt{f_c'}}{1000} + 0.3 f_{pc})bd_p + V_p \qquad (D.31)$$

$$f_{pc} = \frac{F_{se}}{A_{nc}} - \frac{F_{se}e(y_{bot-c} - y_{bot-nc})}{I_{nc}} - \frac{M_{DL}(y_{bot-c} - y_{bot-nc})}{I_{nc}} \qquad (D.32)$$

Based on the required shear, $V_u$, the spreadsheet determined the shear to be carried by shear stirrups, $V_s$, using equation D.33.

$$V_s = \frac{V_u - V_c}{\phi_s} \qquad (D.33)$$

The required minimum stirrup spacing, s, was calculated based on several criteria as specified in equations D.34 through D.35. If $V_s > 8 \, (f_c')^{1/2} \, bd_p$, web crushing was considered a potential a problem. The girder section was not adequate to handle the shear force. If $V_s > 4 \, (f_c')^{1/2} \, bd_p$, the value from D.34 was divided by 2. The resulting minimum stirrup spacing was the minimum of equations D.34 and D.35.

$$s_{max} = MAX(0.75h_{g-c}, 24 \ inches) \qquad (D.34)$$

$$s = \frac{A_v f_y d_p}{V_s} \qquad (D.35)$$

## D.8 Worksheet 7 - Girder Shear Design (Right of Load)

Worksheet 7 shown in Table D.7 performed the same calculations as Worksheet 6 at $10^{th}$ points from the load to the right support. The distance from the load to the right support was "b."

391

## D.9 Worksheet 8 – Interface Shear Check

Worksheet 8 shown in Table D.8 performed calculations to insure adequate capacity existed at the interface between the girder and deck. The basic interface shear capacity, $V_{nh}$, was determined based on the condition of the surface of the girder and the contact area using equation D.36.

$$V_{nh} = v_{nh} A_c \qquad (D.36)$$

$$A_{v-\min} = \frac{50bs}{f_y} \frac{1}{s} \qquad (D.37)$$

Based on the cleanliness and roughness of the contact surface and the inclusion of minimum shear reinforcement steel per linear inch of girder according to equation D.37, the spreadsheet listed the basic interface shear stress, $v_{nh}$, the maximum value being 350 psi. The contact area, $A_c$, was determined as the interface shear contact width (width of the top of girder in this case) multiplied by the contact length, d, which was the distance from the point load to the closest support or one tenth of the span length, $L_l$, whichever was less. For this research, the length "d" was typically taken as one tenth of the span. The basic interface shear capacity was compared with the shear at the left support (worst case based on the configuration of this spreadsheet). If the basic capacity exceeded the worst-case shear, no further steel was required. If the basic capacity was inadequate, the added capacity of the shear steel was calculated.

The added capacity was calculated based on the amount of steel beyond the code-specified minimum in equation D.37. For every one percent of steel provided beyond the minimum, the interface shear capacity increased by an amount calculated in equation D.38.

$$Additional\ V_{nh}\ per\ one\ \%\ steel = \left(\frac{160 f_y}{40,000}\right) bd \qquad (D.38)$$

In most cases, as was true in this research, the steel provided by minimum shear reinforcement more than satisfied the requirement. No additional steel was required to meet interface shear requirements.

On the right-hand side of worksheet 8 are calculations for tensile stress at the shear interface. These calculations were provided to check the resulting tensile stress under maximum live load for comparison with acceptable levels. Acceptable levels were defined as $7.5 * \lambda * (f_c')^{1/2}$. For slab concrete which was assumed to be normal weight concrete, $\lambda = 1$. For the girder which was constructed with HSLC, $\lambda = 0.85$. Using a Mohr's circle calculation to determine tensile stress at the interface, the result was compared with the acceptable levels for both the slab and girder. If the tensile stress was less than both levels, the indicator window indicated, "Tensile Stress at Interface is OK."

Table D.1  Section and Material Properties for Girder Design

## Section and Material Properties for Pretensioned Girder Design

### Glc-West

**Deck Variables**

| Description | Symbol | Value | Unit |
|---|---|---|---|
| Deck Thickness | $t_d$ | 7.5 | IN |
| Deck Width | $W_f$ | 40 | IN |
| Concrete Strength | $f'_c$ | 3500 | PSI |
| Concrete Weight | $W_c$ | 145 | PCF |

**Girder Cross Section Variables**

| Description | Symbol | Value | Unit |
|---|---|---|---|
| Girder Type | | 2 | 1-5,BT |
| Girder Top Flange Width | | 12 | IN |
| Concrete Design Strength | $f'_c$ | 8000 | PSI |
| Concrete Equilibrium Weight | $W_c$ | 155 | PCF |
| % Concrete Strength at Release | | 75% | % |
| LWC Reduction Factor | $\lambda$ | 0.85 | None |
| Strand Diameter | $d_b$ | 0.6 | IN |
| Strand C/S Area | $A_{st}$ | 0.217 | $IN^2$ |
| Strand Ultimate Strength | $f_{pu}$ | 270 | KSI |
| Strand Yield as % of Ultimate | | 0.9 | None |
| Strand Modulus of Elasticity | $E_{ps}$ | 28500 | KSI |
| Stirrup Size | | 4 | # |
| Stirrup Yield Strength | $f_y$ | 75 | KSI |
| Distance from End to COB | XDIST | 6.00 | IN |
| Percent Strand Ultimate at Jacking | | 75% | % |
| Top of Beam to Top Strands | TCL | 2.50 | IN |
| Bottom of Beam to Bottom Strands | BCL | 3.00 | IN |
| Strand Spacing | SPAC | 2.00 | IN |

**Miscellaneous Variables Normally Constant**

| Description | Symbol | Value | Unit |
|---|---|---|---|
| Steel Weight Allowance / Cubic Ft | | 3.0 | PCF |
| Prestress stress for $l_d$ calculation | $f_{ps}$ | 270 | KSI |
| Ratio of Prestressed Reinforcement | $\phi_s$ | 1.00 | None |
| Shear Strength Reduction Factor | $\phi_s$ | 1.00 | None |
| Flexural Strength Reduction Factor | $\phi_f$ | 1.00 | None |

**Elasticity Modulus Values**

| Description | Symbol | Value | Unit |
|---|---|---|---|
| Deck Modulus | $E_{cd}$ | 3.41E+06 | PSI |
| Girder Modulus | $E_{cg}$ | 3.59E+06 | PSI |
| Modular Ratio ($E_{cd}/E_{cg}$) | $\eta$ | 0.950 | None |

**Non-Composite Girder Properties**

| Description | Symbol | Value | Unit |
|---|---|---|---|
| Moment of Inertia | $I_{nc}$ | 50979 | $IN^4$ |
| Distance from Centroid to Top of Beam | $Y_{top-nc}$ | 20.17 | IN |
| Distance from Centroid to Bot. of Beam | $Y_{bot-nc}$ | 15.83 | IN |
| Section Modulus (Top) | $S_{top-nc}$ | 2527.47 | $IN^3$ |
| Section Modulus (Bot) | $S_{bot-nc}$ | 3220.40 | $IN^3$ |
| Cross Sectional Area | $A_{g-nc}$ | 369 | $IN^2$ |
| Weight per Foot (Concrete & Steel) | $W_{g-nc}$ | 0.305 | K/FT |
| Web Thickness | $b$ | 6 | IN |
| Height of Girder | $h_{g-nc}$ | 36 | IN |

**Composite Girder Properties**

| Description | Symbol | Value | Unit |
|---|---|---|---|
| Moment of Inertia | $I_c$ | 142547.25 | $IN^4$ |
| Distance from Centroid to Top of Beam | $Y_{top-c}$ | 10.84 | IN |
| Distance from Centroid to Bot. of Beam | $Y_{bot-c}$ | 25.16 | IN |
| Section Modulus (Bot) | $S_{bot-c}$ | 5664.62 | $IN^3$ |
| Cross Sectional Area | $A_{g-c}$ | 576.68 | $IN^2$ |
| Weight per Foot (Concrete & Steel) | $W_{g-c}$ | 0.5295 | K/FT |
| First Moment of Deck About Centroid | $Q_d$ | 3444.42 | $IN^3$ |
| Overall Depth of Composite Girder | $h_{g-c}$ | 47.5 | IN |

**Miscellaneous Properties**

| Description | Symbol | Value | Unit |
|---|---|---|---|
| Stirrup Area | $A_v$ | 0.4 | $IN^2$ |
| Depth to Prestressing Steel | $d_p$ | 38.4 | IN |
| Ratio of Prestressed Reinforcement | $\rho_p$ | 0.0030 | None |
| Strand Yield to Ultimate Factor | $\gamma_p$ | 0.28 | None |
| Ratio of a/c (Based on Deck Concrete) | $\beta_1$ | 0.85 | None |

**Strand Data (No Drape)**

| Ref. # | Dist. IN | Nbr # | % $l_{ps}$ % | $F_{ps}$ KIP | $F_{ps}d$ KIP-IN |
|---|---|---|---|---|---|
| 18 | TOP 33.5 | 2 | 0.75 | 87.89 | 2944.1 |
| 17 | | 0 | 0.00 | 0.00 | 0.0 |
| 16 | | 0 | 0.00 | 0.00 | 0.0 |
| 15 | 31.0 | 0 | 0.00 | 0.00 | 0.0 |
| 14 | 29.0 | 0 | 0.00 | 0.00 | 0.0 |
| 13 | 27.0 | 0 | 0.00 | 0.00 | 0.0 |
| 12 | 25.0 | 0 | 0.00 | 0.00 | 0.0 |
| 11 | 23.0 | 0 | 0.00 | 0.00 | 0.0 |
| 10 | 21.0 | 0 | 0.00 | 0.00 | 0.0 |
| 9 | 19.0 | 0 | 0.00 | 0.00 | 0.0 |
| 8 | 17.0 | 0 | 0.00 | 0.00 | 0.0 |
| 7 | 15.0 | 0 | 0.00 | 0.00 | 0.0 |
| 6 | 13.0 | 0 | 0.00 | 0.00 | 0.0 |
| 5 | 11.0 | 0 | 0.00 | 0.00 | 0.0 |
| 4 | 9.0 | 0 | 0.00 | 0.00 | 0.0 |
| 3 | 7.0 | 0 | 0.00 | 0.00 | 0.0 |
| 2 | 5.0 | 0 | 0.00 | 0.00 | 0.0 |
| 1 | 3.0 | 8 | 0.75 | 351.54 | 1054.6 |

**Eccentricity from NC Centroid**

| | | |
|---|---|---|
| Distance | -6.73 | IN |

**Strand Development Length**

| | | |
|---|---|---|
| AASHTO-STD (96) | 96.14 | IN |
| Dist. from Bearing | 90.14 | IN |

**Strand Transfer Length**

| | | |
|---|---|---|
| AASHTO-STD (96) | 38.04 | IN |

394

Table D.2  Support Conditions, Calculation of Moment Furnished and Predicted Ultimate Load

| G1C-West | | Support Conditions, Applied Load (KIP) and Moment Furnished (FT-KIP) | | | | | | | | | | | | | | | | | | | |
|---|---|---|---|---|---|---|---|---|---|---|---|---|---|---|---|---|---|---|---|---|---|
| REF | BRNG | 0.05L | 0.10L | 0.15L | 0.20L | 0.25L | 0.30L | 0.35L | 0.40L | 0.45L | 0.50L | 0.55L | 0.60L | 0.65L | 0.70L | 0.75L | 0.80L | 0.85L | 0.90L | 0.95L | BRNG |
| FT | 0.00 | 2.10 | 4.20 | 6.30 | 8.40 | 10.50 | 12.60 | 14.70 | 16.80 | 18.90 | 21.00 | 23.10 | 25.20 | 27.30 | 29.40 | 31.50 | 33.60 | 35.70 | 37.80 | 39.90 | 42.00 |
| IN | 0.00 | 25.20 | 50.40 | 75.60 | 100.80 | 126.00 | 151.20 | 176.40 | 201.60 | 226.80 | 252.00 | 277.20 | 302.40 | 327.60 | 352.80 | 378.00 | 403.20 | 428.40 | 453.60 | 478.80 | 504.00 |

Number of Strands Developed Assuming $l_d$

| | BRNG | 0.05L | 0.10L | 0.15L | 0.20L | 0.25L | 0.30L | 0.35L | 0.40L | 0.45L | 0.50L | 0.55L | 0.60L | 0.65L | 0.70L | 0.75L | 0.80L | 0.85L | 0.90L | 0.95L | BRNG |
|---|---|---|---|---|---|---|---|---|---|---|---|---|---|---|---|---|---|---|---|---|---|---|
| # Top | 0.12 | 0.65 | 1.17 | 1.70 | 2.00 | 2.00 | 2.00 | 2.00 | 2.00 | 2.00 | 2.00 | 2.00 | 2.00 | 2.00 | 2.00 | 2.00 | 2.00 | 1.70 | 1.17 | 0.65 | 0.12 |
| # Bot | 0.50 | 2.60 | 4.69 | 6.79 | 8.00 | 8.00 | 8.00 | 8.00 | 8.00 | 8.00 | 8.00 | 8.00 | 8.00 | 8.00 | 8.00 | 8.00 | 8.00 | 6.79 | 4.69 | 2.60 | 0.50 |
| $M_f$ | 94.7 | 492.3 | 889.9 | 1287.5 | 1516.9 | 1516.9 | 1516.9 | 1516.9 | 1516.9 | 1516.9 | 1516.9 | 1516.9 | 1516.9 | 1516.9 | 1516.9 | 1516.9 | 1516.9 | 1287.5 | 889.9 | 492.3 | 94.7 |

Max Load (KIPS): 233

| Type of Load | L Support Reaction (KIPS) | R Support Reaction (KIPS) |
|---|---|---|
| Dead | 11.38 | 11.38 |
| Point | 193.46 | 39.25 |
| Total | 204.85 | 50.63 |

UNBRACED CONSTRUCTION

| | | | | | |
|---|---|---|---|---|---|
| a | Distance from left support to point load | 85.0 | IN | 7.08 | FT |
| $L_1$ | Distance from left support to right support | 504.0 | IN | 42.00 | FT |
| $L_2$ | Distance from left COB to left support | 0.00 | IN | 0.00 | FT |
| L | Overall Length of Beam (COB-COB) | 504.0 | IN | 42.00 | FT |
| b | Distance from point load to right support | 419.0 | IN | 34.92 | FT |
| $L_3$ | Distance from right support to right COB | 0.0 | IN | 0.00 | FT |
| a/d | Ratio of shear distance to depth | 2.36 | NA | | |

| $M_f$ (Max) Calculations | | |
|---|---|---|
| $d_p$ | 38.40 | IN |
| $\rho_p$ | 0.00297 | None |
| $f_{ps}$ | 249.6 | KSI |
| $\omega_p$ | 0.2121 | .36$\beta_1$ | 0.306 |
| Beam is Under-reinforced | | |
| a < Deck Thickness | | |
| a | 9.58 | IN |
| $M_f$ | 1516.9 | FT-KIP |

DECK

BEAM

SUPT 1

Table D.3 Loss Calculations

## Prestressed Girder Loss Calculations

### G1C-West

**Beam Values**

| Description | Symbol | Value | Units |
|---|---|---|---|
| Girder Length (COB-COB) | $L$ | 42.00 | FT |
| Girder Cross Sectional Area | $A_{g-nc}$ | 369 | $IN^2$ |
| NC Moment of Inertia | $I_{nc}$ | 50979 | $IN^4$ |
| NC Section Modulus (Top) | $S_{top-nc}$ | 2527.47 | $IN^3$ |
| NC Section Modulus (Bot) | $S_{bot-nc}$ | 3220.40 | $IN^3$ |
| Strand Eccentricity from NC Centroid | $e$ | -6.73 | IN |
| NC Girder Weight / Foot (Concrete & Steel) | $W_D$ | 0.305 | K/FT |
| Deck Weight / Foot (Concrete & Steel) | $W_{SD}$ | 0.225 | K/FT |

**Steel Values**

| Description | Symbol | Value | Units |
|---|---|---|---|
| Area of Prestressing Steel | $A_{ps}$ | 2.17 | $IN^2$ |
| Strand Ultimate Strength | $f_{pu}$ | 270 | KSI |
| Strand Yield Strength | $f_{py}$ | 243 | KSI |
| Strand Modulus of Elasticity | $E_{ps}$ | 28500 | KSI |
| Percent Strand Ultimate at Jacking | % | 0.75 | None |
| Strand Jacking Stress | $f_{si}$ | 202.5 | KSI |

**Concrete Values**

| Description | Symbol | Value | Units |
|---|---|---|---|
| Girder Concrete Design Strength | $f'_c$ | 8000 | PSI |
| Girder Design Modulus | $E_{cg}$ | 3.59E+06 | PSI |
| % Girder Concrete Strength at Release | % | 75% | % |
| Girder Concrete Strength at Release | $f'_{ci}$ | 6000 | PSI |
| Girder Modulus at Release | $E_{cig}$ | 3.43E+06 | PSI |

**ES-Elastic Shortening (Release)**

| Description | Symbol | Value | Units |
|---|---|---|---|
| Radius of Gyration | $r_{nc}^2$ | 138.2 | $IN^2$ |
| Initial Jacking Force | $P_i$ | 439.4 | KIPS |
| Est. Jacking Force Loss | OK | -5.7% | % |
| Final Jacking Force | $P_i$ | 414.4 | KIPS |
| MAX Dead Load Moment | $M_D$ | 806.9 | IN-KIPS |
| Stress at Steel Centroid | $f_{cir}$ | -1.385 | KSI |
| Modular Ratio ($E_{ps}/E_{cig}$) | $\eta$ | 8.30 | None |
| ES Losses (KSI - %) | $\Delta_{pES}$ | -11.49 | -5.7% |

**R-Steel Stress Relax (Release)**

| Description | Symbol | Value | Units |
|---|---|---|---|
| % Relax at Release | | 40% | % |
| Time (Jack to Release) | $t_{rel}$ | 24 | HRS |
| R Losses (KSI - %) | $\Delta_{pR}$ | -0.81 | -0.4% |

**R-Steel Stress Relax (Deck Placement)**

| Description | Symbol | Value | Units |
|---|---|---|---|
| % Relax at Release | | 60% | % |
| Time (Release to Slab) | $t_{slab}$ | 30 | DAYS |
| R Losses (KSI - %) | $\Delta_{pR}$ | -1.62 | -0.8% |

**R-Steel Stress Relax (Testing)**

| Description | Symbol | Value | Units |
|---|---|---|---|
| % Relax at Release | | 40% | % |
| Time (Release to Test) | $t_{test}$ | 60 | DAYS |
| R Losses (KSI - %) | $\Delta_{pR}$ | -0.27 | -0.1% |

**CR-Creep (Deck Placement)**

| Description | Symbol | Value | Units |
|---|---|---|---|
| Modular Ratio ($E_{ps}/E_{cb}$) | $\eta$ | 7.95 | None |
| Stress at Steel Centroid | $f_{cir}$ | -1.385 | KSI |
| Addl. DL Since Release | $W_{SD}$ | 0.000 | K/FT |
| Moment due to $W_{SD}$ | $M_{SD}$ | 0.0 | IN-KIP |
| Stress at Steel Centroid | $f_{csd}$ | 0.000 | KSI |
| LWC Factor | | 1.0 | None |
| Creep Factor | $K_{CR}$ | 1.0 | None |
| CR Losses (KSI - %) | $\Delta_{pCR}$ | -16.62 | -8.2% |

**CR-Creep (Testing)**

| Description | Symbol | Value | Units |
|---|---|---|---|
| Modular Ratio ($E_{ps}/E_{cb}$) | $\eta$ | 7.95 | None |
| Stress at Steel Centroid | $f_{cir}$ | -1.385 | KSI |
| Addl. DL Since Release | $W_{SD}$ | 0.225 | K/FT |
| Moment due to $W_{SD}$ | $M_{SD}$ | 594.2 | IN-KIP |
| Stress at Steel Centroid | $f_{csd}$ | 0.078 | KSI |
| LWC Factor | | 1.0 | None |
| Creep Factor | $K_{CR}$ | 1.0 | None |
| CR Losses (KSI - %) | $\Delta_{pCR}$ | -0.55 | -0.3% |

**SH-Shrinkage (Deck Placement)**

| Description | Symbol | Value | Units |
|---|---|---|---|
| Shrinkage Factor | $K_{SH}$ | 1.0 | None |
| Relative Humidity | RH | 70 | % |
| SH Losses (KSI - %) | $\Delta_{pSH}$ | -6.50 | -3.2% |

**Steel Stress Relaxation Percentages-OK**

**Consolidated Loss Calculations**

| Stage | Total KSI Loss | % Loss |
|---|---|---|
| 1. At Release | -12.30 | -6% |
| 2. At Deck Placement | -37.03 | -18% |
| 3. At Testing | -37.85 | -19% |

**Remaining Prestress (KSI)**

| Symbol | Value | Losses |
|---|---|---|
| $f_{ps}$ | 190.20 | ES & R |
| $f_{se}$ | 165.47 | CR, SH & R |
| $f_{se}$ | 164.65 | CR & R |

396

## Table D.4 Non-Composite Stress Calculations

**G1C-West — Non-Composite Girder Stresses at Stages 1 and 2 of Construction**

| REF | BRNG | 0.05L | 0.10L | 0.15L | 0.20L | 0.25L | 0.30L | 0.35L | 0.40L | 0.45L | 0.50L | 0.55L | 0.60L | 0.65L | 0.70L | 0.75L | 0.80L | 0.85L | 0.90L | 0.95L | BRNG |
|---|---|---|---|---|---|---|---|---|---|---|---|---|---|---|---|---|---|---|---|---|---|
| FT | 0.00 | 2.10 | 4.20 | 6.30 | 8.40 | 10.50 | 12.60 | 14.70 | 16.80 | 18.90 | 21.00 | 23.10 | 25.20 | 27.30 | 29.40 | 31.50 | 33.60 | 35.70 | 37.80 | 39.90 | 42.00 |
| IN | 0.00 | 25.20 | 50.40 | 75.60 | 100.80 | 126.00 | 151.20 | 176.40 | 201.60 | 226.80 | 252.00 | 277.20 | 302.40 | 327.60 | 352.80 | 378.00 | 403.20 | 428.40 | 453.60 | 478.80 | 504.00 |

**Number of Strands Developed Assuming $l_t$**

| | BRNG | 0.05L | 0.10L | 0.15L | 0.20L | 0.25L | 0.30L | 0.35L | 0.40L | 0.45L | 0.50L | 0.55L | 0.60L | 0.65L | 0.70L | 0.75L | 0.80L | 0.85L | 0.90L | 0.95L | BRNG |
|---|---|---|---|---|---|---|---|---|---|---|---|---|---|---|---|---|---|---|---|---|---|
| # Top | 0.32 | 1.64 | 2.00 | 2.00 | 2.00 | 2.00 | 2.00 | 2.00 | 2.00 | 2.00 | 2.00 | 2.00 | 2.00 | 2.00 | 2.00 | 2.00 | 2.00 | 2.00 | 2.00 | 1.64 | 0.32 |
| # Bot | 1.26 | 6.56 | 8.00 | 8.00 | 8.00 | 8.00 | 8.00 | 8.00 | 8.00 | 8.00 | 8.00 | 8.00 | 8.00 | 8.00 | 8.00 | 8.00 | 8.00 | 8.00 | 8.00 | 6.56 | 1.26 |

DECK 0.2246 K/FT

BEAM 0.3049 K/FT

**1 — Stresses in Non-Composite Beam due to Effective Prestress & Beam DL (At Release) After Initial Losses Have Occurred (ES & R) Assuming $l_t$ (KSI)**

| | BRNG | 0.05L | 0.10L | 0.15L | 0.20L | 0.25L | 0.30L | 0.35L | 0.40L | 0.45L | 0.50L | 0.55L | 0.60L | 0.65L | 0.70L | 0.75L | 0.80L | 0.85L | 0.90L | 0.95L | BRNG |
|---|---|---|---|---|---|---|---|---|---|---|---|---|---|---|---|---|---|---|---|---|---|
| Axial | -0.176 | -0.917 | -1.119 | -1.119 | -1.119 | -1.119 | -1.119 | -1.119 | -1.119 | -1.119 | -1.119 | -1.119 | -1.119 | -1.119 | -1.119 | -1.119 | -1.119 | -1.119 | -1.119 | -0.917 | -0.176 |
| Fe (T) | 0.173 | 0.901 | 1.099 | 1.099 | 1.099 | 1.099 | 1.099 | 1.099 | 1.099 | 1.099 | 1.099 | 1.099 | 1.099 | 1.099 | 1.099 | 1.099 | 1.099 | 1.099 | 1.099 | 0.901 | 0.173 |
| Fe (B) | -0.136 | -0.707 | -0.863 | -0.863 | -0.863 | -0.863 | -0.863 | -0.863 | -0.863 | -0.863 | -0.863 | -0.863 | -0.863 | -0.863 | -0.863 | -0.863 | -0.863 | -0.863 | -0.863 | -0.707 | -0.136 |
| DL (T) | 0.000 | -0.061 | -0.115 | -0.163 | -0.204 | -0.239 | -0.268 | -0.291 | -0.306 | -0.316 | -0.319 | -0.316 | -0.306 | -0.291 | -0.268 | -0.239 | -0.204 | -0.163 | -0.115 | -0.061 | 0.000 |
| DL (B) | 0.000 | 0.048 | 0.090 | 0.128 | 0.160 | 0.188 | 0.210 | 0.228 | 0.241 | 0.248 | 0.251 | 0.248 | 0.241 | 0.228 | 0.210 | 0.188 | 0.160 | 0.128 | 0.090 | 0.048 | 0.000 |
| Tot (T) | -0.003 | -0.077 | -0.134 | -0.182 | -0.224 | -0.259 | -0.288 | -0.310 | -0.326 | -0.336 | -0.339 | -0.336 | -0.326 | -0.310 | -0.288 | -0.259 | -0.224 | -0.182 | -0.134 | -0.077 | -0.003 |
| Tot (B) | -0.312 | -1.577 | -1.891 | -1.853 | -1.821 | -1.793 | -1.771 | -1.753 | -1.741 | -1.733 | -1.731 | -1.733 | -1.741 | -1.753 | -1.771 | -1.793 | -1.821 | -1.853 | -1.891 | -1.577 | -0.312 |

**2 — Stresses in Non-Composite Beam due to Effective Prestress & All Permanent DL after Slab Placement (ES, R, CR & SH) Assuming $l_t$ (KSI)**

| | BRNG | 0.05L | 0.10L | 0.15L | 0.20L | 0.25L | 0.30L | 0.35L | 0.40L | 0.45L | 0.50L | 0.55L | 0.60L | 0.65L | 0.70L | 0.75L | 0.80L | 0.85L | 0.90L | 0.95L | BRNG |
|---|---|---|---|---|---|---|---|---|---|---|---|---|---|---|---|---|---|---|---|---|---|
| Axial | -0.153 | -0.798 | -0.973 | -0.973 | -0.973 | -0.973 | -0.973 | -0.973 | -0.973 | -0.973 | -0.973 | -0.973 | -0.973 | -0.973 | -0.973 | -0.973 | -0.973 | -0.973 | -0.973 | -0.798 | -0.153 |
| Fe (T) | 0.151 | 0.784 | 0.956 | 0.956 | 0.956 | 0.956 | 0.956 | 0.956 | 0.956 | 0.956 | 0.956 | 0.956 | 0.956 | 0.956 | 0.956 | 0.956 | 0.956 | 0.956 | 0.956 | 0.784 | 0.151 |
| Fe (B) | -0.118 | -0.615 | -0.750 | -0.750 | -0.750 | -0.750 | -0.750 | -0.750 | -0.750 | -0.750 | -0.750 | -0.750 | -0.750 | -0.750 | -0.750 | -0.750 | -0.750 | -0.750 | -0.750 | -0.615 | -0.118 |
| DL (T) | 0.000 | -0.105 | -0.200 | -0.283 | -0.355 | -0.416 | -0.466 | -0.504 | -0.532 | -0.549 | -0.554 | -0.549 | -0.532 | -0.504 | -0.466 | -0.416 | -0.355 | -0.283 | -0.200 | -0.105 | 0.000 |
| DL (B) | 0.000 | 0.083 | 0.157 | 0.222 | 0.278 | 0.326 | 0.365 | 0.396 | 0.418 | 0.431 | 0.435 | 0.431 | 0.418 | 0.396 | 0.365 | 0.326 | 0.278 | 0.222 | 0.157 | 0.083 | 0.000 |
| Tot (T) | -0.003 | -0.119 | -0.217 | -0.300 | -0.372 | -0.433 | -0.483 | -0.521 | -0.549 | -0.566 | -0.571 | -0.566 | -0.549 | -0.521 | -0.483 | -0.433 | -0.372 | -0.300 | -0.217 | -0.119 | -0.003 |
| Tot (B) | -0.272 | -1.331 | -1.567 | -1.502 | -1.445 | -1.397 | -1.358 | -1.328 | -1.306 | -1.293 | -1.288 | -1.293 | -1.306 | -1.328 | -1.358 | -1.397 | -1.445 | -1.502 | -1.567 | -1.331 | -0.272 |

Table D.5 Composite Stress Calculations

| G1C-West | | | | | | | | | | Composite Beam Stresses at Stage 3 of Construction (Testing) | | | | | | | | | | | |
|---|---|---|---|---|---|---|---|---|---|---|---|---|---|---|---|---|---|---|---|---|---|
| REF | BRNG | 0.05L | 0.10L | 0.15L | 0.20L | 0.25L | 0.30L | 0.35L | 0.40L | 0.45L | 0.50L | 0.55L | 0.60L | 0.65L | 0.70L | 0.75L | 0.80L | 0.85L | 0.90L | 0.95L | BRNG |
| FT | 0.00 | 2.10 | 4.20 | 6.30 | 8.40 | 10.50 | 12.60 | 14.70 | 16.80 | 18.90 | 21.00 | 23.10 | 25.20 | 27.30 | 29.40 | 31.50 | 33.60 | 35.70 | 37.80 | 39.90 | 42.00 |

Number of Strands Developed Assuming $l_d$

| | BRNG | 0.05L | 0.10L | 0.15L | 0.20L | 0.25L | 0.30L | 0.35L | 0.40L | 0.45L | 0.50L | 0.55L | 0.60L | 0.65L | 0.70L | 0.75L | 0.80L | 0.85L | 0.90L | 0.95L | BRNG |
|---|---|---|---|---|---|---|---|---|---|---|---|---|---|---|---|---|---|---|---|---|---|
| # Top | 0.12 | 0.65 | 1.17 | 1.70 | 2.00 | 2.00 | 2.00 | 2.00 | 2.00 | 2.00 | 2.00 | 2.00 | 2.00 | 2.00 | 2.00 | 2.00 | 2.00 | 1.70 | 1.17 | 0.65 | 0.12 |
| # Bot | 0.50 | 2.60 | 4.69 | 6.79 | 8.00 | 8.00 | 8.00 | 8.00 | 8.00 | 8.00 | 8.00 | 8.00 | 8.00 | 8.00 | 8.00 | 8.00 | 8.00 | 6.79 | 4.69 | 2.60 | 0.50 |

Max Load (KIPS)  233

SUPT

1

DECK  0.2246  K/FT

BEAM  0.3049  K/FT

3  Stresses in Composite Beam due to Prestressing, Permanent DL and Point Load with Above Support Conditions (All Losses) Assuming $l_d$ (KSI)

| REF | BRNG | 0.05L | 0.10L | 0.15L | 0.20L | 0.25L | 0.30L | 0.35L | 0.40L | 0.45L | 0.50L | 0.55L | 0.60L | 0.65L | 0.70L | 0.75L | 0.80L | 0.85L | 0.90L | 0.95L | BRNG |
|---|---|---|---|---|---|---|---|---|---|---|---|---|---|---|---|---|---|---|---|---|---|---|
| $M_{DL}$ | 0.0 | 22.2 | 42.0 | 59.5 | 74.7 | 87.6 | 98.1 | 106.2 | 112.1 | 115.6 | 116.8 | 115.6 | 112.1 | 106.2 | 98.1 | 87.6 | 74.7 | 59.5 | 42.0 | 22.2 | 0.0 |
| $M_{LL}$ | 0.0 | 406.3 | 812.5 | 1218.8 | 1318.7 | 1236.3 | 1153.9 | 1071.4 | 989.0 | 906.6 | 824.2 | 741.8 | 659.3 | 576.9 | 494.5 | 412.1 | 329.7 | 247.3 | 164.8 | 82.4 | 0.0 |
| Axial | -0.060 | -0.314 | -0.568 | -0.822 | -0.968 | -0.968 | -0.968 | -0.968 | -0.968 | -0.968 | -0.968 | -0.968 | -0.968 | -0.968 | -0.968 | -0.968 | -0.968 | -0.822 | -0.568 | -0.314 | -0.060 |
| Fe (T) | 0.059 | 0.309 | 0.558 | 0.808 | 0.951 | 0.951 | 0.951 | 0.951 | 0.951 | 0.951 | 0.951 | 0.951 | 0.951 | 0.951 | 0.951 | 0.951 | 0.951 | 0.808 | 0.558 | 0.309 | 0.059 |
| Fe (B) | -0.047 | -0.242 | -0.438 | -0.634 | -0.747 | -0.747 | -0.747 | -0.747 | -0.747 | -0.747 | -0.747 | -0.747 | -0.747 | -0.747 | -0.747 | -0.747 | -0.747 | -0.634 | -0.438 | -0.242 | -0.047 |
| DL-T | 0.000 | -0.105 | -0.200 | -0.283 | -0.355 | -0.416 | -0.466 | -0.504 | -0.532 | -0.549 | -0.554 | -0.549 | -0.532 | -0.504 | -0.466 | -0.416 | -0.355 | -0.283 | -0.200 | -0.105 | 0.000 |
| DL-B | 0.000 | 0.083 | 0.157 | 0.222 | 0.278 | 0.326 | 0.365 | 0.396 | 0.418 | 0.431 | 0.435 | 0.431 | 0.418 | 0.396 | 0.365 | 0.326 | 0.278 | 0.222 | 0.157 | 0.083 | 0.000 |
| LL-T | 0.000 | -0.371 | -0.741 | -1.112 | -1.203 | -1.128 | -1.053 | -0.977 | -0.902 | -0.827 | -0.752 | -0.677 | -0.601 | -0.526 | -0.451 | -0.376 | -0.301 | -0.226 | -0.150 | -0.075 | 0.000 |
| LL-B | 0.000 | 0.861 | 1.721 | 2.582 | 2.794 | 2.619 | 2.444 | 2.270 | 2.095 | 1.921 | 1.746 | 1.571 | 1.397 | 1.222 | 1.048 | 0.873 | 0.698 | 0.524 | 0.349 | 0.175 | 0.000 |
| Grd-T | -0.001 | -0.481 | -0.951 | -1.409 | -1.575 | -1.560 | -1.535 | -1.499 | -1.451 | -1.393 | -1.323 | -1.242 | -1.150 | -1.048 | -0.934 | -0.809 | -0.672 | -0.523 | -0.360 | -0.186 | -0.001 |
| Grd-B | -0.107 | 0.387 | 0.872 | 1.348 | 1.357 | 1.230 | 1.095 | 0.951 | 0.798 | 0.636 | 0.466 | 0.287 | 0.099 | -0.097 | -0.302 | -0.516 | -0.738 | -0.710 | -0.500 | -0.299 | -0.107 |
| Deck-T | 0.000 | -0.764 | -1.528 | -2.292 | -2.479 | -2.325 | -2.170 | -2.015 | -1.860 | -1.705 | -1.550 | -1.395 | -1.240 | -1.085 | -0.930 | -0.775 | -0.620 | -0.465 | -0.310 | -0.155 | 0.000 |
| Deck-B | 0.000 | -0.371 | -0.741 | -1.112 | -1.203 | -1.128 | -1.053 | -0.977 | -0.902 | -0.827 | -0.752 | -0.677 | -0.601 | -0.526 | -0.451 | -0.376 | -0.301 | -0.226 | -0.150 | -0.075 | 0.000 |

Table D.6  Girder Shear Design Calculations (Left of Load)

| G1C-West | | | | | | | | **Girder Shear Design (Left of Load)** | | | | |
|---|---|---|---|---|---|---|---|---|---|---|---|---|
| | IN | L-SUPT | 0.1 a | 0.2 a | 0.3 a | 0.4 a | 0.5 a | 0.6 a | 0.7 a | 0.8 a | 0.9 a | P-LOAD |
| Distance from Left Support (Inches) | | 0.00 | 8.50 | 17.00 | 25.50 | 34.00 | 42.50 | 51.00 | 59.50 | 68.00 | 76.50 | 85.00 |
| Ultimate Moment Furnished | FT-KIP | 94.67 | 228.79 | 362.91 | 497.02 | 631.14 | 765.26 | 899.38 | 1033.49 | 1167.61 | 1301.73 | 1435.85 |
| Transferred Strands Factor | | 0.16 | 0.38 | 0.60 | 0.83 | 1.00 | 1.00 | 1.00 | 1.00 | 1.00 | 1.00 | 1.00 |
| Transferred # Top Strands | # | 0.32 | 0.76 | 1.21 | 1.66 | 2.00 | 2.00 | 2.00 | 2.00 | 2.00 | 2.00 | 2.00 |
| Transferred # Bottom Strands | # | 1.26 | 3.05 | 4.84 | 6.62 | 8.00 | 8.00 | 8.00 | 8.00 | 8.00 | 8.00 | 8.00 |
| Developed Strands Factor | | 0.06 | 0.15 | 0.24 | 0.33 | 0.42 | 0.50 | 0.59 | 0.68 | 0.77 | 0.86 | 0.95 |
| Developed # Top Strands | # | 0.12 | 0.30 | 0.48 | 0.66 | 0.83 | 1.01 | 1.19 | 1.36 | 1.54 | 1.72 | 1.89 |
| Developed # Bottom Strands | # | 0.50 | 1.21 | 1.91 | 2.62 | 3.33 | 4.04 | 4.74 | 5.45 | 6.16 | 6.87 | 7.57 |
| Non-composite DL Moment (BM+SL) | FT-KIP | 0.00 | 7.74 | 15.22 | 22.43 | 29.38 | 36.06 | 42.48 | 48.63 | 54.51 | 60.13 | 65.48 |
| Total DL Shear (BM+SL) | KIP | 11.38 | 11.01 | 10.63 | 10.26 | 9.88 | 9.51 | 9.13 | 8.76 | 8.38 | 8.01 | 7.63 |
| Available Moment Capacity | FT-KIP | 94.67 | 221.04 | 347.68 | 474.59 | 601.76 | 729.20 | 856.90 | 984.87 | 1113.10 | 1241.60 | 1370.36 |
| Ultimate Moment, $M_u$ | FT-KIP | 0.00 | 144.78 | 289.29 | 433.54 | 577.53 | 721.24 | 864.70 | 1007.88 | 1150.80 | 1293.46 | 1435.85 |
| Ultimate Shear, $V_u$ | KIP | 204.85 | 204.47 | 204.10 | 203.72 | 203.35 | 202.97 | 202.60 | 202.22 | 201.85 | 201.47 | 201.10 |
| $f_d$ | KSI | 0.000 | 0.029 | 0.057 | 0.084 | 0.109 | 0.134 | 0.158 | 0.181 | 0.203 | 0.224 | 0.244 |
| SFPF (Based on $l_d$) | KIPS | 22.30 | 53.89 | 85.48 | 117.07 | 148.66 | 180.25 | 211.84 | 243.43 | 275.01 | 306.60 | 338.19 |
| $f_{pe}$ | KSI | -0.107 | -0.259 | -0.410 | -0.562 | -0.714 | -0.865 | -1.017 | -1.168 | -1.320 | -1.472 | -1.623 |
| $M_{CR}$ | FT-KIP | 265.85 | 323.81 | 382.23 | 441.12 | 500.47 | 560.30 | 620.59 | 681.34 | 742.57 | 804.26 | 866.42 |
| $V_{ci}$ (Flexure Shear) | KIPS | 29.78 | 478.83 | 290.81 | 228.05 | 196.61 | 177.70 | 165.05 | 155.97 | 149.14 | 149.14 | 143.79 | 139.49 |
| FPF (Based on $l_t$) | KIPS | 56.35 | 136.19 | 216.03 | 295.86 | 357.29 | 357.29 | 357.29 | 357.29 | 357.29 | 357.29 | 357.29 |
| $f_{pc}$ | KSI | -0.083 | -0.218 | -0.353 | -0.486 | -0.593 | -0.607 | -0.621 | -0.635 | -0.648 | -0.660 | -0.672 |
| $V_{cw}$ (Web Shear) | KIPS | 67.06 | 76.39 | 85.68 | 94.93 | 102.26 | 103.28 | 104.25 | 105.19 | 106.08 | 106.93 | 107.75 |
| $V_c$ | KIPS | 29.78 | 76.39 | 85.68 | 94.93 | 102.26 | 103.28 | 104.25 | 105.19 | 106.08 | 106.93 | 107.75 |
| $V_u/\phi$ | KIPS | 204.85 | 204.47 | 204.10 | 203.72 | 203.35 | 202.97 | 202.60 | 202.22 | 201.85 | 201.47 | 201.10 |
| Shear Steel Beyond Minimum Required | Y/N | YES | YES | YES | YES | YES | YES | YES | YES | YES | YES | YES |
| Web Crushing | | CRUSH | OK | OK | OK | OK | OK | OK | OK | OK | OK | OK |
| Required Strength of Steel, $V_s$ | KIPS | 175.07 | 128.08 | 118.41 | 108.79 | 101.08 | 99.69 | 98.34 | 97.04 | 95.77 | 94.54 | 93.35 |
| Required Stirrup Spacing, s | IN | 6.58 | 8.99 | 9.73 | 10.59 | 11.40 | 11.56 | 11.71 | 11.87 | 12.00 | 12.00 | 12.00 |

Table D.7  Girder Shear Design Calculations (Right of Load)

| G1C-West | | Girder Shear Design (Right of Load) | | | | | | | | | | |
|---|---|---|---|---|---|---|---|---|---|---|---|---|
| Distance from Left Support (Inches) | IN | P-LOAD | 0.1 b | 0.2 b | 0.3 b | 0.4 b | 0.5 b | 0.6 b | 0.7 b | 0.8 b | 0.9 b | R-SUPT |
| | | 85.00 | 126.90 | 168.80 | 210.70 | 252.60 | 294.50 | 336.40 | 378.30 | 420.20 | 462.10 | 504.00 |
| Ultimate Moment Furnished | FT-KIP | 1435.85 | 1516.94 | 1516.94 | 1516.94 | 1516.94 | 1516.94 | 1516.94 | 1516.94 | 1416.91 | 755.79 | 94.67 |
| Transferred Strands Factor | | 1.00 | 1.00 | 1.00 | 1.00 | 1.00 | 1.00 | 1.00 | 1.00 | 1.00 | 1.00 | 0.16 |
| Transferred # Top Strands | # | 2.00 | 2.00 | 2.00 | 2.00 | 2.00 | 2.00 | 2.00 | 2.00 | 2.00 | 2.00 | 0.32 |
| Transferred # Bottom Strands | # | 8.00 | 8.00 | 8.00 | 8.00 | 8.00 | 8.00 | 8.00 | 8.00 | 8.00 | 8.00 | 1.26 |
| Developed Strands Factor | | 0.95 | 1.00 | 1.00 | 1.00 | 1.00 | 1.00 | 1.00 | 1.00 | 0.93 | 0.50 | 0.06 |
| Developed # Top Strands | # | 1.89 | 2.00 | 2.00 | 2.00 | 2.00 | 2.00 | 2.00 | 2.00 | 1.87 | 1.00 | 0.12 |
| Developed # Bottom Strands | # | 7.57 | 8.00 | 8.00 | 8.00 | 8.00 | 8.00 | 8.00 | 8.00 | 7.47 | 3.99 | 0.50 |
| Non-composite DL Moment (BM+SL) | FT-KIP | 65.48 | 87.98 | 104.03 | 113.62 | 116.76 | 113.44 | 103.66 | 87.43 | 64.74 | 35.60 | 0.00 |
| Total DL Shear (BM+SL) | KIP | 7.63 | 5.78 | 3.94 | 2.09 | 0.24 | -1.61 | -3.46 | -5.31 | -7.16 | -9.01 | -10.85 |
| Available Moment Capacity | FT-KIP | 1370.36 | 1428.95 | 1412.91 | 1403.32 | 1400.18 | 1403.50 | 1413.28 | 1429.51 | 1352.17 | 720.19 | 94.67 |
| Ultimate Moment, $M_u$ | FT-KIP | 1435.85 | 1321.31 | 1200.32 | 1072.88 | 938.97 | 798.62 | 651.81 | 498.54 | 338.81 | 172.63 | 0.00 |
| Ultimate Shear, $V_u$ | KIP | 31.61 | 33.46 | 35.31 | 37.16 | 39.01 | 40.86 | 42.71 | 44.56 | 46.40 | 48.25 | 50.10 |
| $f_d$ | KSI | 0.244 | 0.328 | 0.388 | 0.423 | 0.435 | 0.423 | 0.386 | 0.326 | 0.241 | 0.133 | 0.000 |
| SFPF (Based on $l_d$) | KIPS | 338.19 | 357.29 | 357.29 | 357.29 | 357.29 | 357.29 | 357.29 | 357.29 | 333.73 | 178.02 | 22.30 |
| $f_{pe}$ | KSI | -1.623 | -1.715 | -1.715 | -1.715 | -1.715 | -1.715 | -1.715 | -1.715 | -1.602 | -0.854 | -0.107 |
| $M_{CR}$ | FT-KIP | 866.42 | 870.12 | 841.89 | 825.02 | 819.50 | 825.34 | 842.54 | 871.09 | 857.62 | 556.06 | 265.85 |
| $V_{ci}$ (Flexure Shear) | KIPS | 37.22 | 38.33 | 39.21 | 41.17 | 44.79 | 51.12 | 62.25 | 83.05 | 120.81 | 156.93 | ######## |
| FPF (Based on $l_t$) | KIPS | 357.29 | 357.29 | 357.29 | 357.29 | 357.29 | 357.29 | 357.29 | 357.29 | 357.29 | 357.29 | 56.35 |
| $f_{pc}$ | KSI | -0.672 | -0.721 | -0.757 | -0.778 | -0.785 | -0.777 | -0.756 | -0.720 | -0.670 | -0.606 | -0.083 |
| $V_{cw}$ (Web Shear) | KIPS | 107.75 | 111.16 | 113.60 | 115.06 | 115.53 | 115.03 | 113.55 | 111.08 | 107.63 | 103.21 | 67.06 |
| $V_c$ | KIPS | 37.22 | 38.33 | 39.21 | 41.17 | 44.79 | 51.12 | 62.25 | 83.05 | 107.63 | 103.21 | 67.06 |
| $V_u/\phi$ | KIPS | 31.61 | 33.46 | 35.31 | 37.16 | 39.01 | 40.86 | 42.71 | 44.56 | 46.40 | 48.25 | 50.10 |
| Shear Steel Beyond Minimum Required | Y/N | NO | NO | NO | NO | NO | NO | NO | NO | NO | NO | NO |
| Web Crushing | | OK | OK | OK | OK | OK | OK | OK | OK | OK | OK | NO |
| Required Strength of Steel, Vs | KIPS | 0.00 | 0.00 | 0.00 | 0.00 | 0.00 | 0.00 | 0.00 | 0.00 | 0.00 | 0.00 | 0.00 |
| Required Stirrup Spacing, s | IN | 24.00 | 24.00 | 24.00 | 24.00 | 24.00 | 24.00 | 24.00 | 24.00 | 24.00 | 24.00 | 24.00 |

Table D.8 Deck / Girder Interface Shear Calculations

| G1C-West | | Deck / Girder Interface Shear Calculations | | | |
|---|---|---|---|---|---|
| **Interface Shear Calculation Values** | | | | **Tensile Stress at Interface** | |
| Lightweight Concrete Reduction Factor | I | 0.85 | None | Deck Concrete Design Strength | $f'_c$ | 3500 | PSI |
| Shear Strength Reduction Factor | $\phi_s$ | 1.00 | None | Maximum Allowable Deck Tensile Stress | | 443.71 | PSI |
| Maximum Unfactored Shear | $V_u$ | 204.85 | KIPS | Girder Concrete Design Strength | $f'_c$ | 8000 | PSI |
| First Moment of Deck About Centroid | QS | 3444.42 | $IN^3$ | Maximum Allowable Beam Tensile Stress | | 570.20 | PSI |
| Composite Moment of Inertia | $I_c$ | 142547 | $IN^4$ | Maximum Interface Shear Stress (VQ/Ib) | $v_h$ | 412.48 | PSI |
| Interface Shear Contact Width | $b_v$ | 12 | IN | Effective Prestress Force | $F_{pe}$ | 338.19 | KIPS |
| Contact Length, d (a+XDIST<=SPAN/10) | Span/10 | 50.40 | IN | Girder Cross Sectional Area | $A_{nc}$ | 369 | $IN^2$ |
| Contact Area ($b_v$*Contact Length) | $A_c$ | 604.8 | $IN^2$ | Strand Eccentricity from NC Centroid | e | -6.73 | IN |
| Yield Strength of Tie Reinforcement | $f_y$ | 75 | KSI | Distance from NC Centroid to Beam Top | $y_{top-nc}$ | 20.17 | IN |
| Stirrup Area | $A_v$ | 0.4 | $IN^2$ | Distance from C Centroid to Beam Top | $y_{top-c}$ | 10.84 | IN |
| | | | | Non-Composite Moment of Inertia | $I_{nc}$ | 50979 | $IN^4$ |
| | | | | Composite Moment of Inertia | $I_c$ | 142547 | $IN^4$ |
| | | | | Dead Load Moment | $M_{DL}$ | 65.48 | FT-KIP |
| | | | | Live Load Moment | $M_{LL}$ | 1370.36 | FT-KIP |
| | | | | Maximum Compressive Stress at Interface | $f_{ca}$ | -1576.88 | PSI |
| | | | | Maximum Tensile Stress at Interface | $f_t$ | 101.381 | PSI |
| | | | | **Tensile Stress at Interface is OK** | | | |

| **Interface Condition** | | | |
|---|---|---|---|
| Contact Surface Clean | | YES | YES/NO |
| Contact Surface Roughened 1/4" | | YES | YES/NO |
| Minimum Ties Provided | | YES | YES/NO |
| Maximum Basic Interface Stress | | 350 | PSI |
| Maximum Basic Interface Force | $V_{nh}$ | 211.68 | KIPS |
| **Basic Interface Shear Capacity Adequate** | | | |

| **Additional Interface Capacity Provided by Shear Reinforcement** | | | |
|---|---|---|---|
| Additional Interface Capacity Required | | 0.00 | KIPS |
| Worst Case Stirrup Spacing over "a" | s | 12.00 | IN |
| Minimum Tie Area per Inch of Beam | | 0.0080 | $IN^2/IN$ |
| Additional $V_{nh}$ Capacity per Percent | | 181.4 | KIPS |
| Additional Percent Required | | 0.00 | % |
| Additional Required Tie Area | | 0.000000 | $IN^2/IN$ |
| Total Tie Area Required | | 0.008000 | $IN^2/IN$ |
| Min. Tie Area Provided by V Reinforcement | | 0.033333 | $IN^2/IN$ |
| Resulting Contact Area Stress | | 338.70 | PSI |
| **Interface Shear Capacity Adequate** | | | |

401

# APPENDIX E

# LOAD CELL CALIBRATION

This Appendix contains the calibration curves for strand load cells used to monitor the force in the prestressing strands from initial tensioning through the time of strand release. Figures E.1 through E.10 show the calibration curves determined for each strand load cell. The following procedure was used in determining the calibration curves.

1. All load cells were connected to the BLH 1225 Portable 10 Channel Switch and Balance Unit, which was connected to a BLH 1200B Portable Digital Strain Indicator. The load cells were a "full-bridge" configuration. The same units used for this calibration were used during girder construction.

2. The load cells were placed individually in an 800 kip SATEK compression testing machine. After being properly positioned, load was applied to the cells slowly through a load of 45 kips, the maximum anticipated load during strand tensioning. At the 10, 20, 30, 40, and 45 kip readings indicated on the SATEK machine, corresponding strain readings were taken from the digital strain indicator.

3. After testing, all load and strain data was entered into an EXCEL spreadsheet and plotted. The slope of each stress vs. strain plot was determined using the linear trendline option in EXCEL. The slope values are listed in the bottom right of each calibration plot.
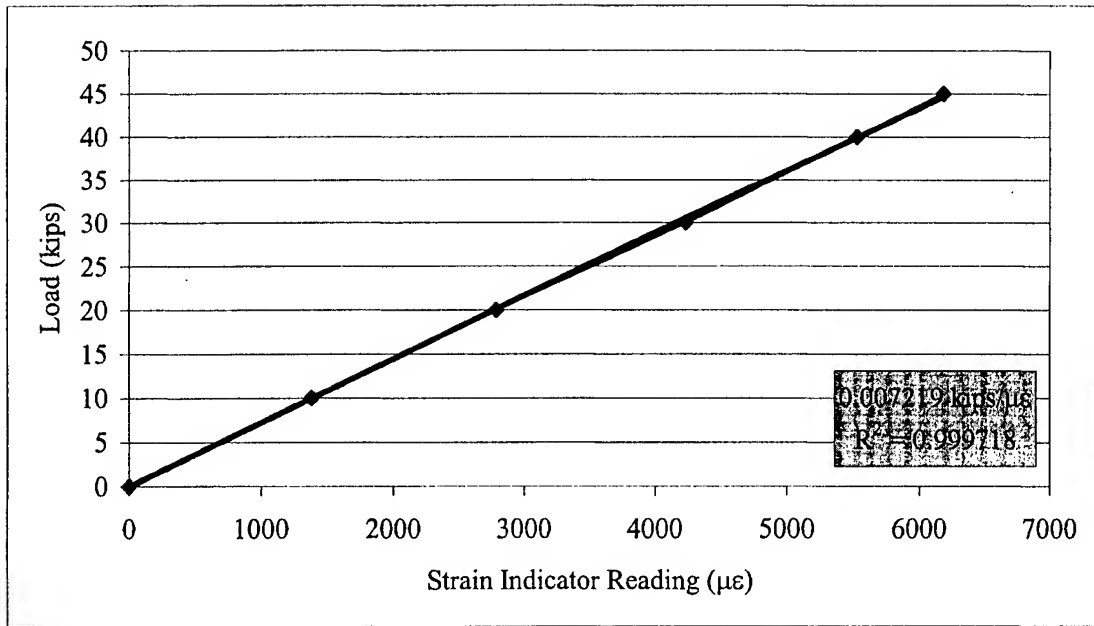
Figure E.1  Calibration Curve for Strand Load Cell # 1
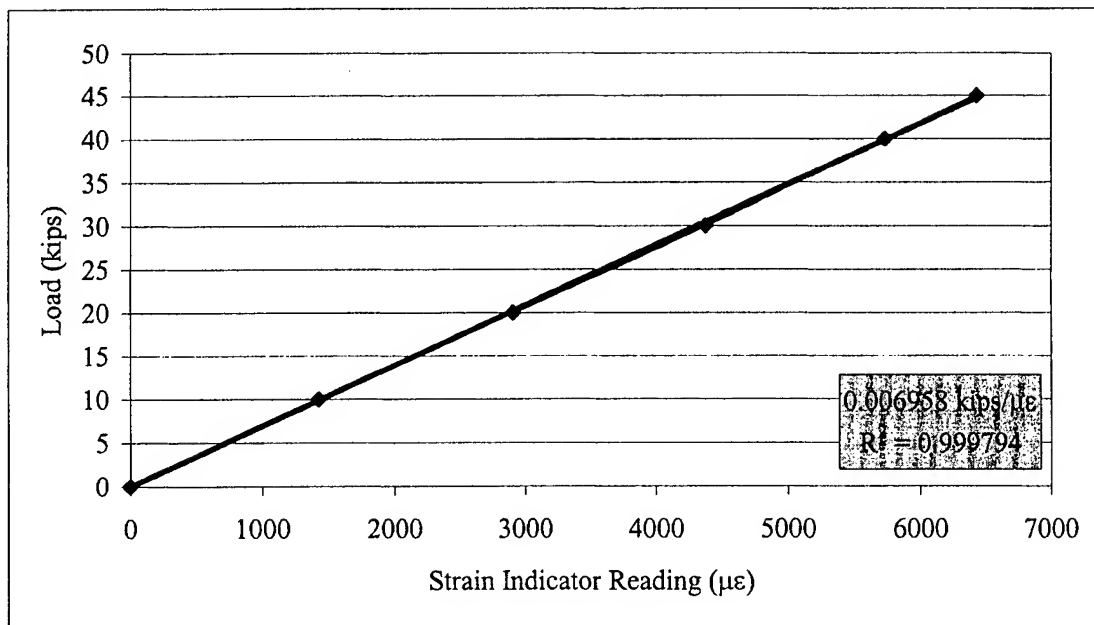


Figure E.2  Calibration Curve for Strand Load Cell # 2
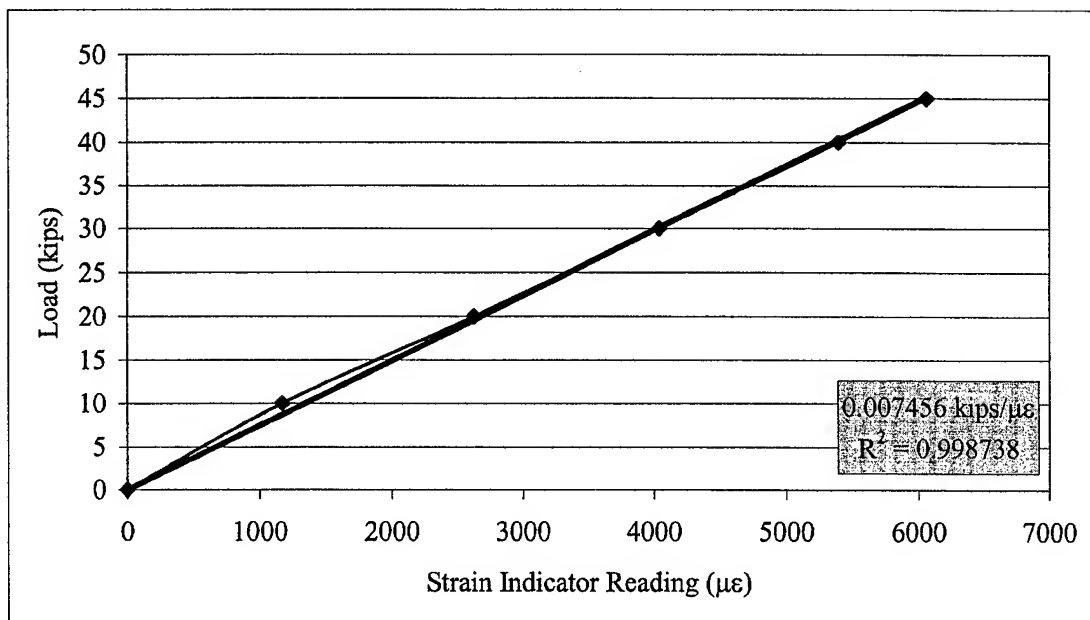
Figure E.3  Calibration Curve for Strand Load Cell # 3
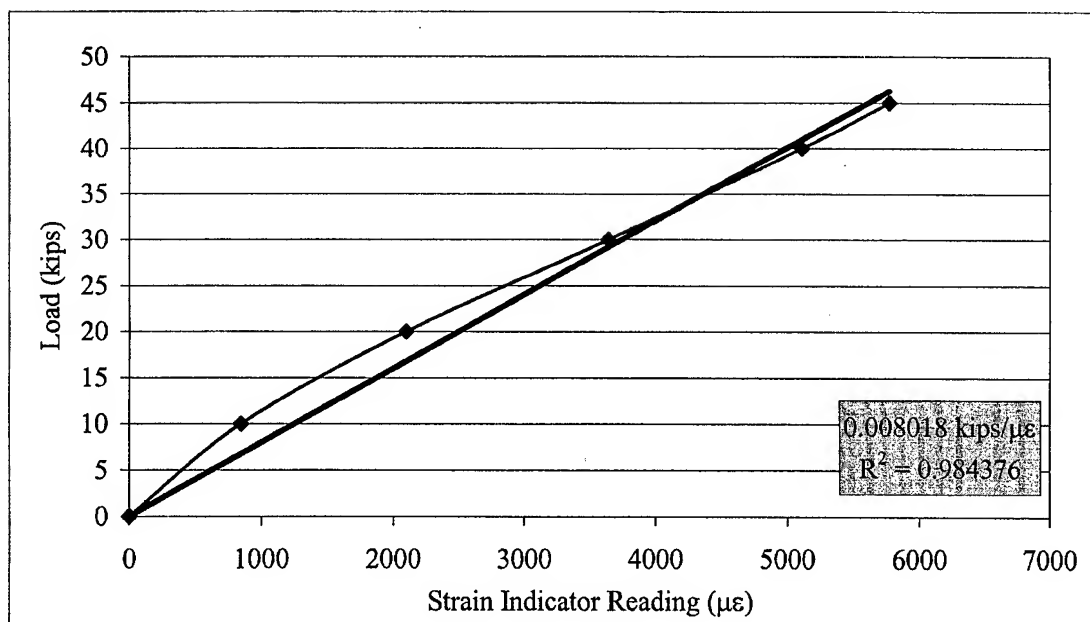


Figure E.4  Calibration Curve for Strand Load Cell # 4

404
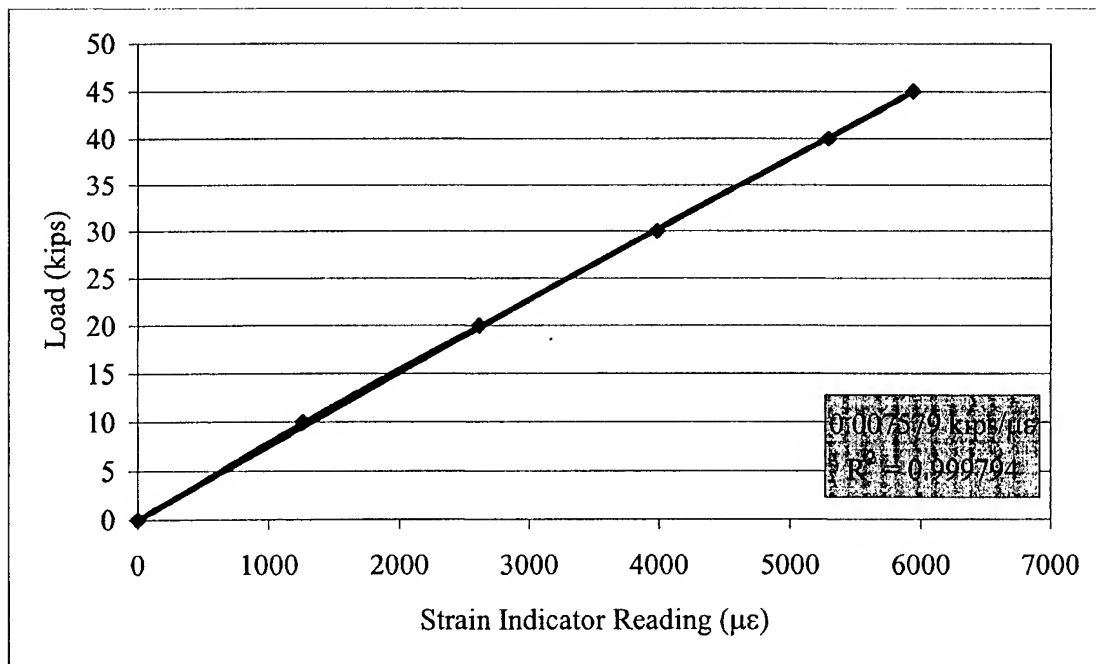
Figure E.5  Calibration Curve for Strand Load Cell # 5
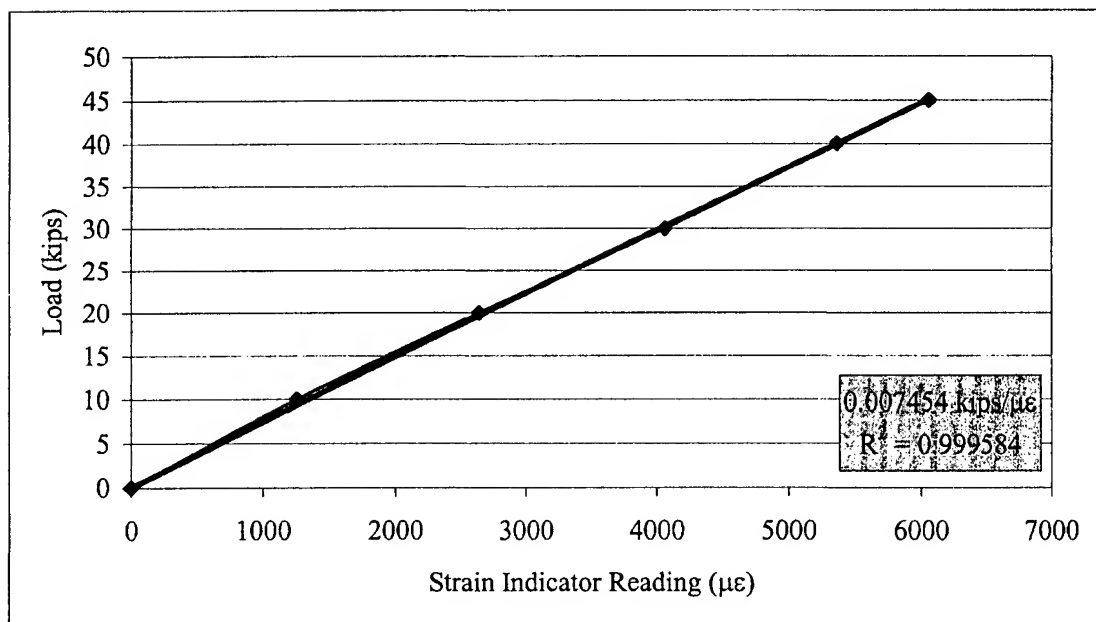


Figure E.6  Calibration Curve for Strand Load Cell # 6
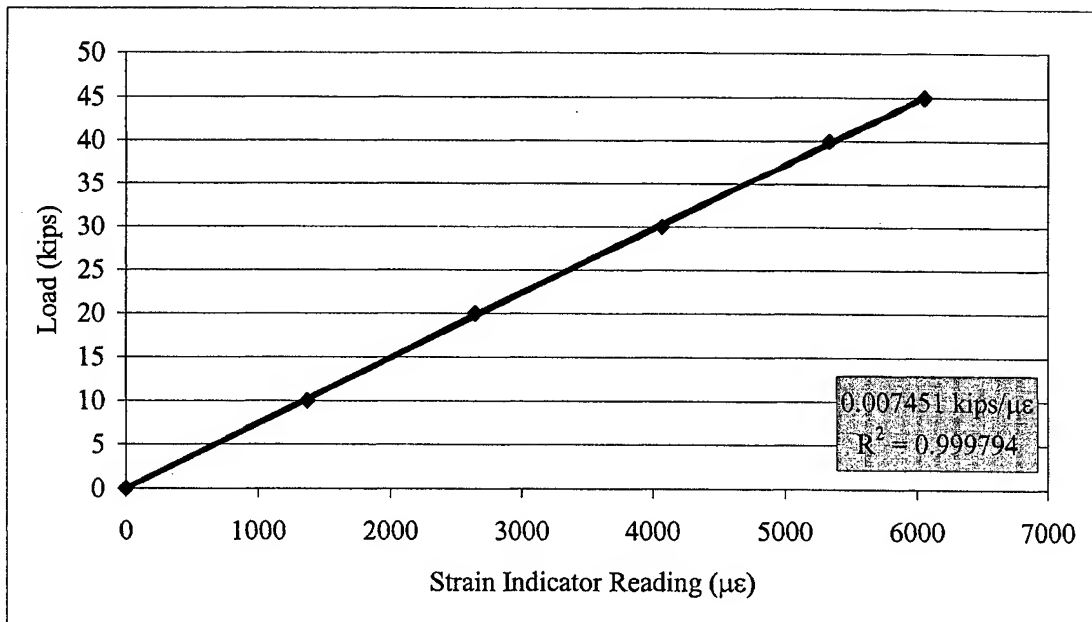
Figure E.7  Calibration Curve for Strand Load Cell # 7
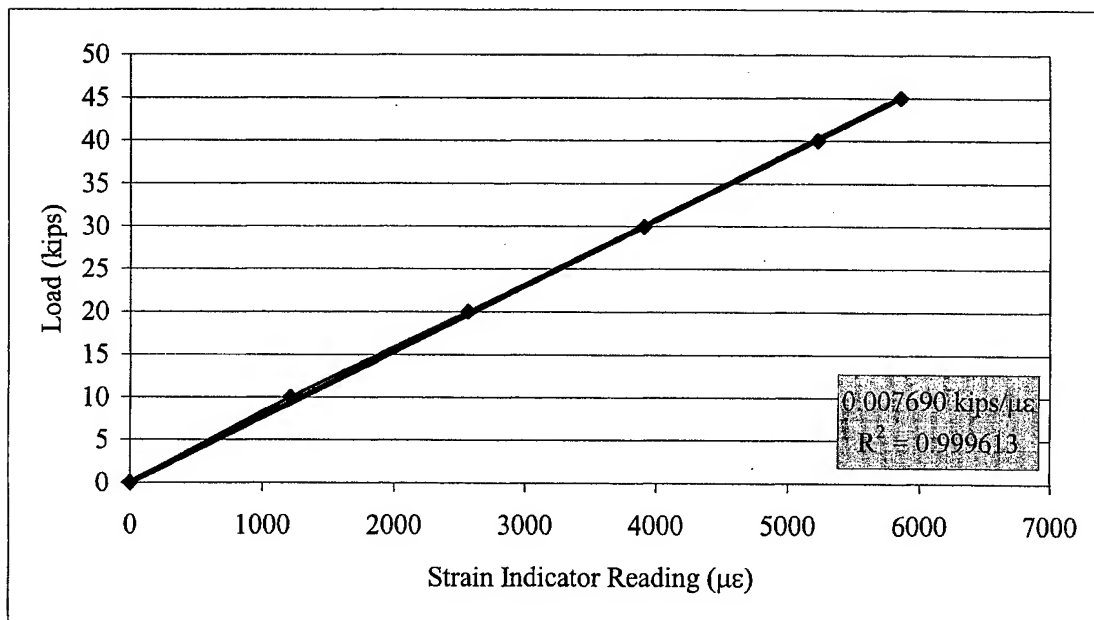


Figure E.8  Calibration Curve for Strand Load Cell # 8

406
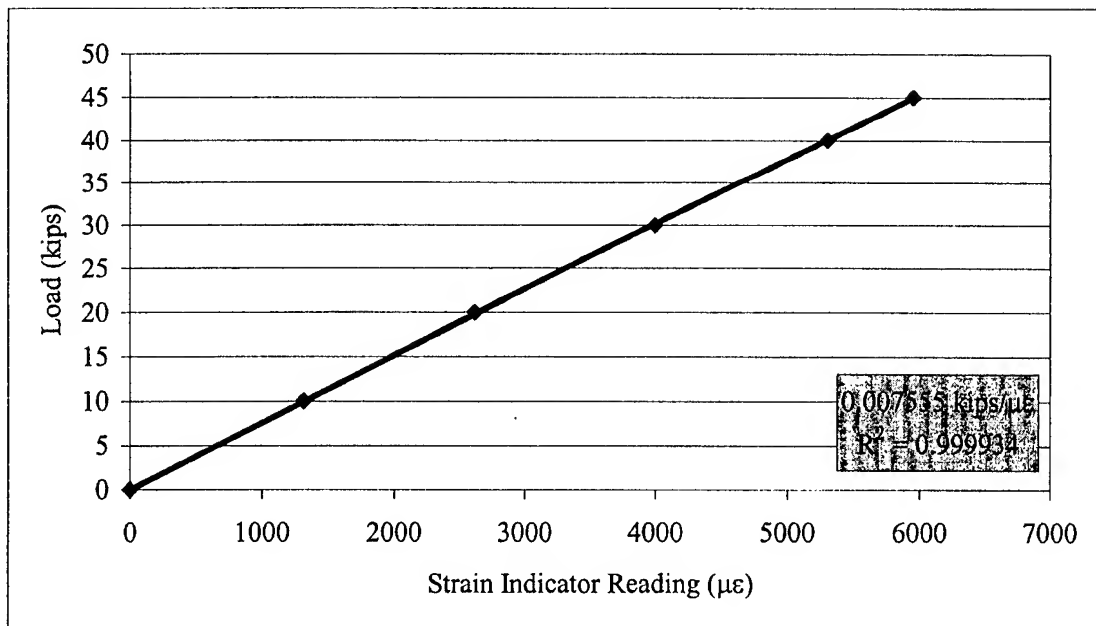
Figure E.9  Calibration Curve for Strand Load Cell # 9
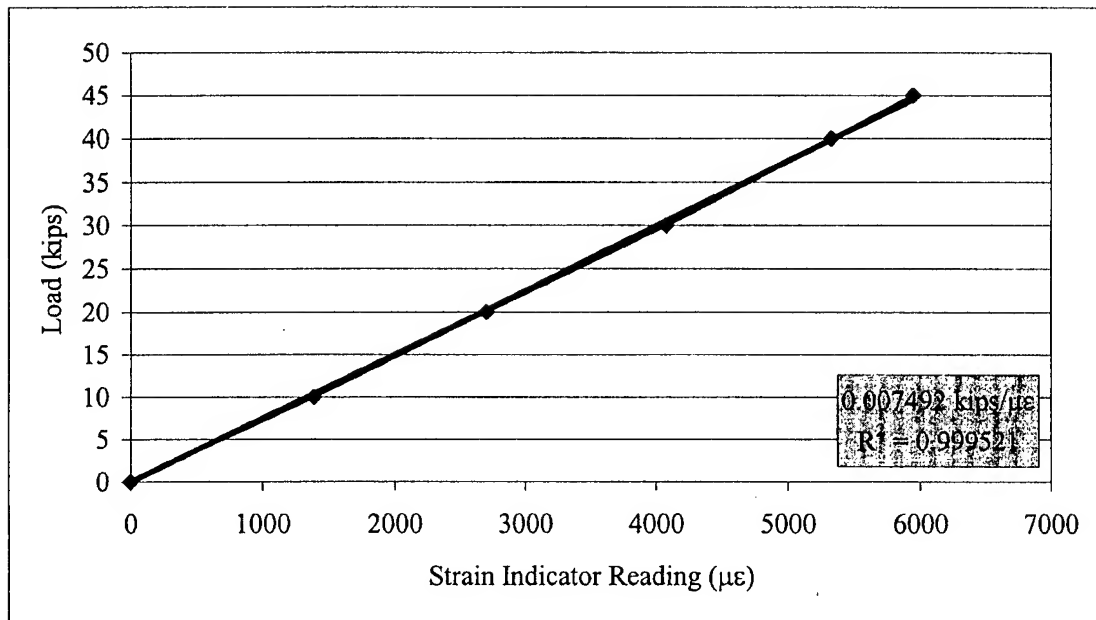


Figure E.10  Calibration Curve for Strand Load Cell # 10

# APPENDIX F

# PRESTRESSING STRESS CALCULATION

This Appendix contains the procedures used to determine the stress in the prestressing strands at initial tensioning of strands, just prior to release of strands, and as necessary at other times during testing.

At the time of strand tensioning and just prior to strand release, strand load cell values were used. Table F.1 shows a spreadsheet listing the calibration constants reported in Appendix E and the load cell strain readings for each series of girders. The resulting stress just prior to release, $f_{pt}$, is listed for each series of girders. The $f_{pt}$ values were used in the transfer length analysis and are reported in Table 9.5.

After release of the strands, the level of prestress was determined with vibrating wire strain gages (VWSG) cast into the girders at midspan at the level of the bottom strands (Figure 8.21). Output from the gages was measured using the device pictured in Figure F.1. The device sent a small excitation voltage to the VWSG causing the wire within to vibrate. The frequency at which the wire in the gage vibrated was based on the amount of tension or compression the gage was experiencing. The values recorded at each measurement were an internal gage resistance used to determine a temperature correction factor and the frequency at which the wire was vibrating. A spreadsheet was created as shown in Table F.2 to determine the strain values.

Table F.1 Prestressing Strand Stress Values at Time of Tensioning and Just Prior to Release

## Strand Load Cell Strain Conversion Factors From Graph Trendlines and PT Forces

| | | Load Cell 1 | Load Cell 2 | Load Cell 3 | Load Cell 4 | Load Cell 5 | Load Cell 6 | Load Cell 7 | Load Cell 8 | Load Cell 9 | Load Cell 10 |
|---|---|---|---|---|---|---|---|---|---|---|---|
| Kips / μ-strain | | 0.007219 | 0.006958 | 0.007456 | 0.008018 | 0.007579 | 0.007454 | 0.007451 | 0.007690 | 0.007555 | 0.007492 |
| Strand Area (in²) | 0.2183 | Strand 1 | Strand 2 | Strand 3 | Strand 4 | Strand 5 | Strand 6 | Strand 7 | Strand 8 | Strand 9 | Strand 10 |
| | | Bottom L | | | | | | | Bottom R | Top L | Top R |
| **Girders G1A / G1B** | | | | | | | | | | | |
| At Stressing | μ-strains | 4533 | 5275 | 5430 | 4975 | 5352 | 5286 | 5206 | 5340 | 5430 | 5532 |
| 392.09 | Kips | 32.72 | 36.70 | 40.49 | 39.89 | 40.56 | 39.40 | 38.79 | 41.06 | 41.02 | 41.45 |
| Before Release | μ-strains | 4513 | 5270 | 5438 | 4960 | 5313 | 5270 | 5150 | 5357 | 5448 | 5479 |
| 390.89 | Kips | 32.58 | 36.67 | 40.55 | 39.77 | 40.27 | 39.28 | 38.37 | 41.20 | 41.16 | 41.05 |
| Bottom / Top Totals | | | | | | 308.68 | | | | 82.21 | |
| $f_{pt}$ (ksi) | 179.06 | | | | | | | | | | |
| **Girders G2A / G2B** | | | | | | | | | | | |
| At Stressing | μ-strains | 6013 | 5107 | 5193 | 4742 | 5516 | 5432 | 5296 | 5452 | 5587 | 5824 |
| 405.21 | Kips | 43.41 | 35.53 | 38.72 | 38.02 | 41.81 | 40.49 | 39.46 | 41.93 | 42.21 | 43.63 |
| Before Release | μ-strains | 6140 | 5310 | 5351 | 4891 | 5727 | 5572 | 5426 | 5612 | 5781 | 6011 |
| 417.62 | Kips | 44.32 | 36.95 | 39.90 | 39.22 | 43.40 | 41.53 | 40.43 | 43.16 | 43.68 | 45.03 |
| Bottom / Top Totals | | | | | | 328.91 | | | | 88.71 | |
| $f_{pt}$ (ksi) | 191.30 | | | | | | | | | | |
| **Girders G1C / G2C** | | | | | | | | | | | |
| At Stressing | μ-strains | 5163 | 5218 | 5640 | 5549 | 5484 | 5456 | 5126 | 5115 | 5489 | 5601 |
| 403.31 | Kips | 37.27 | 36.31 | 42.05 | 44.49 | 41.56 | 40.67 | 38.19 | 39.33 | 41.47 | 41.96 |
| Before Release | μ-strains | 4989 | 5023 | 5387 | 5406 | 5279 | 5309 | 5000 | 4970 | 5387 | 5443 |
| 391.01 | Kips | 36.02 | 34.95 | 40.17 | 43.35 | 40.01 | 39.57 | 37.26 | 38.22 | 40.70 | 40.78 |
| Bottom / Top Totals | | | | | | 309.53 | | | | 81.48 | |
| $f_{pt}$ (ksi) | 179.12 | | | | | | | | | | |
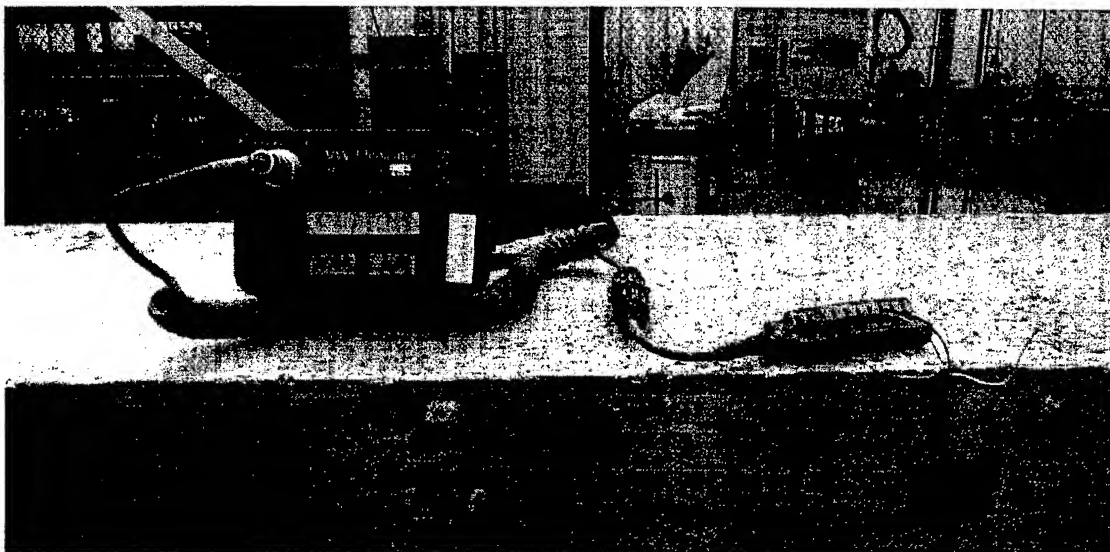
Figure F.1  Vibrating Wire Strain Gage Reader

To convert the frequency readings (Hz) to strains, Equation F.1 was used where

$\varepsilon_{Apparent}$ was the uncorrected strain value, GF was the gage factor provided by the

manufacturer (0.9996), and HZ was the wire vibration frequency read by the gage reader.

$$\varepsilon_{Apparent} = 0.003304\, GF\, (Hz)^2 \qquad\qquad (F.1)$$

To calculate temperature from the gage resistance reading ($\Omega$WG), Equation F.2

was used where $T_t$ was the temperature and $\Omega$WG was the gage resistance in ohms.

$$T_t = \frac{1}{(0.0014051 + 0.0002369\ln(\Omega WG) + 0.0000001019\ln(\Omega WG)^3)} - 273.2 \qquad (F.2)$$

To correct the strain reading for temperature effects, Equation F.3 was used where $\varepsilon_{Initial}$ was the strain reading taken just prior to strand release, $T_{Initial}$ was the temperature of the gage when the first strain reading was taken, and the CTE values are the coefficients of thermal expansion for steel and concrete, 12.2 and 10.2 $\mu\varepsilon/^{\circ}C$, respectively.

$$\varepsilon_{Corrected} = (\varepsilon_{Apparent} - \varepsilon_{Initial})GF + (T_t - T_{Initial})(CTE_{Steel} - CTE_{Concrete}) \qquad (F.3)$$

The temperature correction was based on changes from the temperature at which the first VWSG reading was taken. In general, a drop in temperature meant a lower strain value; an increase in temperature meant a higher strain.

The force in the prestressing strand at any time after strand release was determined using the three equations shown in Figure F.2. The appropriate equation was determined depending on whether $\varepsilon_{Corrected}$ was in the elastic (0 - 0.7135 percent strain), transition (0.7135 – 1.25 percent strain), or plastic (> 1.25 percent strain) portion of the force vs. strain curve. Once the force was determined, the stress was calculated by dividing the strand force by the area of the strand, 0.2183 in$^2$. The shape of the curve in Figure F.2 was determined using the actual force vs. strain curve from the strand manufacturer.

Table F.2 Calcultion of Prestressing Strand Stress Values for Girder Test G1C-West

## Determination of Initial Strand Strain Due to Prestressing

| Strand # | 1 | 2 | 3 | 4 | 5 | 6 | 7 | 8 | 9 | 10 | TOTAL |
|---|---|---|---|---|---|---|---|---|---|---|---|
| | | | | Prestressing Values Reported by Tindall QC | | | | | | | |
| Elongation (In) | 10.625 | 9.875 | 9.75 | 9.875 | 9.875 | 10.125 | 9.875 | 10.25 | 10.125 | 10.25 | (Kips) |
| Tensioning Load (Kip) | 45 | 45 | 45 | 45 | 45 | 45 | 45 | 45 | 45 | 45 | 450.00 |

Prestressing Values Read From Strain Boxes Using Load Cells

| | 1 | 2 | 3 | 4 | 5 | 6 | 7 | 8 | 9 | 10 | TOTAL |
|---|---|---|---|---|---|---|---|---|---|---|---|
| kips/μ-strain | 0.007219 | 0.006958 | 0.007456 | 0.008018 | 0.007579 | 0.007454 | 0.007451 | 0.007690 | 0.007555 | 0.007492 | TOTAL |
| μ-strains at Tensioning | 5163 | 5218 | 5640 | 5549 | 5484 | 5456 | 5126 | 5115 | 5489 | 5601 | (Kips) |
| Tensioning Load (Kip) | 37.27 | 36.31 | 42.05 | 44.49 | 41.56 | 40.67 | 38.19 | 39.33 | 41.47 | 41.96 | 403.31 |
| μ-strains at Release | 4989 | 5023 | 5387 | 5406 | 5279 | 5309 | 5000 | 4970 | 5387 | 5443 | (Kips) |
| Release Load (Kip) | 36.02 | 34.95 | 40.17 | 43.35 | 40.01 | 39.57 | 37.26 | 38.22 | 40.70 | 40.78 | 391.01 |

Values Used to Calculate Strain in Strand at Prestressing and Just Before Release (Enter Tindall or Load Cell)   **Load Cell**

Initial Strand Strain Values

| | 1 | 2 | 3 | 4 | 5 | 6 | 7 | 8 | 9 | 10 | Average |
|---|---|---|---|---|---|---|---|---|---|---|---|
| % Strain at Release | 0.56 | 0.55 | 0.63 | 0.68 | 0.63 | 0.62 | 0.58 | 0.60 | 0.64 | 0.64 | 0.61 |
| Strand Ult Stress, $f_{pu}$ | 283.20 | KSI | Strand Area, $A_s$ | 0.2183 | $IN^2$ | | Level of Prestressing as % of $f_{pu}$ | | | | 63.25% |

## Vibrating Wire Strain Gage Readings and Strand Strain/Force Values

| Vibrating Wire Strain Gage Factor - Enter Value from Strain Gage Certification Sheet | 0.9996 | CTE Steel | 12.2 | CTE Conc | 10.2 |
|---|---|---|---|---|---|

| Time of Reading | Vibrating Wire Strain Gage Values | | | | | | Prestressing Strand Strain / Force / Stress | | | | |
|---|---|---|---|---|---|---|---|---|---|---|---|
| | Hz | WWG (Ohms) | Temp (deg C) | Apparent ε (μ-strains) | Temp Corr (μ-strains) | Corrected ε (μ-strains) | $f_{pt}$ = Before Release, $f_{si}$ = $f_{pt}$ - ES, $f_{se}$ = $f_{pt}$ - ES - CR - SH | | | | |
| | | | | | | | μ-strains | % Strain | Force (K) | Stress (ksi) | Value |
| Before Release (I) | 902.66 | 1308 | 44.99 | 2691 | NA | 2691 | 6131 | 0.61 | 39.10 | 179.11 | $f_{pt}$ |
| Just After Release | 799.65 | 1387 | 43.49 | 2112 | -3 | 2109 | 5550 | 0.55 | 35.39 | 162.11 | $f_{si}$ |
| 1 Day | 791.59 | 2407 | 30.04 | 2070 | -30 | 2040 | 5480 | 0.55 | 34.95 | 160.09 | |
| 7 Days | 762.00 | 2868 | 25.97 | 1918 | -38 | 1880 | 5320 | 0.53 | 33.93 | 155.42 | |
| 14 Days | 749.82 | 2863 | 26.01 | 1857 | -38 | 1819 | 5260 | 0.53 | 33.54 | 153.65 | $f_{se}$ |
| Just Before Testing | 708.37 | 3360 | 22.38 | 1657 | -45 | 1612 | 5053 | 0.51 | 32.22 | 147.61 | $f_{test}$ |

412
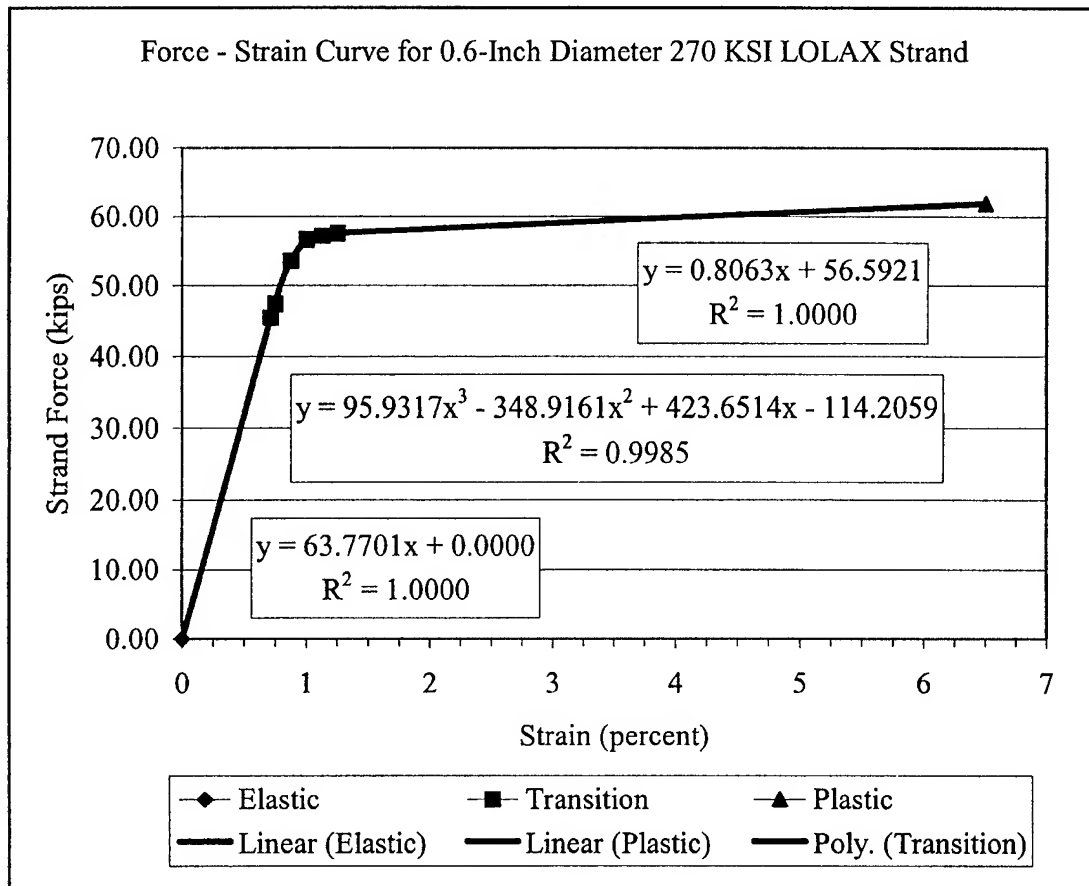
Figure F.2  Strand Force vs. Strain Curve for Prestressing Strand

# APPENDIX G

## TRANSFER LENGTH CALCULATION SPREADSHEET

Appendix G contains the individual pages from the Transfer Length Calculation Spreadsheet. The entire set of worksheet pages is provided for Girder G1C. The pages are listed in the order the calculations occur. A similar series of worksheets was prepared for each girder to determine transfer lengths. Listed below are the individual worksheets within the overall spreadsheet and a brief description of the worksheet's function.

**Table G.1 - Data Taking Sheet** – Used to record CSS readings taken with DEMEC gages.

**Table G.2 – Data Worksheet** – Worksheet used to enter background data information on girder readings to include times, temperatures, strain readings and jacking forces.

**Tables G.3-G.4 – Gage Locations, North & South** – Worksheets used to enter distances to ends of embedment strips. Initial gage lengths calculated.

**Tables G.5-G.16 - CSS Reading Sheets** – Data entry worksheets for each embedment strip (12 total). Readings entered from **Data Taking Sheets**.

**Tables G.17-G.18 - Raw CSS Data Sheets, North & South** – Worksheets listing raw strain data calculated from CSS readings and initial gage lengths.

414

**Tables G.19-G.20 – Smoothed CSS Data Sheets, North & South** – Worksheets listing smoothed strain data determined by a three-point floating average.

**Table G.21 - Average Raw Transfer Length Plot Data** – Worksheets averaging North and South raw data.

**Figures G.1-G.2 - Raw Plots East and West** – Raw CSS plots for East and West ends.

**Table G.22 - Average Smoothed Plot Data** – Worksheets averaging North and South smoothed data.

**Figures G.3-G.4 - Smoothed Plots East and West** – Smoothed CSS plots for East and West ends.

**Figures G.5-G.6 - Transfer Length Plots East and West** – 14-day transfer length calculation plots based on the 95% AMS Method.

**NOTE ON DATA COLLECTION**: Prior to girder construction, it was decided that CSS data collection and recording would be made more consistent and "foolproof" by establishing a basic rule. The rule was that all CSS readings would be taken from LEFT to RIGHT as the data taker looked at the embedment strip. The CSS data form (Table G.1) was configured such that the table provided areas for data entry that matched the location of the embedment strips on the girder. The LEFT to RIGHT rule applied to both sides of the girder. This was done to help alleviate errors from occurring in the field.

Table G.1 Transfer Length Data Taking Sheet

| Beam Number | | Beam Side | | | Take Readings From Left to Right on Each Plate | | | |
|---|---|---|---|---|---|---|---|---|

Dates, Times and Notes for Readings - Gage Length is 8" on DEMEC Gage Reader - Zero Gage on Bar Before Taking Readings

| Reading # | Date | Time | Deflection | TCA | TCI | Hz | 103Hz2 | WWG | Notes |
|---|---|---|---|---|---|---|---|---|---|
| 1 | | | | | | | | | |
| 2 | | | | | | | | | |
| 3 | | | | | | | | | |
| 4 | | | | | | | | | |
| 5 | | | | | | | | | |

| Reading 1 | Reading 2 | Reading 3 | Reading 4 | Reading 5 | Reading 1 | Reading 2 | Reading 3 | Reading 4 | Reading 5 |
|---|---|---|---|---|---|---|---|---|---|

30 Inch Top Left

30 Inch Top Center

30 Inch Top Right

26 Inch Top Center

48 Inch Bottom Left

26 Inch Bottom Center

48 Inch Bottom Right

48 Inch Bottom Center

Table G.2  Data Worksheet for Girder G1C

| Beam # | G1C | Raw Data for Transfer and Development Length | | | | | | | |
|---|---|---|---|---|---|---|---|---|---|

| Reading # | Date (DD/MM/YY) | Time | Midspan Deflection (Inches) | Ambient Temperature (Degrees F) | Internal Temperature (Degrees F) | Vibrating Wire Strain Gage Data | | | Notes |
|---|---|---|---|---|---|---|---|---|---|
| | | | | | | HZ | $10^3HZ^2$ | W WG | |
| Initial 1 | 07/18/2001 | 12:10 | 2.031 | 85.0 | 117.4 | 902.66 | 814.85 | 1308 | Initial Reading 1, Sunny |
| Initial 2 | 07/18/2001 | 12:10 | 2.031 | 85.0 | 117.4 | 902.66 | 814.85 | 1308 | Initial Reading 2, Sunny |
| Release | 07/18/2001 | 15:15 | 2.453 | 87.8 | 108.5 | 799.65 | 639.55 | 1387 | After Cutting Strand, Cloudy |
| 1-Day | 07/19/2001 | 7:08 | 2.469 | 74.2 | 84.6 | 791.59 | 626.65 | 2407 | 1-Day, At Sunrise, Dry and Clear |
| 2-Day | 07/20/2001 | 6:53 | 2.484 | 73.6 | 83.5 | 784.09 | 614.80 | 2514 | 2-Day, At Sunrise, Dry and Clear |
| 3-Day | 07/21/2001 | 6:50 | 2.500 | 72.5 | 79.0 | 780.30 | 608.70 | 2829 | 3-Day, At Sunrise, Overcast |
| 7-Day | 07/25/2001 | 7:10 | 2.531 | 73.8 | 78.7 | 762.00 | 580.60 | 2868 | 7-Day, At Sunrise, Overcast |
| 14-Day | 08/01/2001 | 6:30 | 2.555 | 72.0 | 78.1 | 749.82 | 563.00 | 2863 | 14-Day, At Sunrise, Mostly Clear |
| 95% | | | | | | | | | |
| Slope | | | | | | | | | |

## Load Cell and Jacking Data

| Load Cell (Strand) # | Time of Stressing (me) | Prior to Release (me) |
|---|---|---|
| 1 | 5163 | 4989 |
| 2 | 5218 | 5023 |
| 3 | 5640 | 5387 |
| 4 | 5549 | 5406 |
| 5 | 5484 | 5279 |
| 6 | 5456 | 5309 |
| 7 | 5126 | 5000 |
| 8 | 5115 | 4970 |
| 9 | 5489 | 5387 |
| 10 | 5601 | 5443 |

| Strand # | Strand Jacking Force (Pounds) | Strand Elongation (Inches) | Date/Time | Temp (Deg F) | Notes |
|---|---|---|---|---|---|
| 1 | 45000 | 9.875 | | | |
| 2 | 45500 | 9.750 | | | |
| 3 | 46000 | 9.750 | | | |
| 4 | 46000 | 9.875 | | | |
| 5 | 46000 | 9.875 | 17 Jul 01 | 75 | |
| 6 | 46000 | 9.875 | | | |
| 7 | 45000 | 10.000 | | | |
| 8 | 45000 | 10.000 | | | |
| 9 | 46000 | 9.750 | | | |
| 10 | 46000 | 9.750 | | | |

417

Table G.3 North Side Gage Locations

# Gages - North

————— Distance from Beam End to 1st Gage (IN) —————

| 1 | | | | 1.25 |
|---|---|---|---|---|
| 33.63 | | | | 33.63 |

| 33.75 | <— Elevation of End Gage (IN) —> | 33.75 | <— Elevation of End Gage (IN) —> | 33.63 |

| 1 | Top-L | 11 | 1 | Top-C | 9 | 1 | Top-R | 11 |
|---|---|---|---|---|---|---|---|---|

Position ————————> ←———————— Position

## G1C-N

| 1 | Bot-L | 20 | 1 | Bot-C | 9 | 1 | Bot-R | 20 |
|---|---|---|---|---|---|---|---|---|

| 3 | 3 | | 3.063 | <— Elevation (IN) —> | 2.938 |
|---|---|---|---|---|---|

| 0.625 | | | 1.5 |
|---|---|---|---|

————— Distance from Beam End to 1st Gage (IN) —————

**30" Top-L**

| Elev | Posn | Init | Lgth |
|---|---|---|---|
| 33.64 | 5.07 | 1420 | 8.14 |
| 33.65 | 7.10 | 1212 | 8.12 |
| 33.66 | 9.13 | 1221 | 8.12 |
| 33.67 | 11.16 | 1208 | 8.12 |
| 33.68 | 13.18 | 843 | 8.08 |
| 33.69 | 15.20 | 874 | 8.09 |
| 33.70 | 17.23 | 809 | 8.08 |
| 33.71 | 19.25 | 959 | 8.10 |
| 33.71 | 21.27 | 989 | 8.10 |
| 33.72 | 23.30 | 1072 | 8.11 |
| 33.73 | 25.33 | 1144 | 8.11 |
| Length => | 28.40 | | IN |

**48" Bot-L**

| Elev | Posn | Init | Lgth |
|---|---|---|---|
| 3.00 | 4.63 | 110 | 8.01 |
| 3.00 | 6.63 | -45 | 8.00 |
| 3.00 | 8.63 | -160 | 7.98 |
| 3.00 | 10.62 | -207 | 7.98 |
| 3.00 | 12.62 | 3 | 8.00 |
| 3.00 | 14.63 | 526 | 8.05 |
| 3.00 | 16.65 | 665 | 8.07 |
| 3.00 | 18.66 | 489 | 8.05 |
| 3.00 | 20.67 | 338 | 8.03 |
| 3.00 | 22.67 | 53 | 8.01 |
| 3.00 | 24.67 | -28 | 8.00 |
| 3.00 | 26.68 | 241 | 8.02 |
| 3.00 | 28.68 | -50 | 8.00 |
| 3.00 | 30.68 | -92 | 8.01 |
| 3.00 | 32.68 | -91 | 7.99 |
| 3.00 | 34.67 | -302 | 7.97 |
| 3.00 | 36.67 | 25 | 8.00 |
| 3.00 | 38.67 | 179 | 8.02 |
| 3.00 | 40.68 | 358 | 8.04 |
| 3.00 | 42.69 | 386 | 8.04 |
| Length => | 46.07 | | IN |

**26" Top-C**

| Elev | Posn | Init | Lgth |
|---|---|---|---|
| 33.75 | 250.0 | -574 | 7.94 |
| 33.75 | 252.0 | -597 | 7.94 |
| 33.75 | 254.0 | -339 | 7.97 |
| 33.75 | 256.0 | -180 | 7.98 |
| 33.75 | 258.0 | -146 | 7.99 |
| 33.75 | 260.0 | -299 | 7.97 |
| 33.75 | 262.0 | -302 | 7.97 |
| 33.75 | 264.0 | -283 | 7.97 |
| 33.75 | 266.0 | -537 | 7.95 |
| Length => | 23.88 | | IN |

**#**

| # |
|---|
| 1 |
| 2 |
| 3 |
| 4 |
| 5 |
| 6 |
| 7 |
| 8 |
| 9 |
| 10 |
| 11 |
| 12 |
| 13 |
| 14 |
| 15 |
| 16 |
| 17 |
| 18 |
| 19 |
| 20 |

**26" Bot-C**

| Elev | Posn | Init | Lgth |
|---|---|---|---|
| 3.01 | 249.9 | 1258 | 8.13 |
| 3.02 | 251.9 | 1166 | 8.12 |
| 3.02 | 253.9 | 909 | 8.09 |
| 3.03 | 256.0 | 1022 | 8.10 |
| 3.03 | 258.0 | 987 | 8.10 |
| 3.04 | 260.0 | 1019 | 8.10 |
| 3.04 | 262.1 | 1620 | 8.16 |
| 3.05 | 264.1 | 1310 | 8.13 |
| 3.05 | 266.1 | 1117 | 8.11 |
| Length => | 24.35 | | IN |

**30" Top-R**

| Elev | Posn | Init | Lgth |
|---|---|---|---|
| 33.63 | 25.46 | 762 | 8.08 |
| 33.63 | 23.44 | 743 | 8.07 |
| 33.63 | 21.42 | 865 | 8.09 |
| 33.63 | 19.40 | 922 | 8.09 |
| 33.63 | 17.38 | 753 | 8.08 |
| 33.63 | 15.36 | 696 | 8.07 |
| 33.63 | 13.35 | 606 | 8.06 |
| 33.63 | 11.33 | 740 | 8.07 |
| 33.63 | 9.31 | 549 | 8.05 |
| 33.63 | 7.30 | 639 | 8.06 |
| 33.63 | 5.29 | 409 | 8.04 |
| Length => | 28.25 | | IN |

**48" Bot-R**

| Elev | Posn | Init | Lgth |
|---|---|---|---|
| 2.99 | 43.53 | 104 | 8.01 |
| 2.99 | 41.53 | 148 | 8.01 |
| 2.99 | 39.52 | 190 | 8.02 |
| 2.99 | 37.52 | 96 | 8.01 |
| 2.98 | 35.52 | 146 | 8.01 |
| 2.98 | 33.51 | 109 | 8.01 |
| 2.98 | 31.52 | -219 | 7.98 |
| 2.98 | 29.52 | -255 | 7.97 |
| 2.97 | 27.54 | -530 | 7.95 |
| 2.97 | 25.55 | -420 | 7.96 |
| 2.97 | 23.55 | 69 | 8.01 |
| 2.96 | 21.54 | 127 | 8.01 |
| 2.96 | 19.53 | 361 | 8.04 |
| 2.96 | 17.53 | 257 | 8.03 |
| 2.96 | 15.53 | 12 | 8.00 |
| 2.95 | 13.53 | 56 | 8.01 |
| 2.95 | 11.52 | 142 | 8.01 |
| 2.95 | 9.52 | 208 | 8.02 |
| 2.95 | 7.51 | 283 | 8.03 |
| 2.94 | 5.51 | 216 | 8.02 |
| Length => | 46.04 | | IN |

| Beam Length | 43.00 | FT |
|---|---|---|
| DEMEC Gage Length | 8.00 | IN |

# Table G.4 South Side Gage Locations

## Beam Gage Locations - South

Distance from Beam End to 1st Gage (IN)

<—— Elevation of End Gage (IN)

| | | 0.875 | 33.88 | | 0.813 | 33.75 |
|---|---|---|---|---|---|---|
| Top - L | 11 | | 33.63 | 33.88 | Top - C | 9 | | Top - R | 11 |
| Bot - L | 20 | | | | Bot - C | 9 | | Bot - R | 20 |

G1C - S

Position —————>      <————— Position

<—— Elevation (IN) ——>

| 3.125 | 3.063 | | 3.125 | 3.375 | | 3.125 | 1.313 |

Distance from Beam End to 1st Gage (IN)

| 3.125 | | 0.75 | | 3.375 |

| Beam Length | 43.00 | FT |
|---|---|---|
| DEMEC Gage Length | 8.00 | IN |

### 30" Top - L

| Elev | Posn | Init | Lgth |
|---|---|---|---|
| 33.86 | 4.90 | 576 | 8.06 |
| 33.85 | 6.92 | 614 | 8.06 |
| 33.84 | 8.94 | 758 | 8.08 |
| 33.83 | 10.95 | 501 | 8.05 |
| 33.82 | 12.96 | 566 | 8.06 |
| 33.81 | 14.98 | 669 | 8.07 |
| 33.80 | 17.00 | 619 | 8.06 |
| 33.79 | 19.02 | 925 | 8.09 |
| 33.79 | 21.04 | 847 | 8.08 |
| 33.78 | 23.06 | 786 | 8.08 |
| 33.77 | 25.08 | 761 | 8.08 |
| Length => | | 28.23 | IN |

### 48" Bot - L

| Elev | Posn | Init | Lgth |
|---|---|---|---|
| 3.12 | 4.73 | -500 | 7.95 |
| 3.12 | 6.72 | -192 | 7.98 |
| 3.11 | 8.72 | -192 | 7.98 |
| 3.11 | 10.72 | 48 | 8.00 |
| 3.11 | 12.72 | 170 | 8.02 |
| 3.11 | 14.72 | -18 | 8.00 |
| 3.10 | 16.72 | -23 | 8.00 |
| 3.10 | 18.72 | -56 | 7.99 |
| 3.10 | 20.71 | -313 | 7.97 |
| 3.10 | 22.71 | -75 | 7.99 |
| 3.09 | 24.71 | -95 | 7.99 |
| 3.09 | 26.70 | -252 | 7.97 |
| 3.09 | 28.71 | 253 | 8.03 |
| 3.08 | 30.71 | -37 | 8.00 |
| 3.08 | 32.70 | -155 | 7.98 |
| 3.08 | 34.70 | -101 | 7.99 |
| 3.08 | 36.68 | -580 | 7.94 |
| 3.07 | 38.67 | -469 | 7.95 |
| 3.07 | 40.67 | -178 | 7.98 |
| 3.07 | 42.67 | -107 | 7.99 |
| Length => | | 45.89 | IN |

### 26" Top - C

| Elev | Posn | Init | Lgth |
|---|---|---|---|
| 33.67 | 249.9 | 1162 | 8.12 |
| 33.69 | 251.9 | 686 | 8.07 |
| 33.71 | 254.0 | 854 | 8.09 |
| 33.73 | 256.0 | 736 | 8.07 |
| 33.75 | 258.0 | 641 | 8.06 |
| 33.77 | 260.0 | 770 | 8.08 |
| 33.79 | 262.0 | 721 | 8.07 |
| 33.81 | 264.1 | 694 | 8.07 |
| 33.83 | 266.1 | 879 | 8.09 |
| Length => | | 24.27 | IN |

### 26" Bot - C

| # | Elev | Posn | Init | Lgth |
|---|---|---|---|---|
| 1 | 3.13 | 249.9 | 911 | 8.09 |
| 2 | 3.13 | 252.0 | 827 | 8.08 |
| 3 | 3.13 | 254.0 | 692 | 8.07 |
| 4 | 3.13 | 256.0 | 626 | 8.06 |
| 5 | 3.13 | 258.0 | 755 | 8.08 |
| 6 | 3.13 | 260.0 | 574 | 8.06 |
| 7 | 3.13 | 262.0 | 715 | 8.07 |
| 8 | 3.13 | 264.1 | 703 | 8.07 |
| 9 | 3.13 | 266.1 | 757 | 8.08 |
| 10 | Length => | | 24.23 | IN |
| 11 | | | | |
| 12 | | | | |
| 13 | | | | |
| 14 | | | | |
| 15 | | | | |
| 16 | | | | |
| 17 | | | | |
| 18 | | | | |
| 19 | | | | |
| 20 | | | | |

### 30" Top - R

| Elev | Posn | Init | Lgth |
|---|---|---|---|
| 33.75 | 25.03 | 686 | 8.07 |
| 33.75 | 23.01 | 677 | 8.07 |
| 33.75 | 20.99 | 802 | 8.08 |
| 33.75 | 18.97 | 786 | 8.08 |
| 33.75 | 16.95 | 798 | 8.08 |
| 33.75 | 14.93 | 779 | 8.08 |
| 33.75 | 12.91 | 776 | 8.08 |
| 33.75 | 10.90 | 678 | 8.07 |
| 33.75 | 8.88 | 623 | 8.06 |
| 33.75 | 6.86 | 670 | 8.07 |
| 33.75 | 4.85 | 691 | 8.07 |
| Length => | | 28.25 | IN |

### 48" Bot - R

| Elev | Posn | Init | Lgth |
|---|---|---|---|
| 3.35 | 43.25 | 1065 | 8.11 |
| 3.34 | 41.24 | 463 | 8.05 |
| 3.33 | 39.23 | 338 | 8.03 |
| 3.32 | 37.22 | 228 | 8.02 |
| 3.31 | 35.21 | 267 | 8.03 |
| 3.30 | 33.21 | 88 | 8.01 |
| 3.29 | 31.21 | -18 | 8.00 |
| 3.28 | 29.22 | -177 | 7.98 |
| 3.27 | 27.22 | -289 | 7.97 |
| 3.26 | 25.23 | -376 | 7.96 |
| 3.24 | 23.24 | -370 | 7.96 |
| 3.23 | 21.26 | -505 | 7.95 |
| 3.22 | 19.28 | -774 | 7.92 |
| 3.21 | 17.29 | -709 | 7.93 |
| 3.20 | 15.31 | -703 | 7.93 |
| 3.19 | 13.33 | -703 | 7.93 |
| 3.18 | 11.34 | -423 | 7.96 |
| 3.17 | 9.35 | -511 | 7.95 |
| 3.16 | 7.36 | -324 | 7.97 |
| 3.15 | 5.37 | -247 | 7.98 |
| Length => | | 45.99 | IN |

Table G.5 CSS Reading Sheet for 30-inch Top Left Embedment Strip on North Side

| Beam Number | | G1C | | Beam Side | | North | | | 30 Inch Top Left | | |
|---|---|---|---|---|---|---|---|---|---|---|---|
| Initial 1 | Initial 2 | Release | 1-Day | 2-Day | 3-Day | 7-Day | 14-Day | 95% | Slope | | |
| 1418 | 1422 | 1422 | 1409 | 1398 | 1402 | 1398 | 1402 | | | | |
| 1209 | 1215 | 1211 | 1198 | 1191 | 1191 | 1186 | 1191 | | | | |
| 1221 | 1220 | 1217 | 1205 | 1192 | 1198 | 1190 | 1191 | | | | |
| 1204 | 1211 | 1206 | 1194 | 1187 | 1189 | 1181 | 1192 | | | | |
| 0844 | 0842 | 0836 | 0824 | 0816 | 0817 | 0805 | 0819 | | | | |
| 0875 | 0873 | 0866 | 0849 | 0843 | 0845 | 0836 | 0844 | | | | |
| 0807 | 0810 | 0800 | 0784 | 0782 | 0784 | 0774 | 0779 | | | | |
| 0963 | 0954 | 0929 | 0940 | 0932 | 0933 | 0914 | 0932 | | | | |
| 0990 | 0987 | 0986 | 0971 | 0964 | 0963 | 0962 | 0965 | | | | |
| 1071 | 1072 | 1066 | 1049 | 1042 | 1046 | 1038 | 1042 | | | | |
| 1143 | 1145 | 1138 | 1119 | 1119 | 1119 | 1111 | 1117 | | | | |

420

Table G.6 CSS Reading Sheet for 48-inch Bottom Left Embedment Strip on North Side

| Beam Number | | G1C | Beam Side | | North | | | 48 Inch Bottom Left | | |
| --- | --- | --- | --- | --- | --- | --- | --- | --- | --- | --- |
| Initial 1 | Initial 2 | Release | 1-Day | 2-Day | 3-Day | 7-Day | 14-Day | 95% | Slope |
| 0110 | 0109 | 0101 | 0086 | 0081 | 0081 | 0072 | 0081 | | |
| -0046 | -0044 | -0057 | -0070 | -0074 | -0070 | -0083 | -0077 | | |
| -0160 | -0160 | -0172 | -0185 | -0203 | -0205 | -0209 | -0196 | | |
| -0196 | -0218 | -0234 | -0258 | -0256 | -0252 | -0256 | -0243 | | |
| 0003 | 0003 | -0021 | -0032 | -0035 | -0038 | -0044 | -0040 | | |
| 0523 | 0529 | 0503 | 0492 | 0481 | 0481 | 0475 | 0482 | | |
| 0665 | 0664 | 0630 | 0615 | 0610 | 0608 | 0603 | 0607 | | |
| 0483 | 0494 | 0463 | 0439 | 0446 | 0429 | 0428 | 0438 | | |
| 0338 | 0338 | 0297 | 0281 | 0275 | 0273 | 0264 | 0266 | | |
| 0049 | 0056 | 0014 | -0013 | -0019 | -0013 | -0028 | -0017 | | |
| -0031 | -0024 | -0070 | -0085 | -0089 | -0086 | -0096 | -0095 | | |
| 0244 | 0237 | 0194 | 0166 | 0163 | 0161 | 0152 | 0154 | | |
| -0049 | -0051 | -0098 | -0115 | -0127 | -0124 | -0135 | -0136 | | |
| 0089 | 0094 | 0033 | -0005 | 0002 | -0017 | -0015 | 0012 | | |
| -0091 | -0091 | -0143 | -0164 | -0179 | -0184 | -0192 | -0194 | | |
| -0303 | -0300 | -0345 | -0365 | -0375 | -0375 | -0383 | -0380 | | |
| 0023 | 0026 | -0017 | -0039 | -0045 | -0051 | -0058 | -0057 | | |
| 0178 | 0179 | 0132 | 0113 | 0109 | 0102 | 0095 | 0101 | | |
| 0358 | 0357 | 0321 | 0289 | 0277 | 0283 | 0273 | 0268 | | |
| 0389 | 0382 | 0339 | 0316 | 0314 | 0303 | 0292 | 0303 | | |

Table G.7 CSS Reading Sheet for 26-inch Top Center Embedment Strip on North Side

| Beam Number | G1C | Beam Side | North | 26 Inch Top Center | | | | | |
|---|---|---|---|---|---|---|---|---|---|
| Initial 1 | Initial 2 | Release | 1-Day | 2-Day | 3-Day | 7-Day | 14-Day | 95% | Slope |
| -0570 | -0577 | -0587 | -0609 | -0610 | -0619 | -0628 | -0624 | | |
| -0596 | -0598 | -0614 | -0641 | -0652 | -0647 | -0658 | -0653 | | |
| -0336 | -0341 | -0353 | -0372 | -0383 | -0380 | -0392 | -0386 | | |
| -0179 | -0181 | -0200 | -0215 | -0223 | -0221 | -0229 | -0228 | | |
| -0145 | -0147 | -0170 | -0199 | -0196 | -0179 | -0209 | -0186 | | |
| -0297 | -0301 | -0315 | -0340 | -0341 | -0335 | -0352 | -0341 | | |
| -0302 | -0301 | -0313 | -0342 | -0345 | -0339 | -0353 | -0339 | | |
| -0281 | -0285 | -0305 | -0326 | -0326 | -0325 | -0334 | -0321 | | |
| -0533 | -0540 | -0557 | -0589 | -0587 | -0586 | -0609 | -0595 | | |

Table G.8  CSS Reading Sheet for 26-inch Bottom Center Embedment Strip on North Side

| Beam Number | G1C | Beam Side | North | 26 Inch Bottom Center | | | | | | |
|---|---|---|---|---|---|---|---|---|---|---|
| Initial 1 | Initial 2 | Release | 1-Day | 2-Day | 3-Day | 7-Day | 14-Day | 95% | Slope |
| 1254 | 1262 | 1272 | 1192 | 1181 | 1180 | 1165 | 1158 | | |
| 1167 | 1164 | 1110 | 1087 | 1078 | 1081 | 1073 | 1072 | | |
| 0911 | 0907 | 0842 | 0839 | 0832 | 0824 | 0813 | 0822 | | |
| 1023 | 1021 | 0971 | 0948 | 0935 | 0919 | 0909 | 0915 | | |
| 0986 | 0988 | 0943 | 0924 | 0922 | 0921 | 0917 | 0920 | | |
| 1020 | 1017 | 0976 | 0964 | 0959 | 0954 | 0942 | 0957 | | |
| 1623 | 1617 | 1567 | 1549 | 1547 | 1546 | 1534 | 1541 | | |
| 1312 | 1307 | 1253 | 1235 | 1243 | 1230 | 1225 | 1228 | | |
| 1117 | 1117 | 1060 | 1044 | 1037 | 1031 | 1013 | 1032 | | |

Table G.9  CSS Reading Sheet for 30-inch Top Right Embedment Strip on North Side

| Beam Number | G1C | Beam Side | North | 30 Inch Top Right | | | | | | |
|---|---|---|---|---|---|---|---|---|---|---|
| Initial 1 | Initial 2 | Release | 1-Day | 2-Day | 3-Day | 7-Day | 14-Day | 95% | Slope | |
| 0763 | 0760 | 0570 | 0730 | 0730 | 0727 | 0721 | 0729 | | | |
| 0742 | 0744 | 0732 | 0712 | 0709 | 0710 | 0702 | 0709 | | | |
| 0865 | 0865 | 0852 | 0833 | 0830 | 0829 | 0820 | 0832 | | | |
| 0926 | 0918 | 0902 | 0893 | 0887 | 0891 | 0882 | 0895 | | | |
| 0752 | 0753 | 0738 | 0722 | 0719 | 0723 | 0714 | 0720 | | | |
| 0697 | 0695 | 0685 | 0667 | 0661 | 0663 | 0658 | 0662 | | | |
| 0605 | 0607 | 0596 | 0579 | 0575 | 0580 | 0573 | 0578 | | | |
| 0740 | 0740 | 0714 | 0693 | 0689 | 0689 | 0686 | 0693 | | | |
| 0548 | 0550 | 0538 | 0522 | 0516 | 0521 | 0514 | 0520 | | | |
| 0639 | 0639 | 0628 | 0614 | 0611 | 0611 | 0604 | 0616 | | | |
| 0409 | 0409 | 0405 | 0388 | 0384 | 0387 | 0379 | 0387 | | | |

424

Table G.10 CSS Reading Sheet for 48-inch Bottom Right Embedment Strip on North Side

| Beam Number | | G1C | Beam Side | North | | | | 48 Inch Bottom Right | | |
| --- | --- | --- | --- | --- | --- | --- | --- | --- | --- | --- |
| Initial 1 | Initial 2 | Release | 1-Day | 2-Day | 3-Day | 7-Day | 14-Day | 95% | Slope |
| 0103 | 0105 | 0041 | 0026 | 0016 | 0016 | 0005 | 0010 | | |
| 0147 | 0149 | 0090 | 0057 | 0059 | 0062 | 0052 | 0054 | | |
| 0188 | 0191 | 0137 | 0123 | 0115 | 0109 | 0103 | 0114 | | |
| 0098 | 0093 | 0042 | 0021 | 0014 | 0016 | 0007 | 0010 | | |
| 0144 | 0148 | 0091 | 0068 | 0063 | 0059 | 0055 | 0066 | | |
| 0107 | 0110 | 0057 | 0049 | 0040 | 0038 | 0028 | 0053 | | |
| -0219 | -0219 | -0278 | -0297 | -0301 | -0306 | -0315 | -0304 | | |
| -0254 | -0256 | -0308 | -0327 | -0336 | -0339 | -0351 | -0341 | | |
| -0524 | -0536 | -0588 | -0610 | -0617 | -0635 | -0643 | -0631 | | |
| -0416 | -0423 | -0507 | -0513 | -0502 | -0504 | -0518 | -0501 | | |
| 0068 | 0070 | 0025 | 0003 | 0000 | -0002 | -0011 | 0006 | | |
| 0128 | 0126 | 0078 | 0059 | 0055 | 0053 | 0047 | 0051 | | |
| 0357 | 0365 | 0316 | 0302 | 0296 | 0298 | 0283 | 0290 | | |
| 0258 | 0256 | 0218 | 0204 | 0201 | 0197 | 0189 | 0198 | | |
| 0014 | 0009 | -0015 | -0017 | -0033 | -0052 | -0052 | -0028 | | |
| 0064 | 0048 | 0031 | 0022 | 0000 | -0003 | 0007 | 0022 | | |
| 0143 | 0141 | 0111 | 0094 | 0092 | 0093 | 0082 | 0095 | | |
| 0203 | 0213 | 0189 | 0168 | 0168 | 0161 | 0149 | 0159 | | |
| 0289 | 0276 | 0258 | 0225 | 0243 | 0224 | 0211 | 0230 | | |
| 0209 | 0223 | 0208 | 0190 | 0191 | 0187 | 0181 | 0204 | | |

Table G.11  CSS Reading Sheet for 30-inch Top Left Embedment Strip on South Side

| Beam Number | | G1C | | Beam Side | | South | | 30 Inch Top Left | |
| --- | --- | --- | --- | --- | --- | --- | --- | --- | --- |
| Initial 1 | Initial 2 | Release | 1-Day | 2-Day | 3-Day | 7-Day | 14-Day | 95% | Slope |
| 0574 | 0578 | 0567 | 0553 | 0554 | 0565 | 0552 | 0554 | | |
| 0615 | 0613 | 0605 | 0594 | 0592 | 0596 | 0587 | 0593 | | |
| 0753 | 0762 | 0749 | 0733 | 0733 | 0741 | 0733 | 0735 | | |
| 0499 | 0503 | 0478 | 0473 | 0472 | 0476 | 0471 | 0467 | | |
| 0568 | 0563 | 0563 | 0550 | 0567 | 0576 | 0568 | 0571 | | |
| 0673 | 0665 | 0661 | 0647 | 0617 | 0652 | 0640 | 0647 | | |
| 0626 | 0611 | 0605 | 0591 | 0590 | 0596 | 0587 | 0590 | | |
| 0922 | 0928 | 0903 | 0894 | 0888 | 0904 | 0899 | 0904 | | |
| 0855 | 0838 | 0806 | 0783 | 0790 | 0802 | 0813 | 0814 | | |
| 0785 | 0787 | 0775 | 0763 | 0759 | 0759 | 0754 | 0757 | | |
| 0760 | 0761 | 0752 | 0735 | 0730 | 0739 | 0729 | 0728 | | |

Table G.12 CSS Reading Sheet for 48-inch Bottom Left Embedment Strip on South Side

| Beam Number | | G1C | Beam Side | | South | | | 48 Inch Bottom Left | | |
| Initial 1 | Initial 2 | Release | 1-Day | 2-Day | 3-Day | 7-Day | 14-Day | 95% | Slope |
|---|---|---|---|---|---|---|---|---|---|
| -0500 | -0500 | -0533 | -0546 | -0545 | -0542 | -0551 | -0545 | | |
| -0192 | -0192 | -0234 | -0244 | -0250 | -0250 | -0252 | -0248 | | |
| -0192 | -0192 | -0222 | -0233 | -0233 | -0233 | -0243 | -0228 | | |
| 0040 | 0056 | 0007 | -0005 | -0009 | -0011 | -0010 | -0014 | | |
| 0170 | 0170 | 0140 | 0135 | 0129 | 0126 | 0115 | 0124 | | |
| -0010 | -0025 | -0068 | -0085 | -0076 | -0086 | -0078 | -0094 | | |
| -0026 | -0019 | -0068 | -0086 | -0089 | -0082 | -0087 | -0089 | | |
| -0055 | -0056 | -0107 | -0123 | -0128 | -0123 | -0138 | -0132 | | |
| -0313 | -0313 | -0353 | -0367 | -0374 | -0370 | -0373 | -0369 | | |
| -0077 | -0073 | -0134 | -0150 | -0157 | -0154 | -0165 | -0160 | | |
| -0095 | -0095 | -0150 | -0171 | -0176 | -0168 | -0182 | -0171 | | |
| -0266 | -0237 | -0329 | -0343 | -0353 | -0348 | -0353 | -0352 | | |
| 0253 | 0253 | 0192 | 0175 | 0167 | 0182 | 0165 | 0166 | | |
| -0038 | -0035 | -0130 | -0141 | -0146 | -0145 | -0154 | -0155 | | |
| -0154 | -0155 | -0203 | -0194 | -0211 | -0210 | -0216 | -0210 | | |
| -0101 | -0100 | -0167 | -0175 | -0184 | -0179 | -0191 | -0188 | | |
| -0580 | -0580 | -0620 | -0636 | -0638 | -0637 | -0647 | -0644 | | |
| -0467 | -0470 | -0500 | -0505 | -0516 | -0512 | -0528 | -0522 | | |
| -0178 | -0178 | -0263 | -0270 | -0276 | -0278 | -0294 | -0283 | | |
| -0108 | -0106 | -0151 | -0159 | -0163 | -0160 | -0174 | -0170 | | |

Table G.13  CSS Reading Sheet for 26-inch Top Center Embedment Strip on South Side

| Beam Number | G1C | Beam Side | South | | 26 Inch Top Center | | | | |
|---|---|---|---|---|---|---|---|---|---|
| Initial 1 | Initial 2 | Release | 1-Day | 2-Day | 3-Day | 7-Day | 14-Day | 95% | Slope |
| 1161 | 1163 | 1147 | 1122 | 1124 | 1124 | 1115 | 1118 | | |
| 0686 | 0686 | 0633 | 0617 | 0614 | 0621 | 0609 | 0613 | | |
| 0861 | 0847 | 0838 | 0815 | 0824 | 0828 | 0817 | 0821 | | |
| 0739 | 0732 | 0726 | 0710 | 0709 | 0720 | 0713 | 0720 | | |
| 0642 | 0639 | 0637 | 0638 | 0621 | 0617 | 0606 | 0613 | | |
| 0770 | 0770 | 0748 | 0754 | 0739 | 0741 | 0729 | 0734 | | |
| 0721 | 0721 | 0705 | 0690 | 0685 | 0688 | 0677 | 0682 | | |
| 0695 | 0693 | 0647 | 0659 | 0660 | 0661 | 0652 | 0654 | | |
| 0881 | 0877 | 0866 | 0845 | 0864 | 0862 | 0852 | 0859 | | |

Table G.14 CSS Reading Sheet for 26-inch Bottom Center Embedment Strip on South Side

| Beam Number | G1C | Beam Side | South | 26 Inch Bottom Center | | | | | |
|---|---|---|---|---|---|---|---|---|---|
| Initial 1 | Initial 2 | Release | 1-Day | 2-Day | 3-Day | 7-Day | 14-Day | 95% | Slope |
| 0913 | 0908 | 0851 | 0840 | 0834 | 0834 | 0824 | 0819 | | |
| 0829 | 0824 | 0769 | 0756 | 0753 | 0755 | 0737 | 0736 | | |
| 0692 | 0692 | 0646 | 0631 | 0630 | 0625 | 0616 | 0619 | | |
| 0635 | 0616 | 0546 | 0565 | 0563 | 0559 | 0549 | 0547 | | |
| 0758 | 0752 | 0702 | 0697 | 0688 | 0680 | 0677 | 0673 | | |
| 0575 | 0572 | 0512 | 0509 | 0498 | 0565 | 0496 | 0508 | | |
| 0716 | 0713 | 0643 | 0644 | 0624 | 0633 | 0619 | 0636 | | |
| 0707 | 0699 | 0667 | 0646 | 0646 | 0640 | 0633 | 0642 | | |
| 0760 | 0753 | 0703 | 0692 | 0687 | 0681 | 0679 | 0681 | | |

Table G.15 CSS Reading Sheet for 30-inch Top Right Embedment Strip on North Side

| Beam Number | G1C | Beam Side | South | | | | 30 Inch Top Right | | |
| --- | --- | --- | --- | --- | --- | --- | --- | --- | --- |
| Initial 1 | Initial 2 | Release | 1-Day | 2-Day | 3-Day | 7-Day | 14-Day | 95% | Slope |
| 0694 | 0678 | 0670 | 0649 | 0654 | 0653 | 0642 | 0647 | | |
| 0673 | 0680 | 0660 | 0639 | 0636 | 0645 | 0636 | 0638 | | |
| 0797 | 0806 | 0779 | 0771 | 0769 | 0776 | 0768 | 0771 | | |
| 0786 | 0785 | 0761 | 0746 | 0747 | 0746 | 0741 | 0742 | | |
| 0799 | 0797 | 0780 | 0763 | 0762 | 0759 | 0764 | 0760 | | |
| 0781 | 0777 | 0758 | 0743 | 0742 | 0748 | 0740 | 0742 | | |
| 0772 | 0779 | 0761 | 0742 | 0740 | 0745 | 0738 | 0741 | | |
| 0678 | 0678 | 0666 | 0647 | 0646 | 0648 | 0643 | 0649 | | |
| 0625 | 0621 | 0610 | 0591 | 0593 | 0594 | 0590 | 0592 | | |
| 0670 | 0670 | 0662 | 0648 | 0645 | 0652 | 0647 | 0650 | | |
| 0696 | 0686 | 0684 | 0670 | 0667 | 0669 | 0664 | 0671 | | |

Table G.16 CSS Reading Sheet for 48-inch Bottom Right Embedment Strip on South Side

| Beam Number | | G1C | Beam Side | | South | | 48 Inch Bottom Right | | |
| --- | --- | --- | --- | --- | --- | --- | --- | --- | --- |
| Initial 1 | Initial 2 | Release | 1-Day | 2-Day | 3-Day | 7-Day | 14-Day | 95% | Slope |
| 1065 | 1065 | 1005 | 0952 | 0949 | 0943 | 0935 | 0935 | | |
| 0469 | 0457 | 0402 | 0381 | 0377 | 0381 | 0371 | 0370 | | |
| 0337 | 0338 | 0281 | 0261 | 0253 | 0255 | 0245 | 0246 | | |
| 0225 | 0230 | 0149 | 0131 | 0133 | 0127 | 0115 | 0120 | | |
| 0270 | 0263 | 0208 | 0188 | 0182 | 0185 | 0174 | 0174 | | |
| 0085 | 0091 | 0034 | 0017 | 0013 | 0010 | 0000 | -0008 | | |
| -0019 | -0016 | -0073 | -0090 | -0096 | -0095 | -0106 | -0107 | | |
| -0178 | -0175 | -0237 | -0249 | -0260 | -0259 | -0273 | -0271 | | |
| -0289 | -0288 | -0366 | -0378 | -0388 | -0387 | -0388 | -0373 | | |
| -0378 | -0373 | -0411 | -0426 | -0450 | -0439 | -0455 | -0449 | | |
| -0369 | -0370 | -0419 | -0436 | -0445 | -0443 | -0454 | -0454 | | |
| -0505 | -0504 | -0550 | -0568 | -0575 | -0572 | -0582 | -0580 | | |
| -0773 | -0775 | -0792 | -0816 | -0831 | -0837 | -0851 | -0837 | | |
| -0712 | -0706 | -0734 | -0759 | -0758 | -0758 | -0765 | -0758 | | |
| -0714 | -0691 | -0721 | -0746 | -0749 | -0746 | -0752 | -0746 | | |
| -0706 | -0699 | -0724 | -0740 | -0746 | -0740 | -0755 | -0742 | | |
| -0426 | -0419 | -0449 | -0459 | -0460 | -0466 | -0484 | -0476 | | |
| -0511 | -0511 | -0514 | -0529 | -0522 | -0532 | -0540 | -0527 | | |
| -0325 | -0322 | -0330 | -0347 | -0347 | -0351 | -0355 | -0348 | | |
| -0244 | -0249 | -0187 | -0215 | -0212 | -0220 | -0222 | -0217 | | |

Table G.17  Raw Concrete Surface Strains for North Side of Girder G1C

Raw Transfer Length Data - North Side of Girder G1C

| Bot-L | CSS - Microstrains | | | | | | | |
|---|---|---|---|---|---|---|---|---|
| Gage # | Release | 1-Day | 2-Day | 3-Day | 7-Day | 14-Day | 95% | Slope |
| 1 | 106 | 293 | 356 | 356 | 468 | 356 | | |
| 2 | 150 | 313 | 363 | 313 | 475 | 400 | | |
| 3 | 150 | 313 | 539 | 564 | 614 | 451 | | |
| 4 | 338 | 639 | 614 | 564 | 614 | 451 | | |
| 5 | 300 | 437 | 475 | 512 | 587 | 537 | | |
| 6 | 286 | 422 | 559 | 559 | 633 | 546 | | |
| 7 | 428 | 614 | 676 | 700 | 762 | 713 | | |
| 8 | 317 | 615 | 528 | 739 | 752 | 627 | | |
| 9 | 510 | 710 | 784 | 809 | 921 | 896 | | |
| 10 | 481 | 818 | 893 | 818 | 1006 | 868 | | |
| 11 | 531 | 719 | 769 | 732 | 857 | 844 | | |
| 12 | 580 | 928 | 966 | 991 | 1103 | 1078 | | |
| 13 | 600 | 813 | 963 | 926 | 1063 | 1076 | | |
| 14 | 730 | 1205 | 1117 | 1355 | 1330 | 993 | | |
| 15 | 651 | 914 | 1101 | 1164 | 1264 | 1289 | | |
| 16 | 546 | 797 | 922 | 922 | 1023 | 985 | | |
| 17 | 519 | 794 | 868 | 943 | 1031 | 1018 | | |
| 18 | 580 | 817 | 867 | 954 | 1041 | 967 | | |
| 19 | 454 | 852 | 1002 | 927 | 1052 | 1114 | | |
| 20 | 578 | 865 | 889 | 1026 | 1163 | 1026 | | |

| Bot-R | CSS - Microstrains | | | | | | | |
|---|---|---|---|---|---|---|---|---|
| Gage # | Release | 1-Day | 2-Day | 3-Day | 7-Day | 14-Day | 95% | Slope |
| 1 | 786 | 974 | 1099 | 1099 | 1236 | 1173 | | |
| 2 | 724 | 1135 | 1110 | 1073 | 1198 | 1173 | | |
| 3 | 655 | 829 | 929 | 1004 | 1079 | 942 | | |
| 4 | 668 | 930 | 1018 | 993 | 1105 | 1067 | | |
| 5 | 686 | 973 | 1036 | 1086 | 1135 | 998 | | |
| 6 | 643 | 743 | 855 | 880 | 1005 | 693 | | |
| 7 | 740 | 978 | 1028 | 1090 | 1203 | 1065 | | |
| 8 | 665 | 903 | 1016 | 1053 | 1204 | 1078 | | |
| 9 | 730 | 1007 | 1095 | 1321 | 1422 | 1271 | | |
| 10 | 1100 | 1175 | 1037 | 1062 | 1238 | 1024 | | |
| 11 | 550 | 824 | 862 | 887 | 999 | 787 | | |
| 12 | 612 | 849 | 899 | 924 | 998 | 948 | | |
| 13 | 560 | 734 | 809 | 784 | 971 | 884 | | |
| 14 | 486 | 660 | 698 | 748 | 847 | 735 | | |
| 15 | 331 | 356 | 556 | 794 | 794 | 494 | | |
| 16 | 312 | 425 | 700 | 737 | 612 | 425 | | |
| 17 | 387 | 599 | 624 | 611 | 749 | 586 | | |
| 18 | 237 | 499 | 499 | 586 | 736 | 611 | | |
| 19 | 305 | 716 | 492 | 729 | 891 | 654 | | |
| 20 | 100 | 324 | 312 | 362 | 436 | 150 | | |

Table G.18 Raw Concrete Surface Strains for South Side of Girder G1C

Raw Transfer Length Data - South Side of Girder G1C

| Bot-L Gage # | Release | 1-Day | 2-Day | 3-Day | 7-Day | 14-Day | 95% | Slope |
|---|---|---|---|---|---|---|---|---|
| | | | | CSS - Microstrains | | | | |
| 1 | 415 | 579 | 566 | 528 | 642 | 566 | | |
| 2 | 526 | 652 | 727 | 727 | 752 | 702 | | |
| 3 | 376 | 514 | 514 | 514 | 639 | 451 | | |
| 4 | 512 | 662 | 712 | 737 | 725 | 775 | | |
| 5 | 374 | 437 | 511 | 549 | 686 | 574 | | |
| 6 | 631 | 844 | 731 | 856 | 756 | 956 | | |
| 7 | 569 | 794 | 831 | 744 | 806 | 831 | | |
| 8 | 644 | 844 | 907 | 844 | 1032 | 957 | | |
| 9 | 502 | 678 | 765 | 715 | 753 | 703 | | |
| 10 | 738 | 938 | 1026 | 988 | 1126 | 1063 | | |
| 11 | 688 | 951 | 1014 | 914 | 1089 | 951 | | |
| 12 | 972 | 1147 | 1273 | 1210 | 1273 | 1260 | | |
| 13 | 760 | 972 | 1072 | 885 | 1097 | 1084 | | |
| 14 | 1169 | 1307 | 1369 | 1357 | 1469 | 1482 | | |
| 15 | 607 | 495 | 708 | 695 | 770 | 695 | | |
| 16 | 832 | 932 | 1045 | 982 | 1133 | 1095 | | |
| 17 | 504 | 705 | 730 | 718 | 844 | 806 | | |
| 18 | 396 | 459 | 597 | 547 | 748 | 673 | | |
| 19 | 1065 | 1153 | 1228 | 1253 | 1453 | 1315 | | |
| 20 | 551 | 651 | 701 | 663 | 839 | 789 | | |

| Bot-R Gage # | Release | 1-Day | 2-Day | 3-Day | 7-Day | 14-Day | 95% | Slope |
|---|---|---|---|---|---|---|---|---|
| | | | | CSS - Microstrains | | | | |
| 1 | 740 | 1394 | 1431 | 1505 | 1604 | 1604 | | |
| 2 | 758 | 1019 | 1069 | 1019 | 1143 | 1156 | | |
| 3 | 703 | 952 | 1052 | 1027 | 1151 | 1139 | | |
| 4 | 978 | 1203 | 1178 | 1253 | 1402 | 1340 | | |
| 5 | 729 | 978 | 1053 | 1015 | 1152 | 1152 | | |
| 6 | 674 | 887 | 936 | 974 | 1099 | 1199 | | |
| 7 | 694 | 906 | 981 | 969 | 1106 | 1119 | | |
| 8 | 758 | 908 | 1046 | 1034 | 1209 | 1184 | | |
| 9 | 972 | 1123 | 1248 | 1236 | 1248 | 1060 | | |
| 10 | 446 | 634 | 936 | 797 | 998 | 923 | | |
| 11 | 622 | 835 | 948 | 923 | 1061 | 1061 | | |
| 12 | 572 | 799 | 887 | 849 | 975 | 950 | | |
| 13 | 227 | 530 | 719 | 795 | 972 | 795 | | |
| 14 | 315 | 631 | 618 | 618 | 706 | 618 | | |
| 15 | 233 | 549 | 586 | 549 | 624 | 549 | | |
| 16 | 271 | 473 | 549 | 473 | 662 | 498 | | |
| 17 | 333 | 459 | 471 | 547 | 773 | 672 | | |
| 18 | 38 | 226 | 138 | 264 | 365 | 201 | | |
| 19 | 82 | 295 | 295 | 345 | 395 | 307 | | |
| 20 | 746 | 395 | 433 | 332 | 307 | 370 | | |

Table G.19  Smoothed Concrete Surface Strains for North Side of Girder G1C

Smoothed Transfer Length Data - North Side of Girder G1C

**Bot-L**

| Gage # | Release | 1-Day | 2-Day | 3-Day | 7-Day | 14-Day | 95% | Slope |
|---|---|---|---|---|---|---|---|---|
| | | | | CSS - Microstrains | | | | |
| 1 | | | | | | | | |
| 2 | 135 | 306 | 419 | 411 | 519 | 402 | | |
| 3 | 213 | 422 | 505 | 480 | 568 | 434 | | |
| 4 | 263 | 463 | 543 | 547 | 605 | 480 | | |
| 5 | 308 | 500 | 549 | 545 | 612 | 512 | | |
| 6 | 338 | 491 | 570 | 591 | 661 | 599 | | |
| 7 | 343 | 550 | 587 | 666 | 716 | 629 | | |
| 8 | 418 | 646 | 663 | 750 | 812 | 745 | | |
| 9 | 436 | 714 | 735 | 789 | 893 | 797 | | |
| 10 | 508 | 749 | 815 | 786 | 928 | 869 | | |
| 11 | 531 | 822 | 876 | 847 | 988 | 930 | | |
| 12 | 570 | 820 | 899 | 883 | 1008 | 999 | | |
| 13 | 637 | 982 | 1015 | 1090 | 1165 | 1049 | | |
| 14 | 661 | 977 | 1061 | 1148 | 1219 | 1119 | | |
| 15 | 642 | 972 | 1047 | 1147 | 1205 | 1089 | | |
| 16 | 572 | 835 | 964 | 1010 | 1106 | 1097 | | |
| 17 | 548 | 802 | 886 | 940 | 1032 | 990 | | |
| 18 | 518 | 821 | 912 | 942 | 1041 | 1033 | | |
| 19 | 538 | 845 | 919 | 969 | 1085 | 1036 | | |
| 20 | | | | | | | | |

**Bot-R**

| Gage # | Release | 1-Day | 2-Day | 3-Day | 7-Day | 14-Day | 95% | Slope |
|---|---|---|---|---|---|---|---|---|
| | | | | CSS - Microstrains | | | | |
| 1 | | | | | | | | |
| 2 | 722 | 979 | 1046 | 1058 | 1171 | 1096 | | |
| 3 | 682 | 965 | 1019 | 1023 | 1127 | 1061 | | |
| 4 | 670 | 911 | 994 | 1027 | 1106 | 1002 | | |
| 5 | 666 | 882 | 969 | 986 | 1082 | 919 | | |
| 6 | 690 | 898 | 973 | 1019 | 1115 | 919 | | |
| 7 | 682 | 874 | 966 | 1008 | 1137 | 946 | | |
| 8 | 711 | 962 | 1046 | 1155 | 1276 | 1138 | | |
| 9 | 831 | 1028 | 1049 | 1145 | 1288 | 1124 | | |
| 10 | 793 | 1002 | 998 | 1090 | 1220 | 1027 | | |
| 11 | 754 | 949 | 932 | 957 | 1078 | 920 | | |
| 12 | 574 | 802 | 856 | 865 | 989 | 873 | | |
| 13 | 552 | 748 | 802 | 818 | 939 | 856 | | |
| 14 | 459 | 584 | 688 | 775 | 871 | 704 | | |
| 15 | 376 | 480 | 651 | 759 | 751 | 551 | | |
| 16 | 343 | 460 | 627 | 714 | 718 | 502 | | |
| 17 | 312 | 507 | 607 | 645 | 699 | 541 | | |
| 18 | 310 | 605 | 538 | 642 | 792 | 617 | | |
| 19 | 214 | 513 | 434 | 559 | 688 | 471 | | |
| 20 | | | | | | | | |

Table G.20  Smoothed Concrete Surface Strains for South Side of Girder G1C

**Smoothed Transfer Length Data - South Side of Girder G1C**

| Bot-L Gage # | Release | 1-Day | 2-Day | 3-Day | 7-Day | 14-Day | 95% | Slope |
|---|---|---|---|---|---|---|---|---|
| | | | CSS - Microstrains | | | | | |
| 1 | | | | | | | | |
| 2 | 439 | 581 | 602 | 590 | 677 | 573 | | |
| 3 | 471 | 609 | 651 | 659 | 705 | 642 | | |
| 4 | 421 | 537 | 579 | 600 | 683 | 600 | | |
| 5 | 506 | 648 | 652 | 714 | 722 | 768 | | |
| 6 | 525 | 691 | 691 | 716 | 750 | 787 | | |
| 7 | 615 | 827 | 823 | 815 | 865 | 915 | | |
| 8 | 572 | 772 | 835 | 768 | 864 | 830 | | |
| 9 | 628 | 820 | 899 | 849 | 970 | 908 | | |
| 10 | 643 | 856 | 935 | 872 | 989 | 906 | | |
| 11 | 799 | 1012 | 1104 | 1037 | 1163 | 1092 | | |
| 12 | 807 | 1023 | 1119 | 1003 | 1153 | 1098 | | |
| 13 | 967 | 1142 | 1238 | 1151 | 1280 | 1275 | | |
| 14 | 846 | 924 | 1050 | 979 | 1112 | 1087 | | |
| 15 | 870 | 911 | 1041 | 1011 | 1124 | 1091 | | |
| 16 | 648 | 711 | 828 | 798 | 916 | 865 | | |
| 17 | 577 | 699 | 791 | 749 | 908 | 858 | | |
| 18 | 655 | 772 | 852 | 839 | 1015 | 931 | | |
| 19 | 671 | 754 | 842 | 821 | 1013 | 926 | | |
| 20 | | | | | | | | |

| Bot-R Gage # | Release | 1-Day | 2-Day | 3-Day | 7-Day | 14-Day | 95% | Slope |
|---|---|---|---|---|---|---|---|---|
| | | | CSS - Microstrains | | | | | |
| 1 | | | | | | | | |
| 2 | 734 | 1122 | 1184 | 1184 | 1299 | 1299 | | |
| 3 | 813 | 1058 | 1100 | 1100 | 1232 | 1212 | | |
| 4 | 804 | 1044 | 1094 | 1098 | 1235 | 1210 | | |
| 5 | 794 | 1022 | 1056 | 1081 | 1218 | 1230 | | |
| 6 | 699 | 924 | 990 | 986 | 1119 | 1157 | | |
| 7 | 709 | 900 | 988 | 992 | 1138 | 1167 | | |
| 8 | 808 | 979 | 1092 | 1079 | 1188 | 1121 | | |
| 9 | 725 | 888 | 1077 | 1022 | 1152 | 1056 | | |
| 10 | 680 | 864 | 1044 | 985 | 1103 | 1015 | | |
| 11 | 547 | 756 | 924 | 857 | 1011 | 978 | | |
| 12 | 474 | 721 | 851 | 856 | 1003 | 935 | | |
| 13 | 372 | 653 | 741 | 754 | 884 | 788 | | |
| 14 | 259 | 570 | 641 | 654 | 767 | 654 | | |
| 15 | 273 | 551 | 584 | 546 | 664 | 555 | | |
| 16 | 279 | 493 | 535 | 523 | 686 | 573 | | |
| 17 | 214 | 386 | 386 | 428 | 600 | 457 | | |
| 18 | 151 | 327 | 302 | 385 | 511 | 394 | | |
| 19 | 288 | 305 | 289 | 314 | 356 | 293 | | |
| 20 | | | | | | | | |

Table G.21 Averaged Raw Concrete Surface Strains for Girder G1C (North Reference)

Averaged Raw Transfer Length Plot Data for Girder G1C - (North Reference)

Bot-L

| Posn | Release | 1-Day | 2-Day | 3-Day | 7-Day | 14-Day | 95% | Slope |
|------|---------|-------|-------|-------|-------|--------|-----|-------|
|  | | CSS - microstrains (Normal Order) | | | | | | |
| 0 | 0 | 0 | 0 | 0 | 0 | 0 | | |
| 5.00 | 426 | 344 | 394 | 344 | 388 | 363 | | |
| 6.99 | 116 | 304 | 329 | 329 | 435 | 354 | | |
| 8.99 | 94 | 270 | 338 | 414 | 489 | 326 | | |
| 10.98 | 336 | 549 | 543 | 555 | 693 | 562 | | |
| 12.97 | 286 | 455 | 512 | 493 | 625 | 518 | | |
| 14.97 | 259 | 485 | 573 | 554 | 629 | 547 | | |
| 16.97 | 371 | 622 | 647 | 659 | 734 | 665 | | |
| 18.97 | 272 | 573 | 624 | 767 | 862 | 711 | | |
| 20.96 | 541 | 754 | 836 | 829 | 948 | 923 | | |
| 22.96 | 551 | 827 | 921 | 871 | 1033 | 965 | | |
| 24.95 | 489 | 677 | 852 | 764 | 927 | 884 | | |
| 26.95 | 776 | 1026 | 1107 | 1113 | 1176 | 1069 | | |
| 28.95 | 679 | 861 | 1005 | 980 | 1136 | 1130 | | |
| 30.95 | 712 | 1056 | 1049 | 1162 | 1218 | 1056 | | |
| 32.94 | 662 | 900 | 1019 | 1069 | 1181 | 1244 | | |
| 34.94 | 637 | 887 | 987 | 969 | 1088 | 1069 | | |
| 36.95 | 749 | 998 | 1023 | 1098 | 1217 | 1179 | | |
| 38.95 | 642 | 885 | 959 | 991 | 1096 | 1053 | | |
| 40.96 | 606 | 936 | 1035 | 973 | 1097 | 1135 | | |
| 42.97 | 659 | 1129 | 1160 | 1266 | 1383 | 1315 | | |

Bot-R

| Posn | Release | 1-Day | 2-Day | 3-Day | 7-Day | 14-Day | 95% | Slope |
|------|---------|-------|-------|-------|-------|--------|-----|-------|
|  | | CSS - microstrains (Reverse Order) | | | | | | |
| 0 | 0 | 0 | 0 | 0 | 0 | 0 | | |
| 5.12 | 257 | 451 | 439 | 445 | 539 | 358 | | |
| 7.12 | 416 | 684 | 609 | 728 | 821 | 678 | | |
| 9.12 | 306 | 506 | 506 | 550 | 687 | 531 | | |
| 11.12 | 450 | 631 | 668 | 674 | 737 | 680 | | |
| 13.12 | 343 | 431 | 605 | 643 | 649 | 499 | | |
| 15.12 | 481 | 600 | 644 | 825 | 775 | 725 | | |
| 17.12 | 527 | 727 | 765 | 746 | 827 | 783 | | |
| 19.13 | 602 | 789 | 858 | 814 | 1001 | 920 | | |
| 21.13 | 557 | 763 | 832 | 819 | 876 | 826 | | |
| 23.13 | 644 | 881 | 944 | 938 | 1063 | 925 | | |
| 25.13 | 894 | 1063 | 1025 | 988 | 1163 | 988 | | |
| 27.12 | 851 | 1077 | 1184 | 1266 | 1347 | 1266 | | |
| 29.12 | 712 | 937 | 1044 | 969 | 1150 | 1081 | | |
| 31.11 | 954 | 1142 | 1199 | 1224 | 1336 | 1274 | | |
| 33.11 | 625 | 619 | 781 | 788 | 888 | 694 | | |
| 35.11 | 759 | 953 | 1040 | 1034 | 1134 | 1047 | | |
| 37.10 | 586 | 818 | 874 | 855 | 974 | 937 | | |
| 39.10 | 525 | 644 | 763 | 775 | 913 | 807 | | |
| 41.10 | 894 | 1144 | 1169 | 1163 | 1326 | 1244 | | |
| 43.10 | 669 | 812 | 900 | 881 | 1037 | 981 | | |

436
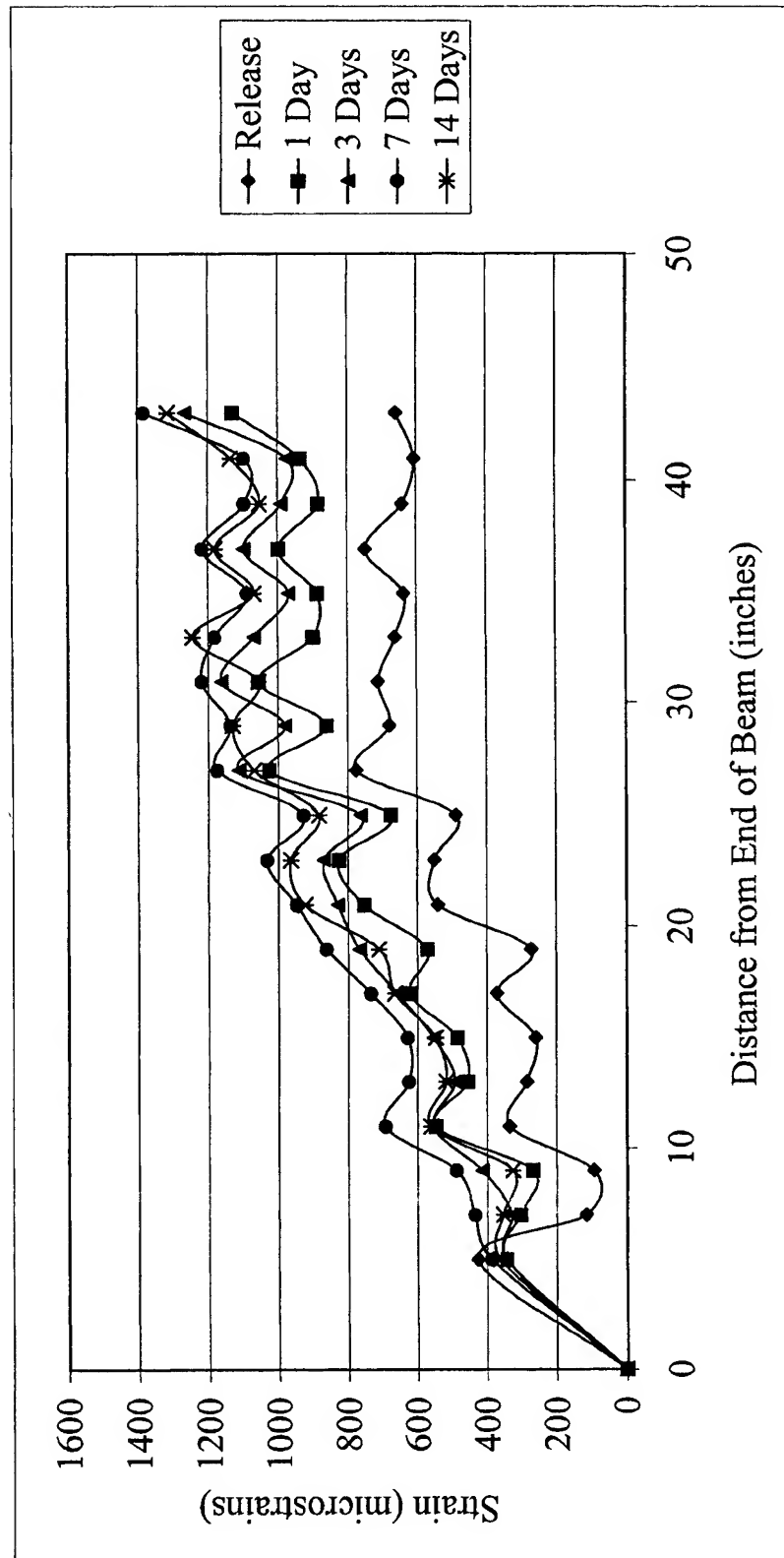
Figure G.1  Raw CSS Data for East End of Girder G1C
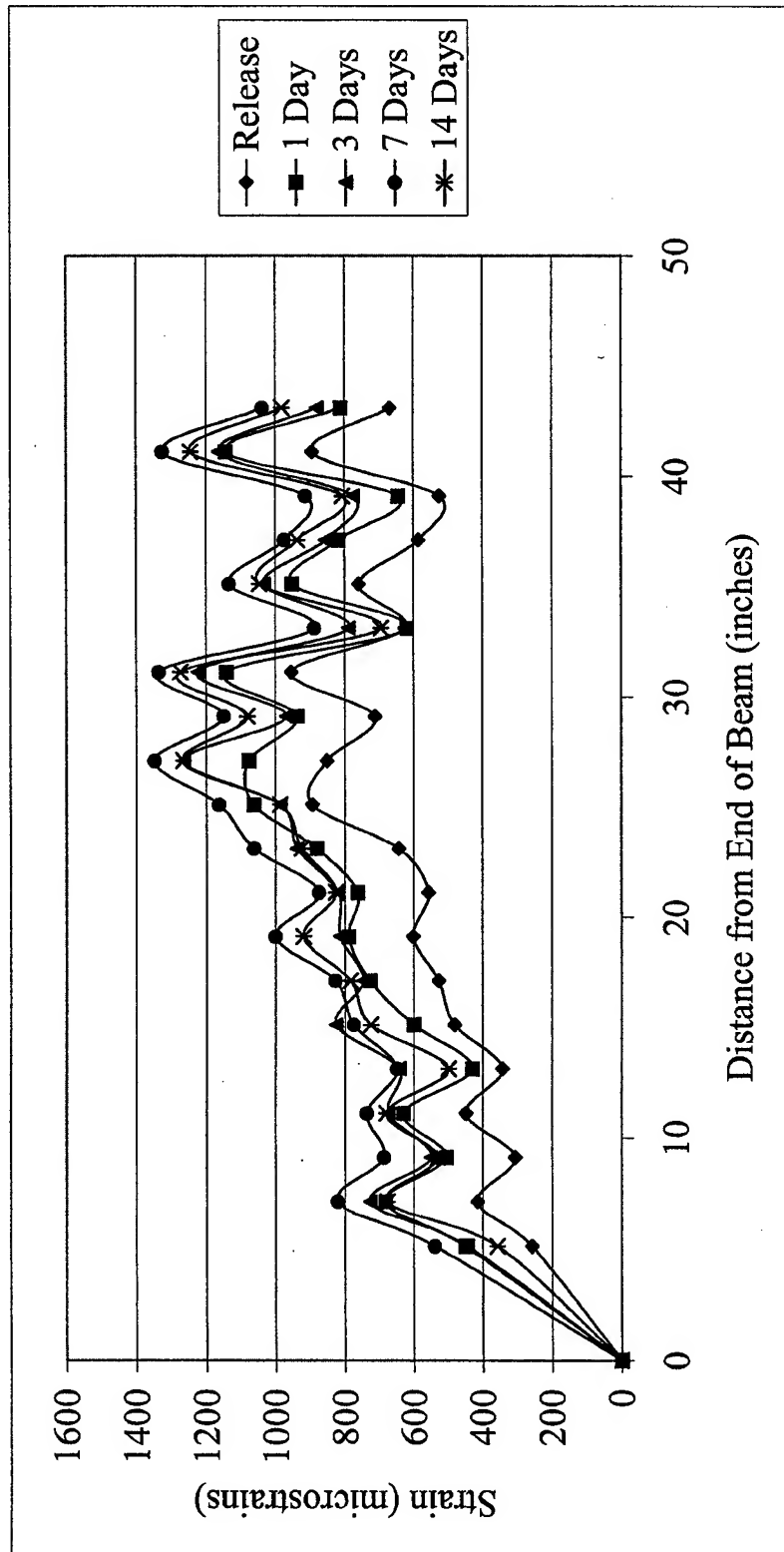
Figure G.2 Raw CSS Data for West End of Girder G1C

438

Table G.22 Averaged Smoothed Concrete Surface Strains for Girder G1C (North Reference)

Averaged Smoothed Transfer Length Plot Data for Girder G1C - (North Reference)

**Bot-L — CSS - microstrains (Normal Order)**

| Posn | Release | 1-Day | 2-Day | 3-Day | 7-Day | 14-Day | 95% | Slope |
|---|---|---|---|---|---|---|---|---|
| 0 | 0 | 0 | 0 | 0 | 0 | 0 | 0 | 0 |
| 6.99 | 212 | 306 | 354 | 362 | 437 | 348 | 1137 | 348 |
| 8.99 | 182 | 374 | 403 | 433 | 539 | 414 | 1137 | 414 |
| 10.98 | 238 | 425 | 464 | 487 | 603 | 469 | 1137 | 469 |
| 12.97 | 294 | 497 | 542 | 534 | 649 | 542 | 1137 | 542 |
| 14.97 | 306 | 521 | 577 | 569 | 663 | 577 | 1137 | 577 |
| 16.97 | 301 | 560 | 614 | 660 | 742 | 641 | 1137 | 641 |
| 18.97 | 395 | 650 | 702 | 752 | 848 | 767 | 1137 | 767 |
| 20.96 | 455 | 718 | 793 | 822 | 948 | 866 | 1137 | 866 |
| 22.96 | 527 | 752 | 869 | 821 | 970 | 924 | 1137 | 924 |
| 24.95 | 605 | 843 | 960 | 916 | 1045 | 972 | 1137 | 972 |
| 26.95 | 648 | 854 | 988 | 952 | 1080 | 1027 | 1137 | |
| 28.95 | 722 | 981 | 1054 | 1085 | 1177 | 1085 | 1137 | |
| 30.95 | 685 | 939 | 1024 | 1070 | 1179 | 1143 | 1137 | |
| 32.94 | 671 | 948 | 1019 | 1067 | 1162 | 1123 | 1137 | |
| 34.94 | 683 | 929 | 1010 | 1045 | 1162 | 1164 | 1137 | |
| 36.95 | 676 | 923 | 990 | 1019 | 1134 | 1100 | 1137 | |
| 38.95 | 665 | 940 | 1006 | 1021 | 1137 | 1122 | 1137 | |
| 40.96 | 636 | 983 | 1052 | 1076 | 1192 | 1168 | 1137 | |
| 42.97 | | | | | | | | |

**Bot-R — CSS - microstrains (Reverse Order)**

| Gage # | Release | 1-Day | 2-Day | 3-Day | 7-Day | 14-Day | 95% | Slope |
|---|---|---|---|---|---|---|---|---|
| 0 | 0 | 0 | 0 | 0 | 0 | 0 | 0 | 0 |
| 7.12 | 327 | 547 | 518 | 574 | 682 | 522 | 975 | 522 |
| 9.12 | 391 | 607 | 595 | 651 | 748 | 630 | 975 | 630 |
| 11.12 | 366 | 522 | 593 | 622 | 691 | 570 | 975 | 570 |
| 13.12 | 425 | 554 | 639 | 714 | 720 | 635 | 975 | 635 |
| 15.12 | 451 | 586 | 671 | 738 | 750 | 669 | 975 | 669 |
| 17.12 | 537 | 706 | 755 | 795 | 868 | 810 | 975 | 810 |
| 19.13 | 562 | 760 | 818 | 793 | 901 | 843 | 975 | 843 |
| 21.13 | 601 | 811 | 878 | 857 | 980 | 890 | 975 | 890 |
| 23.13 | 698 | 903 | 934 | 915 | 1034 | 913 | 975 | 913 |
| 25.13 | 796 | 1007 | 1051 | 1064 | 1191 | 1059 | 975 | 1059 |
| 27.12 | 819 | 1026 | 1084 | 1074 | 1220 | 1111 | 975 | |
| 29.12 | 839 | 1052 | 1142 | 1153 | 1278 | 1207 | 975 | |
| 31.11 | 764 | 899 | 1008 | 993 | 1125 | 1016 | 975 | |
| 33.11 | 780 | 905 | 1007 | 1015 | 1119 | 1005 | 975 | |
| 35.11 | 657 | 796 | 899 | 892 | 999 | 892 | 975 | |
| 37.10 | 623 | 805 | 892 | 888 | 1007 | 930 | 975 | |
| 39.10 | 668 | 869 | 935 | 931 | 1071 | 996 | 975 | |
| 41.10 | 696 | 867 | 944 | 940 | 1092 | 1011 | 975 | |
| 43.10 | | | | | | | | |
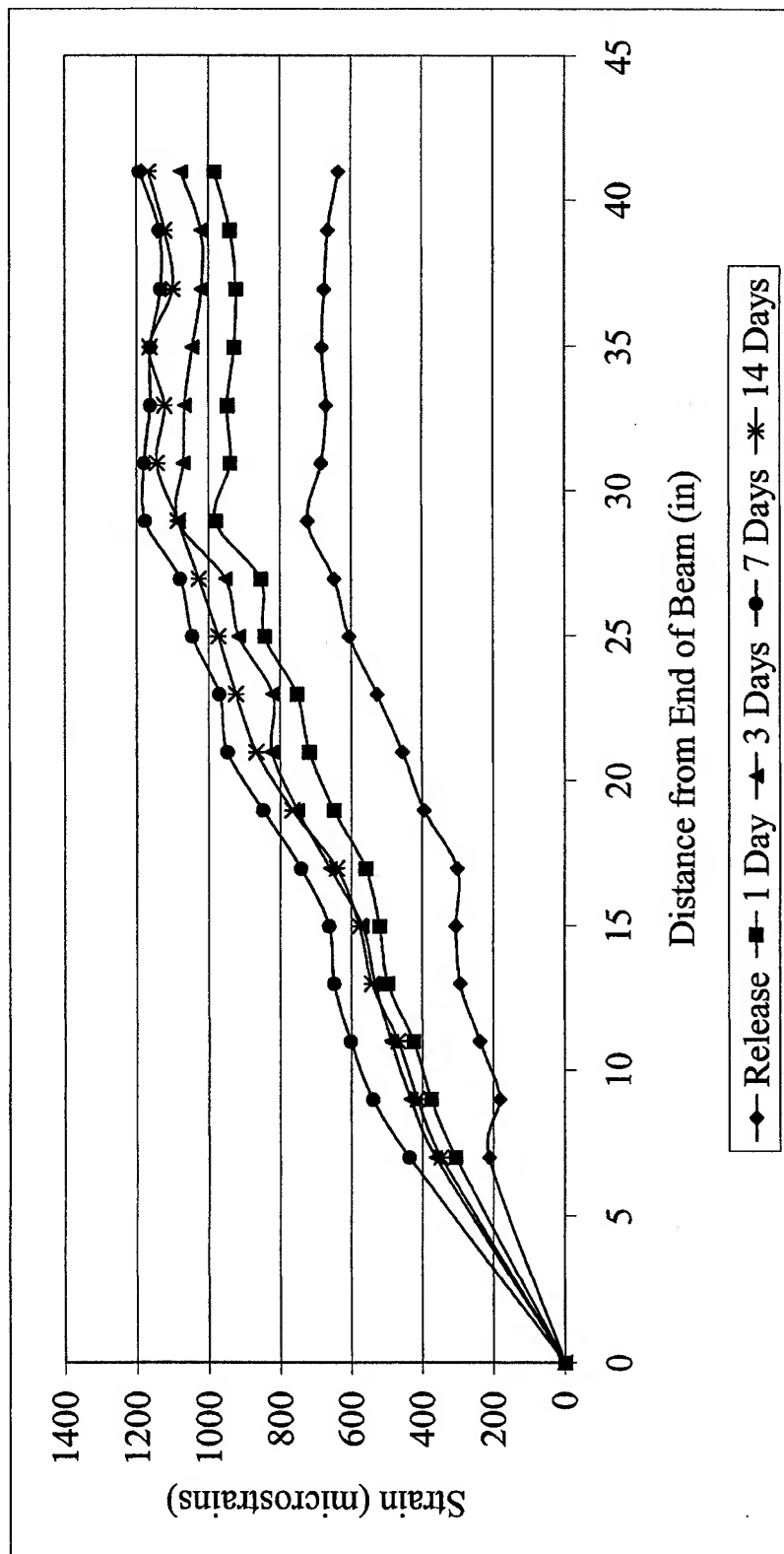
Figure G.3 Smoothed CSS Data for East End of Girder G1C
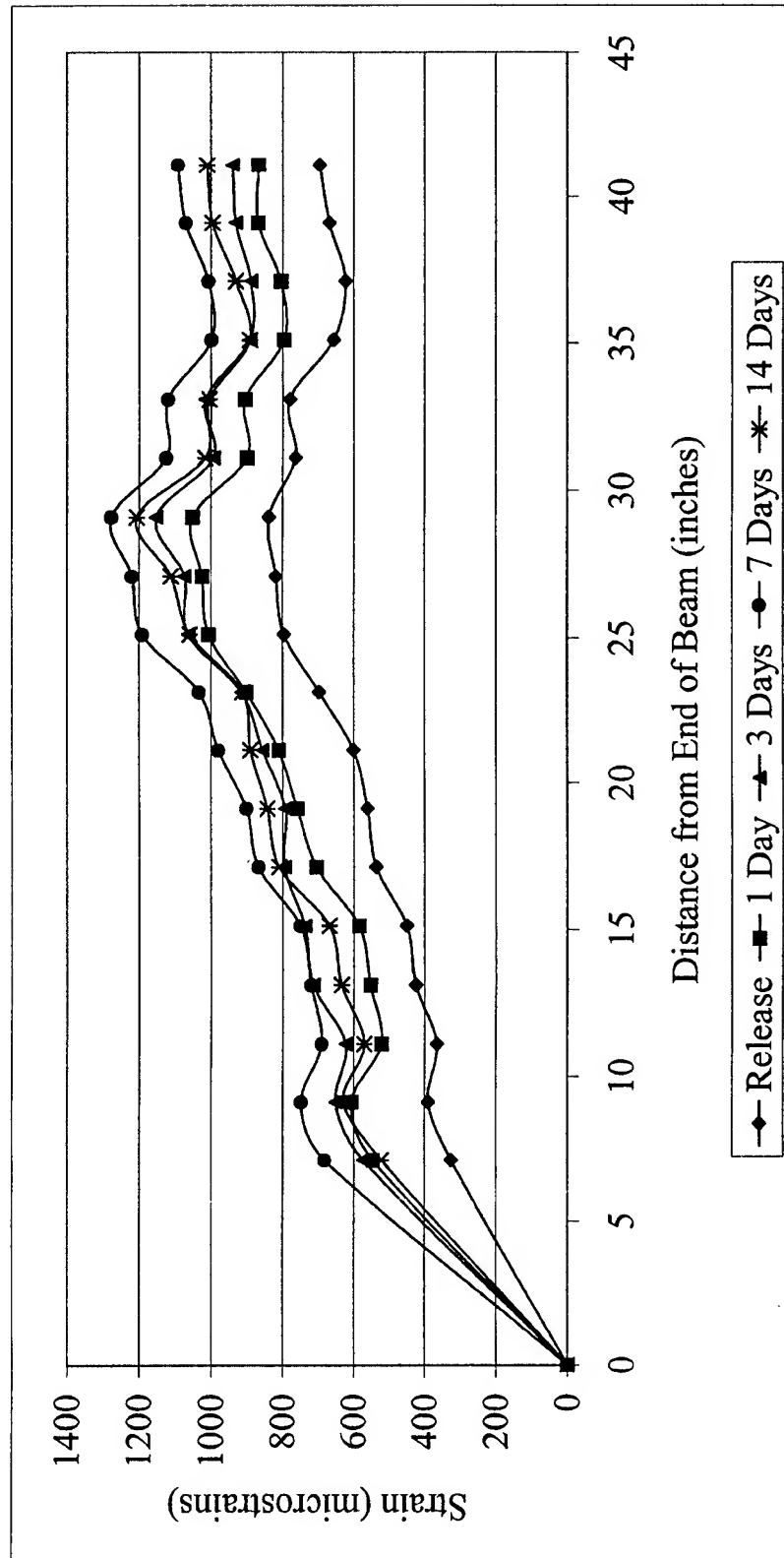
Figure G.4  Smoothed CSS Data for West End of Girder G1C

441
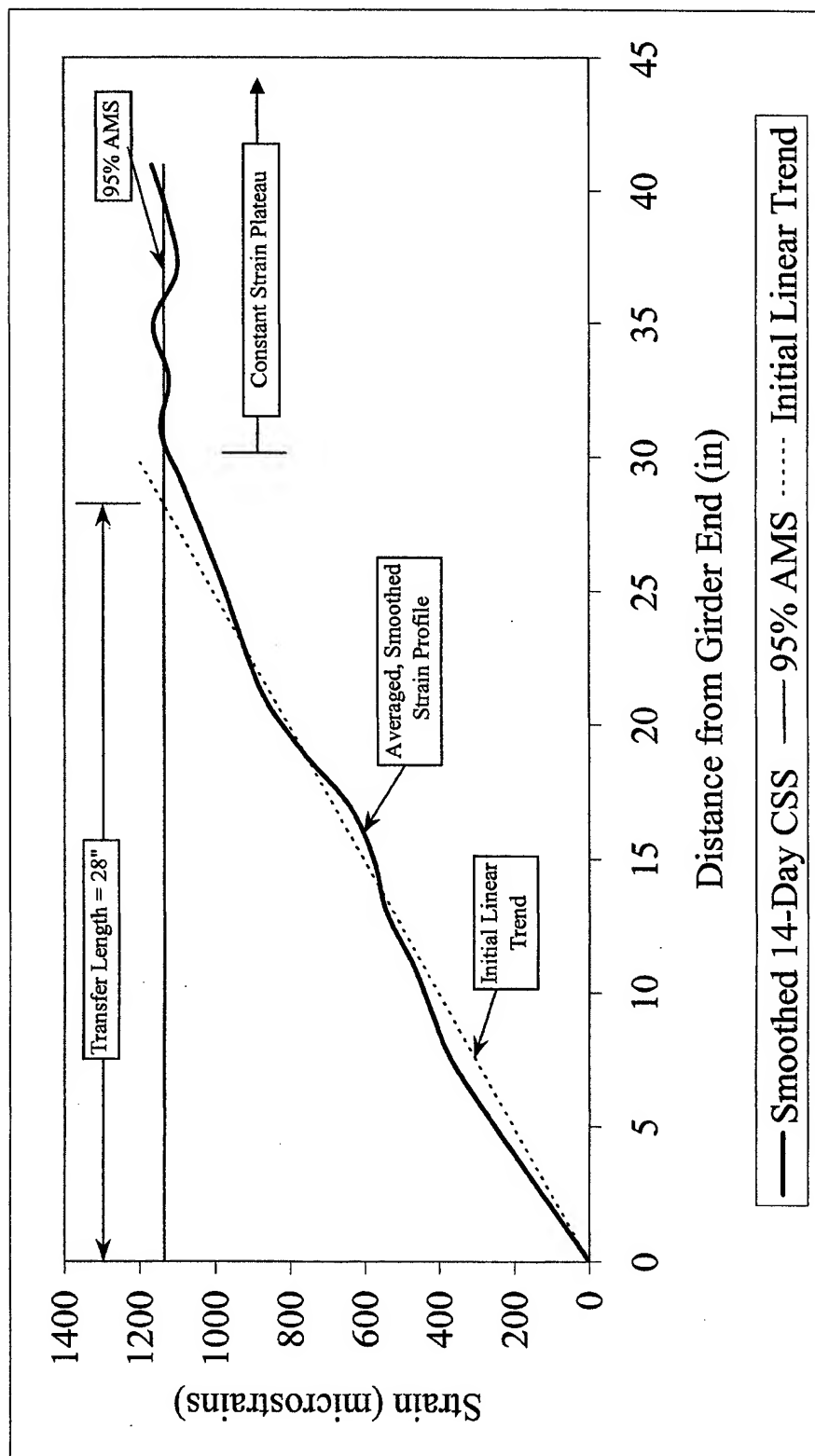
Figure G.5  Transfer Length Determined Using 95% AMS Method for East End of Girder G1C
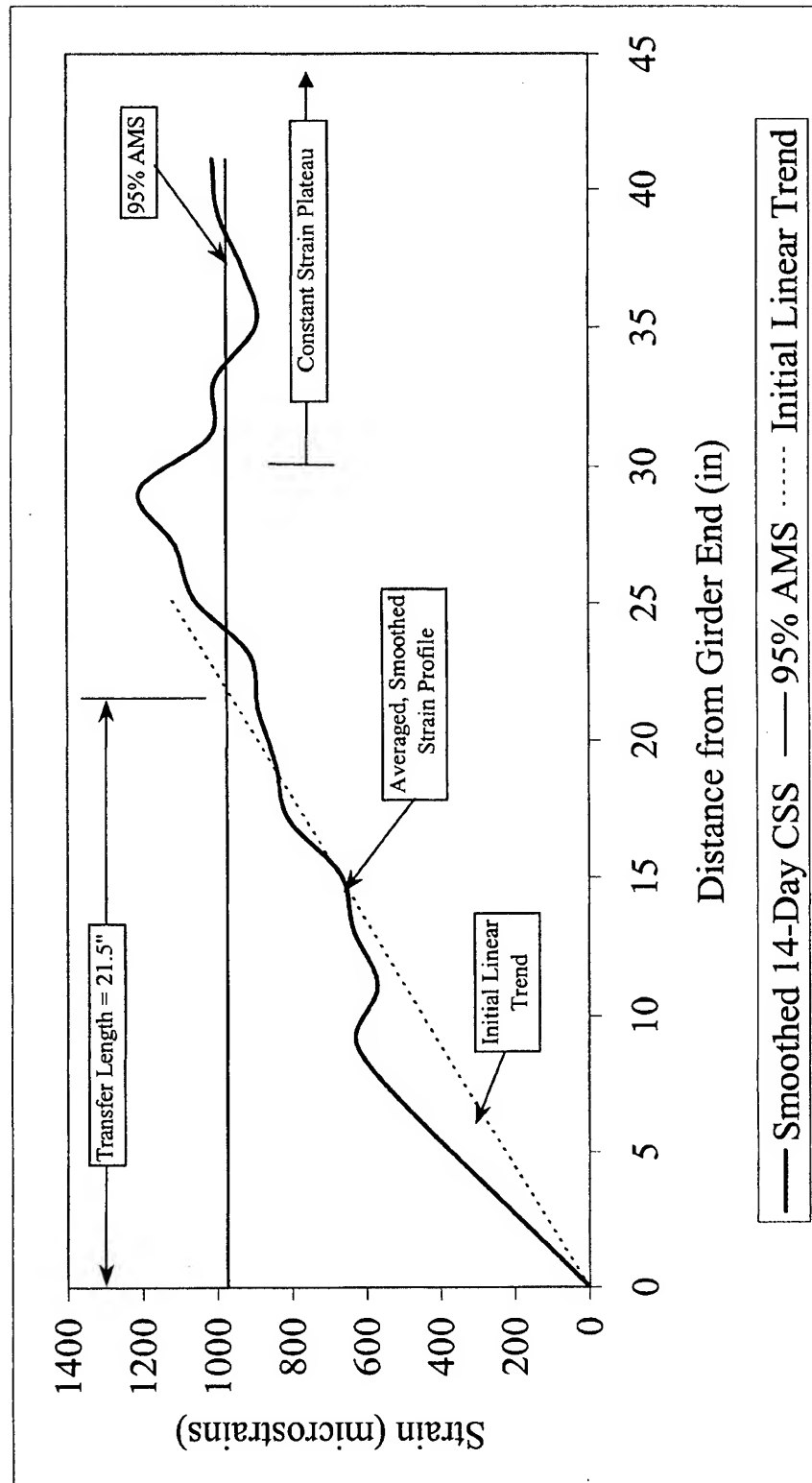
Figure G.6 Transfer Length Determined Using 95% AMS Method for West End of Girder G1C

# APPENDIX H

## CONCRETE SURFACE STRAIN AND OTHER DATA

This Appendix contains raw data for each girder. The following data items were recorded before strand release (initial), just after release, and 1, 2, 3, 7 and 14-days after strand release. The data taken through 14 days were used to determine transfer length.

Date and time

Midspan deflection

Ambient temperature

Internal girder temperature

Reading in hertz from the vibrating wire strain gage at midspan

Resistance reading from the thermistor in the vibrating wire strain gage

CSS readings from each embedment strip

The following values were also recorded for each girder at the time of strand tensioning.

Strain reading from strand load cell

Strand jacking force

Strand elongation

Date and time

Ambient temperature

Strand load cell readings were also recorded immediately prior to strand release for comparison with initial load cell readings. The sections correspond with the individual girders as follows:

**Section H.1** – Girder G1A

**Section H.2** – Girder G1B

**Section H.3** – Girder G1C

**Section H.4** – Girder G2A

**Section H.5** – Girder G2B

**Section H.6** – Girder G2C

The directions North and South refer to girder sides based on orientation at time of construction. East and West refer to girder ends. The gage positions on embedment strips are always referenced from left to right as shown in Figures G.3 and G.4. Gage locations are numbered from 1 to 20 meaning there are 20 CSS readings taken on each bottom embedment strip. The embedment strips are located at the ends of the girders on both sides at the level of the bottom row of prestressing strands. Positive CSS values indicate a compressive strain.

## H.1 Girder G1A

### Table H.1  G1A Girder Data

| Girder # | | G1A | Raw Data for Transfer and Development Length | | | | |
|---|---|---|---|---|---|---|---|
| Reading # | Date (m/dd/yy) | Time (24 hr) | Midspan Deflection (inches) | Ambient Temp (Deg F) | Internal Temp (Deg F) | VWSG Data | |
| | | | | | | Hz | ΩWG |
| Initial 1 | 7/10/01 | 11:30 | 1.703 | 80.0 | | 924.84 | 2128 |
| Initial 2 | 7/10/01 | 12:10 | 1.703 | 80.0 | | 924.84 | 2128 |
| Release | 7/10/01 | 15:07 | 2.063 | 90.0 | | 822.05 | 2128 |
| 1-Day | 7/11/01 | 7:40 | 2.078 | 75.0 | | | |
| 2-Day | 7/12/01 | 7:45 | 2.094 | 75.0 | 73.8 | 809.31 | 2470 |
| 3-Day | 7/13/01 | 7:05 | 2.094 | 74.7 | 72.2 | 802.80 | 2515 |
| 7-Day | 7/17/01 | 6:30 | 2.109 | 72.4 | 67.0 | 790.57 | 2884 |
| 14-Day | 7/24/01 | 6:55 | 2.125 | 74.5 | 68.4 | 778.42 | 2568 |

| Strand Jacking Data from Load Cells and Tensioning Machine | | | | | | |
|---|---|---|---|---|---|---|
| | Load Cell Readings | | Tension Machine Readings | | Date and Time Of Tensioning (m/dd/yy) (24 hr) | Ambient Temp (Deg F) |
| Load Cell (Strand) # | At Time of Stressing (με) | Prior To Release (με) | Strand Jacking Force (lbs) | Strand Elongation (inches) | | |
| 1 | 4533 | 4513 | 45000 | 10.250 | | |
| 2 | 5275 | 5270 | 45000 | 9.875 | | |
| 3 | 5430 | 5438 | 45000 | 10.125 | | |
| 4 | 4975 | 4960 | 45000 | 9.875 | | |
| 5 | 5352 | 5313 | 45000 | 9.875 | 9 Jul 01 11:30 | 90 |
| 6 | 5286 | 5270 | 45000 | 9.750 | | |
| 7 | 5206 | 5150 | 45500 | 9.875 | | |
| 8 | 5340 | 5357 | 45000 | 10.625 | | |
| 9 | 5430 | 5448 | 45000 | 10.250 | | |
| 10 | 5532 | 5479 | 45000 | 10.125 | | |

Table H.2  Raw Concrete Surface Strain Data for Girder G1A-North

| East Gage # | Raw CSS - microstrains | | | | | |
|---|---|---|---|---|---|---|
| | Release | 1-Day | 2-Day | 3-Day | 7-Day | 14-Day |
| 1 | 157 | 244 | 307 | 269 | 420 | 457 |
| 2 | 250 | 350 | 463 | 375 | 550 | 600 |
| 3 | 237 | 350 | 412 | 375 | 525 | 637 |
| 4 | 243 | 380 | 405 | 380 | 480 | 517 |
| 5 | 450 | 512 | 587 | 525 | 774 | 837 |
| 6 | 344 | 432 | 407 | 382 | 545 | 632 |
| 7 | 419 | 557 | 632 | 594 | 695 | 720 |
| 8 | 344 | 444 | 557 | 507 | 895 | 682 |
| 9 | 456 | 780 | 905 | 818 | 955 | 1030 |
| 10 | 482 | 657 | 757 | 707 | 932 | 1007 |
| 11 | 499 | 674 | 699 | 737 | 861 | 886 |
| 12 | 468 | 643 | 693 | 705 | 942 | 980 |
| 13 | 356 | 494 | 544 | 556 | 744 | 606 |
| 14 | 531 | 681 | 644 | 631 | 794 | 869 |
| 15 | 451 | 488 | 576 | 589 | 902 | 764 |
| 16 | 513 | 738 | 851 | 876 | 964 | 1101 |
| 17 | 457 | 569 | 632 | 644 | 845 | 1082 |
| 18 | 449 | 674 | 736 | 736 | 936 | 1010 |
| 19 | 475 | 674 | 737 | 724 | 1086 | 1149 |
| 20 | 431 | 281 | 807 | 757 | 857 | 957 |

| West Gage # | Raw CSS - microstrains | | | | | |
|---|---|---|---|---|---|---|
| | Release | 1-Day | 2-Day | 3-Day | 7-Day | 14-Day |
| 1 | 401 | 526 | 514 | 526 | 764 | 777 |
| 2 | 450 | 801 | 901 | 813 | 1063 | 1088 |
| 3 | 632 | 944 | 1019 | 957 | 1182 | 1294 |
| 4 | 588 | 639 | 751 | 676 | 964 | 1014 |
| 5 | 514 | 564 | 740 | 765 | 1003 | 1053 |
| 6 | 358 | 421 | 484 | 409 | 861 | 987 |
| 7 | 88 | 615 | 615 | 615 | 640 | 678 |
| 8 | 407 | 707 | 745 | 795 | 907 | 982 |
| 9 | 501 | 739 | 939 | 814 | 1052 | 1127 |
| 10 | 592 | 879 | 941 | 792 | 555 | 1203 |
| 11 | 639 | 551 | 639 | 701 | 1139 | 1152 |
| 12 | 263 | 313 | 489 | 489 | 890 | 1065 |
| 13 | 382 | 495 | 557 | 570 | 795 | 708 |
| 14 | 413 | 125 | 276 | 363 | 651 | 614 |
| 15 | 318 | 517 | 580 | 580 | 704 | 754 |
| 16 | 589 | 288 | 175 | 63 | 100 | 251 |
| 17 | 407 | 307 | 319 | 357 | 369 | 457 |
| 18 | 281 | 432 | 444 | 469 | 557 | 544 |
| 19 | 19 | 144 | 19 | 6 | 169 | 257 |
| 20 | 162 | 37 | 287 | 249 | 336 | 448 |

## Table H.3  Raw Concrete Surface Strain Data for Girder G1A-South

| East Gage # | Raw CSS - microstrains | | | | | |
|---|---|---|---|---|---|---|
| | Release | 1-Day | 2-Day | 3-Day | 7-Day | 14-Day |
| 1 | 411 | 722 | 760 | 772 | 872 | 897 |
| 2 | 618 | 693 | 843 | 830 | 930 | 955 |
| 3 | 468 | 805 | 855 | 855 | 967 | 992 |
| 4 | 588 | 763 | 825 | 800 | 900 | 925 |
| 5 | 474 | 699 | 736 | 724 | 611 | 649 |
| 6 | 530 | 629 | 729 | 754 | 854 | 854 |
| 7 | 455 | 679 | 804 | 791 | 854 | 916 |
| 8 | 610 | 722 | 834 | 809 | 909 | 984 |
| 9 | 978 | 916 | 1190 | 1265 | 1277 | 1240 |
| 10 | 529 | 754 | 754 | 816 | 754 | 828 |
| 11 | 473 | 771 | 821 | 809 | 846 | 833 |
| 12 | 416 | 714 | 702 | 640 | 665 | 677 |
| 13 | 497 | 634 | 721 | 671 | 696 | 671 |
| 14 | 542 | 879 | 941 | 904 | 1003 | 1041 |
| 15 | 306 | 892 | 917 | 892 | 980 | 830 |
| 16 | 256 | 693 | 768 | 756 | 831 | 843 |
| 17 | 256 | 493 | 430 | 493 | 468 | 443 |
| 18 | 330 | 542 | 492 | 504 | 529 | 156 |
| 19 | 100 | 338 | 563 | 438 | 701 | 688 |
| 20 | 94 | 357 | 408 | 395 | 508 | 508 |

| West Gage # | Raw CSS - microstrains | | | | | |
|---|---|---|---|---|---|---|
| | Release | 1-Day | 2-Day | 3-Day | 7-Day | 14-Day |
| 1 | 75 | 300 | 325 | 275 | 613 | 526 |
| 2 | 232 | 545 | 557 | 307 | 820 | 770 |
| 3 | 224 | 511 | 499 | 499 | 499 | 524 |
| 4 | 312 | 561 | 598 | 524 | 661 | 686 |
| 5 | 319 | 731 | 706 | 406 | 643 | 818 |
| 6 | 437 | 762 | 787 | 824 | 837 | 824 |
| 7 | 507 | 745 | 845 | 883 | 1033 | 1083 |
| 8 | 530 | 830 | 880 | 892 | 980 | 992 |
| 9 | 527 | 765 | 1003 | 1078 | 1191 | 1179 |
| 10 | 502 | 765 | 803 | 803 | 891 | 916 |
| 11 | 784 | 1034 | 934 | 1047 | 884 | 884 |
| 12 | 510 | 863 | 876 | 914 | 939 | 989 |
| 13 | 532 | 757 | 770 | 845 | 882 | 607 |
| 14 | 532 | 832 | 857 | 895 | 983 | 970 |
| 15 | 381 | 731 | 744 | 756 | 719 | 669 |
| 16 | 548 | 810 | 847 | 872 | 959 | 959 |
| 17 | 486 | 910 | 997 | 1096 | 1184 | 1258 |
| 18 | 491 | 802 | 827 | 1286 | 988 | 827 |
| 19 | 690 | 1150 | 1200 | 1225 | 1324 | 1312 |
| 20 | 584 | 870 | 895 | 920 | 1045 | 1007 |

## H.2 Girder G1B

### Table H.4 G1B Girder Data

| Girder # | G1B | | Raw Data for Transfer and Development Length | | | | |
|---|---|---|---|---|---|---|---|
| Reading # | Date (m/dd/yy) | Time (24 hr) | Midspan Deflection (inches) | Ambient Temp (Deg F) | Internal Temp (Deg F) | VWSG Data | |
| | | | | | | Hz | WG |
| Initial 1 | 7/10/01 | 11:30 | 1.938 | 80.0 | | 929.61 | 2009 |
| Initial 2 | 7/10/01 | 12:10 | 1.938 | 80.0 | | 929.61 | 2009 |
| Release | 7/10/01 | 15:25 | 2.250 | 90.0 | | 822.64 | 2009 |
| 1-Day | 7/11/01 | 7:55 | 2.266 | 75.0 | | | |
| 2-Day | 7/12/01 | 7:50 | 2.297 | 75.0 | 85.3 | 808.81 | 2448 |
| 3-Day | 7/13/01 | 7:45 | 2.297 | 77.2 | 82.6 | 802.40 | 2534 |
| 7-Day | 7/17/01 | 7:30 | 2.320 | 70.0 | 78.5 | 788.66 | 2905 |
| 14-Day | 7/24/01 | 7:00 | 2.328 | 75.6 | 83.0 | 775.01 | 2499 |

| Strand Jacking Data from Load Cells and Tensioning Machine | | | | | | |
|---|---|---|---|---|---|---|
| | Load Cell Readings | | Tension Machine Readings | | Date and Time Of | Ambient Temp |
| Load Cell (Strand) # | At Time of Stressing ($\mu\epsilon$) | Prior To Release ($\mu\epsilon$) | Strand Jacking Force (lbs) | Strand Elongation (inches) | Tensioning (m/dd/yy) (24 hr) | (Deg F) |
| 1 | 4533 | 4513 | 45000 | 10.250 | | |
| 2 | 5275 | 5270 | 45000 | 9.875 | | |
| 3 | 5430 | 5438 | 45000 | 10.125 | | |
| 4 | 4975 | 4960 | 45000 | 9.875 | | |
| 5 | 5352 | 5313 | 45000 | 9.875 | 9 Jul 01 | 90 |
| 6 | 5286 | 5270 | 45000 | 9.750 | 11:30 | |
| 7 | 5206 | 5150 | 45500 | 9.875 | | |
| 8 | 5340 | 5357 | 45000 | 10.625 | | |
| 9 | 5430 | 5448 | 45000 | 10.250 | | |
| 10 | 5532 | 5479 | 45000 | 10.125 | | |

449

## Table H.5  Raw Concrete Surface Strain Data for Girder G1B-North

| East Gage # | Raw CSS - microstrains | | | | | |
|---|---|---|---|---|---|---|
| | Release | 1-Day | 2-Day | 3-Day | 7-Day | 14-Day |
| 1 | 37 | 174 | 224 | 199 | 422 | 497 |
| 2 | 6 | 156 | 193 | 193 | 380 | 430 |
| 3 | 337 | 175 | 912 | 212 | 237 | 62 |
| 4 | 256 | 169 | 219 | 169 | 156 | 219 |
| 5 | 75 | 38 | 126 | 113 | 414 | 477 |
| 6 | 87 | 500 | 512 | 500 | 612 | 700 |
| 7 | 424 | 649 | 711 | 836 | 998 | 973 |
| 8 | 238 | 450 | 500 | 488 | 663 | 801 |
| 9 | 243 | 593 | 456 | 418 | 655 | 805 |
| 10 | 350 | 350 | 413 | 388 | 588 | 725 |
| 11 | 419 | 618 | 743 | 743 | 806 | 906 |
| 12 | 535 | 573 | 797 | 834 | 759 | 909 |
| 13 | 478 | 763 | 813 | 850 | 999 | 1073 |
| 14 | 224 | 385 | 509 | 559 | 832 | 584 |
| 15 | 453 | 552 | 639 | 614 | 925 | 1011 |
| 16 | 494 | 569 | 656 | 669 | 844 | 881 |
| 17 | 539 | 627 | 727 | 702 | 928 | 966 |
| 18 | 533 | 445 | 771 | 720 | 1121 | 1422 |
| 19 | 444 | 657 | 732 | 720 | 895 | 932 |
| 20 | 537 | 599 | 724 | 674 | 1011 | 1024 |

| West Gage # | Raw CSS - microstrains | | | | | |
|---|---|---|---|---|---|---|
| | Release | 1-Day | 2-Day | 3-Day | 7-Day | 14-Day |
| 1 | 381 | 618 | 705 | 705 | 930 | 955 |
| 2 | 312 | 599 | 661 | 661 | 811 | 874 |
| 3 | 343 | 580 | 580 | 605 | 855 | 892 |
| 4 | 462 | 487 | 549 | 574 | 874 | 824 |
| 5 | 357 | 532 | 607 | 644 | 832 | 882 |
| 6 | 368 | 630 | 667 | 692 | 867 | 904 |
| 7 | 383 | 458 | 558 | 608 | 822 | 834 |
| 8 | 301 | 690 | 652 | 527 | 928 | 941 |
| 9 | 478 | 578 | 692 | 754 | 918 | 993 |
| 10 | 126 | 604 | 579 | 717 | 805 | 918 |
| 11 | 343 | 618 | 705 | 705 | 1005 | 1217 |
| 12 | 381 | 644 | 744 | 656 | 982 | 1032 |
| 13 | 392 | 702 | 802 | 1001 | 963 | 1001 |
| 14 | 137 | 337 | 411 | 349 | 623 | 773 |
| 15 | 300 | 512 | 612 | 587 | 849 | 887 |
| 16 | 50 | 237 | 200 | 225 | 437 | 575 |
| 17 | 150 | 287 | 400 | 412 | 562 | 612 |
| 18 | 181 | 355 | 418 | 430 | 530 | 630 |
| 19 | 62 | 312 | 374 | 361 | 374 | 399 |
| 20 | 106 | 44 | 181 | 156 | 243 | 243 |

450

Table H.6  Raw Concrete Surface Strain Data for Girder G1B-South

| East Gage # | Raw CSS - microstrains | | | | | |
|---|---|---|---|---|---|---|
| | Release | 1-Day | 2-Day | 3-Day | 7-Day | 14-Day |
| 1 | 553 | 452 | 515 | 917 | 666 | 766 |
| 2 | 723 | 911 | 999 | 987 | 1163 | 1213 |
| 3 | 545 | 859 | 946 | 972 | 1072 | 1034 |
| 4 | 490 | 842 | 968 | 930 | 1069 | 1081 |
| 5 | 661 | 837 | 1039 | 1089 | 1177 | 1328 |
| 6 | 763 | 1078 | 1216 | 1166 | 1191 | 1254 |
| 7 | 391 | 858 | 1022 | 1073 | 1148 | 1249 |
| 8 | 581 | 961 | 1024 | 1011 | 1138 | 1188 |
| 9 | 541 | 906 | 1007 | 981 | 1095 | 1120 |
| 10 | 490 | 653 | 741 | 402 | 502 | 578 |
| 11 | 509 | 760 | 860 | 747 | 835 | 873 |
| 12 | 383 | 483 | 508 | 445 | 571 | 596 |
| 13 | 408 | 633 | 872 | 784 | 922 | 959 |
| 14 | 519 | 795 | 895 | 857 | 995 | 958 |
| 15 | 507 | 569 | 682 | 607 | 594 | 532 |
| 16 | 274 | 449 | 6043 | 473 | 473 | 473 |
| 17 | 193 | 442 | 492 | 417 | 542 | 529 |
| 18 | 361 | 274 | 460 | 361 | 448 | 410 |
| 19 | 56 | 43 | 155 | 192 | 354 | 329 |
| 20 | 346 | 136 | 333 | 197 | 148 | 309 |

| West Gage # | Raw CSS - microstrains | | | | | |
|---|---|---|---|---|---|---|
| | Release | 1-Day | 2-Day | 3-Day | 7-Day | 14-Day |
| 1 | 38 | 163 | 250 | 225 | 463 | 338 |
| 2 | 13 | 138 | 413 | 188 | 263 | 238 |
| 3 | 131 | 344 | 319 | 294 | 406 | 344 |
| 4 | 287 | 449 | 424 | 499 | 687 | 612 |
| 5 | 281 | 582 | 544 | 544 | 582 | 544 |
| 6 | 263 | 501 | 538 | 538 | 714 | 601 |
| 7 | 457 | 820 | 832 | 870 | 958 | 882 |
| 8 | 532 | 857 | 882 | 920 | 970 | 970 |
| 9 | 476 | 839 | 889 | 1001 | 1026 | 1014 |
| 10 | 394 | 732 | 757 | 732 | 844 | 807 |
| 11 | 470 | 846 | 871 | 883 | 984 | 1009 |
| 12 | 389 | 703 | 741 | 766 | 879 | 879 |
| 13 | 439 | 777 | 827 | 802 | 927 | 902 |
| 14 | 726 | 801 | 852 | 826 | 952 | 889 |
| 15 | 451 | 889 | 977 | 1002 | 1140 | 1140 |
| 16 | 450 | 775 | 813 | 813 | 938 | 888 |
| 17 | 558 | 846 | 947 | 909 | 1085 | 1147 |
| 18 | 666 | 1005 | 1419 | 1608 | 1633 | 1620 |
| 19 | 438 | 676 | 714 | 726 | 827 | 827 |
| 20 | 495 | 746 | 821 | 821 | 1272 | 1147 |

## H.3 Girder G1C

### Table H.7 G1C Girder Data

| Girder # | | G1C | Raw Data for Transfer and Development Length | | | | |
|---|---|---|---|---|---|---|---|
| Reading # | Date (m/dd/yy) | Time (24 hr) | Midspan Deflection (inches) | Ambient Temp (Deg F) | Internal Temp (Deg F) | VWSG Data | |
| | | | | | | Hz | WG |
| Initial 1 | 7/18/01 | 12:10 | 2.031 | 85.0 | 117.4 | 902.66 | 1308 |
| Initial 2 | 7/18/01 | 12:10 | 2.031 | 85.0 | 117.4 | 902.66 | 1308 |
| Release | 7/18/01 | 15:15 | 2.453 | 87.8 | 108.5 | 799.65 | 1387 |
| 1-Day | 7/19/01 | 7:08 | 2.469 | 74.2 | 84.6 | 791.59 | 2407 |
| 2-Day | 7/20/01 | 6:53 | 2.484 | 73.6 | 83.5 | 784.09 | 2514 |
| 3-Day | 7/21/01 | 6:50 | 2.500 | 72.5 | 79.0 | 780.30 | 2829 |
| 7-Day | 7/25/01 | 7:10 | 2.531 | 73.8 | 78.7 | 762.00 | 2868 |
| 14-Day | 8/1/01 | 6:30 | 2.555 | 72.0 | 78.1 | 749.82 | 2863 |

| Strand Jacking Data from Load Cells and Tensioning Machine | | | | | | |
|---|---|---|---|---|---|---|
| | Load Cell Readings | | Tension Machine Readings | | Date and Time Of | Ambient Temp |
| Load Cell (Strand) # | At Time of Stressing (με) | Prior To Release (με) | Strand Jacking Force (lbs) | Strand Elongation (inches) | Tensioning (m/dd/yy) (24 hr) | (Deg F) |
| 1 | 5163 | 4989 | 45000 | 9.875 | | |
| 2 | 5218 | 5023 | 45500 | 9.750 | | |
| 3 | 5640 | 5387 | 46000 | 9.750 | | |
| 4 | 5549 | 5406 | 46000 | 9.875 | | |
| 5 | 5484 | 5279 | 46000 | 9.875 | 17 Jul 01 9:40 | 75 |
| 6 | 5456 | 5309 | 46000 | 9.875 | | |
| 7 | 5126 | 5000 | 45000 | 10.000 | | |
| 8 | 5115 | 4970 | 45000 | 10.000 | | |
| 9 | 5489 | 5387 | 46000 | 9.750 | | |
| 10 | 5601 | 5443 | 46000 | 9.750 | | |

452

Table H.8  Raw Concrete Surface Strain Data for Girder G1C-North

| East | Raw CSS - microstrains | | | | | |
|------|---------|-------|-------|-------|-------|--------|
| Gage # | Release | 1-Day | 2-Day | 3-Day | 7-Day | 14-Day |
| 1 | 106 | 293 | 356 | 356 | 468 | 356 |
| 2 | 150 | 313 | 363 | 313 | 475 | 400 |
| 3 | 150 | 313 | 539 | 564 | 614 | 451 |
| 4 | 338 | 639 | 614 | 564 | 614 | 451 |
| 5 | 300 | 437 | 475 | 512 | 587 | 537 |
| 6 | 286 | 422 | 559 | 559 | 633 | 546 |
| 7 | 428 | 614 | 676 | 700 | 762 | 713 |
| 8 | 317 | 615 | 528 | 739 | 752 | 627 |
| 9 | 510 | 710 | 784 | 809 | 921 | 896 |
| 10 | 481 | 818 | 893 | 818 | 1006 | 868 |
| 11 | 531 | 719 | 769 | 732 | 857 | 844 |
| 12 | 580 | 928 | 966 | 991 | 1103 | 1078 |
| 13 | 600 | 813 | 963 | 926 | 1063 | 1076 |
| 14 | 730 | 1205 | 1117 | 1355 | 1330 | 993 |
| 15 | 651 | 914 | 1101 | 1164 | 1264 | 1289 |
| 16 | 546 | 797 | 922 | 922 | 1023 | 985 |
| 17 | 519 | 794 | 868 | 943 | 1031 | 1018 |
| 18 | 580 | 817 | 867 | 954 | 1041 | 967 |
| 19 | 454 | 852 | 1002 | 927 | 1052 | 1114 |
| 20 | 578 | 865 | 889 | 1026 | 1163 | 1026 |

| West | Raw CSS - microstrains | | | | | |
|------|---------|-------|-------|-------|-------|--------|
| Gage # | Release | 1-Day | 2-Day | 3-Day | 7-Day | 14-Day |
| 1 | 786 | 974 | 1099 | 1099 | 1236 | 1173 |
| 2 | 724 | 1135 | 1110 | 1073 | 1198 | 1173 |
| 3 | 655 | 829 | 929 | 1004 | 1079 | 942 |
| 4 | 668 | 930 | 1018 | 993 | 1105 | 1067 |
| 5 | 686 | 973 | 1036 | 1086 | 1135 | 998 |
| 6 | 643 | 743 | 855 | 880 | 1005 | 693 |
| 7 | 740 | 978 | 1028 | 1090 | 1203 | 1065 |
| 8 | 665 | 903 | 1016 | 1053 | 1204 | 1078 |
| 9 | 730 | 1007 | 1095 | 1321 | 1422 | 1271 |
| 10 | 1100 | 1175 | 1037 | 1062 | 1238 | 1024 |
| 11 | 550 | 824 | 862 | 887 | 999 | 787 |
| 12 | 612 | 849 | 899 | 924 | 998 | 948 |
| 13 | 560 | 734 | 809 | 784 | 971 | 884 |
| 14 | 486 | 660 | 698 | 748 | 847 | 735 |
| 15 | 331 | 356 | 556 | 794 | 794 | 494 |
| 16 | 312 | 425 | 700 | 737 | 612 | 425 |
| 17 | 387 | 599 | 624 | 611 | 749 | 586 |
| 18 | 237 | 499 | 499 | 586 | 736 | 611 |
| 19 | 305 | 716 | 492 | 729 | 891 | 654 |
| 20 | 100 | 324 | 312 | 362 | 436 | 150 |

453

## Table H.9  Raw Concrete Surface Strain Data for Girder G1C-South

| East Gage # | Raw CSS - microstrains | | | | | |
|---|---|---|---|---|---|---|
| | Release | 1-Day | 2-Day | 3-Day | 7-Day | 14-Day |
| 1 | 740 | 1394 | 1431 | 1505 | 1604 | 1604 |
| 2 | 758 | 1019 | 1069 | 1019 | 1143 | 1156 |
| 3 | 703 | 952 | 1052 | 1027 | 1151 | 1139 |
| 4 | 978 | 1203 | 1178 | 1253 | 1402 | 1340 |
| 5 | 729 | 978 | 1053 | 1015 | 1152 | 1152 |
| 6 | 674 | 887 | 936 | 974 | 1099 | 1199 |
| 7 | 694 | 906 | 981 | 969 | 1106 | 1119 |
| 8 | 758 | 908 | 1046 | 1034 | 1209 | 1184 |
| 9 | 972 | 1123 | 1248 | 1236 | 1248 | 1060 |
| 10 | 446 | 634 | 936 | 797 | 998 | 923 |
| 11 | 622 | 835 | 948 | 923 | 1061 | 1061 |
| 12 | 572 | 799 | 887 | 849 | 975 | 950 |
| 13 | 227 | 530 | 719 | 795 | 972 | 795 |
| 14 | 315 | 631 | 618 | 618 | 706 | 618 |
| 15 | 233 | 549 | 586 | 549 | 624 | 549 |
| 16 | 271 | 473 | 549 | 473 | 662 | 498 |
| 17 | 333 | 459 | 471 | 547 | 773 | 672 |
| 18 | 38 | 226 | 138 | 264 | 365 | 201 |
| 19 | 82 | 295 | 295 | 345 | 395 | 307 |
| 20 | 746 | 395 | 433 | 332 | 307 | 370 |

| West Gage # | Raw CSS - microstrains | | | | | |
|---|---|---|---|---|---|---|
| | Release | 1-Day | 2-Day | 3-Day | 7-Day | 14-Day |
| 1 | 415 | 579 | 566 | 528 | 642 | 566 |
| 2 | 526 | 652 | 727 | 727 | 752 | 702 |
| 3 | 376 | 514 | 514 | 514 | 639 | 451 |
| 4 | 512 | 662 | 712 | 737 | 725 | 775 |
| 5 | 374 | 437 | 511 | 549 | 686 | 574 |
| 6 | 631 | 844 | 731 | 856 | 756 | 956 |
| 7 | 569 | 794 | 831 | 744 | 806 | 831 |
| 8 | 644 | 844 | 907 | 844 | 1032 | 957 |
| 9 | 502 | 678 | 765 | 715 | 753 | 703 |
| 10 | 738 | 938 | 1026 | 988 | 1126 | 1063 |
| 11 | 688 | 951 | 1014 | 914 | 1089 | 951 |
| 12 | 972 | 1147 | 1273 | 1210 | 1273 | 1260 |
| 13 | 760 | 972 | 1072 | 885 | 1097 | 1084 |
| 14 | 1169 | 1307 | 1369 | 1357 | 1469 | 1482 |
| 15 | 607 | 495 | 708 | 695 | 770 | 695 |
| 16 | 832 | 932 | 1045 | 982 | 1133 | 1095 |
| 17 | 504 | 705 | 730 | 718 | 844 | 806 |
| 18 | 396 | 459 | 597 | 547 | 748 | 673 |
| 19 | 1065 | 1153 | 1228 | 1253 | 1453 | 1315 |
| 20 | 551 | 651 | 701 | 663 | 839 | 789 |

## H.4  Girder G2A

### Table H.10  G2A Girder Data

| Girder # | G2A | | Raw Data for Transfer and Development Length | | | | |
|---|---|---|---|---|---|---|---|
| Reading # | Date | Time | Midspan Deflection (inches) | Ambient Temp (Deg F) | Internal Temp (Deg F) | VWSG Data | |
| | (m/dd/yy) | (24 hr) | | | | Hz | WG |
| Initial 1 | 7/13/01 | 10:15 | 2.047 | 82.8 | 112.0 | 920.40 | 1377 |
| Initial 2 | 7/13/01 | 10:15 | 2.047 | 82.8 | 112.0 | 920.40 | 1377 |
| Release | 7/13/01 | 15:30 | 2.359 | 98.8 | 106.4 | 846.40 | 1410 |
| 1-Day | 7/14/01 | 7:25 | 2.313 | 73.6 | 81.0 | 844.75 | 2771 |
| 2-Day | | | | | | | |
| 3-Day | 7/16/01 | 6:40 | 2.320 | 75.3 | 80.5 | 843.64 | 2813 |
| 7-Day | 7/20/01 | 7:55 | 2.344 | 74.2 | 82.3 | 838.23 | 2556 |
| 14-Day | 7/27/01 | 6:55 | 2.344 | 73.1 | 78.7 | 839.09 | 2759 |

| Strand Jacking Data from Load Cells and Tensioning Machine | | | | | | |
|---|---|---|---|---|---|---|
| | Load Cell Readings | | Tension Machine Readings | | Date and Time Of | Ambient Temp |
| Load Cell (Strand) # | At Time of Stressing (με) | Prior To Release (με) | Strand Jacking Force (lbs) | Strand Elongation (inches) | Tensioning (m/dd/yy) (24 hr) | (Deg F) |
| 1 | 6013 | 6140 | 45000 | 10.500 | | |
| 2 | 5107 | 5310 | 45500 | 9.875 | | |
| 3 | 5193 | 5351 | 45500 | 10.000 | | |
| 4 | 4742 | 4891 | 45000 | 10.000 | | |
| 5 | 5516 | 5727 | 45000 | 9.750 | 12 Jul 01 11:30 | 95 |
| 6 | 5432 | 5572 | 45000 | 9.750 | | |
| 7 | 5296 | 5426 | 45000 | 9.875 | | |
| 8 | 5452 | 5612 | 45000 | 10.000 | | |
| 9 | 5587 | 5781 | 45500 | 10.500 | | |
| 10 | 5824 | 6011 | 45500 | 10.375 | | |

455

Table H.11  Raw Concrete Surface Strain Data for Girder G2A-North

| East | Raw CSS - microstrains | | | | | |
|------|---------|-------|-------|-------|-------|--------|
| Gage # | Release | 1-Day | 2-Day | 3-Day | 7-Day | 14-Day |
| 1 | 205 | 441 | | 541 | 553 | 665 |
| 2 | 479 | 653 | | 727 | 653 | 715 |
| 3 | 318 | 518 | | 555 | 568 | 555 |
| 4 | 375 | 525 | | 338 | 350 | 300 |
| 5 | 351 | 627 | | 715 | 690 | 777 |
| 6 | 437 | 687 | | 825 | 837 | 862 |
| 7 | 200 | 474 | | 723 | 624 | 723 |
| 8 | 718 | 1343 | | 1318 | 1381 | 1531 |
| 9 | 281 | 505 | | 455 | 318 | 405 |
| 10 | 582 | 819 | | 894 | 894 | 1044 |
| 11 | 800 | 963 | | 1038 | 1026 | 1213 |
| 12 | 454 | 728 | | 778 | 703 | 790 |
| 13 | 584 | 733 | | 819 | 844 | 1018 |
| 14 | 452 | 614 | | 564 | 490 | 614 |
| 15 | 459 | 645 | | 632 | 620 | 694 |
| 16 | 487 | 761 | | 936 | 923 | 1023 |
| 17 | 795 | 1095 | | 1158 | 1158 | 1233 |
| 18 | 494 | 782 | | 857 | 845 | 945 |
| 19 | 375 | 663 | | 726 | 726 | 763 |
| 20 | 399 | 624 | | 611 | 636 | 711 |

| West | Raw CSS - microstrains | | | | | |
|------|---------|-------|-------|-------|-------|--------|
| Gage # | Release | 1-Day | 2-Day | 3-Day | 7-Day | 14-Day |
| 1 | 474 | 924 | | 1048 | 1036 | 1136 |
| 2 | 443 | 855 | | 855 | 818 | 905 |
| 3 | 462 | 774 | | 761 | 774 | 848 |
| 4 | 543 | 668 | | 705 | 705 | 880 |
| 5 | 606 | 831 | | 918 | 931 | 981 |
| 6 | 537 | 800 | | 837 | 812 | 887 |
| 7 | 332 | 759 | | 759 | 796 | 846 |
| 8 | 407 | 658 | | 720 | 670 | 733 |
| 9 | 521 | 823 | | 923 | 898 | 973 |
| 10 | 308 | 659 | | 709 | 684 | 785 |
| 11 | 1456 | 1244 | | 1156 | 1206 | 1131 |
| 12 | 719 | 906 | | 969 | 981 | 1069 |
| 13 | 467 | 790 | | 828 | 815 | 877 |
| 14 | 518 | 767 | | 817 | 829 | 904 |
| 15 | 431 | 843 | | 905 | 918 | 1005 |
| 16 | 319 | 644 | | 706 | 656 | 706 |
| 17 | 331 | 543 | | 543 | 531 | 581 |
| 18 | 268 | 455 | | 480 | 443 | 493 |
| 19 | 318 | 567 | | 505 | 517 | 630 |
| 20 | 380 | 355 | | 430 | 380 | 442 |

Table H.12 Raw Concrete Surface Strain Data for Girder G2A-South

| East Gage # | Raw CSS - microstrains | | | | | |
|---|---|---|---|---|---|---|
| | Release | 1-Day | 2-Day | 3-Day | 7-Day | 14-Day |
| 1 | 339 | 740 | | 916 | 991 | 891 |
| 2 | 232 | 508 | | 1022 | 1060 | 822 |
| 3 | 207 | 570 | | 695 | 833 | 620 |
| 4 | 577 | 1080 | | 1230 | 716 | 1193 |
| 5 | 283 | 674 | | 674 | 1177 | 699 |
| 6 | 359 | 801 | | 901 | 990 | 788 |
| 7 | 411 | 790 | | 853 | 878 | 828 |
| 8 | 398 | 727 | | 968 | 1081 | 1006 |
| 9 | 283 | 586 | | 674 | 774 | 724 |
| 10 | 246 | 497 | | 573 | 636 | 548 |
| 11 | 333 | 696 | | 797 | 885 | 809 |
| 12 | 376 | 714 | | 840 | 1015 | 902 |
| 13 | 332 | 1210 | | 1310 | 1285 | 1298 |
| 14 | 262 | 600 | | 762 | 825 | 787 |
| 15 | 188 | 551 | | 576 | 639 | 651 |
| 16 | 230 | 479 | | 529 | 542 | 616 |
| 17 | 118 | 629 | | 753 | 716 | 790 |
| 18 | 56 | 292 | | 367 | 379 | 317 |
| 19 | 6 | 217 | | 254 | 378 | 353 |
| 20 | 49 | 234 | | 296 | 308 | 247 |

| West Gage # | Raw CSS - microstrains | | | | | |
|---|---|---|---|---|---|---|
| | Release | 1-Day | 2-Day | 3-Day | 7-Day | 14-Day |
| 1 | 100 | 150 | | 363 | 163 | 138 |
| 2 | 213 | 413 | | 575 | 638 | 651 |
| 3 | 0 | 13 | | 225 | 213 | 325 |
| 4 | 237 | 449 | | 537 | 424 | 337 |
| 5 | 200 | 475 | | 650 | 700 | 587 |
| 6 | 382 | 733 | | 858 | 870 | 1008 |
| 7 | 288 | 738 | | 926 | 1026 | 1013 |
| 8 | 351 | 438 | | 576 | 739 | 613 |
| 9 | 395 | 758 | | 1022 | 1084 | 1034 |
| 10 | 332 | 607 | | 882 | 920 | 807 |
| 11 | 201 | 590 | | 728 | 803 | 728 |
| 12 | 263 | 564 | | 715 | 727 | 589 |
| 13 | 282 | 582 | | 595 | 708 | 595 |
| 14 | 300 | 526 | | 663 | 638 | 538 |
| 15 | 219 | 443 | | 606 | 618 | 518 |
| 16 | 225 | 514 | | 651 | 702 | 601 |
| 17 | 207 | 470 | | 582 | 595 | 507 |
| 18 | 232 | 496 | | 672 | 722 | 621 |
| 19 | 188 | 464 | | 539 | 539 | 501 |
| 20 | 257 | 495 | | 633 | 633 | 558 |

## H.5  Girder G2B

Table H.13  G2B Girder Data

| Girder # | | G2B | Raw Data for Transfer and Development Length | | | | |
|---|---|---|---|---|---|---|---|
| Reading # | Date (m/dd/yy) | Time (24 hr) | Midspan Deflection (inches) | Ambient Temp (Deg F) | Internal Temp (Deg F) | VWSG Data | |
| | | | | | | Hz | WG |
| Initial 1 | 7/13/01 | 10:50 | 1.875 | 82.8 | 112.0 | 900.40 | 1363 |
| Initial 2 | 7/13/01 | 10:50 | 1.875 | 82.8 | 112.0 | 900.40 | 1363 |
| Release | 7/13/01 | 15:50 | 2.172 | 98.8 | 107.1 | 826.40 | 1396 |
| 1-Day | 7/14/01 | 7:46 | 2.094 | 73.6 | 82.6 | 823.30 | 2653 |
| 2-Day | | | | | | | |
| 3-Day | 7/16/01 | 6:40 | 2.117 | 75.8 | 80.6 | 822.40 | 2789 |
| 7-Day | 7/20/01 | 7:57 | 2.148 | 75.4 | 81.5 | 818.38 | 2614 |
| 14-Day | 7/27/01 | 7:02 | 2.164 | 73.1 | 78.5 | 817.30 | 2797 |

| Strand Jacking Data from Load Cells and Tensioning Machine | | | | | | |
|---|---|---|---|---|---|---|
| | Load Cell Readings | | Tension Machine Readings | | Date and Time Of Tensioning | Ambient Temp |
| Load Cell (Strand) # | At Time of Stressing ($\mu\varepsilon$) | Prior To Release ($\mu\varepsilon$) | Strand Jacking Force (lbs) | Strand Elongation (inches) | (m/dd/yy) (24 hr) | (Deg F) |
| 1 | 6013 | 6140 | 45000 | 10.500 | | |
| 2 | 5107 | 5310 | 45500 | 9.875 | | |
| 3 | 5193 | 5351 | 45500 | 10.000 | | |
| 4 | 4742 | 4891 | 45000 | 10.000 | | |
| 5 | 5516 | 5727 | 45000 | 9.750 | 12 Jul 01 11:30 | 95 |
| 6 | 5432 | 5572 | 45000 | 9.750 | | |
| 7 | 5296 | 5426 | 45000 | 9.875 | | |
| 8 | 5452 | 5612 | 45000 | 10.000 | | |
| 9 | 5587 | 5781 | 45500 | 10.500 | | |
| 10 | 5824 | 6011 | 45500 | 10.375 | | |

Table H.14 Raw Concrete Surface Strain Data for Girder G2B-North

| East Gage # | Raw CSS - microstrains | | | | | |
|---|---|---|---|---|---|---|
| | Release | 1-Day | 2-Day | 3-Day | 7-Day | 14-Day |
| 1 | 269 | 282 | | 394 | 232 | 407 |
| 2 | 218 | 368 | | 456 | 418 | 493 |
| 3 | 188 | 538 | | 613 | 575 | 588 |
| 4 | 362 | 562 | | 487 | 512 | 562 |
| 5 | 306 | 643 | | 718 | 718 | 755 |
| 6 | 307 | 846 | | 896 | 896 | 921 |
| 7 | 357 | 745 | | 833 | 858 | 870 |
| 8 | 482 | 670 | | 745 | 732 | 845 |
| 9 | 426 | 764 | | 751 | 802 | 802 |
| 10 | 387 | 562 | | 624 | 761 | 699 |
| 11 | 443 | 643 | | 717 | 680 | 705 |
| 12 | 412 | 750 | | 775 | 800 | 787 |
| 13 | 425 | 575 | | 675 | 712 | 725 |
| 14 | 526 | 751 | | 776 | 801 | 801 |
| 15 | 495 | 608 | | 758 | 821 | 808 |
| 16 | 387 | 600 | | 637 | 687 | 675 |
| 17 | 431 | 731 | | 831 | 881 | 881 |
| 18 | 443 | 693 | | 768 | 793 | 793 |
| 19 | 411 | 648 | | 686 | 711 | 711 |
| 20 | 469 | 770 | | 895 | 907 | 995 |

| West Gage # | Raw CSS - microstrains | | | | | |
|---|---|---|---|---|---|---|
| | Release | 1-Day | 2-Day | 3-Day | 7-Day | 14-Day |
| 1 | 577 | 903 | | 916 | 903 | 966 |
| 2 | 469 | 932 | | 770 | 745 | 982 |
| 3 | 294 | 620 | | 632 | 620 | 645 |
| 4 | 269 | 694 | | 756 | 794 | 781 |
| 5 | 432 | 807 | | 969 | 982 | 1007 |
| 6 | 345 | 697 | | 860 | 848 | 948 |
| 7 | 470 | 808 | | 871 | 908 | 996 |
| 8 | 414 | 927 | | 815 | 1053 | 1028 |
| 9 | 426 | 751 | | 751 | 751 | 776 |
| 10 | 156 | 730 | | 630 | 755 | 780 |
| 11 | 457 | 909 | | 909 | 1021 | 1084 |
| 12 | 457 | 733 | | 771 | 821 | 796 |
| 13 | 464 | 639 | | 765 | 790 | 740 |
| 14 | 370 | 683 | | 770 | 846 | 921 |
| 15 | 337 | 511 | | 499 | 598 | 548 |
| 16 | 31 | 570 | | 570 | 608 | 608 |
| 17 | 131 | 407 | | 457 | 469 | 544 |
| 18 | 150 | 250 | | 462 | 575 | 837 |
| 19 | 125 | 501 | | 551 | 614 | 614 |
| 20 | 137 | 436 | | 535 | 510 | 660 |

459

Table H.15  Raw Concrete Surface Strain Data for Girder G2B-South

| East Gage # | Raw CSS - microstrains | | | | | |
|---|---|---|---|---|---|---|
| | Release | 1-Day | 2-Day | 3-Day | 7-Day | 14-Day |
| 1 | 486 | 786 | | 698 | 748 | 673 |
| 2 | 274 | 474 | | 548 | 524 | 548 |
| 3 | 306 | 656 | | 793 | 780 | 705 |
| 4 | 262 | 637 | | 749 | 861 | 811 |
| 5 | 212 | 623 | | 511 | 561 | 387 |
| 6 | 262 | 674 | | 712 | 762 | 737 |
| 7 | 424 | 523 | | 573 | 561 | 573 |
| 8 | 299 | 585 | | 623 | 685 | 623 |
| 9 | 243 | 841 | | 865 | 828 | 940 |
| 10 | 317 | 678 | | 703 | 753 | 753 |
| 11 | 311 | 646 | | 658 | 671 | 646 |
| 12 | 298 | 634 | | 621 | 845 | 659 |
| 13 | 261 | 573 | | 623 | 747 | 685 |
| 14 | 224 | 623 | | 623 | 760 | 660 |
| 15 | 244 | 582 | | 569 | 607 | 569 |
| 16 | 300 | 550 | | 625 | 737 | 687 |
| 17 | 641 | 928 | | 803 | 878 | 803 |
| 18 | 44 | 342 | | 330 | 280 | 243 |
| 19 | 25 | 375 | | 450 | 537 | 462 |
| 20 | 38 | 388 | | 401 | 489 | 401 |

| West Gage # | Raw CSS - microstrains | | | | | |
|---|---|---|---|---|---|---|
| | Release | 1-Day | 2-Day | 3-Day | 7-Day | 14-Day |
| 1 | 38 | 263 | | 389 | 363 | 38 |
| 2 | 131 | 281 | | 269 | 306 | 31 |
| 3 | 19 | 393 | | 455 | 417 | 368 |
| 4 | 243 | 1028 | | 1028 | 1003 | 941 |
| 5 | 187 | 674 | | 724 | 612 | 749 |
| 6 | 294 | 606 | | 606 | 556 | 444 |
| 7 | 163 | 539 | | 639 | 601 | 639 |
| 8 | 256 | 656 | | 631 | 618 | 568 |
| 9 | 376 | 689 | | 777 | 752 | 765 |
| 10 | 351 | 740 | | 715 | 690 | 652 |
| 11 | 219 | 621 | | 596 | 771 | 583 |
| 12 | 321 | 736 | | 736 | 799 | 723 |
| 13 | 256 | 569 | | 557 | 607 | 507 |
| 14 | 545 | 1108 | | 1146 | 1196 | 1171 |
| 15 | 237 | 587 | | 550 | 562 | 537 |
| 16 | 293 | 681 | | 730 | 743 | 730 |
| 17 | 305 | 417 | | 455 | 505 | 480 |
| 18 | 329 | 652 | | 615 | 665 | 652 |
| 19 | 292 | 728 | | 790 | 865 | 740 |
| 20 | 242 | 640 | | 677 | 776 | 665 |

460

## H.6 Girder G2C

### Table H.16 G2C Girder Data

| Girder # | G2C | | Raw Data for Transfer and Development Length | | | | |
|---|---|---|---|---|---|---|---|
| Reading # | Date (m/dd/yy) | Time (24 hr) | Midspan Deflection (inches) | Ambient Temp (Deg F) | Internal Temp (Deg F) | VWSG Data | |
| | | | | | | Hz | WG |
| Initial 1 | 7/18/01 | 12:40 | 2.047 | 85.0 | 125.5 | 913.36 | 1427 |
| Initial 2 | 7/18/01 | 12:40 | 2.047 | 85.0 | 125.5 | 913.36 | 1427 |
| Release | 7/18/01 | 15:00 | 2.469 | 87.8 | 108.9 | 827.12 | 1428 |
| 1-Day | 7/19/01 | 6:55 | 2.438 | 74.2 | 86.0 | 817.71 | 2353 |
| 2-Day | 7/20/01 | 6:55 | 2.469 | 73.6 | 84.6 | 814.71 | 2469 |
| 3-Day | 7/21/01 | 6:50 | 2.453 | 72.5 | 78.8 | 813.58 | 2807 |
| 7-Day | 7/25/01 | 7:10 | 2.469 | 73.8 | 78.0 | 806.60 | 2886 |
| 14-Day | 8/1/01 | 6:30 | 2.477 | 72.0 | 78.5 | 802.68 | 2850 |

| Strand Jacking Data from Load Cells and Tensioning Machine | | | | | | |
|---|---|---|---|---|---|---|
| | Load Cell Readings | | Tension Machine Readings | | Date and Time Of | Ambient Temp |
| Load Cell (Strand) # | At Time of Stressing ($\mu\varepsilon$) | Prior To Release ($\mu\varepsilon$) | Strand Jacking Force (lbs) | Strand Elongation (inches) | Tensioning (m/dd/yy) (24 hr) | (Deg F) |
| 1 | 5163 | 4989 | 45000 | 9.875 | | |
| 2 | 5218 | 5023 | 45500 | 9.750 | | |
| 3 | 5640 | 5387 | 46000 | 9.750 | | |
| 4 | 5549 | 5406 | 46000 | 9.875 | | |
| 5 | 5484 | 5279 | 46000 | 9.875 | 17 Jul 01 9:40 | 75 |
| 6 | 5456 | 5309 | 46000 | 9.875 | | |
| 7 | 5126 | 5000 | 45000 | 10.000 | | |
| 8 | 5115 | 4970 | 45000 | 10.000 | | |
| 9 | 5489 | 5387 | 46000 | 9.750 | | |
| 10 | 5601 | 5443 | 46000 | 9.750 | | |

461

Table H.17  Raw Concrete Surface Strain Data for Girder G2C-North

| East Gage # | Raw CSS - microstrains | | | | | |
|---|---|---|---|---|---|---|
| | Release | 1-Day | 2-Day | 3-Day | 7-Day | 14-Day |
| 1 | 100 | 251 | 276 | 238 | 226 | 138 |
| 2 | 200 | 437 | 499 | 537 | 562 | 387 |
| 3 | 44 | 469 | 582 | 506 | 619 | 256 |
| 4 | 281 | 505 | 443 | 568 | 555 | 418 |
| 5 | 431 | 668 | 743 | 781 | 756 | 643 |
| 6 | 445 | 632 | 632 | 658 | 670 | 582 |
| 7 | 494 | 1220 | 782 | 807 | 794 | 569 |
| 8 | 513 | 789 | 852 | 952 | 952 | 801 |
| 9 | 519 | 706 | 831 | 819 | 844 | 719 |
| 10 | 543 | 756 | 818 | 831 | 856 | 731 |
| 11 | 649 | 899 | 899 | 924 | 936 | 861 |
| 12 | 512 | 662 | 699 | 737 | 749 | 587 |
| 13 | 506 | 706 | 718 | 743 | 731 | 643 |
| 14 | 532 | 669 | 794 | 845 | 870 | 719 |
| 15 | 457 | 682 | 670 | 670 | 720 | 545 |
| 16 | 444 | 619 | 694 | 719 | 694 | 656 |
| 17 | 500 | 700 | 800 | 825 | 825 | 738 |
| 18 | 468 | 668 | 693 | 755 | 780 | 693 |
| 19 | 369 | 693 | 731 | 781 | 818 | 668 |
| 20 | 494 | 757 | 769 | 769 | 832 | 669 |

| West Gage # | Raw CSS - microstrains | | | | | |
|---|---|---|---|---|---|---|
| | Release | 1-Day | 2-Day | 3-Day | 7-Day | 14-Day |
| 1 | 370 | 633 | 684 | 633 | 734 | 408 |
| 2 | 395 | 595 | 620 | 570 | 570 | 369 |
| 3 | 307 | 632 | 657 | 670 | 695 | 532 |
| 4 | 444 | 607 | 732 | 657 | 657 | 444 |
| 5 | 445 | 670 | 746 | 758 | 758 | 696 |
| 6 | 433 | 659 | 671 | 671 | 696 | 533 |
| 7 | 419 | 620 | 532 | 532 | 557 | 394 |
| 8 | 463 | 776 | 739 | 638 | 689 | 488 |
| 9 | 469 | 681 | 669 | 656 | 694 | 569 |
| 10 | 604 | 779 | 779 | 804 | 804 | 629 |
| 11 | 539 | 765 | 802 | 840 | 903 | 752 |
| 12 | 771 | 846 | 771 | 796 | 921 | 407 |
| 13 | 558 | 758 | 796 | 896 | 846 | 683 |
| 14 | 388 | 551 | 589 | 639 | 664 | 501 |
| 15 | 386 | 586 | 536 | 549 | 573 | 474 |
| 16 | 113 | 138 | 476 | 513 | 476 | 13 |
| 17 | 338 | 489 | 439 | 489 | 464 | 188 |
| 18 | 344 | 494 | 469 | 507 | 507 | 382 |
| 19 | 169 | 332 | 419 | 382 | 394 | 194 |
| 20 | 93 | 429 | 728 | 641 | 740 | 292 |

Table H.18  Raw Concrete Surface Strain Data for Girder G2C-South

| East | Raw CSS - microstrains | | | | | |
|---|---|---|---|---|---|---|
| Gage # | Release | 1-Day | 2-Day | 3-Day | 7-Day | 14-Day |
| 1 | 673 | 798 | 760 | 873 | 873 | 661 |
| 2 | 573 | 773 | 835 | 860 | 823 | 723 |
| 3 | 687 | 850 | 887 | 925 | 962 | 875 |
| 4 | 506 | 681 | 730 | 743 | 768 | 693 |
| 5 | 531 | 731 | 881 | 918 | 1055 | 818 |
| 6 | 593 | 780 | 767 | 917 | 867 | 730 |
| 7 | 574 | 686 | 711 | 736 | 748 | 711 |
| 8 | 747 | 846 | 846 | 871 | 871 | 859 |
| 9 | 591 | 740 | 1014 | 765 | 765 | 728 |
| 10 | 629 | 803 | 828 | 853 | 903 | 928 |
| 11 | 547 | 671 | 759 | 846 | 821 | 746 |
| 12 | 640 | 776 | 751 | 963 | 925 | 813 |
| 13 | 560 | 734 | 784 | 871 | 883 | 833 |
| 14 | 137 | 200 | 462 | 499 | 524 | 424 |
| 15 | 512 | 624 | 787 | 799 | 961 | 861 |
| 16 | 269 | 331 | 469 | 569 | 669 | 506 |
| 17 | 112 | 224 | 312 | 474 | 424 | 436 |
| 18 | 137 | 261 | 485 | 386 | 435 | 249 |
| 19 | 0 | 163 | 250 | 288 | 275 | 288 |
| 20 | 44 | 169 | 282 | 357 | 407 | 294 |

| West | Raw CSS - microstrains | | | | | |
|---|---|---|---|---|---|---|
| Gage # | Release | 1-Day | 2-Day | 3-Day | 7-Day | 14-Day |
| 1 | 6 | 220 | 270 | 270 | 408 | 245 |
| 2 | 62 | 262 | 337 | 337 | 425 | 375 |
| 3 | 81 | 106 | 5254 | 243 | 280 | 168 |
| 4 | 144 | 406 | 431 | 369 | 494 | 469 |
| 5 | 368 | 455 | 543 | 555 | 618 | 580 |
| 6 | 357 | 482 | 545 | 545 | 632 | 482 |
| 7 | 350 | 475 | 538 | 551 | 638 | 576 |
| 8 | 462 | 612 | 649 | 674 | 749 | 699 |
| 9 | 376 | 476 | 527 | 564 | 664 | 501 |
| 10 | 514 | 577 | 665 | 614 | 677 | 702 |
| 11 | 508 | 571 | 709 | 684 | 709 | 696 |
| 12 | 887 | 510 | 787 | 1001 | 711 | 1001 |
| 13 | 719 | 669 | 706 | 706 | 844 | 832 |
| 14 | 550 | 676 | 738 | 776 | 813 | 713 |
| 15 | 550 | 512 | 662 | 675 | 762 | 675 |
| 16 | 462 | 75 | 562 | 662 | 699 | 412 |
| 17 | 405 | 467 | 604 | 617 | 692 | 480 |
| 18 | 447 | 423 | 534 | 559 | 646 | 534 |
| 19 | 559 | 622 | 584 | 647 | 709 | 572 |
| 20 | 379 | 553 | 553 | 602 | 714 | 577 |

# APPENDIX I

## SMOOTHED CONCRETE SURFACE STRAIN PROFILES AND DETERMINATION OF TRANSFER LENGTH

This Appendix contains smoothed CSS profiles for each girder end as well as

plots showing the determination of transfer length based on 14-day CSS data.

## I.1  Girder G1A-East
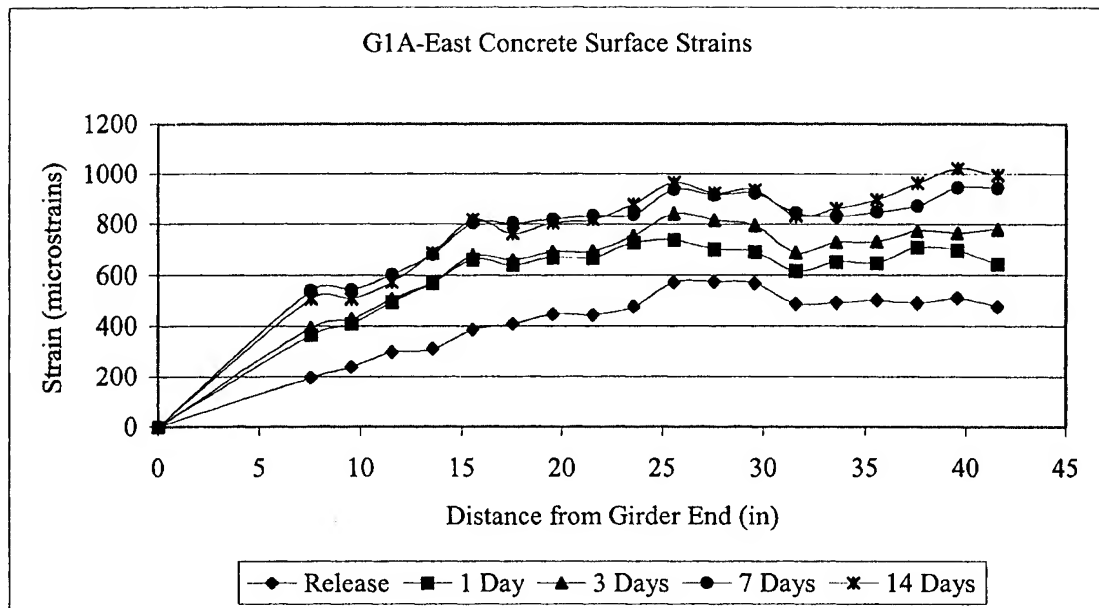


Figure I.1  Concrete Surface Strains for G1A-East
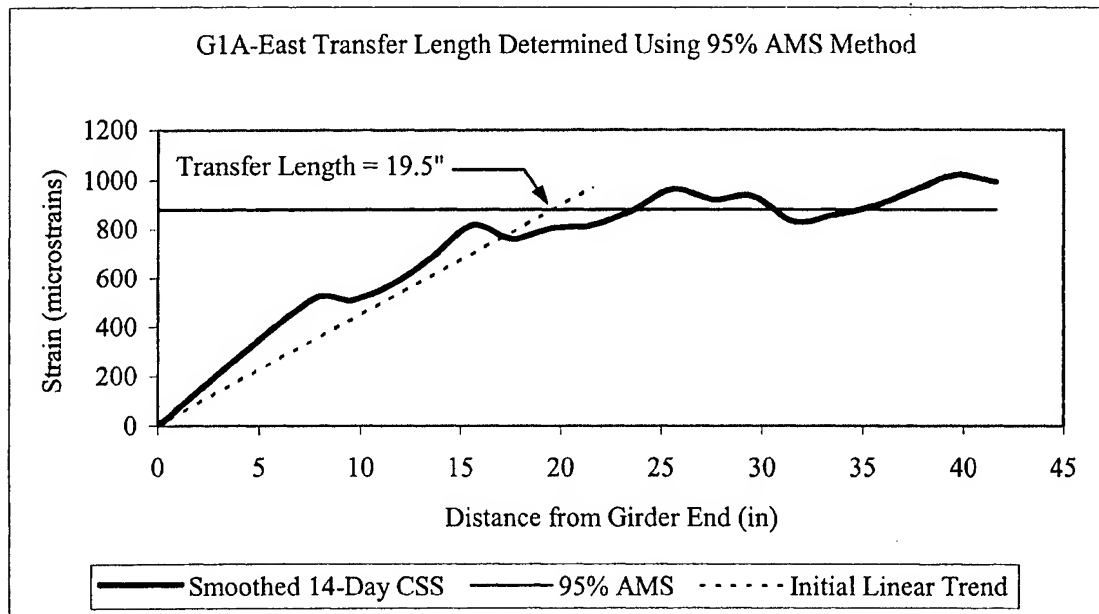


Figure I.2  14-Day Transfer Length Determined for G1A-East

465
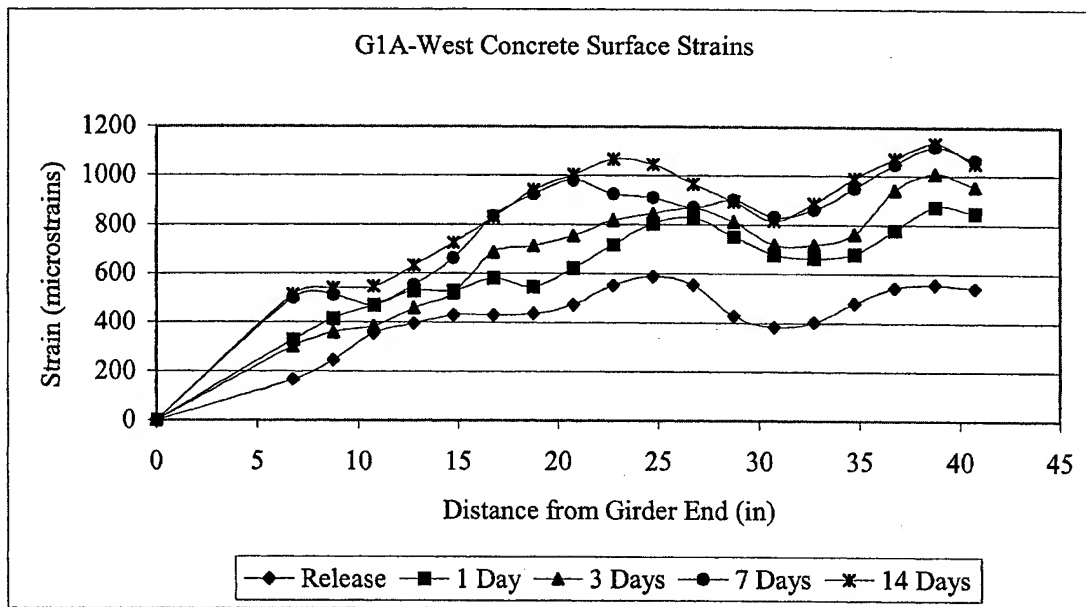
## I.2 Girder G1A-West



Figure I.3  Concrete Surface Strains for G1A-West
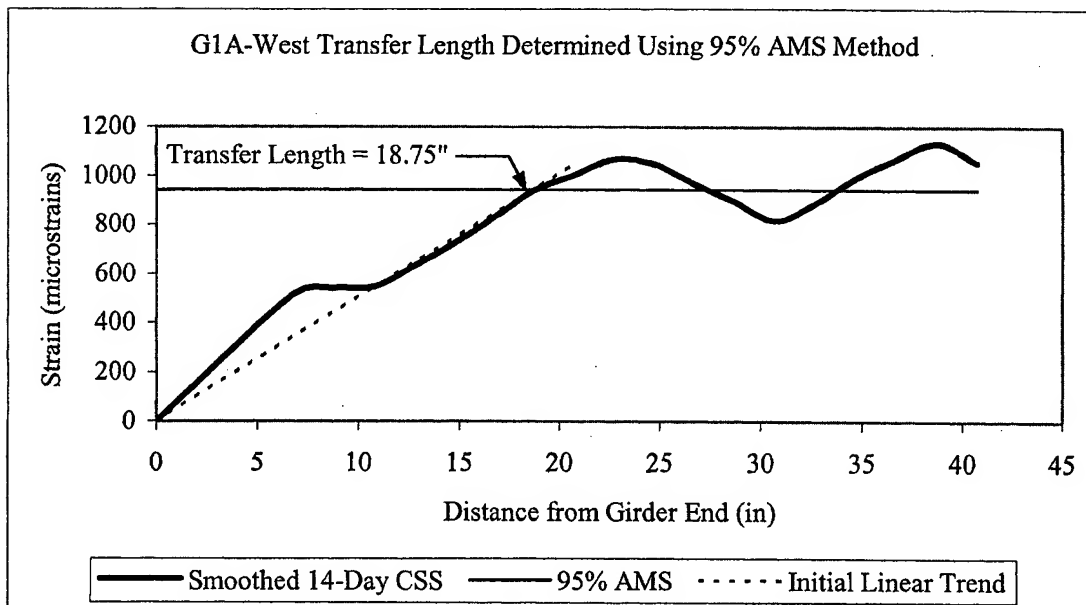


Figure I.4  14-Day Transfer Length Determined for G1A-West

466
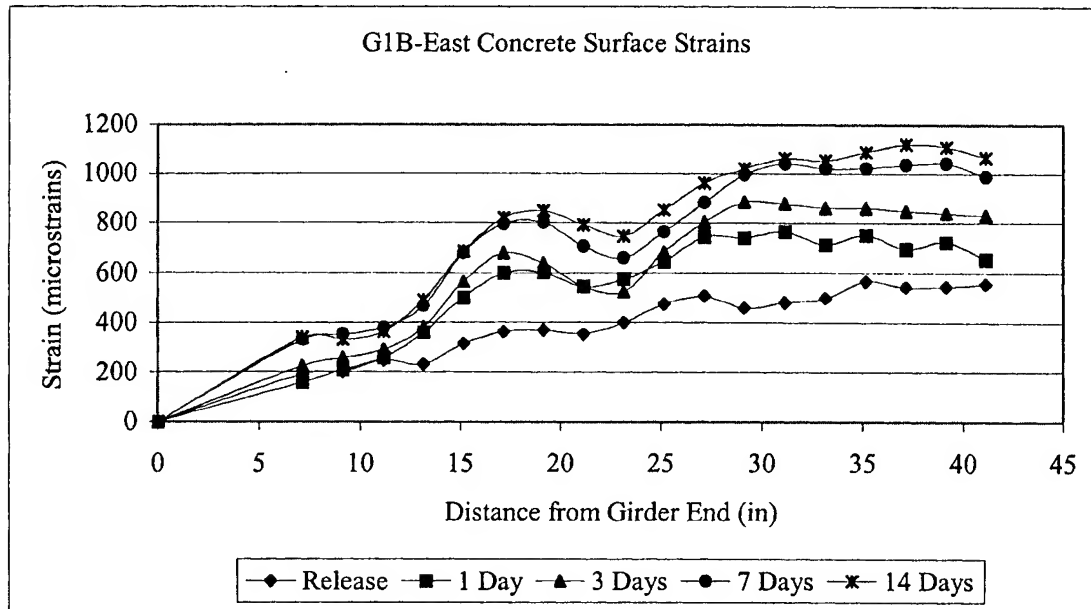
## I.3 Girder G1B-East



Figure I.5  Concrete Surface Strains for G1B-East
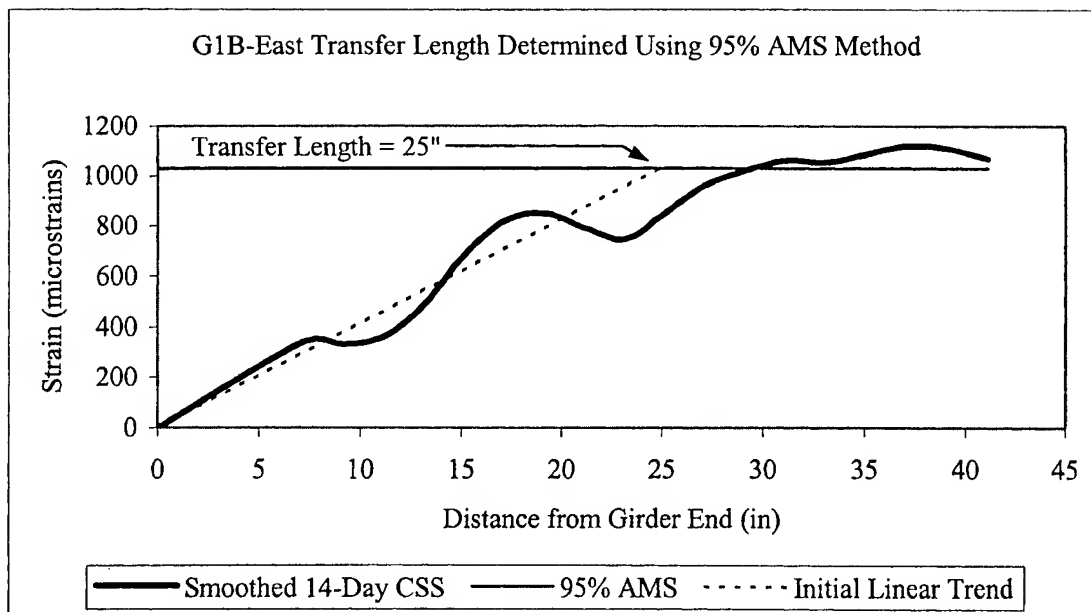


Figure I.6  14-Day Transfer Length Determined for G1B-East

467
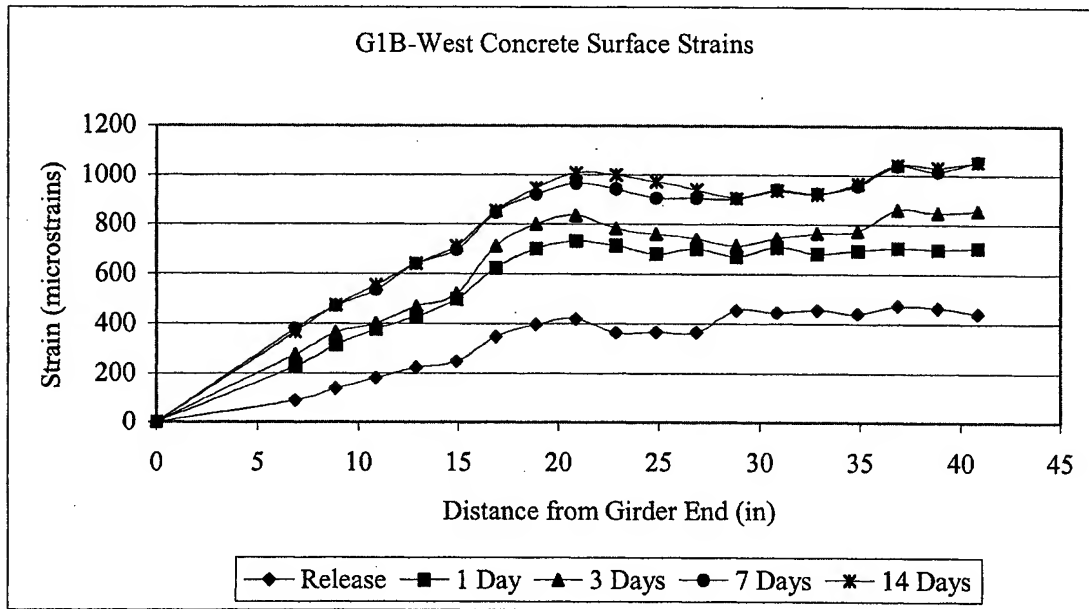
## I.4  Girder G1B-West



Figure I.7  Concrete Surface Strains for G1B-West
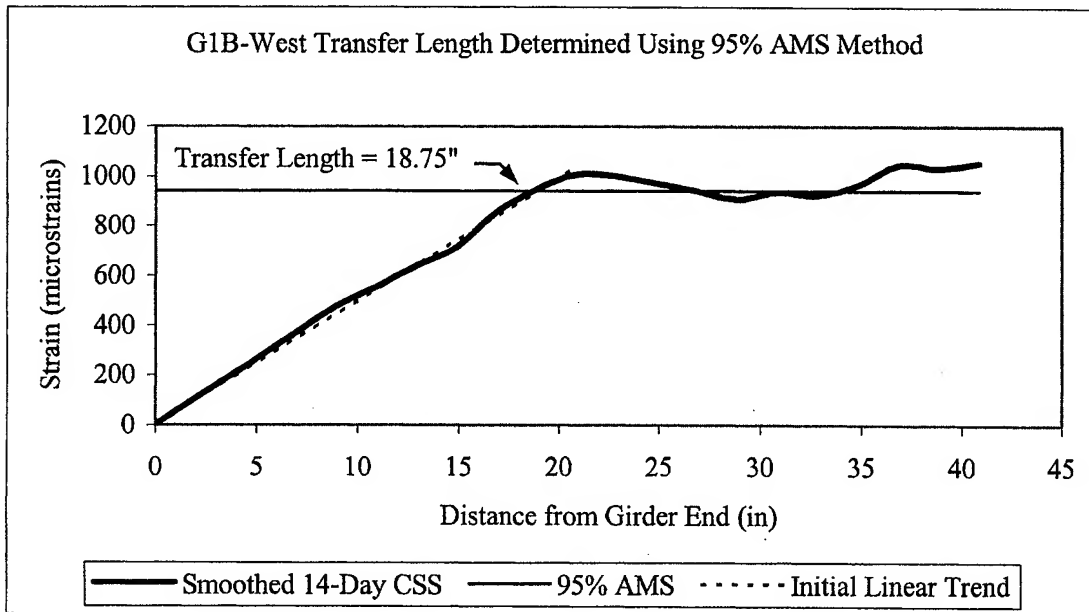


Figure I.8  14-Day Transfer Length Determined for G1B-West

## I.5 Girder G1C-East
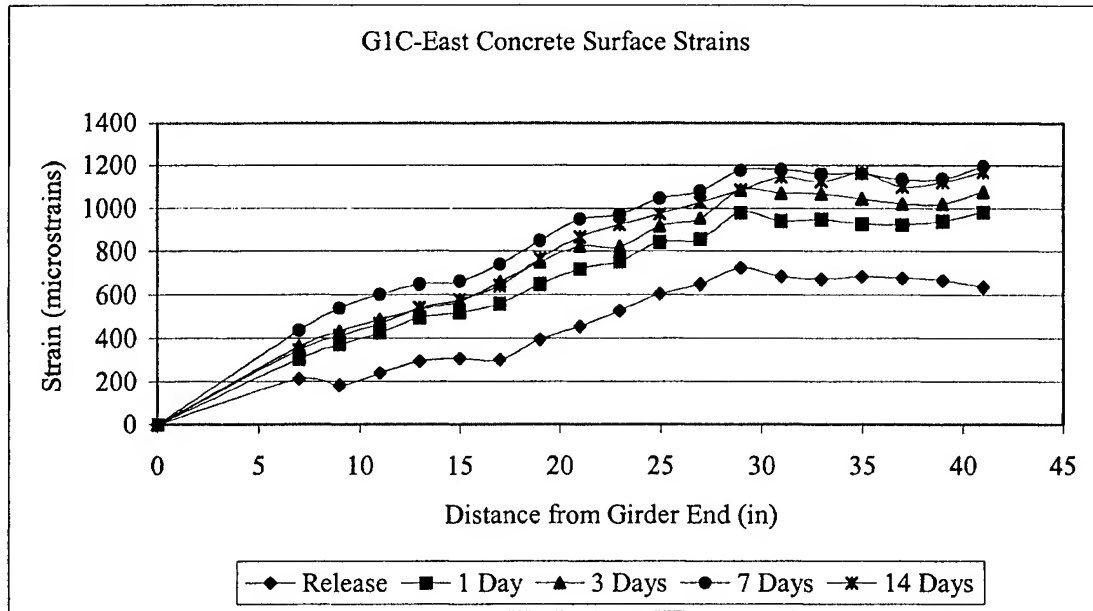


Figure I.9 Concrete Surface Strains for G1C-East
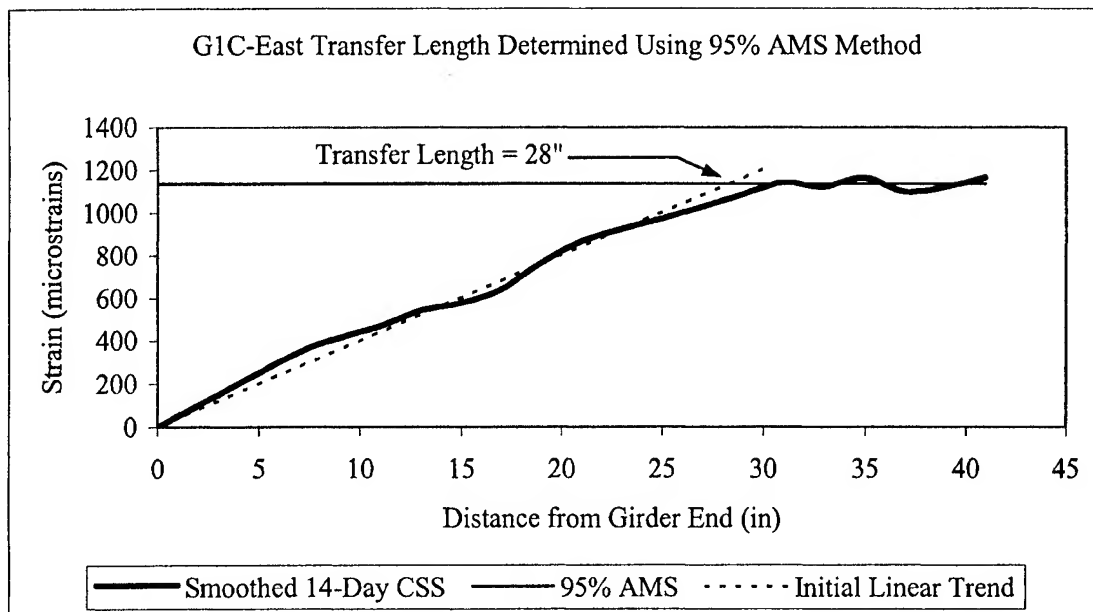


Figure I.10 14-Day Transfer Length Determined for G1C-East

469
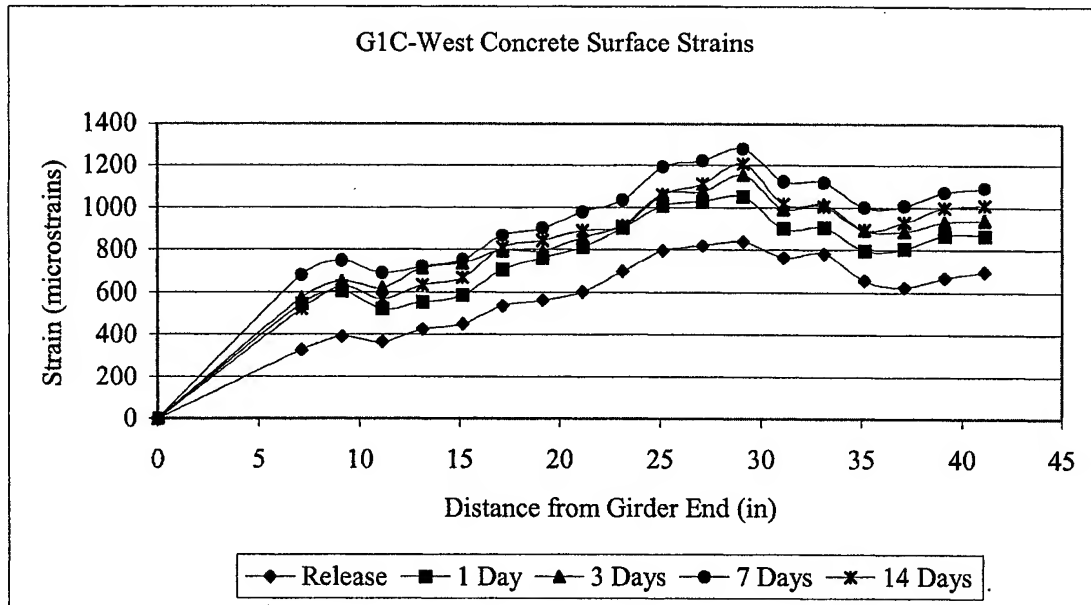
## I.6 Girder G1C-West



Figure I.11 Concrete Surface Strains for G1C-West
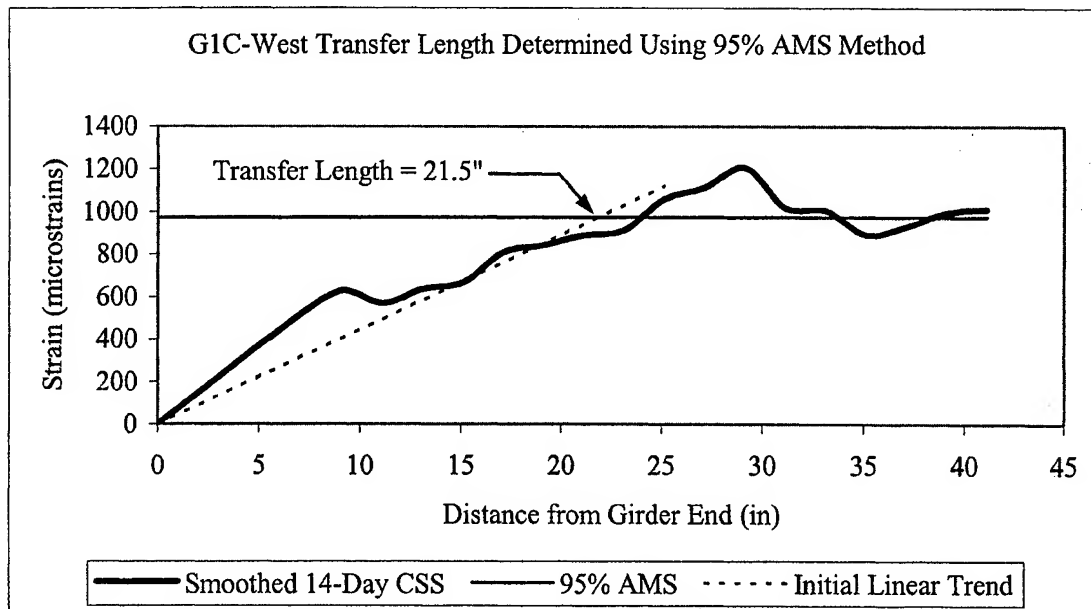


Figure I.12 14-Day Transfer Length Determined for G1C-West

470

## I.7  Girder G2A-East

**G2A-East Smoothed Concrete Surface Strains**
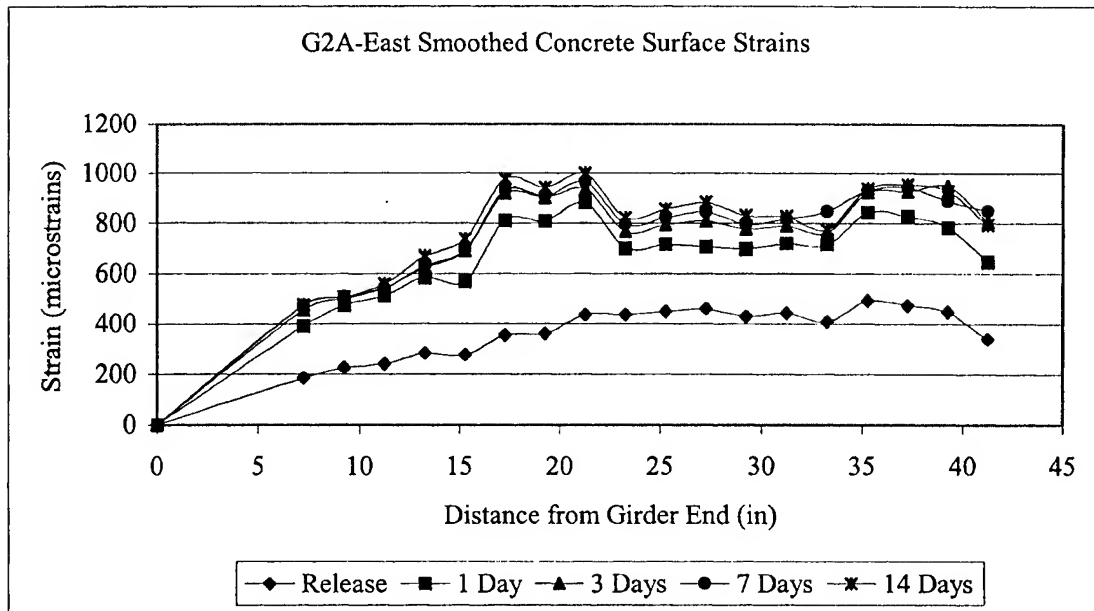


Figure I.13  Concrete Surface Strains for G2A-East

**G2A-East Transfer Length Determined Using 95% AMS Method**
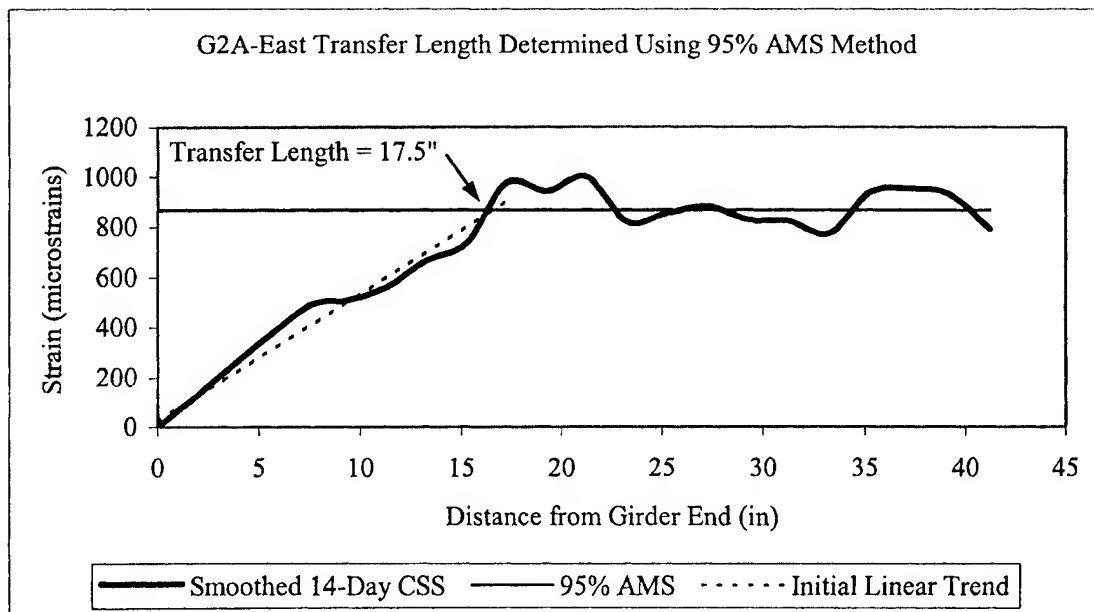


Figure I.14  14-Day Transfer Length Determined for G2A-East

## I.8 Girder G2A-West
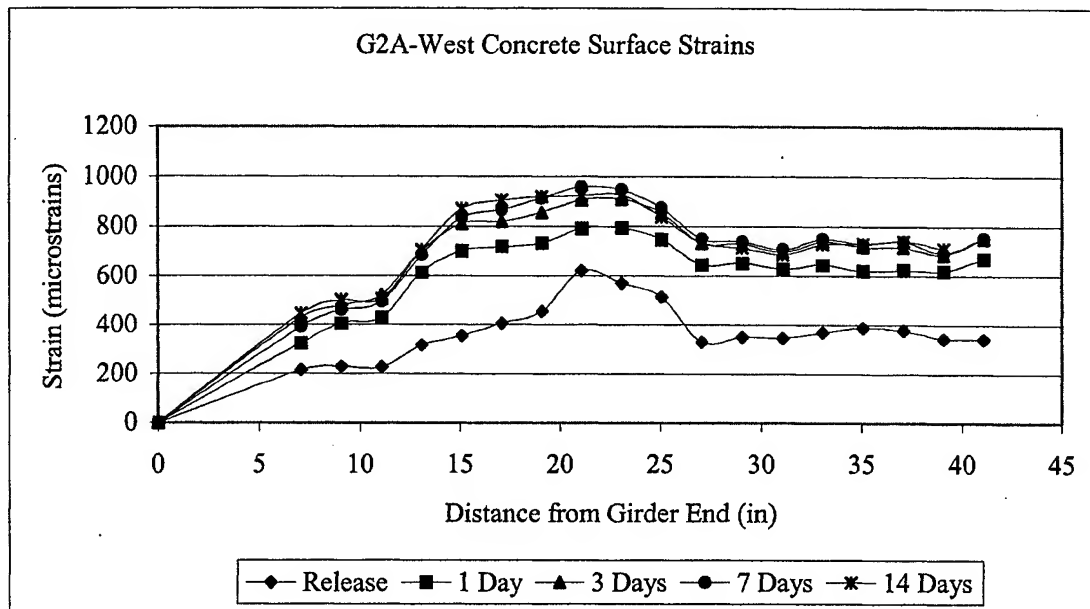


Figure I.15 Concrete Surface Strains for G2A-West
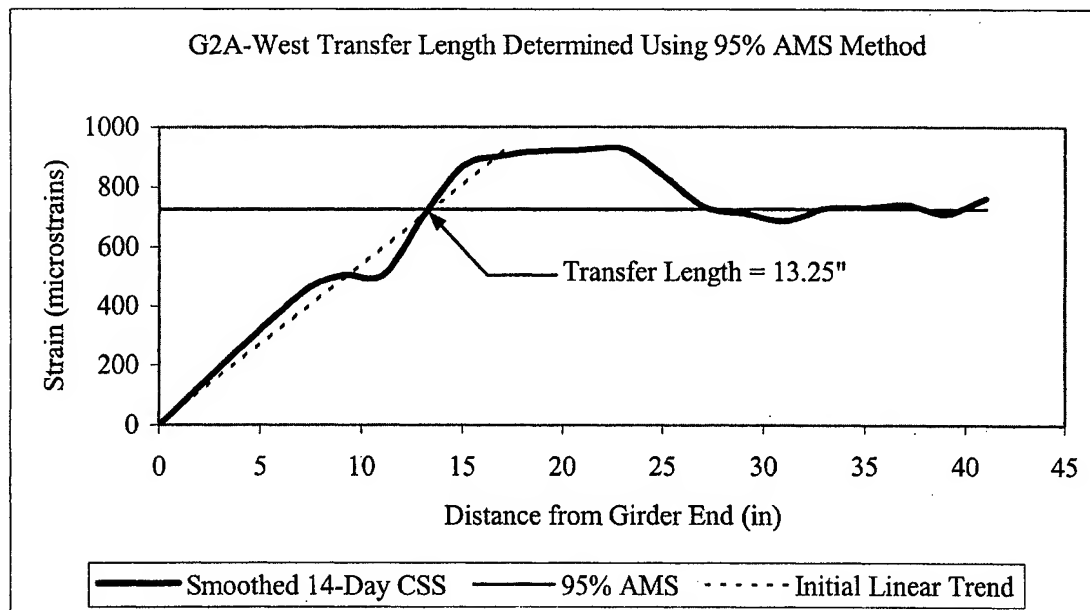


Figure I.16 14-Day Transfer Length Determined for G2A-West

472
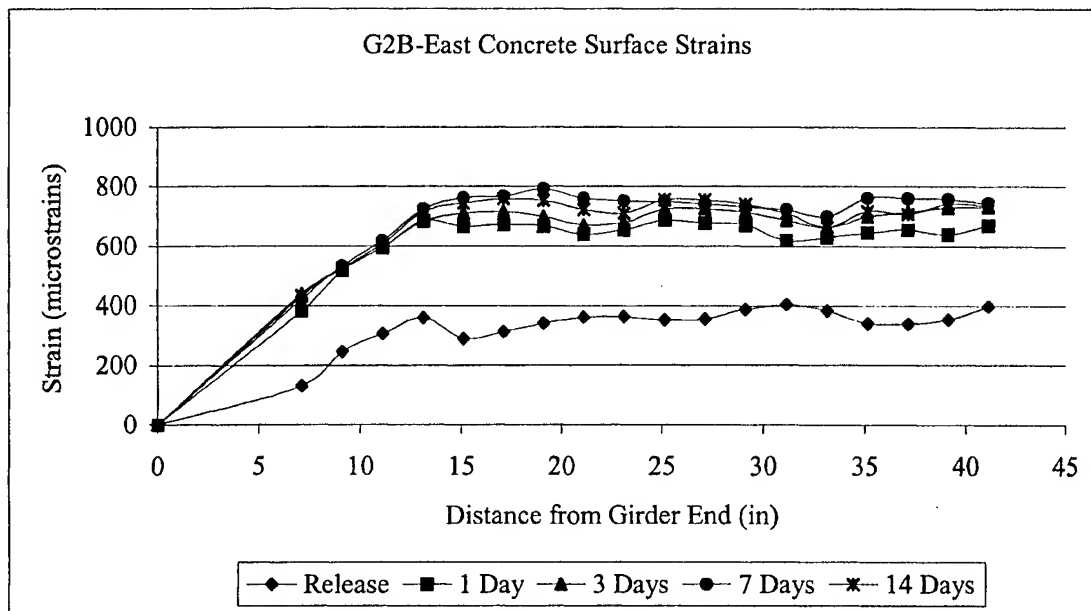
## I.9 Girder G2B-East



Figure I.17 Concrete Surface Strains for G2B-East
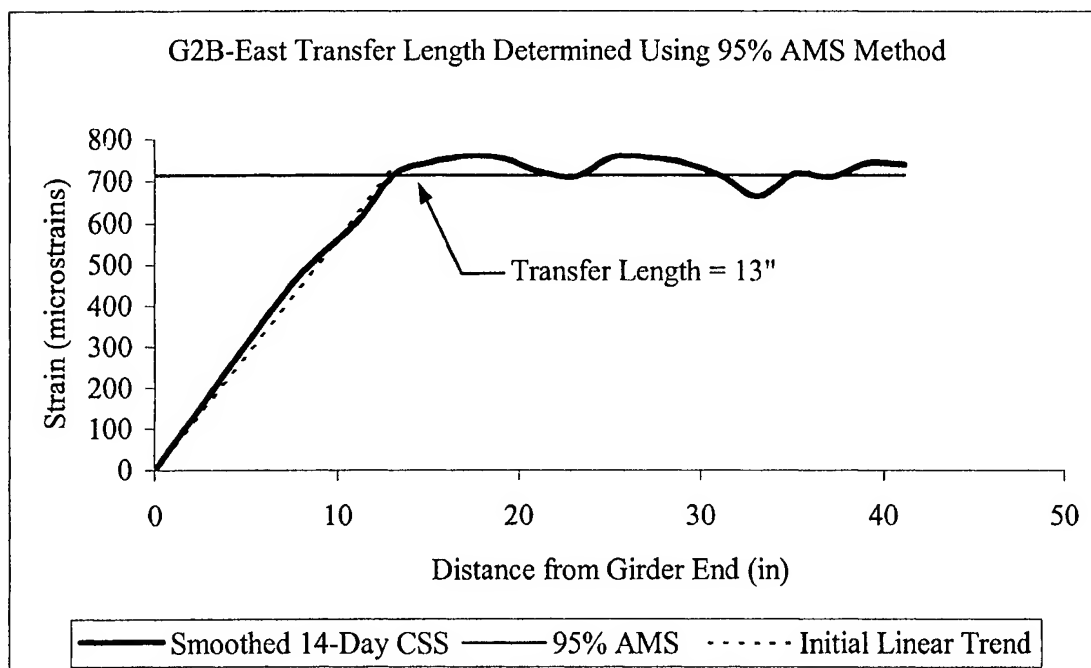


Figure I.18 14-Day Transfer Length Determined for G2B-East

473

## I.10 Girder G2B-West
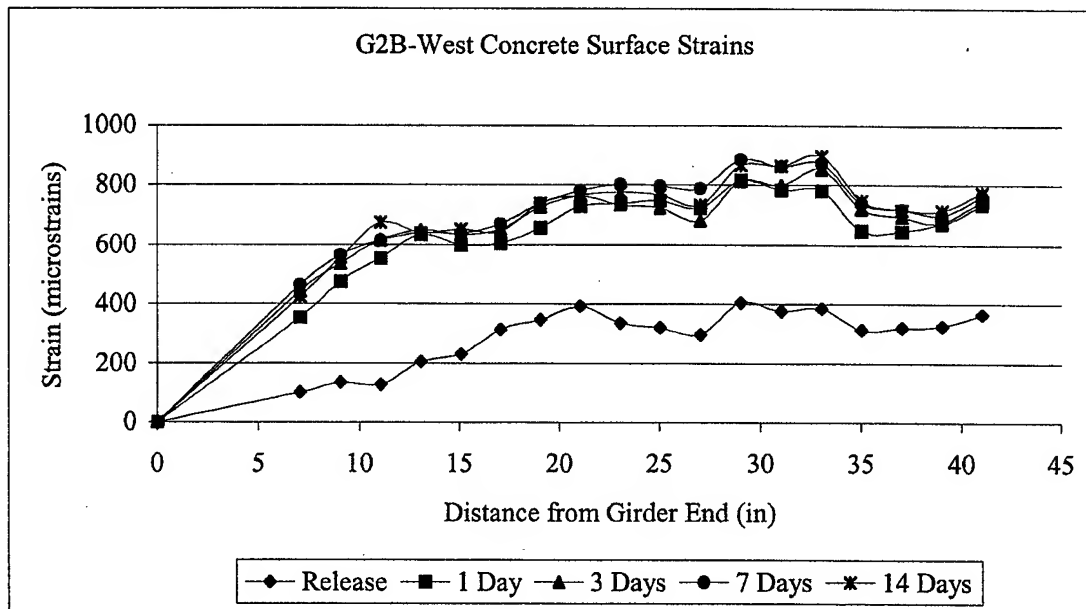


Figure I.19 Concrete Surface Strains for G2B-West
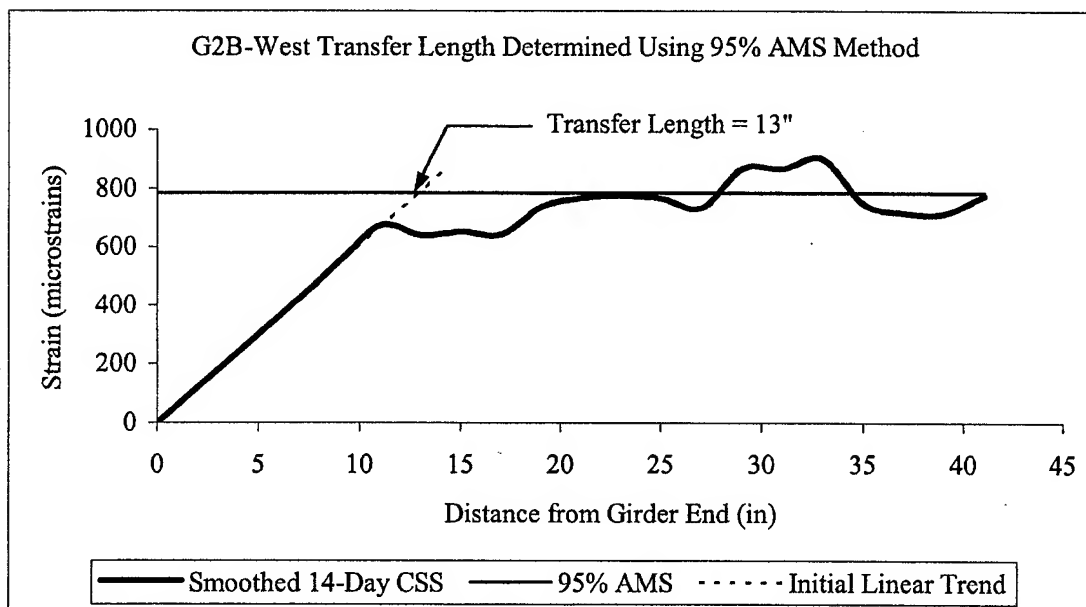


Figure I.20 14-Day Transfer Length Determined for G2B-West

474

## I.11 Girder G2C-East
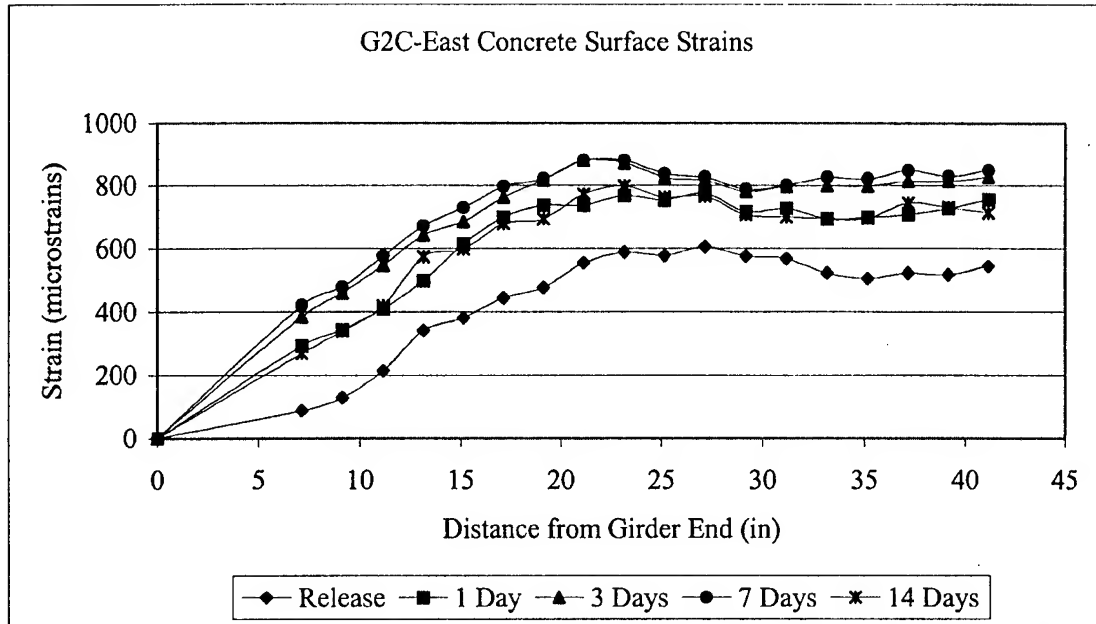


Figure I.21 Concrete Surface Strains for G2C-East
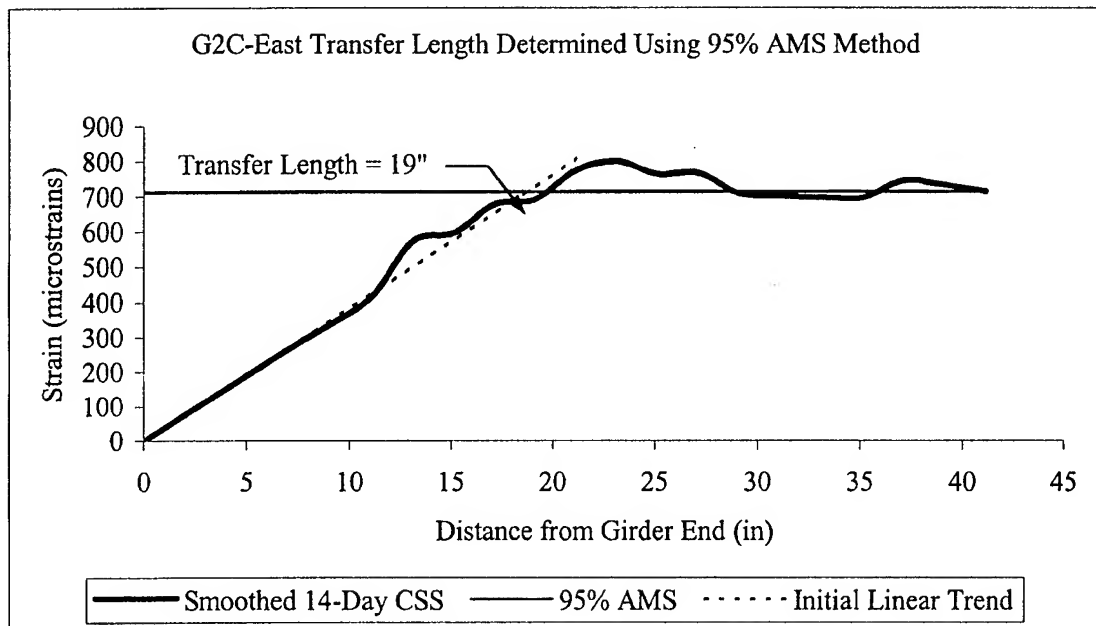


Figure I.22 14-Day Transfer Length Determined for G2C-East

## I.12  Girder G2C-West
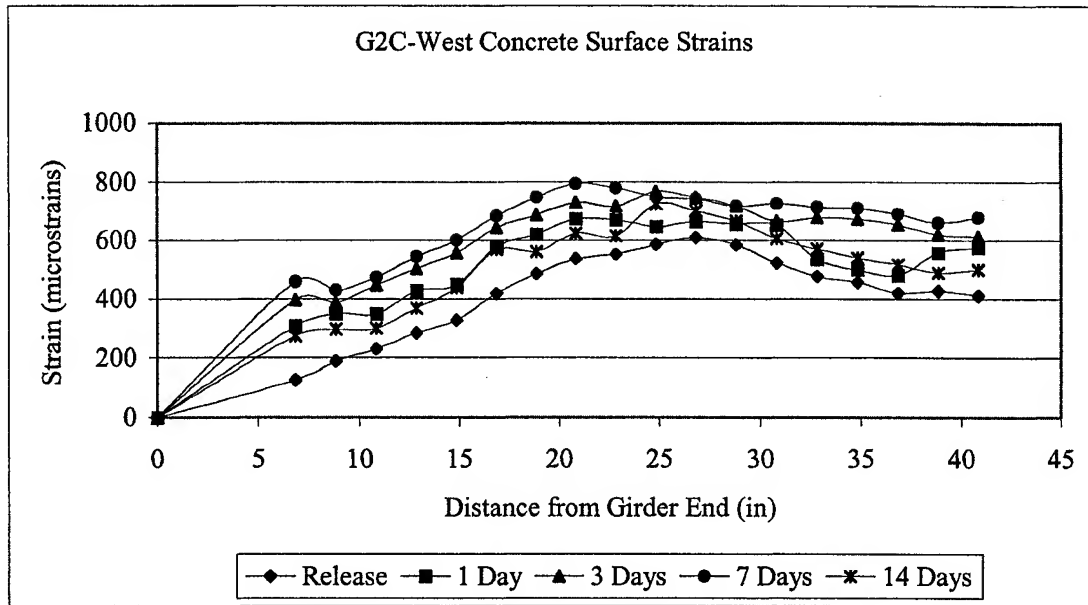


Figure I.23  Concrete Surface Strains for G2C-West
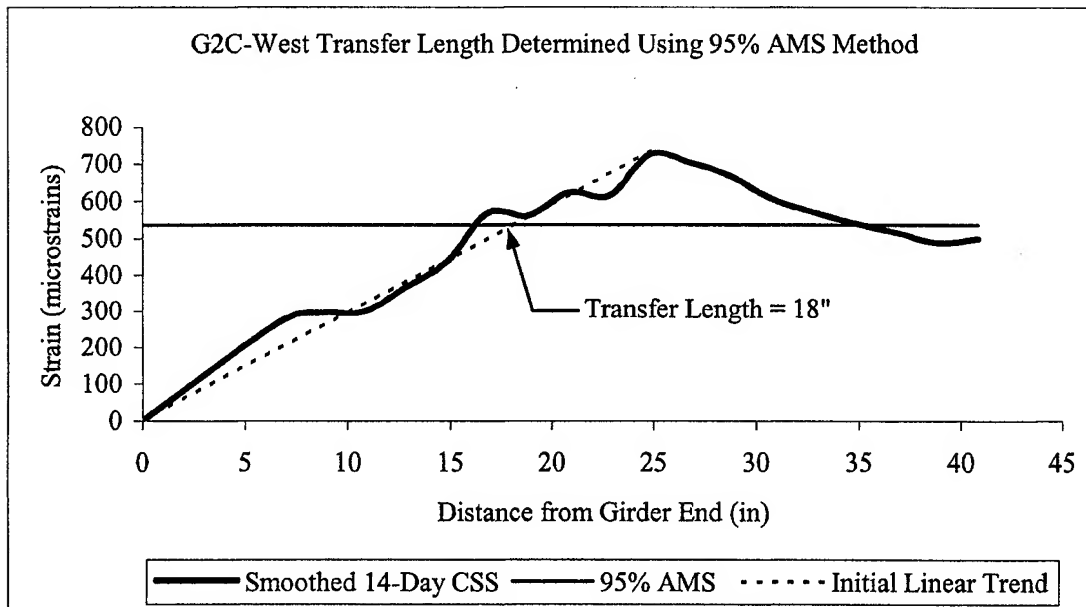


Figure I.24  14-Day Transfer Length Determined for G2C-West

476

# APPENDIX J

# TRANSFER LENGTH DATA FROM OTHER RESEARCHERS

This Appendix contains transfer length data from this project and other researchers. All transfer length data is based on the use of 0.6-inch prestressing strand. The data were used to evaluate the usefulness of the transfer length equations based on initial concrete compressive strength developed in Section 9.9.

Table J.1 Transfer Length Data from Researchers Using 0.6" Strand

| Specimen # | Name of Researcher | Concrete (LWC or NWC) | Specimen Cross Section | # Strands | Transfer Length (in) | $f_{ci}'$ (psi) |
|---|---|---|---|---|---|---|
| G1A-E | Meyer | LWC | AASHTO Type II | 8 | 19.50 | 7465 |
| G1A-W | Meyer | LWC | AASHTO Type II | 8 | 18.75 | 7465 |
| G1B-E | Meyer | LWC | AASHTO Type II | 8 | 25.00 | 7465 |
| G1B-W | Meyer | LWC | AASHTO Type II | 8 | 18.75 | 7465 |
| G1C-E | Meyer | LWC | AASHTO Type II | 8 | 28.00 | 6315 |
| G1C-W | Meyer | LWC | AASHTO Type II | 8 | 21.50 | 6315 |
| G2A-E | Meyer | LWC | AASHTO Type II | 8 | 17.50 | 9640 |
| G2A-W | Meyer | LWC | AASHTO Type II | 8 | 13.25 | 9640 |
| G2B-E | Meyer | LWC | AASHTO Type II | 8 | 13.00 | 9640 |
| G2B-W | Meyer | LWC | AASHTO Type II | 8 | 13.00 | 9640 |
| G2C-E | Meyer | LWC | AASHTO Type II | 8 | 19.00 | 8261 |
| G2C-W | Meyer | LWC | AASHTO Type II | 8 | 18.00 | 8261 |
| FA4601N | Russell | NWC | AASHTO Type | 4 | 24.00 | 4900 |
| FA4601S | Russell | NWC | AASHTO Type | 4 | 44.00 | 4900 |
| FA4602N | Russell | NWC | AASHTO Type | 4 | 33.00 | 4450 |
| FA4602S | Russell | NWC | AASHTO Type | 4 | 34.00 | 4450 |
| FA4603N | Russell | NWC | AASHTO Type | 4 | 32.00 | 4450 |
| FA4603S | Russell | NWC | AASHTO Type | 4 | 33.00 | 4450 |
| FA4604N | Russell | NWC | AASHTO Type | 4 | 25.00 | 4900 |
| FA4604S | Russell | NWC | AASHTO Type | 4 | 30.00 | 4900 |
| FA4605N | Russell | NWC | AASHTO Type | 4 | 33.00 | 4700 |
| FA4605S | Russell | NWC | AASHTO Type | 4 | 37.00 | 4700 |
| FA4606N | Russell | NWC | AASHTO Type | 4 | 33.00 | 4700 |
| FA4606S | Russell | NWC | AASHTO Type | 4 | 30.00 | 4700 |
| 6-1-EXT | Deatherage | NWC | AASHTO Type I | 7 | 25.00 | 4100 |
| 6-1-INT | Deatherage | NWC | AASHTO Type I | 7 | 27.00 | 4100 |
| 6-2-EXT | Deatherage | NWC | AASHTO Type I | 7 | 30.00 | 4280 |
| 6-2-INT | Deatherage | NWC | AASHTO Type I | 7 | 24.00 | 4280 |
| 6-3-EXT | Deatherage | NWC | AASHTO Type I | 7 | 23.00 | 5230 |
| 6-3-INT | Deatherage | NWC | AASHTO Type I | 7 | 21.00 | 5230 |
| 6-4-EXT | Deatherage | NWC | AASHTO Type I | 7 | 22.00 | 5450 |
| 6-4-INT | Deatherage | NWC | AASHTO Type I | 7 | 23.00 | 5450 |
| LOB-A | Barnes | NWC | AASHTO Type I | 6 | 26.00 | 4240 |
| LOB-B | Barnes | NWC | AASHTO Type I | 6 | 25.00 | 4240 |
| LOB-C | Barnes | NWC | AASHTO Type I | 6 | 30.00 | 4240 |
| LOB-D | Barnes | NWC | AASHTO Type I | 6 | 36.00 | 4240 |
| MOB-A | Barnes | NWC | AASHTO Type I | 8 | 22.00 | 6610 |
| MOB-B | Barnes | NWC | AASHTO Type I | 8 | 19.00 | 6610 |
| MOB-C | Barnes | NWC | AASHTO Type I | 8 | 18.00 | 6610 |
| MOB-D | Barnes | NWC | AASHTO Type I | 8 | 16.00 | 6610 |
| HOB-A | Barnes | NWC | AASHTO Type I | 8 | 15.00 | 11030 |
| HOB-B | Barnes | NWC | AASHTO Type I | 8 | 16.00 | 11030 |
| HOB-C | Barnes | NWC | AASHTO Type I | 8 | 16.00 | 11030 |
| HOB-D | Barnes | NWC | AASHTO Type I | 8 | 17.00 | 11030 |

Table J.1  Transfer Length Data from Researchers Using 0.6" Strand (Cont.)

| Specimen # | Name of Researcher | Concrete (LWC or NWC) | Specimen Cross Section | # Strands | Transfer Length (in) | $f_{ci}'$ (psi) |
|---|---|---|---|---|---|---|
| G2A-S | Reutlinger | NWC | AASHTO Type II | 8 | 15.40 | 14989 |
| G2A-N | Reutlinger | NWC | AASHTO Type II | 8 | 17.00 | 12379 |
| G2B-S | Reutlinger | NWC | AASHTO Type II | 8 | 17.90 | 12379 |
| G2B-N | Reutlinger | NWC | AASHTO Type II | 8 | 17.80 | 11721 |
| G4A-S | Reutlinger | NWC | AASHTO Type II | 8 | 16.70 | 14675 |
| G4A-N | Reutlinger | NWC | AASHTO Type II | 8 | 13.80 | 14395 |
| G4B-S | Reutlinger | NWC | AASHTO Type II | 8 | 13.50 | 14395 |
| G4B-N | Reutlinger | NWC | AASHTO Type II | 8 | 13.40 | 14610 |
| KLM1-C | Kaar | NWC | | | 51.50 | 2220 |
| KLM1-D | Kaar | NWC | | | 33.50 | 2220 |
| KLM2-C | Kaar | NWC | | | 52.00 | 2410 |
| KLM2-D | Kaar | NWC | | | 41.50 | 2410 |
| KLM3-C | Kaar | NWC | | | 49.00 | 3180 |
| KLM3-D | Kaar | NWC | | | 42.50 | 3180 |
| KLM4-C | Kaar | NWC | | | 36.00 | 4070 |
| KLM4-D | Kaar | NWC | | | 29.00 | 4070 |
| KLM5-C | Kaar | NWC | | | 39.50 | 5465 |
| KLM5-D | Kaar | NWC | | | 27.50 | 5465 |
| Mayfield - A1 | Mayfield | NWC | | | 16.73 | 7120 |
| Mayfield - A2 | Mayfield | NWC | | | 16.73 | 7120 |
| Mayfield - A3 | Mayfield | NWC | | | 16.73 | 7120 |
| Mayfield - A4 | Mayfield | NWC | | | 16.73 | 7120 |
| Mayfield - A5 | Mayfield | NWC | | | 16.73 | 7120 |
| Mayfield - A6 | Mayfield | NWC | | | 16.73 | 7120 |
| Mayfield - A7 | Mayfield | NWC | | | 16.73 | 7120 |
| Mayfield - B1 | Mayfield | NWC | | | 26.07 | 7120 |
| Mayfield - B2 | Mayfield | NWC | | | 26.07 | 7120 |
| Mayfield - B3 | Mayfield | NWC | | | 26.07 | 7120 |
| Mayfield - B4 | Mayfield | NWC | | | 26.07 | 7120 |
| Mayfield - B5 | Mayfield | NWC | | | 26.07 | 7120 |
| Mayfield - B6 | Mayfield | NWC | | | 26.07 | 7120 |
| Mayfield - B7 | Mayfield | NWC | | | 26.07 | 7120 |
| Mayfield - B8 | Mayfield | NWC | | | 26.07 | 7120 |
| Mayfield - C1 | Mayfield | NWC | | | 29.53 | 6120 |
| Mayfield - C2 | Mayfield | NWC | | | 29.53 | 6120 |
| Mayfield - C3 | Mayfield | NWC | | | 29.53 | 6120 |
| Mayfield - C4 | Mayfield | NWC | | | 29.53 | 6120 |
| Mayfield - C5 | Mayfield | NWC | | | 29.53 | 6120 |
| Mayfield - C6 | Mayfield | NWC | | | 29.53 | 6120 |
| Mayfield - C7 | Mayfield | NWC | | | 29.53 | 6120 |
| Mayfield - C8 | Mayfield | NWC | | | 29.53 | 6120 |
| Mayfield - C9 | Mayfield | NWC | | | 29.53 | 6120 |

Table J.1  Transfer Length Data from Researchers Using 0.6" Strand (Cont.)

| Specimen # | Name of Researcher | Concrete (LWC or NWC) | Specimen Cross Section | # Strands | Transfer Length (in) | $f_{ci}$' (psi) |
|---|---|---|---|---|---|---|
| 16/31-1865 A | Mitchell | NWC | Rectangular | 1 | 32.90 | 3000 |
| 16/31-1500 A | Mitchell | NWC | Rectangular | 1 | 35.90 | 3000 |
| 16/31-1500 B | Mitchell | NWC | Rectangular | 1 | 38.20 | 3000 |
| 16/65-1150 A | Mitchell | NWC | Rectangular | 1 | 20.80 | 6950 |
| 16/65-1150 B | Mitchell | NWC | Rectangular | 1 | 16.80 | 6950 |
| 16/65-725-A | Mitchell | NWC | Rectangular | 1 | 21.10 | 6950 |
| 16/65-725-B | Mitchell | NWC | Rectangular | 1 | 17.10 | 6950 |
| 16/89-675B | Mitchell | NWC | Rectangular | 1 | 16.10 | 7310 |
| 16/89-975B | Mitchell | NWC | Rectangular | 1 | 13.60 | 7310 |
| FC160-12 N | Russell | NWC | Rectangular | 1 | 48.00 | 3853 |
| FC160-12 S | Russell | NWC | Rectangular | 1 | 46.00 | 3853 |
| FC360-1 N | Russell | NWC | Rectangular | 3 | 42.00 | 4201 |
| FC360-1 S | Russell | NWC | Rectangular | 3 | 41.00 | 4201 |
| FC360-2 N | Russell | NWC | Rectangular | 3 | 37.00 | 4201 |
| FC360-2 N | Russell | NWC | Rectangular | 3 | 48.00 | 4201 |
| FCT360-3 N | Russell | NWC | Rectangular | 3 | 40.00 | 4201 |
| FCT360-3 S | Russell | NWC | Rectangular | 3 | 46.00 | 4201 |
| FCT360-4 N | Russell | NWC | Rectangular | 3 | 51.00 | 4792 |
| FCT360-4 S | Russell | NWC | Rectangular | 3 | 42.00 | 4792 |
| FCT362-11 N | Russell | NWC | Rectangular | 3 | 46.00 | 4759 |
| FCT362-11 S | Russell | NWC | Rectangular | 3 | 44.00 | 4759 |
| FCT362-12 N | Russell | NWC | Rectangular | 3 | 44.00 | 4759 |
| FCT362-12 S | Russell | NWC | Rectangular | 3 | 42.00 | 4759 |
| FCT362-13 N | Russell | NWC | Rectangular | 3 | 42.00 | 4759 |
| FCT362-13 S | Russell | NWC | Rectangular | 3 | 40.00 | 4759 |
| FC560-1 S | Russell | NWC | Rectangular | 5 | 46.00 | 4481 |
| FC560-1 N | Russell | NWC | Rectangular | 5 | 37.00 | 4481 |
| FCT560-2 S | Russell | NWC | Rectangular | 5 | 48.00 | 4481 |
| FCT560-2 N | Russell | NWC | Rectangular | 5 | 47.00 | 4481 |
| FC560-3 S | Russell | NWC | Rectangular | 5 | 48.00 | 4481 |
| FC560-3 N | Russell | NWC | Rectangular | 5 | 52.00 | 4481 |

# APPENDIX K

## GIRDER "AS-BUILT" ANALYSIS SPREADSHEET

Appendix K contains the individual pages from the Girder "AS-BUILT" Analysis

Spreadsheet. This sheet was used to process the DAQ output from the 18 girder tests

based on "as-built" girder characteristics. The entire set of worksheet pages is provided

from girder test G1C-W. A similar series of worksheets was prepared for each of the 18

girder tests. Listed below are the individual worksheets within the overall spreadsheet

and a brief description of the worksheet's function.

**Table K.1 – DAQ Output** – A sample of the raw data output from the data acquisition

system. Only a small percentage of the total number of DAQ lines is shown.

**Table K.2 – Load, Shear, Moment, Deflection, Strain and Curvature Values** – The

values are calculated based on DAQ and other user input values regarding the test. Only

a small percentage of the total number of lines in this worksheet is shown.

**Table K.3 – Calculated Principal Strains, Angles and Maximum Shear Strain** – The

values are calculated based on DAQ and other user input values regarding the test. Only

a small percentage of the total number of lines in this worksheet is shown.

**Table K.4 – Input Values for Girder Test** – The user enters values in the shaded cells

for LVDT gage length, test configuration and prestressing values.

**Table K.5 – Section Properties for Girder "AS-BUILT"** – The user enters all values in the table. The shaded values are the ones that change between tests.

**Table K.6 – Support Conditions, Reactions, Max Load and Moment Furnished** – The user enters values in the shaded areas. All other values are calculated automatically based on input and values from other worksheets. This worksheet provides a visual depiction of the support conditions to verify their location.

**Table K.7 – AASHTO Loss Calculations** – This worksheet calculates losses using the AASHTO[152] 1996 Standard Specifications. The user enters values in the shaded cells. Iteration may be required to determine the elastic shortening loss.

**Table K.8 – Girder Shear Capacity by 1996 AASHTO[40] Standard Procedure** – This worksheet calculates girder shear capacity at the tenth points of the shear span based on the 1996 AASHTO Standard Specification. The user enters the stirrup spacing in the shaded box.

**Table K.9 – Deflection Calculations** – This worksheet calculates predicted deflections at cracking and at ultimate condition.

**Table K.10 – Variable Angle Truss Model** – This worksheet determines the shear capacity of the girder, the angle of the compression strut, forces in the prestressing strand and bond stress using the variable angle truss model.

**Figure K.1 – Force in Prestressing Strand vs. Distance from Girder End**

**Figure K.2 – Bond Stress of Prestressing Strand vs. Distance from Girder End**

**Table K.11 – Theoretical Moment-Curvature Stages 1-3** – This worksheet calculates moment and curvature for the elastic stages.

**Table K.12 - Theoretical Moment-Curvature Stages 4-6** – This worksheet calculates moment and curvature for the stages after cracking; top of deck strain equal to 0.001, 0.002, 0.003 in/in. The user must enter values in the shaded boxes until the compression force and tension force are equal. $(F_{se} = F_c)$

**Figure K.3 – Moment-Curvature Plot**

**Table K.13 – Girder Shear Capacity by 1998 AASHTO[92] LRFD Procedure** – This worksheet calculates girder shear capacity at the tenth points of the shear span based on the 1998 AASHTO LRFD Specification. The user enters the values in the shaded boxes for crack angle, then the β value from the chart in the specification.

**Table K.14 – Girder-Deck Interface Shear Calculations** – This worksheet determines the interface shear adequacy between the girder and deck. The user enters values in the shaded boxes.

**Table K.15 – Prestressing Strand Tension Curve** – This worksheet provides a mathematical depiction of the stress strain curve for the prestressing strand. It is based on the actual curve received from the manufacturer.

**Table K.16 – Principal Strain and Maximum Shear Strain Plots** – Provides a visual depiction of the progression of principal strain angles and values as well as maximum shear strain. The user enters values for $V_{crack}$ and the low and high values of crack angles.

**Figure K.4 – Load vs. Displacement Plot**

**Table K.17 – Overview of Girder Test Results** – This worksheet provides an overview of the most important values from the girder test. It is meant to provide a snapshot of the test output.

483

Table K.1 DAQ Output

| 11/02/2001 Load Cell | 12:07 PM LVDT Top | LVDT Bottom | Wire Pot | LVDT 0 | LVDT 45 | LVDT 90 |
|---|---|---|---|---|---|---|
| 11.442372 | -0.00048 | -0.001137 | 2.465919 | -0.00249 | -0.002784 | -0.001542 |
| 13.463793 | -0.00056 | -0.001176 | 2.461571 | -0.002496 | -0.00279 | -0.001566 |
| 16.630684 | -0.000659 | -0.00129 | 2.455239 | -0.002484 | -0.002856 | -0.001548 |
| 27.815872 | -0.000462 | -0.001888 | 2.433496 | -0.002496 | -0.0031 | -0.001554 |
| 35.0256 | 0.000148 | -0.00232 | 2.415492 | -0.002477 | -0.003245 | -0.001554 |
| 34.789768 | 0.000173 | -0.00232 | 2.415569 | -0.002484 | -0.00327 | -0.00156 |
| 39.236893 | 0.000457 | -0.002524 | 2.410762 | -0.002471 | -0.003343 | -0.001548 |
| 45.536983 | 0.001055 | -0.002905 | 2.396878 | -0.002477 | -0.003495 | -0.001566 |
| 48.872326 | 0.001227 | -0.003109 | 2.392224 | -0.002465 | -0.003543 | -0.001548 |
| 48.653339 | 0.00127 | -0.003121 | 2.392148 | -0.002496 | -0.003562 | -0.001554 |
| 55.509319 | 0.001424 | -0.003541 | 2.377653 | -0.002459 | -0.00372 | -0.001573 |
| 61.371441 | 0.002059 | -0.003808 | 2.368269 | -0.002453 | -0.003841 | -0.001517 |
| 71.697525 | 0.002632 | -0.004393 | 2.349273 | -0.002399 | -0.004096 | -0.001542 |
| 75.369766 | 0.003138 | -0.004635 | 2.340576 | -0.002405 | -0.004175 | -0.001554 |
| 78.907257 | 0.003428 | -0.0048 | 2.332566 | -0.002393 | -0.004248 | -0.001535 |
| 83.1017 | 0.003797 | -0.005105 | 2.326692 | -0.002375 | -0.004364 | -0.001542 |
| 82.832176 | 0.003841 | -0.005105 | 2.326615 | -0.002381 | -0.004364 | -0.001548 |
| 82.663727 | 0.003834 | -0.005131 | 2.326615 | -0.002363 | -0.004364 | -0.001535 |
| 86.20121 | 0.004118 | -0.005334 | 2.321809 | -0.002357 | -0.004431 | -0.001529 |
| 89.233345 | 0.004291 | -0.005474 | 2.313188 | -0.002357 | -0.004491 | -0.00156 |
| 92.753983 | 0.004475 | -0.005652 | 2.308458 | -0.00232 | -0.004577 | -0.001548 |
| 92.551834 | 0.004728 | -0.00569 | 2.308382 | -0.002332 | -0.004583 | -0.001542 |
| 92.383385 | 0.004549 | -0.005652 | 2.308382 | -0.002314 | -0.004577 | -0.001554 |
| 92.248627 | 0.004697 | -0.005716 | 2.308458 | -0.002332 | -0.004589 | -0.001554 |
| 92.181244 | 0.004636 | -0.005678 | 2.308535 | -0.00235 | -0.004589 | -0.001542 |
| 92.063324 | 0.004697 | -0.005703 | 2.308306 | -0.002338 | -0.004577 | -0.001542 |
| 91.945412 | 0.004586 | -0.005716 | 2.308229 | -0.002332 | -0.004589 | -0.001554 |
| 91.878029 | 0.00463 | -0.00569 | 2.308382 | -0.002326 | -0.004577 | -0.00156 |

484

Table K.2 Calculated Load, Shear, Moment, Strain and Curvature Values

| Data Point # | Applied Load (Kips) | Applied Shear (Kips) | Total Moment (ft-kips) | Top LVDT (Inches) Compression ε = (-) | Top Strain (m-strain) Compression ε = (-) | Bot LVDT (Inches) Tension ε = (+) | Bot Strain (m-strain) Tension ε = (+) | Vertical Deflection (Inches) | Neutral Axis Location (In from Bot) | Top of Slab (+) = Comp (in/in) | At Level of Bot Strands (in/in) | Total Strand Strain (in/in) | Phi (rad/in) |
|---|---|---|---|---|---|---|---|---|---|---|---|---|---|
| 0 | 0.0 | 0.0 | 67.2 | 0.000000 | 0.00 | 0.000000 | 0.00 | 0.000000 | NA | 0.00 | 0.00 | 0.00505 | 0.000000 |
| 1 | 2.0 | 1.7 | 79.1 | -0.000080 | 3.33 | -0.000039 | 1.63 | 0.004348 | 17.38 | 0.00000 | 0.00000 | 0.00505 | 0.000000 |
| 2 | 5.2 | 4.3 | 97.8 | -0.000179 | 7.46 | -0.000153 | 6.38 | 0.010680 | 23.22 | -0.00001 | 0.00001 | 0.00506 | 0.000000 |
| 3 | 16.4 | 13.6 | 163.6 | 0.000018 | -0.75 | -0.000751 | 31.29 | 0.032423 | 45.85 | 0.00000 | 0.00003 | 0.00508 | 0.000001 |
| 4 | 23.6 | 19.6 | 206.1 | 0.000628 | -26.17 | -0.001183 | 49.29 | 0.050427 | 31.66 | 0.00003 | 0.00005 | 0.00510 | 0.000002 |
| 5 | 23.3 | 19.4 | 204.7 | 0.000653 | -27.21 | -0.001183 | 49.29 | 0.050350 | 31.27 | 0.00003 | 0.00005 | 0.00510 | 0.000002 |
| 6 | 27.8 | 23.1 | 230.9 | 0.000937 | -39.04 | -0.001387 | 57.79 | 0.055157 | 29.19 | 0.00004 | 0.00006 | 0.00511 | 0.000002 |
| 7 | 34.1 | 28.3 | 268.0 | 0.001535 | -63.96 | -0.001768 | 73.67 | 0.069041 | 26.49 | 0.00007 | 0.00007 | 0.00513 | 0.000003 |
| 8 | 37.4 | 31.1 | 287.6 | 0.001707 | -71.13 | -0.001972 | 82.17 | 0.073695 | 26.52 | 0.00007 | 0.00008 | 0.00514 | 0.000003 |
| 9 | 37.2 | 30.9 | 286.3 | 0.001750 | -72.92 | -0.001984 | 82.67 | 0.073771 | 26.31 | 0.00008 | 0.00008 | 0.00514 | 0.000004 |
| 10 | 44.1 | 36.6 | 326.7 | 0.001904 | -79.33 | -0.002404 | 100.17 | 0.088266 | 27.48 | 0.00008 | 0.00010 | 0.00515 | 0.000004 |
| 11 | 49.9 | 41.5 | 361.2 | 0.002539 | -105.79 | -0.002671 | 111.29 | 0.097650 | 25.49 | 0.00011 | 0.00011 | 0.00516 | 0.000005 |
| 12 | 60.3 | 50.1 | 422.0 | 0.003112 | -129.67 | -0.003256 | 135.67 | 0.116646 | 25.43 | 0.00014 | 0.00014 | 0.00519 | 0.000006 |
| 13 | 63.9 | 53.1 | 443.7 | 0.003618 | -150.75 | -0.003498 | 145.75 | 0.125343 | 24.57 | 0.00016 | 0.00015 | 0.00520 | 0.000007 |
| 14 | 67.5 | 56.1 | 464.5 | 0.003908 | -162.83 | -0.003663 | 152.63 | 0.133353 | 24.23 | 0.00017 | 0.00015 | 0.00521 | 0.000007 |
| 15 | 71.7 | 59.6 | 489.2 | 0.004277 | -178.21 | -0.003968 | 165.33 | 0.139227 | 24.12 | 0.00019 | 0.00017 | 0.00522 | 0.000008 |
| 16 | 71.4 | 59.3 | 487.6 | 0.004321 | -180.04 | -0.003968 | 165.33 | 0.139304 | 24.00 | 0.00019 | 0.00017 | 0.00522 | 0.000008 |
| 17 | 71.2 | 59.2 | 486.6 | 0.004314 | -179.75 | -0.003994 | 166.42 | 0.139304 | 24.09 | 0.00019 | 0.00017 | 0.00522 | 0.000008 |
| 18 | 74.8 | 62.2 | 507.4 | 0.004598 | -191.58 | -0.004197 | 174.88 | 0.144110 | 23.94 | 0.00020 | 0.00017 | 0.00523 | 0.000008 |
| 19 | 77.8 | 64.7 | 525.3 | 0.004771 | -198.79 | -0.004337 | 180.71 | 0.152731 | 23.89 | 0.00021 | 0.00018 | 0.00523 | 0.000009 |
| 20 | 81.3 | 67.6 | 546.0 | 0.004955 | -206.46 | -0.004515 | 188.13 | 0.157461 | 23.92 | 0.00022 | 0.00019 | 0.00524 | 0.000009 |
| 21 | 81.1 | 67.4 | 544.8 | 0.005208 | -217.00 | -0.004553 | 189.71 | 0.157537 | 23.47 | 0.00023 | 0.00019 | 0.00524 | 0.000009 |
| 22 | 80.9 | 67.3 | 543.8 | 0.005029 | -209.54 | -0.004515 | 188.13 | 0.157537 | 23.76 | 0.00022 | 0.00019 | 0.00524 | 0.000009 |
| 23 | 80.8 | 67.2 | 543.1 | 0.005177 | -215.71 | -0.004579 | 190.79 | 0.157461 | 23.59 | 0.00022 | 0.00019 | 0.00524 | 0.000009 |
| 24 | 80.7 | 67.1 | 542.7 | 0.005116 | -213.17 | -0.004541 | 189.21 | 0.157384 | 23.63 | 0.00022 | 0.00019 | 0.00524 | 0.000009 |
| 25 | 80.6 | 67.0 | 542.0 | 0.005177 | -215.71 | -0.004566 | 190.25 | 0.157613 | 23.56 | 0.00022 | 0.00019 | 0.00524 | 0.000009 |
| 26 | 80.5 | 66.9 | 541.3 | 0.005066 | -211.08 | -0.004579 | 190.79 | 0.157690 | 23.83 | 0.00022 | 0.00019 | 0.00524 | 0.000009 |
| 27 | 80.4 | 66.9 | 540.9 | 0.005110 | -212.92 | -0.004553 | 189.71 | 0.157537 | 23.67 | 0.00022 | 0.00019 | 0.00524 | 0.000009 |
| 28 | 80.4 | 66.8 | 540.4 | 0.005060 | -210.83 | -0.004528 | 188.67 | 0.157384 | 23.72 | 0.00022 | 0.00019 | 0.00524 | 0.000009 |
| 29 | 80.3 | 66.7 | 540.0 | 0.005110 | -212.92 | -0.004528 | 188.67 | 0.157461 | 23.61 | 0.00022 | 0.00019 | 0.00524 | 0.000009 |
| 30 | 80.1 | 66.6 | 539.2 | 0.005079 | -211.63 | -0.004528 | 188.67 | 0.157613 | 23.68 | 0.00022 | 0.00019 | 0.00524 | 0.000009 |
| 31 | 80.1 | 66.6 | 538.9 | 0.005227 | -217.79 | -0.004503 | 187.63 | 0.157461 | 23.31 | 0.00023 | 0.00019 | 0.00524 | 0.000009 |
| 32 | 80.1 | 66.6 | 538.7 | 0.005171 | -215.46 | -0.004528 | 188.67 | 0.157537 | 23.48 | 0.00022 | 0.00019 | 0.00524 | 0.000009 |
| 33 | 80.0 | 66.5 | 538.3 | 0.005060 | -210.83 | -0.004528 | 188.67 | 0.157537 | 23.72 | 0.00022 | 0.00019 | 0.00524 | 0.000009 |
| 34 | 79.9 | 66.4 | 537.9 | 0.005060 | -210.83 | -0.004464 | 186.00 | 0.157537 | 23.56 | 0.00022 | 0.00019 | 0.00524 | 0.000009 |

Table K.3 Calculated Principal Strains, Angles and Maximum Shear Strain

| Data Point | Load | Shear | LVDT 0 | LVDT 45 | LVDT 90 | Shear Zone Strain 45 | Strain XX | Strain YY | Strain XY | θp | Principal Strains Tension ε=(+) ε₁ | θp1 | Comp ε=(-) ε₂ | θp2 | γmax |
|---|---|---|---|---|---|---|---|---|---|---|---|---|---|---|---|
| # | (Kips) | (Kips) | (Inches) | (Inches) | (Inches) | (m-strain) Compression ε=(-) | (m-strain) Compression ε=(-) | (m-strain) Tension ε=(+) | (m-rads) Tension ε=(+) | (degrees) | (m-strain) | (deg) | (m-strain) | (deg) | (m-rads) |
| 0 | 0.0 | 0.0 | 0.000000 | 0.000000 | 0.000000 | 0.00 | -236.42 | 0.00 | 236.42 | NA | 48.96 | NA | -285.39 | NA | 334.35 |
| 1 | 2.0 | 1.7 | -0.000006 | -0.000006 | -0.000024 | 0.37 | -235.86 | 2.26 | 232.86 | -22.18 | 49.73 | 67.82 | -283.33 | -22.18 | 333.05 |
| 2 | 5.2 | 4.3 | 0.000006 | -0.000072 | -0.000006 | 4.43 | -236.99 | 0.56 | 227.56 | -21.88 | 46.27 | 68.12 | -282.69 | -21.88 | 328.96 |
| 3 | 16.4 | 13.6 | -0.000006 | -0.000316 | -0.000012 | 19.45 | -235.86 | 1.13 | 195.84 | -19.78 | 36.35 | 70.22 | -271.08 | -19.78 | 307.43 |
| 4 | 23.6 | 19.6 | 0.000013 | -0.000461 | -0.000012 | 28.37 | -237.65 | 1.13 | 179.78 | -18.49 | 31.19 | 71.51 | -267.70 | -18.49 | 298.89 |
| 5 | 23.3 | 19.4 | 0.000006 | -0.000486 | -0.000018 | 29.91 | -236.99 | 1.69 | 175.48 | -18.16 | 30.48 | 71.84 | -265.77 | -18.16 | 296.25 |
| 6 | 27.8 | 23.1 | 0.000019 | -0.000559 | -0.000006 | 34.40 | -238.21 | 0.56 | 168.85 | -17.63 | 27.40 | 72.37 | -265.05 | -17.63 | 292.44 |
| 7 | 34.1 | 28.3 | 0.000013 | -0.000711 | -0.000024 | 43.75 | -237.65 | 2.26 | 147.88 | -15.83 | 23.22 | 74.17 | -258.61 | -15.83 | 281.82 |
| 8 | 37.4 | 31.1 | 0.000025 | -0.000759 | -0.000006 | 46.71 | -238.78 | 0.56 | 144.80 | -15.59 | 20.76 | 74.41 | -258.97 | -15.59 | 279.73 |
| 9 | 37.2 | 30.9 | -0.000006 | -0.000778 | -0.000012 | 47.88 | -235.86 | 0.56 | 138.98 | -15.19 | 20.00 | 74.81 | -254.73 | -15.19 | 274.73 |
| 10 | 44.1 | 36.6 | 0.000031 | -0.000936 | -0.000031 | 57.60 | -239.34 | 2.92 | 121.22 | -13.29 | 17.24 | 76.71 | -253.66 | -13.29 | 270.90 |
| 11 | 49.9 | 41.5 | 0.000037 | -0.001057 | 0.000025 | 65.05 | -239.91 | -2.35 | 112.17 | -12.64 | 10.22 | 77.36 | -252.48 | -12.64 | 262.70 |
| 12 | 60.3 | 50.1 | 0.000091 | -0.001312 | 0.000000 | 80.74 | -244.99 | 0.00 | 83.51 | -9.41 | 6.92 | 80.59 | -251.91 | -9.41 | 258.83 |
| 13 | 63.9 | 53.1 | 0.000085 | -0.001391 | -0.000012 | 85.60 | -244.42 | 1.13 | 72.09 | -8.18 | 6.31 | 81.82 | -249.61 | -8.18 | 255.92 |
| 14 | 67.5 | 56.1 | 0.000097 | -0.001464 | 0.000007 | 90.09 | -245.55 | -0.66 | 66.03 | -7.54 | 3.71 | 82.46 | -249.93 | -7.54 | 253.64 |
| 15 | 71.7 | 59.6 | 0.000115 | -0.001580 | 0.000000 | 97.23 | -247.25 | 0.00 | 52.79 | -6.03 | 2.79 | 83.97 | -250.03 | -6.03 | 252.82 |
| 16 | 71.4 | 59.3 | 0.000109 | -0.001580 | -0.000006 | 97.23 | -246.68 | 0.56 | 51.66 | -5.90 | 3.23 | 84.10 | -249.35 | -5.90 | 252.59 |
| 17 | 71.2 | 59.2 | 0.000127 | -0.001580 | 0.000007 | 97.23 | -248.38 | -0.66 | 54.57 | -6.21 | 2.31 | 83.79 | -251.35 | -6.21 | 253.66 |
| 18 | 74.8 | 62.2 | 0.000133 | -0.001647 | 0.000013 | 101.35 | -248.94 | -1.22 | 47.46 | -5.42 | 1.03 | 84.58 | -251.19 | -5.42 | 252.22 |
| 19 | 77.8 | 64.7 | 0.000133 | -0.001707 | -0.000018 | 105.05 | -248.94 | 1.69 | 37.16 | -4.22 | 3.06 | 85.78 | -250.31 | -4.22 | 253.37 |
| 20 | 81.3 | 67.6 | 0.000170 | -0.001799 | -0.000006 | 110.34 | -252.42 | 0.56 | 31.18 | -3.51 | 1.52 | 86.49 | -253.38 | -3.51 | 254.90 |
| 21 | 81.1 | 67.4 | 0.000158 | -0.001799 | 0.000000 | 110.71 | -251.29 | 0.00 | 29.88 | -3.39 | 0.89 | 86.61 | -252.18 | -3.39 | 253.06 |
| 22 | 80.9 | 67.3 | 0.000176 | -0.001793 | -0.000012 | 110.34 | -252.99 | 1.13 | 31.18 | -3.50 | 2.08 | 86.50 | -253.94 | -3.50 | 256.02 |
| 23 | 80.8 | 67.2 | 0.000158 | -0.001805 | -0.000012 | 111.08 | -251.29 | 1.13 | 28.01 | -3.17 | 1.90 | 86.83 | -252.07 | -3.17 | 253.97 |
| 24 | 80.7 | 67.1 | 0.000140 | -0.001805 | 0.000000 | 111.08 | -249.60 | 0.00 | 27.45 | -3.14 | 0.75 | 86.86 | -250.35 | -3.14 | 251.10 |
| 25 | 80.6 | 67.0 | 0.000152 | -0.001793 | 0.000000 | 110.34 | -250.73 | 0.00 | 30.05 | -3.42 | 0.90 | 86.58 | -251.63 | -3.42 | 252.52 |
| 26 | 80.5 | 66.9 | 0.000158 | -0.001805 | -0.000012 | 111.08 | -251.29 | 1.13 | 28.01 | -3.17 | 1.90 | 86.83 | -252.07 | -3.17 | 253.97 |
| 27 | 80.4 | 66.9 | 0.000164 | -0.001793 | -0.000018 | 110.34 | -251.86 | 1.69 | 29.49 | -3.32 | 2.55 | 86.68 | -252.71 | -3.32 | 255.26 |
| 28 | 80.4 | 66.8 | 0.000170 | -0.001786 | -0.000012 | 109.91 | -252.42 | 1.13 | 31.48 | -3.54 | 2.10 | 86.46 | -253.40 | -3.54 | 255.50 |
| 29 | 80.3 | 66.7 | 0.000158 | -0.001793 | 0.000025 | 110.34 | -251.29 | -2.35 | 32.97 | -3.77 | -1.27 | 86.23 | -252.38 | -3.77 | 251.12 |
| 30 | 80.1 | 66.6 | 0.000164 | -0.001786 | -0.000006 | 109.91 | -251.86 | 0.56 | 31.48 | -3.55 | 1.54 | 86.45 | -252.84 | -3.55 | 254.38 |
| 31 | 80.1 | 66.6 | 0.000158 | -0.001805 | -0.000006 | 111.08 | -251.29 | 0.56 | 28.58 | -3.24 | 1.37 | 86.76 | -252.10 | -3.24 | 253.48 |
| 32 | 80.1 | 66.6 | 0.000164 | -0.001768 | 0.000000 | 108.80 | -251.86 | 0.00 | 34.26 | -3.87 | 1.16 | 86.13 | -253.02 | -3.87 | 254.18 |
| 33 | 80.0 | 66.5 | 0.000146 | -0.001786 | 0.000000 | 109.91 | -250.17 | 0.00 | 30.35 | -3.46 | 0.92 | 86.54 | -251.08 | -3.46 | 252.00 |
| 34 | 79.9 | 66.4 | 0.000146 | -0.001786 | -0.000012 | 109.91 | -250.17 | 1.13 | 29.22 | -3.32 | 1.98 | 86.68 | -251.01 | -3.32 | 252.99 |

486

Table K.4  Input Values for Girder Test

## G1C-W

## Girder Test Information

| | |
|---|---|
| Test Configuration # | 4 |
| Stirrup Density | Single |
| Date | 02-Nov-01 |

Enter values in shaded fields and adjust limits of functions to include all data points in DAQ file.

| | | |
|---|---|---|
| LVDT 0 Length | 10.625 | Inches |
| LVDT 45 Length | 16.250 | Inches |
| LVDT 90 Length | 10.625 | Inches |

| | | |
|---|---|---|
| Top LVDT Length | 21.00 | Inches |
| Top Edge Distance | 1.00 | Inches |

— Top LVDT —

| | | |
|---|---|---|
| Initial Cracking Load | $P_{cr}$ | 195.00 | Kips |
| Cracking Moment | $M_{cr}$ | 1144.85 | Ft-Kips |
| Cracking Deflection | $\delta_{cr}$ | 0.44 | Inches |
| Max Applied Load | $P_{max}$ | 299.04 | Kips |
| Nominal Moment | $M_{n}$ | 1828.17 | Ft-Kips |
| Max Deflection | $\delta_{max}$ | 2.27 | Inches |
| Max Deck Strain | $\varepsilon_{cu}$ | 0.0036 | in/in |
| Max Bot Strand Strn | $\varepsilon_{ps}$ | 1.3960 | Percent |
| Max Bot Strand Force | $F_{ps}$ | 57.72 | Kips |

| Actual Strand Prestressing Values (ksi) | | |
|---|---|---|
| Jacking Stress | $f_{pt}$ | 179.11 |
| Stress After Release | $f_{si}$ | 167.11 |
| Stress at 14 Days | $f_{se}$ | 153.65 |
| Strain at Test (µε) | $\varepsilon_{se}$ | 5053 |
| Stress At Testing | $f_{se}$ | 147.61 |
| Actual Girder Prestressing Values | | |
| Initial X-X Stress (ksi) | $f_{pc\,INT}$ | 0.87 |
| Initial X-X Strain (me) | $\varepsilon_{cipx}$ | 2.36E-04 |

| | | |
|---|---|---|
| Bottom LVDT Length | 14.00 | Inches |
| Bot Edge Distance | 5.00 | Inches |

— Bot LVDT —

| | | |
|---|---|---|
| Measured Transfer Length | 21.5 | Inches |
| Actual Development Length | 0.1 | Inches |

The $M_{cr}$ and $M_{n}$ values include the $M_{DL}$ value.

0
45
90
+

Table K.5  Section Properties for Girder "AS BUILT"

## G1C-W — Section Properties for "AS BUILT" Prestressed Girder Analysis

### Deck Variables

| Description | Symbol | Value | Unit |
|---|---|---|---|
| Deck Thickness | $t_d$ | (illegible) | IN |
| Deck Width | $W_f$ | (illegible) | IN |
| Concrete Actual Strength | $f'_c$ | (illegible) | PSI |
| Concrete Weight | $W_c$ | (illegible) | PCF |

### Beam Cross Section Variables

| Description | Symbol | Value | Unit |
|---|---|---|---|
| Girder Type | | 2 | 1-5,BT |
| Girder Top Flange Width | | 12 | IN |
| Concrete Strength at Release | $f'_{ci}$ | (illegible) | PSI |
| Concrete Actual Strength | $f'_c$ | (illegible) | PSI |
| Concrete Equilibrium Weight | $W_c$ | (illegible) | PCF |
| LWC Reduction Factor | $\lambda$ | 0.85 | None |
| Strand Diameter | $d_b$ | 0.6 | IN |
| Strand C/S Area | $A_{st}$ | 0.2183 | IN$^2$ |
| Strand Ultimate Strength | $f_{pu}$ | 283.25 | KSI |

### Miscellaneous Variables Normally Constant

| Description | Symbol | Value | Unit |
|---|---|---|---|
| Strand Yield as % of Ultimate | | 0.9 | None |
| Strand Modulus of Elasticity | $E_{ps}$ | 29000 | KSI |
| Stirrup Size | | 4 | # |
| Stirrup Yield Strength | $f_y$ | 62 | KSI |
| Distance from End to COB | XDIST | 6.00 | IN |
| Tension Strength Factor | a | 7.50 | |
| Top of Beam to Top Strands | TCL | 2.50 | IN |
| Bottom of Beam to Bottom Strands | BCL | 3.00 | IN |
| Strand Spacing | SPAC | 2.00 | IN |
| Steel Weight Allowance / Cubic Ft | | 3.0 | PCF |
| Prestress stress for $l_d$ calculation | $f_{ps}$ | 266 | KSI |
| Ratio of Prestressed Reinforcement | p* | 0.0029 | None |
| Strand Yield to Ultimate Factor | $Y_p$ | 0.28 | None |
| Ratio of a/c (Based on Beam Concrete) | $\beta_1$ | 1.00 | None |

### Elasticity Modulus Values

| Description | Symbol | Value | Unit |
|---|---|---|---|
| Deck Mod. of Elast. at Testing (Actual) | $E_{cd}$ | 3.85E+06 | PSI |
| Beam Mod. Of Elast. At Testing (Est) | $E_{cg}$ | 3.69E+06 | PSI |
| Modular Ratio ($E_{cd}/E_{cb}$) | $\eta$ | 0.907 | None |

### Non-Composite Beam Properties

| Description | Symbol | Value | Unit |
|---|---|---|---|
| Moment of Inertia | $I_{nc}$ | 50979 | IN$^4$ |
| Distance from Centroid to Top of Beam | $Y_{top}$ | 20.17 | IN |
| Distance from Centroid to Bot. of Beam | $Y_{bot}$ | 15.83 | IN |
| Section Modulus (Top) | $S_{top}$ | 2527.47 | IN$^3$ |
| Section Modulus (Bot) | $S_{bot}$ | 3220.40 | IN$^3$ |
| Cross Sectional Area | $A_{bm}$ | 369 | IN$^2$ |
| Weight per Foot (Concrete & Steel) | $W_D$ | 0.307 | K/FT |
| Web Thickness | WS | 0.6 | IN |
| Height of Beam | DB | 36 | IN |

### Composite Beam Properties

| Description | Symbol | Value | Unit |
|---|---|---|---|
| Moment of Inertia | $I_c$ | 144285.39 | IN$^4$ |
| Distance from Centroid to Top of Beam | $Y_{top}$ | 10.74 | IN |
| Distance from Centroid to Bot. of Beam | $Y_{bot}$ | 25.26 | IN |
| Section Modulus (Bot) | $S_{bot}$ | 5711.81 | IN$^3$ |
| Cross Sectional Area | $A_{bm}$ | 577.68 | IN$^2$ |
| Weight per Foot (Concrete & Steel) | $W_D$ | 0.5435 | K/FT |
| First Moment of Deck About Centroid | QS | 3480.00 | IN$^3$ |
| Overall Depth of Composite Beam | H | 47.875 | IN |

### Miscellaneous Properties

| Description | Symbol | Value | Unit |
|---|---|---|---|
| Stirrup Area | $A_v$ | 0.4 | IN$^2$ |
| Depth to Prestressing Steel | $d_p$ | 38.78 | IN |
| Ratio of Prestressed Reinforcement | p* | 0.0029 | None |
| Strand Yield to Ultimate Factor | $Y_p$ | 0.28 | None |
| Ratio of a/c (Based on Beam Concrete) | $\beta_1$ | 0.65 | None |

### Strand Data (No Drape)

| Ref. # | Dist. IN | Nbr # | % $f_{pu}$ % | $F_{ps}$ KIP | $F_{ps}d$ KIP-IN |
|---|---|---|---|---|---|
| TOP | 33.5 | 2 | 0.63 | 78.20 | 2619.7 |
| 18 | | 0 | 0.00 | 0.00 | 0.0 |
| 17 | | 0 | 0.00 | 0.00 | 0.0 |
| 16 | | 0 | 0.00 | 0.00 | 0.0 |
| 15 | 31.0 | 0 | 0.00 | 0.00 | 0.0 |
| 14 | 29.0 | 0 | 0.00 | 0.00 | 0.0 |
| 13 | 27.0 | 0 | 0.00 | 0.00 | 0.0 |
| 12 | 25.0 | 0 | 0.00 | 0.00 | 0.0 |
| 11 | 23.0 | 0 | 0.00 | 0.00 | 0.0 |
| 10 | 21.0 | 0 | 0.00 | 0.00 | 0.0 |
| 9 | 19.0 | 0 | 0.00 | 0.00 | 0.0 |
| 8 | 17.0 | 0 | 0.00 | 0.00 | 0.0 |
| 7 | 15.0 | 0 | 0.00 | 0.00 | 0.0 |
| 6 | 13.0 | 0 | 0.00 | 0.00 | 0.0 |
| 5 | 11.0 | 0 | 0.00 | 0.00 | 0.0 |
| 4 | 9.0 | 0 | 0.00 | 0.00 | 0.0 |
| 3 | 7.0 | 0 | 0.00 | 0.00 | 0.0 |
| 2 | 5.0 | 0 | 0.00 | 0.00 | 0.0 |
| 1 | 3.0 | 8 | 0.63 | 312.80 | 938.4 |

**Eccentricity from NC Centroid:** Distance = -6.73 IN

**Development Length (Inches):** AASHTO 100.56 | Actual 91.00 ; COB Dist. 94.56 | COB 85.00

**Transfer Length (Inches):** AASHTO 30.73 | Actual 21.50

Table K.6 Support Conditions, Reactions, Max Load and Moment Furnished

| G1C-W | | Support Conditions, Applied Load (KIP) and Moment Furnished (FT-KIP) | | | | | | | | | | | | | | | | | | | |
|---|---|---|---|---|---|---|---|---|---|---|---|---|---|---|---|---|---|---|---|---|---|
| REF | BRNG | 0.05L | 0.10L | 0.15L | 0.20L | 0.25L | 0.30L | 0.35L | 0.40L | 0.45L | 0.50L | 0.55L | 0.60L | 0.65L | 0.70L | 0.75L | 0.80L | 0.85L | 0.90L | 0.95L | BRNG |
| FT | 0.00 | 2.10 | 4.20 | 6.30 | 8.40 | 10.50 | 12.60 | 14.70 | 16.80 | 18.90 | 21.00 | 23.10 | 25.20 | 27.30 | 29.40 | 31.50 | 33.60 | 35.70 | 37.80 | 39.90 | 42.00 |
| IN | 0.00 | 25.20 | 50.40 | 75.60 | 100.80 | 126.00 | 151.20 | 176.40 | 201.60 | 226.80 | 252.00 | 277.20 | 302.40 | 327.60 | 352.80 | 378.00 | 403.20 | 428.40 | 453.60 | 478.80 | 504.00 |

Number of Strands Developed Assuming $l_d$

| | BRNG | 0.05L | 0.10L | 0.15L | 0.20L | 0.25L | 0.30L | 0.35L | 0.40L | 0.45L | 0.50L | 0.55L | 0.60L | 0.65L | 0.70L | 0.75L | 0.80L | 0.85L | 0.90L | 0.95L | BRNG |
|---|---|---|---|---|---|---|---|---|---|---|---|---|---|---|---|---|---|---|---|---|---|
| # Top | 0.13 | 0.69 | 1.24 | 1.79 | 2.00 | 2.00 | 2.00 | 2.00 | 2.00 | 2.00 | 2.00 | 2.00 | 2.00 | 2.00 | 2.00 | 2.00 | 2.00 | 1.79 | 1.24 | 0.69 | 0.13 |
| # Bot | 0.53 | 2.74 | 4.96 | 7.17 | 8.00 | 8.00 | 8.00 | 8.00 | 8.00 | 8.00 | 8.00 | 8.00 | 8.00 | 8.00 | 8.00 | 8.00 | 8.00 | 7.17 | 4.96 | 2.74 | 0.53 |
| $M_r$ | 112.7 | 586.2 | 1059.6 | 1533.0 | 1709.6 | 1709.6 | 1709.6 | 1709.6 | 1709.6 | 1709.6 | 1709.6 | 1709.6 | 1709.6 | 1709.6 | 1709.6 | 1709.6 | 1709.6 | 1533.0 | 1059.6 | 586.2 | 112.7 |

Max Load (KIPS)

279

SUPT 1

DECK

BEAM

| Type of Load | L Support Reaction (KIPS) | R Support Reaction (KIPS) |
|---|---|---|
| Dead | 11.68 | 11.68 |
| Point | 231.87 | 47.04 |
| Total | 243.55 | 58.72 |

| Strength Reduction for Shear Cap. | |
|---|---|
| STD,LRFD | STD |
| 0.930 | |

| a | Distance from left support to point load | 85.0 | IN | 7.08 | FT |
|---|---|---|---|---|---|
| $L_1$ | Distance from left support to right support | 504.00 | IN | 42.00 | FT |
| $L_2$ | Distance from left COB to left support | 0.00 | IN | 0.00 | FT |
| L | Overall Length of Beam (COB-COB) | 504.00 | IN | 42.00 | FT |
| b | Distance from point load to right support | 419.0 | IN | 34.92 | FT |
| $L_3$ | Distance from right support to right COB | 0.0 | IN | 0.00 | FT |
| a/d | Ratio of shear distance to depth | 2.36 | | NA | |

| MAX LOAD | 259 | KIPS | SHEAR CTRLS |
|---|---|---|---|

| $M_r$ (Max) Calculations | | |
|---|---|---|
| $d_p$ | 38.78 | IN |
| $p^*$ | 0.00291 | None |
| $f^*_{su}$ | 264.60 | KSI |
| $w_p$ | 0.1428 | .36$b_1$ | 0.234 |
| Beam is Under-reinforced | | |
| a < Deck Thickness | | |
| a | 6.51 | IN |
| $M_f$ | 1709.6 | FT-KIP |

O

Table K.7  Prestressed Beam Loss Calculations (AASHTO-STD '96)

## G1C-W — Prestressed Beam Loss Calculations (AASHTO-STD '96)

### Beam Values

| | | | |
|---|---|---|---|
| Beam Length (COB-COB) | L | 42.00 | FT |
| Beam Cross Sectional Area | $A_{bm}$ | 369 | IN² |
| NC Moment of Inertia | $I_{nc}$ | 50979 | IN⁴ |
| NC Section Modulus (Top) | $S_{top}$ | 2527.47 | IN³ |
| NC Section Modulus (Bot) | $S_{bot}$ | 3220.40 | IN³ |
| Strand Eccentricity from NC Centroid | e | -6.73 | IN |
| Beam Weight / Foot (Concrete & Steel) | $W_D$ | 0.307 | K/FT |
| Deck Weight / Foot (Concrete & Steel) | $W_{SD}$ | 0.236 | K/FT |

### ES-Elastic Shortening (Release)

| | | | |
|---|---|---|---|
| Radius of Gyration | $r^2$ | 138.2 | IN² |
| Initial Jacking Force | $P_j$ | 391.0 | KIPS |
| Est. Jacking Force Loss | OK | ░░░ | % |
| Final Jacking Force | $P_i$ | 368.7 | KIPS |
| MAX Dead Load Moment | $M_D$ | 812.3 | IN-KIPS |
| Stress at Steel Centroid | $f_{cir}$ | -1.220 | KSI |
| Modular Ratio ($E_{py}/E_{cb}$) | n | 9.67 | None |
| ES Losses (KSI - %) | $\Delta_{pES}$ | -11.79 | -6.6% |

### CR-Creep (Slab Placement)

| | | | |
|---|---|---|---|
| Modular Ratio ($E_{ps}/E_{cb}$) | $\eta$ | 7.85 | None |
| Stress at Steel Centroid | $f_{cir}$ | -1.220 | KSI |
| Addl. DL Since Release | $W_{SD}$ | 0.000 | K/FT |
| Moment due to $W_{SD}$ | $M_{SD}$ | 0.0 | IN-KIP |
| Stress at Steel Centroid | $f_{csd}$ | 0.000 | KSI |
| LWC Factor | | 1.0 | None |
| Creep Factor | $K_{CR}$ | 1.0 | None |
| CR Losses (KSI - %) | $\Delta_{pCR}$ | -14.63 | -8.2% |

### Steel Values

| | | | |
|---|---|---|---|
| Area of Prestressing Steel | Aps | 2.183 | IN² |
| Strand Ultimate Strength | $f_{pu}$ | 283.25 | KSI |
| Strand Yield Strength | $f_{py}$ | 254.925 | KSI |
| Strand Modulus of Elasticity | $E_{ps}$ | 29000 | KSI |
| Percent Strand Ultimate at Jacking | % | 0.63 | None |
| Strand Jacking Stress | $f_{pt}$ | 179.11 | KSI |

### R-Steel Stress Relax (Release)

| | | | |
|---|---|---|---|
| % Relax at Release | | 30% | % |
| Time (Jack to Release) | $t_{rel}$ | 24 | HRS |
| R Losses (KSI - %) | $\Delta_{pR}$ | -0.83 | -0.5% |

### R-Steel Stress Relax (Slab Placement)

| | | | |
|---|---|---|---|
| % Relax at Release | | 60% | % |
| Time (Release to Slab) | $t_{slab}$ | 30 | DAYS |
| R Losses (KSI - %) | $\Delta_{pR}$ | -1.66 | -0.9% |

### SH-Shrinkage (Slab Placement)

| | | | |
|---|---|---|---|
| Shrinkage Factor | $K_{SH}$ | 1.0 | None |
| Relative Humidity | RH | 70 | % |
| SH Losses (KSI - %) | $\Delta_{pSH}$ | -6.50 | -3.6% |

### R-Steel Stress Relax (Testing)

| | | | |
|---|---|---|---|
| % Relax at Release | | 10% | % |
| Time (Release to Test) | $t_{test}$ | 120 | DAYS |
| R Losses (KSI - %) | $\Delta_{pR}$ | -0.28 | -0.2% |

### Concrete Values

| | | | |
|---|---|---|---|
| Beam Concrete Design Strength | $f'_c$ | 8911 | PSI |
| Beam Design Modulus | $E_{cb}$ | 3.69E+06 | PSI |
| % Beam Concrete Strength at Release | | 71% | % |
| Beam Concrete Strength at Release | $f'_{ci}$ | 6315 | PSI |
| Beam Mod. Of Elast. at Release (Act) | $E_{cb}$ | ░░░░ | PSI |

### Steel Stress Relaxation Percentages-OK

AASHTO Loss Calculations and PT (KSI)

| Stage | % | Loss | PT |
|---|---|---|---|
| At Release, $f_{si}$ | -7% | -12.62 | 166.49 |
| At Slab Placement, $f_{se}$ | -20% | -35.41 | 143.70 |
| At Testing, $f_{se}$ | -20% | -35.69 | 143.42 |

### Shrinkage Factors-OK

Actual Losses and PT (KSI)

| Stage | % | Loss | PT |
|---|---|---|---|
| At Release, $f_{si}$ | -9% | -17.00 | 162.1 |
| At 14 Days, $f_{se}$ | -14% | -25.46 | 153.7 |
| At Testing, $f_{se}$ | -18% | -31.50 | 147.6 |

Table K.8  Girder Shear Capacity by 1996 AASHTO[40] Standard Procedure

| G1C-W | | Girder Shear Capacity AASHTO STD-96 (Left of Point Load) | | | | | | | | | | |
|---|---|---|---|---|---|---|---|---|---|---|---|---|
| | IN | L-SUPT | 0.1 a | 0.2 a | 0.3 a | 0.4 a | 0.5 a | 0.6 a | 0.7 a | 0.8 a | 0.9 a | P-LOAD |
| Distance from Left Support (Inches) | IN | 0.00 | 8.50 | 17.00 | 25.50 | 34.00 | 42.50 | 51.00 | 59.50 | 68.00 | 76.50 | 85.00 |
| Ultimate Moment Furnished | FT-KIP | 112.72 | 272.42 | 432.11 | 591.80 | 751.50 | 911.19 | 1070.88 | 1230.58 | 1390.27 | 1549.96 | 1709.64 |
| Transferred Strands Factor | | 0.28 | 0.67 | 1.00 | 1.00 | 1.00 | 1.00 | 1.00 | 1.00 | 1.00 | 1.00 | 1.00 |
| Transferred # Top Strands | # | 0.56 | 1.35 | 2.00 | 2.00 | 2.00 | 2.00 | 2.00 | 2.00 | 2.00 | 2.00 | 2.00 |
| Transferred # Bottom Strands | # | 2.23 | 5.40 | 8.00 | 8.00 | 8.00 | 8.00 | 8.00 | 8.00 | 8.00 | 8.00 | 8.00 |
| Developed Strands Factor | | 0.07 | 0.16 | 0.25 | 0.35 | 0.44 | 0.53 | 0.63 | 0.72 | 0.81 | 0.91 | 1.00 |
| Developed # Top Strands | # | 0.13 | 0.32 | 0.51 | 0.69 | 0.88 | 1.07 | 1.25 | 1.44 | 1.63 | 1.81 | 2.00 |
| Developed # Bottom Strands | # | 0.53 | 1.27 | 2.02 | 2.77 | 3.52 | 4.26 | 5.01 | 5.76 | 6.51 | 7.25 | 8.00 |
| Non-composite DL Moment (BM+SL) | FT-KIP | 0.00 | 7.95 | 15.62 | 23.02 | 30.15 | 37.01 | 43.60 | 49.91 | 55.95 | 61.71 | 67.21 |
| Total DL Shear (BM+SL) | KIP | 11.68 | 11.30 | 10.91 | 10.53 | 10.14 | 9.76 | 9.37 | 8.99 | 8.60 | 8.22 | 7.83 |
| Available Moment Capacity | FT-KIP | 112.72 | 264.47 | 416.49 | 568.78 | 721.34 | 874.18 | 1027.29 | 1180.67 | 1334.32 | 1488.25 | 1642.43 |
| Ultimate Moment, $M_u$ | FT-KIP | 0.00 | 172.19 | 344.11 | 515.75 | 687.13 | 858.23 | 1029.05 | 1199.61 | 1369.89 | 1539.90 | 1709.64 |
| Ultimate Shear, $V_u$ | KIP | 243.55 | 243.17 | 242.78 | 242.40 | 242.01 | 241.63 | 241.24 | 240.86 | 240.47 | 240.09 | 239.70 |
| $f_d$ | KSI | 0.000 | 0.030 | 0.058 | 0.086 | 0.112 | 0.138 | 0.162 | 0.186 | 0.208 | 0.230 | 0.250 |
| SFPF (Based on $l_d$) | KIPS | 21.25 | 51.34 | 81.44 | 111.54 | 141.64 | 171.74 | 201.84 | 231.94 | 262.04 | 292.13 | 322.23 |
| $f_{pe}$ | KSI | -0.102 | -0.246 | -0.391 | -0.535 | -0.680 | -0.824 | -0.969 | -1.113 | -1.258 | -1.402 | -1.547 |
| $M_{CR}$ | FT-KIP | 277.69 | 332.36 | 387.51 | 443.15 | 499.27 | 555.87 | 612.96 | 670.53 | 728.58 | 787.12 | 846.13 |
| $V_d$ (Flexure Shear) | KIPS | 31.73 | 491.86 | 295.52 | 230.01 | 197.19 | 177.46 | 164.27 | 154.82 | 147.70 | 142.14 | 137.67 |
| FPF (Based on $l_b$) | KIPS | 89.92 | 217.32 | 322.23 | 322.23 | 322.23 | 322.23 | 322.23 | 322.23 | 322.23 | 322.23 | 322.23 |
| $f_{pc}$ | KSI | -0.132 | -0.336 | -0.507 | -0.523 | -0.539 | -0.554 | -0.569 | -0.583 | -0.596 | -0.609 | -0.621 |
| $V_{cw}$ (Web Shear) | KIPS | 74.53 | 88.79 | 100.70 | 101.85 | 102.96 | 104.02 | 105.04 | 106.02 | 106.95 | 107.85 | 108.70 |
| $V_c$ | KIPS | 31.73 | 88.79 | 100.70 | 101.85 | 102.96 | 104.02 | 105.04 | 106.02 | 106.95 | 107.85 | 108.70 |
| $V_u/\phi$ | KIPS | 243.55 | 243.17 | 242.78 | 242.40 | 242.01 | 241.63 | 241.24 | 240.86 | 240.47 | 240.09 | 239.70 |
| Shear Steel Beyond Minimum Required | Y/N | YES | YES | YES | YES | YES | YES | YES | YES | YES | YES | YES |
| Web Crushing | | CRUSH | CRUSH | OK | OK | OK | OK | OK | OK | OK | OK | OK |
| Required Strength of Steel, Vs | KIPS | 211.82 | 154.38 | 142.08 | 140.55 | 139.06 | 137.61 | 136.21 | 134.84 | 133.52 | 132.24 | 131.01 |
| Required Stirrup Spacing, s | IN | 4.54 | 6.23 | 6.77 | 6.84 | 6.92 | 6.99 | 7.06 | 7.13 | 7.20 | 7.27 | 7.34 |
| Actual Stirrup Spacing, s | IN | 2.00 | | | | | | 7.00 | | | | |
| Strength of Steel, Vs | KIPS | 480.81 | 137.37 | 137.37 | 137.37 | 137.37 | 137.37 | 137.37 | 137.37 | 137.37 | 137.37 | 137.37 |
| Total Beam Shear Strength, Vc + Vs | KIPS | 512.54 | 226.16 | 238.08 | 239.23 | 240.33 | 241.39 | 242.41 | 243.39 | 244.33 | 245.22 | 246.07 |
| Beam "AS BUILT" Shear Capacity | P/F | PASS | FAIL | FAIL | FAIL | FAIL | FAIL | PASS | PASS | PASS | PASS | PASS |
| Ratio of (Vc + Vs)/(Vu/$\phi$) | NONE | 2.10 | 0.93 | 0.98 | 0.99 | 0.99 | 1.00 | 1.00 | 1.01 | 1.02 | 1.02 | 1.03 |

491

Table K.9 Deflection Calculations

## G1C-W — Predicted Approximate Deflection Calculations

### Member and Section Dimensions

| Description | Symbol | Value | Units |
|---|---|---|---|
| Distance from Left Support to Load | a | 85.001 | IN |
| Distance from Load to Right Support | b | 418.999 | IN |
| Distance Between Supports | $L_1$ | 504 | IN |
| Height of Beam | DB | 36 | IN |
| Deck Thickness | $t_d$ | 11.875 | IN |
| Bottom of Beam to Bottom Strands | BCL | 3.00 | IN |
| Moment of Inertia | $I_c$ | 144285 | $IN^4$ |
| Beam Mod. Of Elast. At Testing (Est) | $E_{cb}$ | 3.69E+06 | PSI |
| Web Thickness | WS | 6 | IN |
| Depth to Prestressing Steel | $d_p$ | 38.78 | IN |
| Shear Modulus Factor (Cracking) | G Factor | | None |
| Shear Modulus Factor (Ultimate) | G Factor | | None |
| Shape Factor for Shear (I Section) | k | 1 | None |
| Length of Plastic Hinge at Point of Loading | $L_{age}$ | 44.88 | IN |

### Girder Predicted Values

| Description | Symbol | Value | Units |
|---|---|---|---|
| Predicted Cracking Moment | $M_{cr}$ | 970.63 | FT-KIP |
| Dead Load Moment | $M_{DL}$ | 67.21 | FT-KIP |
| Predicted Applied Cracking Load | $P_{cr}$ | 153.41 | KIP |
| Predicted L Support Reaction at Cracking | $R_{lcr}$ | 127.54 | KIP |
| Predicted R Support Reaction at Cracking | $R_{rcr}$ | 25.87 | KIP |
| Predicted Curvature at Cracking | $\phi_{cr}$ | 0.000013 | RAD/IN |

### Girder Predicted Ultimate Values Using a Cracked Section Analysis

| Description | Symbol | Value | Units |
|---|---|---|---|
| Maximum Experimentally Applied Load | $P_{alt}$ | 290.31 | KIP |
| Maximum Left Support Reaction | $R_l$ | 241.35 | KIP |
| Maximum Right Support Reaction | $R_r$ | 48.96 | KIP |
| Predicted Curvature at Ultimate | $\phi_{alt}$ | 0.000358 | RAD/IN |

### First Moment WRT Right Support

| | Dist From L Supt (IN) | Area of Section (RAD) | | Dist Cent to R Supt (IN) | | A*C (IN) |
|---|---|---|---|---|---|---|
| $X_1$ | 44.92 | $A_1$ | 0.0002944 | $C_1$ | 474.05 | 0.1396 |
| $X_2$ | 62.56 | $A_2$ | 0.0002313 | $C_2$ | 450.26 | 0.1041 |
| $X_3$ | 85.00 | $A_3$ | 0.0030466 | $C_3$ | 447.32 | 1.3628 |
| $X_4$ | 107.44 | $A_4$ | 0.0080421 | $C_4$ | 430.22 | 3.4599 |
| $X_5$ | 282.58 | $A_5$ | 0.0080421 | $C_5$ | 407.78 | 3.2794 |
| $X_6$ | 504.00 | $A_6$ | 0.0022959 | $C_6$ | 308.99 | 0.7094 |
| | | $A_7$ | 0.0302401 | $C_7$ | 338.18 | 10.2266 |
| | | $A_8$ | 0.0014512 | $C_8$ | 147.61 | 0.2142 |

| | | |
|---|---|---|
| $\theta_L$*L (IN) | | 19.4960 |
| $\theta_L$ (RAD) | | 0.0387 |
| $\theta_L$*a (IN) | | 3.2881 |

### First Moment WRT Point of Loading

| Area of Section (RAD) | | Dist Cent to Load (IN) | | A*C (IN) |
|---|---|---|---|---|
| $A_1$ | 0.0002944 | $CP_1$ | 55.06 | 0.0162 |
| $A_2$ | 0.0002313 | $CP_2$ | 31.26 | 0.0072 |
| $A_3$ | 0.0030466 | $CP_3$ | 28.32 | 0.0863 |
| $A_4$ | 0.0080421 | $CP_4$ | 11.22 | 0.0902 |
| | | $\Delta P_\theta$ | | 0.1999 |

### Deflections Due to Predicted Loads at Cracking and Ultimate

| Stage of Loading | Flexure | Shear | Flexure + Shear | Units |
|---|---|---|---|---|
| Cracking | 0.241 | 0.03154 | 0.273 | IN |
| Ultimate | 3.088 | 0.05968 | 3.148 | IN |

492

Table K.10  Variable Angle Truss Model

## Variable Angle Truss Model

### G1C-W — Variables and Values

| Variable | Value | Units |
|---|---|---|
| $V_{ult} = V_{DL} + V_{applied}$ | 260.29 | KIPS |
| Shear Area, $A_v$ | 0.4 | IN² |
| Yield Strength of Stirrups, $f_y$ | 62 | KSI |
| Top of Deck to Centroid of PT, $d_p$ | 38.78 | IN |
| Maximum Depth of RSB, $a$ | 6.51 | IN |
| $f^*_{su}$ | 264.60 | KSI |
| Stirrup Spacing | 7.00 | IN |
| Shear Span | 85.00 | IN |
| XDIST | 6.00 | IN |
| Maximum Crack Angle | 70 | Deg |
| Minimum Crack Angle (A2.5) | 25 | Deg |
| $F_{stirrup}$ | 24.8 | KIPS |
| Min 1st Stirrup Distance from Load | 12.93 | IN |
| Max Nth Stirrup Distance from Load | 76.17 | IN |
| Maximum Stirrups in Fan | 9 | EACH |
| # Stirrups Req'd for $V_{ult}$ | 11 | EACH |
| Total Stirrups Available | 11 | EACH |
| Internal Moment Arm, jd | 35.52 | IN |
| Total Strand Force Based on $f_{su}^*$, $f_{se}$ | 526.54 | KIPS |
| Nominal Strand Circumference | 1.885 | IN |
| Maximum VATM Predicted Shear | 223.2 | KIPS |
| Maximum VATM Predicted Moment | 1581.0 | FT-KIP |
| Compression Field Crack Angle θ | 29.41 | DEG |
| **Compression Strut (Based on $V_{ult}$)** | | |
| Width of Strut (jd cos θ) | 30.94 | IN |
| Compressive Force D | 530.01 | KIPS |
| Compressive Stress in Strut, $f_{cd}$ | 2.86 | KSI |
| Lightweight Concrete Factor, l | 0.85 | None |
| Allowable Stress in Strut, A3.2 | 3.86 | KSI |
| **VATM IS CONSERVATIVE** | | |

### Variable Angle Truss Model

| Stirrup # | Distance From Load (IN) | Stirrup Force (KIPS) | X/jd | $F_{strand}$ Reduction (KIPS) | $F_{strand}$ Remaining (KIPS) |
|---|---|---|---|---|---|
| 1 | 15.00 | 24.80 | 0.422 | 10.47 | 516.06 |
| 2 | 22.00 | 24.80 | 0.619 | 15.36 | 500.70 |
| 3 | 29.00 | 24.80 | 0.817 | 20.25 | 480.45 |
| 4 | 36.00 | 24.80 | 1.014 | 25.14 | 455.32 |
| 5 | 43.00 | 24.80 | 1.211 | 30.03 | 425.29 |
| 6 | 50.00 | 24.80 | 1.408 | 34.91 | 390.38 |
| 7 | 57.00 | 24.80 | 1.605 | 39.80 | 350.58 |
| 8 | 64.00 | 24.80 | 1.802 | 44.69 | 305.89 |
| 9 | 71.00 | 24.80 | 1.999 | 49.58 | 256.31 |
| 10 | 78.00 | 24.80 | 1.774 | 43.99 | 212.32 |
| 11 | 85.00 | 24.80 | 1.774 | 43.99 | 168.33 |

### Plot Data

| Distance (IN) | $F_{strand}$ (KIPS) | $l_e$ (IN) | $\sigma_{bond}$ (KSI) |
|---|---|---|---|
| 85.00 | 526.54 | 91.00 | 0.3070 |
| 70.00 | 526.54 | 76.00 | 0.3675 |
| 70.00 | 516.06 | 76.00 | 0.3602 |
| 63.00 | 516.06 | 69.00 | 0.3968 |
| 63.00 | 500.70 | 69.00 | 0.3850 |
| 56.00 | 500.70 | 62.00 | 0.4284 |
| 56.00 | 480.45 | 62.00 | 0.4111 |
| 49.00 | 480.45 | 55.00 | 0.4634 |
| 49.00 | 455.32 | 55.00 | 0.4392 |
| 42.00 | 455.32 | 48.00 | 0.5032 |
| 42.00 | 425.29 | 48.00 | 0.4700 |
| 35.00 | 425.29 | 41.00 | 0.5503 |
| 35.00 | 390.38 | 41.00 | 0.5051 |
| 28.00 | 390.38 | 34.00 | 0.6091 |
| 28.00 | 350.58 | 34.00 | 0.5470 |
| 21.00 | 350.58 | 27.00 | 0.6888 |
| 21.00 | 305.89 | 27.00 | 0.6010 |
| 14.00 | 305.89 | 20.00 | 0.8114 |
| 14.00 | 256.31 | 20.00 | 0.6799 |
| 7.00 | 256.31 | 13.00 | 1.3075 |
| 7.00 | 212.32 | 13.00 | 1.0831 |
| 0.00 | 212.32 | 6.00 | 2.3467 |
| 0.00 | 168.33 | 6.00 | 1.8605 |
|  | 168.33 |  |  |

Angle minimum and maximum values and the allowable stress in the compressive strut are based on ACI318-02. Changes are in CI, June 2001, pp. 125-132. Bond stress inside 1 stirrup space from the support is based on only the bottom 8 strands. Stirrup spacing initiates at the support and moves to the load. All plot data is based on the ultimate (experimental) shear value.

493
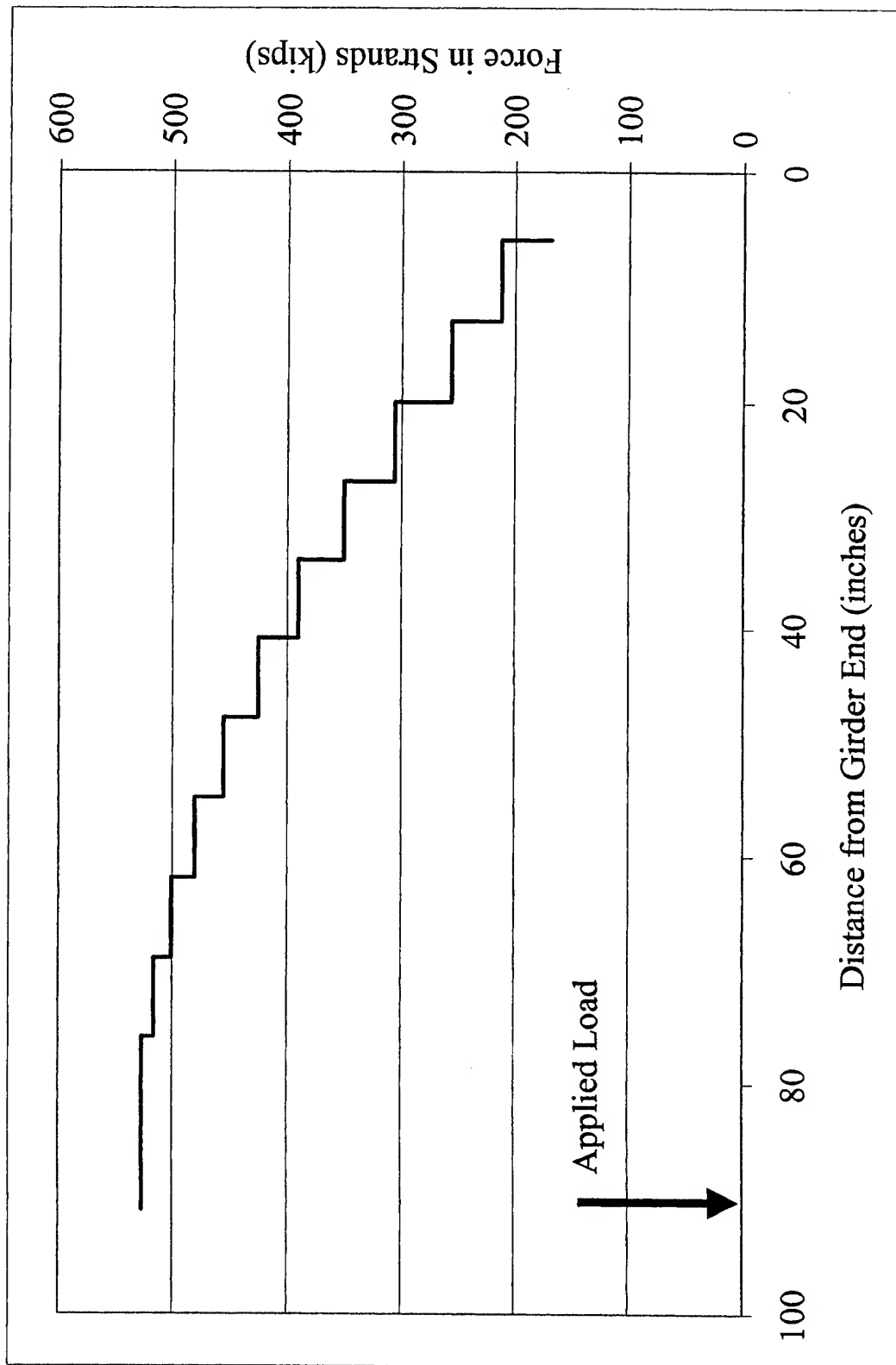
Figure K.1  Force in Prestressing Strands vs. Distance From Girder End
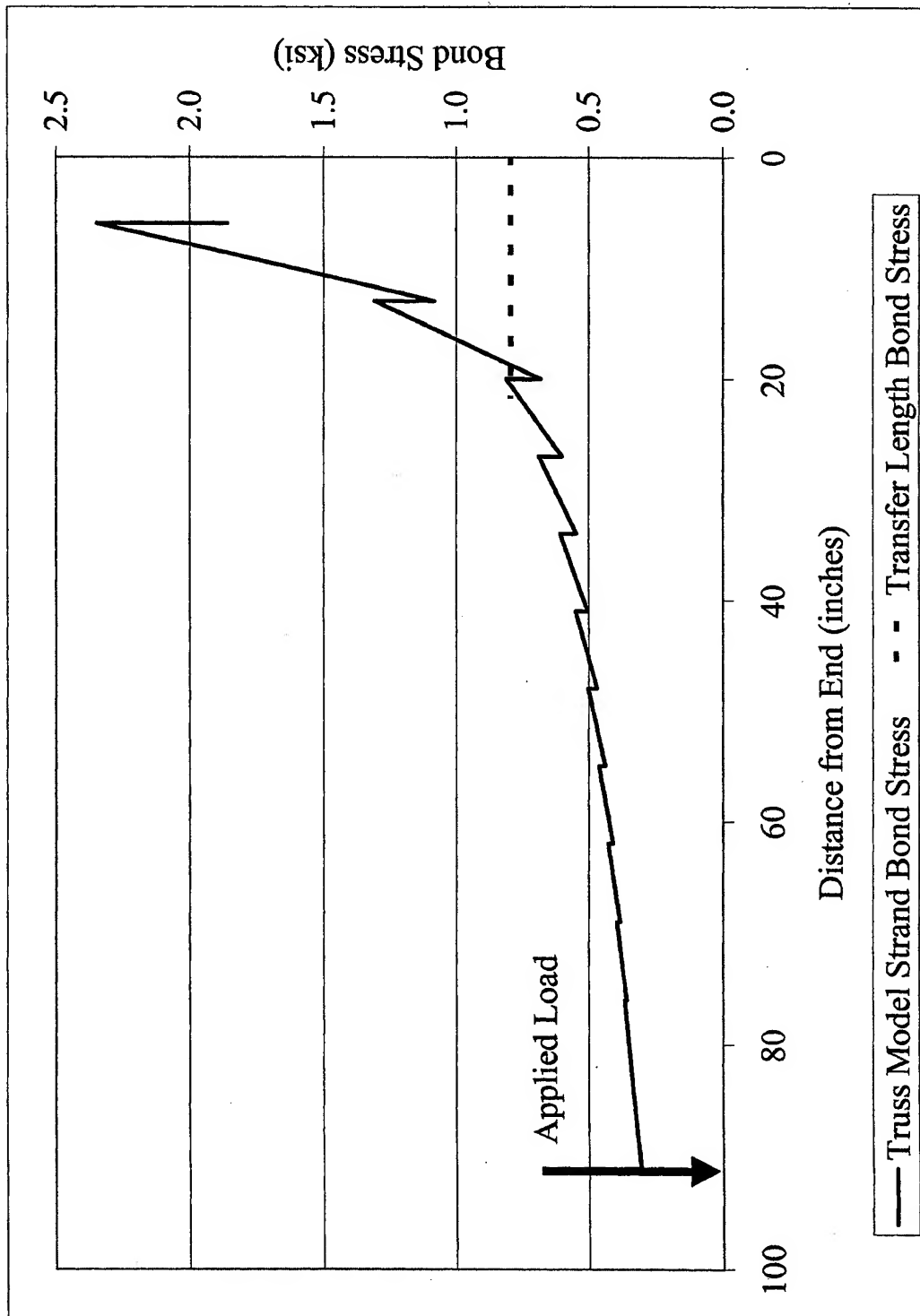
Figure K.2 Prestressing Strand Bond Stress vs. Distance From Girder End

495

Table K.11 Theoretical Moment-Curvature Stages 1 - 3 (Elastic Portion)

## Theoretical Moment-Curvature (Elastic Portion)

### G1C-W

**Stage 1 - No Load**

| Description | Symbol | Value | Units |
|---|---|---|---|
| NC Moment of Inertia | $I_{nc}$ | 50979 | $IN^4$ |
| NC Section Modulus (Top) | $S_{top-nc}$ | 2527.47 | $IN^3$ |
| NC Section Modulus (Bot) | $S_{bot-nc}$ | 3220.40 | $IN^3$ |
| NC Girder Area | $A_{nc}$ | 369 | $IN^2$ |
| NC Girder Height | DB | 36 | IN |
| Ecc from NC Centroid | e | -6.73 | IN |
| Girder $E_c$ (Est) | $E_{cg}$ | 3.69E+06 | PSI |
| Effective PT Force | $F_{se}$ | 322.23 | KIPS |
| $M_{DL}$ | $M_{DL}$ | 67.21 | FT-KIP |

| NC Girder Stress | TOP | BOTTOM | |
|---|---|---|---|
| Axial Prestress | -0.873 | -0.873 | KSI |
| Eccentricity Prestress | 0.858 | -0.673 | KSI |
| Dead Load Moment | -0.319 | 0.250 | KSI |
| Total Concrete Stress | -0.334 | -1.296 | KSI |
| Total Concrete Strain | -90.5 | -350.9 | µe |
| Conc Strain at Bot Strands | $\varepsilon_{ce}$ | -329.2 | µe |
| Conc Stress at Bot Strands | $\sigma_{ce}$ | -1.2161 | KSI |
| Steel Strain in Bot Strands | $\varepsilon_{se}$ | 5053.0 | µe |
| Curvature of Girder | -7.23E-06 | | rad/in |

**Stage 2 - Zero Strain in Conc at Bot Strand Level**

| Description | Symbol | Value | Units |
|---|---|---|---|
| C Moment of Inertia | $I_c$ | 144285 | $IN^4$ |
| C Section Modulus (Girder) | $S_{top-c}$ | 13436 | $IN^3$ |
| C Section Modulus (Girder) | $S_{bot-c}$ | 5712 | $IN^3$ |
| C Girder Area | $A_c$ | 577.68 | $IN^2$ |
| Deck Thickness | $t_d$ | 11.875 | IN |
| C Centroid to NC Girder Bot | $Y_{bot-c}$ | 25.26 | IN |
| NC Girder Top to Top Strds | TCL | 2.50 | IN |
| NC Girder Bot to Bot Strds | BCL | 3.00 | IN |
| Required Additional Moment | $M_2$ | 656.83 | FT-KIP |
| Total Moment $(M_{DL}+M_2)$ | | 724.04 | FT-KIP |

| NC Girder Stress | TOP | BOTTOM | |
|---|---|---|---|
| Axial Prestress | -0.873 | -0.873 | KSI |
| Eccentricity Prestress | 0.858 | -0.673 | KSI |
| Dead Load Moment | -0.319 | 0.250 | KSI |
| Additional Moment $M_2$ | -0.587 | 1.380 | KSI |
| Total Concrete Stress | -0.921 | 0.084 | KSI |
| Total Concrete Strain | -249 | 23 | µe |
| Steel Strain in Bot Strands | $\varepsilon_{s2}$ | 5382.2 | µe |
| Curvature of Girder | 7.56E-06 | | rad/in |

**Stage 3 - Cracking on Bottom Fiber**

| Description | Symbol | Value | Units |
|---|---|---|---|
| Tension Strength Factor | a | 7.5 | None |
| LWC Reduction Factor | 1 | 0.85 | None |
| Concrete Actual Strength | $f'_c$ | 8911 | PSI |
| Rupture Stress | $f_r$ | 0.602 | KSI |
| Required Addl Stress | $f_3$ | 0.518 | KSI |
| Required Addl Moment | $M_3$ | 246.59 | FT-KIP |
| Total Moment $(M_{DL}+M_2+M_3)=M_{CR}$ | | 970.63 | FT-KIP |

| NC Girder Stress | TOP | BOTTOM | |
|---|---|---|---|
| Axial Prestress | -0.873 | -0.873 | KSI |
| Eccentricity Prestress | 0.858 | -0.673 | KSI |
| Dead Load Moment | -0.319 | 0.250 | KSI |
| Additional Moment $M_2$ | -0.587 | 1.380 | KSI |
| Additional Moment $M_3$ | -0.22 | 0.518 | KSI |
| Total Concrete Stress | -1.141 | 0.602 | KSI |
| Total Concrete Strain | -309.0 | 162.9 | me |
| Conc Strain at Bot Strands | $\varepsilon_{ce}$ | 123.6 | me |
| Conc Strain on Top of Deck | $\varepsilon_{cd}$ | -460.0 | me |
| Steel Strain in Bot Strands | $\varepsilon_{s3}$ | 5505.8 | me |
| Curvature of Girder | 1.31E-05 | | rad/in |

Table K.12  Theoretical Moment-Curvature Stages 4-6 (Cracked Portion)

**G1C-W — Theoretical Moment-Curvature (Cracked Portion)**

| Parameter | Symbol | Stage 4 – Deck Strain = 1000 | units | Stage 5 – Deck Strain = 2000 | units | Stage 6 – Deck Strain = 3000 | units |
|---|---|---|---|---|---|---|---|
| Conc Strain on Top of Deck | $\varepsilon_{cd}$ | 1000.0 | με | 2000.0 | με | 3000.0 | με |
| Guess for NA Depth "c" | $c$ | (5.500) | IN | (9.80) | IN | | IN |
| Resulting Top Strand Strain | $\varepsilon_{set}$ | 5011.3 | με | 6216.4 | με | 7698.8 | με |
| Resulting Top Strand Stress | $\sigma_{set}$ | 146.39 | KSI | 181.59 | KSI | 224.10 | KSI |
| Resulting Top Strand Force | $F_{set}$ | 63.91 | KIPS | 79.28 | KIPS | 97.84 | KIPS |
| Bot Strand Strain Increase | $\varepsilon_{sebi}$ | 2991.7 | με | 9074.8 | με | 16084.2 | με |
| Resulting Bot Strand Strain | $\varepsilon_{seb}$ | 8373.9 | με | 14457.1 | με | 21466.5 | με |
| Resulting Bot Strand Stress | $\sigma_{seb}$ | 239.20 | KSI | 264.58 | KSI | 267.17 | KSI |
| Resulting Bot Strand Force | $F_{seb}$ | 417.73 | KIPS | 462.06 | KIPS | 466.58 | KIPS |
| Resulting Strand Force | $F_{se}$ | 481.65 | KIPS | 541.34 | KIPS | 564.42 | KIPS |
| Resulting Concrete Force | $F_c$ | 481.22 | KIPS | 542.26 | KIPS | 564.83 | KIPS |
| Within Tolerance | | YES | Y/N | YES | Y/N | YES | Y/N |
| Resulting Moment | $M_4$ / $M_5$ / $M_6$ | 1433.0012 | FT-KIP | 1661.3037 | FT-KIP | 1709.5994 | FT-KIP |
| Curvature of Girder | | 6.67E-05 | rad/in | 2.02E-04 | rad/in | 3.58E-04 | rad/in |
| Todeschini Variable | $f''_c$ | 4845.6 | PSI | 4845.6 | PSI | 4845.6 | PSI |
| Todeschini Variable | $\varepsilon_0$ | 2748.3 | με | 2748.3 | με | 2748.3 | με |
| Todeschini Variable | $x$ | 0.364 | None | 0.728 | None | 1.092 | None |
| Todeschini Variable | $\beta_1$ | 0.342 | None | 0.584 | None | 0.719 | None |
| Todeschini Variable | $k_2$ | 0.342 | None | 0.362 | None | 0.387 | None |
| Average Stress | $\sigma_{avg}$ | 1656 | PSI | 2830 | PSI | 3483 | PSI |

497

Figure K.3 Moment-Curvature Plot

Table K.13  Girder Shear Capacity by 1998 AASHTO[92] LRFD Procedure

| G1C-W | | Beam Shear Capacity AASHTO LRFD-98 (Left of Point Load) | | | | | | | | | | |
|---|---|---|---|---|---|---|---|---|---|---|---|---|
| | IN | L-SUPT | 0.1 a | 0.2 a | 0.3 a | 0.4 a | 0.5 a | 0.6 a | 0.7 a | 0.8 a | 0.9 a | P-LOAD |
| Distance from Left Support (Inches) | IN | 0.00 | 8.50 | 17.00 | 25.50 | 34.00 | 42.50 | 51.00 | 59.50 | 68.00 | 76.50 | 85.00 |
| Ultimate Moment Furnished | FT-KIP | 112.72 | 272.42 | 432.11 | 591.80 | 751.50 | 911.19 | 1070.88 | 1230.58 | 1390.27 | 1549.96 | 1709.64 |
| Developed # Top Strands | # | 0.13 | 0.32 | 0.51 | 0.69 | 0.88 | 1.07 | 1.25 | 1.44 | 1.63 | 1.81 | 2.00 |
| Developed # Bottom Strands | # | 0.53 | 1.27 | 2.02 | 2.77 | 3.52 | 4.26 | 5.01 | 5.76 | 6.51 | 7.25 | 8.00 |
| Non-composite DL Moment (BM+SL) | FT-KIP | 0.00 | 7.95 | 15.62 | 23.02 | 30.15 | 37.01 | 43.60 | 49.91 | 55.95 | 61.71 | 67.21 |
| Total DL Shear (BM+SL) | KIP | 11.68 | 11.30 | 10.91 | 10.53 | 10.14 | 9.76 | 9.37 | 8.99 | 8.60 | 8.22 | 7.83 |
| Available Moment Capacity | FT-KIP | 112.72 | 264.47 | 416.49 | 568.78 | 721.34 | 874.18 | 1027.29 | 1180.67 | 1334.32 | 1488.25 | 1642.43 |
| Ultimate Moment, $M_u$ | FT-KIP | 0.00 | 172.19 | 344.11 | 515.75 | 687.13 | 858.23 | 1029.05 | 1199.61 | 1369.89 | 1539.90 | 1709.64 |
| Ultimate Shear, $V_u$ | KIP | 243.55 | 243.17 | 242.78 | 242.40 | 242.01 | 241.63 | 241.24 | 240.86 | 240.47 | 240.09 | 239.70 |
| Stress in Prestressing Strands at $M_u$, $f_{ps}$ | KSI | 9.73 | 23.52 | 37.31 | 51.10 | 64.88 | 78.67 | 92.46 | 106.25 | 120.03 | 133.82 | 264.60 |
| Depth of Compression Block, a | IN | 0.24 | 0.58 | 0.92 | 1.26 | 1.60 | 1.94 | 2.28 | 2.62 | 2.96 | 3.29 | 6.51 |
| Effective Shear Depth, $d_v$ | IN | 38.66 | 38.49 | 38.32 | 38.15 | 37.98 | 37.81 | 37.64 | 37.47 | 37.30 | 37.13 | 35.52 |
| Effective Area of Prestress, $A_{pse}$ | IN² | 0.12 | 0.28 | 0.44 | 0.60 | 0.77 | 0.93 | 1.09 | 1.26 | 1.42 | 1.58 | 1.75 |
| Shear Stress on Concrete, $v / f'_c$ | None | 0.118 | 0.118 | 0.119 | 0.119 | 0.119 | 0.120 | 0.120 | 0.120 | 0.121 | 0.121 | 0.126 |
| Measured θ From Beam | DEG | 30.? | 30.? | 30.? | 30.? | 30.? | 30.? | 30.? | 30.? | 30.? | 30.? | 30.? |
| Strain in Reinforcement, $\varepsilon_{x, Actual}$ | IN/IN | 0.0581 | 0.0277 | 0.0198 | 0.0161 | 0.0141 | 0.0128 | 0.0118 | 0.0112 | 0.0107 | 0.0103 | 0.0104 |
| Strain in Reinforcement, $\varepsilon_{x, Allowed}$ | IN/IN | 0.0020 | 0.0020 | 0.0020 | 0.0020 | 0.0020 | 0.0020 | 0.0020 | 0.0020 | 0.0020 | 0.0020 | 0.0020 |
| Adjustment Factor for "-" Value, $F_e$ | None | NA | NA | NA | NA | NA | NA | NA | NA | NA | NA | NA |
| Strain in Reinforcement, $\varepsilon_{x, Allowed}$ | IN/IN | 0.0020 | 0.0020 | 0.0020 | 0.0020 | 0.0020 | 0.0020 | 0.0020 | 0.0020 | 0.0020 | 0.0020 | 0.0020 |
| Value of β From Figure | None | ? | ? | ? | ? | ? | ? | ? | ? | ? | ? | ? |
| Shear Strength of Concrete, $V_c$ | KIPS | 24.18 | 24.07 | 23.96 | 23.86 | 23.75 | 23.64 | 23.54 | 23.43 | 23.33 | 23.22 | 22.21 |
| Stirrup Spacing, s | IN | 2.00 | 7.00 | 7.00 | 7.00 | 7.00 | 7.00 | 7.00 | 7.00 | 7.00 | 7.00 | 7.00 |
| Strength of Steel, $V_s$ | KIPS | 830.21 | 236.16 | 235.12 | 234.08 | 233.04 | 232.00 | 230.95 | 229.91 | 228.87 | 227.83 | 217.95 |
| Total Beam Shear Strength, $V_c + V_s$ | KIPS | 854.39 | 260.23 | 259.08 | 257.94 | 256.79 | 255.64 | 254.49 | 253.35 | 252.20 | 251.05 | 240.16 |
| Beam "AS BUILT" Shear Capacity | P/F | PASS | PASS | PASS | PASS | PASS | PASS | PASS | PASS | PASS | PASS | PASS |
| Ratio of $(V_c + V_s) / (V_u / \phi)$ | NONE | 3.51 | 1.07 | 1.07 | 1.06 | 1.06 | 1.06 | 1.05 | 1.05 | 1.05 | 1.05 | 1.00 |
| Longitudinal Reinforcement Satisfied | Y/N | YES | NO | NO | NO | NO | NO | NO | NO | NO | NO | NO |
| Addl Non-Prestressed Steel Required | IN² | NA | 3.17 | 3.35 | 3.54 | 3.73 | 3.93 | 4.14 | 4.35 | 4.57 | 4.80 | 5.52 |

Table K.14  Girder-Deck Interface Shear Calculations

| G1C-W | Deck / Beam Interface Shear Calculations (AASHTO-STD '96) | | |
|---|---|---|---|

**Interface Shear Calculation Values**

| Description | Symbol | Value | Units |
|---|---|---|---|
| Lightweight Concrete Reduction Factor | | 0.85 | None |
| Shear Strength Reduction Factor | $\phi_s$ | 1.00 | None |
| Maximum Unfactored Shear | $V_u$ | 243.55 | KIPS |
| First Moment of Deck About Centroid | QS | 3480.00 | IN³ |
| Composite Moment of Inertia | $I_c$ | 144285 | IN⁴ |
| Interface Shear Contact Width | $b_v$ | 12 | IN |
| Contact Length, d (a+XDIST<=SPAN/10) | Span/10 | 50.40 | IN |
| Contact Area ($b_v$*Contact Length) | $A_c$ | 604.8 | IN² |
| Yield Strength of Tie Reinforcement | $f_y$ | 62 | KSI |
| Stirrup Area | $A_v$ | 0.4 | IN² |

**Interface Condition**

| Description | Symbol | Value | Units |
|---|---|---|---|
| Contact Surface Clean | | | YES/NO |
| Contact Surface Roughened 1/4" | | | YES/NO |
| Minimum Ties Provided | | YES | YES/NO |
| Maximum Basic Interface Stress | | 350 | PSI |
| Maximum Basic Interface Force | $V_{nh}$ | 211.68 | KIPS |
| **Basic Interface Shear Capacity Inadequate** | | | |

**Tensile Stress at Interface**

| Description | Symbol | Value | Units |
|---|---|---|---|
| Deck Concrete Actual Strength | $f'_c$ | 5384 | PSI |
| Maximum Allowable Deck Tensile Stress | | 550.32 | PSI |
| Beam Concrete Actual Strength | $f'_c$ | 8911 | PSI |
| Maximum Allowable Beam Tensile Stress | | 601.79 | PSI |
| Maximum Interface Shear Stress (VQ/Ib) | $v_h$ | 489.52 | PSI |
| Effective Prestress Force | $F_{se}$ | 322.23 | KIPS |
| Beam Cross Sectional Area | $A_{bm}$ | 369 | IN² |
| Strand Eccentricity from NC Centroid | e | -6.73 | IN |
| Distance from NC Centroid to Beam Top | $y_{top}$ | 20.17 | IN |
| Distance from C Centroid to Beam Top | $y_{top}$ | 10.74 | IN |
| Non-Composite Moment of Inertia | $I_{nc}$ | 50979 | IN⁴ |
| Composite Moment of Inertia | $I_c$ | 144285 | IN⁴ |
| Dead Load Moment | $M_{DL}$ | 67.21 | FT-KIP |
| Live Load Moment | $M_{LL}$ | 1642.43 | FT-KIP |
| Maximum Compressive Stress at Interface | $f_{ca}$ | -1801.27 | PSI |
| Maximum Tensile Stress at Interface | $f_t$ | 124.438 | PSI |
| **Tensile Stress at Interface is OK** | | | |

**Additional Interface Capacity Provided by Shear Reinforcement**

| Description | Symbol | Value | Units |
|---|---|---|---|
| Additional Interface Capacity Required | | 31.87 | KIPS |
| Worst Case Stirrup Spacing over "a" | s | 7.00 | IN |
| Minimum Tie Area per Inch of Beam | | 0.0097 | IN²/IN |
| Additional $V_{nh}$ Capacity per Percent | | 150.0 | KIPS |
| Additional Percent Required | | 0.21 | % |
| Additional Required Tie Area | | 0.000021 | IN²/IN |
| Total Tie Area Required | | 0.009698 | IN²/IN |
| Min. Tie Area Provided by V Reinforcement | | 0.057143 | IN²/IN |
| Resulting Contact Area Stress | | 402.70 | PSI |
| **Interface Shear Capacity Adequate** | | | |

Table K.15  Prestressing Strand Tension Test Curve

## Prestressing Strand Tension Test Curve and Zone Limit Data

Strain -Stress Curve for 0.6-Inch Diameter 270 KSI LOLAX Strand

$y = 0.8063x + 56.5921$
$R^2 = 1.0000$

$y = 95.9317x^3 - 348.9161x^2 + 423.6514x - 114.2059$
$R^2 = 0.9985$

$y = 63.7701x + 0.0000$
$R^2 = 1.0000$

Strain (percent)

Strand Force (kips)

◆ Elastic   ■ Transition   ▲ Plastic   —— Linear (Elastic)   —— Linear (Plastic)   —— Poly. (Transition)

| Prestressing Strand Loading Data | | |
|---|---|---|
| Point of Loading | Strain (%) | Load (Kips) |
| Start of Elastic | 0 | 0.00 |
| End of Elastic | 0.7135 | 45.50 |
| Transition 1 | 0.7500 | 47.45 |
| Transition 2 | 0.8750 | 53.63 |
| Transition 3 | 1.0000 | 56.67 |
| Transition 4 | 1.1250 | 57.20 |
| Start of Plastic | 1.2500 | 57.60 |
| End of Plastic | 6.5000 | 61.83 |

| Zone | Percent Strain | | |
|---|---|---|---|
| Elastic | 0 | < e < | 0.7135 |
| Transition | 0.7135 | < e < | 1.2500 |
| Plastic | 1.2500 | > e | |

| Zone | Load | | |
|---|---|---|---|
| Elastic | 0 | < Kips < | 45.50 |
| Transition | 45.50 | < Kips < | 57.60 |
| Plastic | 57.60 | > Kips | |

Table K.16  Principal Strain and Maximum Shear Strain Plots

Figure K.4  Load Displacement Plot

Table K.17 Overview of Girder Test Results

| G1C-W | 4 | Single | 02-Nov-01 | | Units |
|---|---|---|---|---|---|
| **Support and Load Dimensions** | | | | | |
| Shear Span | a | 85.001 | IN | | |
| Distance Between Supports | L1 | 504 | IN | | |
| **Deck Variables** | | | | | |
| Deck Thickness | $t_d$ | 11.875 | IN | | |
| Deck Width | $W_f$ | 19.375 | IN | | |
| Concrete Strength at Testing | $f'_c$ | 5384 | PSI | | |
| Elasticity Modulus at Testing | $E_{cd}$ | 3.35E+06 | PSI | | |
| **Girder Variables** | | | | | |
| Concrete Strength at Release | $f'_{ci}$ | 6315 | PSI | | |
| Concrete Strength at Testing | $f'_c$ | 8911 | PSI | | |
| Concrete Equilibrium Weight | $W_c$ | 116.8 | PCF | | |
| Lightweight Concrete Factor | 1 | 0.85 | None | | |
| Elasticity Modulus at Release | $E_{ci}$ | 3.00E+06 | PSI | | |
| Elasticity Modulus at Test (Est) | $E_{cb}$ | 3.69E+06 | PSI | | |
| **Prestressing Strand Variables** | | | | | |
| Strand C/S Area | $A_{st}$ | 0.2183 | $IN^2$ | | |
| Strand Ultimate Strength | $f_{pu}$ | 283.25 | KSI | | |
| Strand Modulus of Elasticity | $E_{ps}$ | 29000 | KSI | | |
| Strand Percent $f_{pu}$ at Jacking | | 63% | % | | |
| Stress at Jacking | $f_{pt}$ | 179.11 | KSI | | |
| Stress after Release | $f_{si}$ | 162.11 | KSI | | |
| Stress after 14 Days | $f_{se}$ | 153.65 | KSI | | |
| Stress at Testing | $f_{se}$ | 147.61 | KSI | | |
| **Stirrup Variables** | | | | | |
| Strain at Testing | $\varepsilon_{se}$ | 5053 | $\mu\varepsilon$ | | |
| Strain at Ultimate Load | $\varepsilon_{ps}$ | 13960 | $\mu\varepsilon$ | | |
| Stirrup Size | | 4 | # | | |
| Stirrup Yield Strength | $f_y$ | 62 | KSI | | |

**Girder Test Overview**

| Value | | Predicted | Experimental | Units |
|---|---|---|---|---|
| Transfer Length | $l_t$ | 30.73 | 21.50 | IN |
| Development Length | $l_d$ | 100.56 | 91.00 | IN |
| Cracking Load | $P_{cr}$ | 153.41 | 183.00 | KIPS |
| Cracking Moment | $M_{cr}$ | 970.63 | 1144.85 | FT-KIPS |
| Rupture Stress | $f_r$ | 601.79 | 967.82 | PSI |
| Ultimate Load (AASHTO-Flexure) | $P_{ult}$ | 278.91 | 299.04 | KIPS |
| Ultimate Moment (AASHTO-Flexure) | $M_{ult}$ | 1709.64 | 1828.17 | FT-KIPS |
| Ultimate Load (Cracked Section) | $P_{ult}$ | 290.31 | 299.04 | KIPS |
| Ultimate Moment (Cracked Section) | $M_{ult}$ | 1709.60 | 1828.17 | FT-KIPS |
| Deflection at Cracking (Flex & Shear) | $\delta cr$ | 0.273 | 0.441 | IN |
| Ultimate Deflection (Flex & Shear) | $\delta ult$ | 3.148 | 2.270 | IN |
| Ultimate Concrete Deck Surface Strain | $\varepsilon_{cu}$ | 0.0030 | 0.0036 | IN/IN |
| Initial Losses on Release | ES | -12.62 | -17.00 | KSI |
| Time Dependant Losses (14-Day) | CR,SH | -35.41 | -25.46 | KSI |
| Time Dependant Losses (Test) | CR,SH | -35.69 | -31.50 | KSI |
| Web Shear Strength ($V_{cw\text{-}ALT}/V_{crack}$) | $V_{cw}$ | 123.3 | 134.2 | KIPS |
| Tensile Strength for Shear Cracking | $f_t''$ | 0.321 | 0.363 | KSI |
| Tensile Strength Factor (Includes $\lambda$) | $\xi_v$ | 4.00 | 4.52 | None |
| Strand Stress at Ultimate Load | $f_{ps}$ | 264.60 | 264.40 | KSI |
| Ultimate Shear Capacity (VATM/$V_{exp}$) | $V_{U\text{-}VATM}$ | 223.20 | 260.29 | KIPS |
| Ultimate Shear Capacity (STD/$V_{exp}$) | $V_{U\text{-}STD}$ | 241.39 | 260.29 | KIPS |
| Comp Field Angle (VATM/Girder) $\theta$ | | 29.4 | 30.0 | DEG |
| LVDT Rosette Tension Crack Angles (Low/High) | | 22.7 | 40.9 | DEG |

The predicted $f_t''$ is based on the ACI alternate technique specified in 11.4.2.2 using a of 4. The regular approach in 11.4.2.2 uses 3.5 as the multiplier as is seen in equation 11-12. a can be changed in the "predicted a" cell. The experimental $V_{cw}$ value is shear at which shear cracking occurred. The predicted $f_t''$ is based on the equation from Burns' book, page 254. The $f_{pc}$ value comes from the STD Shear Page at the 0.5a location.

# APPENDIX L

## MOMENT vs. CURVATURE PLOTS
## AND
## LOAD vs. DEFLECTION PLOTS


Appendix L contains moment vs. curvature plots and load vs. displacement plots

for each girder test. The predicted and experimental values are listed on both plots. The

following sections describe the calculations required for both plots.

### L.1 Moment-Curvature

Predicted moment and curvature values were determined at several stages

progressing from zero applied load to the ultimate applied load. The predicted moment

and curvature values were then used to predict deflections at the point of loading and for

comparison with experimental values. The process for calculating moment and curvature

values can be found in *Design of Prestressed Concrete Structures*, T.Y. Lin and Ned H.

Burns.[126] The process for determining stresses in a composite section can be found in

*Prestressed Concrete Structures*, Michael P. Collins and Denis Mitchell.[145] Several

assumptions were made to determine the values.

1. The concrete and prestressing strands were considered perfectly bonded.

Strains in the concrete and steel were considered to be the same.

2. The stress-strain relationship was known for the concrete and steel.

3. Strains were distributed linearly over the height of the girder.

4. The girder was in static equilibrium.

A Todeschini[151] stress distribution was assumed for the deck during the cracked section analysis. Moment and curvature values were determined at six specific points as described in the following sections. Tables K.11 and K.12 show calculation of moment and curvature values. Variables are defined in Appendix T.

### L.1.1  Stage 1 - Zero Applied Load

The following procedure was used to determine curvature with zero applied load.

$$f_{top} = -\frac{F_{se}}{A_{nc}} - \frac{F_{se}e}{S_{top-nc}} - \frac{M_{DL}}{S_{top-nc}} \qquad (L.1)$$

$$f_{bot} = -\frac{F_{se}}{A_{nc}} + \frac{F_{se}e}{S_{bot-nc}} + \frac{M_{DL}}{S_{bot-nc}} \qquad (L.2)$$

Strains at the top and bottom of the girder were calculated with the following equations:

$$\varepsilon_{top} = \frac{f_{top}}{E_{cg}} \qquad (L.3)$$

$$\varepsilon_{bot} = \frac{f_{bot}}{E_{cg}} \qquad (L.4)$$

The predicted curvature at Stage 1 was calculated with the following equation:

$$\phi = \frac{-(\varepsilon_{top} - \varepsilon_{bot})}{h_{g-nc}} \qquad (L.5)$$

The resulting stress in the concrete at the level of the bottom strands was calculated as:

$$\sigma_{ce} = \frac{(\varepsilon_{top} + (\varepsilon_{bot} - \varepsilon_{top})) * (h_{g-nc} - BCL)}{h_{g-nc}} * E_{cg} \qquad (L.6)$$

## L.1.2  Stage 2 – Zero Concrete Strain at the Level of Bottom Strands

The following procedure was used to determine the curvature at the point where the applied load produced zero concrete strain at the level of the bottom strands. This point is known as the "decompression load." The effect of the applied load was determined using the composite section properties. The effects of prestressing and any dead load moment were the same as in Stage 1. The effect of the applied load was added to the Stage 1 values to determine the total affect. To determine the applied moment required, $M_2$, to produce zero strain and thus zero stress in the concrete at the level of the bottom strands, the following equation was used. Refer to Table K.11.

$$M_2 = \frac{-\sigma_{ce} I_c}{(y_{bot-c} + BCL)} \qquad (L.7)$$

507

The resulting stresses at the top and bottom of the girder were calculated with the following equations:

$$f_{top} = -\frac{F_{se}}{A_{nc}} - \frac{F_{se}\,e}{S_{top-nc}} - \frac{M_{DL}}{S_{top-nc}} - \frac{M_2}{S_{top-c}} \qquad (L.8)$$

$$f_{bot} = -\frac{F_{se}}{A_{nc}} + \frac{F_{se}\,e}{S_{bot-nc}} + \frac{M_{DL}}{S_{bot-nc}} + \frac{M_2}{S_{bot-c}} \qquad (L.9)$$

The resulting strains at the top and bottom of the girder were calculated using equations L.3 and L.4. The resulting strain in the bottom strands was calculated using the following equation where the effective strain prior to applying load, $\varepsilon_{se}$, was determined from VWSG readings prior to girder testing.

$$\varepsilon_{s2} = \varepsilon_{se} - \frac{\sigma_{ce}}{E_{cg}} \qquad (L.10)$$

Curvature was calculated using equation L.5.

### L.1.3  Stage 3 – Cracking Stress on Bottom Fiber

The following procedure was used to determine the curvature at the point where the additional applied load produced a stress at the bottom fiber equal to the predicted

cracking stress, $f_{cr}$. The moment that produces the cracking stress on the bottom fiber is the cracking moment, $M_{cr}$. The predicted cracking stress was calculated using the following equation:

$$f_{cr} = 7.5\lambda\sqrt{f_c'}$$ (L.11)

The effect of the applied load was determined using the composite section properties. The effects of prestressing and any dead load moment were the same as in Stage 1. The effect of the applied load was added to the Stage 1 values to determine the total effect. To determine the additional applied moment required, $M_3$, to produce $M_{cr}$ and the cracking stress, $f_{cr}$, at the bottom fiber, the following equation was used. The subscript "-2" indicates the bottom stress from Stage 2.

$$M_3 = (f_{cr} - f_{bot-2})S_{bot-c}$$ (L.12)

The cracking moment, $M_{cr}$, was determined with the following equation:

$$M_{cr} = M_{DL} + M_2 + M_3$$ (L.13)

The total concrete stress at the top and bottom of the girder were calculated with the following equations:

509

$$f_{top} = -\frac{F_{se}}{A_{nc}} - \frac{F_{se}e}{S_{top-nc}} - \frac{M_{DL}}{S_{top-nc}} - \frac{M_2}{S_{top-c}} - \frac{M_3}{S_{top-c}} \qquad (L.14)$$

$$f_{bot} = -\frac{F_{se}}{A_{nc}} + \frac{F_{se}e}{S_{bot-nc}} + \frac{M_{DL}}{S_{bot-nc}} + \frac{M_2}{S_{bot-c}} + \frac{M_3}{S_{bot-c}} \qquad (L.15)$$

The resulting strains at the top and bottom of the girder were calculated with equations L.3 and L.4. The resulting strain in the bottom strands, $\varepsilon_{s3}$, was calculated with the following equation:

$$\varepsilon_{s3} = \varepsilon_{s2} + \frac{(f_{cr} - f_{bot-2})}{E_{cg}} * \left( \frac{y_{bot-c} - BCL}{y_{bot-c}} \right) \qquad (L.16)$$

Curvature was calculated using equation L.5.

## L.1.4 Cracked Section Analysis

Force equilibrium was used to calculate the moment and curvature values after cracking occurred. Once a strain on the surface of the deck or in the prestressing strand was assumed, the depth to the neutral axis was determined which balanced the tension and compression forces. The procedure was identical for the assumed deck strains, $\varepsilon_{cd}$, of 0.001 in/in (Stage 4), 0.002 in/in (Stage 6) and 0.003 in/in (Stage 7). Stage 5 was the point at which the strand was at a strain of 0.01 in/in and began to yield. To approximate the stress distribution for the deck, a Todeschini[151] distribution was used since the deck

510

concrete was a normal weight concrete with less than 6,000 psi compressive strength.

Details of the Todeschini distribution are shown in Figure L.1
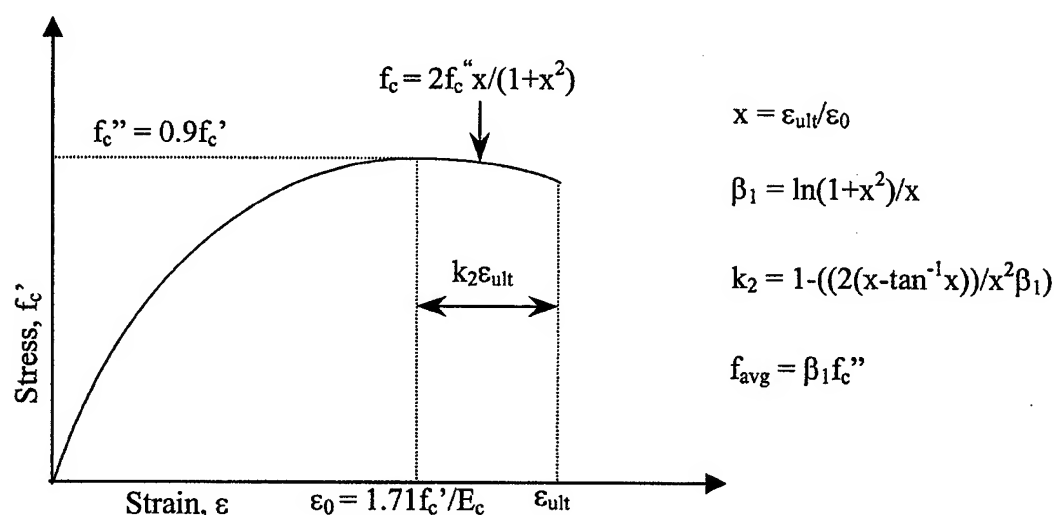


Figure L.1  Todeschini Stress Distribution

Once a deck surface strain or prestressing strand strain was selected and an

estimate entered for the depth to the neutral axis, c, it was necessary to determine the

force in the prestressing strands.  After Stage 3, the strain in the bottom strands, $\varepsilon_{s3}$, was

known.  Since there was very little rotation in the girder up to the cracking load, it was

assumed that the strain in the top strands at $M_{cr}$ was the effective prestress strain, $\varepsilon_{se}$.  An

"if" statement was used in the spreadsheet to calculate resulting strand forces in the top

strands based on the location of the assumed neutral axis relative to the top strands.  If the

neutral axis fell below the top strands, there would be a reduction in strand strain as

calculated below:

511

$$\varepsilon_{set} = \varepsilon_{se} - \frac{(c - (t_d + TCL))}{c} \varepsilon_{cd} \qquad (L.17)$$

If the neutral axis fell above the top strands, there would be an increase in strand strain as calculated below:

$$\varepsilon_{set} = \varepsilon_{se} + \frac{(t_d + TCL - c)}{(t_d + h_{g-nc} - c - BCL)} \varepsilon_{sebi} \qquad (L.18)$$

The force in the top strands was then calculated using the prestressing strand stress-strain plot described in Chapter 8. The strain in the bottom strands was calculated using the following equations:

$$\varepsilon_{seb} = \frac{(t_d + h_{g-nc} - BCL)}{c} \varepsilon_{cd} + \varepsilon_{se2} \qquad (L.19)$$

$$\varepsilon_{sebi} = \varepsilon_{seb} - \varepsilon_{se2} \qquad (L.20)$$

The force in the bottom strands was then calculated using the prestressing strand tension curve plot seen in Table K.15. The total tension force, $F_s$, was the sum of the force in the top strands and the force in the bottom strands.

The concrete compression force, $F_c$, was calculated using the Todeschini technique. Referring to Figure L.1, the compressive force was calculated as below:

512

$$F_c = f_{avg} W_f c \qquad (L.21)$$

Values of "c" were varied until $F_c$ was within 1 kip of $F_s$.

The resulting moment was calculated using the equation below based on the force in the top and bottom strands.

$$M_{4,5,6} = F_{top}(t_d + TCL - k_2 c) + F_{bot}(t_d + h_{g-nc} - BCL - k_2 c) \qquad (L.22)$$

The curvature was calculated using the equation:

$$\phi_{4,5,6,7} = \frac{\varepsilon_{cd}}{c} \qquad (L.23)$$

This procedure was used for each of the selected deck strain values. The girder's ultimate moment and curvature values were determined at a deck surface strain of 0.003 in/in.

## L.1.5 Experimental Moment-Curvature

The experimental moment and curvature were calculated using the equations below:

$$M_{exp} = M_{DL} + P\frac{(L_1 - a)}{L_1}a \qquad (L.24)$$

513

$$\phi = \frac{\varepsilon_{bot} - \varepsilon_{top}}{h_g} \qquad (L.25)$$

$M_{DL}$ is the dead load moment caused by the girder and deck. P is the applied

load. $L_1$ and "a" are the distance between supports and shear span respectively. $\varepsilon_{bot}$ and

$\varepsilon_{top}$ are the strains at the bottom and top of the composite girder that were calculated from

strain readings recorded using LVDTs placed close to the bottom and top of the

composite girder assuming a linear strain distribution. Table L.1 lists the $L_1$ and "a"

distances for each girder test.

The predicted plot begins with a negative curvature reflecting the initial upward

camber due to prestressing. The moment value also starts above zero in most cases

reflecting the initial dead load moment.

Table L.1  Dimensions "a" and $L_1$ for Girder Tests

| Girder Test # | Configuration # | Shear Span "a" (inches) | Support to Support Distance $L_1$ (inches) |
|---|---|---|---|
| G1A-East, G2A-East | 2 | 61 | 316 |
| G1A-West, G2A-West | 1 | 90 | 456 |
| G1A-Center, G2A-Center | 7 | 82 | 185 |
| G1B-East, G2B-East | 5 | 61 | 456, 321 |
| G1B-West, G2B-West | 3 | 75 | 345, 456 |
| G1B-Center, G2B-Center | 8 | 96 | 210 |
| G1C-East, G2C-East | 6 | 75 | 369 |
| G1C-West, G2C-West | 4 | 85 | 504 |
| G1C-Center, G2C-Center | 9 | 120 | 244 |

## L.2 Deflection

Calculations for deflection at cracking and at ultimate were compared to experimental results. An elastic technique was used to calculate the deflection at cracking and a moment area technique was used for the ultimate deflection. The moment area technique used provided a good estimate but was not an exact solution. Table K.9 provides details on deflection calculations. Table K.2 shows experimental deflections.

### L.2.1 Calculations for Deflection at Flexural Cracking

An elastic technique was used to predict the deflection at initial flexural cracking as specified in *Mechanics of Materials*, Gere and Timoshenko.[124] Table K.9 provides details on elastic deflection calculations. Included in the elastic deflection calculations were components due to both flexure and shear. Figure L.2 provides a diagram of variables used in calculating elastic deflections.
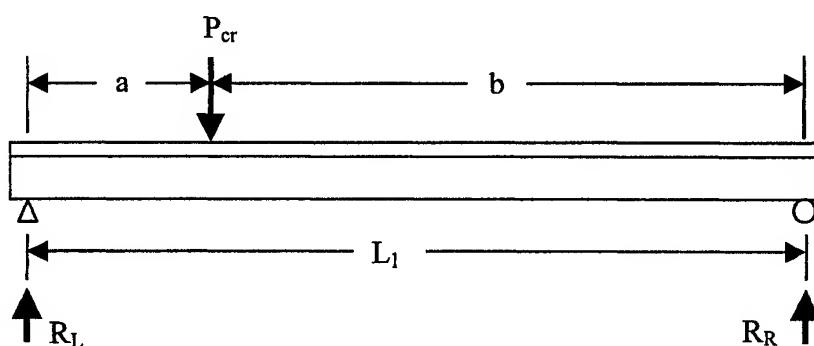


Figure L.2  Diagram Showing Variables for Elastic Deflection Calculations

$P_{cr}$ was the predicted cracking load. The value of $0.4 E_{cg}$ was used for the shear modulus, G. The cracking deflection at the point of load application was calculated with the following equations for flexural deflection and shear deflection:

$$\delta_{cr-flex} = \frac{P_{cr}ba}{6E_{cg}I_cL_1}(L_1^2 - b^2 - a^2)$$

(L.26)

$$\delta_{cr-shear} = R_L \frac{a}{0.4E_{cg}\,b\,d_p}$$

(L.27)

The total elastic cracking deflection was the sum of the flexural and shear deflections.

## L.2.2 Calculations for Ultimate Deflection

A moment area technique was used to calculate deflection at the ultimate condition as described in *Mechanics of Materials*, Gere and Timoshenko.[124] At the ultimate condition, a plastic hinge forms at the point of load application. The length of the plastic hinge was assumed to equal the distance from the surface of the deck to the bottom strands. Over the plastic hinge, the curvature was assumed to be at $\phi_{ult}$ as described in Section L.1.4. The variables shown in Figure L.2 also apply during the ultimate deflection calculations.

Two different curvature diagrams were required for ultimate deflection calculations. The diagram shown in Figure L.3, the "modified" curvature diagram, applied when distances from the point of loading to a support were small. The hinge

region effectively encompassed the region where a yielding curvature point, $\phi_y$, would be considered. Figure L.4, the "normal" curvature diagram, applied when the distances from the point of loading to a support would allow consideration of a yielding curvature point, $\phi_y$. The yielding curvature, $\phi_y$, was the point at which the prestressing strand first yielded. The curvature value, $\phi_{cr}$, was the curvature at initial flexural cracking. The curvature value, $\phi_{ult}$ was the curvature at ultimate. The calculations in Table K.9 automatically determined the characteristics of the curvature diagram based on the dimensions of the girder test and curvature values. In most cases, the diagram to the left of the load was the modified diagram and to the right of the load was the normal diagram
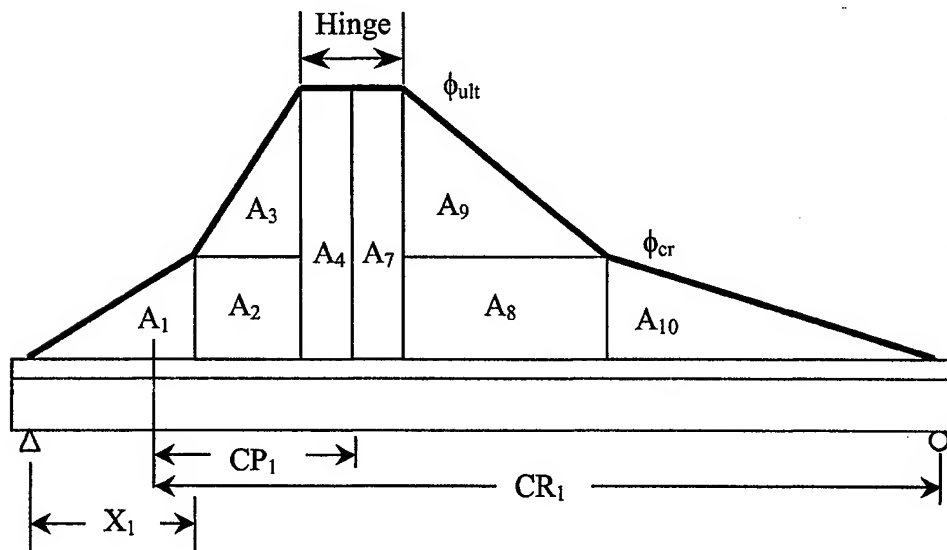


Figure L.3 "Modified" Curvature Diagram for Ultimate Deflection Calculations

517
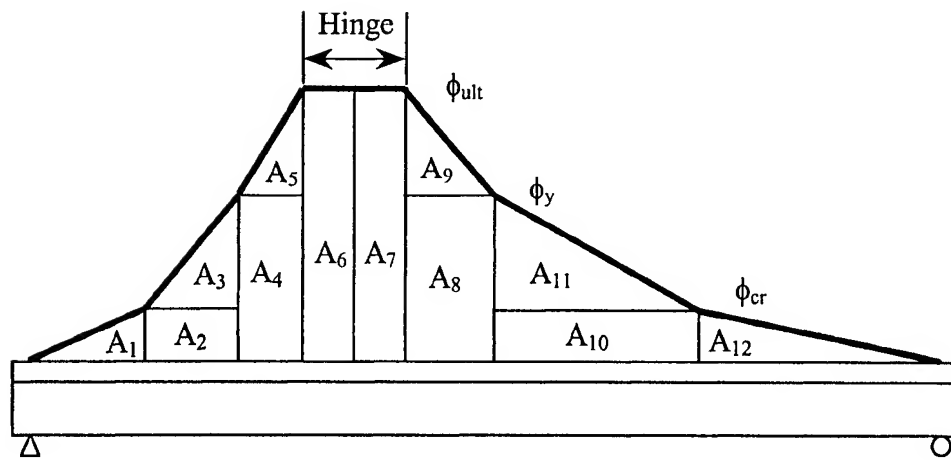
Figure L.4 "Normal" Curvature Diagram for Ultimate Deflection Calculations

The values $X_x$, $CR_x$ and $CP_x$, and $A_x$ are referenced in Table K.9 and shown in Figure L.3. The same definitions apply to Figure L.4. The X distances are distances from the left support to the far side of a particular area. The CR values measure the distance from the centroid of an area to the right support. The CP values measure the distance from the centroid of an area to the point of load application.

Figure L.5 shows a diagram describing the calculation of deflections. It is important to emphasize again that the resulting ultimate deflection calculation was a good estimate, but not an exact value.
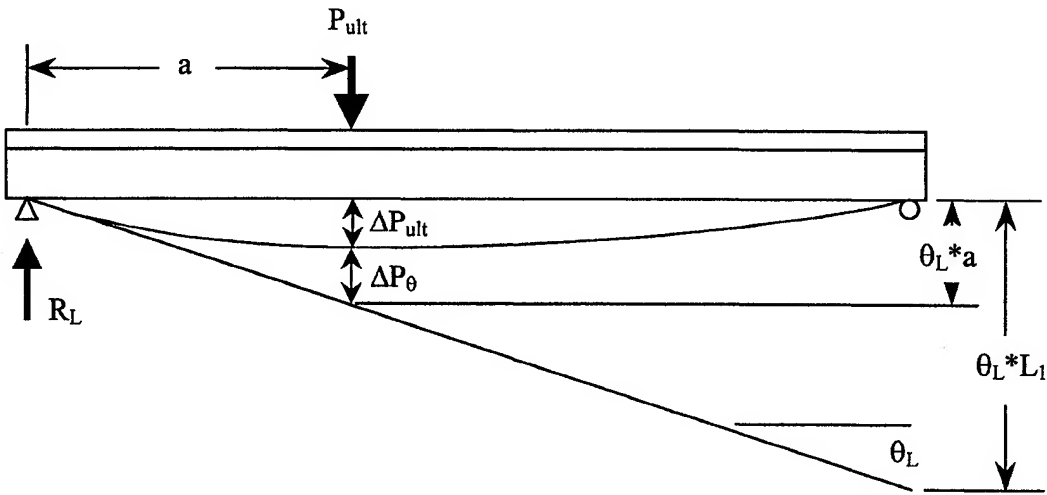
Figure L.5 Diagram Showing Ultimate Deflection Calculation

The following equations were used to calculate the ultimate deflection, $\Delta P_{ult}$:

$$\theta_L a = \sum A_x CR_x \frac{a}{L_1} \qquad (L.28)$$

$$\Delta_{p\theta} = \sum A_x CP_x \qquad (L.29)$$

$$\Delta P_{ult} = \theta_L a - \Delta P_\theta + R_L \frac{a}{0.4 E_{cg} b d_p} \qquad (L.30)$$

Equation L.30 reflects the deflection component due to shear deformation. The percentage of total deflection due to shear is much less in the ultimate deflection; however, it must be included for accuracy. The value $0.4E_{cg}$ used in the denominator represents the shear modulus, G. If cracking was extreme during a test, this value was reduced to $0.2E_{cg}$ to reflect a reduced shear modulus.

### L.2.3 Experimental Deflections

Measurement of experimental deflections was accomplished with a wire potentiometer placed under girder at the point of load application.

## L.3 Girder Test G1A-East
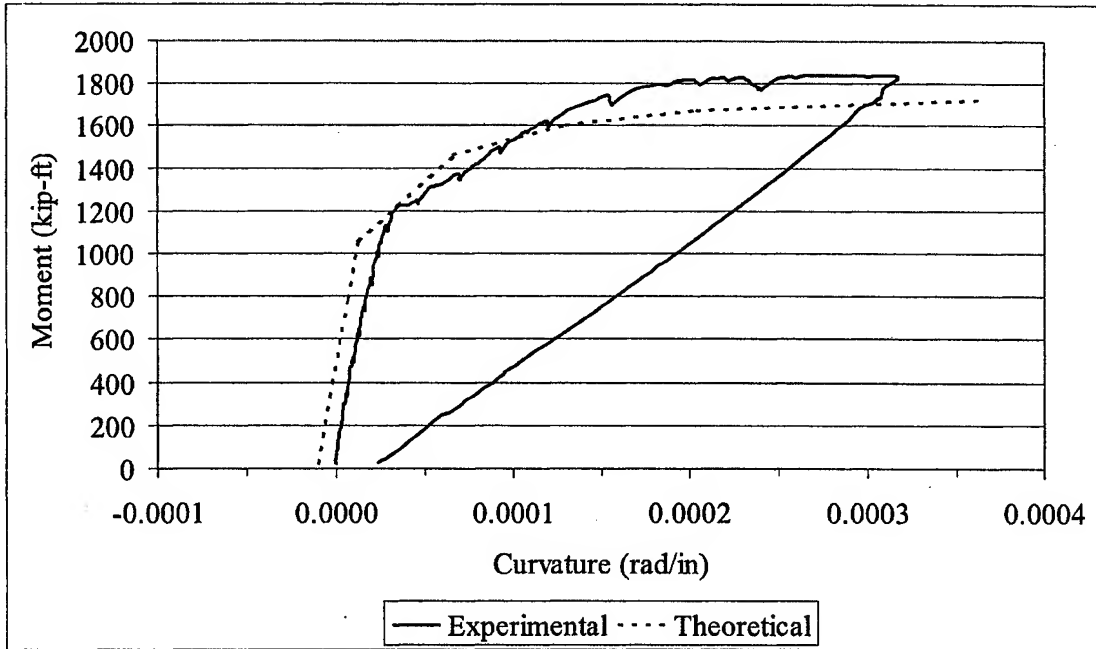


Figure L.6  G1A-East Moment vs. Curvature Plot
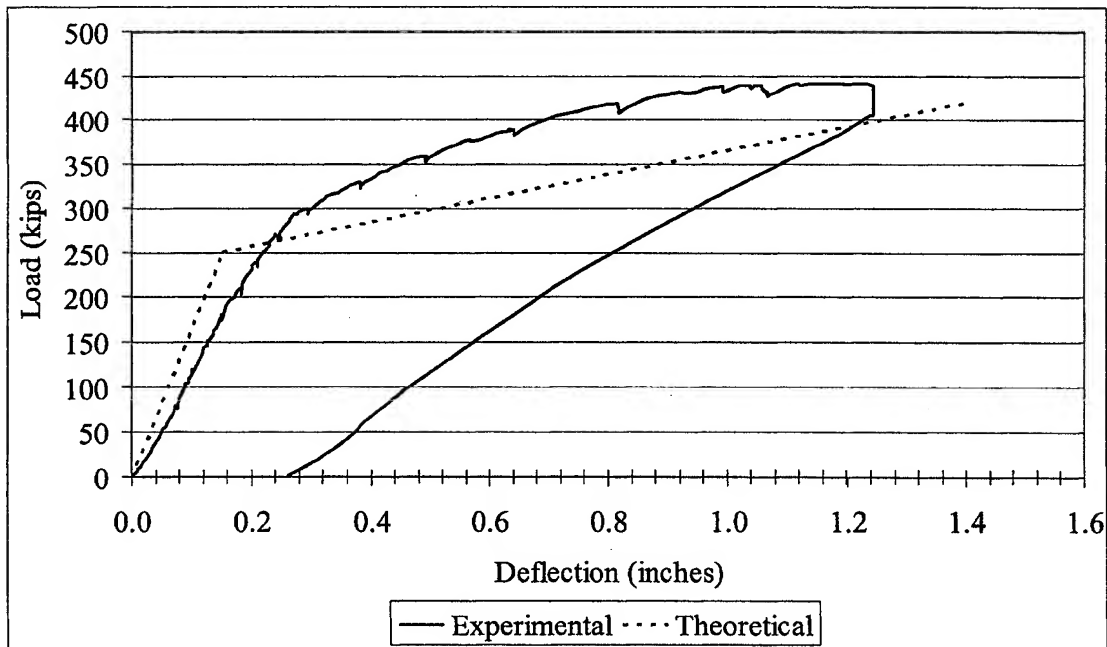


Figure L.7  G1A-East Load vs. Deflection Plot

521

## L.4 Girder Test G1A-West
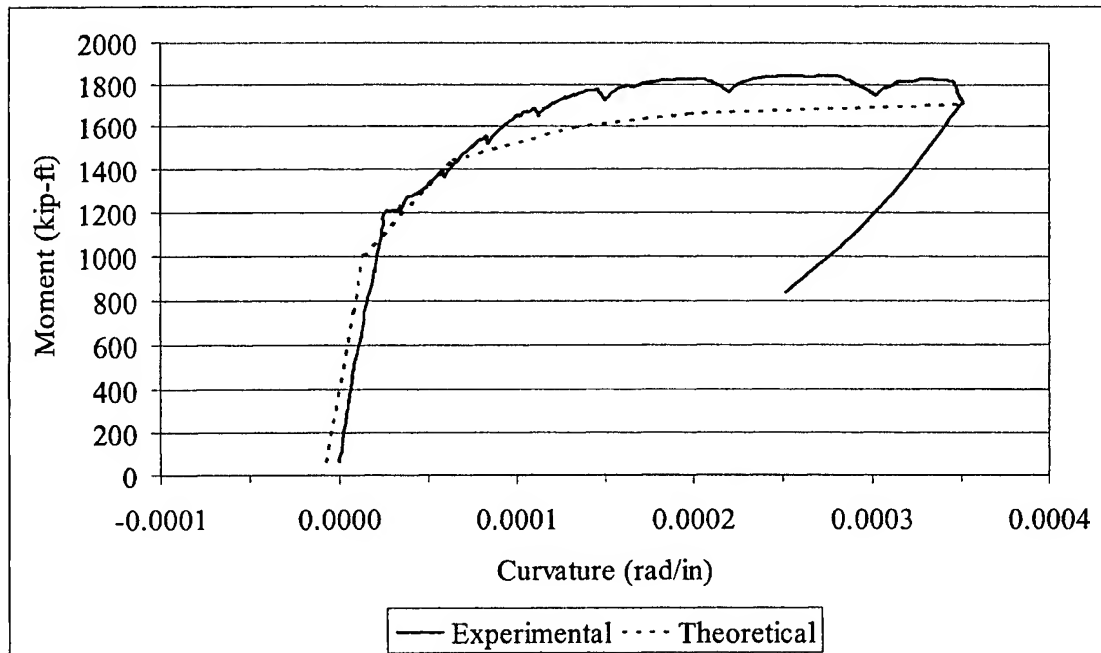


Figure L.8  G1A-West Moment vs. Curvature Plot
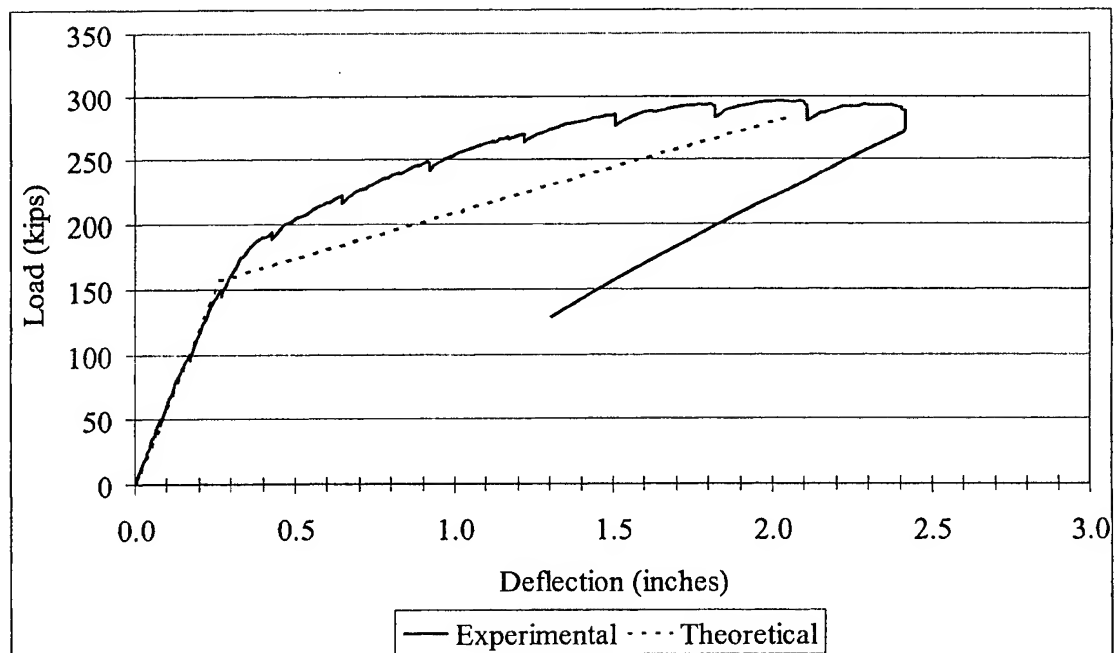


Figure L.9  G1A-West Load vs. Deflection Plot

522

## L.5 Girder Test G1A-Center
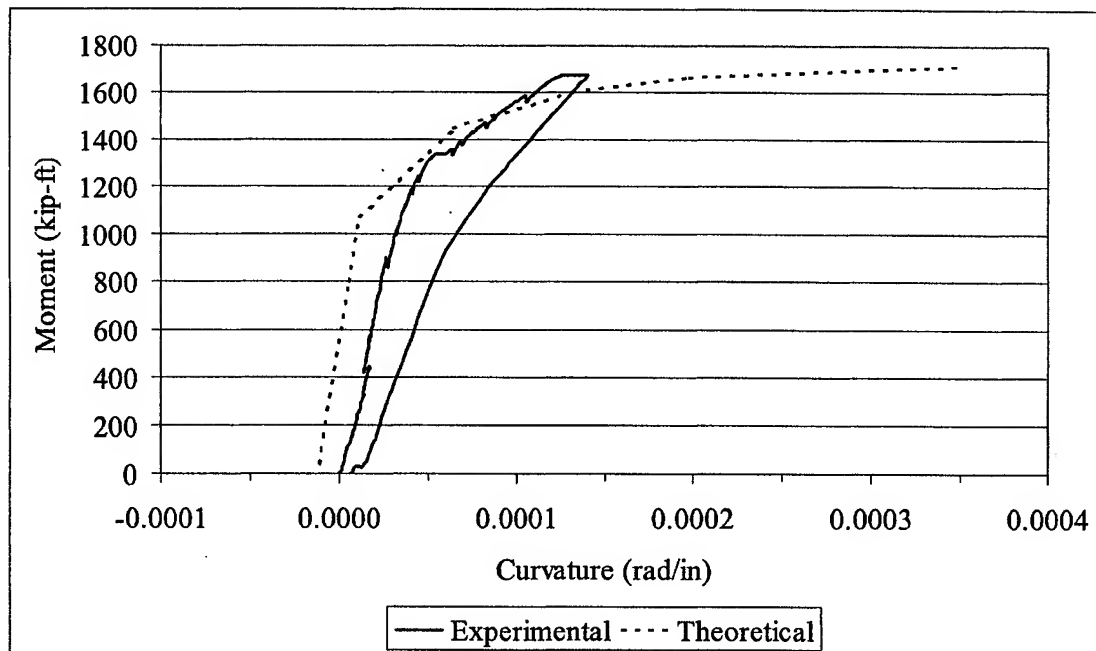


Figure L.10  G1A-Center Moment vs. Curvature Plot
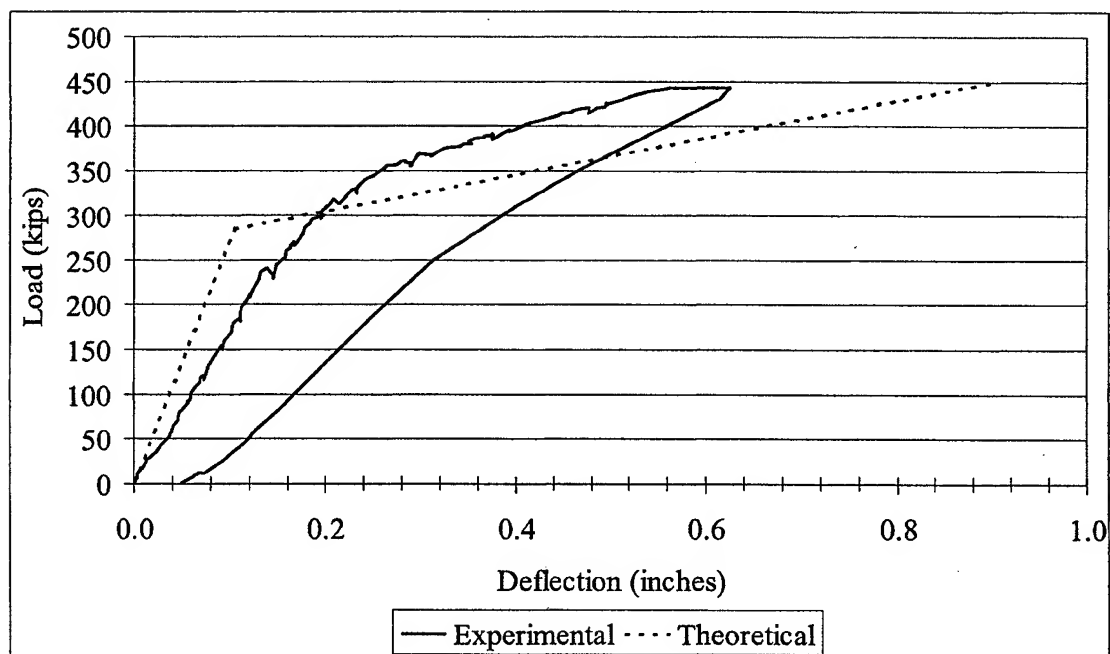


Figure L.11  G1A-Center Load vs. Deflection Plot

## L.6 Girder Test G1B-East
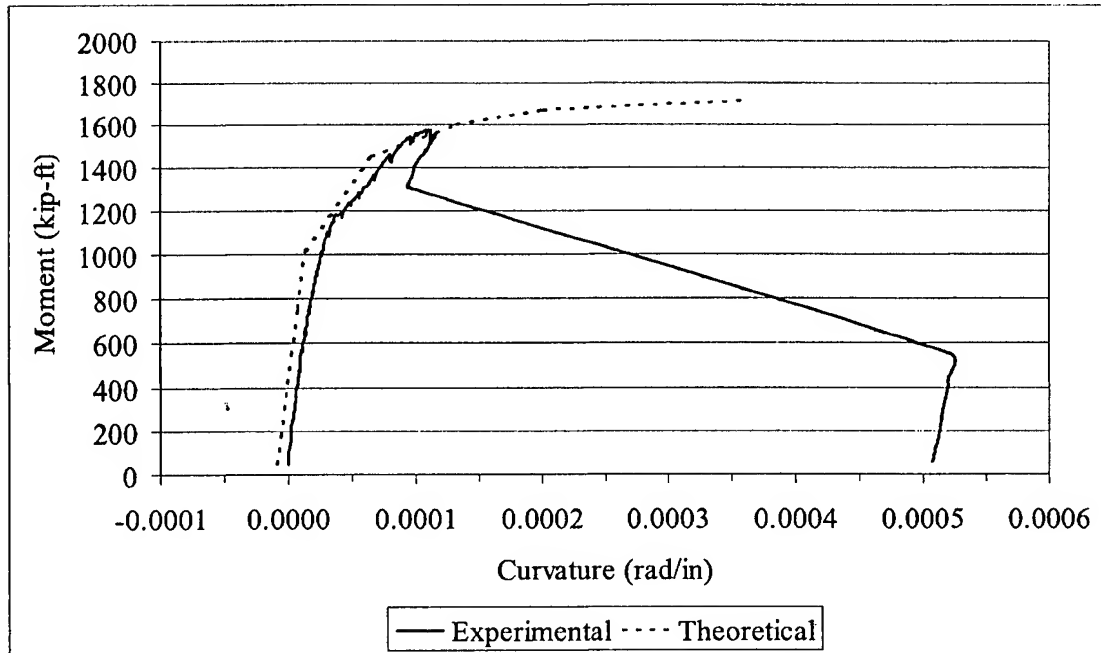


Figure L.12 G1B-East Moment vs. Curvature Plot
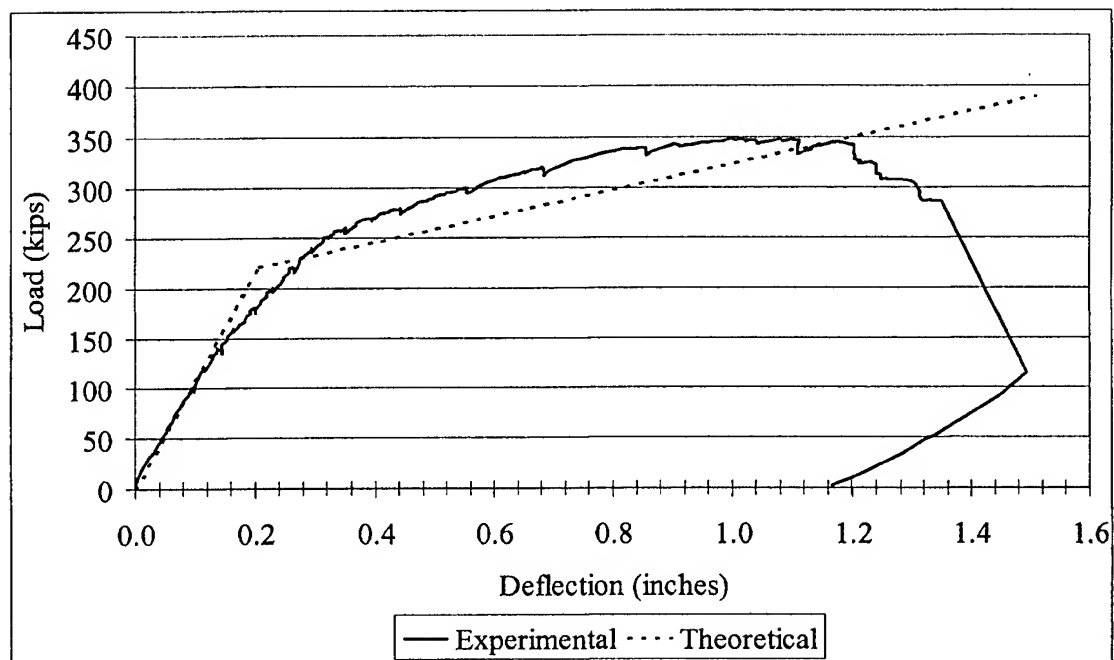


Figure L.13 G1B-East Load vs. Deflection Plot

## L.7  Girder Test G1B-West
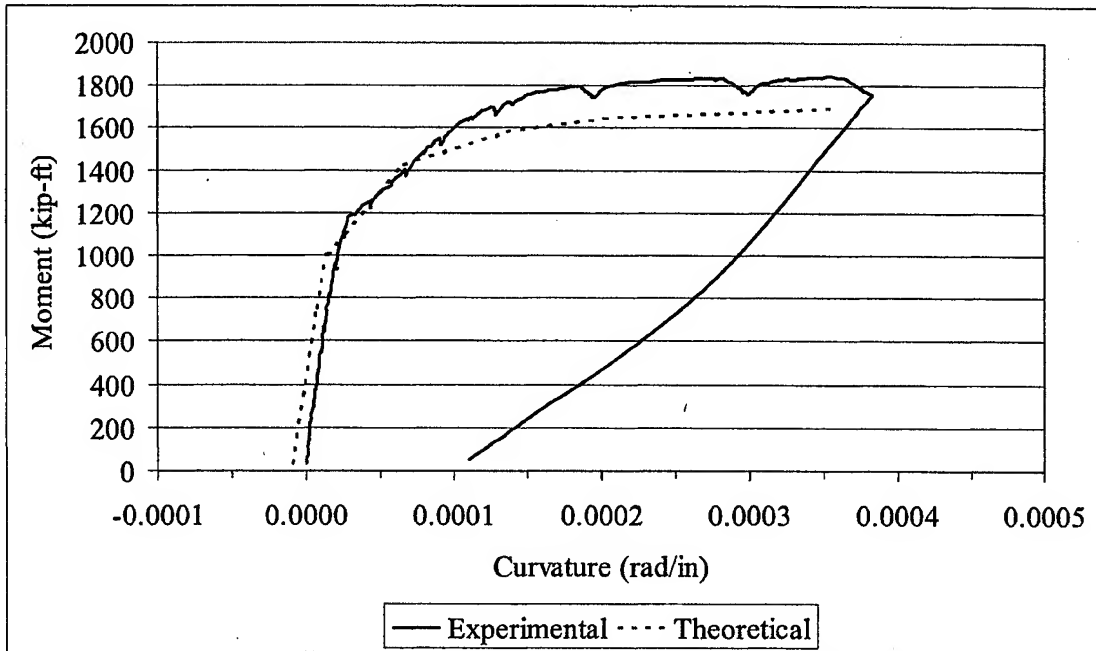


Figure L.14  G1B-West Moment vs. Curvature Plot
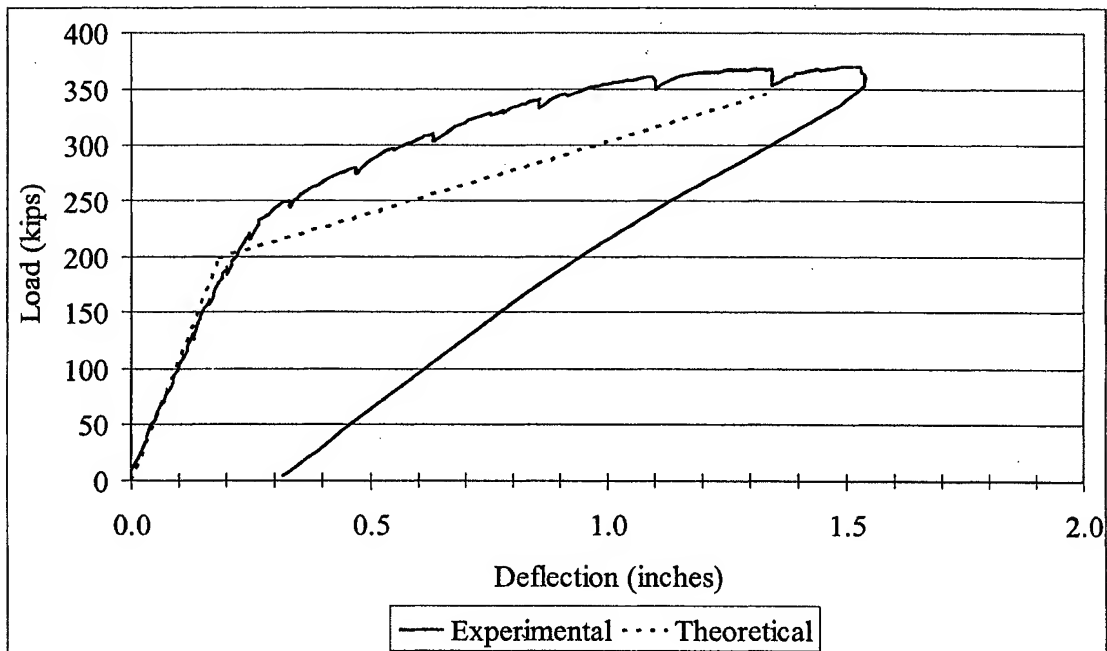


Figure L.15  G1B-West Load vs. Deflection Plot

## L.8 Girder Test G1B-Center
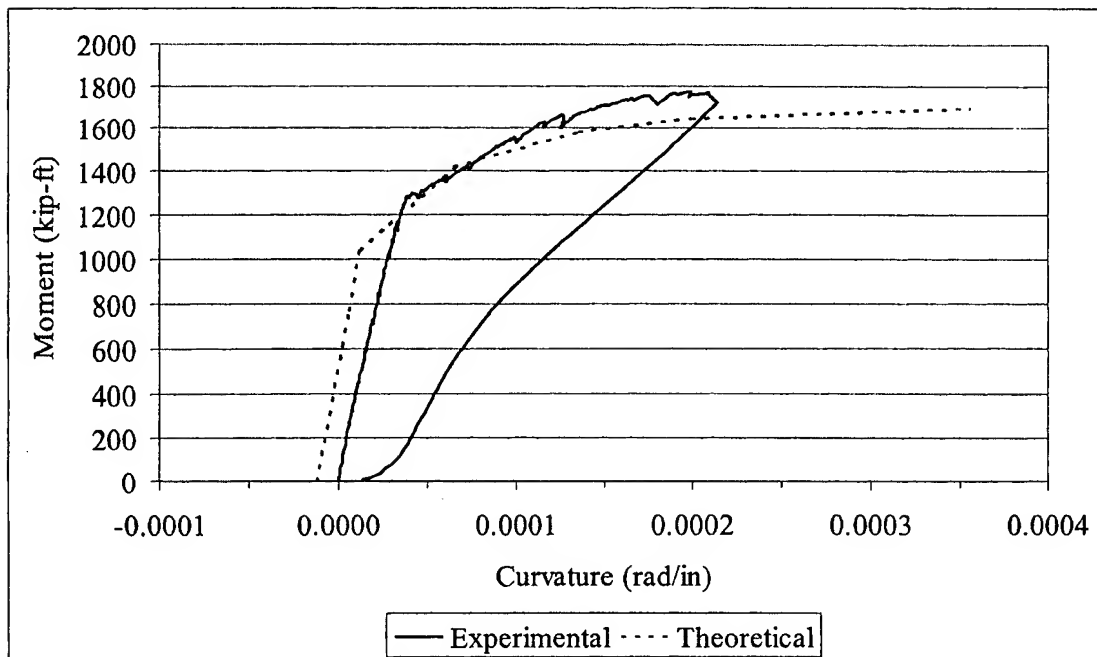


Figure L.16  G1B-Center Moment vs. Curvature Plot
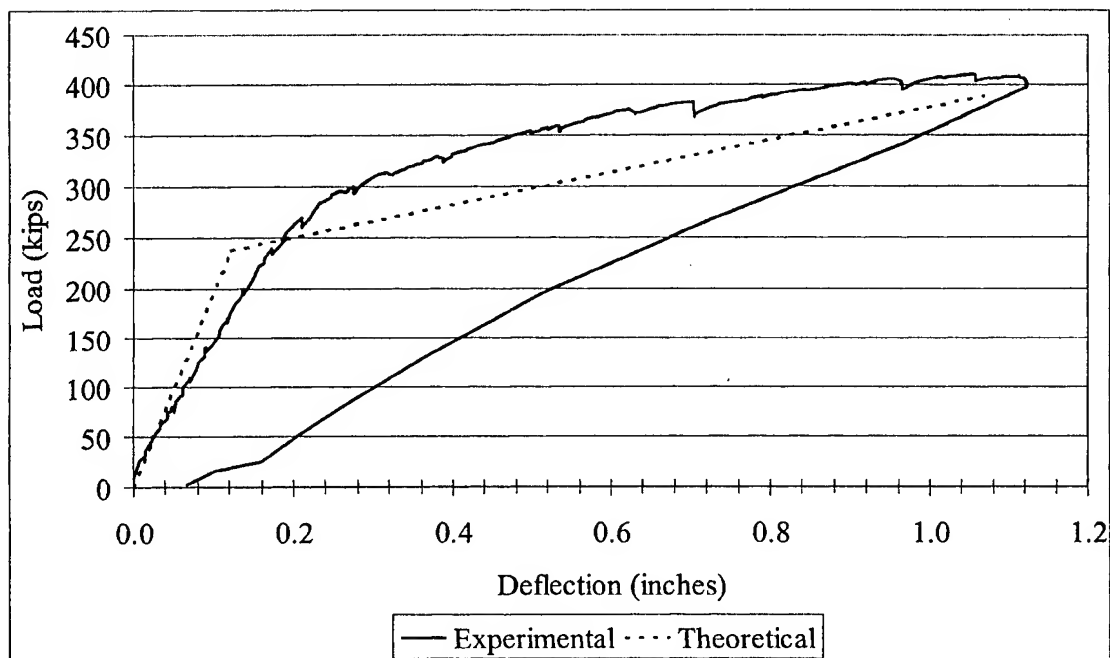


Figure L.17  G1B-Center Load vs. Deflection Plot

526

## L.9 Girder Test G1C-East
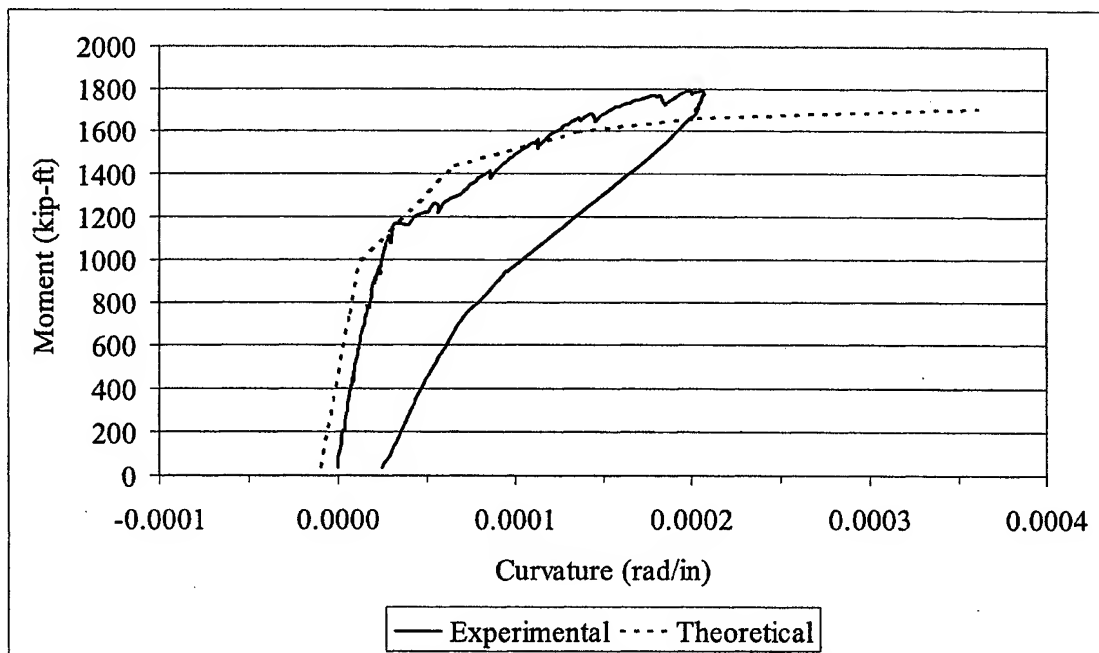


Figure L.18 G1C-East Moment vs. Curvature Plot
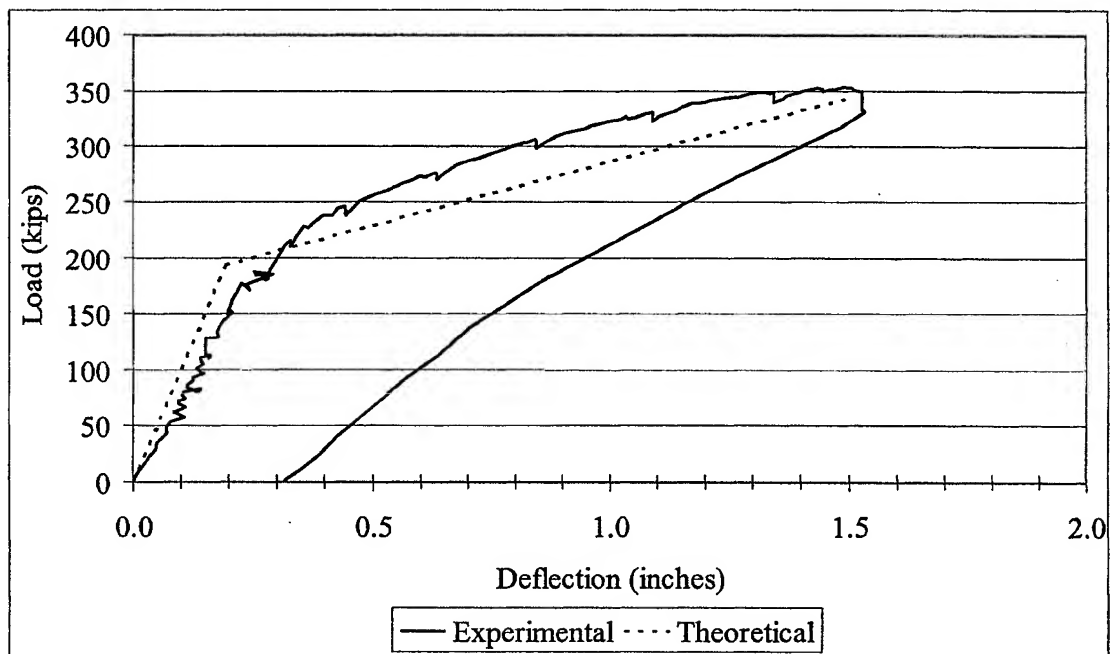


Figure L.19 G1C-East Load vs. Deflection Plot

527

## L.10  Girder Test G1C-West
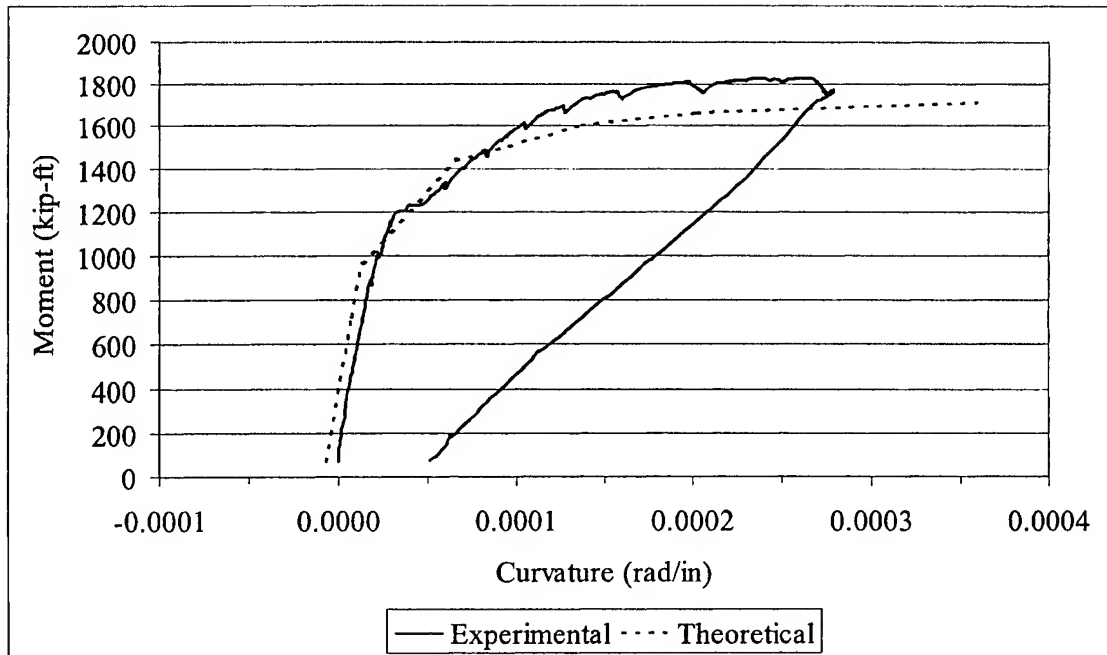


Figure L.20  G1C-West Moment vs. Curvature Plot
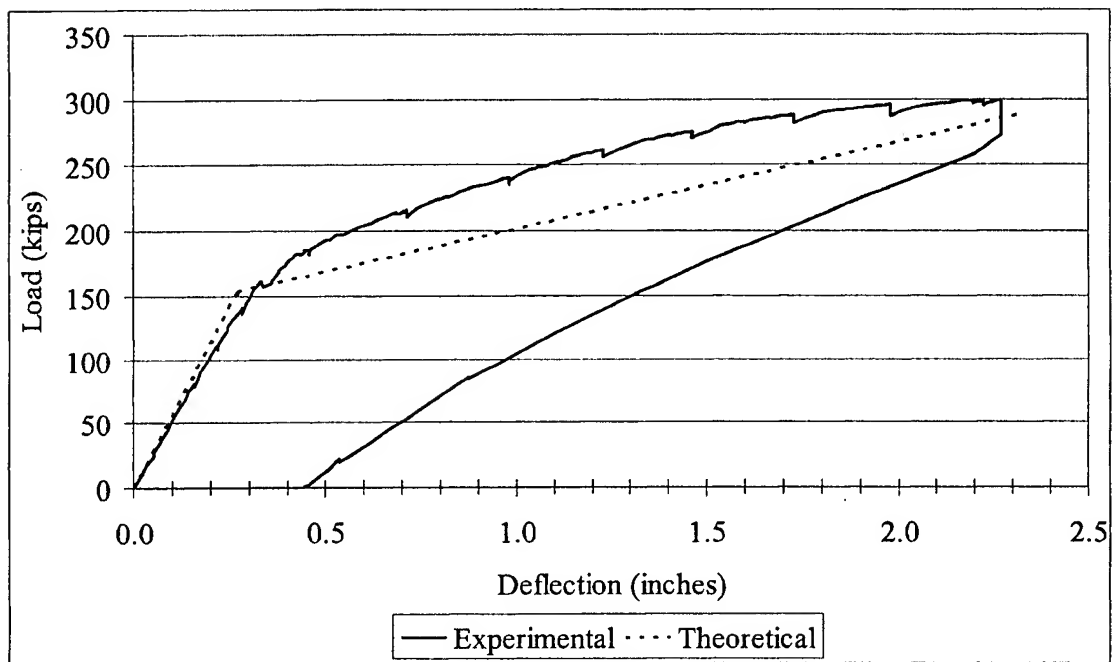


Figure L.21  G1C-West Load vs. Deflection Plot

## L.11 Girder Test G1C-Center
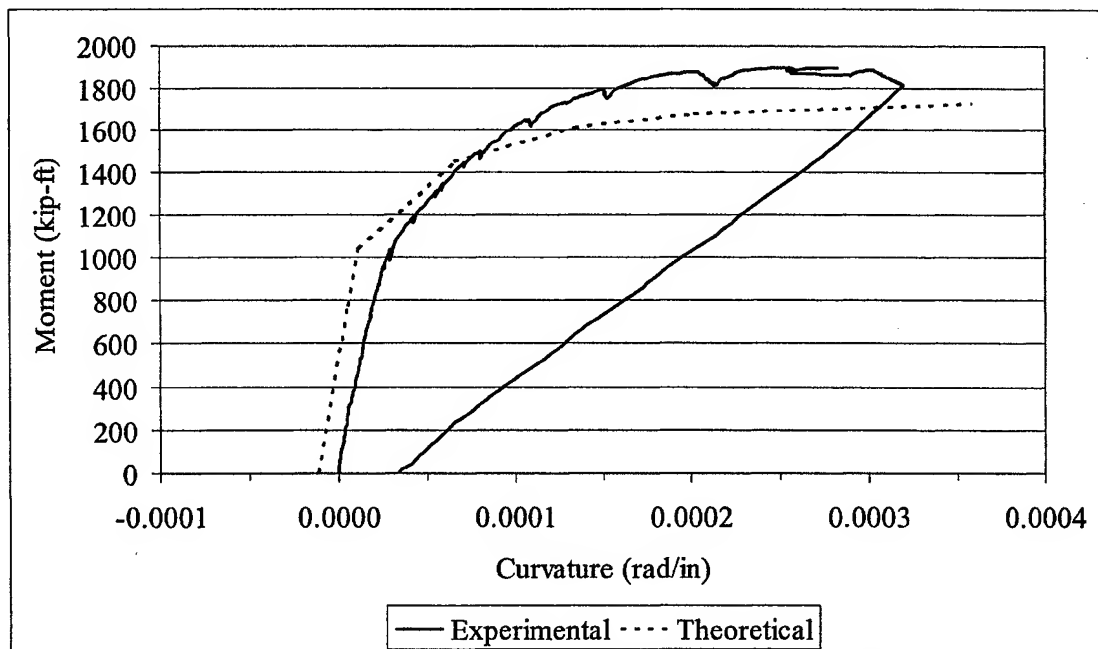


Figure L.22 G1C-Center Moment vs. Curvature Plot
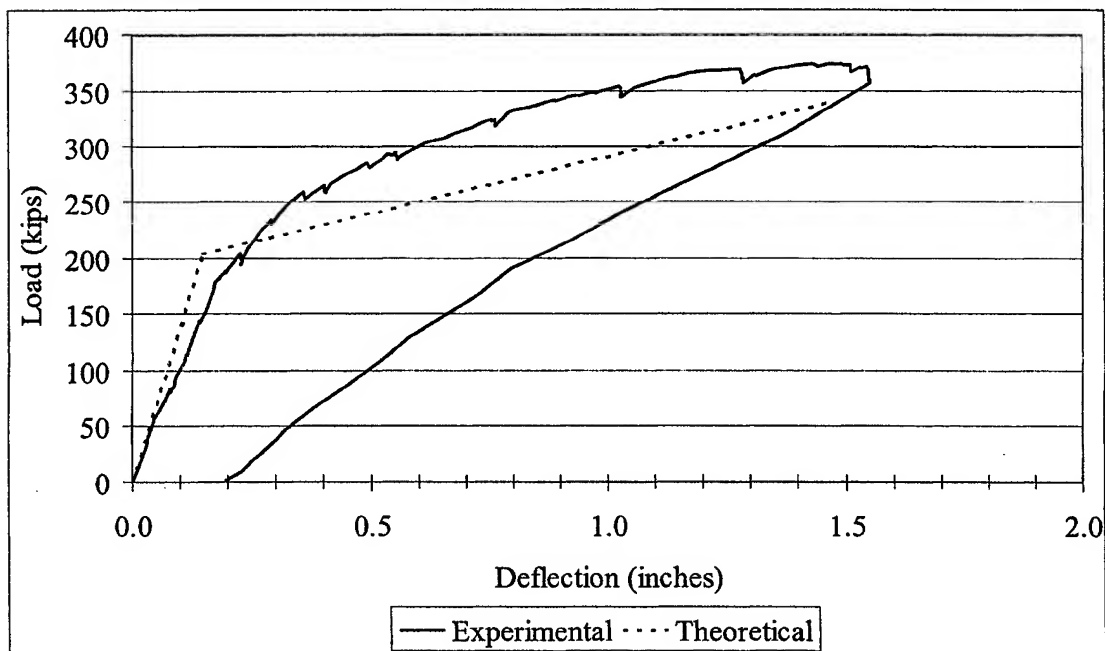


Figure L.23 G1C-Center Load vs. Deflection Plot

529

## L.12  Girder Test G2A-East
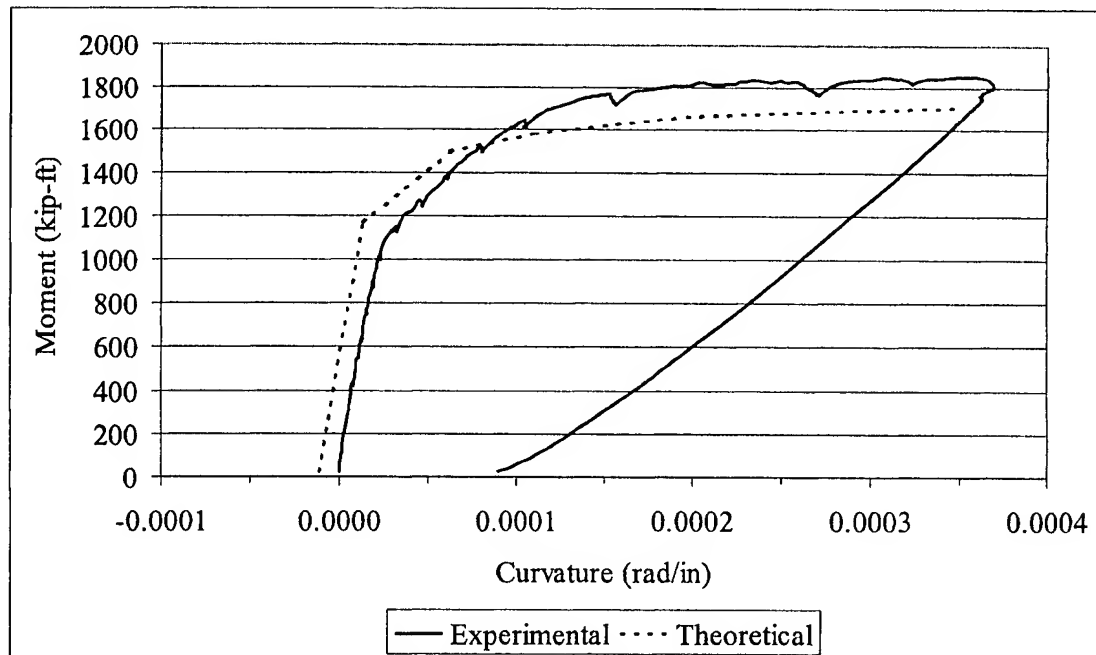


Figure L.24  G2A-East Moment vs. Curvature Plot
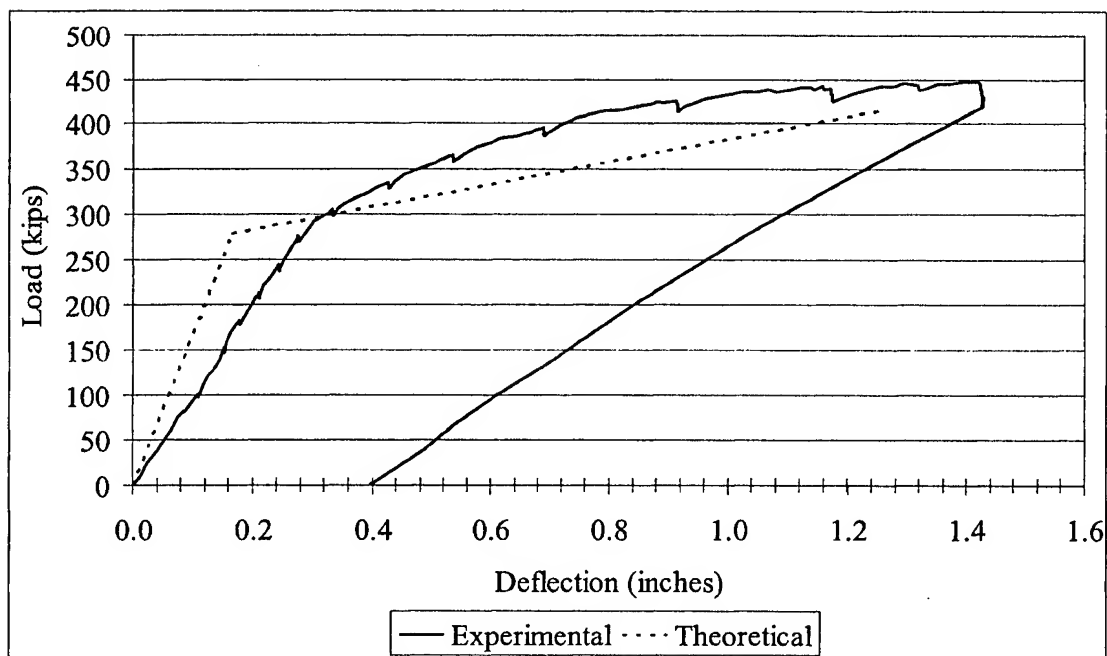


Figure L.25  G2A-East Load vs. Deflection Plot

## L.13 Girder Test G2A-West
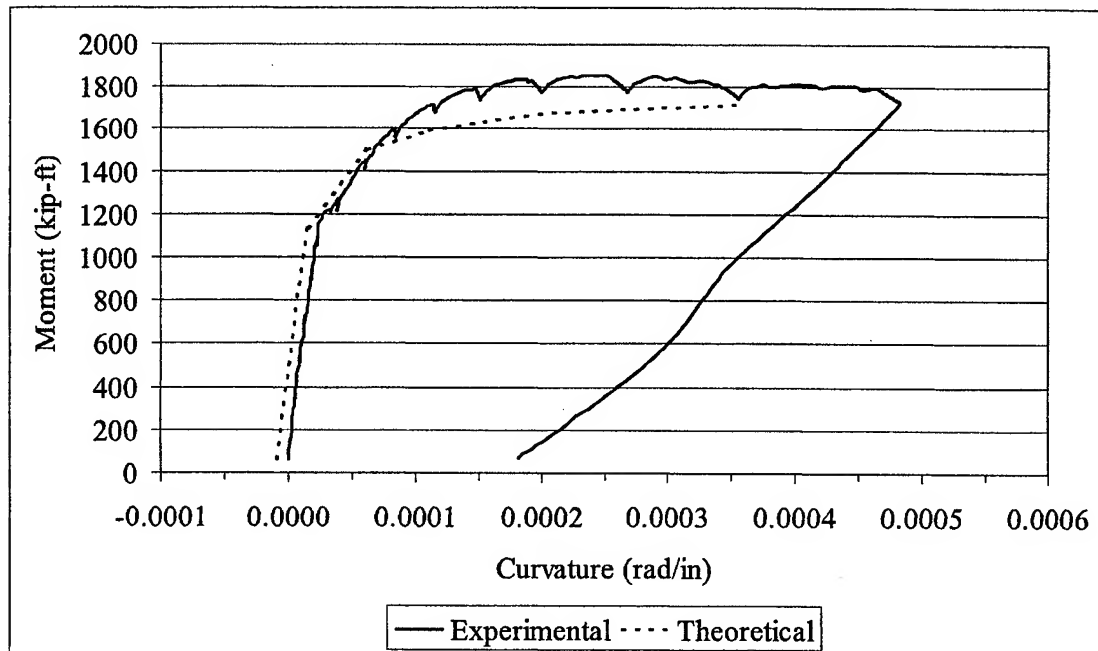


Figure L.26 G2A-West Moment vs. Curvature Plot
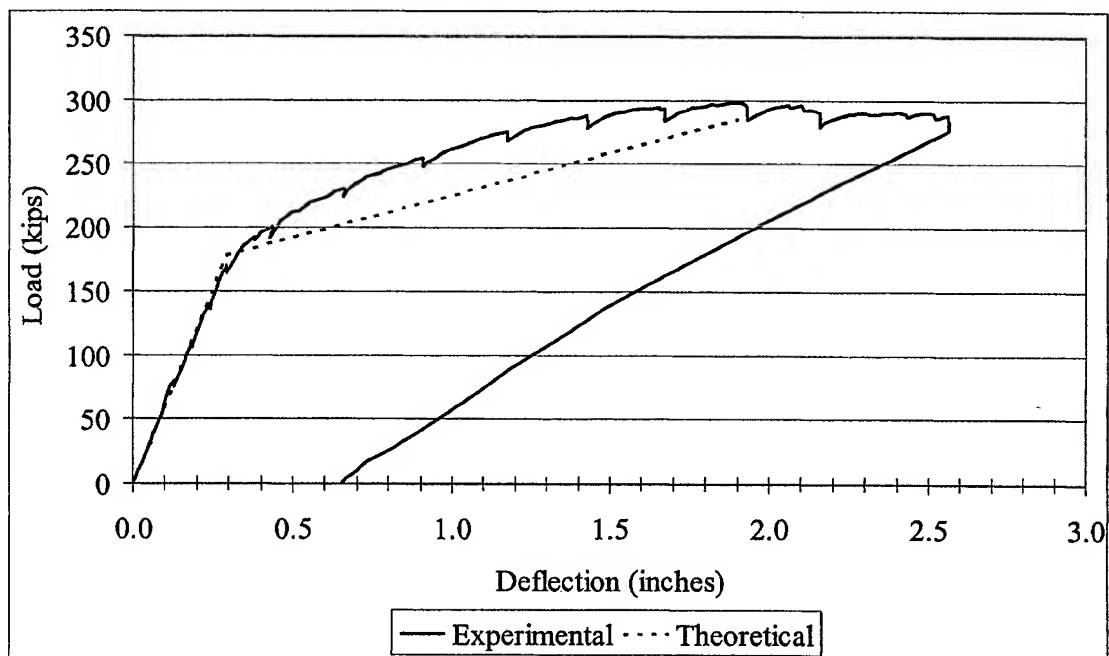


Figure L.27 G2A-West Load vs. Deflection Plot

531

## L.14 Girder Test G2A-Center
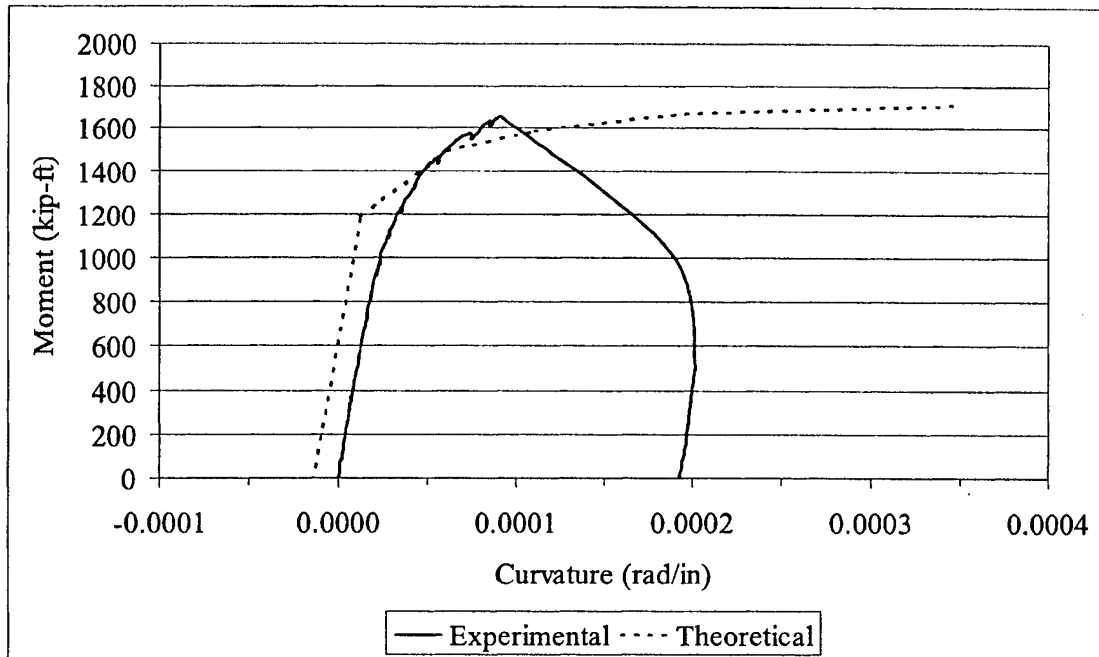


Figure L.28  G2A-Center Moment vs. Curvature Plot
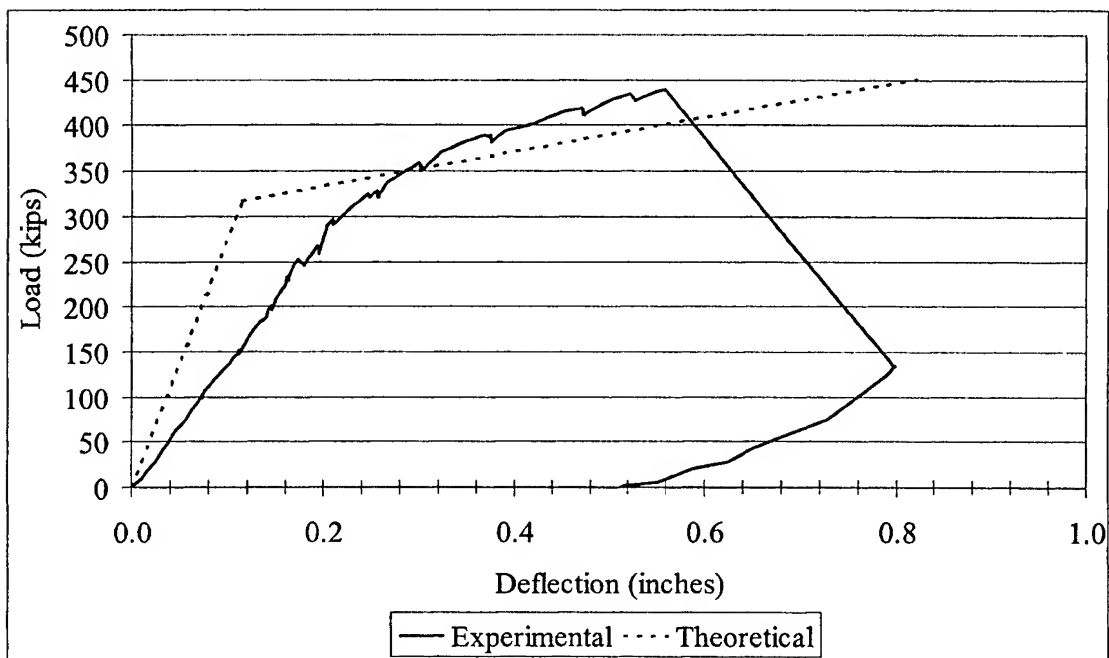


Figure L.29  G2A-Center Load vs. Deflection Plot

532

## L.15  Girder Test G2B-East
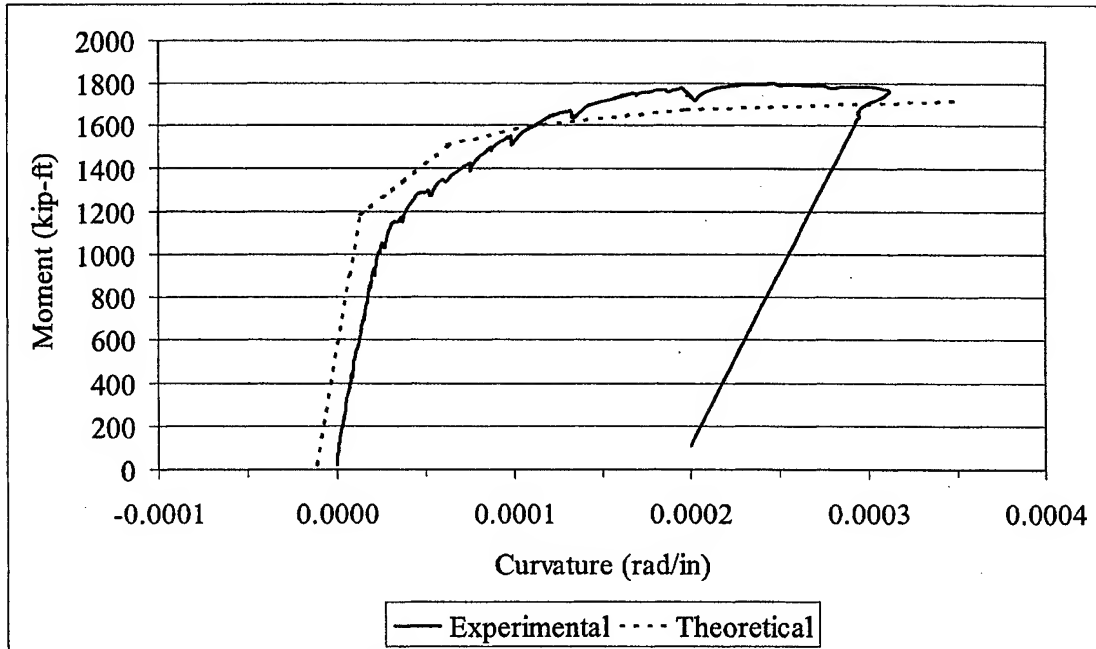


Figure L.30  G2B-East Moment vs. Curvature Plot
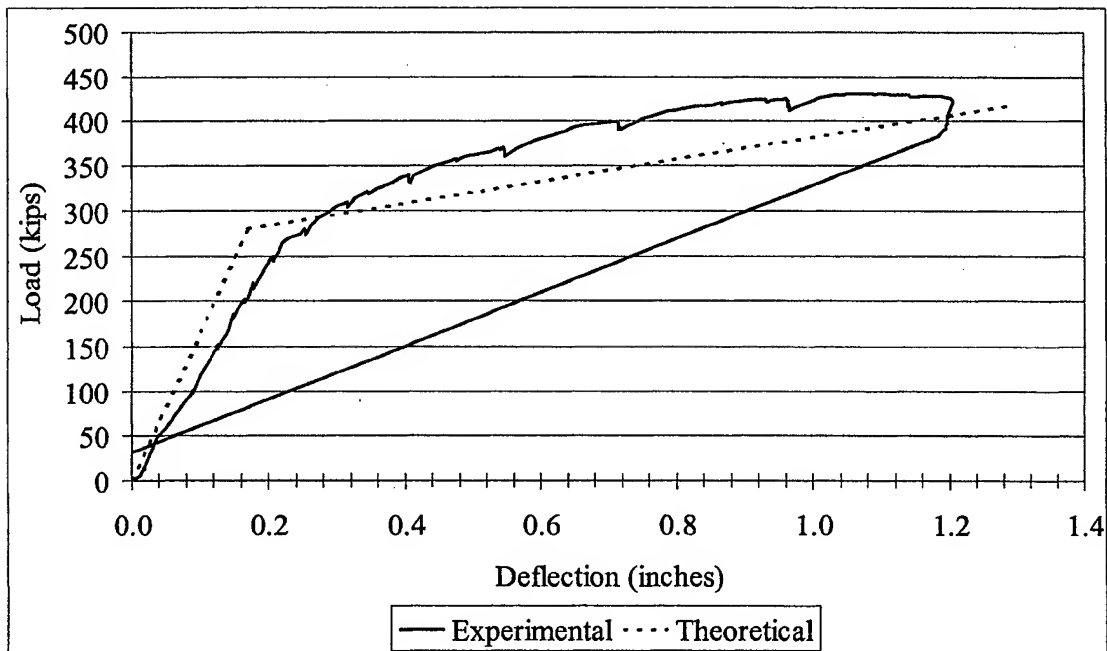


Figure L.31  G2B-East Load vs. Deflection Plot

533

## L.16 Girder Test G2B-West
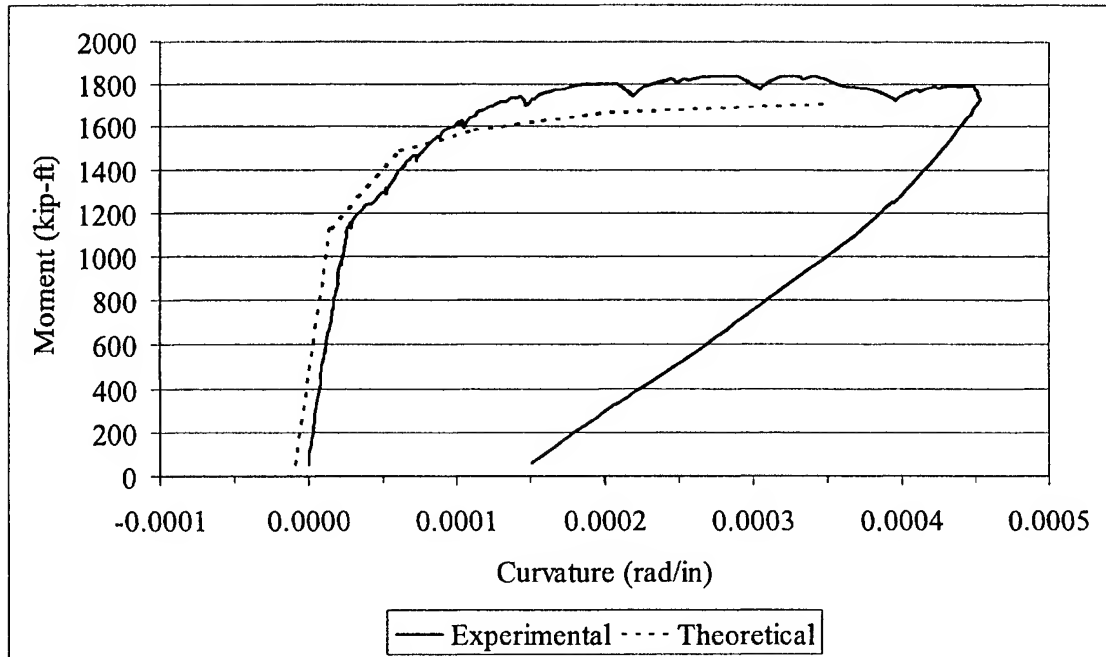


Figure L.32 G2B-West Moment vs. Curvature Plot
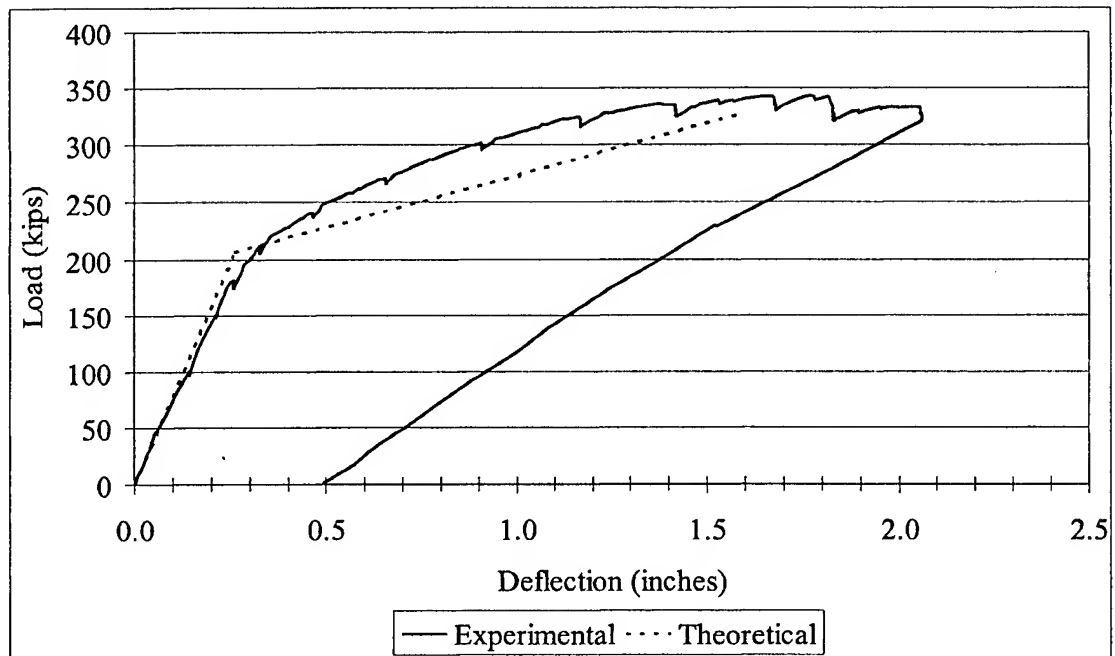


Figure L.33 G2B-West Load vs. Deflection Plot

534

## L.17 Girder Test G2B-Center
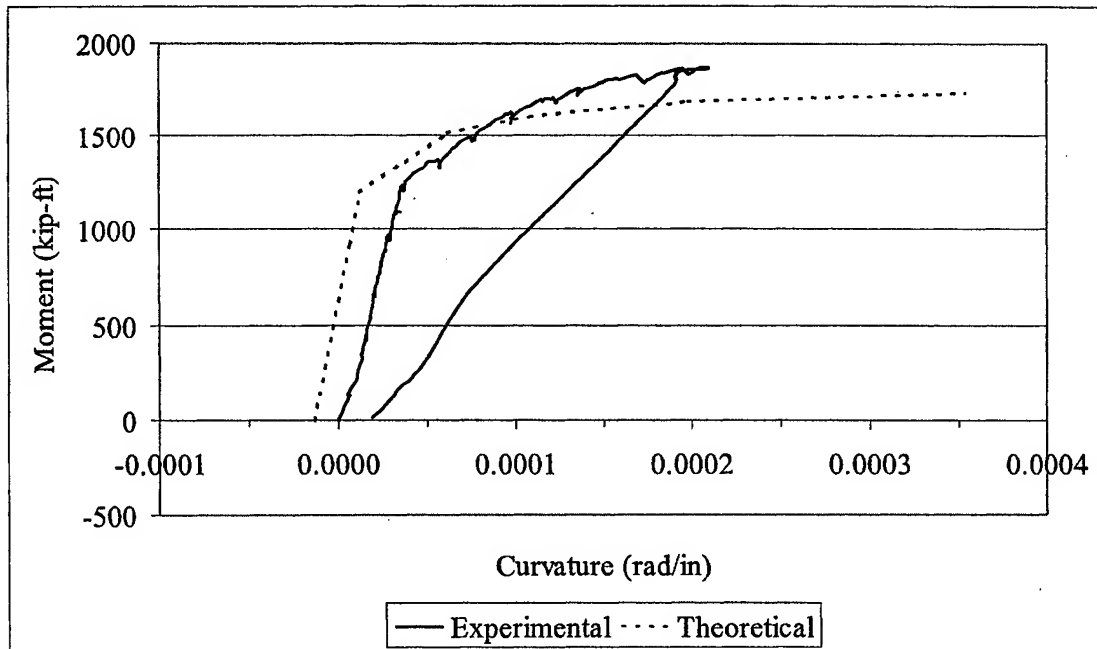


Figure L.34 G2B-Center Moment vs. Curvature Plot
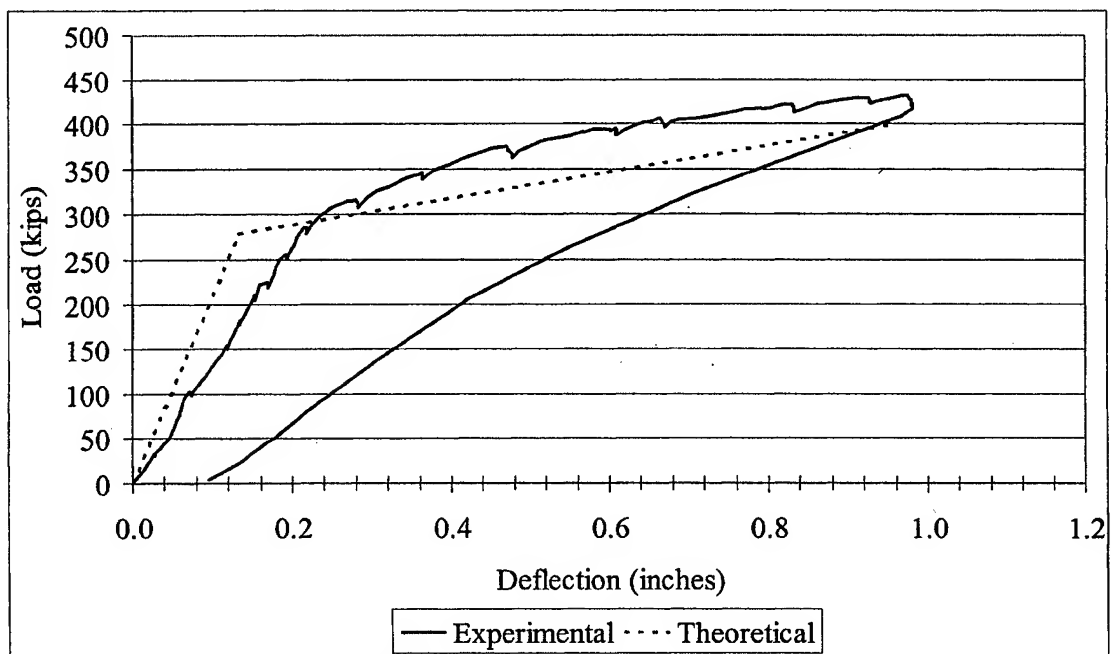


Figure L.35 G2B-Center Load vs. Deflection Plot

## L.18 Girder Test G2C-East
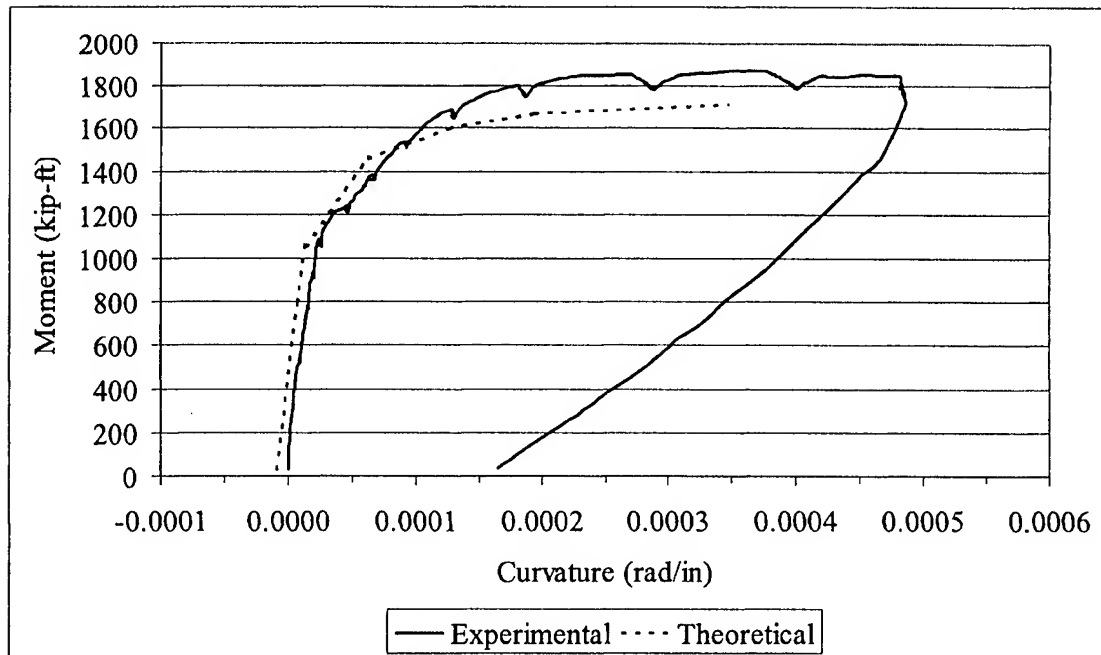


Figure L.36 G2C-East Moment vs. Curvature Plot
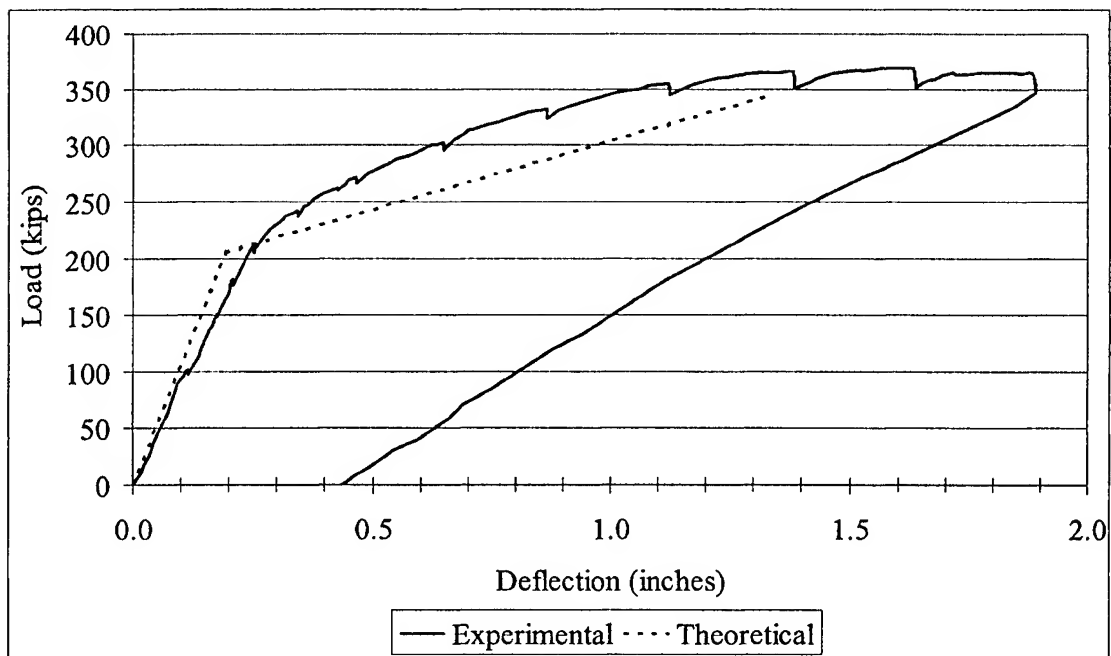


Figure L.37 G2C-East Load vs. Deflection Plot

536

## L.19 Girder Test G2C-West
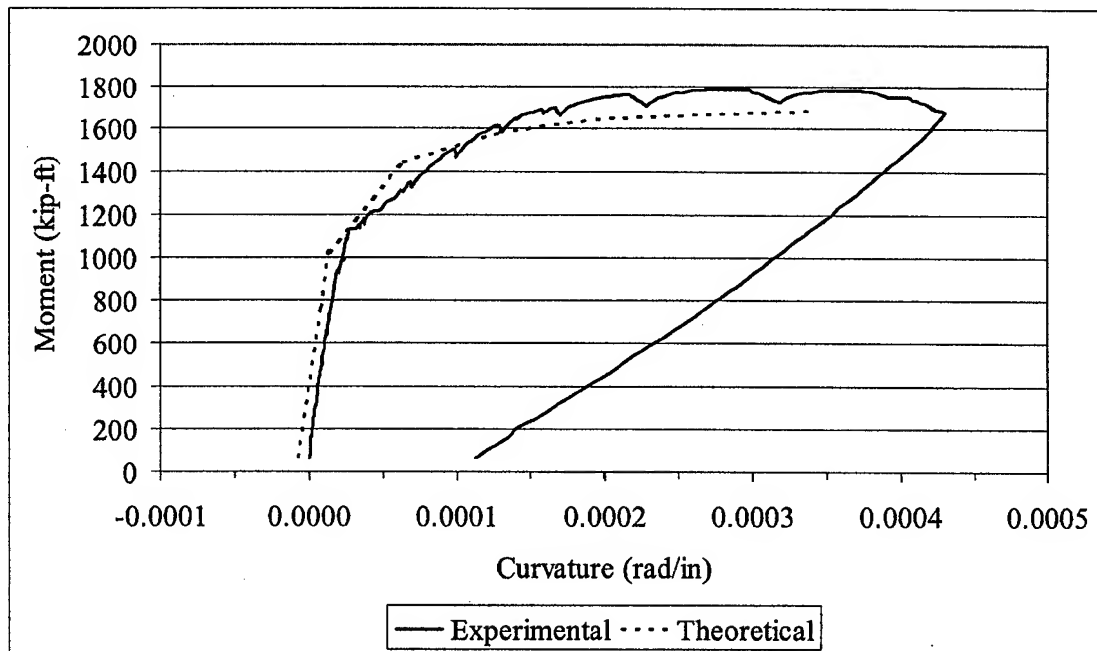


Figure L.38  G2C-West Moment vs. Curvature Plot
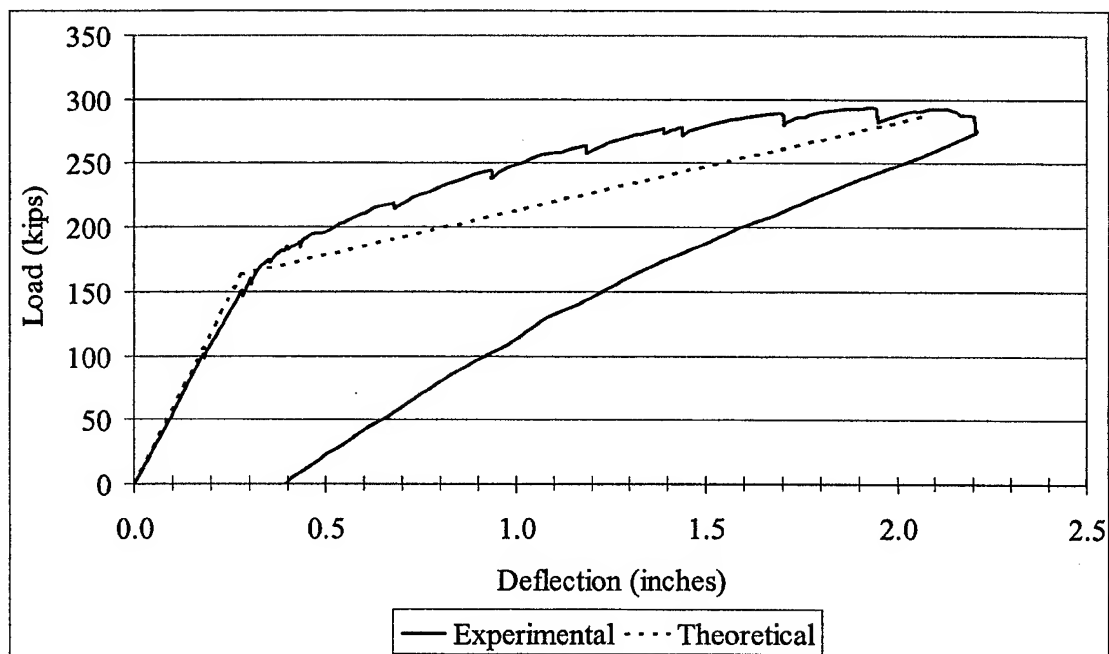


Figure L.39  G2C-West Load vs. Deflection Plot

## L.20  Girder Test G2C-Center
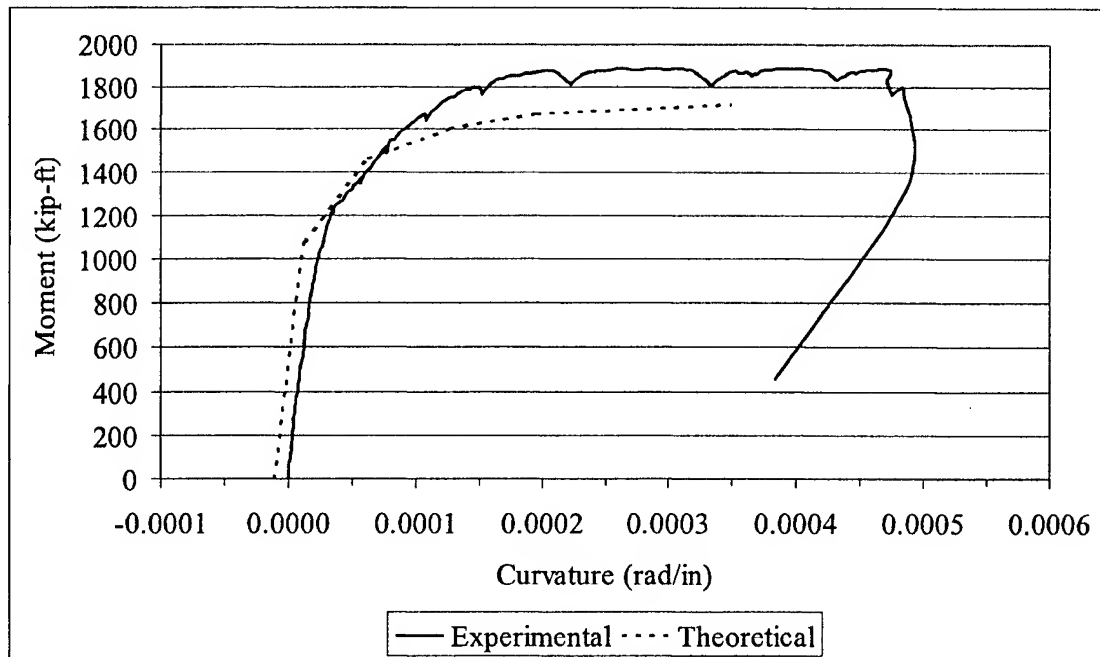


Figure L.40  G2C-Center Moment vs. Curvature Plot
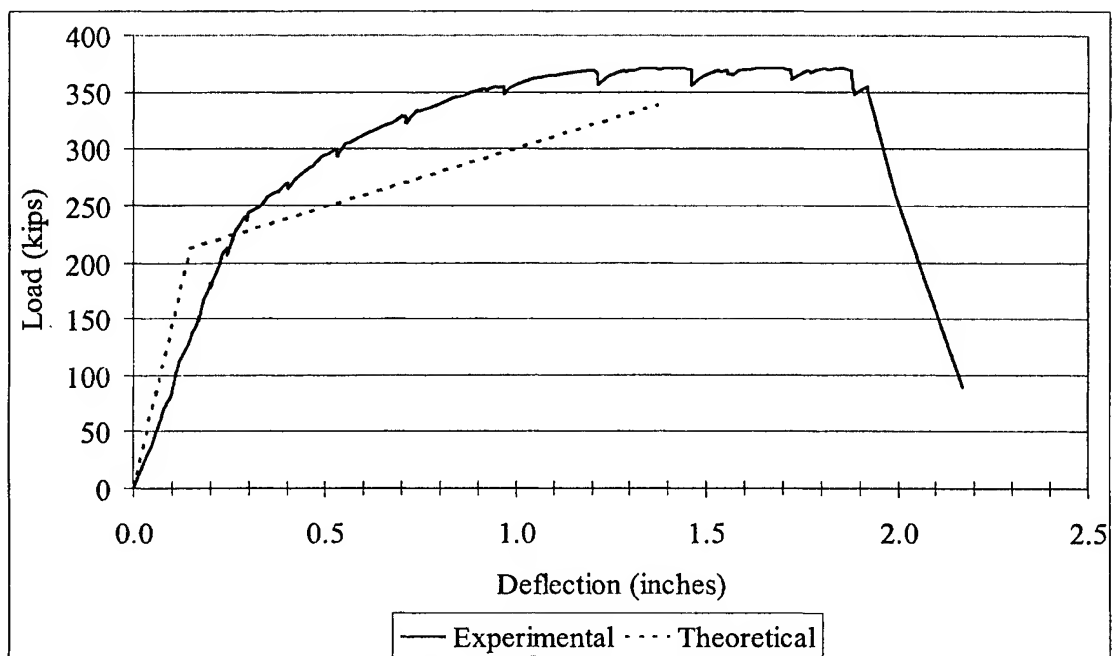


Figure L.41  G2C-Center Load vs. Deflection Plot

538

# APPENDIX M

# PHOTOS OF GIRDER CENTER SPAN TESTS

Appendix M contains photos from each center span girder test. Photos of the girder end spans are located in Appendix Q. The photos in this appendix are matched by test configuration. For example, Girder tests G1A-Center and G2A-Center are shown on the same page to allow comparison of test results between the two grades of HSLC.

## M.1 Girder Test G1A-Center
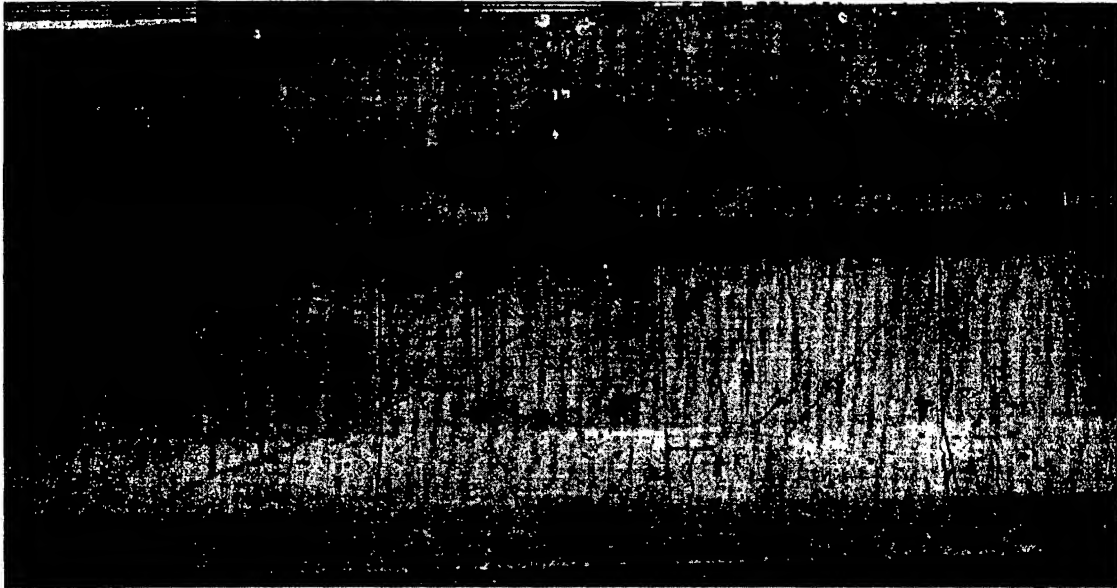


Figure M.1  G1A-Center Crack Patterns


## M.2 Girder Test G2A-Center
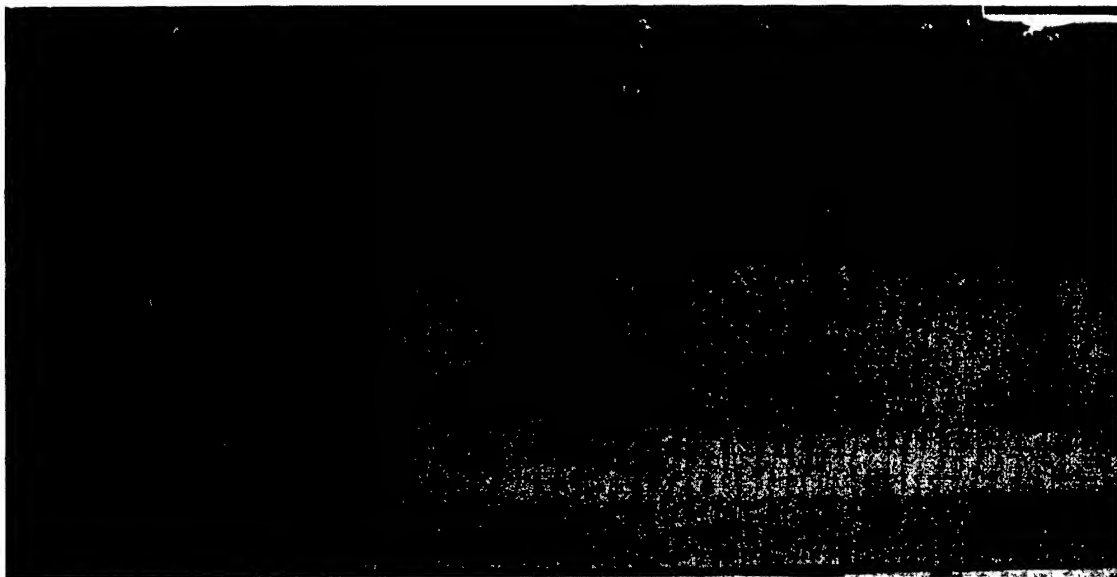


Figure M.2  G2A-Center Crack Patterns

## M.3  Girder Test G1B-Center
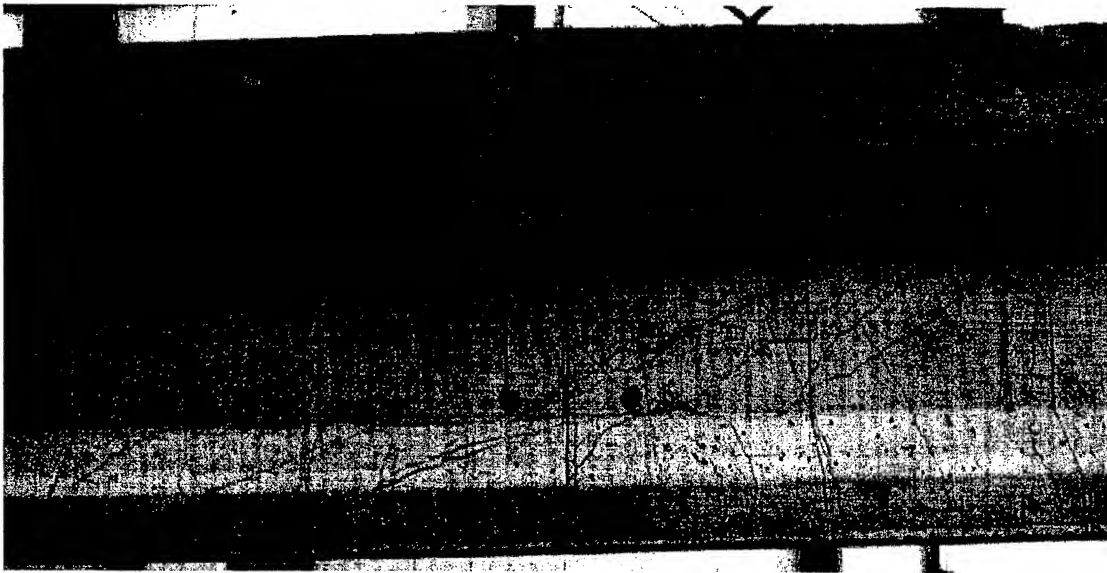


Figure M.3  G1B-Center Crack Patterns

## M.4  Girder Test G2B-Center
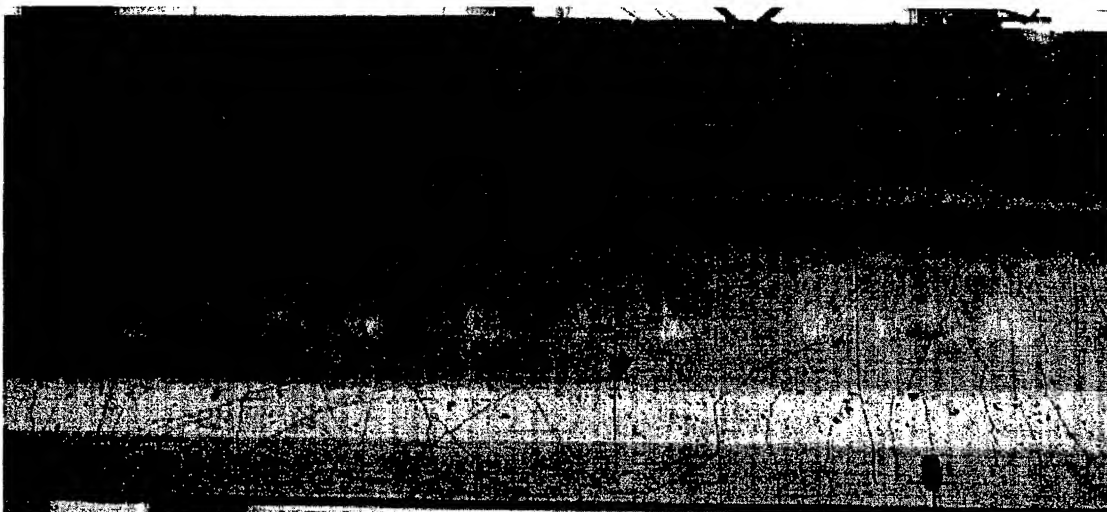


Figure M.4  G2B-Center Crack Patterns

## M.5  Girder Test G1C-Center
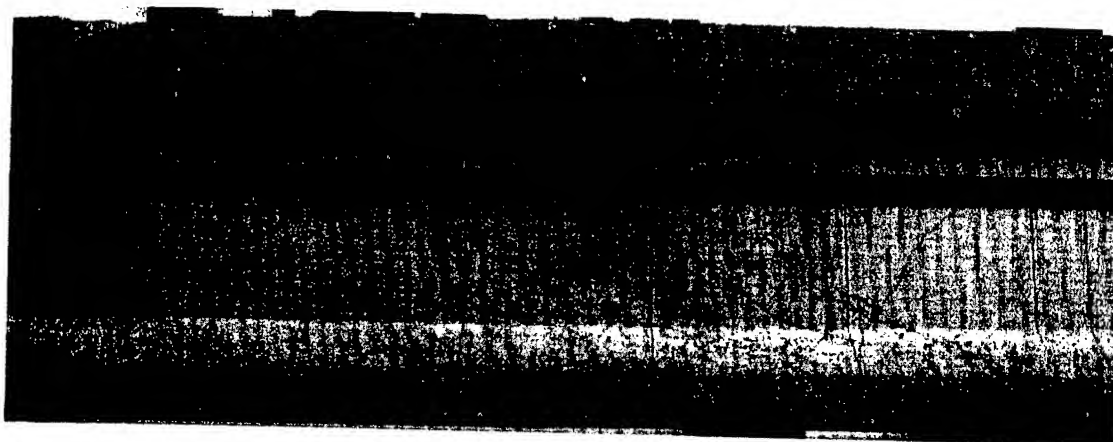


Figure M.5  G1C-Center Crack Patterns

## M.6  Girder Test G2C-Center
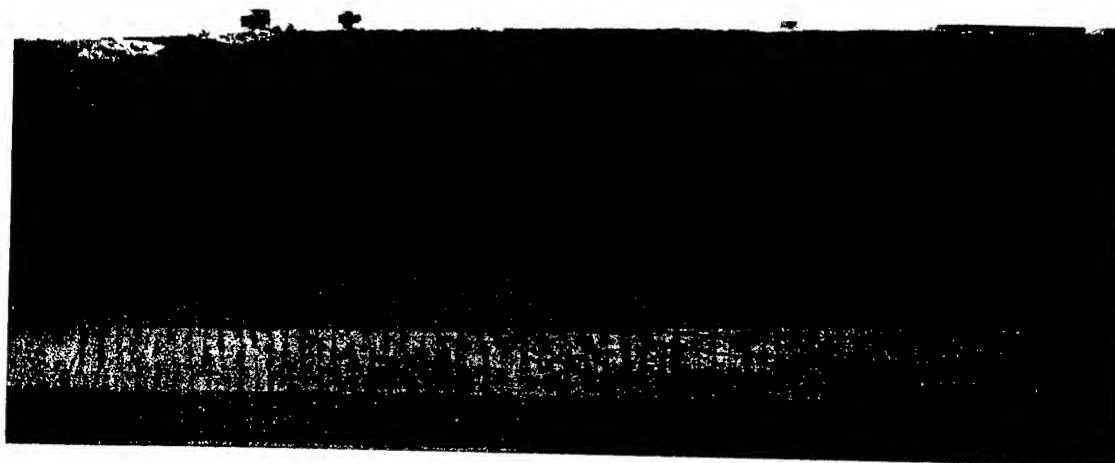


Figure M.6  G2C-Center Crack Patterns

542

# APPENDIX N


# VARIABLE ANGLE TRUSS MODEL PLOTS
## OF
## STRAND FORCE AND BOND STRESS


Appendix N contains plots of strand force and bond stress as predicted using the variable angle truss model for girder tests that failed due to shear induced by strand slip. For the girder tests, it was assumed that once the strands were within a distance equal to one stirrup space from the support that only the bottom eight strands carried the strand force.

## N.1 Girder Test G1A-East
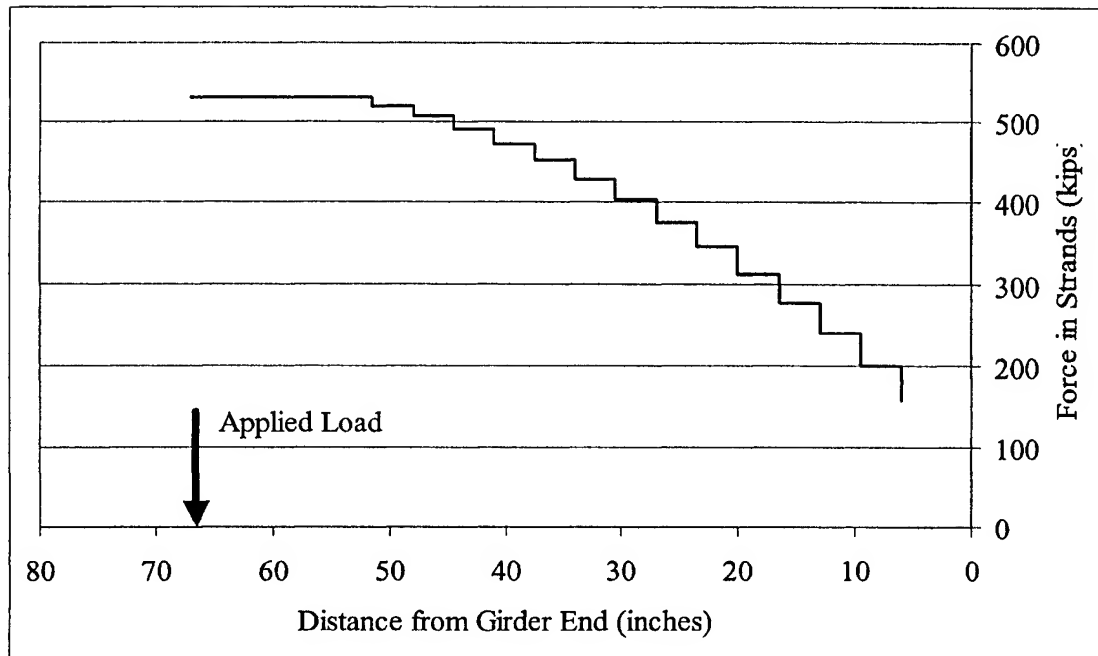


Figure N.1  G1A-East Strand Force Plot
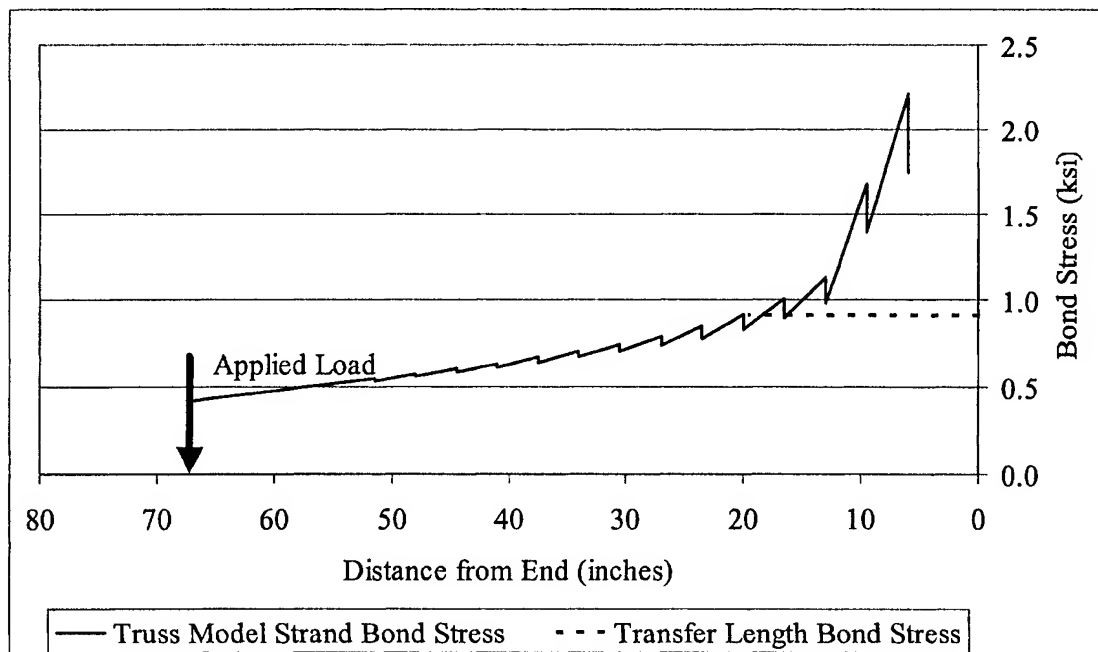


Figure N.2  G1A-East Bond Stress Plot

## N.2 Girder Test G1B-East
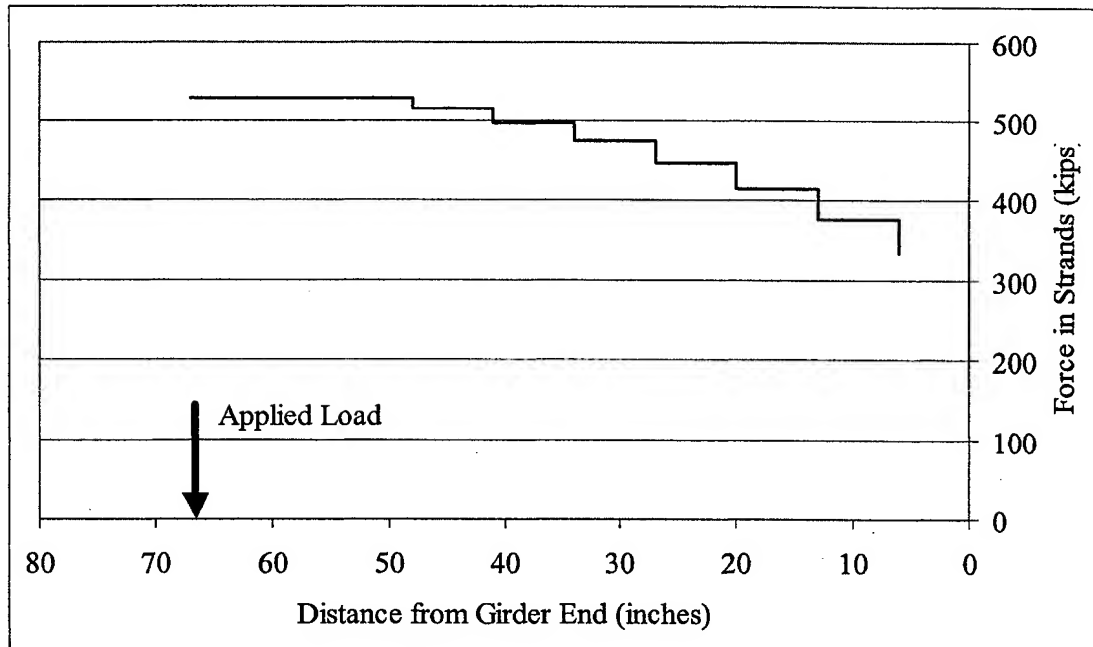


Figure N.3 G1B-East Strand Force Plot
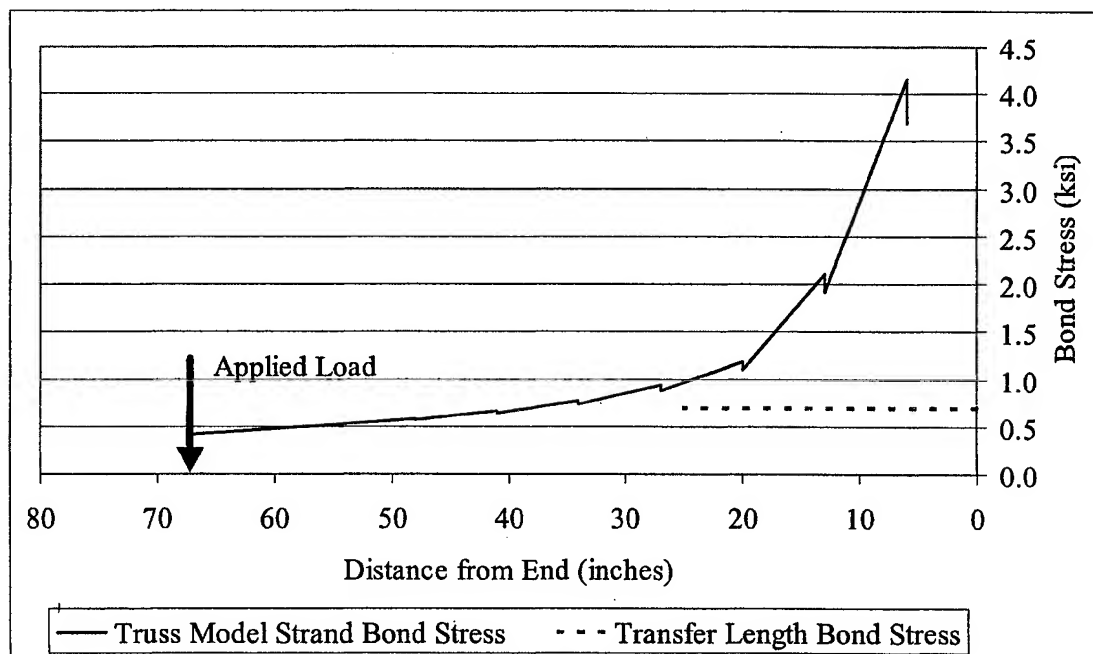


Figure N.4 G1B-East Bond Stress Plot

## N.3  Girder Test G1C-East
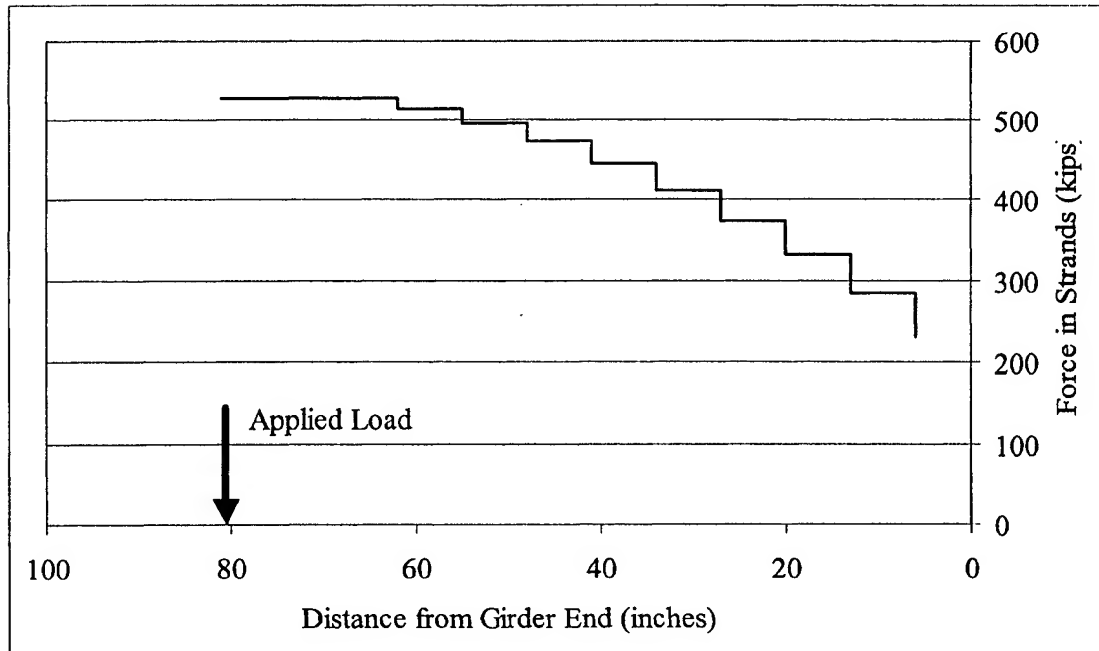


Figure N.5  G1C-East Strand Force Plot
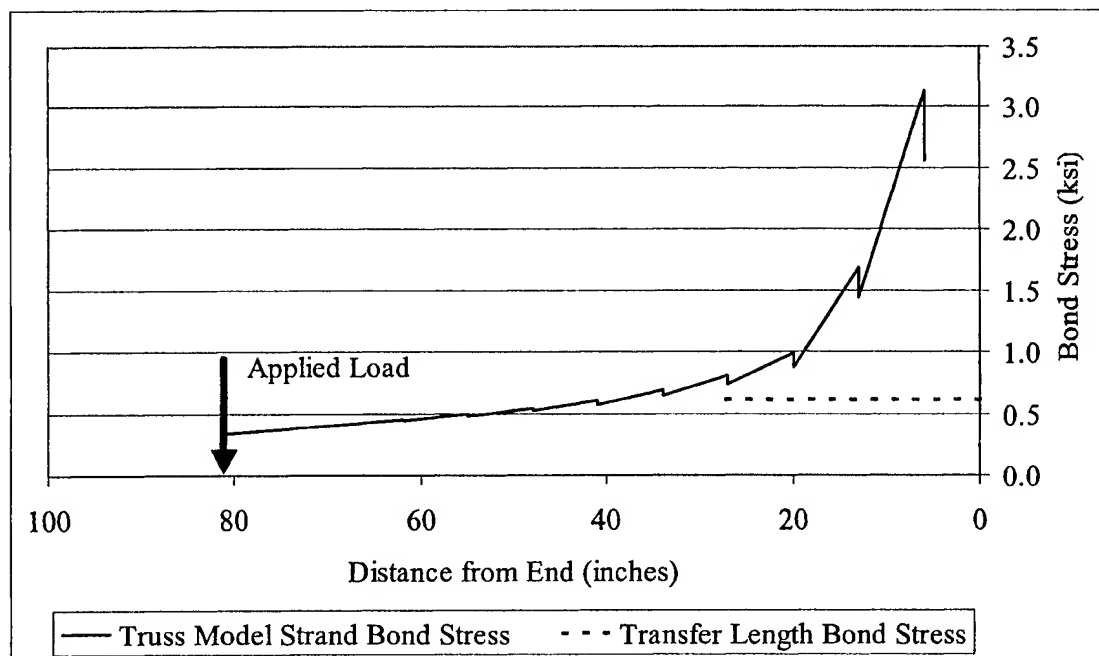


Figure N.6  G1C-East Bond Stress Plot

# APPENDIX O

## DEVELOPMENT LENGTH DAQ OUTPUT PROCESSING SPREADSHEET

Appendix O contains the individual pages from the Development Length DAQ Output Processing Spreadsheet. This sheet was used to process the DAQ output from the 12 development length tests. The entire set of worksheet pages is provided from development length test G1C-W. The pages are listed in the order the calculations occur. A similar series of worksheets was prepared for each development length test. Listed below are the individual worksheets within the overall spreadsheet and a brief description of the worksheet's function.

**Table O.1 – Input Variables** – Used to enter information about the development length test. The user enters values in the shaded fields. All other fields are automatic and provide key information about the test. The value for $P_{crack}$ must be determined and entered by the user from the load-displacement curve.

**Table O.2 – DAQ Output** – A sample of the raw data output from the data acquisition system. Only a small percentage of the total number of DAQ lines is shown.

**Table O.3 – Prestressing Strand Tension Test Curve** – Used to determine forces and stresses in prestressing strand based on strand strain data.

547

**Table O.4 – Load, Strain, Deflection and Strain Values** – Calculates applied load and shear, vertical deflection, and strain values on the top surface of the deck and at bottom strand level. Calculates the position of the neutral axis based on a linear strain distribution assumption.

**Table O.5 – Strand Slip** – Calculates strand slip values for each strand and the average slip.

**Figure O.1 – Load vs. Vertical Displacement Plot**

**Figure O.2 – Applied Shear vs. Average Strand Slip**

**Figure O.3 – Load vs. Top of Deck Strain**

**Figure O.4 – Load vs. Strand Strain** – Calculates total strain in strand by adding the strain due to effective prestressing and flexural strain due to load application.

Table O.1 Input Variables

# Input Variables

| Beam # | GHCW | | Test Configuration # | 4 | | Date | 02-Nov-01 |

Enter values in blue fields and adjust limits of functions to include all data points in DAQ file.

| Support Span | $L_j$ | 50400? | Inches |
| Shear Distance | a | 85.00 | Inches |
| Beam Height | | 36.00 | Inches |
| Composite Bm Ht | H | 47.88? | Inches |
| Deck Width | $W_D$ | 103.75 | Inches |

| Top Strand Height | 33.50 | Inches |

Top LVDT

| Gage Length | 24.00? | Inches |
| Top Edge Distance | 1.00 | Inches |

| Stirrup Design | Single |

### Girder Test Values

| | | | |
|---|---|---|---|
| Initial Cracking Load | $P_{crack}$ | 183.00 | Kips |
| Cracking Moment | $M_{cr}$ | 1077.64 | Ft-Kips |
| Max Applied Load | $P_{max}$ | 299.04 | Kips |
| Nominal Moment | $M_n$ | 1760.95 | Ft-Kips |
| Max Deflection | $d_{max}$ | 2.27 | Inches |
| Max Deck Strain | $e_{cu}$ | 0.0036 | in/in |
| Max Strand Strain | $e_{ps}$ | 1.3960 | Percent |
| Max Strand Force | $F_{ps}$ | 57.72 | Kips |

### Maximum Strand Slip

| | | |
|---|---|---|
| Strand 0 | 0.0011 | |
| Strand 1 | 0.0018 | |
| Strand 2 | 0.0003 | |
| Strand 3 | 0.0001 | |
| Strand 4 | 0.0002 | Inches |
| Strand 5 | 0.0001 | |
| Strand 6 | 0.0001 | |
| Strand 7 | 0.0002 | |

| Max Avg Strand Slip | | |
|---|---|---|
| 0.0001 | Inches |

Bot LVDT

| Gage Length | 24.00? | Inches |
| Bot Edge Distance | 3.00 | Inches |

| Bot Strand Height | 3.00? | Inches |
| Effective Strand Strain | 5053 | me |

0

45

90

Table O.2 DAQ Output

| 11/02/2001 Load Cell | 12:07 PM LVDT Top | LVDT Bot | Wire Pot | LVDT 0 | LVDT 45 | LVDT 90 | LIN 0 | LIN 1 | LIN 2 | LIN 3 | LIN 4 | LIN 5 | LIN 6 | LIN 7 |
|---|---|---|---|---|---|---|---|---|---|---|---|---|---|---|
| 11.442372 | -0.00048 | -0.001137 | 2.465919 | -0.00249 | -0.002784 | -0.001542 | 0.002204 | 0.001449 | 0.000915 | 0.000915 | 0.000883 | 0.000946 | 0.000915 | 0.000946 |
| 13.463793 | -0.00056 | -0.001176 | 2.461571 | -0.002496 | -0.00279 | -0.001566 | 0.002267 | 0.001386 | 0.000883 | 0.000915 | 0.000883 | 0.000978 | 0.000946 | 0.001041 |
| 16.630684 | -0.000659 | -0.00129 | 2.455239 | -0.002484 | -0.002856 | -0.001548 | 0.002046 | 0.001418 | 0.001009 | 0.000883 | 0.000852 | 0.000978 | 0.000978 | 0.001009 |
| 27.815872 | -0.000462 | -0.001888 | 2.433496 | -0.002496 | -0.0031 | -0.001554 | 0.002172 | 0.001512 | 0.000978 | 0.000978 | 0.000915 | 0.001072 | 0.000978 | 0.000946 |
| 35.0256 | 0.000148 | -0.00232 | 2.415492 | -0.002477 | -0.003245 | -0.001554 | 0.002172 | 0.001449 | 0.000946 | 0.000883 | 0.000852 | 0.001009 | 0.001009 | 0.000946 |
| 34.789768 | 0.000173 | -0.00232 | 2.415569 | -0.002484 | -0.00327 | -0.00156 | 0.002172 | 0.001355 | 0.000915 | 0.000883 | 0.000915 | 0.000978 | 0.000852 | 0.000915 |
| 39.236893 | 0.000457 | -0.002524 | 2.410762 | -0.002471 | -0.003343 | -0.001548 | 0.002204 | 0.001386 | 0.001009 | 0.000852 | 0.000852 | 0.000946 | 0.000915 | 0.000978 |
| 45.536983 | 0.001055 | -0.002905 | 2.396878 | -0.002477 | -0.003495 | -0.001566 | 0.002046 | 0.001481 | 0.001009 | 0.000852 | 0.000789 | 0.001009 | 0.000915 | 0.000978 |
| 48.872326 | 0.001227 | -0.003109 | 2.392224 | -0.002465 | -0.003543 | -0.001548 | 0.002078 | 0.001386 | 0.000946 | 0.000978 | 0.000821 | 0.001072 | 0.000883 | 0.000915 |
| 48.653339 | 0.00127 | -0.003121 | 2.392148 | -0.002459 | -0.003562 | -0.001554 | 0.002109 | 0.001386 | 0.000883 | 0.000978 | 0.000821 | 0.001009 | 0.000915 | 0.000978 |
| 55.509319 | 0.001424 | -0.003541 | 2.377653 | -0.002459 | -0.00372 | -0.001573 | 0.002015 | 0.001386 | 0.000821 | 0.000883 | 0.000821 | 0.001072 | 0.000883 | 0.000946 |
| 61.371441 | 0.002059 | -0.003808 | 2.368269 | -0.002453 | -0.003841 | -0.001517 | 0.002204 | 0.001386 | 0.001009 | 0.000978 | 0.000821 | 0.000946 | 0.000915 | 0.000978 |
| 71.697525 | 0.002632 | -0.004393 | 2.349273 | -0.002399 | -0.004096 | -0.001542 | 0.002141 | 0.001449 | 0.000946 | 0.000978 | 0.000695 | 0.000978 | 0.000883 | 0.000946 |
| 75.369766 | 0.003138 | -0.004635 | 2.340576 | -0.002405 | -0.004175 | -0.001554 | 0.002046 | 0.001386 | 0.000946 | 0.000946 | 0.000883 | 0.000946 | 0.000915 | 0.000946 |
| 78.907257 | 0.003428 | -0.0048 | 2.332566 | -0.002393 | -0.004248 | -0.001535 | 0.002046 | 0.001449 | 0.001009 | 0.000915 | 0.000883 | 0.000978 | 0.000946 | 0.000915 |
| 83.1017 | 0.003797 | -0.005105 | 2.326692 | -0.002375 | -0.004364 | -0.001542 | 0.002204 | 0.001386 | 0.001009 | 0.000852 | 0.000852 | 0.001009 | 0.000915 | 0.000978 |
| 82.832176 | 0.003841 | -0.005105 | 2.326615 | -0.002381 | -0.004364 | -0.001548 | 0.002046 | 0.001418 | 0.000883 | 0.000915 | 0.000821 | 0.000978 | 0.000883 | 0.001009 |
| 82.663727 | 0.003834 | -0.005131 | 2.326615 | -0.002363 | -0.004364 | -0.001535 | 0.002046 | 0.001386 | 0.000946 | 0.000915 | 0.000821 | 0.000946 | 0.000915 | 0.000946 |
| 86.20121 | 0.004118 | -0.005334 | 2.321809 | -0.002357 | -0.004431 | -0.001529 | 0.002015 | 0.001449 | 0.000946 | 0.000883 | 0.000821 | 0.001041 | 0.000946 | 0.000946 |
| 89.233345 | 0.004291 | -0.005474 | 2.313188 | -0.002357 | -0.004491 | -0.00156 | 0.002046 | 0.001481 | 0.000915 | 0.000883 | 0.000789 | 0.000946 | 0.000883 | 0.000883 |
| 92.753983 | 0.004475 | -0.005652 | 2.308458 | -0.00232 | -0.004577 | -0.001548 | 0.002109 | 0.001355 | 0.000946 | 0.000883 | 0.000821 | 0.000978 | 0.000852 | 0.001009 |
| 92.551834 | 0.004728 | -0.00569 | 2.308382 | -0.002332 | -0.004583 | -0.001542 | 0.002046 | 0.001386 | 0.001009 | 0.000883 | 0.000883 | 0.001009 | 0.000883 | 0.000883 |
| 92.383385 | 0.004549 | -0.005652 | 2.308382 | -0.002314 | -0.004577 | -0.001554 | 0.002046 | 0.001323 | 0.000946 | 0.000946 | 0.000821 | 0.000946 | 0.000978 | 0.000946 |
| 92.248627 | 0.004697 | -0.005716 | 2.308458 | -0.002332 | -0.004589 | -0.001554 | 0.002078 | 0.001418 | 0.001041 | 0.000946 | 0.000852 | 0.000946 | 0.000852 | 0.000978 |
| 92.181244 | 0.004636 | -0.005678 | 2.308535 | -0.00235 | -0.004589 | -0.001542 | 0.002015 | 0.001355 | 0.001072 | 0.000978 | 0.000852 | 0.000978 | 0.000946 | 0.000946 |
| 92.063324 | 0.004697 | -0.005703 | 2.308306 | -0.002338 | -0.004577 | -0.001542 | 0.002015 | 0.001386 | 0.000946 | 0.000946 | 0.000852 | 0.000978 | 0.000852 | 0.000978 |
| 91.945412 | 0.004586 | -0.005716 | 2.308229 | -0.002332 | -0.004589 | -0.001554 | 0.002078 | 0.001386 | 0.000915 | 0.000852 | 0.000821 | 0.000883 | 0.000915 | 0.000978 |
| 91.878029 | 0.00463 | -0.00569 | 2.308535 | -0.002326 | -0.004577 | -0.00156 | 0.002015 | 0.001386 | 0.000946 | 0.000915 | 0.000946 | 0.000946 | 0.000946 | 0.000978 |
| 91.7938 | 0.00458 | -0.005665 | 2.308535 | -0.00232 | -0.00457 | -0.001554 | 0.002046 | 0.001323 | 0.001009 | 0.000883 | 0.000883 | 0.001041 | 0.000978 | 0.000978 |
| 91.726425 | 0.00463 | -0.005665 | 2.308458 | -0.002332 | -0.004577 | -0.001517 | 0.001984 | 0.001292 | 0.001009 | 0.000883 | 0.000821 | 0.000946 | 0.000883 | 0.000946 |
| 91.591667 | 0.004599 | -0.005665 | 2.308306 | -0.002326 | -0.00457 | -0.001548 | 0.002015 | 0.001449 | 0.000946 | 0.000978 | 0.000852 | 0.000915 | 0.000946 | 0.000883 |
| 91.541122 | 0.004747 | -0.00564 | 2.308306 | -0.002332 | -0.004589 | -0.001548 | 0.001952 | 0.001449 | 0.000915 | 0.000883 | 0.000852 | 0.000978 | 0.000946 | 0.000978 |
| 91.507439 | 0.004691 | -0.005665 | 2.308458 | -0.002326 | -0.004552 | -0.001542 | 0.002015 | 0.001386 | 0.000883 | 0.000946 | 0.000852 | 0.000978 | 0.000915 | 0.000978 |
| 91.440056 | 0.00458 | -0.005665 | 2.308382 | -0.002344 | -0.00457 | -0.001542 | 0.001984 | 0.001355 | 0.000978 | 0.000946 | 0.000852 | 0.000883 | 0.000915 | 0.000915 |
| 91.372681 | 0.00458 | -0.005601 | 2.308382 | -0.002344 | -0.00457 | -0.001554 | 0.001984 | 0.001418 | 0.001009 | 0.000946 | 0.000789 | 0.001009 | 0.000852 | 0.001009 |
| 91.30529 | 0.004389 | -0.005678 | 2.308535 | -0.00235 | -0.00457 | -0.00156 | 0.001984 | 0.001481 | 0.000978 | 0.000883 | 0.000852 | 0.001041 | 0.000915 | 0.000915 |
| 91.288452 | 0.004482 | -0.005652 | 2.308382 | -0.002332 | -0.004564 | -0.001554 | 0.002078 | 0.001418 | 0.000978 | 0.000978 | 0.000821 | 0.001009 | 0.000946 | 0.000946 |
| 91.187378 | 0.004531 | -0.005665 | 2.308382 | -0.002332 | -0.004546 | -0.001548 | 0.002046 | 0.001418 | 0.000915 | 0.000915 | 0.000789 | 0.000978 | 0.000852 | 0.000915 |
| 91.120003 | 0.004475 | -0.005652 | 2.308535 | -0.002296 | -0.004552 | -0.001554 | 0.001984 | 0.001386 | 0.000946 | 0.000978 | 0.000883 | 0.000946 | 0.000915 | 0.000883 |

Table O.3  Prestressing Strand Tension Curve

## Prestressing Strand Tension Test Curve and Zone Limit Data



Strain -Stress Curve for 0.6" 270 KSI LOLAX Strand

$y = 0.8063x + 56.5921$
$R^2 = 1.0000$

$y = 95.9317x^3 - 348.9161x^2 + 423.6514x - 114.2059$
$R^2 = 0.9985$

$y = 63.7701x + 0.0000$
$R^2 = 1.0000$

Load (Kips) vs. Strain (Percent)

◆ Elastic   ■ Transition   ▲ Plastic   — Transition   — Linear (Elastic)   — Linear (Plastic)   — Poly. (Transition)

| Prestressing Strand Loading Data | | |
| --- | --- | --- |
| Point of Loading | Strain (%) | Load (Kips) |
| Start of Elastic | 0 | 0.00 |
| End of Elastic | 0.7135 | 45.50 |
| Transition 1 | 0.7500 | 47.45 |
| Transition 2 | 0.8750 | 53.63 |
| Transition 3 | 1.0000 | 56.67 |
| Transition 4 | 1.1250 | 57.20 |
| Start of Plastic | 1.2500 | 57.60 |
| End of Plastic | 6.5000 | 61.83 |

| Zone | Percent Strain | | |
| --- | --- | --- | --- |
| Elastic | 0 | <e< | 0.7135 |
| Transition | 0.7135 | <e< | 1.2500 |
| Plastic | 1.2500 | >e | |

| Zone | Load | | |
| --- | --- | --- | --- |
| Elastic | 0 | <Kips< | 45.50 |
| Transition | 45.50 | <Kips< | 57.60 |
| Plastic | 57.60 | >Kips | |

Table O.4 Load, Shear, Deflection and Strain Values

## Load, Shear, Deflection and Strain Values

| Data Point # | At Point of Loading | | | | | | | Neutral Axis Location | Adjusted Values (Linear Assumption) | | |
|---|---|---|---|---|---|---|---|---|---|---|---|
| | Load | Shear | Top LVDT (Inches) | Top Strain (m-strain) | Bot LVDT (Inches) | Bot Strain (m-strain) | Vertical Deflection | | Top of Slab | At Level of Bottom Strands | Total Strand Strain |
| | (Kips) | (Kips) | Compression e = (-) | Compression e = (-) | Tension e = (+) | Tension e = (+) | (Inches) | (Inches from Bot) | (in/in) | (m-strain) | (percent strain) |
| 0 | 0.0 | 0.0 | 0.000000 | 0.00 | 0.000000 | 0.00 | 0.000000 | NA | 0.00 | 0.00 | 0.505 |
| 1 | 2.0 | 1.7 | -0.000080 | 3.33 | -0.000039 | 1.63 | 0.004348 | 17.38 | 0.00000 | 1.63 | 0.505 |
| 2 | 5.2 | 4.3 | -0.000179 | 7.46 | -0.000153 | 6.38 | 0.010680 | 23.22 | -0.00001 | 6.38 | 0.506 |
| 3 | 16.4 | 13.6 | 0.000018 | -0.75 | -0.000751 | 31.29 | 0.032423 | 45.85 | 0.00000 | 31.29 | 0.508 |
| 4 | 23.6 | 19.6 | 0.000628 | -26.17 | -0.001183 | 49.29 | 0.050427 | 31.66 | 0.00003 | 49.29 | 0.510 |
| 5 | 23.3 | 19.4 | 0.000653 | -27.21 | -0.001183 | 49.29 | 0.050350 | 31.27 | 0.00003 | 49.29 | 0.510 |
| 6 | 27.8 | 23.1 | 0.000937 | -39.04 | -0.001387 | 57.79 | 0.055157 | 29.19 | 0.00004 | 57.79 | 0.511 |
| 7 | 34.1 | 28.3 | 0.001535 | -63.96 | -0.001768 | 73.67 | 0.069041 | 26.49 | 0.00007 | 73.67 | 0.513 |
| 8 | 37.4 | 31.1 | 0.001707 | -71.13 | -0.001972 | 82.17 | 0.073695 | 26.52 | 0.00007 | 82.17 | 0.514 |
| 9 | 37.2 | 30.9 | 0.001750 | -72.92 | -0.001984 | 82.67 | 0.073771 | 26.31 | 0.00008 | 82.67 | 0.514 |
| 10 | 44.1 | 36.6 | 0.001904 | -79.33 | -0.002404 | 100.17 | 0.088266 | 27.48 | 0.00008 | 100.17 | 0.515 |
| 11 | 49.9 | 41.5 | 0.002539 | -105.79 | -0.002671 | 111.29 | 0.097650 | 25.49 | 0.00011 | 111.29 | 0.516 |
| 12 | 60.3 | 50.1 | 0.003112 | -129.67 | -0.003256 | 135.67 | 0.116646 | 25.43 | 0.00014 | 135.67 | 0.519 |
| 13 | 63.9 | 53.1 | 0.003618 | -150.75 | -0.003498 | 145.75 | 0.125343 | 24.57 | 0.00016 | 145.75 | 0.520 |
| 14 | 67.5 | 56.1 | 0.003908 | -162.83 | -0.003663 | 152.63 | 0.133353 | 24.23 | 0.00017 | 152.63 | 0.521 |
| 15 | 71.7 | 59.6 | 0.004277 | -178.21 | -0.003968 | 165.33 | 0.139227 | 24.12 | 0.00019 | 165.33 | 0.522 |
| 16 | 71.4 | 59.3 | 0.004321 | -180.04 | -0.003968 | 165.33 | 0.139304 | 24.00 | 0.00019 | 165.33 | 0.522 |
| 17 | 71.2 | 59.2 | 0.004314 | -179.75 | -0.003994 | 166.42 | 0.139304 | 24.09 | 0.00019 | 166.42 | 0.522 |
| 18 | 74.8 | 62.2 | 0.004598 | -191.58 | -0.004197 | 174.88 | 0.144110 | 23.94 | 0.00020 | 174.88 | 0.523 |
| 19 | 77.8 | 64.7 | 0.004771 | -198.79 | -0.004337 | 180.71 | 0.152731 | 23.89 | 0.00021 | 180.71 | 0.523 |
| 20 | 81.3 | 67.6 | 0.004955 | -206.46 | -0.004515 | 188.13 | 0.157461 | 23.92 | 0.00022 | 188.13 | 0.524 |
| 21 | 81.1 | 67.4 | 0.005208 | -217.00 | -0.004553 | 189.71 | 0.157537 | 23.47 | 0.00023 | 189.71 | 0.524 |
| 22 | 80.9 | 67.3 | 0.005029 | -209.54 | -0.004515 | 188.13 | 0.157537 | 23.76 | 0.00022 | 188.13 | 0.524 |
| 23 | 80.8 | 67.2 | 0.005177 | -215.71 | -0.004579 | 190.79 | 0.157461 | 23.59 | 0.00022 | 190.79 | 0.524 |
| 24 | 80.7 | 67.1 | 0.005116 | -213.17 | -0.004541 | 189.21 | 0.157384 | 23.63 | 0.00022 | 189.21 | 0.524 |
| 25 | 80.6 | 67.0 | 0.005177 | -215.71 | -0.004566 | 190.25 | 0.157613 | 23.56 | 0.00022 | 190.25 | 0.524 |
| 26 | 80.5 | 66.9 | 0.005066 | -211.08 | -0.004579 | 190.79 | 0.157690 | 23.83 | 0.00022 | 190.79 | 0.524 |
| 27 | 80.4 | 66.9 | 0.005110 | -212.92 | -0.004553 | 189.71 | 0.157537 | 23.67 | 0.00022 | 189.71 | 0.524 |
| 28 | 80.4 | 66.8 | 0.005060 | -210.83 | -0.004528 | 188.67 | 0.157384 | 23.72 | 0.00022 | 188.67 | 0.524 |
| 29 | 80.3 | 66.7 | 0.005110 | -212.92 | -0.004528 | 188.67 | 0.157461 | 23.61 | 0.00022 | 188.67 | 0.524 |
| 30 | 80.1 | 66.6 | 0.005079 | -211.63 | -0.004528 | 188.67 | 0.157613 | 23.68 | 0.00022 | 188.67 | 0.524 |
| 31 | 80.1 | 66.6 | 0.005227 | -217.79 | -0.004503 | 187.63 | 0.157613 | 23.31 | 0.00023 | 187.63 | 0.524 |
| 32 | 80.1 | 66.6 | 0.005171 | -215.46 | -0.004528 | 188.67 | 0.157461 | 23.48 | 0.00022 | 188.67 | 0.524 |
| 33 | 80.0 | 66.5 | 0.005060 | -210.83 | -0.004528 | 188.67 | 0.157537 | 23.72 | 0.00022 | 188.67 | 0.524 |
| 34 | 79.9 | 66.4 | 0.005060 | -210.83 | -0.004464 | 186.00 | 0.157537 | 23.56 | 0.00022 | 186.00 | 0.524 |

Table O.5 Strand Slip

## Strand Slip

| Data Point # | Applied Shear (kips) | Strand Slip Indicators | | | | | | | | Avg Slip (Inches) |
|---|---|---|---|---|---|---|---|---|---|---|
| | | LIN 0 (Inches) | LIN 1 (Inches) | LIN 2 (Inches) | LIN 3 (Inches) | LIN 4 (Inches) | LIN 5 (Inches) | LIN 6 (Inches) | LIN 7 (Inches) | |
| 0 | 0.0 | 0.000000 | 0.000000 | 0.000000 | 0.000000 | 0.000000 | 0.000000 | 0.000000 | 0.000000 | 0.000000 |
| 1 | 1.7 | 0.000063 | -0.000063 | -0.000032 | 0.000000 | 0.000000 | 0.000032 | 0.000031 | 0.000095 | 0.000016 |
| 2 | 4.3 | -0.000158 | -0.000031 | 0.000094 | -0.000032 | -0.000031 | 0.000032 | 0.000063 | 0.000063 | 0.000000 |
| 3 | 13.6 | -0.000032 | 0.000063 | 0.000063 | 0.000063 | 0.000032 | 0.000126 | 0.000063 | 0.000000 | 0.000047 |
| 4 | 19.6 | -0.000032 | 0.000000 | 0.000031 | -0.000032 | -0.000031 | 0.000063 | 0.000094 | 0.000031 | 0.000012 |
| 5 | 19.4 | -0.000032 | -0.000094 | 0.000000 | -0.000032 | 0.000032 | 0.000032 | -0.000063 | -0.000031 | -0.000024 |
| 6 | 23.1 | 0.000000 | -0.000063 | 0.000094 | -0.000063 | -0.000031 | 0.000063 | 0.000000 | 0.000032 | -0.000004 |
| 7 | 28.3 | -0.000158 | 0.000032 | 0.000094 | -0.000063 | -0.000094 | 0.000126 | 0.000000 | 0.000032 | -0.000012 |
| 8 | 31.1 | -0.000126 | -0.000063 | 0.000031 | 0.000063 | -0.000062 | 0.000126 | -0.000032 | -0.000031 | -0.000012 |
| 9 | 30.9 | -0.000095 | -0.000063 | -0.000032 | 0.000063 | -0.000062 | 0.000000 | 0.000000 | 0.000032 | -0.000020 |
| 10 | 36.6 | -0.000189 | -0.000063 | 0.000063 | -0.000032 | -0.000062 | 0.000126 | -0.000032 | 0.000000 | -0.000024 |
| 11 | 41.5 | 0.000000 | -0.000063 | 0.000094 | -0.000032 | -0.000188 | 0.000032 | -0.000032 | 0.000032 | -0.000020 |
| 12 | 50.1 | -0.000063 | -0.000063 | 0.000031 | 0.000063 | 0.000000 | 0.000000 | 0.000000 | 0.000000 | -0.000004 |
| 13 | 53.1 | -0.000158 | 0.000000 | 0.000031 | 0.000031 | 0.000000 | 0.000063 | 0.000031 | 0.000000 | 0.000000 |
| 14 | 56.1 | -0.000158 | -0.000063 | 0.000094 | 0.000000 | 0.000000 | 0.000032 | 0.000000 | -0.000031 | -0.000015 |
| 15 | 59.6 | 0.000000 | -0.000031 | 0.000063 | -0.000063 | -0.000031 | 0.000063 | -0.000032 | 0.000032 | 0.000000 |
| 16 | 59.3 | -0.000158 | -0.000031 | -0.000032 | 0.000000 | -0.000062 | 0.000032 | 0.000000 | 0.000063 | -0.000024 |
| 17 | 59.2 | -0.000158 | -0.000063 | 0.000031 | 0.000000 | -0.000062 | 0.000000 | -0.000063 | 0.000000 | -0.000039 |
| 18 | 62.2 | -0.000189 | 0.000000 | 0.000031 | 0.000063 | -0.000062 | 0.000095 | 0.000031 | 0.000000 | -0.000020 |
| 19 | 64.7 | -0.000158 | 0.000032 | 0.000000 | -0.000032 | 0.000000 | 0.000000 | -0.000032 | -0.000063 | -0.000043 |
| 20 | 67.6 | -0.000095 | -0.000094 | 0.000031 | -0.000032 | -0.000062 | 0.000032 | -0.000063 | 0.000063 | -0.000028 |
| 21 | 67.4 | -0.000158 | -0.000063 | 0.000094 | -0.000032 | 0.000000 | 0.000063 | -0.000032 | -0.000063 | -0.000024 |
| 22 | 67.3 | -0.000158 | -0.000126 | 0.000031 | -0.000063 | -0.000062 | 0.000000 | 0.000063 | 0.000000 | -0.000028 |
| 23 | 67.2 | -0.000126 | -0.000031 | 0.000126 | 0.000031 | -0.000031 | 0.000000 | -0.000063 | 0.000032 | -0.000008 |
| 24 | 67.1 | -0.000189 | -0.000094 | 0.000157 | 0.000063 | -0.000031 | 0.000032 | 0.000031 | 0.000000 | -0.000004 |
| 25 | 67.0 | -0.000189 | -0.000063 | 0.000031 | 0.000031 | -0.000031 | 0.000032 | -0.000063 | 0.000000 | -0.000032 |
| 26 | 66.9 | -0.000126 | -0.000063 | 0.000000 | -0.000063 | -0.000062 | -0.000063 | 0.000000 | 0.000032 | -0.000043 |
| 27 | 66.9 | -0.000189 | -0.000063 | 0.000031 | 0.000000 | 0.000063 | 0.000000 | 0.000031 | 0.000032 | -0.000012 |
| 28 | 66.8 | -0.000158 | -0.000126 | 0.000094 | 0.000031 | 0.000000 | 0.000095 | 0.000031 | 0.000032 | 0.000000 |
| 29 | 66.7 | -0.000220 | -0.000157 | 0.000094 | -0.000032 | -0.000062 | 0.000000 | 0.000063 | 0.000000 | -0.000039 |
| 30 | 66.6 | -0.000189 | 0.000000 | 0.000031 | 0.000063 | -0.000031 | 0.000000 | -0.000032 | 0.000063 | -0.000032 |
| 31 | 66.6 | -0.000252 | 0.000000 | 0.000000 | 0.000032 | -0.000031 | 0.000031 | 0.000031 | 0.000032 | -0.000028 |
| 32 | 66.6 | -0.000189 | -0.000063 | -0.000032 | 0.000031 | -0.000031 | 0.000032 | 0.000000 | 0.000032 | -0.000028 |
| 33 | 66.5 | -0.000220 | -0.000094 | 0.000063 | 0.000031 | -0.000031 | -0.000063 | 0.000000 | -0.000031 | -0.000043 |
| 34 | 66.4 | -0.000220 | -0.000031 | 0.000094 | 0.000031 | -0.000094 | 0.000063 | -0.000063 | 0.000063 | -0.000020 |
| 35 | 66.4 | -0.000220 | 0.000032 | 0.000063 | -0.000032 | -0.000031 | 0.000095 | 0.000000 | -0.000031 | -0.000016 |

553
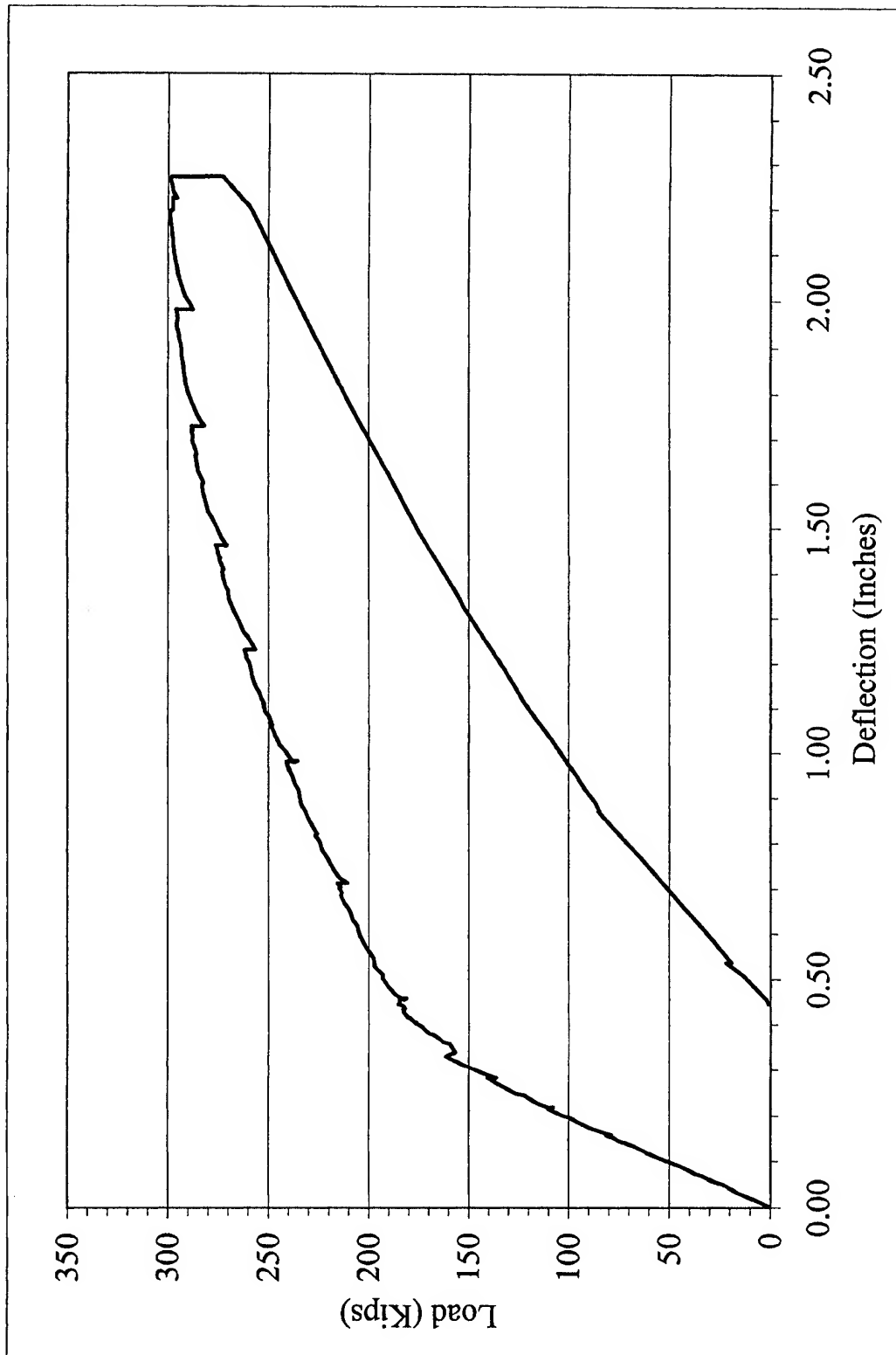
Figure O.1  Load vs. Vertical Deflection Plot for Girder Test G1C–West
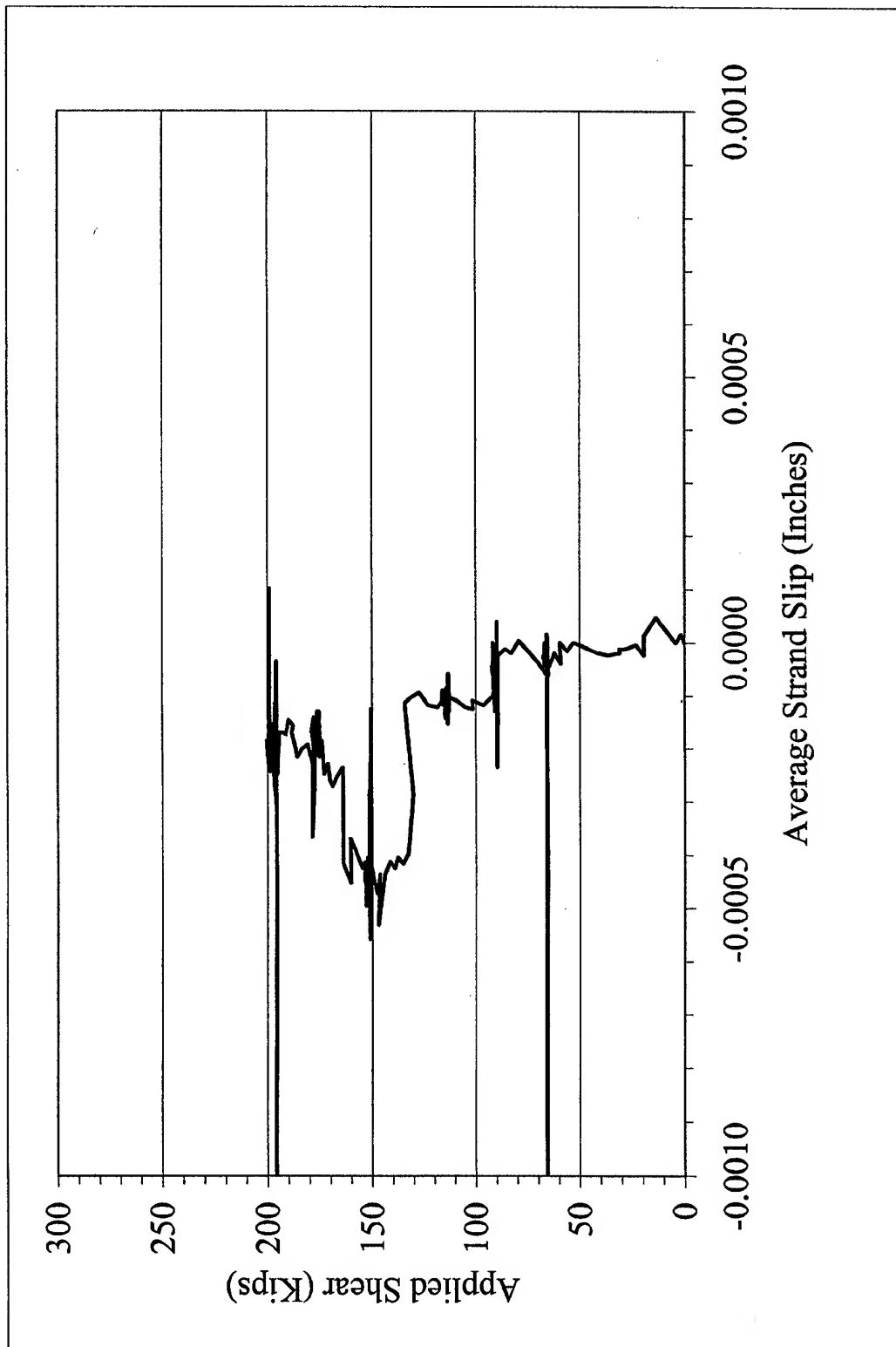
Figure O.2 Applied Shear vs. Average Strand Slip for Girder Test G1C-West
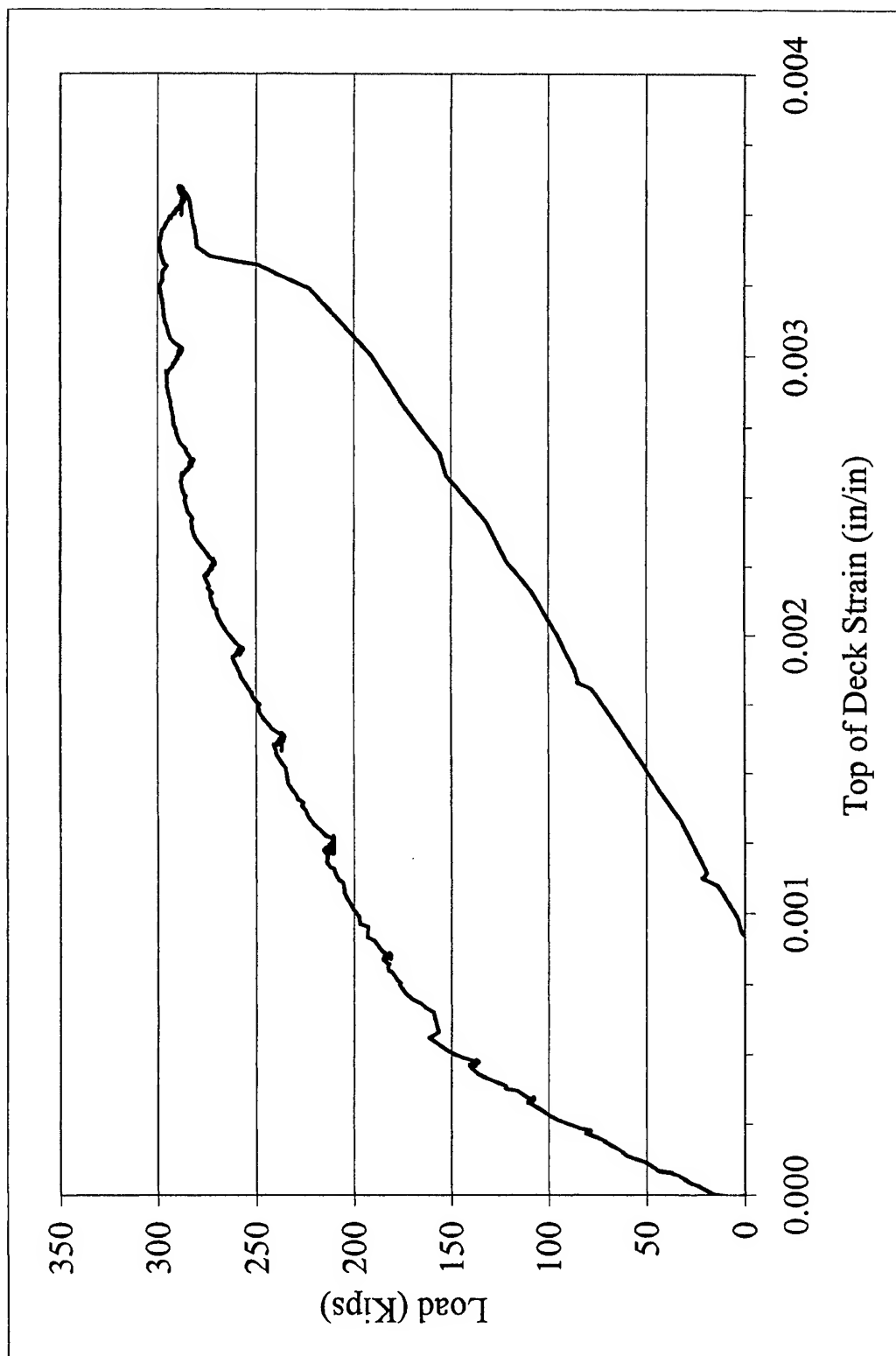
Figure O.3 Load vs. Top of Deck Strain for Girder Test G1C-West
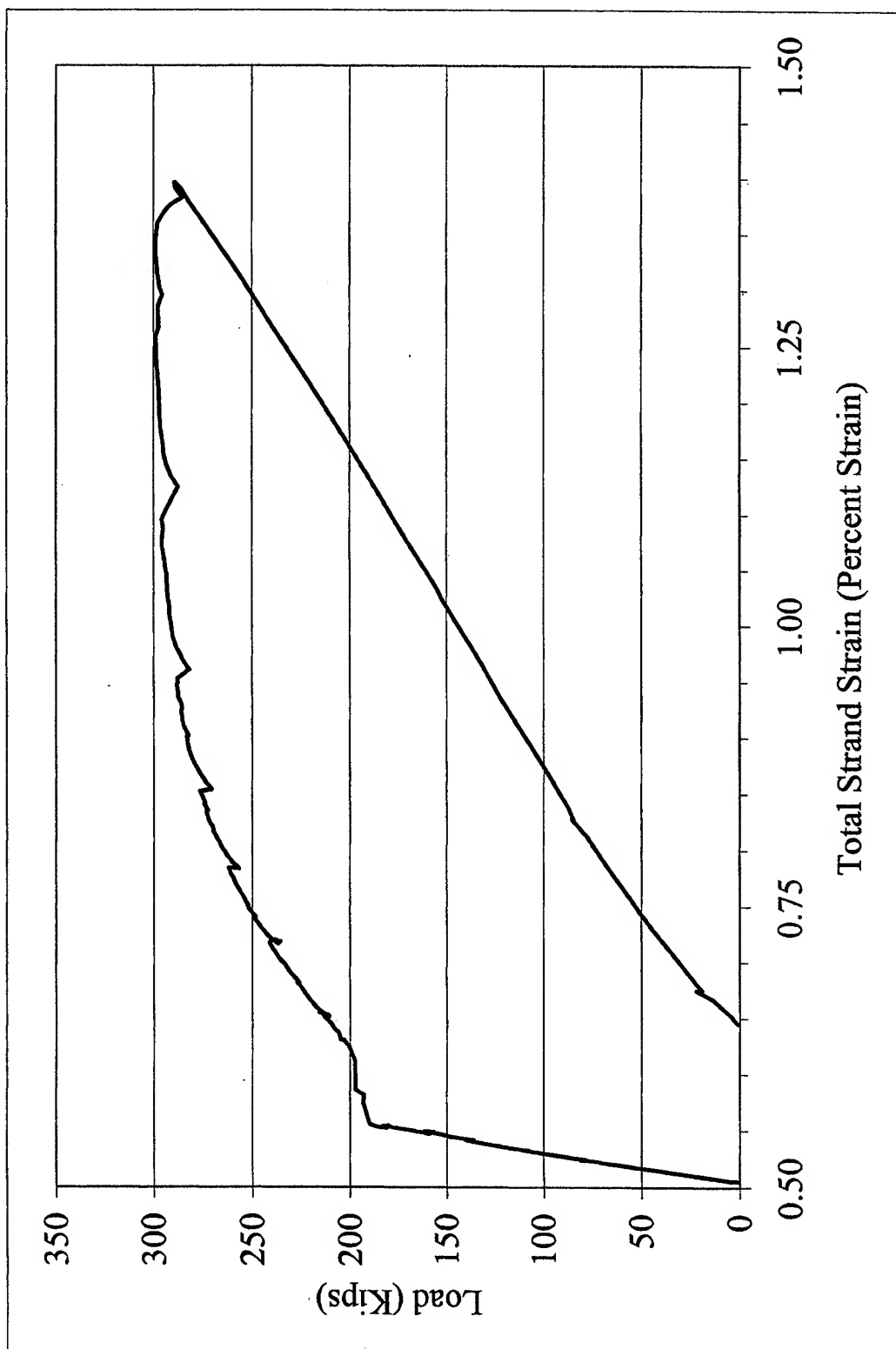
Figure O.4 Load vs. Total Strand Strain for Girder Test G1C-West

# APPENDIX P

## DEVELOPMENT LENGTH CSS DATA PROCESSING SPREADSHEET

Appendix P contains the individual pages from the Development Length CSS Data Processing Spreadsheet. This sheet was used to process the CSS data collected before and during the 12 development length tests. The entire set of worksheet pages is provided from development length test G1C-West. The pages are listed in the order the calculations occur. A similar series of worksheets was prepared for each development length test. Listed below are the individual worksheets within the overall spreadsheet and a brief description of the worksheet's function.

**Table P.1 – Girder Information Sheet** – Used to enter information about the girder end being tested. The diagram depicts both sides of the girder end being tested. The user enters values in the shaded boxes. The program automatically calculates the values that are displayed in unshaded boxes.

**Table P.2, Table P.3 – Initial Readings (Release and Testing) and 14-Day Readings** – Used to enter CSS readings just before strand release, 14 days after strand release, and just prior to testing. Table P.2 is for the North side of the girder; Table P.3 is for the South side.

**Table P.4, Table P.5 – CSS Data Taken During Development Length Test** – Used to record CSS data during the development length test. Table P.4 is for the North side of the girder; Table P.5 is for the South side of the girder.

**Table P.6, Table P.7 – Calculated Raw Strains** - Table P.6 is for the North side of the girder; Table P.7 is for the South side of the girder.

**Table P.8 – Average Raw Strains** – Averages raw strains from Tables P.6 and P.7.

**Table P.9 – Smoothed Strains** – Calculates a three point floating average of the average raw strain values from Table P.8.

**Table P.10 – Strand Stress Values Based on Smoothed CSS Values** – Calculates the total strand strain based on the smoothed CSS values from Table P.9 and the initial strand strain due to the effective prestress.

**Figure P.1 – Plot of Strand Stress vs. Distance from Girder End** – Plots stress in the strand at the following stress levels:

- When the strand stress is at effective prestress.

- When the strand stress at the point of loading is approximately at yield stress.

- When the strand stress at the point of loading is at ultimate stress.

- The ultimate stress the strand reaches at the point of loading

The plot also indicates locations where shear cracking passed through bottom layer of strands.

**Table P.11 – Smoothed CSS Data for Tracking Effect of Surface Cracking** – Lists pure CSS data for tracking the effect of shear cracking.

559

**Table P.12 – Plot of CSS with Information About Crack Formation** – The user enters data into the shaded fields reference the location of shear cracks in or near the transfer length region at the level of the bottom strands. The plot indicates CSS data at key applied shear levels that coincide with the formation of shear cracks. Also depicted in the plot is the transfer length, and the location of cracks.

**Table P.13 – Prestressing Strand Tension Curve** – Used to determine forces and stresses in prestressing strand based on strand strain data.

Table P.1  Girder Information Sheet

## Girder Information for Development Length Plots

**G1C-W  4**

Left diagram (SW):

| 1 | Top - L | 11 | 1 | Top - C | 9 |
|---|---------|----|---|---------|---|
| Position ------> | | | | | |
| 1 | Bot - L | 20 | 1 | Bot - C | 9 |

<-- Elevation (IN) ----->

3.125   0.75

Right diagram (NW):

| 1 | Top - C | 9 | NW | 1 | Top - R | 11 |
|---|---------|---|----|---|---------|----|
| | | | | | Position | |
| 1 | Bot - C | 9 | 5 | 1 | Bot - R | 20 |

<---- Elevation (IN) ----->

2.938   1.5

Distance from Beam End to 1st Gage (IN) ------>

---

### 48" Bot - L

| Elev | Posn | Init | Lgth |
|------|------|------|------|
| 3.12 | 4.76 | 154 | 8.02 |
| 3.12 | 6.75 | -263 | 7.97 |
| 3.11 | 8.74 | -248 | 7.98 |
| 3.11 | 10.74 | -42 | 8.00 |
| 3.11 | 12.75 | 100 | 8.01 |
| 3.11 | 14.74 | -111 | 7.99 |
| 3.10 | 16.74 | -112 | 7.98 |
| 3.10 | 18.74 | -156 | 7.96 |
| 3.10 | 20.73 | -401 | 7.98 |
| 3.10 | 22.72 | -188 | 7.98 |
| 3.09 | 24.72 | -206 | 7.98 |
| 3.09 | 26.71 | -380 | 7.96 |
| 3.09 | 28.71 | 151 | 8.02 |
| 3.08 | 30.71 | -180 | 7.98 |
| 3.08 | 32.70 | -241 | 7.98 |
| 3.08 | 34.70 | -213 | 7.98 |
| 3.08 | 36.68 | -673 | 7.93 |
| 3.07 | 38.67 | -548 | 7.95 |
| 3.07 | 40.66 | -307 | 7.97 |
| 3.07 | 42.65 | -192 | 7.98 |
| | Length => | 45.91 | IN |

### 48" Bot - R

| Elev | Posn | Init | Lgth |
|------|------|------|------|
| 2.99 | 43.48 | -17 | 8.00 |
| 2.99 | 41.48 | 32 | 8.00 |
| 2.99 | 39.48 | 86 | 8.01 |
| 2.99 | 37.48 | -19 | 8.00 |
| 2.98 | 35.48 | 44 | 8.00 |
| 2.98 | 33.48 | 13 | 8.00 |
| 2.98 | 31.48 | -331 | 7.97 |
| 2.98 | 29.49 | -367 | 7.96 |
| 2.97 | 27.51 | -659 | 7.93 |
| 2.97 | 25.52 | -527 | 7.95 |
| 2.97 | 23.52 | -30 | 8.00 |
| 2.96 | 21.52 | 36 | 8.00 |
| 2.96 | 19.52 | 276 | 8.03 |
| 2.96 | 17.51 | 188 | 8.02 |
| 2.96 | 15.51 | -48 | 8.00 |
| 2.95 | 13.51 | -11 | 8.00 |
| 2.95 | 11.51 | 70 | 8.01 |
| 2.95 | 9.51 | 136 | 8.01 |
| 2.95 | 7.50 | 205 | 8.02 |
| 2.94 | 5.50 | 154 | 8.02 |
| | Length => | 45.98 | IN |

---

**Initial Gage Lengths are Based on Readings Taken Just Prior to Girder Testing**

| Date of Strand Release | 17-Jul-01 |
|------------------------|-----------|
| Date of Girder End Test | 02-Nov-01 |
| Age at Testing (Days) | 107 |

14-Day Transfer Lgth (in)

| Strand Initial Strain (me) | 6503 |
|----------------------------|------|
| From Prestress Force Calc Spreadsheet | |

| Load at ~1% Strain (kips) | |
|---------------------------|------|
| Ultimate Load (kips) | 299 |
| Ultimate CSS (me) | 8907 |
| From DAQ Spreadsheet | |

| Embedment Length (in) | |
|-----------------------|------|
| Shear Span "a" (in) | 85 |
| Supt to Supt Dist. (in) | 504 |
| Strand Area (in²) | 0.2183 |

---

| f_se | 147.6 | ksi |
|------|-------|-----|
| f_ps | 264.4 | ksi |

| F_se | 32.2 | kips |
|------|------|------|
| F_ps | 57.7 | kips |

| Gage Lgth | | IN |
|-----------|--|----|

**NW**

| Beam Lgth | | FT |
|-----------|--|----|

**SW**

Table P.2  Initial Readings Prior to Testing, Initial Readings Prior to Release and 14 Day Readings (North Side)

| Beam # | G1C-W | Beam Side | North | Test # | 4 | Read LEFT to RIGHT |
|---|---|---|---|---|---|---|

**Initial Readings Just Prior to Testing, Initial Readings Prior to Release and 14-Day Readings**

Notes for Readings - Gage Length is 8" on DEMEC Gage Reader - Zero Gage on Bar Before Taking Readings

30 Inch Top Left

| 26 Inch Top Center | | 30 Inch Top Right | |
|---|---|---|---|
| Test # 1 | Test # 2 | Test # 1 | Test # 2 |

48 Inch Bottom Left

| 26 Inch Bottom Center | | 48 Inch Bottom Right | | | |
|---|---|---|---|---|---|
| Test # 1 | Test # 2 | Test # 1 | Test # 2 | Rel # 1 | Rel # 2 | 14-Day |

Table P.3  Initial Readings Prior to Testing, Initial Readings Prior to Release and 14 Day Readings (South Side)

| Beam # | G1C-W | Beam Side | South | Test # | 4 | Read LEFT to RIGHT |
|---|---|---|---|---|---|---|

**Initial Readings Just Prior to Testing, Initial Readings Prior to Release and 14-Day Readings**

Notes for Readings - Gage Length is 8" on DEMEC Gage Reader - Zero Gage on Bar Before Taking Readings

### 30 Inch Top Left

| Test # 1 | Test # 2 |
|---|---|
|  | .0541 |
| .0586 | .0583 |
| .0630 | .0721 |
|  |  |
|  | .0561 |
| .0655 | .0621 |
| .0523 | .0565 |
| .0567 | .0583 |
| .0583 | .0680 |
|  | .0754 |
| .0709 | .0709 |

### 26 Inch Top Center

| Test # 1 | Test # 2 |
|---|---|
|  | .0086 |
| .0583 | .0578 |
| .0253 | .0286 |
|  | .0685 |
| .0685 | .0586 |
| .0695 | .0590 |
| .0649 | .0644 |
| .0661 | .0619 |
| .0822 | .0817 |

### 30 Inch Top Right

(no data)

### 48 Inch Bottom Left

| Test # 1 | Test # 2 | Rel # 1 | Rel # 2 | 14-Day |
|---|---|---|---|---|
|  | .0157 | .0100 | .0000 |  |
| .0264 | .0262 | .0197 | .0192 | .0248 |
| .0249 | .0247 | .0196 | .0192 | .0248 |
| .0642 | .0042 | .0040 | .0050 | .0012 |
| .0100 | .0100 | .0170 | .0170 | .0129 |
| .0104 | .0115 | .0010 | .0019 | .0109 |
| .0112 | .0112 | .0028 | .0019 | .0089 |
| .0056 | .0155 | .0155 | .0056 | .0159 |
| .0397 | .0403 | .0331 | .0331 | .0369 |
| .0187 | .0188 | .0077 | .0075 | .0160 |
| .0204 | .0207 | .0095 | .0095 | .0176 |
| .0385 | .0381 | .0266 | .0232 | .035 |
| .0153 | .0151 | .0123 | .0255 | .0160 |
| .0427 | .0178 | .0098 | .0035 | .0155 |
| .0289 | .0242 | .0154 | .0156 | .0210 |
| .0211 | .0213 | .0101 | .0100 | .0188 |
| .0671 | .0671 | .0580 | .0580 | .0617 |
| .0546 | .0549 | .0467 | .0470 | .0524 |
| .0305 | .0309 | .0178 | .0178 | .0248 |
| .0193 | .0193 | .0108 | .0105 | .0101 |

### 26 Inch Bottom Center

| Test # 1 | Test # 2 |
|---|---|
| .0807 | .0800 |
| .0710 | .0709 |
| .0595 | .0596 |
| .0513 | .0518 |
| .0699 | .0648 |
| .0473 | .0472 |
| .0598 | .0596 |
| .0605 | .0606 |
| .0649 | .0647 |

### 48 Inch Bottom Right

(no data)

Table P.4 CSS Data Taken During Development Length Testing (North Side)

| Beam # | G1C-W | | | | Side | | North | | | Test # | | 4 | | | Read LEFT to RIGHT | | | |
|---|---|---|---|---|---|---|---|---|---|---|---|---|---|---|---|---|---|---|
| | Notes for Readings - Gage Length is 8" on DEMEC Gage Reader - Zero Gage on Bar Before Taking Readings | | | | | | | | | | | | | | | | | |
| Reading | 1 | 2 | 3 | 4 | 5 | 6 | 7 | 8 | 9 | 10 | 11 | 12 | 13 | 14 | 15 | 16 | 17 |
| Load (K) | | | | | | | | | | | | | | | | | |
| Gage # | | | | | | | | | | | | | | | | | |
| 1 | | | | | | | | | | | | | | | | | |
| 2 | | | | | | | | | | | | | | | | | |
| 3 | | | | | | | | | | | | | | | | | |
| 4 | | | | | | | | | | | | | | | | | |
| 5 | | | | | | | | | | | | | | | | | |
| 6 | | | | | | | | | | | | | | | | | |
| 7 | | | | | | | | | | | | | | | | | |
| 8 | | | | | | | | | | | | | | | | | |
| 9 | | | | | | | | | | | | | | | | | |
| 10 | | | | | | | | | | | | | | | | | |
| 11 | | | | | | | | | | | | | | | | | |
| 12 | | | | | | | | | | | | | | | | | |
| 13 | | | | | | | | | | | | | | | | | |
| 14 | | | | | | | | | | | | | | | | | |
| 15 | | | | | | | | | | | | | | | | | |
| 16 | | | | | | | | | | | | | | | | | |
| 17 | | | | | | | | | | | | | | | | | |
| 18 | | | | | | | | | | | | | | | | | |
| 19 | | | | | | | | | | | | | | | | | |
| 20 | | | | | | | | | | | | | | | | | |

Table P.5 CSS Data Taken During Development Length Testing (South Side)

| Beam # | G1C-W | | | Side | | | South | | Test # | | | 4 | Read LEFT to RIGHT | | | | |
|---|---|---|---|---|---|---|---|---|---|---|---|---|---|---|---|---|---|
| | | Notes for Readings - Gage Length is 8" on DEMEC Gage Reader - Zero Gage on Bar Before Taking Readings | | | | | | | | | | | | | | | | |
| Reading | 1 | 2 | 3 | 4 | 5 | 6 | 7 | 8 | 9 | 10 | 11 | 12 | 13 | 14 | 15 | 16 | 17 |
| Load (K) | 80 | 110 | 140 | 155 | 184 | 215 | 240 | 261 | 276 | 287 | 295 | 296 | | | | | |

Gage #

| 1 | 2 | 3 | 4 | 5 | 6 | 7 | 8 | 9 | 10 | 11 | 12 | 13 | 14 | 15 | 16 | 17 | 18 | 19 | 20 |
|---|---|---|---|---|---|---|---|---|---|---|---|---|---|---|---|---|---|---|---|

565

Table P.6 Calculated Raw Strains (North Side)

| G1C-W | 48" | | | | | | | | | | | | | | | | | | | |
|---|---|---|---|---|---|---|---|---|---|---|---|---|---|---|---|---|---|---|---|---|
| | | Transfer Length | | | Raw Strains - North Side CSS Reading (microstrains) Development Length | | | | | | | | | | | | | | | |
| Gage Point Load | Rel | 14-Day | Test | 1 | 2 | 3 | 4 | 5 | 6 | 7 | 8 | 9 | 10 | 11 | 12 | 13 | 14 | 15 | 16 | 17 |
| | 0 | 0 | 0 | 80 | 110 | 140 | 155 | 184 | 215 | 240 | 261 | 276 | 287 | 295 | 296 | 0 | 0 | 0 | 0 | 0 |
| 1 | 0 | 1175 | 1507 | 194 | 194 | 231 | 369 | 381 | 469 | 556 | 944 | 1769 | 2469 | 2694 | 3057 | | | | | |
| 2 | 0 | 1175 | 1456 | 219 | 231 | 294 | 381 | 469 | 569 | 668 | 1056 | 1881 | 2693 | 2830 | 3043 | | | | | |
| 3 | 0 | 943 | 1299 | 219 | 243 | 268 | 368 | 418 | 518 | 581 | 1130 | 2042 | 2966 | 3153 | 3515 | | | | | |
| 4 | 0 | 1069 | 1432 | 175 | 188 | 213 | 313 | 388 | 488 | 550 | 713 | 1013 | 1500 | 1600 | 1688 | | | | | |
| 5 | 0 | 999 | 1274 | 187 | 175 | 237 | 275 | 362 | 425 | 487 | 700 | 800 | 1049 | 1049 | 775 | | | | | |
| 6 | 0 | 694 | 1194 | 200 | 250 | 275 | 337 | 425 | 500 | 562 | 700 | 875 | 1450 | 1662 | 1700 | | | | | |
| 7 | 0 | 1067 | 1400 | 207 | 207 | 220 | 320 | 383 | 408 | 483 | 533 | 496 | 973 | 1462 | 1789 | | | | | |
| 8 | 0 | 1080 | 1400 | 182 | 107 | 220 | 295 | 333 | 358 | 446 | 496 | 496 | 1036 | 1965 | 10894 | | | | | |
| 9 | 0 | 1273 | 1620 | 158 | 208 | 208 | 296 | 372 | 359 | 410 | 485 | 460 | 1002 | 1909 | 11211 | | | | | |
| 10 | 0 | 1026 | 1353 | 138 | 164 | 189 | 277 | 352 | 340 | 440 | 466 | 528 | 617 | 1208 | 10532 | | | | | |
| 11 | 0 | 788 | 1232 | 156 | 194 | 194 | 281 | 394 | 381 | 456 | 506 | 556 | 594 | 844 | 10110 | | | | | |
| 12 | 0 | 950 | 1143 | 169 | 169 | 181 | 244 | 356 | 369 | 394 | 444 | 519 | 444 | 431 | 668 | | | | | |
| 13 | 0 | 884 | 1059 | 149 | 187 | 224 | 336 | 461 | 436 | 498 | 573 | 698 | 2952 | 5568 | 6054 | | | | | |
| 14 | 0 | 736 | 867 | 143 | 143 | 118 | 218 | 330 | 368 | 405 | 443 | 555 | 3087 | 5967 | 6553 | | | | | |
| 15 | 0 | 494 | 738 | 119 | 106 | 6 | 106 | 231 | 344 | 1132 | 1832 | 2583 | 5247 | 8586 | 9024 | | | | | |
| 16 | 0 | 425 | 838 | 138 | 213 | 138 | 175 | 200 | 388 | 1088 | 1750 | 2513 | 5288 | 8589 | 9089 | | | | | |
| 17 | 0 | 587 | 899 | 112 | 125 | 100 | 162 | 200 | 412 | 1062 | 1711 | 2410 | 2897 | 3547 | 3622 | | | | | |
| 18 | 0 | 611 | 898 | 62 | 50 | 12 | 237 | 537 | 1048 | 1809 | 2533 | 3369 | 3594 | 4218 | 3968 | | | | | |
| 19 | 0 | 655 | 973 | 131 | 268 | 118 | 305 | 605 | 1004 | 916 | 1054 | 1166 | 1315 | 1390 | 1365 | | | | | |
| 20 | 0 | 150 | 774 | 175 | 137 | 162 | 362 | 661 | 948 | 1023 | 1060 | 1198 | 1223 | 1260 | 1310 | | | | | |
| Compression + | | | | | | | | | | | | Tension + | | | | | | | | |

566

Table P.7 Calculated Raw Strains (South Side)

**G1C-W**    48"

**Raw Strains - South Side**

CSS Reading (microstrains)

| Gage Point | Transfer Length | | | Development Length | | | | | | | | | | | | | | | | |
|---|---|---|---|---|---|---|---|---|---|---|---|---|---|---|---|---|---|---|---|---|
| Load | Rel | 14-Day | Test | 1 | 2 | 3 | 4 | 5 | 6 | 7 | 8 | 9 | 10 | 11 | 12 | 13 | 14 | 15 | 16 | 17 |
|  | 0 | 0 | 0 | 80 | 110 | 140 | 155 | 184 | 215 | 240 | 261 | 276 | 287 | 295 | 296 | 0 | 0 | 0 | 0 | 0 |
| 1 | 0 | -561 | -674 | 175 | 137 | 162 | 362 | 661 | 948 | 1023 | 1060 | 1198 | 1223 | 1260 | 1310 | | | | | |
| 2 | 0 | 702 | 890 | 113 | 163 | 201 | 451 | 564 | 564 | 640 | 702 | 790 | 890 | 916 | 966 | | | | | |
| 3 | 0 | 451 | 696 | -6 | 132 | 94 | 445 | 520 | 533 | 596 | 646 | 746 | 871 | 934 | 947 | | | | | |
| 4 | 0 | 775 | 1126 | 88 | 63 | 75 | 100 | 213 | 963 | 1463 | 1976 | 2601 | 4940 | 5403 | 5390 | | | | | |
| 5 | 0 | 574 | 874 | 75 | 62 | 25 | 100 | 674 | 1411 | 2047 | 2697 | 3296 | 5730 | 5630 | 5543 | | | | | |
| 6 | 0 | 958 | 1170 | -13 | 50 | 75 | 150 | 751 | 1477 | 2115 | 2866 | 3918 | 6647 | 8837 | 9013 | | | | | |
| 7 | 0 | 832 | 1120 | 63 | 75 | 50 | 125 | 764 | 1540 | 2191 | 2904 | 3918 | 6672 | 9200 | 9363 | | | | | |
| 8 | 0 | 958 | 1252 | 106 | 106 | 144 | 169 | 570 | 695 | 820 | 1046 | 1346 | 1860 | 3901 | 4064 | | | | | |
| 9 | 0 | 704 | 1106 | 75 | 88 | 88 | 151 | 138 | 151 | 201 | 276 | 528 | 678 | 3467 | 3731 | | | | | |
| 10 | 0 | 1065 | 1410 | 94 | 94 | 94 | 182 | 106 | 119 | 157 | 182 | 194 | 157 | 232 | 219 | | | | | |
| 11 | 0 | 952 | 1385 | 157 | 132 | 132 | 207 | 169 | 207 | 320 | 232 | 269 | 583 | 2137 | 7726 | | | | | |
| 12 | 0 | 1262 | 1608 | 69 | 107 | 144 | 182 | 82 | 82 | 157 | 157 | 182 | 546 | 2531 | 8647 | | | | | |
| 13 | 0 | 1085 | 1273 | 162 | 150 | 162 | 237 | 125 | 299 | 287 | 299 | 274 | 711 | 2645 | 12514 | | | | | |
| 14 | 0 | 1485 | 1798 | 113 | 150 | 163 | 238 | 213 | 238 | 238 | 326 | 376 | 802 | 2869 | 12704 | | | | | |
| 15 | 0 | 696 | 1078 | 107 | 94 | 119 | 169 | 157 | 132 | 244 | 169 | 445 | 809 | 1147 | 5598 | | | | | |
| 16 | 0 | 1097 | 1410 | 88 | 100 | 138 | 288 | 238 | 263 | 363 | 514 | 752 | 965 | 990 | 4725 | | | | | |
| 17 | 0 | 807 | 1166 | 95 | 120 | 158 | 233 | 208 | 221 | 271 | 460 | 662 | 952 | 1103 | 977 | | | | | |
| 18 | 0 | 673 | 994 | 94 | 107 | 132 | 220 | 208 | 208 | 308 | 447 | 673 | 875 | 1064 | 1466 | | | | | |
| 19 | 0 | 1318 | 1619 | 176 | 176 | 188 | 251 | 238 | 314 | 402 | 979 | 1443 | 1907 | 2133 | 2409 | | | | | |
| 20 | 0 | 789 | 1065 | 138 | 175 | 213 | 301 | 313 | 338 | 464 | 890 | 1328 | 1854 | 2118 | 2531 | | | | | |

Compression +          Tension +

567

Table P.8  Average Raw Strains

| G1C-W | | | | | | | | | | | | | | | | | | | | |
|---|---|---|---|---|---|---|---|---|---|---|---|---|---|---|---|---|---|---|---|---|
| 48" | | | Average of North and South Data (From North Perspective) | | | | | | | | | | | | | | | | | |
| | Transfer Length | | | CSS Reading (microstrains) | | | | | | | | | | | | | | | | |
| | | | | | | | | | Development Length | | | | | | | | | | |
| Gage Point | Rel | 14-Day | Test | 1 | 2 | 3 | 4 | 5 | 6 | 7 | 8 | 9 | 10 | 11 | 12 | 13 | 14 | 15 | 16 | 17 |
| Load | 0 | 0 | 0 | 80 | 110 | 140 | 155 | 184 | 215 | 240 | 261 | 276 | 287 | 295 | 296 | 0 | 0 | 0 | 0 | 0 |
| 1 | 0 | 982 | 1286 | 166 | 185 | 222 | 335 | 347 | 404 | 510 | 917 | 1549 | 2162 | 2406 | 2794 | | | | | |
| 2 | 0 | 1246 | 1537 | 197 | 203 | 241 | 316 | 353 | 441 | 535 | 1017 | 1662 | 2300 | 2482 | 2726 | | | | | |
| 3 | 0 | 808 | 1146 | 156 | 175 | 200 | 294 | 313 | 363 | 444 | 788 | 1357 | 1920 | 2108 | 2491 | | | | | |
| 4 | 0 | 938 | 1299 | 135 | 154 | 185 | 273 | 298 | 354 | 411 | 586 | 837 | 1226 | 1352 | 1332 | | | | | |
| 5 | 0 | 1048 | 1342 | 138 | 138 | 188 | 282 | 300 | 344 | 425 | 607 | 776 | 1007 | 1020 | 2750 | | | | | |
| 6 | 0 | 695 | 1136 | 153 | 172 | 197 | 253 | 291 | 316 | 403 | 435 | 660 | 1129 | 1405 | 3649 | | | | | |
| 7 | 0 | 1276 | 1599 | 160 | 179 | 191 | 279 | 298 | 323 | 361 | 430 | 436 | 887 | 2166 | 7246 | | | | | |
| 8 | 0 | 1083 | 1336 | 172 | 128 | 191 | 266 | 229 | 329 | 366 | 398 | 385 | 874 | 2305 | 11704 | | | | | |
| 9 | 0 | 1268 | 1614 | 113 | 157 | 176 | 239 | 227 | 220 | 283 | 321 | 321 | 774 | 2220 | 9929 | | | | | |
| 10 | 0 | 989 | 1369 | 148 | 148 | 160 | 242 | 261 | 273 | 380 | 349 | 399 | 600 | 1672 | 9129 | | | | | |
| 11 | 0 | 926 | 1321 | 125 | 144 | 144 | 232 | 250 | 250 | 307 | 344 | 375 | 375 | 538 | 5165 | | | | | |
| 12 | 0 | 827 | 1124 | 122 | 128 | 135 | 197 | 247 | 260 | 297 | 360 | 523 | 561 | 1949 | 2200 | | | | | |
| 13 | 0 | 921 | 1156 | 128 | 147 | 184 | 253 | 515 | 566 | 659 | 809 | 1022 | 2406 | 4735 | 5059 | | | | | |
| 14 | 0 | 784 | 994 | 103 | 109 | 84 | 172 | 547 | 954 | 1298 | 1673 | 2236 | 4879 | 7584 | 7958 | | | | | |
| 15 | 0 | 726 | 954 | 53 | 78 | 41 | 128 | 491 | 911 | 1624 | 2349 | 3250 | 5947 | 8712 | 9018 | | | | | |
| 16 | 0 | 500 | 856 | 106 | 137 | 81 | 137 | 437 | 899 | 1568 | 2223 | 2904 | 5509 | 7110 | 7316 | | | | | |
| 17 | 0 | 681 | 1012 | 100 | 94 | 87 | 131 | 206 | 688 | 1262 | 1844 | 2506 | 3919 | 4475 | 4506 | | | | | |
| 18 | 0 | 531 | 797 | 28 | 91 | 53 | 341 | 528 | 791 | 1203 | 1589 | 2058 | 2233 | 2576 | 2457 | | | | | |
| 19 | 0 | 678 | 931 | 122 | 216 | 160 | 378 | 585 | 784 | 778 | 878 | 978 | 1103 | 1153 | 1165 | | | | | |
| 20 | 0 | -206 | 50 | 175 | 137 | 162 | 362 | 661 | 948 | 1023 | 1060 | 1198 | 1223 | 1260 | 1310 | | | | | |
| | Compression + | | | | | | | | | | | | | | Tension + | | | | | |

568

Table P.9 Smoothed Strains

**G1C-W — Smoothed Average Plot Data From the SOUTH Perspective**

Strain Readings (microstrains)

| 48" Gage Point | Distance From End (inches) | Transfer Lgth CSS Rel | 14-Day | Test | Strand Initial | Test | Development Length Test CSS + Initial Strand Strain Due to Pretensioning |  |  |  |  |  |  |  |  |  |  |  |  |  |  |  |  |
|---|---|---|---|---|---|---|---|---|---|---|---|---|---|---|---|---|---|---|---|---|---|---|---|
|  |  |  |  |  |  |  | 1 | 2 | 3 | 4 | 5 | 6 | 7 | 8 | 9 | 10 | 11 | 12 | 13 | 14 | 15 | 16 | 17 |
| Load |  | 0 | 0 | 0 | 0 | 0 | 80 | 110 | 140 | 155 | 184 | 215 | 240 | 261 | 276 | 287 | 295 | 296 | 0 | 0 | 0 | 0 | 0 |
| 0 | 0 | 0 | 0 | 0 | 0 | 0 | 0 | 0 | 0 | 0 | 0 | 0 | 0 | 0 | 0 | 0 | 0 | 0 |  |  |  |  |  |
| 2 | 7.13 | 0 | 335 | 593 | 1675 |  | 1783 | 1823 | 1800 | 2035 | 2266 | 2516 | 2676 | 2851 | 3086 | 3194 | 3338 | 3319 |  |  |  |  |  |
| 3 | 9.13 | 0 | 630 | 914 | 2145 |  | 2228 | 2278 | 2245 | 2429 | 2585 | 2899 | 3226 | 3582 | 3992 | 4563 | 4880 | 4855 |  |  |  |  |  |
| 4 | 11.13 | 0 | 571 | 888 | 2615 |  | 2693 | 2723 | 2689 | 2819 | 3006 | 3408 | 3959 | 4501 | 5105 | 6502 | 7335 | 7375 |  |  |  |  |  |
| 5 | 13.13 | 0 | 636 | 941 | 3086 |  | 3172 | 3189 | 3156 | 3218 | 3464 | 3918 | 4570 | 5225 | 5973 | 8211 | 9851 | 10033 |  |  |  |  |  |
| 6 | 15.13 | 0 | 670 | 934 | 3556 |  | 3643 | 3664 | 3624 | 3701 | 4047 | 4477 | 5052 | 5638 | 6353 | 9001 | 11357 | 11653 |  |  |  |  |  |
| 7 | 17.13 | 0 | 810 | 1034 | 4025 |  | 4120 | 4136 | 4128 | 4209 | 4543 | 4835 | 5219 | 5636 | 6195 | 8436 | 11035 | 11370 |  |  |  |  |  |
| 8 | 19.13 | 0 | 844 | 1091 | 4495 |  | 4613 | 4623 | 4630 | 4702 | 4932 | 5088 | 5247 | 5443 | 5756 | 7111 | 9251 | 9568 |  |  |  |  |  |
| 9 | 21.13 | 0 | 891 | 1200 | 4965 |  | 5090 | 5105 | 5119 | 5192 | 5302 | 5323 | 5386 | 5469 | 5605 | 6079 | 7372 | 9106 |  |  |  |  |  |
| 10 | 23.12 | 0 | 914 | 1271 | 5053 |  | 5185 | 5193 | 5199 | 5277 | 5306 | 5314 | 5381 | 5404 | 5485 | 5565 | 6439 | 10551 |  |  |  |  |  |
| 11 | 25.12 | 0 | 1061 | 1434 | 5053 |  | 5182 | 5203 | 5213 | 5290 | 5299 | 5301 | 5376 | 5391 | 5418 | 5636 | 6530 | 13127 |  |  |  |  |  |
| 12 | 27.11 | 0 | 1113 | 1440 | 5053 |  | 5197 | 5197 | 5229 | 5302 | 5292 | 5327 | 5396 | 5409 | 5421 | 5802 | 7119 | 15307 |  |  |  |  |  |
| 13 | 29.10 | 0 | 1209 | 1516 | 5053 |  | 5201 | 5208 | 5239 | 5314 | 5304 | 5344 | 5390 | 5436 | 5434 | 5898 | 7283 | 14679 |  |  |  |  |  |
| 14 | 31.10 | 0 | 1018 | 1357 | 5053 |  | 5215 | 5213 | 5246 | 5319 | 5326 | 5375 | 5430 | 5474 | 5547 | 6016 | 7011 | 12586 |  |  |  |  |  |
| 15 | 33.09 | 0 | 1006 | 1359 | 5053 |  | 5203 | 5216 | 5245 | 5324 | 5349 | 5381 | 5449 | 5543 | 5677 | 6061 | 6583 | 9601 |  |  |  |  |  |
| 16 | 35.09 | 0 | 894 | 1259 | 5053 |  | 5195 | 5207 | 5243 | 5322 | 5349 | 5391 | 5466 | 5596 | 5811 | 6174 | 6312 | 7630 |  |  |  |  |  |
| 17 | 37.08 | 0 | 931 | 1262 | 5053 |  | 5196 | 5208 | 5244 | 5336 | 5357 | 5407 | 5480 | 5714 | 6043 | 6437 | 6546 | 7244 |  |  |  |  |  |
| 18 | 39.07 | 0 | 997 | 1327 | 5053 |  | 5216 | 5230 | 5262 | 5347 | 5374 | 5439 | 5516 | 5850 | 6339 | 6868 | 7034 | 7236 |  |  |  |  |  |
| 19 | 41.07 | 0 | 1012 | 1323 | 5053 |  | 5226 | 5241 | 5274 | 5368 | 5391 | 5456 | 5549 | 5961 | 6576 | 7180 | 7385 | 7723 |  |  |  |  |  |
| 20 | 43.07 | 0 |  |  |  |  |  |  |  |  |  |  |  |  |  |  |  |  |  |  |  |  |  |

Compression +        Tension +

569

Table P.10  Strand Stress Values Based on Smoothed CSS Values

**G1C-W — Smoothed Average Plot Data From SOUTH Perspective**

Stress in Strand due to Effective Prestress and Load Applied to Girder

| 48" Gage Point Load | Distance From End (inches) | 1 | 2 | 3 | 4 | 5 | 6 | 7 | 8 | 9 | 10 | 11 | 12 | 13 | 14 | 15 | 16 | 17 |
|---|---|---|---|---|---|---|---|---|---|---|---|---|---|---|---|---|---|---|
| | | 80 | 110 | 140 | 155 | 184 | 215 | 240 | 261 | 276 | 287 | 295 | 296 | 0 | 0 | 0 | 0 | 0 |
| 0 | 0 | 0 | 0 | 0 | 0 | 0 | 0 | 0 | 0 | 0 | 0 | 0 | 0 | 0 | 0 | 0 | 0 | 0 |
| 2 | 7.13 | 52.09 | 53.25 | 52.58 | 59.46 | 66.21 | 73.50 | 78.18 | 83.28 | 90.15 | 93.32 | 97.51 | 96.96 | | | | | |
| 3 | 9.13 | 65.09 | 66.55 | 65.58 | 70.94 | 75.50 | 84.69 | 94.24 | 104.64 | 116.62 | 133.30 | 142.54 | 141.81 | | | | | |
| 4 | 11.13 | 78.68 | 79.53 | 78.56 | 82.34 | 87.81 | 99.55 | 115.66 | 131.48 | 149.12 | 189.94 | 213.82 | 215.02 | | | | | |
| 5 | 13.13 | 92.67 | 93.16 | 92.18 | 94.01 | 101.19 | 114.46 | 133.51 | 152.62 | 174.47 | 235.99 | 257.63 | 258.83 | | | | | |
| 6 | 15.13 | 106.42 | 107.03 | 105.87 | 108.12 | 118.23 | 130.77 | 147.58 | 164.69 | 185.57 | 249.16 | 263.03 | 263.26 | | | | | |
| 7 | 17.13 | 120.35 | 120.83 | 120.59 | 122.96 | 132.71 | 141.24 | 152.45 | 164.63 | 180.96 | 240.34 | 262.57 | 263.04 | | | | | |
| 8 | 19.13 | 134.75 | 135.06 | 135.24 | 137.37 | 144.07 | 148.64 | 153.27 | 159.00 | 168.14 | 207.72 | 252.20 | 255.37 | | | | | |
| 9 | 21.13 | 148.69 | 149.11 | 149.54 | 151.67 | 154.90 | 155.51 | 153.33 | 159.77 | 163.73 | 177.58 | 214.94 | 250.50 | | | | | |
| 10 | 23.12 | 151.45 | 151.70 | 151.88 | 154.14 | 154.99 | 155.23 | 157.19 | 157.86 | 160.24 | 162.56 | 188.11 | 261.28 | | | | | |
| 11 | 25.12 | 151.37 | 151.98 | 152.29 | 154.55 | 154.79 | 154.85 | 157.05 | 157.48 | 158.27 | 164.64 | 190.75 | 264.09 | | | | | |
| 12 | 27.11 | 151.82 | 151.83 | 152.74 | 154.88 | 154.58 | 155.62 | 157.63 | 158.00 | 158.37 | 169.49 | 207.96 | 264.89 | | | | | |
| 13 | 29.10 | 151.95 | 152.13 | 153.05 | 155.25 | 154.94 | 156.10 | 157.45 | 158.79 | 158.73 | 172.29 | 212.21 | 264.66 | | | | | |
| 14 | 31.10 | 152.33 | 152.27 | 153.25 | 155.38 | 155.57 | 157.03 | 158.62 | 159.90 | 162.03 | 175.75 | 204.82 | 263.89 | | | | | |
| 15 | 33.09 | 152.00 | 152.36 | 153.22 | 155.53 | 156.26 | 157.18 | 159.19 | 161.93 | 165.83 | 177.05 | 192.30 | 255.67 | | | | | |
| 16 | 35.09 | 151.75 | 152.12 | 153.16 | 155.47 | 156.26 | 157.48 | 159.68 | 163.46 | 169.74 | 180.35 | 184.38 | 222.28 | | | | | |
| 17 | 37.08 | 151.78 | 152.15 | 153.19 | 155.48 | 156.48 | 157.94 | 160.08 | 166.90 | 176.53 | 188.05 | 191.23 | 210.98 | | | | | |
| 18 | 39.07 | 152.36 | 152.79 | 153.71 | 156.21 | 157.00 | 158.89 | 161.14 | 170.90 | 185.16 | 200.64 | 205.46 | 210.72 | | | | | |
| 19 | 41.07 | 152.67 | 153.09 | 154.07 | 156.81 | 157.48 | 159.37 | 162.11 | 174.12 | 192.09 | 208.94 | 215.32 | 224.73 | | | | | |
| 20 | 43.07 | | | | | | | | | | | | | | | | | |

**G1C-W — Plot Data for Strand Stress vs Distance from Girder End**

| | Distance From Girder End (in) | Strain in Strand (me) | Stress in Strand (ksi) |
|---|---|---|---|
| Girder End | 0 | 0 | 0 |
| Transfer Lgth | 21.5 | 5053 | 147.61 |
| End of Plot | 109.2 | 5053 | 147.61 |
| e_ps-ULT | 91 | 13960 | 264.40 |

| Load at ~1% Strand Strain | 291 | Kips |
|---|---|---|

570
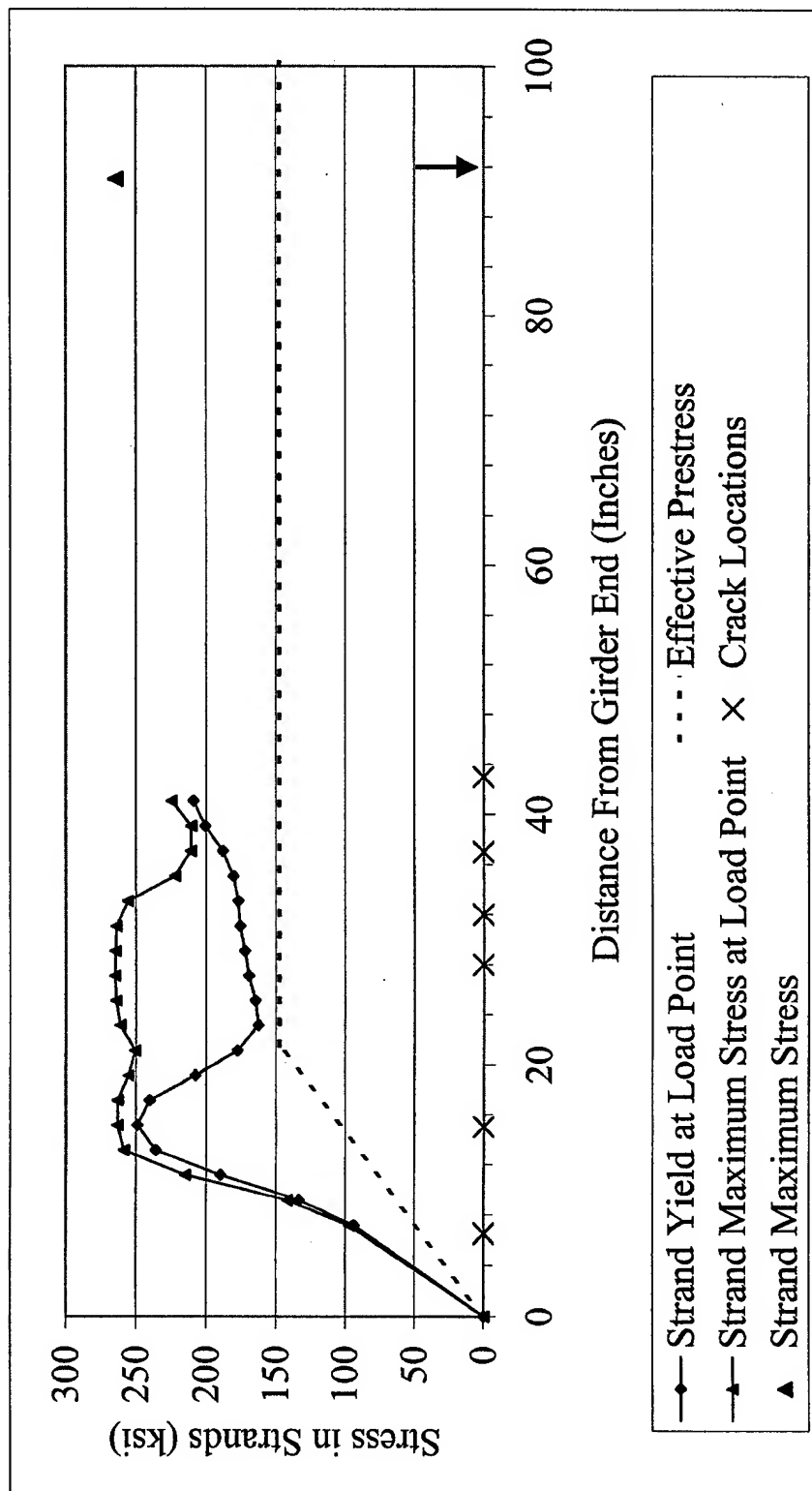
Figure P.1 Plot of Strand Stress vs. Distance From Girder End

Table P.11  Smoothed CSS Data for Tracking Effect of Surface Cracking

**G1C-W**  Smoothed Average Plot Data From the  SOUTH  Perspective  (CSS Only)

Strain Readings (microstrains)
Development Length Test CSS

| 48" Gage Point | Distance From End (inches) | Strand Initial | 1 | 2 | 3 | 4 | 5 | 6 | 7 | 8 | 9 | 10 | 11 | 12 | 13 | 14 | 15 | 16 | 17 |
|---|---|---|---|---|---|---|---|---|---|---|---|---|---|---|---|---|---|---|---|
| Load | | 0 | 80 | 110 | 140 | 155 | 184 | 215 | 240 | 261 | 276 | 287 | 295 | 296 | 0 | 0 | 0 | 0 | 0 |
| 0 | 0 | 0 | 0 | 0 | 0 | 0 | 0 | 0 | 0 | 0 | 0 | 0 | 0 | 1 | | | | | |
| 2 | 7.13 | 0 | 108 | 148 | 125 | 360 | 591 | 841 | 1001 | 1176 | 1411 | 1519 | 1663 | 1644 | | | | | |
| 3 | 9.13 | 0 | 83 | 133 | 100 | 284 | 440 | 754 | 1081 | 1437 | 1847 | 2418 | 2735 | 2710 | | | | | |
| 4 | 11.13 | 0 | 78 | 107 | 74 | 203 | 391 | 792 | 1344 | 1885 | 2489 | 3887 | 4720 | 4760 | | | | | |
| 5 | 13.13 | 0 | 86 | 103 | 70 | 132 | 378 | 832 | 1485 | 2139 | 2887 | 5125 | 6765 | 6947 | | | | | |
| 6 | 15.13 | 0 | 87 | 108 | 69 | 146 | 492 | 921 | 1496 | 2082 | 2797 | 5445 | 7802 | 8097 | | | | | |
| 7 | 17.13 | 0 | 95 | 111 | 103 | 184 | 518 | 810 | 1194 | 1611 | 2170 | 4411 | 7010 | 7345 | | | | | |
| 8 | 19.13 | 0 | 118 | 128 | 134 | 207 | 437 | 593 | 752 | 948 | 1261 | 2615 | 4756 | 5072 | | | | | |
| 9 | 21.13 | 0 | 125 | 140 | 154 | 227 | 338 | 358 | 421 | 504 | 640 | 1114 | 2407 | 4141 | | | | | |
| 10 | 23.12 | 0 | 132 | 140 | 146 | 224 | 253 | 261 | 328 | 351 | 432 | 512 | 1386 | 5498 | | | | | |
| 11 | 25.12 | 0 | 129 | 150 | 160 | 237 | 246 | 248 | 323 | 338 | 365 | 583 | 1477 | 8074 | | | | | |
| 12 | 27.11 | 0 | 144 | 144 | 176 | 249 | 239 | 274 | 343 | 356 | 368 | 749 | 2066 | 10254 | | | | | |
| 13 | 29.10 | 0 | 148 | 155 | 186 | 261 | 251 | 291 | 337 | 383 | 381 | 845 | 2230 | 9626 | | | | | |
| 14 | 31.10 | 0 | 162 | 160 | 193 | 266 | 273 | 322 | 377 | 421 | 494 | 963 | 1958 | 7533 | | | | | |
| 15 | 33.09 | 0 | 150 | 163 | 192 | 271 | 296 | 328 | 396 | 490 | 624 | 1008 | 1530 | 4548 | | | | | |
| 16 | 35.09 | 0 | 142 | 154 | 190 | 269 | 296 | 338 | 413 | 543 | 758 | 1121 | 1259 | 2577 | | | | | |
| 17 | 37.08 | 0 | 143 | 155 | 191 | 283 | 304 | 354 | 427 | 661 | 990 | 1384 | 1493 | 2191 | | | | | |
| 18 | 39.07 | 0 | 163 | 177 | 209 | 294 | 321 | 386 | 463 | 797 | 1286 | 1815 | 1981 | 2183 | | | | | |
| 19 | 41.07 | 0 | 173 | 188 | 221 | 315 | 338 | 403 | 496 | 908 | 1523 | 2127 | 2332 | 2670 | | | | | |
| 20 | 43.07 | | | | | | | | | | | | | | | | | | |

Tension +

**G1C-W**  Plotting Data for Transfer Length on Crack ID Plot

| | Distance From Girder End (in) | Plot Data |
|---|---|---|
| Girder End | 0 | 0 |
| Transfer Lgth | 21.5 | 0 |

572

Table P.12  Plot of CSS with Information About Crack Formation

| G1C-W | | | | | | | | | |
| --- | --- | --- | --- | --- | --- | --- | --- | --- | --- |
| **Crack Data - Enter Location of Cracks Crossing DEMEC Gage Strips** | | | | | | | | | |
| Crack Number | 1 | 2 | 3 | 4 | 5 | 6 | 7 | 8 | 9 | 10 |
| Distance from Girder End (in) | 6.5 | | | | | | | | | |
| Load at Which Crack Crosses Strand | 184 | 184 | 296 | 296 | 240 | 296 | | | | |
| Shear at Which Crack Crosses Strand | 153 | 153 | 246 | 246 | 200 | 246 | 0 | 0 | 0 | 0 |
| Plotting Data for Y-Axis | 0 | 0 | 0 | 0 | 0 | 0 | 0 | 0 | 0 | 0 |

| Load Step vs Shear | |
| --- | --- |
| Step | Shear (kips) |
| 1 | 67 |
| 2 | 91 |
| 3 | 116 |
| 4 | 129 |
| 5 | 153 |
| 6 | 179 |
| 7 | 200 |
| 8 | 217 |
| 9 | 229 |
| 10 | 239 |
| 11 | 245 |
| 12 | 246 |
| 13 | 0 |
| 14 | 0 |
| 15 | 0 |



CSS vs Distance From Girder End

Legend: × Crack; Lt; V=153 K; V=200 K; V=246 K

Y-axis: CSS at Level of Bottom Strands (με)
X-axis: Distance From Girder End (Inches)

573

Table P.13 Prestressing Strand Tension Curve

## Prestressing Strand Tension Test Curve and Zone Limit Data



Strain -Stress Curve for 0.6" 270 KSI LOLAX Strand

$y = 0.8063x + 56.5921$
$R^2 = 1.0000$

$y = 95.9317x^3 - 348.9161x^2 + 423.6514x - 114.2059$
$R^2 = 0.9985$

$y = 63.7701x + 0.0000$
$R^2 = 1.0000$

Strain (Percent)

Load (Kips)

◆ Elastic    ■ Transition    ▲ Plastic    —— Linear (Elastic)

—— Linear (Plastic)    —— Poly. (Transition)    —— Linear (Plastic)

### Prestressing Strand Loading Data

| Point of Loading | Strain (%) | Load (Kips) |
|---|---|---|
| Start of Elastic | 0 | 0.00 |
| End of Elastic | 0.7135 | 45.50 |
| Transition 1 | 0.7500 | 47.45 |
| Transition 2 | 0.8750 | 53.63 |
| Transition 3 | 1.0000 | 56.67 |
| Transition 4 | 1.1250 | 57.20 |
| Start of Plastic | 1.2500 | 57.60 |
| End of Plastic | 6.5000 | 61.83 |

| Zone | Percent Strain | | |
|---|---|---|---|
| Elastic | 0 | < e < | 0.7135 |
| Transition | 0.7135 | < e < | 1.2500 |
| Plastic | 1.2500 | > e | |

| Zone | Load | | |
|---|---|---|---|
| Elastic | 0 | < Kips < | 45.50 |
| Transition | 45.50 | < Kips < | 57.60 |
| Plastic | 57.60 | > Kips | |

# APPENDIX Q

## PHOTOS AND STRAND STRESS PLOTS FROM DEVELOPMENT LENGTH TESTS

Appendix Q contains a photo and a plot of stress in the prestressing strand from each of the 12 development length tests. The stress increase in the prestressing strand during loading was determined with concrete surface strain (CSS) data taken at the level of the bottom strands over the initial 48 inches of the girder. The CSS data was measured using DEMEC points with an 8-inch gage length; a three gage moving average was used to determine each value. This additional stress due to loading was added to the effective prestress to plot the resulting strand stress. The following items are shown on each plot.

- Effective stress due to prestressing over entire embedment length (dashed line)

- Stress in the strand over the initial 48 inches of the girder when the strand begins to yield at the point of load application (line with diamonds)

- Stress in the strand over the initial 48 inches of the girder when the strand is at ultimate stress at the point of load application (line with triangles)

- Stress in the strand at ultimate load at the point of load application (triangle). The CSS data at the load point was found using an LVDT with a gage length of 24 inches.

- Point of load application indicator (downward arrow along x-axis)

- Cracks passing through the level of the bottom strands along the initial 48 inches of the girder (marked with X along x-axis)

In the tests where the average strand end slip is over 0.01" (G1A-East, G1B-East and G1C-East), the level of stress indicated in the strand indicated is not considered accurate. With slip between the strand and concrete, it is impossible to know with any certainty the level of stress in the strand using CSS data. If the level of average strand end slip is less than 0.01 inches, it is assumed the resulting strand stress plots are reasonable because the affect on strand stress calculations would be less than 0.015 percent. On the plots, cracking in the girder causes the peaks and valleys. The sections correspond with the individual development length tests as follows:

**Section Q.1** – Test G1A-East

**Section Q.2** – Test G1A-West

**Section Q.3** – Test G1B-East

**Section Q.4** – Test G1B-West

**Section Q.5** – Test G1C-East

**Section Q.6** – Test G1C-West

**Section Q.7** – Test G2A-East

**Section Q.8** – Test G2A-West

**Section Q.9** – Test G2B-East

**Section Q.10** – Test G2B-West

**Section Q.11** – Test G2C-East

**Section Q.12** – Test G2C-West

576

## Q.1 Development Length Test G1A-East
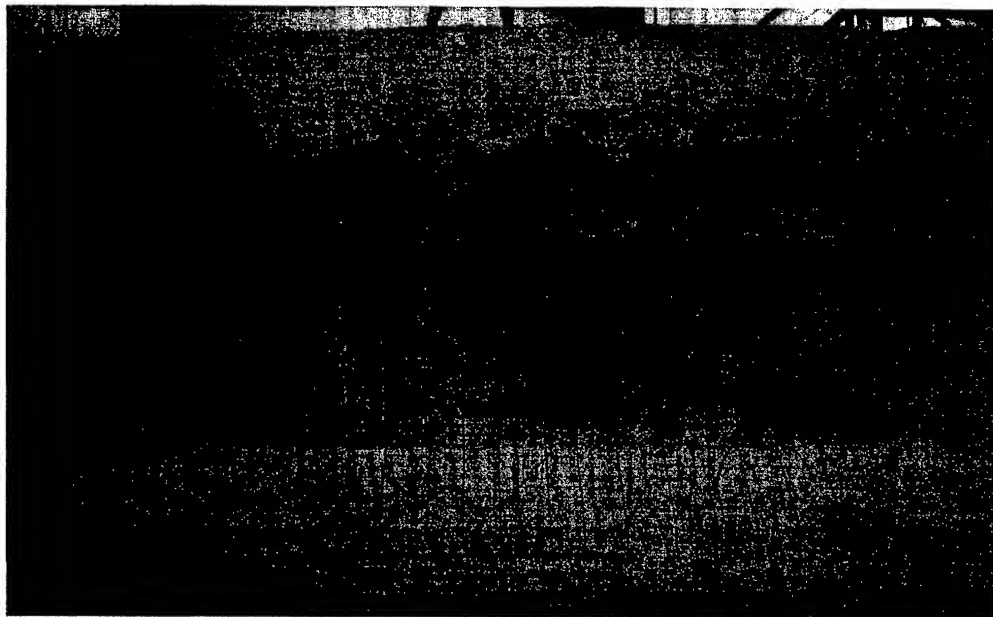


Figure Q.1 G1A-East Crack Patterns from Development Length Test
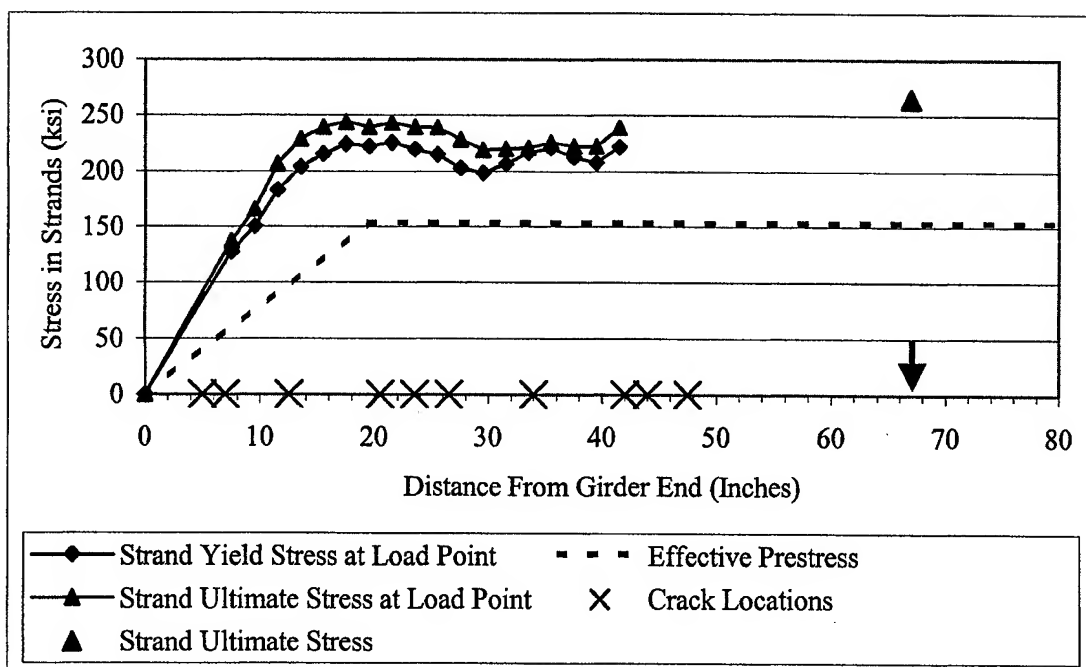


Figure Q.2 G1A-East Strand Stress vs Distance from Girder End

## Q.2 Development Length Test G1A-West
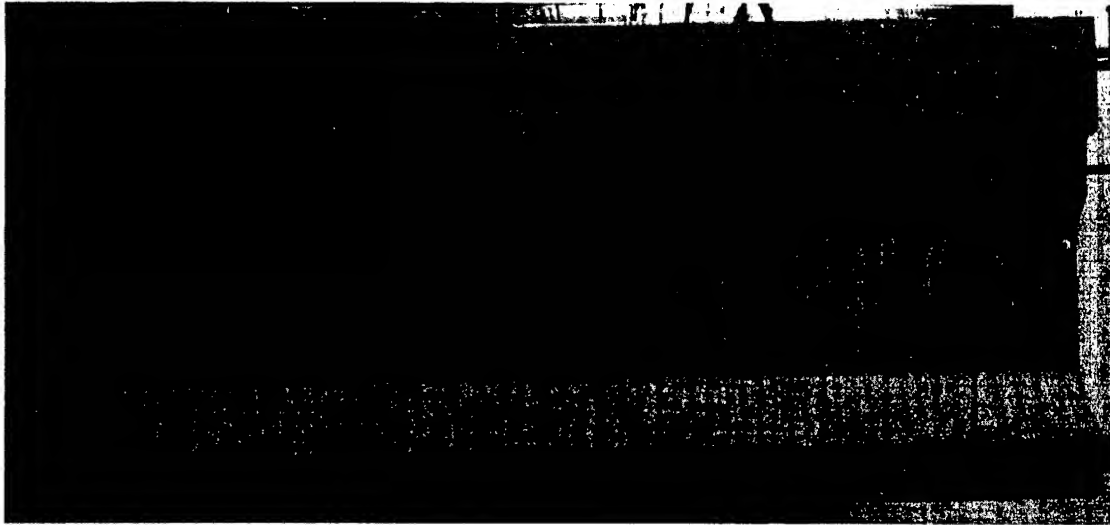


Figure Q.3  G1A-West Crack Patterns from Development Length Test
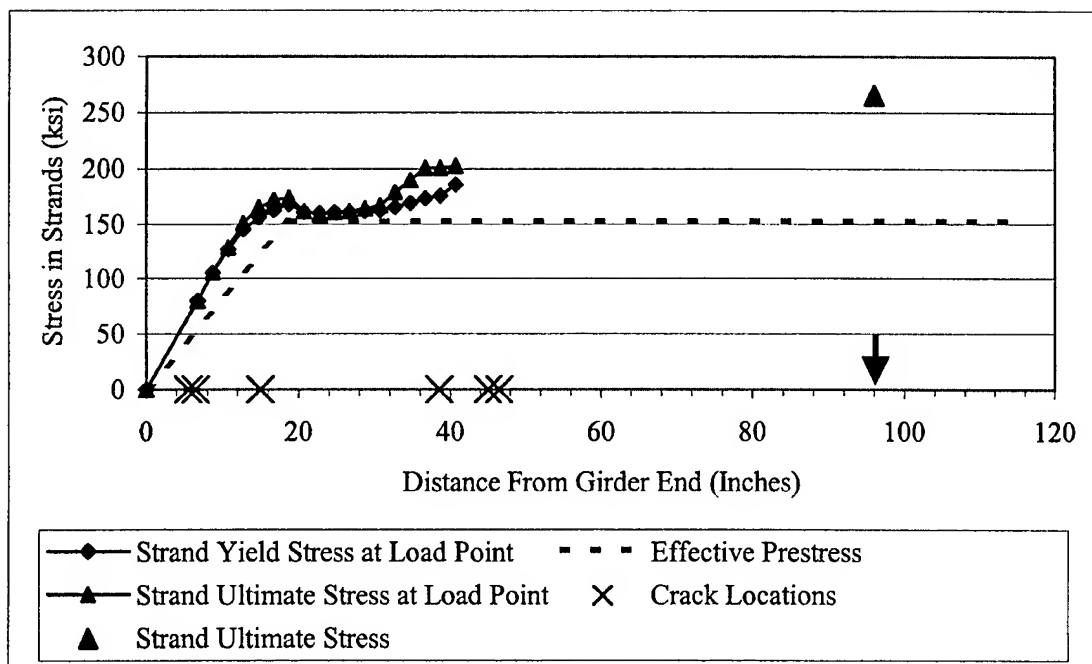


Figure Q.4  G1A-West Strand Stress vs Distance from Girder End

## Q.3 Development Length Test G1B-East
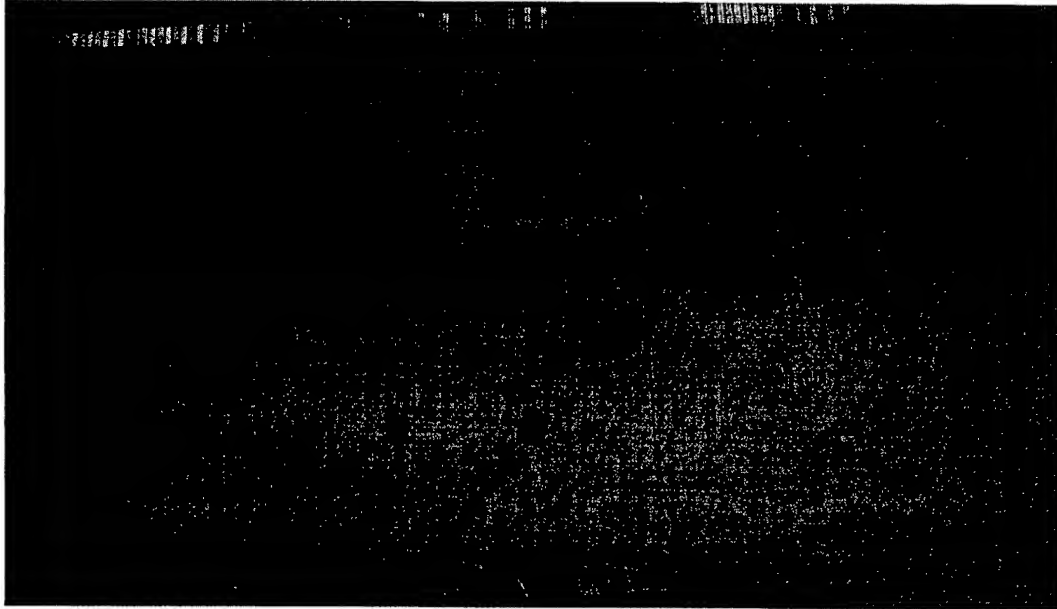


Figure Q.5  G1B-East Crack Patterns from Development Length Test
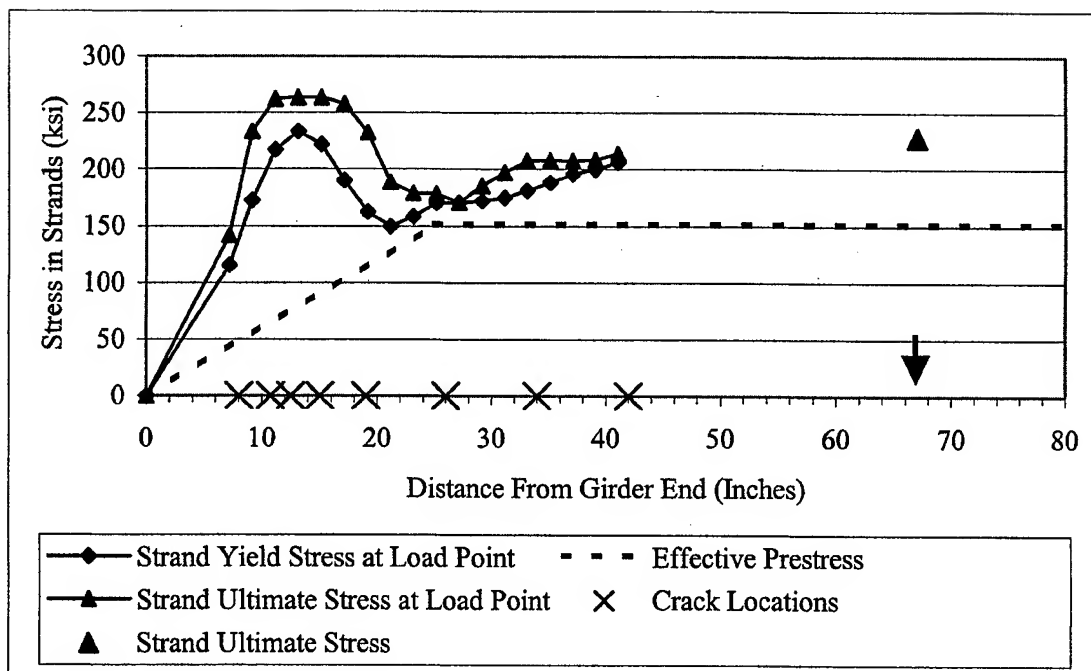


Figure Q.6  G1B-East Strand Stress vs Distance from Girder End

## Q.4 Development Length Test G1B-West
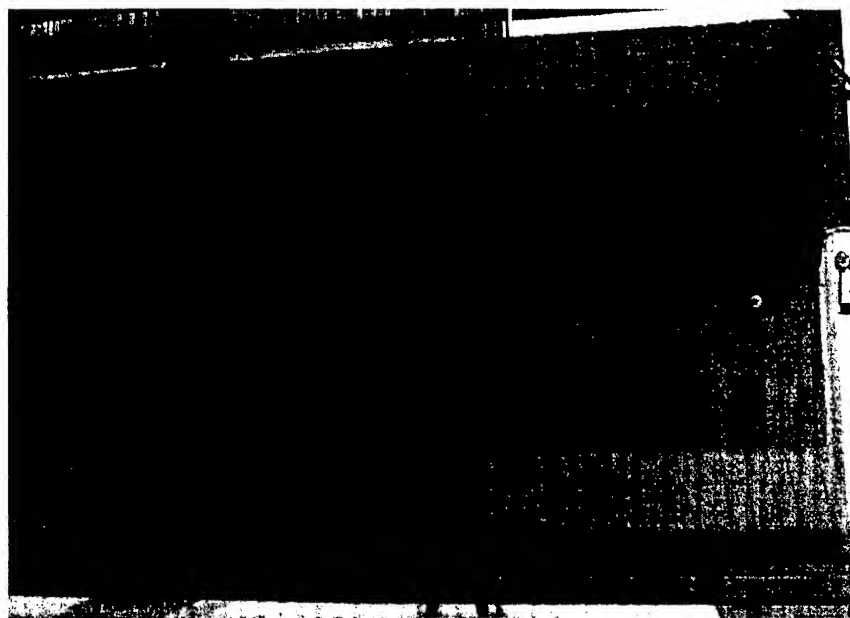


Figure Q.7  G1B-West Crack Patterns from Development Length Test
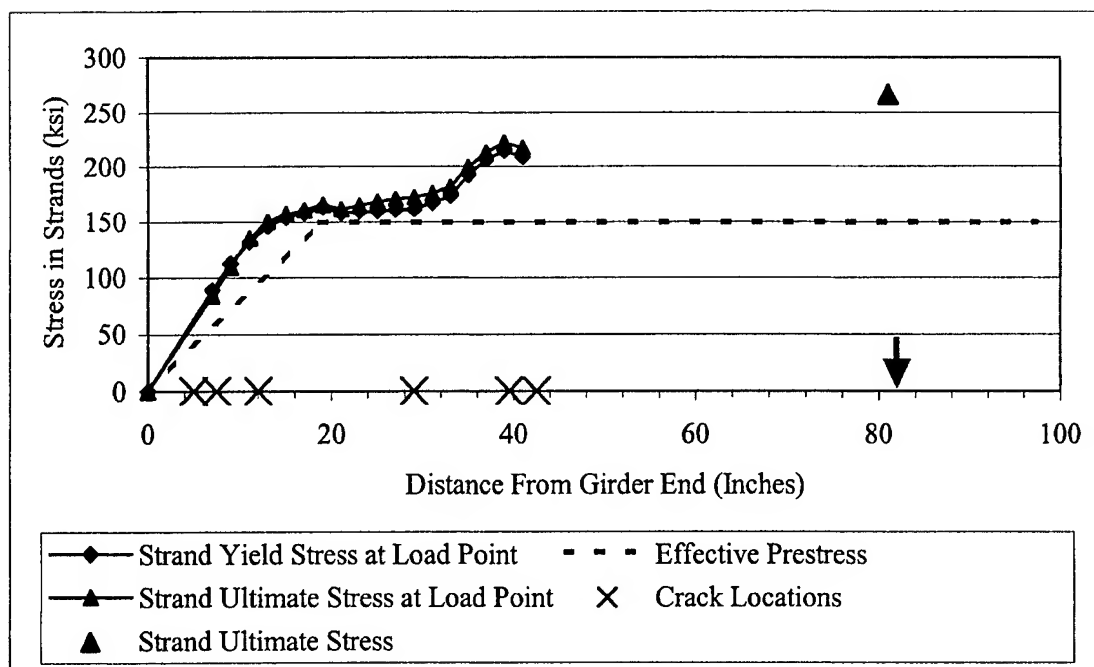


Figure Q.8  G1B-West Strand Stress vs Distance from Girder End

580

## Q.5  Development Length Test G1C-East
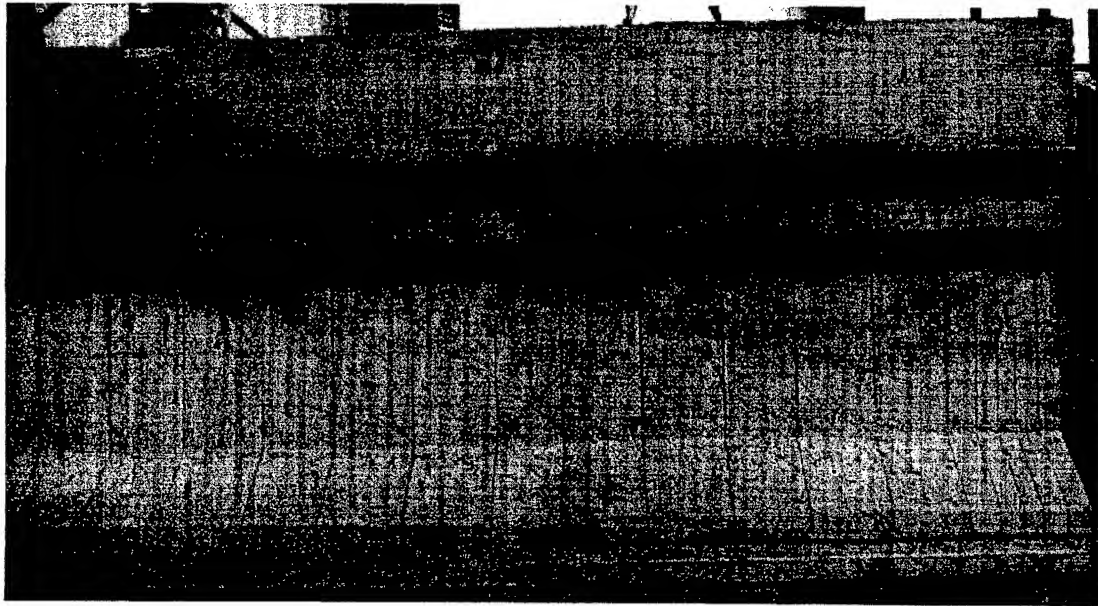


Figure Q.9  G1C-East Crack Patterns from Development Length Test
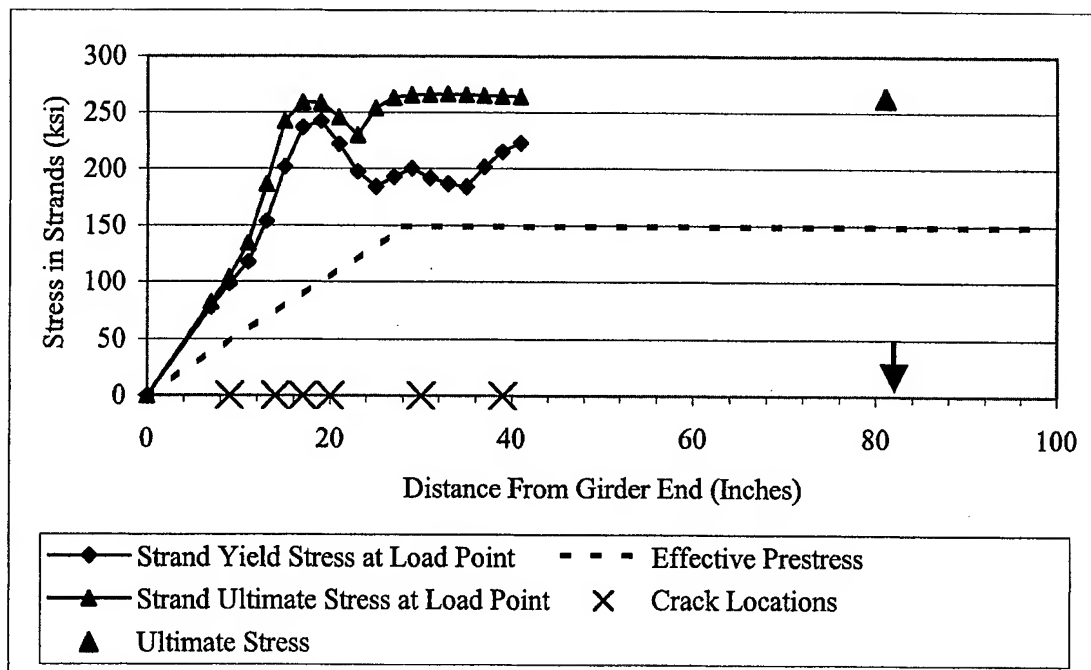


Figure Q.10  G1C-East Strand Stress vs Distance from Girder End

## Q.6 Development Length Test G1C-West
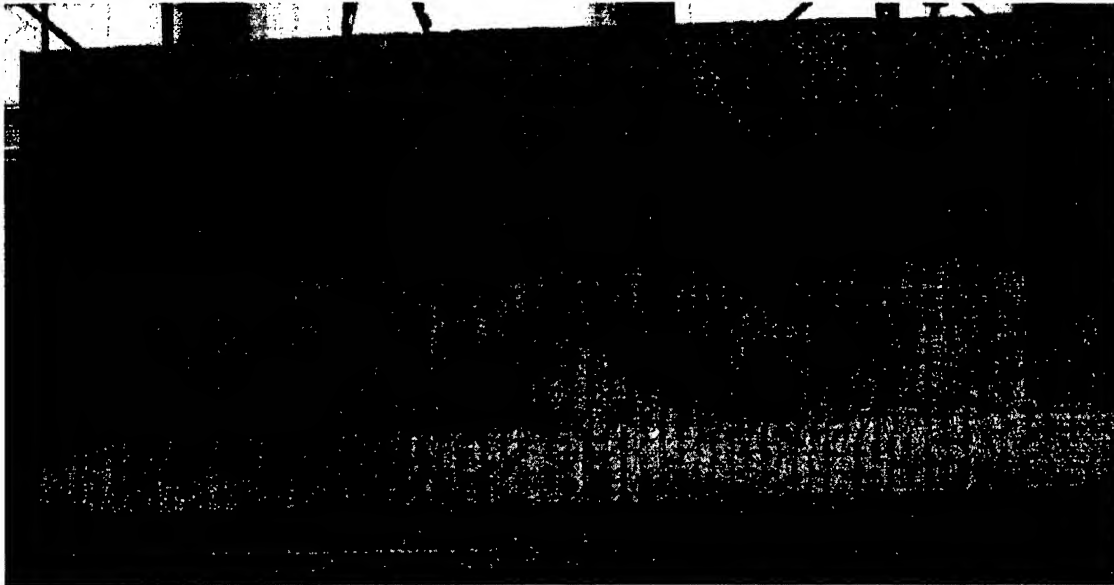


Figure Q.11  G1C-West Crack Patterns from Development Length Test
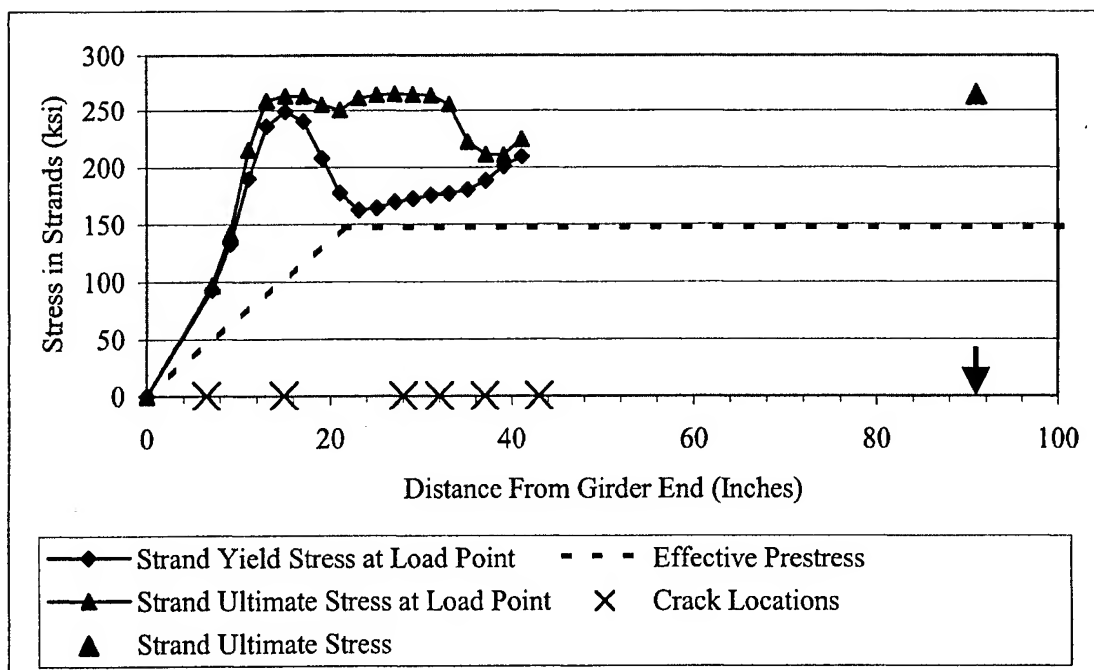


Figure Q.12  G1C-West Strand Stress vs Distance from Girder End

## Q.7 Development Length Test G2A-East
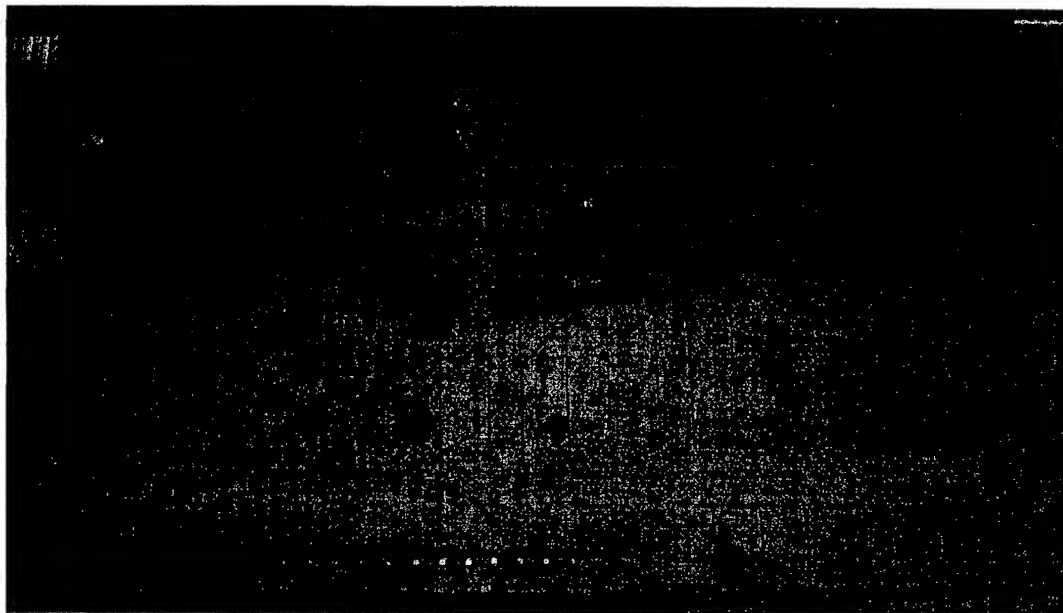


Figure Q.13  G2A-East Crack Patterns from Development Length Test
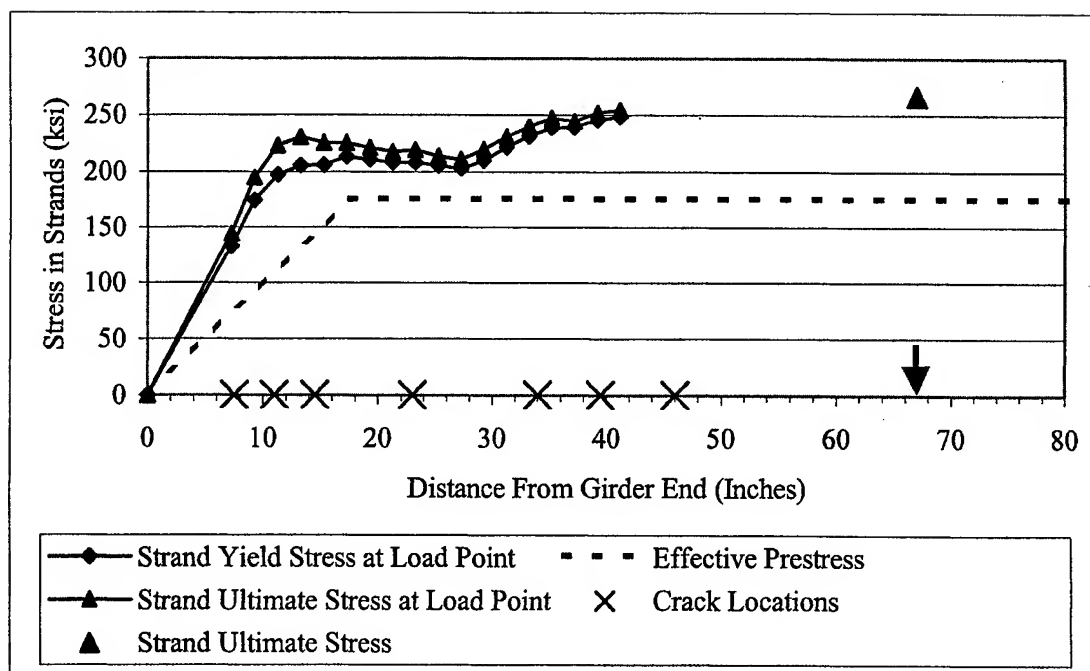


Figure Q.14  G2A-East Strand Stress vs Distance from Girder End

## Q.8 Development Length Test G2A-West
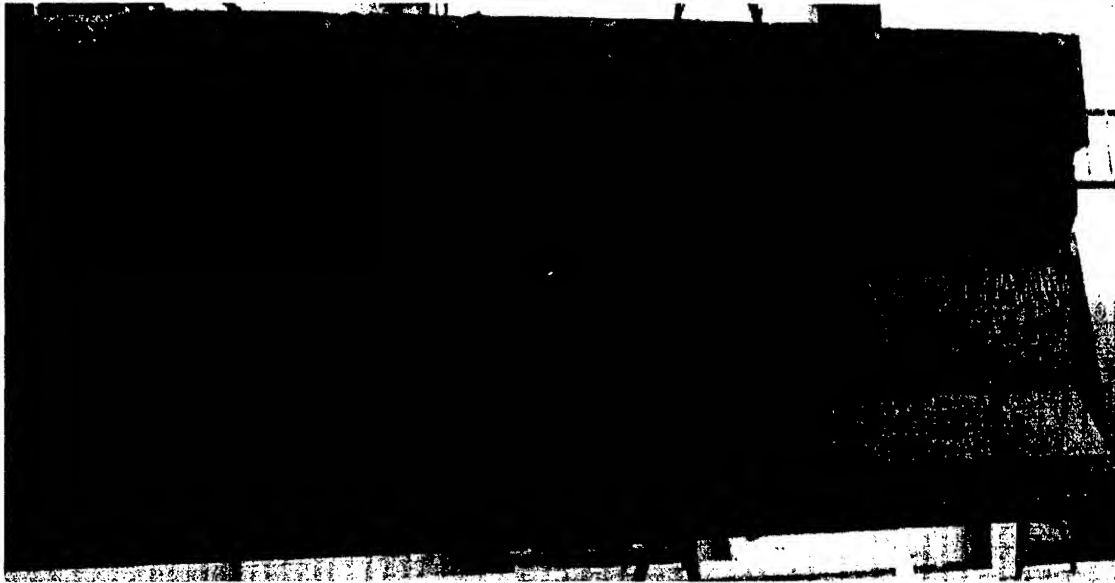


Figure Q.15  G2A-West Crack Patterns from Development Length Test
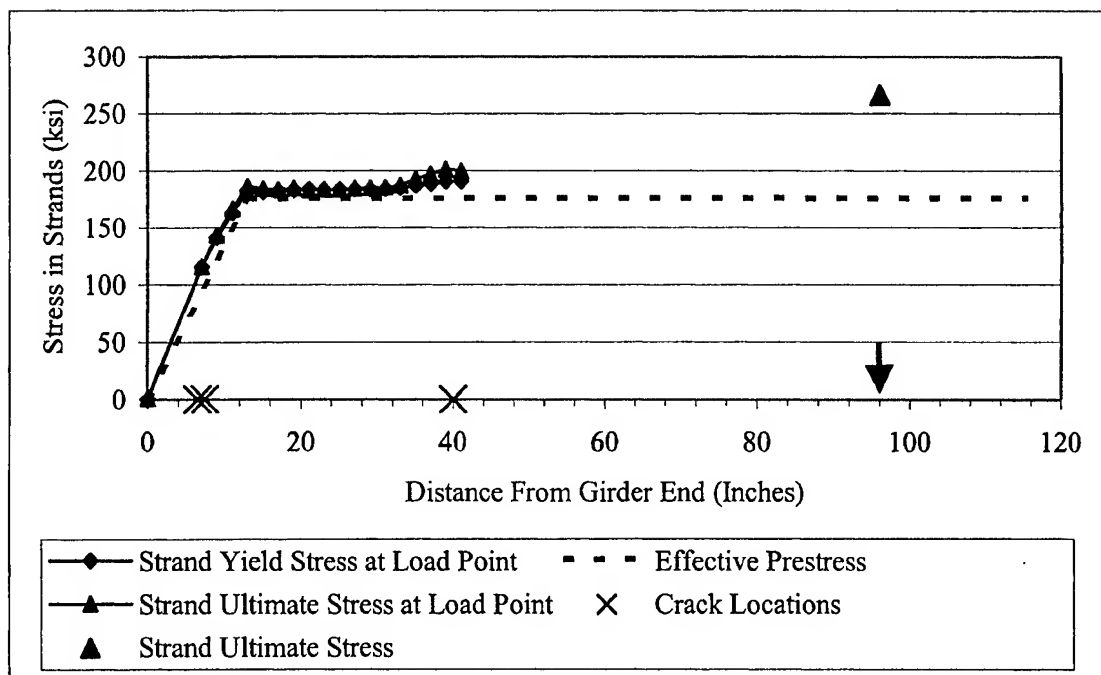


Figure Q.16  G2A-West Strand Stress vs Distance from Girder End

## Q.9  Development Length Test G2B-East
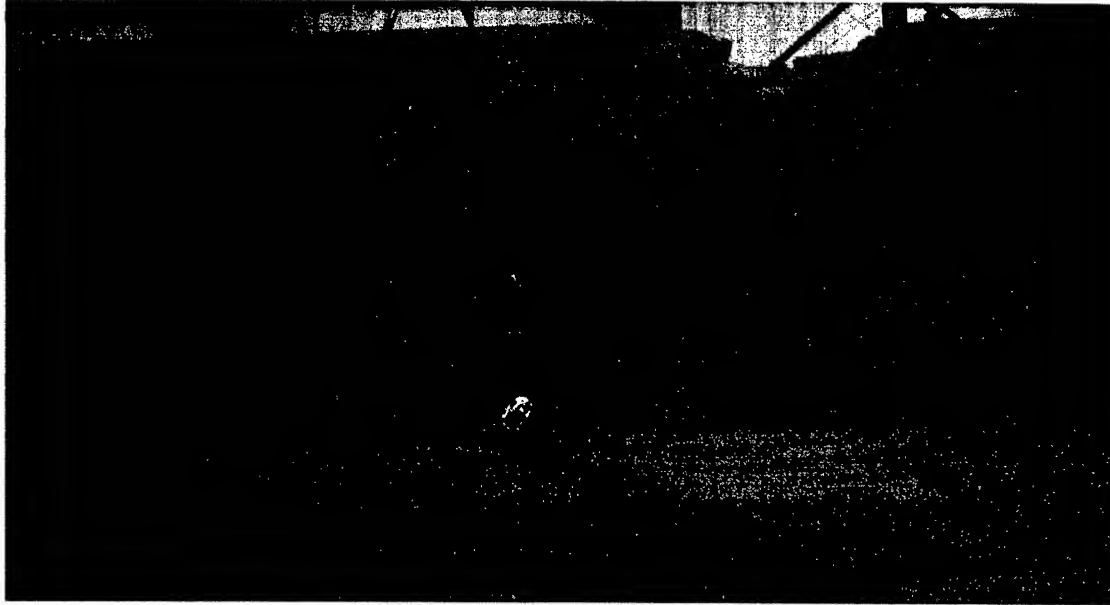


Figure Q.17  G2B-East Crack Patterns from Development Length Test
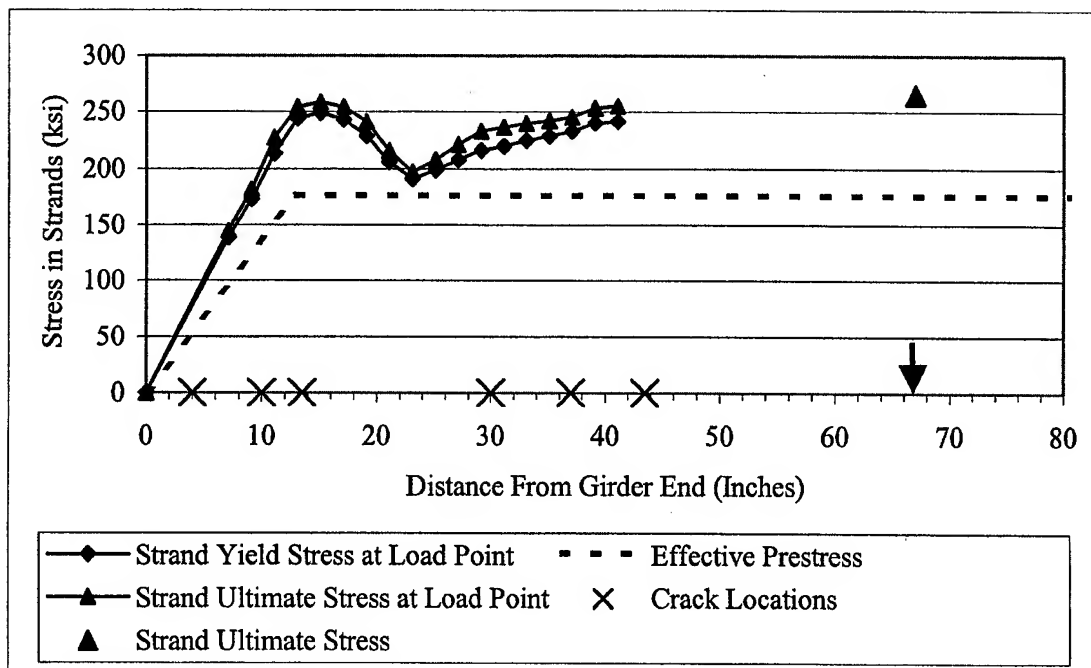


Figure Q.18  G2B-East Strand Stress vs Distance from Girder End

## Q.10 Development Length Test G2B-West
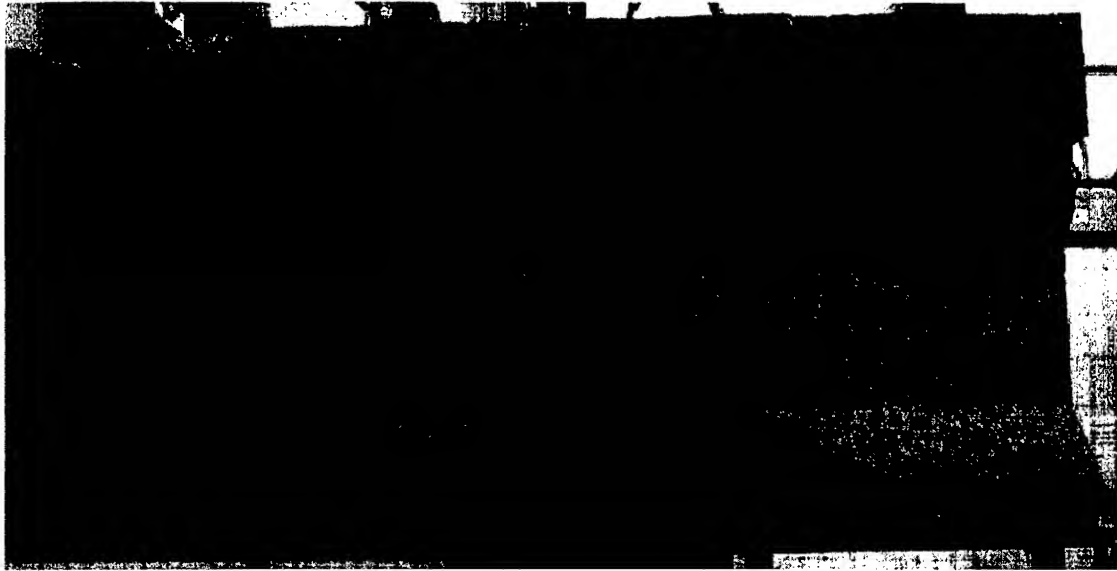


Figure Q.19 G2B-West Crack Patterns from Development Length Test
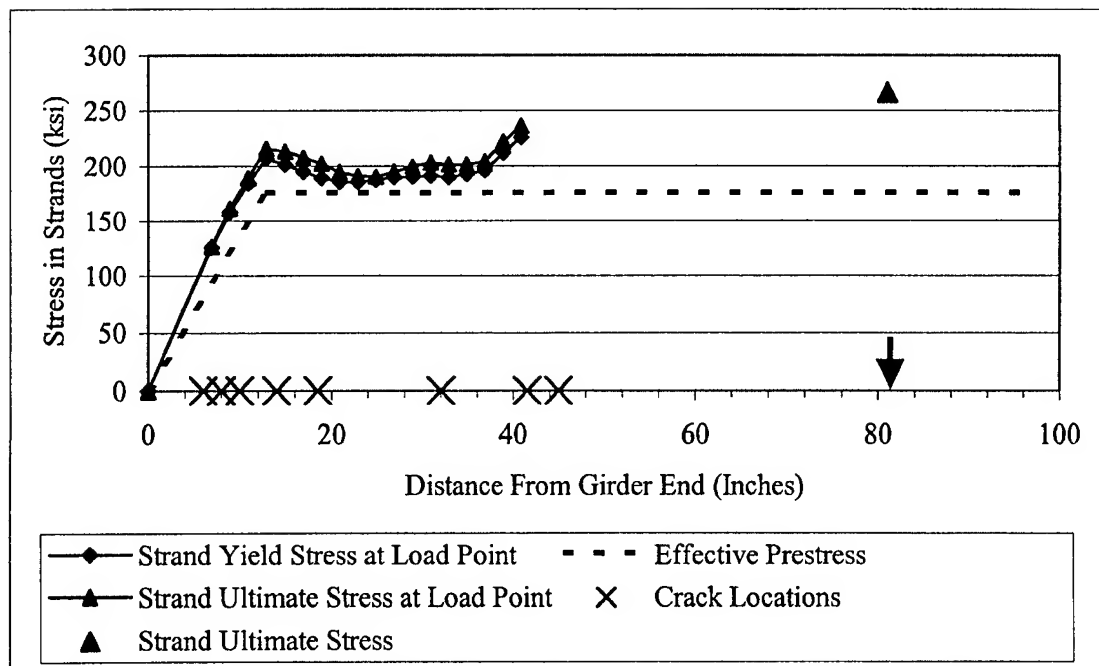


Figure Q.20 G2B-West Strand Stress vs Distance from Girder End

586

## Q.11 Development Length Test G2C-East
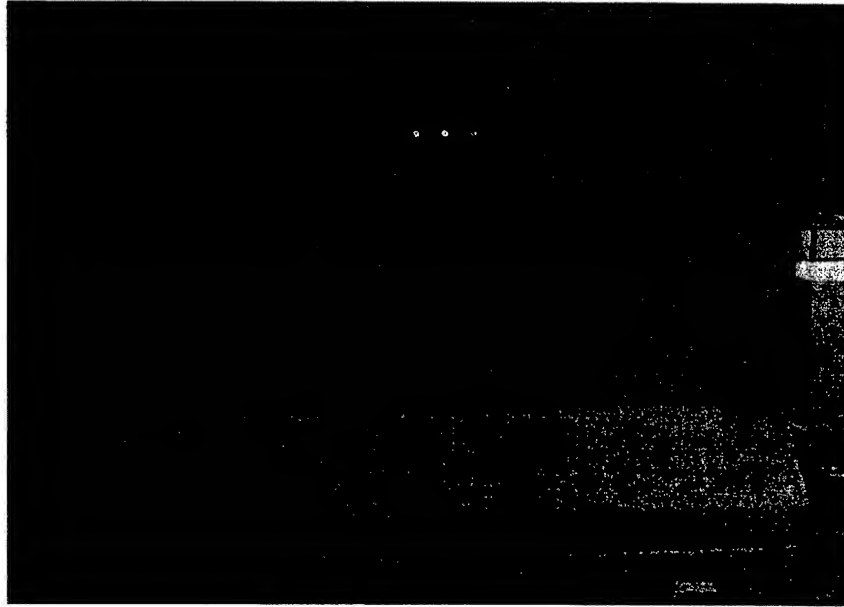


Figure Q.21  G2C-East Crack Patterns from Development Length Test
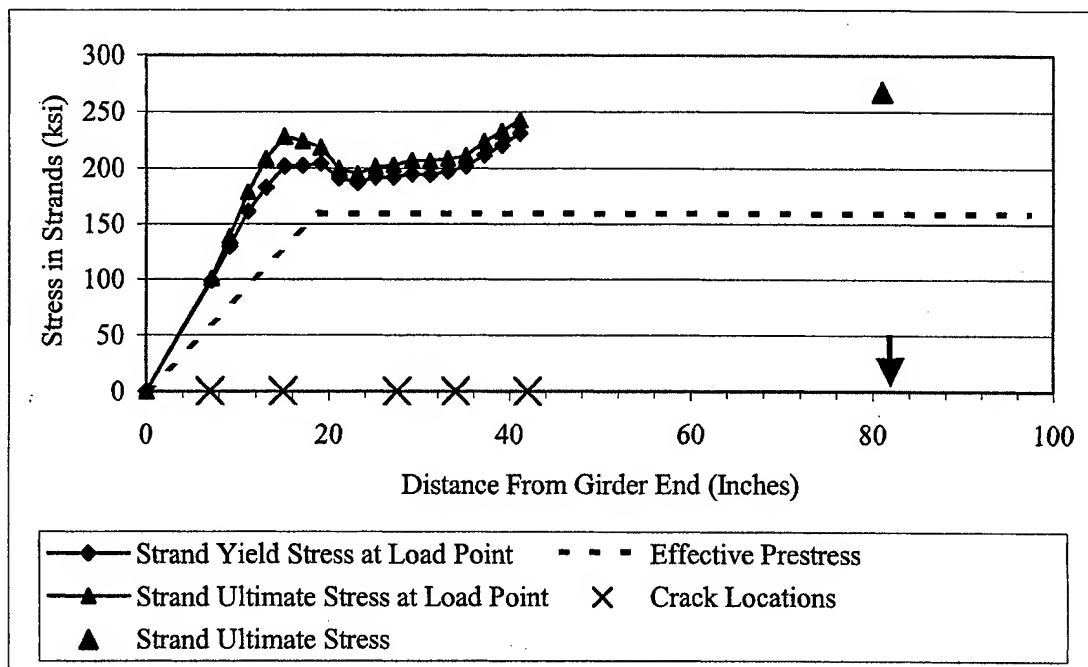


Figure Q.22  G2C-East Strand Stress vs Distance from Girder End

587

## Q.12 Development Length Test G2C-West
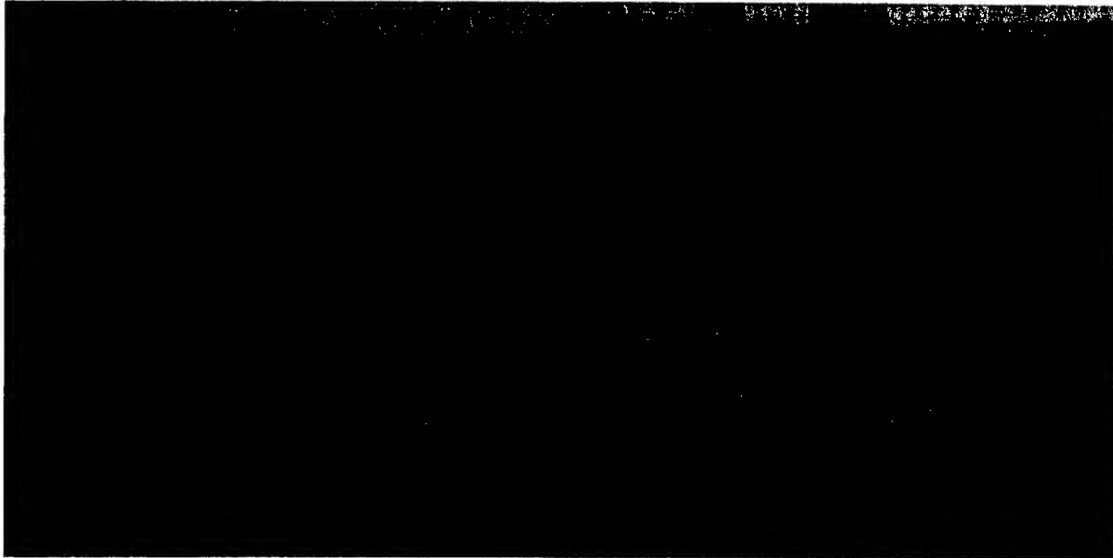


Figure Q.23  G2C-West Crack Patterns from Development Length Test
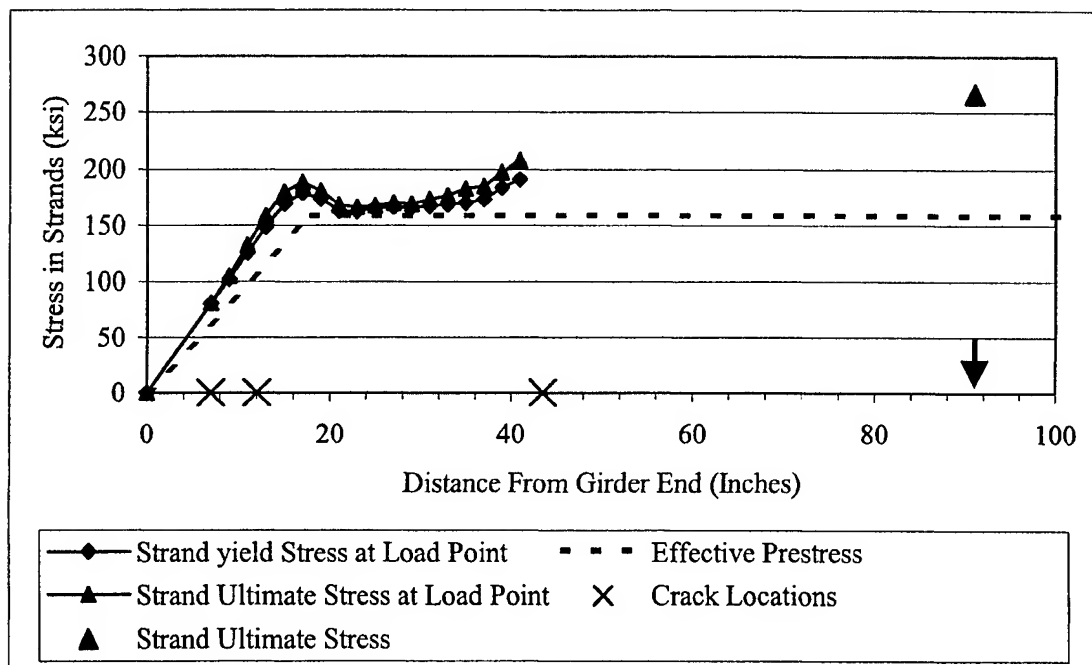


Figure Q.24  G2C-West Strand Stress vs Distance from Girder End

# APPENDIX R

## SHEAR vs. STRAND SLIP PLOTS
## AND
## CSS vs. DISTANCE FROM GIRDER END PLOTS
## FROM
## DEVELOPMENT LENGTH TESTS

Appendix R contains a plot comparing the applied shear vs. average strand slip

and CSS vs. distance from girder ends for each development length test. For many of the

applied shear vs. average strand slip plots, there is no definitive point where strand slip

begins. The scatter of data on the graph as the applied shear increased due to variability

in the data acquisition system and noise. In most cases, the variability of the data is less

than 0.0006 inches, which essentially indicates "zero slip." On the CSS vs. distance from

girder end plots, the CSS data were collected after each load step. Only the plots at

applied shear levels where cracking occurred through the initial 48 inches of the girder at

the lower strand level are shown. The sections correspond with the individual

development length tests as follows:

**Section R.1** – Test G1A-East

**Section R.2** – Test G1A-West

**Section R.3** – Test G1B-East

**Section R.4** – Test G1B-West

**Section R.5** – Test G1C-East

589

## R.1 Development Length Test G1A-East
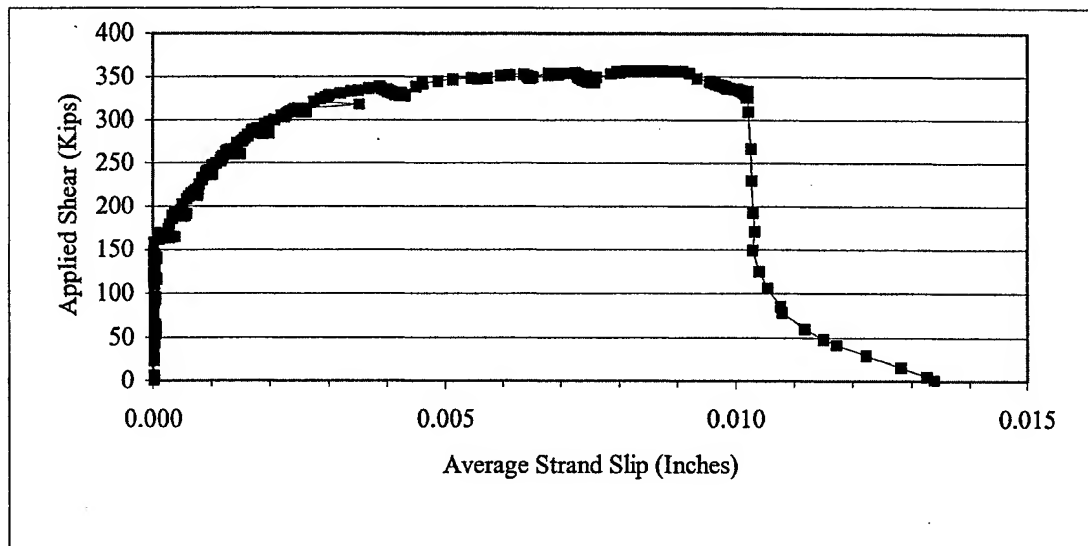


Figure R.1 G1A-East Applied Shear vs. Average Strand Slip
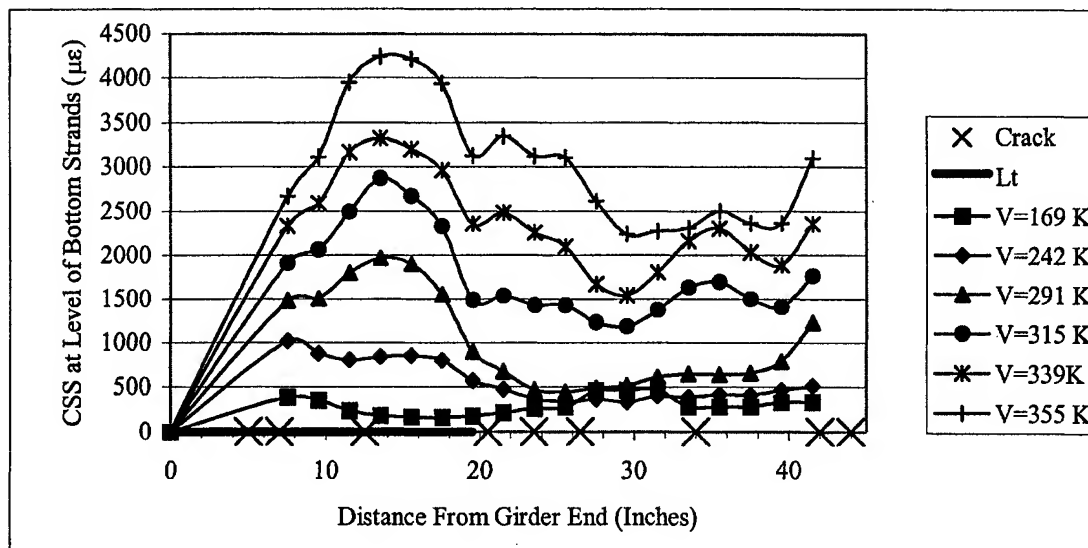


| Shear Crack Data | | | | | | | | | | |
|---|---|---|---|---|---|---|---|---|---|---|
| Distance From End (Inches) | 5.0 | 7.0 | 12.5 | 20.5 | 23.5 | 26.5 | 34.0 | 42.0 | 44.0 | 47.5 |
| Applied Shear at Cracking (Kips) | 169 | 315 | 242 | 339 | 315 | 355 | 339 | 339 | 291 | 355 |

Figure R.2 G1A-East CSS and Shear Cracking vs. Distance from Girder End

591

## R.2 Development Length Test G1A-West
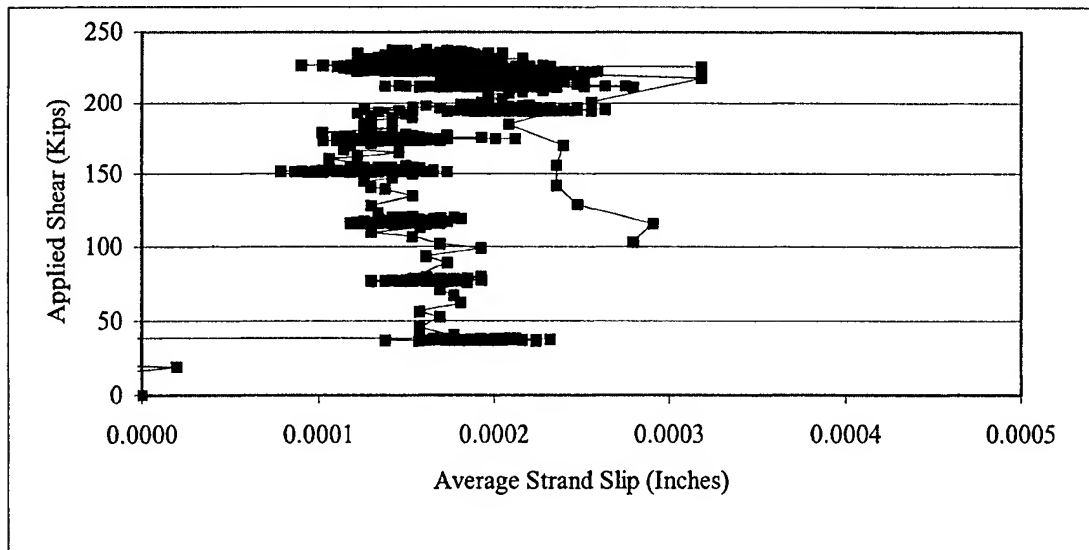


Figure R.3  G1A-West Applied Shear vs. Average Strand Slip
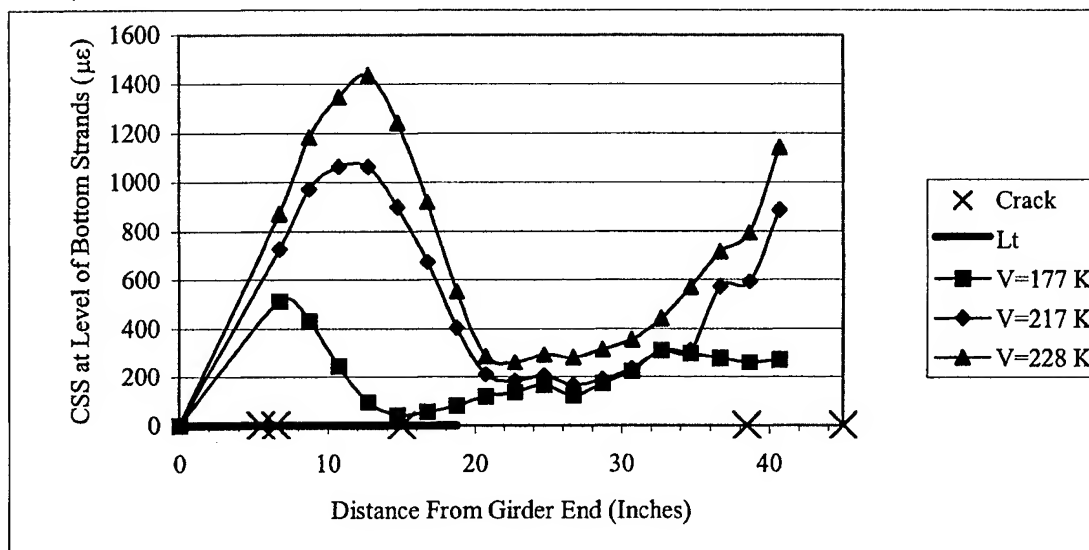


| Shear Crack Data | | | | | | | | | |
|---|---|---|---|---|---|---|---|---|---|
| Distance From End (Inches) | 5.5 | 6.5 | 15.0 | 38.5 | 45.0 | 46.5 | | | |
| Applied Shear at Cracking (Kips) | 177 | 177 | 217 | 228 | 228 | 217 | | | |

Figure R.4  G1A-West CSS and Shear Cracking vs. Distance from Girder End

## R.3 Development Length Test G1B-East
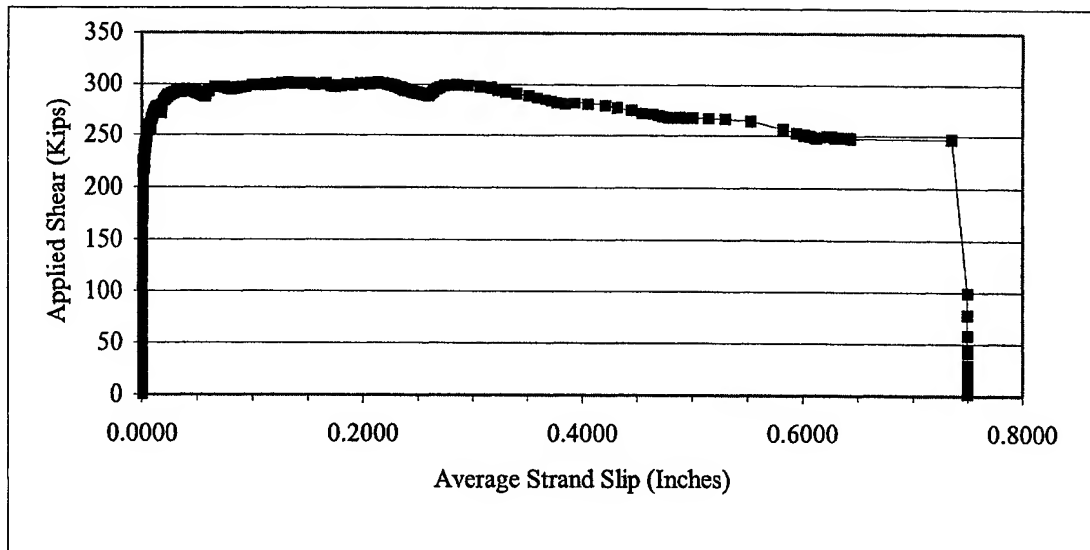


Figure R.5  G1B-East Applied Shear vs. Average Strand Slip
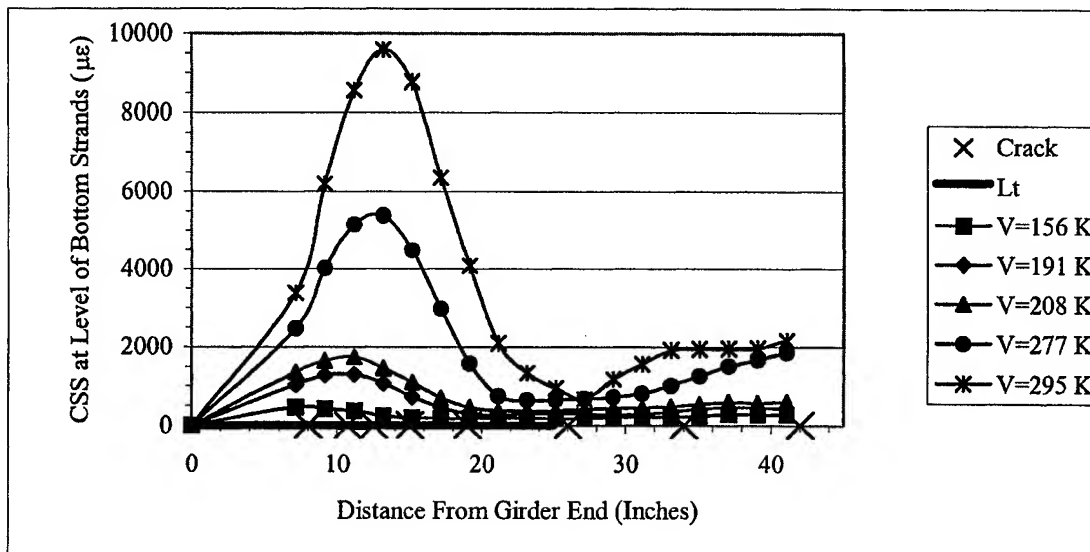


| Shear Crack Data | | | | | | | | | | |
|---|---|---|---|---|---|---|---|---|---|---|
| Distance From End (Inches) | 8 | 10.75 | 12.5 | 15 | 19 | 26 | 34 | 42 | | |
| Applied Shear at Cracking (Kips) | 156 | 191 | 208 | 295 | 295 | 295 | 295 | 277 | | |

Figure R.6  G1B-East CSS and Shear Cracking vs. Distance from Girder End

593

## R.4 Development Length Test G1B-West
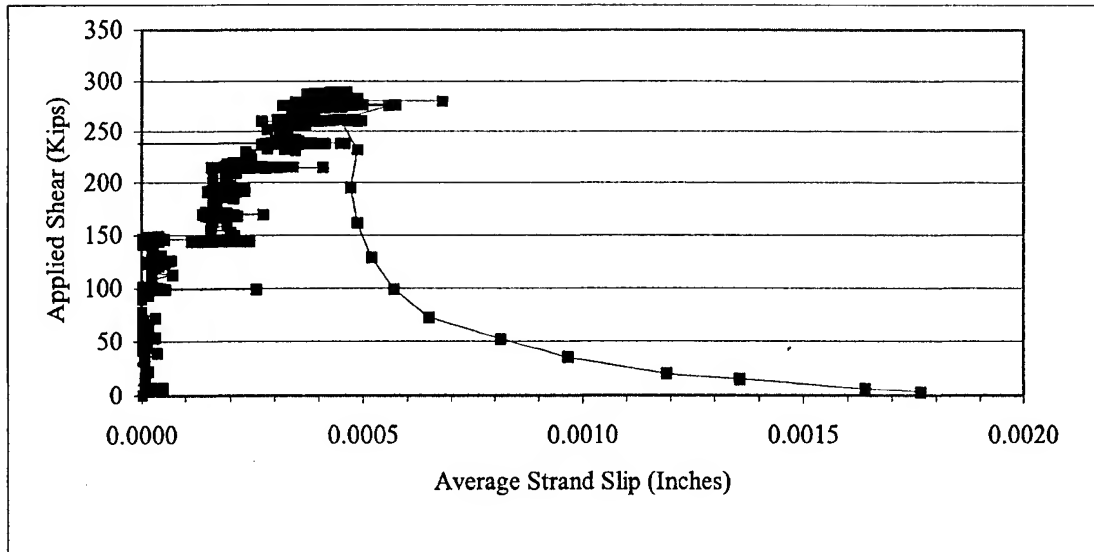


Figure R.7  G1B-West Applied Shear vs. Average Strand Slip
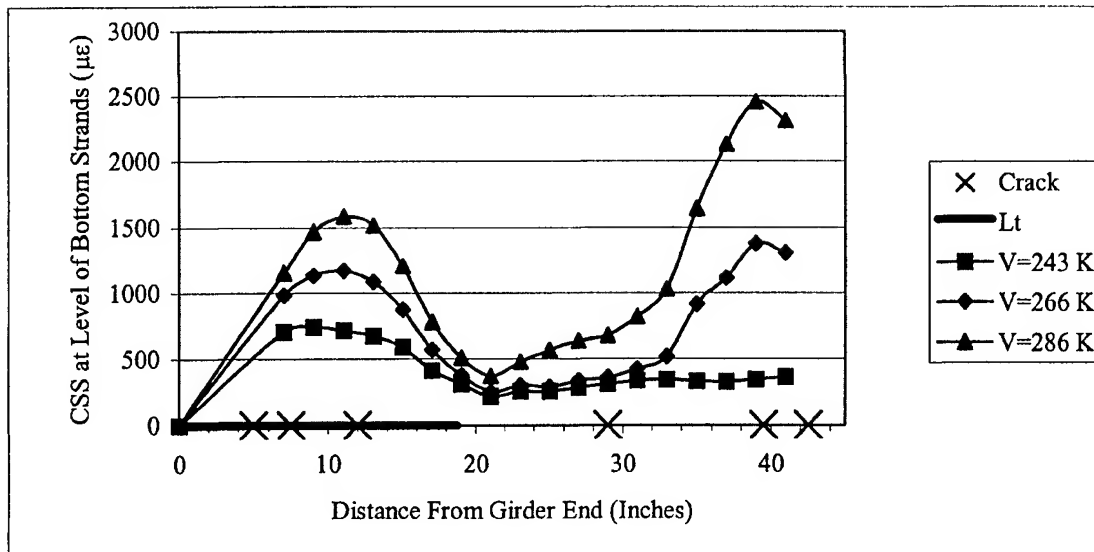


| Shear Crack Data | | | | | | | | | |
|---|---|---|---|---|---|---|---|---|---|
| Distance From End (Inches) | 5 | 7.5 | 12 | 29 | 39.5 | 42.5 | | | |
| Applied Shear at Cracking (Kips) | 243 | 266 | 266 | 286 | 286 | 286 | | | |

Figure R.8  G1B-West CSS and Shear Cracking vs. Distance from Girder End

594

## R.5  Development Length Test G1C-East
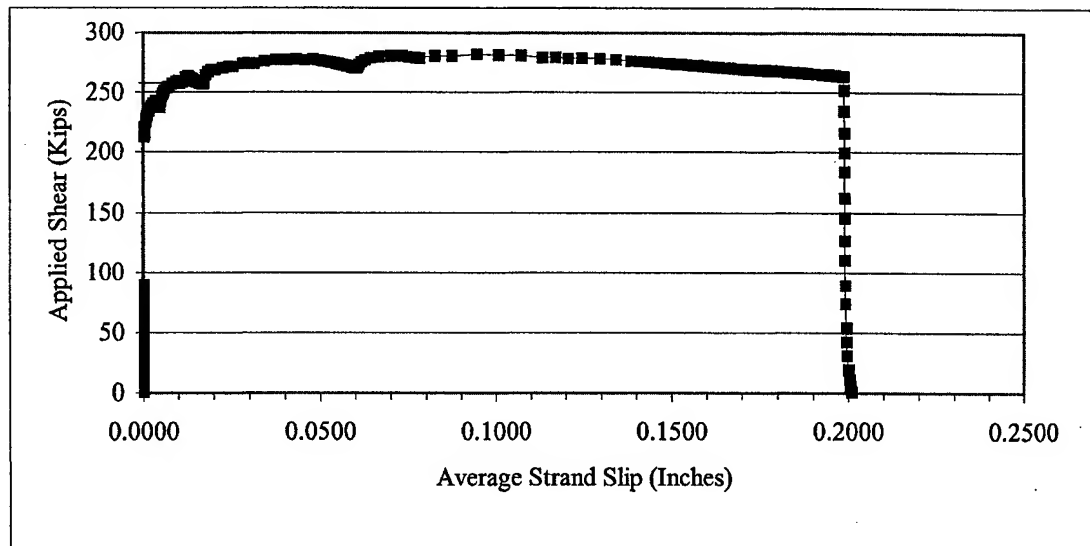


Figure R.9  G1C-East Applied Shear vs. Average Strand Slip
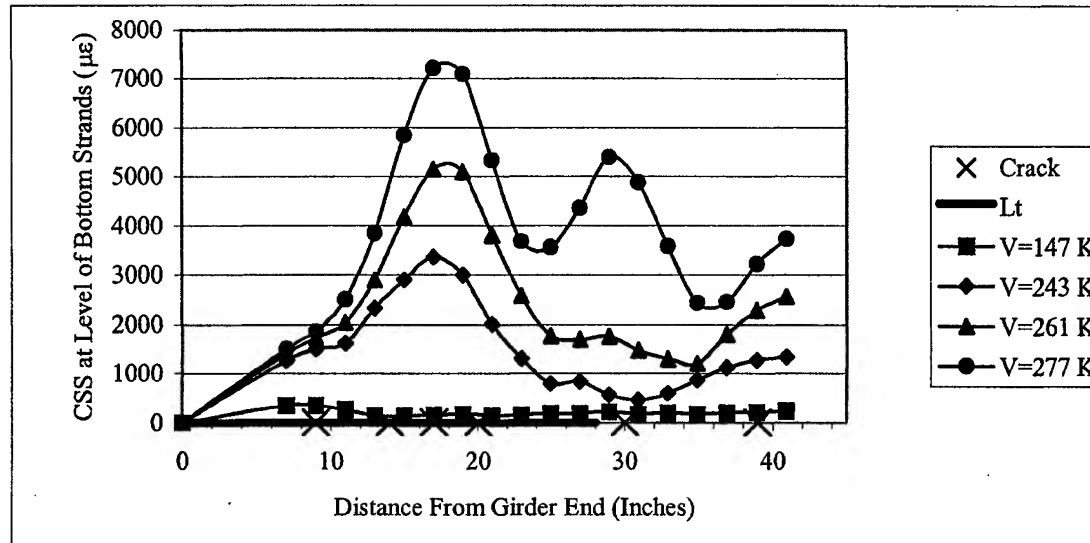


| Shear Crack Data | | | | | | | | | | |
|---|---|---|---|---|---|---|---|---|---|---|
| Distance From End (Inches) | 9 | 14 | 17 | 20 | 30 | 39 | | | | |
| Applied Shear at Cracking (Kips) | 147 | 261 | 243 | 261 | 261 | 277 | | | | |

Figure R.10  G1C-East CSS and Shear Cracking vs. Distance from Girder End

595

## R.6 Development Length Test G1C-West
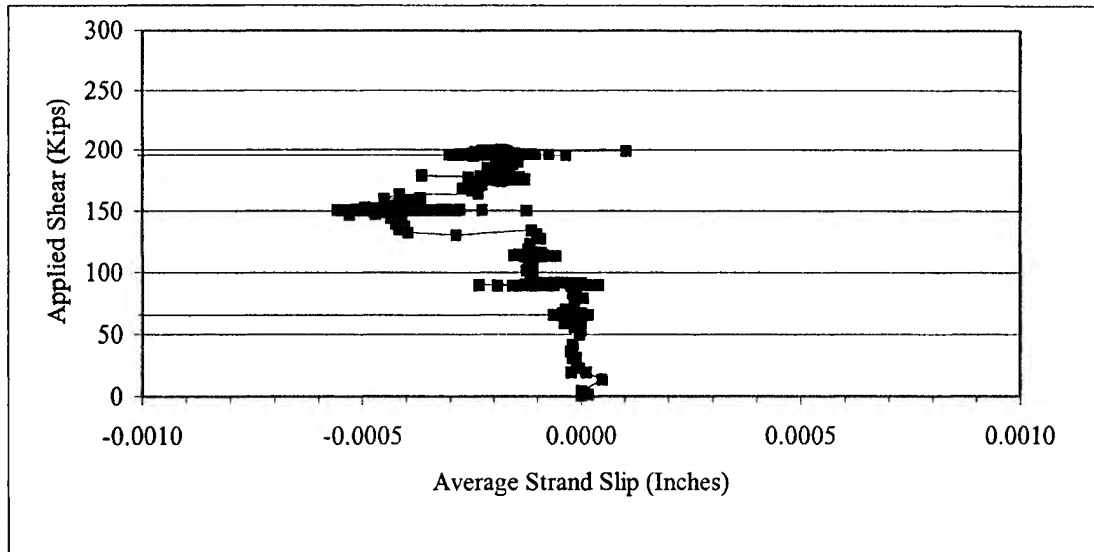


Figure R.11  G1C-West Applied Shear vs. Average Strand Slip
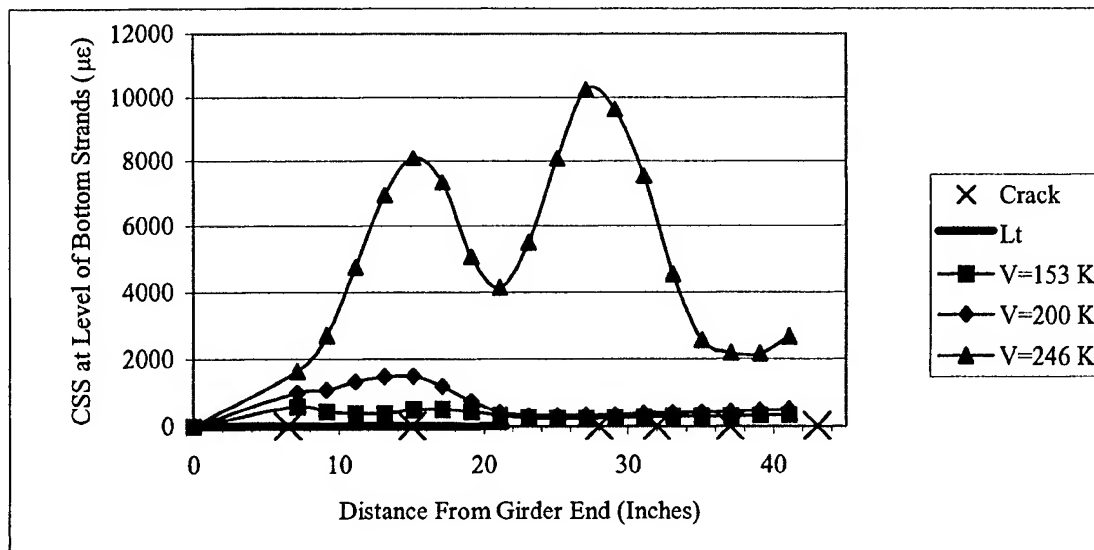


| Shear Crack Data | | | | | | | | | | |
|---|---|---|---|---|---|---|---|---|---|---|
| Distance From End (Inches) | 6.5 | 15 | 28 | 32 | 37 | 43 | | | | |
| Applied Shear at Cracking (Kips) | 153 | 153 | 246 | 246 | 200 | 246 | | | | |

Figure R.12  G1C-West CSS and Shear Cracking vs. Distance from Girder End

596

## R.7 Development Length Test G2A-East
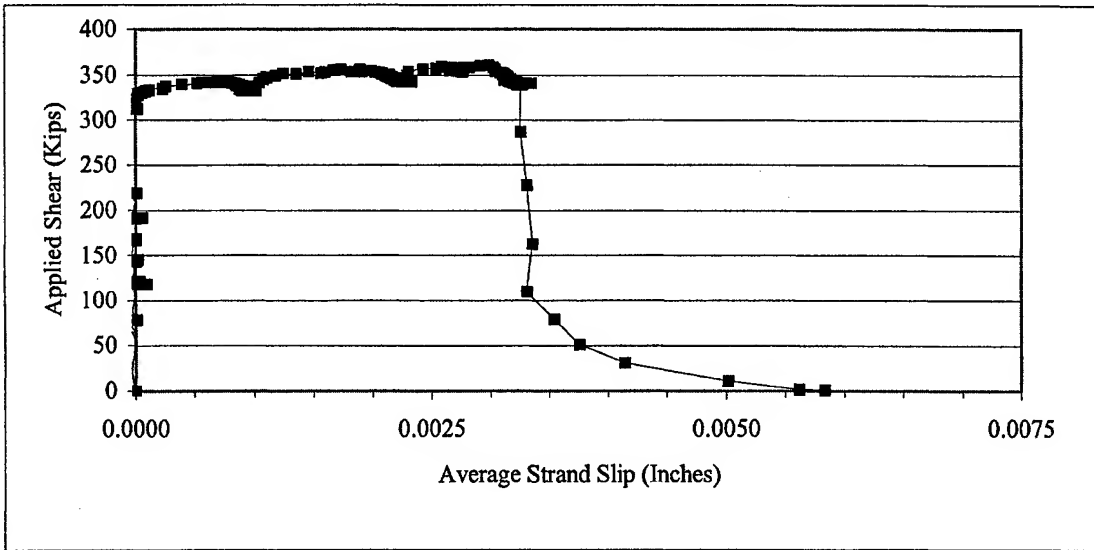


Figure R.13  G2A-East Applied Shear vs. Average Strand Slip
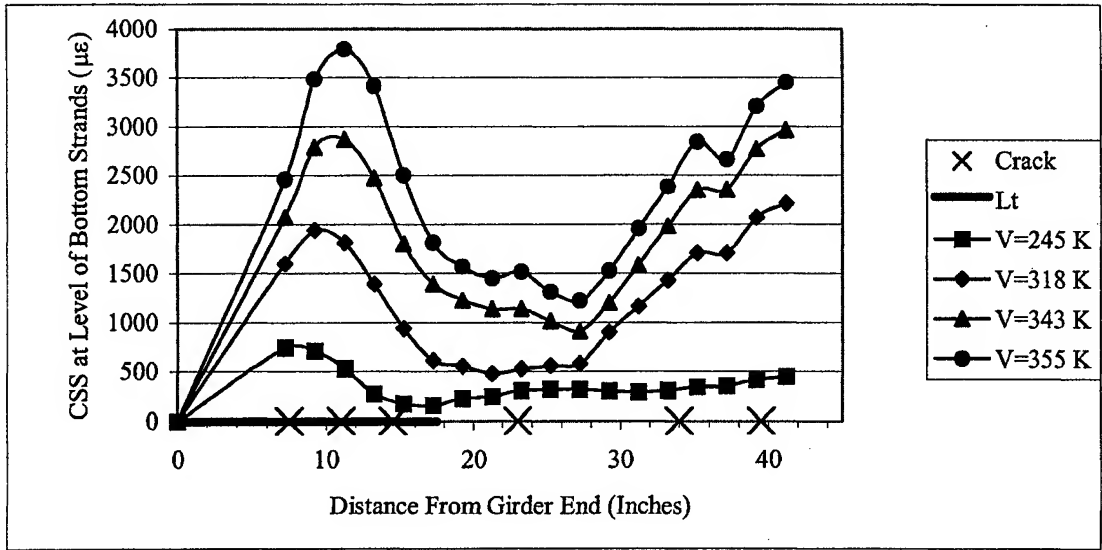


| Shear Crack Data | | | | | | | | | | |
|---|---|---|---|---|---|---|---|---|---|---|
| Distance From End (Inches) | 7.5 | 11 | 14.5 | 23 | 34 | 39.5 | 46 | | | |
| Applied Shear at Cracking (Kips) | 245 | 355 | 343 | 343 | 318 | 318 | 355 | | | |

Figure R.14  G2A-East CSS and Shear Cracking vs. Distance from Girder End

597

## R.8 Development Length Test G2A-West
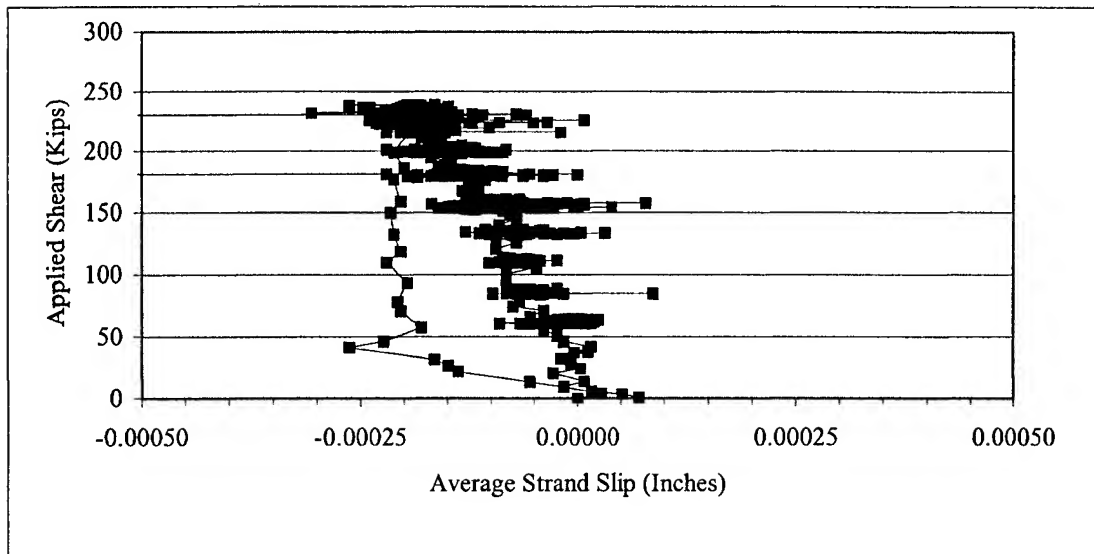


Figure R.15  G2A-West Applied Shear vs. Average Strand Slip
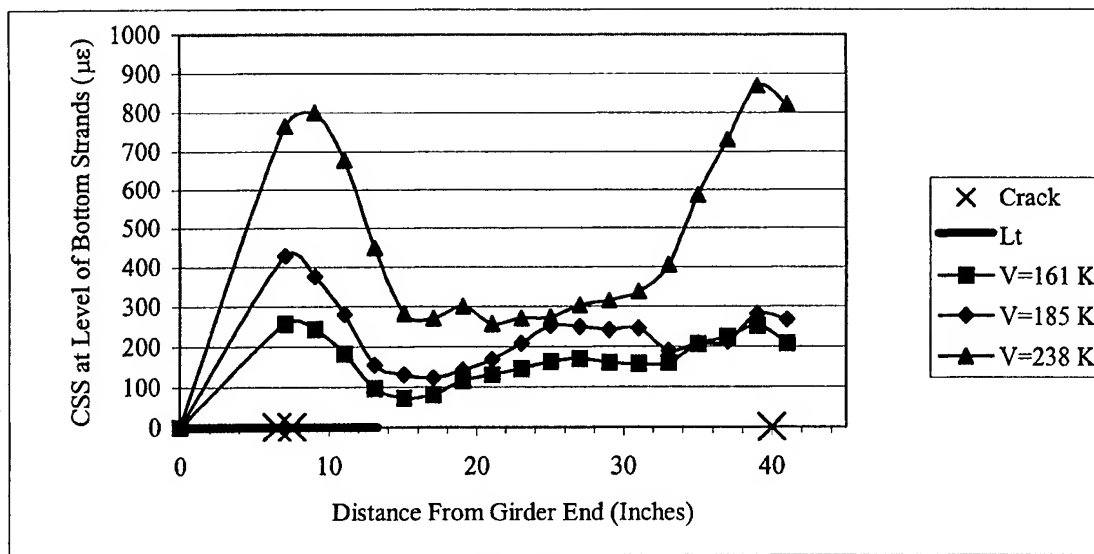


| Shear Crack Data | | | | | | | | | | |
|---|---|---|---|---|---|---|---|---|---|---|
| Distance From End (Inches) | 6.5 | 7.5 | 40 | | | | | | | |
| Applied Shear at Cracking (Kips) | 161 | 185 | 238 | | | | | | | |

Figure R.16  G2A-West CSS and Shear Cracking vs. Distance from Girder End

598

## R.9 Development Length Test G2B-East
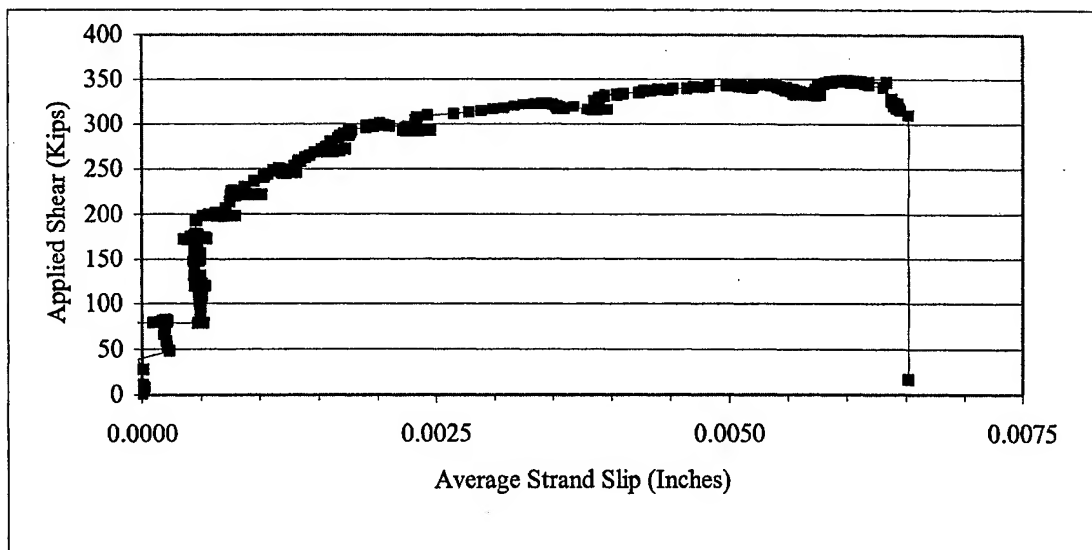


Figure R.17 G2B-East Applied Shear vs. Average Strand Slip
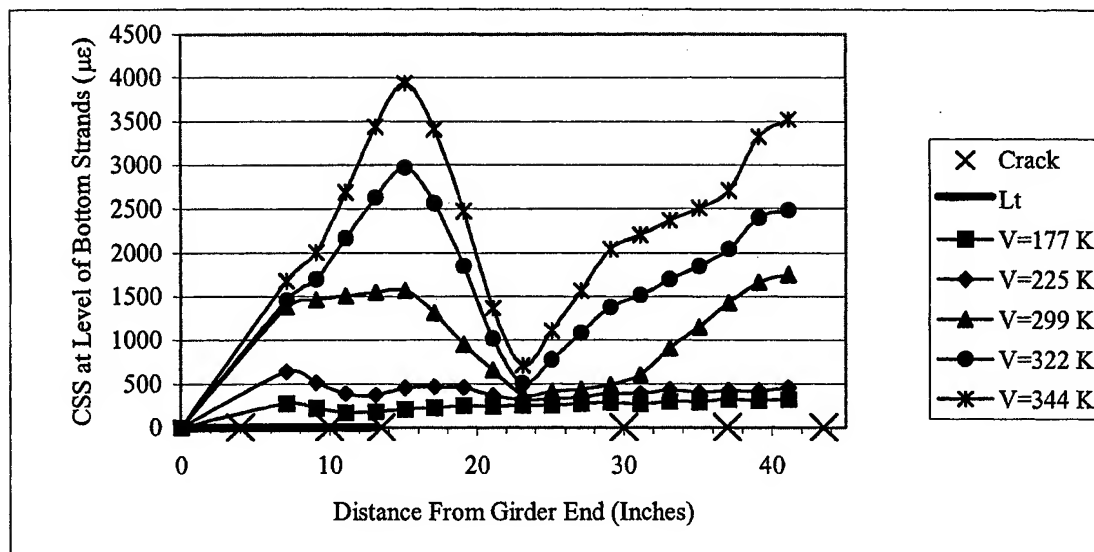


| Shear Crack Data | | | | | | | | | |
|---|---|---|---|---|---|---|---|---|---|
| Distance From End (Inches) | 4 | 10 | 13.5 | 30 | 37 | 43.5 | | | |
| Applied Shear at Cracking (Kips) | 177 | 225 | 322 | 344 | 299 | 299 | | | |

Figure R.18 G2B-East CSS and Shear Cracking vs. Distance from Girder End

## R.10 Development Length Test G2B-West
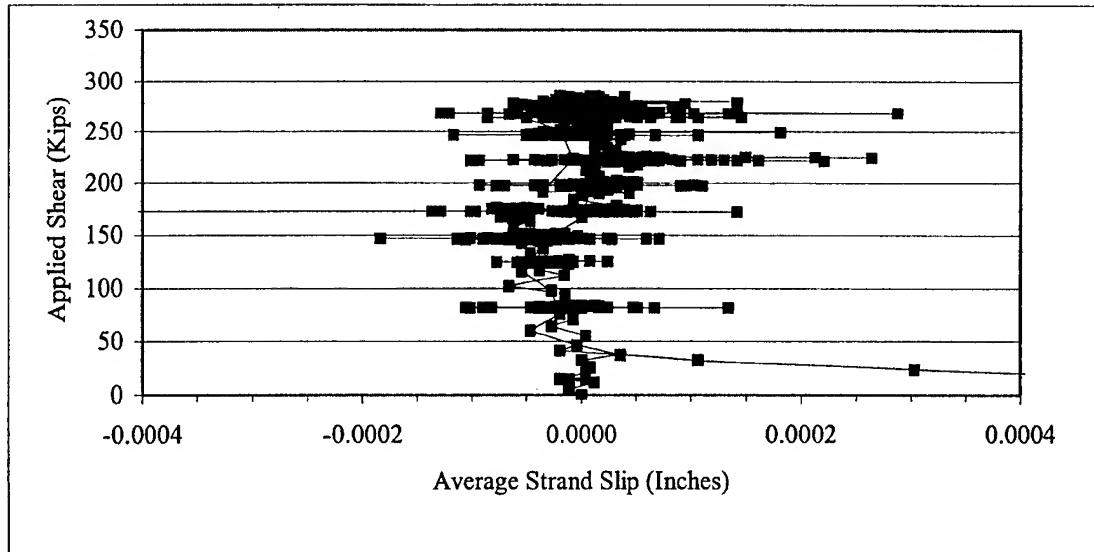


Figure R.19 G2B-West Applied Shear vs. Average Strand Slip
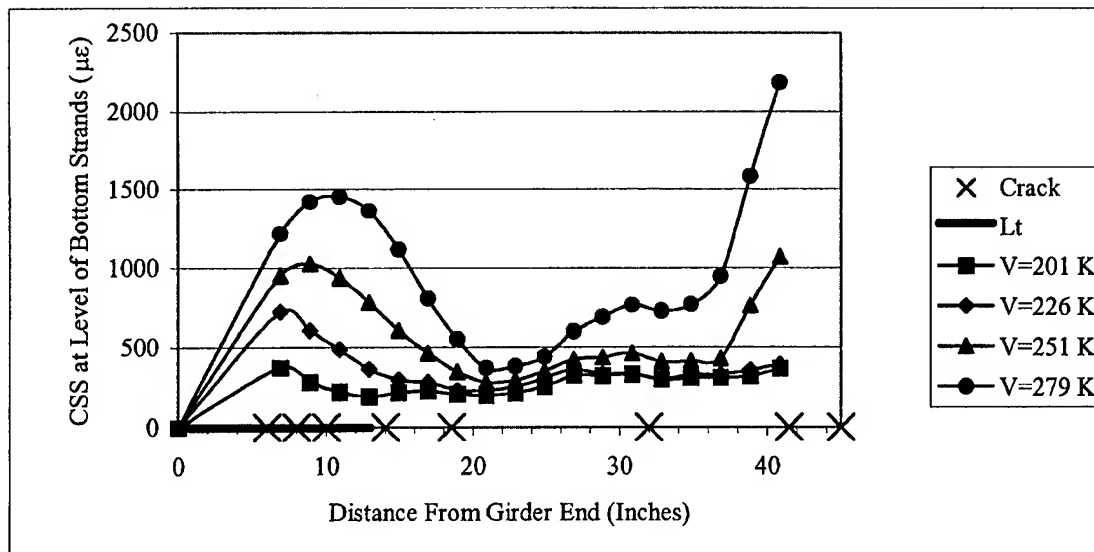


| Shear Crack Data | | | | | | | | | | |
|---|---|---|---|---|---|---|---|---|---|---|
| Distance From End (Inches) | 6 | 8 | 10 | 14 | 18.5 | 32 | 41.5 | 45 | | |
| Applied Shear at Cracking (Kips) | 201 | 226 | 251 | 251 | 279 | 279 | 279 | 251 | | |

Figure R.20 G2B-West CSS and Shear Cracking vs. Distance from Girder End

600

## R.11 Development Length Test G2C-East
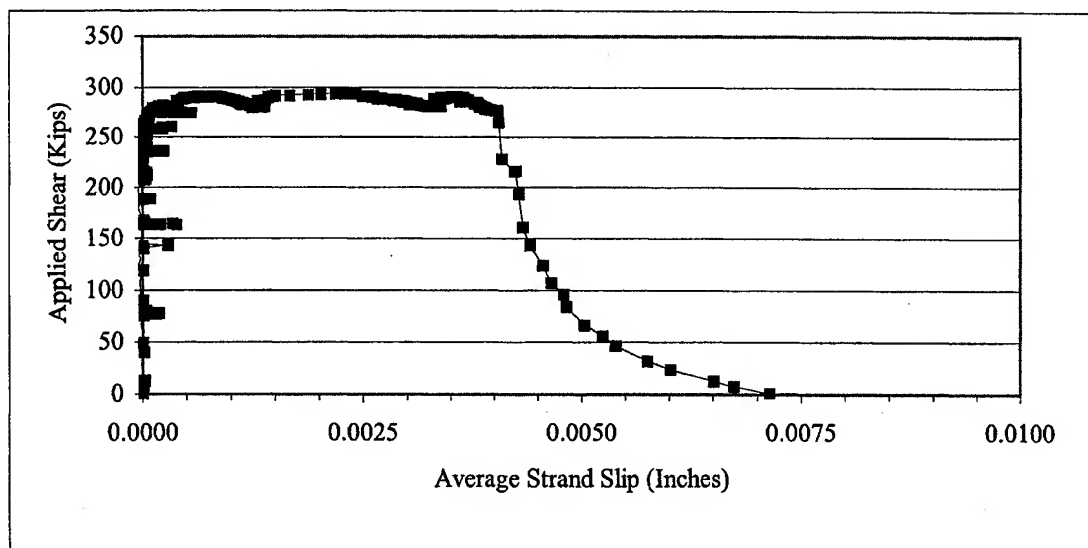


Figure R.21  G2C-East Applied Shear vs. Average Strand Slip
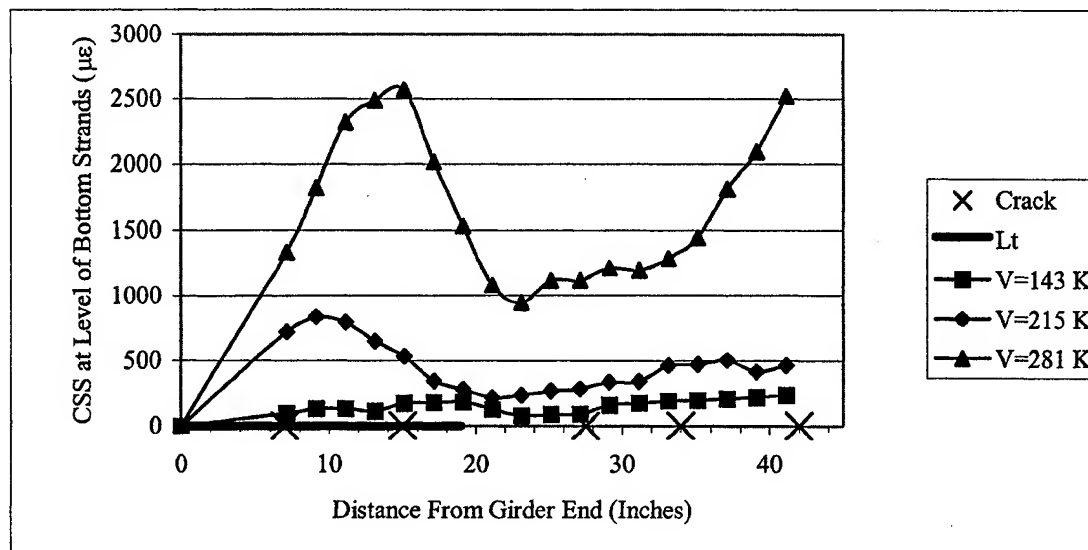


| Shear Crack Data | | | | | | | | | | |
|---|---|---|---|---|---|---|---|---|---|---|
| Distance From End (Inches) | 7 | 15 | 27.5 | 34 | 42 | | | | | |
| Applied Shear at Cracking (Kips) | 143 | 215 | 281 | 281 | 281 | | | | | |

Figure R.22  G2C-East CSS and Shear Cracking vs. Distance from Girder End

601

## R.12 Development Length Test G2C-West
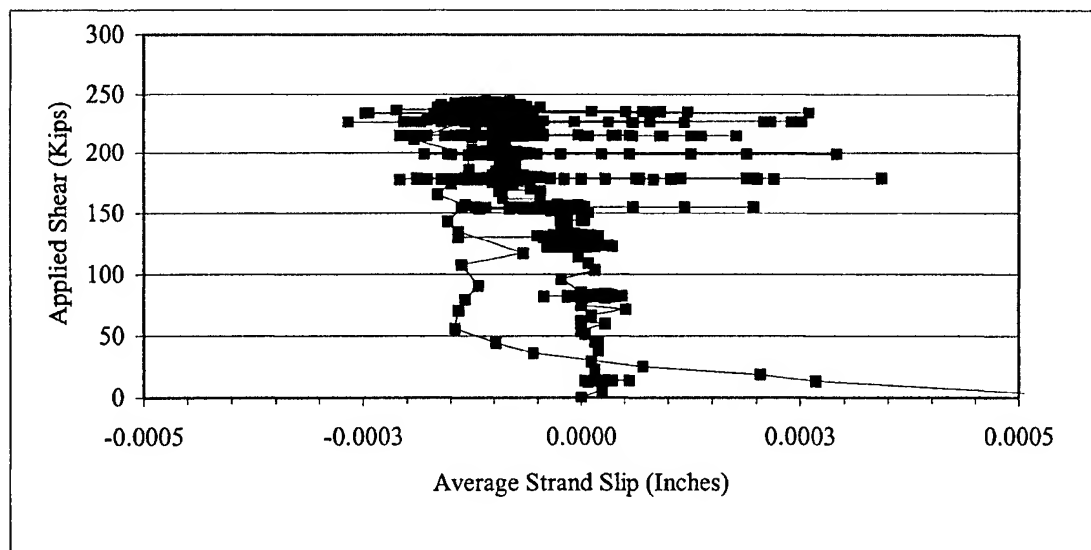


Figure R.23 G2C-West Applied Shear vs. Average Strand Slip
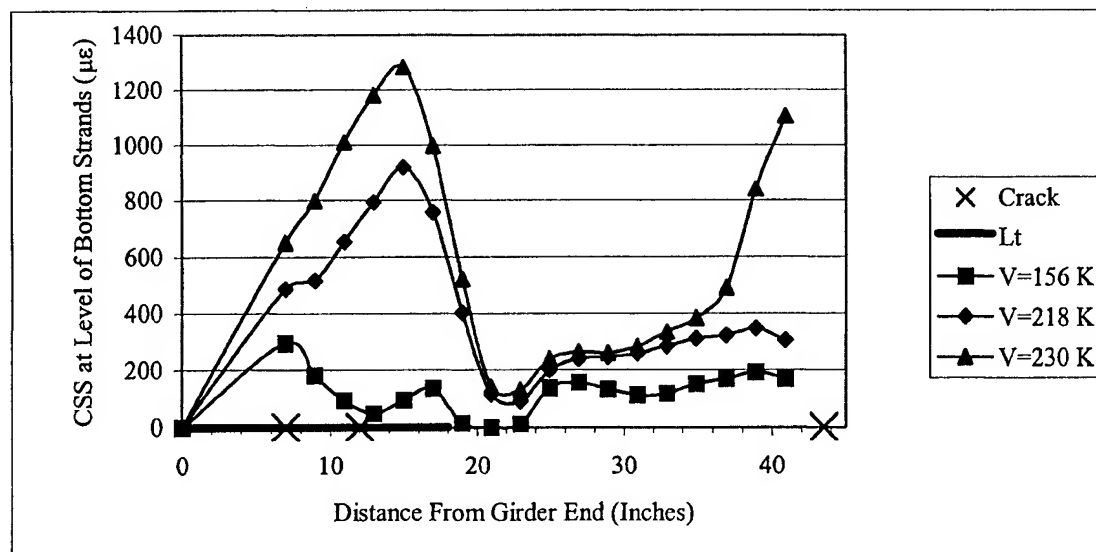


| Shear Crack Data | | | | | | | | | | |
|---|---|---|---|---|---|---|---|---|---|---|
| Distance From End (Inches) | 7 | 12 | 43.5 | | | | | | | |
| Applied Shear at Cracking (Kips) | 156 | 218 | 230 | | | | | | | |

Figure R.24 G2C-West CSS and Shear Cracking vs. Distance from Girder End

602

# APPENDIX S

## VWSG AND CONCRETE SURFACE STRAIN DATA FROM DEVELOPMENT LENGTH TESTS

Appendix S contains raw data for each development length test. Prior to a test, values from the vibrating wire strain gage (VWSG) were recorded. During the test, CSS readings were taken at the tested end and at midspan at the level of the top and bottom strands. The sections correspond with the individual development length tests as follows

**Section S.1** – Consolidated VWSG Data

**Section S.2** – Test G1A-East

**Section S.3** – Test G1A-West

**Section S.4** – Test G1B-East

**Section S.5** – Test G1B-West

**Section S.6** – Test G1C-East

**Section S.7** – Test G1C-West

**Section S.8** – Test G2A-East

**Section S.9** – Test G2A-West

**Section S.10** – Test G2B-East

**Section S.11** – Test G2B-West

**Section S.12** – Test G2C-East

**Section S.13** – Test G2C-West

## S.1 Consolidated Vibrating Wire Strain Gage Data

Table S.1  Vibrating Wire Strain Gage Data From Development Length Tests

| Development Length Test # | Vibrating Wire Strain Gage Reading (Hz) | Thermistor Reading (ohms) | Strain in Concrete At Bottom Strands (microstrains) | Effective Stress In Bottom Strands $f_{se}$ (ksi) |
|---|---|---|---|---|
| G1A-East | 774.77 | 3780 | -378.9 | 153.7 |
| G1A-West | 763.93 | 3131 | -343.7 | 152.3 |
| G1B-East | 762.59 | 3035 | -353.8 | 151.2 |
| G1B-West | 754.38 | 3770 | -360.4 | 149.7 |
| G1C-East | 718.33 | 3410 | -359.4 | 149.0 |
| G1C-West | 708.37 | 3360 | -329.2 | 147.6 |
| G2A-East | 836.69 | 3450 | -418.9 | 175.8 |
| G2A-West | 836.12 | 3450 | -387.4 | 175.7 |
| G2B-East | 817.63 | 3760 | -418.6 | 176.2 |
| G2B-West | 813.30 | 3550 | -393.9 | 175.6 |
| G2C-East | 801.33 | Inoperative | -350.8 | 159.3 |
| G2C-West | 797.96 | Inoperative | -327.2 | 158.8 |

## S.2 G1A-East

Table S.2 Raw Concrete Surface Strains Data for Development Length Test G1A-East

| Step | 1 | 2 | 3 | 4 | 5 | 6 | 7 | 8 | 9 | 10 | 11 | 12 | 13 |
|------|---|---|---|---|---|---|---|---|---|----|----|----|----|
| Load (Kips) | 80 | 120 | 150 | 180 | 210 | 241 | 270 | 300 | 330 | 360 | 390 | 420 | 440 |

| Gage | North Side CSS - microstrains | | | | | | | | | | | | |
|------|-----|-----|-----|-----|-----|-----|-----|------|------|------|------|------|------|
| 1 | 113 | 113 | 113 | 138 | 363 | 564 | 965 | 1178 | 1253 | 1404 | 1742 | 2068 | 2319 |
| 2 | 94 | 181 | 181 | 206 | 457 | 632 | 995 | 1145 | 1183 | 1370 | 1733 | 1996 | 2246 |
| 3 | 113 | 125 | 150 | 150 | 188 | 163 | 363 | 800 | 1551 | 2239 | 3339 | 4565 | 5865 |
| 4 | 112 | 137 | 137 | 137 | 150 | 162 | 262 | 723 | 1509 | 2233 | 3056 | 3967 | 5251 |
| 5 | 119 | 169 | 169 | 181 | 181 | 181 | 306 | 756 | 1556 | 2419 | 3157 | 4044 | 5369 |
| 6 | 144 | 207 | 182 | 257 | 282 | 219 | 470 | 933 | 1773 | 2600 | 3427 | 4354 | 5795 |
| 7 | 125 | 125 | 150 | 175 | 175 | 175 | 225 | 213 | 301 | 376 | 426 | 1340 | 2831 |
| 8 | 94 | 219 | 232 | 269 | 282 | 219 | 194 | 320 | 470 | 457 | 1021 | 1923 | 2863 |
| 9 | 131 | 181 | 194 | 306 | 331 | 344 | 381 | 419 | 519 | 481 | 1281 | 2094 | 3044 |
| 10 | 113 | 163 | 188 | 238 | 276 | 263 | 288 | 338 | 363 | 413 | 1177 | 2142 | 4045 |
| 11 | 187 | 250 | 275 | 337 | 375 | 412 | 400 | 487 | 525 | 575 | 1312 | 1625 | 2500 |
| 12 | 112 | 162 | 237 | 287 | 350 | 337 | 337 | 412 | 387 | 512 | 787 | 1062 | 2087 |
| 13 | 150 | 163 | 200 | 250 | 225 | 275 | 363 | 388 | 401 | 388 | 601 | 864 | 2003 |
| 14 | 44 | 181 | 131 | 257 | 307 | 369 | 407 | 332 | 469 | 619 | 1608 | 2196 | 2459 |
| 15 | 100 | 201 | 213 | 288 | 326 | 313 | 389 | 426 | 426 | 527 | 1630 | 2320 | 2382 |
| 16 | 144 | 169 | 194 | 219 | 257 | 307 | 357 | 395 | 407 | 570 | 1560 | 2250 | 2287 |
| 17 | 132 | 182 | 207 | 294 | 332 | 357 | 407 | 445 | 470 | 620 | 1509 | 2211 | 2298 |
| 18 | 150 | 187 | 225 | 275 | 312 | 337 | 412 | 425 | 437 | 762 | 1137 | 1536 | 1998 |
| 19 | 188 | 175 | 263 | 313 | 363 | 388 | 463 | 550 | 563 | 1588 | 2326 | 3064 | 3914 |
| 20 | 157 | 194 | 244 | 294 | 369 | 407 | 457 | 570 | 607 | 1521 | 2248 | 3199 | 4238 |
| Gage | South Side CSS - microstrains | | | | | | | | | | | | |
| 1 | 125 | 162 | 224 | 287 | 324 | 449 | 486 | 586 | 1134 | 2419 | 3154 | 4239 | 5286 |
| 2 | 87 | 112 | 437 | 475 | 362 | 387 | 450 | 487 | 487 | 525 | 587 | 700 | 1037 |
| 3 | 112 | 137 | 187 | 312 | 300 | 375 | 450 | 462 | 487 | 587 | 1137 | 1400 | 2100 |
| 4 | 138 | 113 | 213 | 275 | 300 | 363 | 438 | 413 | 438 | 663 | 1777 | 2403 | 2841 |
| 5 | 87 | 100 | 162 | 175 | 200 | 325 | 387 | 350 | 537 | 774 | 1861 | 2398 | 2648 |
| 6 | 106 | 106 | 293 | 206 | 293 | 468 | 355 | 480 | 443 | 717 | 1802 | 2264 | 2538 |
| 7 | 162 | 50 | 225 | 225 | 312 | 324 | 349 | 337 | 362 | 699 | 1322 | 1572 | 1559 |
| 8 | 94 | 81 | 181 | 231 | 1378 | 318 | 393 | 430 | 393 | 729 | 1265 | 1602 | 2724 |
| 9 | 231 | 144 | 131 | 306 | 218 | 393 | 368 | 106 | 343 | 181 | 1541 | 1941 | 2627 |
| 10 | 118 | 118 | 218 | 268 | 206 | 368 | 330 | 380 | 393 | 542 | 1876 | 2936 | 3722 |
| 11 | 68 | 255 | 143 | 193 | 243 | 305 | 342 | 305 | 392 | 479 | 1861 | 2882 | 3629 |
| 12 | 25 | 99 | 249 | 199 | 174 | 187 | 311 | 286 | 336 | 336 | 1069 | 1865 | 1790 |
| 13 | 81 | 131 | 180 | 193 | -19 | 56 | 815 | 1213 | 1524 | 1910 | 2793 | 4000 | 4697 |
| 14 | 69 | 44 | 106 | 144 | 131 | 106 | 543 | 967 | 1279 | 1841 | 2340 | 2939 | 3525 |
| 15 | 81 | 144 | 231 | 119 | 94 | 231 | 681 | 1156 | 1518 | 2131 | 3968 | 3218 | 3930 |
| 16 | 13 | 88 | 75 | 138 | 113 | 138 | 525 | 1113 | 1488 | 2038 | 2700 | 3275 | 3800 |
| 17 | 25 | 212 | 300 | 312 | 287 | 300 | 387 | 387 | 549 | 387 | 936 | 1061 | 1286 |
| 18 | 6 | 168 | 156 | 68 | 492 | 616 | 953 | 1052 | 1326 | 1476 | 1774 | 2048 | 2123 |
| 19 | 107 | 194 | 232 | 357 | 545 | 758 | 871 | 1159 | 1172 | 1334 | 1560 | 1898 | 1886 |
| 20 | 63 | 88 | 113 | 50 | 289 | 577 | 728 | 778 | 929 | 1067 | 1305 | 1443 | 1606 |

605

## S.3 G1A-West

Table S.3 Raw Concrete Surface Strains Data for Development Length Test G1A-West

| Step | 1 | 2 | 3 | 4 | 5 | 6 | 7 | 8 | 9 | 10 | 11 |
|---|---|---|---|---|---|---|---|---|---|---|---|
| Load (Kips) | 50 | 100 | 150 | 194 | 221 | 248 | 270 | 284 | 292 | 294 | 290 |

| Gage | North Side CSS - microstrains | | | | | | | | | | |
|---|---|---|---|---|---|---|---|---|---|---|---|
| 1 | 94 | 144 | 207 | 307 | 370 | 495 | 1059 | 1987 | 1849 | 1949 | 1812 |
| 2 | 88 | 100 | 200 | 225 | 301 | 401 | 476 | 764 | 1565 | 1828 | 1778 |
| 3 | 88 | 75 | 163 | 250 | 301 | 388 | 1703 | 714 | 1540 | 1741 | 1728 |
| 4 | 63 | 113 | 163 | 226 | 276 | 338 | 439 | 765 | 1617 | 1855 | 1805 |
| 5 | 94 | 119 | 195 | 270 | 320 | 420 | 345 | 195 | 1525 | 1537 | 1512 |
| 6 | 88 | 138 | 164 | 239 | 252 | 340 | 315 | 340 | 378 | 466 | 491 |
| 7 | 188 | 201 | 239 | 289 | 364 | 402 | 389 | 490 | 502 | 615 | 628 |
| 8 | 69 | 81 | 106 | 182 | 182 | 269 | 282 | 332 | 370 | 382 | 395 |
| 9 | 38 | 75 | 100 | 138 | 176 | 251 | 238 | 276 | 301 | 313 | 288 |
| 10 | 81 | 81 | 119 | 243 | 281 | 343 | 343 | 381 | 443 | 443 | 406 |
| 11 | 119 | 157 | 207 | 257 | 244 | 332 | 307 | 407 | 432 | 357 | 395 |
| 12 | 44 | 82 | 107 | 157 | 157 | 194 | 207 | 220 | 257 | 232 | 270 |
| 13 | 75 | 63 | 88 | 75 | 213 | 276 | 376 | 326 | 288 | 288 | 451 |
| 14 | 0 | 50 | 38 | 113 | 138 | 301 | 890 | 1266 | 1530 | 1655 | 1655 |
| 15 | 37 | 37 | 12 | 62 | 62 | 287 | 923 | 1273 | 1535 | 1635 | 1647 |
| 16 | 31 | 94 | 81 | 157 | 144 | 407 | 959 | 1359 | 1547 | 1410 | 1673 |
| 17 | 38 | 63 | 113 | 88 | 125 | 651 | 1139 | 1690 | 1940 | 1815 | 1490 |
| 18 | 31 | 44 | 44 | 232 | 444 | 807 | 983 | 1020 | 995 | 995 | 945 |
| 19 | 0 | 50 | 63 | 251 | 790 | 752 | 840 | 865 | 840 | 865 | 990 |
| 20 | 12 | 37 | 12 | 187 | 399 | 648 | 499 | 785 | 773 | 785 | 773 |
| Gage | South Side CSS - microstrains | | | | | | | | | | |
| 1 | 56 | 6 | 31 | 332 | 557 | 720 | 683 | 833 | 833 | 795 | 946 |
| 2 | 94 | 132 | 56 | 244 | 457 | 633 | 457 | 720 | 633 | 708 | 733 |
| 3 | 25 | -12 | -12 | 237 | 424 | 748 | 898 | 1010 | 1010 | 998 | 1048 |
| 4 | 19 | -44 | -31 | 143 | 343 | 842 | 1503 | 1790 | 1790 | 1728 | 1728 |
| 5 | -13 | -75 | -138 | -163 | -13 | 325 | 888 | 1200 | 1463 | 1526 | 1601 |
| 6 | -19 | 6 | -56 | -81 | -81 | 319 | 956 | 1306 | 1556 | 1606 | 1656 |
| 7 | 50 | 0 | -25 | -38 | 0 | 351 | 777 | 1041 | 1542 | 1442 | 1780 |
| 8 | 56 | 19 | -31 | -19 | 6 | 56 | 119 | 306 | 556 | 731 | 818 |
| 9 | 69 | -69 | 56 | -19 | -31 | 82 | 44 | 157 | 144 | 44 | 182 |
| 10 | 44 | 69 | 69 | 107 | 132 | 195 | 220 | 295 | 308 | 232 | 308 |
| 11 | 157 | 31 | 107 | 132 | 31 | 6 | -19 | 107 | 144 | 56 | 282 |
| 12 | 82 | 120 | 132 | 107 | 132 | 196 | 145 | 284 | 360 | 322 | 423 |
| 13 | 169 | 219 | 132 | 69 | -56 | 319 | 6 | 307 | 432 | 420 | 432 |
| 14 | 94 | 107 | 94 | 107 | 244 | 295 | 81 | 194 | 357 | 332 | 370 |
| 15 | 88 | 113 | 113 | 100 | 363 | 388 | 325 | 463 | 538 | 713 | 688 |
| 16 | 62 | 75 | 112 | 137 | 312 | 374 | 399 | 973 | 1559 | 1771 | 1808 |
| 17 | 62 | 25 | 112 | 62 | 262 | 225 | 37 | 686 | 1447 | 1347 | 1285 |
| 18 | 93 | 118 | 205 | 193 | 193 | 504 | 504 | 964 | 1599 | 1686 | 1736 |
| 19 | 249 | 374 | 237 | 249 | 224 | 411 | 399 | 872 | 1445 | 1495 | 1520 |
| 20 | 162 | -37 | 174 | 162 | 237 | 349 | 1170 | 1544 | 1668 | 1606 | 1693 |

606

## S.4  G1B-East

Table S.4  Raw Concrete Surface Strains Data for Development Length Test G1B-East

| Step | 1 | 2 | 3 | 4 | 5 | 6 | 7 | 8 | 9 | 10 | 11 | 12 | 13 |
|---|---|---|---|---|---|---|---|---|---|---|---|---|---|
| Load (Kips) | 100 | 120 | 140 | 160 | 180 | 200 | 220 | 240 | 260 | 280 | 300 | 320 | 340 |

| Gage | North Side CSS - microstrains | | | | | | | | | | | | |
|---|---|---|---|---|---|---|---|---|---|---|---|---|---|
| 1 | -31 | -31 | -44 | -56 | 168 | 454 | 479 | 479 | 466 | 541 | 752 | 963 | 1187 |
| 2 | -19 | -31 | -44 | -118 | 193 | 642 | 1066 | 1514 | 1726 | 1789 | 2175 | 2973 | 3745 |
| 3 | 112 | 162 | 162 | 137 | 425 | 987 | 1524 | 1961 | 2586 | 3386 | 4098 | 5722 | 7696 |
| 4 | 106 | 94 | 119 | 106 | 319 | 1007 | 1483 | 1984 | 2697 | 3623 | 4436 | 6051 | 9129 |
| 5 | -50 | 0 | 38 | 25 | 38 | 364 | 829 | 1344 | 1935 | 3154 | 4021 | 5817 | 9461 |
| 6 | 38 | 38 | 63 | 75 | 75 | 250 | 300 | 400 | 763 | 1951 | 2651 | 3939 | 6966 |
| 7 | -94 | -31 | -31 | -19 | 219 | 181 | 106 | 81 | 56 | 556 | 943 | 1443 | 5654 |
| 8 | -25 | -38 | -13 | -13 | 50 | 88 | 88 | 113 | 113 | 338 | 614 | 1077 | 4045 |
| 9 | 131 | 106 | 119 | 144 | 219 | 244 | 269 | 306 | 281 | 306 | 343 | 518 | 2841 |
| 10 | 94 | 81 | 106 | 144 | 181 | 207 | 219 | 257 | 257 | 294 | 344 | 507 | 2772 |
| 11 | 0 | -25 | 38 | 50 | -25 | 175 | 188 | 188 | 200 | 263 | 375 | 538 | 438 |
| 12 | 50 | 50 | 87 | 75 | 125 | 199 | 224 | 237 | 262 | 312 | 411 | 436 | 461 |
| 13 | 99 | 124 | 137 | 149 | 199 | 248 | 286 | 360 | 311 | 410 | 472 | 460 | 783 |
| 14 | 143 | 155 | 193 | 205 | 267 | 329 | 354 | 379 | 391 | 416 | 540 | 764 | 1361 |
| 15 | 75 | 62 | 99 | 137 | 75 | 236 | 286 | 323 | 286 | 385 | 447 | 559 | 1242 |
| 16 | 106 | 106 | 156 | 131 | 194 | 319 | 344 | 407 | 394 | 469 | 557 | 845 | 1445 |
| 17 | 107 | 94 | 69 | 119 | 119 | 295 | 270 | 333 | 370 | 496 | 634 | 1601 | 2216 |
| 18 | 19 | 82 | 119 | 157 | 207 | 282 | 333 | 383 | 408 | 533 | 621 | 1374 | 1563 |
| 19 | 132 | 169 | 194 | 219 | 269 | 382 | 370 | 432 | 482 | 645 | 808 | 1760 | 2224 |
| 20 | 88 | 113 | 163 | 175 | 200 | 300 | 300 | 388 | 363 | 538 | 1013 | 1875 | 2288 |
| Gage | South Side CSS - microstrains | | | | | | | | | | | | |
| 1 | 220 | 321 | 321 | 321 | 396 | 572 | 522 | 937 | 786 | 723 | 1075 | 2597 | 3163 |
| 2 | 113 | 201 | 176 | 252 | 239 | 415 | 516 | 705 | 1032 | 793 | 768 | 1851 | 1737 |
| 3 | 264 | 352 | 326 | 377 | 427 | 515 | 615 | 778 | 979 | 866 | 916 | 1770 | 1958 |
| 4 | 340 | 302 | 327 | 365 | 390 | 504 | 617 | 818 | 1095 | 718 | 995 | 1699 | 2027 |
| 5 | 334 | 334 | 372 | 359 | 385 | 624 | 586 | 864 | 498 | 889 | 1255 | 1835 | 2566 |
| 6 | 227 | 240 | 164 | 328 | 265 | 492 | 467 | 505 | 821 | 606 | 644 | 1073 | 2159 |
| 7 | 126 | 139 | 126 | 38 | 177 | 215 | 38 | 442 | 1175 | 720 | 581 | 1112 | 2768 |
| 8 | 190 | 203 | 228 | 215 | 354 | 354 | 329 | 671 | 874 | 798 | 494 | 899 | 1165 |
| 9 | 139 | 164 | 113 | 76 | 151 | 340 | 340 | 567 | 617 | 529 | 277 | 655 | 554 |
| 10 | 145 | 182 | 233 | 170 | 295 | 270 | 459 | 471 | 735 | 773 | 446 | 1075 | 622 |
| 11 | 220 | 220 | 220 | 270 | 308 | 333 | 409 | 547 | 710 | 597 | 622 | 723 | 798 |
| 12 | 126 | 163 | 151 | 213 | 239 | 213 | 264 | 452 | 477 | 477 | 402 | 465 | 590 |
| 13 | 132 | 195 | 132 | 69 | 207 | 333 | 257 | 596 | 835 | 835 | 1337 | 1162 | 1526 |
| 14 | 56 | 94 | 119 | 69 | 182 | 620 | 821 | 1259 | 1911 | 2788 | 3677 | 4893 | 9804 |
| 15 | 94 | 106 | 144 | 131 | 307 | 758 | 1121 | 1697 | 2398 | 3212 | 4389 | 5278 | 10112 |
| 16 | 193 | 206 | 218 | 256 | 393 | 892 | 1203 | 1827 | 2326 | 3498 | 4046 | 5480 | 10680 |
| 17 | 112 | 199 | 212 | 125 | 312 | 1184 | 1583 | 1571 | 2593 | 3678 | 4613 | 5661 | 11184 |
| 18 | 336 | -62 | 461 | 174 | 784 | 1195 | 1208 | 1755 | 1992 | 1992 | 2291 | 2141 | 3174 |
| 19 | 205 | 130 | 242 | 168 | 528 | 615 | 826 | 1174 | 1546 | 1745 | 1521 | 1571 | 2229 |
| 20 | 228 | 204 | 315 | 327 | 673 | 1118 | 1105 | 1315 | 1525 | 1575 | 1809 | 1402 | 2217 |

## S.5 G1B-West

Table S.5  Raw Concrete Surface Strains Data for Development Length Test G1B-West

| Step | 1 | 2 | 3 | 4 | 5 | 6 | 7 | 8 | 9 | 10 | 11 | 12 |
|------|---|---|---|---|---|---|---|---|---|----|----|----|
| Load (Kips) | 77 | 130 | 160 | 190 | 220 | 250 | 280 | 310 | 340 | 360 | 365 | 367 |

| Gage | North Side CSS - microstrains | | | | | | | | | | | |
|------|------|------|------|------|------|------|------|------|------|------|------|------|
| 1 | 94 | 169 | 144 | 194 | 244 | 281 | 356 | 406 | 1144 | 1506 | 1731 | 1793 |
| 2 | 75 | 125 | 150 | 200 | 237 | 262 | 350 | 387 | 1437 | 1936 | 2224 | 2286 |
| 3 | 56 | -6 | 56 | 219 | 281 | 269 | 343 | 443 | 1505 | 2317 | 2654 | 2741 |
| 4 | 63 | 113 | 125 | 150 | 213 | 225 | 275 | 338 | 1488 | 2175 | 2275 | 2313 |
| 5 | 50 | 113 | 125 | 163 | 200 | 250 | 301 | 388 | 864 | 1340 | 1440 | 1465 |
| 6 | 62 | 75 | 100 | 150 | 175 | 225 | 300 | 350 | 524 | 787 | 1099 | 1224 |
| 7 | 94 | 107 | 119 | 170 | 195 | 245 | 270 | 308 | 383 | 433 | 672 | 810 |
| 8 | 6 | 56 | 56 | 157 | 195 | 119 | 282 | 345 | 446 | 571 | 709 | 785 |
| 9 | 57 | 94 | 69 | 145 | 245 | 233 | 233 | 283 | 359 | 409 | 661 | 812 |
| 10 | 63 | 88 | 88 | 126 | 151 | 164 | 214 | 264 | 264 | 327 | 340 | 353 |
| 11 | 0 | 25 | 75 | 100 | 162 | 175 | 187 | 262 | 225 | 325 | 337 | 375 |
| 12 | 69 | 69 | 81 | 119 | 119 | 156 | 219 | 207 | 244 | 282 | 357 | 369 |
| 13 | 50 | 62 | 62 | 62 | 87 | 112 | 162 | 187 | 199 | 249 | 299 | 324 |
| 14 | 62 | 62 | 112 | 50 | 137 | 137 | 212 | 249 | 237 | 399 | 462 | 549 |
| 15 | 38 | 63 | 38 | 50 | 75 | 100 | 100 | 275 | 438 | 638 | 763 | 813 |
| 16 | 63 | 75 | 25 | 25 | 88 | 88 | 138 | 450 | 838 | 1150 | 1238 | 1375 |
| 17 | 50 | 63 | 50 | 75 | 113 | 100 | 138 | 700 | 1263 | 1588 | 1775 | 1850 |
| 18 | 25 | 37 | 25 | 50 | 75 | 75 | 87 | 699 | 1198 | 1435 | 1523 | 1585 |
| 19 | 6 | 31 | 19 | 81 | 181 | 306 | 468 | 1004 | 1353 | 1552 | 1627 | 542 |
| 20 | 56 | 69 | 56 | 143 | 218 | 330 | 480 | 791 | 953 | 1028 | 1052 | 1115 |
| Gage | South Side CSS - microstrains | | | | | | | | | | | |
| 1 | -56 | -94 | -44 | -19 | 44 | 294 | 457 | 545 | 707 | 720 | 707 | 695 |
| 2 | -88 | -326 | -288 | -163 | 75 | 213 | 426 | 476 | 539 | 639 | 652 | 601 |
| 3 | -13 | 13 | 13 | 150 | 288 | 488 | 550 | 725 | 1163 | 1376 | 1376 | 1301 |
| 4 | 0 | 75 | -12 | -12 | 25 | 150 | 225 | 849 | 1312 | 1749 | 1861 | 1786 |
| 5 | 6 | -69 | -6 | 44 | 81 | 257 | 219 | 895 | 1271 | 1671 | 1721 | 1734 |
| 6 | 25 | 63 | -25 | -75 | 25 | 213 | 226 | 877 | 1416 | 1729 | 1729 | 1830 |
| 7 | -13 | -13 | -38 | 25 | 63 | 251 | 263 | 814 | 1053 | 1341 | 1328 | 1341 |
| 8 | 125 | 50 | 50 | 63 | 113 | 63 | 25 | 100 | 88 | 113 | 125 | 125 |
| 9 | 232 | 132 | 182 | 169 | 207 | 257 | 219 | 320 | 457 | 345 | 507 | 545 |
| 10 | 19 | 31 | 94 | 44 | 194 | 144 | 207 | 244 | 294 | 382 | 607 | 645 |
| 11 | 38 | 63 | 50 | 63 | 201 | 138 | 163 | 238 | 314 | 289 | 728 | 778 |
| 12 | 19 | -57 | -19 | 69 | 233 | 107 | 195 | 245 | 283 | 258 | 723 | 823 |
| 13 | 44 | 69 | 144 | 182 | 220 | 220 | 295 | 320 | 358 | 395 | 684 | 722 |
| 14 | 63 | 75 | 150 | 75 | 176 | 50 | 251 | 364 | 326 | 326 | 639 | 652 |
| 15 | 0 | -13 | 63 | 88 | 138 | 138 | 301 | 326 | 502 | 1003 | 1141 | 1192 |
| 16 | 225 | 75 | 150 | 188 | 225 | 275 | 325 | 338 | 526 | 1014 | 1202 | 1239 |
| 17 | 132 | -6 | 257 | 82 | 220 | 232 | 144 | 245 | 1588 | 2505 | 2706 | 2794 |
| 18 | 101 | -63 | -25 | 176 | 252 | 289 | 201 | 214 | 717 | 2378 | 2504 | 2617 |
| 19 | 157 | 119 | 144 | 107 | 295 | 245 | 270 | 433 | 1511 | 2100 | 2364 | 2213 |
| 20 | 107 | 31 | 132 | 182 | 220 | 245 | 471 | 295 | 1538 | 2078 | 2392 | 2341 |

608

## S.6 G1C-East

Table S.6 Raw Concrete Surface Strains Data for Development Length Test G1C-East

| Step | 1 | 2 | 3 | 4 | 5 | 6 | 7 | 8 | 9 | 10 | 11 |
|---|---|---|---|---|---|---|---|---|---|---|---|
| Load (Kips) | 81 | 112 | 152 | 185 | 215 | 245 | 275 | 305 | 328 | 348 | 349 |

| Gage | North Side CSS - microstrains | | | | | | | | | | |
|---|---|---|---|---|---|---|---|---|---|---|---|
| 1 | -119 | -6 | -19 | 256 | 431 | 568 | 606 | 856 | 693 | 681 | 681 |
| 2 | -94 | -44 | 31 | 319 | 482 | 607 | 720 | 920 | 1258 | 1445 | 1495 |
| 3 | -25 | 113 | 88 | 414 | 627 | 689 | 652 | 1015 | 1341 | 1516 | 1579 |
| 4 | 31 | 82 | 132 | 420 | 633 | 696 | 872 | 1047 | 1398 | 1524 | 1612 |
| 5 | -63 | -50 | 13 | 75 | 88 | 50 | 75 | 125 | 638 | 1051 | 1288 |
| 6 | -50 | 0 | 37 | 37 | 683 | 1566 | 2436 | 3890 | 4424 | 5431 | 5269 |
| 7 | -12 | 37 | 62 | 124 | 757 | 1563 | 2432 | 3809 | 5149 | 7345 | 6849 |
| 8 | 25 | 62 | 112 | 149 | 808 | 1728 | 2562 | 3867 | 5135 | 7510 | 6938 |
| 9 | 12 | -199 | 87 | 125 | 822 | 1719 | 2592 | 4386 | 5607 | 7600 | 6903 |
| 10 | 56 | 69 | 81 | 119 | 244 | 294 | 319 | 694 | 1307 | 2695 | 3233 |
| 11 | 50 | 163 | 175 | 200 | 275 | 325 | 488 | 1202 | 2654 | 5020 | 6434 |
| 12 | 44 | 6 | 69 | 181 | 156 | 193 | 356 | 1167 | 2852 | 5273 | 6471 |
| 13 | 69 | 81 | 169 | 232 | 257 | 282 | 407 | 758 | 2586 | 5104 | 6720 |
| 14 | 25 | 125 | 138 | 288 | 113 | 125 | 238 | 600 | 2501 | 5890 | 17432 |
| 15 | 0 | 38 | -13 | -25 | 150 | 138 | 326 | 414 | 714 | 1479 | 11557 |
| 16 | 38 | 38 | 113 | 251 | 264 | 289 | 402 | 1068 | 930 | 1457 | 11244 |
| 17 | 0 | 0 | 100 | 213 | 150 | 225 | 163 | 663 | 1051 | 2465 | 15578 |
| 18 | -81 | 19 | 156 | 169 | 144 | 231 | 343 | 1205 | 2679 | 4265 | 8049 |
| 19 | 31 | 93 | 193 | 280 | 318 | 417 | 542 | 1663 | 2747 | 4492 | 8242 |
| 20 | -69 | 44 | 118 | 181 | 218 | 280 | 492 | 1115 | 2410 | 4790 | 8265 |
| Gage | South Side CSS - microstrains | | | | | | | | | | |
| 1 | 136 | 136 | 247 | 346 | 383 | 470 | 630 | 1113 | 2225 | 2905 | 7145 |
| 2 | 112 | 124 | 187 | 261 | 349 | 436 | 697 | 1556 | 2689 | 3038 | 7271 |
| 3 | 81 | 118 | 131 | 181 | 268 | 405 | 605 | 1378 | 2600 | 2912 | 7151 |
| 4 | 81 | 144 | 156 | 206 | 268 | 393 | 631 | 1143 | 1929 | 2179 | 11595 |
| 5 | 100 | 175 | 212 | 225 | 324 | 374 | 537 | 1236 | 1610 | 1435 | 7026 |
| 6 | 100 | 125 | 175 | 238 | 300 | 338 | 388 | 713 | 988 | 5603 | 16535 |
| 7 | 88 | 163 | 175 | 263 | 276 | 363 | 438 | -438 | 1077 | 5661 | 16694 |
| 8 | -19 | 157 | 169 | 107 | 245 | 232 | 433 | 709 | 960 | 5553 | 10334 |
| 9 | 138 | 226 | 289 | 302 | 390 | 452 | 578 | 628 | 616 | 4914 | 9991 |
| 10 | 88 | 126 | 151 | 151 | 239 | 365 | 428 | 566 | 503 | 302 | 428 |
| 11 | 119 | 107 | 145 | 208 | 233 | 296 | 396 | 522 | 2685 | 3188 | 2710 |
| 12 | 63 | 101 | 139 | 176 | 202 | 252 | 365 | 479 | 2759 | 3250 | 2797 |
| 13 | -25 | 25 | 51 | 101 | 13 | 164 | 379 | 2061 | 5360 | 7749 | 7256 |
| 14 | 32 | 95 | 133 | 196 | 398 | 638 | 1534 | 3150 | 6370 | 8858 | 8378 |
| 15 | 0 | 50 | 101 | 126 | 379 | 593 | 1553 | 3131 | 4242 | 6148 | 6931 |
| 16 | 19 | 95 | 120 | 69 | 410 | 638 | 1496 | 3099 | 4021 | 6015 | 6015 |
| 17 | 82 | 132 | 170 | 522 | 1151 | 1830 | 2774 | 3013 | 3038 | 3277 | 3353 |
| 18 | 38 | 88 | 126 | 415 | 869 | 1284 | 1511 | 1775 | 2090 | 2014 | 2115 |
| 19 | -6 | 19 | 57 | 383 | 735 | 1137 | 1375 | 1576 | 1551 | 1715 | 1802 |
| 20 | -31 | 6 | 31 | 295 | 696 | 1072 | 1298 | 1474 | 1499 | 1637 | 1649 |

609

## S.7 G1C-West

Table S.7  Raw Concrete Surface Strains Data for Development Length Test G1C-West

| Step | 1 | 2 | 3 | 4 | 5 | 6 | 7 | 8 | 9 | 10 | 11 | 12 |
|---|---|---|---|---|---|---|---|---|---|---|---|---|
| Load (Kips) | 80 | 110 | 140 | 155 | 184 | 215 | 240 | 261 | 276 | 287 | 295 | 296 |

| Gage | North Side CSS - microstrains | | | | | | | | | | | |
|---|---|---|---|---|---|---|---|---|---|---|---|---|
| 1 | 194 | 194 | 231 | 369 | 381 | 469 | 556 | 944 | 1769 | 2469 | 2694 | 3057 |
| 2 | 219 | 231 | 294 | 381 | 469 | 569 | 668 | 1056 | 1881 | 2693 | 2830 | 3043 |
| 3 | 219 | 243 | 268 | 368 | 418 | 518 | 581 | 1130 | 2042 | 2966 | 3153 | 3515 |
| 4 | 175 | 188 | 213 | 313 | 388 | 488 | 550 | 713 | 1013 | 1500 | 1600 | 1688 |
| 5 | 187 | 175 | 237 | 275 | 362 | 425 | 487 | 700 | 800 | 1049 | 1049 | 775 |
| 6 | 200 | 250 | 275 | 337 | 425 | 500 | 562 | 700 | 875 | 1450 | 1662 | 1700 |
| 7 | 207 | 207 | 220 | 320 | 383 | 408 | 483 | 533 | 496 | 973 | 1462 | 1789 |
| 8 | 182 | 107 | 220 | 295 | 333 | 358 | 446 | 496 | 496 | 1036 | 1965 | 10894 |
| 9 | 158 | 208 | 208 | 296 | 372 | 359 | 410 | 485 | 460 | 1002 | 1909 | 11211 |
| 10 | 138 | 164 | 189 | 277 | 352 | 340 | 440 | 466 | 528 | 617 | 1208 | 10532 |
| 11 | 156 | 194 | 194 | 281 | 394 | 381 | 456 | 506 | 556 | 594 | 844 | 10110 |
| 12 | 169 | 169 | 181 | 244 | 356 | 369 | 394 | 444 | 519 | 444 | 431 | 668 |
| 13 | 149 | 187 | 224 | 336 | 461 | 436 | 498 | 573 | 698 | 2952 | 5568 | 6054 |
| 14 | 143 | 143 | 118 | 218 | 330 | 368 | 405 | 443 | 555 | 3087 | 5967 | 6553 |
| 15 | 119 | 106 | 6 | 106 | 231 | 344 | 1132 | 1832 | 2583 | 5247 | 8586 | 9024 |
| 16 | 138 | 213 | 138 | 175 | 200 | 388 | 1088 | 1750 | 2513 | 5288 | 8589 | 9089 |
| 17 | 112 | 125 | 100 | 162 | 200 | 412 | 1062 | 1711 | 2410 | 2897 | 3547 | 3622 |
| 18 | 62 | 50 | 12 | 237 | 537 | 1048 | 1809 | 2533 | 3369 | 3594 | 4218 | 3968 |
| 19 | 131 | 268 | 118 | 305 | 605 | 1004 | 916 | 1054 | 1166 | 1315 | 1390 | 1365 |
| 20 | 175 | 137 | 162 | 362 | 661 | 948 | 1023 | 1060 | 1198 | 1223 | 1260 | 1310 |
| Gage | South Side CSS - microstrains | | | | | | | | | | | |
| 1 | 175 | 137 | 162 | 362 | 661 | 948 | 1023 | 1060 | 1198 | 1223 | 1260 | 1310 |
| 2 | 113 | 163 | 201 | 451 | 564 | 564 | 640 | 702 | 790 | 890 | 916 | 966 |
| 3 | -6 | 132 | 94 | 445 | 520 | 533 | 596 | 646 | 746 | 871 | 934 | 947 |
| 4 | 88 | 63 | 75 | 100 | 213 | 963 | 1463 | 1976 | 2601 | 4940 | 5403 | 5390 |
| 5 | 75 | 62 | 25 | 100 | 674 | 1411 | 2047 | 2697 | 3296 | 5730 | 5630 | 5543 |
| 6 | -13 | 50 | 75 | 150 | 751 | 1477 | 2115 | 2866 | 3918 | 6647 | 8837 | 9013 |
| 7 | 63 | 75 | 50 | 125 | 764 | 1540 | 2191 | 2904 | 3918 | 6672 | 9200 | 9363 |
| 8 | 106 | 106 | 144 | 169 | 570 | 695 | 820 | 1046 | 1346 | 1860 | 3901 | 4064 |
| 9 | 75 | 88 | 88 | 151 | 138 | 151 | 201 | 276 | 528 | 678 | 3467 | 3731 |
| 10 | 94 | 94 | 94 | 182 | 106 | 119 | 157 | 182 | 194 | 157 | 232 | 219 |
| 11 | 157 | 132 | 132 | 207 | 169 | 207 | 320 | 232 | 269 | 583 | 2137 | 7726 |
| 12 | 69 | 107 | 144 | 182 | 82 | 82 | 157 | 157 | 182 | 546 | 2531 | 8647 |
| 13 | 162 | 150 | 162 | 237 | 125 | 299 | 287 | 299 | 274 | 711 | 2645 | 12514 |
| 14 | 113 | 150 | 163 | 238 | 213 | 238 | 238 | 326 | 376 | 802 | 2869 | 12704 |
| 15 | 107 | 94 | 119 | 169 | 157 | 132 | 244 | 169 | 445 | 809 | 1147 | 5598 |
| 16 | 88 | 100 | 138 | 288 | 238 | 263 | 363 | 514 | 752 | 965 | 990 | 4725 |
| 17 | 95 | 120 | 158 | 233 | 208 | 221 | 271 | 460 | 662 | 952 | 1103 | 977 |
| 18 | 94 | 107 | 132 | 220 | 208 | 208 | 308 | 447 | 673 | 875 | 1064 | 1466 |
| 19 | 176 | 176 | 188 | 251 | 238 | 314 | 402 | 979 | 1443 | 1907 | 2133 | 2409 |
| 20 | 138 | 175 | 213 | 301 | 313 | 338 | 464 | 890 | 1328 | 1854 | 2118 | 2531 |

## S.8  G2A-East

Table S.8  Raw Concrete Surface Strains Data for Development Length Test G2A-East

| Step | 1 | 2 | 3 | 4 | 5 | 6 | 7 | 8 | 9 | 10 | 11 | 12 | 13 |
|---|---|---|---|---|---|---|---|---|---|---|---|---|---|
| Load (Kips) | 100 | 151 | 181 | 211 | 244 | 274 | 304 | 334 | 364 | 394 | 425 | 439 | 440 |

| Gage | North Side CSS - microstrains | | | | | | | | | | | | |
|---|---|---|---|---|---|---|---|---|---|---|---|---|---|
| 1 | 37 | 62 | 50 | 87 | 286 | 436 | 709 | 896 | 1058 | 1244 | 1356 | 1356 | 1419 |
| 2 | -6 | 19 | 106 | 180 | 504 | 603 | 1114 | 1425 | 1785 | 2022 | 2408 | 2706 | 2793 |
| 3 | 106 | 119 | 156 | 219 | 493 | 606 | 1168 | 1567 | 2029 | 2416 | 2741 | 2966 | 3165 |
| 4 | 94 | 106 | 144 | 94 | 194 | 181 | 869 | 1394 | 2282 | 2920 | 4282 | 4995 | 5508 |
| 5 | 31 | 94 | 107 | 94 | 182 | 458 | 521 | 772 | 1374 | 1863 | 3093 | 3808 | 4222 |
| 6 | 44 | 94 | 69 | 69 | 119 | 144 | 169 | 356 | 844 | 1207 | 2183 | 2658 | 2971 |
| 7 | 50 | 100 | 100 | 150 | 200 | 262 | 250 | 399 | 811 | 1161 | 2247 | 2696 | 3021 |
| 8 | 69 | 94 | 106 | 131 | 169 | 219 | 219 | 244 | 319 | 419 | 1195 | 1370 | 1433 |
| 9 | 150 | 212 | 249 | 312 | 362 | 437 | 449 | 499 | 574 | 649 | 1272 | 1609 | 1659 |
| 10 | 100 | 125 | 113 | 138 | 225 | 275 | 263 | 288 | 426 | 501 | 1227 | 1402 | 1452 |
| 11 | 119 | 169 | 157 | 194 | 232 | 282 | 369 | 332 | 419 | 482 | 1196 | 1459 | 1596 |
| 12 | 106 | 156 | 193 | 243 | 268 | 380 | 405 | 417 | 455 | 442 | 442 | 479 | 579 |
| 13 | 62 | 62 | -25 | 25 | 137 | 149 | 211 | 186 | 236 | 249 | 373 | 448 | 398 |
| 14 | 43 | 130 | 93 | 143 | 192 | 291 | 291 | 391 | 416 | 1209 | 1743 | 1991 | 2053 |
| 15 | 112 | 174 | 161 | 273 | 310 | 372 | 409 | 447 | 509 | 1278 | 1762 | 1985 | 2035 |
| 16 | 81 | 106 | 144 | 181 | 219 | 331 | 343 | 381 | 531 | 1268 | 1780 | 1980 | 2042 |
| 17 | 81 | 119 | 169 | 207 | 219 | 332 | 370 | 470 | 696 | 2325 | 3152 | 3640 | 3803 |
| 18 | 88 | 138 | 163 | 163 | 1027 | 388 | 426 | 451 | 576 | 1453 | 1842 | 2105 | 2205 |
| 19 | 113 | 125 | 150 | 213 | 263 | 363 | 438 | 463 | 789 | 1716 | 2204 | 2580 | 2642 |
| 20 | 50 | 137 | 212 | 225 | 312 | 387 | 425 | 425 | 1161 | 2510 | 3471 | 4045 | 4158 |
| Gage | South Side CSS - microstrains | | | | | | | | | | | | |
| 1 | 119 | 107 | 182 | 195 | 270 | 408 | 571 | 848 | 2066 | 2995 | 3924 | 4640 | 4866 |
| 2 | 31 | -44 | -94 | 19 | -207 | 207 | 508 | 609 | 1839 | 3119 | 4223 | 5177 | 5428 |
| 3 | 19 | -44 | 94 | 82 | 56 | 194 | 320 | 458 | 859 | 1498 | 2113 | 2502 | 1398 |
| 4 | 63 | 88 | 101 | 176 | 201 | 226 | 452 | 427 | 905 | 2313 | 3067 | 3507 | 3771 |
| 5 | 57 | -44 | 6 | -6 | 145 | 82 | 221 | 271 | 447 | 1380 | 2199 | 2161 | 2741 |
| 6 | 76 | 38 | 50 | 189 | 189 | 215 | 290 | 353 | 416 | 1679 | 2158 | 2486 | 2650 |
| 7 | 63 | 63 | 63 | 190 | 164 | 291 | 316 | 455 | 544 | 1758 | 2277 | 2517 | 2795 |
| 8 | 51 | 13 | 38 | 165 | 241 | 114 | 228 | 329 | 228 | 798 | 1190 | 1431 | 1811 |
| 9 | 32 | 6 | 183 | 233 | 158 | 271 | 359 | 384 | 435 | 964 | 1178 | 1494 | 1531 |
| 10 | -44 | 19 | 57 | 195 | 183 | 284 | 359 | 460 | 435 | 561 | 1103 | 1229 | 1418 |
| 11 | 19 | 107 | 44 | 107 | 157 | 220 | 182 | 258 | 345 | 408 | 948 | 1162 | 1300 |
| 12 | -6 | 44 | 19 | 270 | 220 | 282 | 220 | 345 | 646 | 571 | 1073 | 1486 | 1650 |
| 13 | 56 | 19 | 107 | 44 | 69 | 119 | 157 | 257 | 282 | 345 | 1111 | 1312 | 1199 |
| 14 | 6 | -44 | 69 | 81 | 56 | 119 | 94 | 169 | 131 | 181 | 457 | 494 | 444 |
| 15 | 0 | -25 | -63 | 50 | -38 | 50 | 63 | 125 | 175 | 363 | 1165 | 1617 | 1805 |
| 16 | -6 | -31 | -56 | 118 | 6 | -19 | -31 | 31 | 455 | 841 | 1676 | 2162 | 2549 |
| 17 | -112 | -12 | -50 | -37 | -25 | 50 | 62 | 37 | -274 | 1159 | 2442 | 3052 | 3426 |
| 18 | 100 | 162 | 149 | 162 | 336 | 261 | 622 | 796 | 1120 | 1692 | 2986 | 3683 | 3882 |
| 19 | 112 | 62 | 12 | 99 | 236 | 409 | 409 | 682 | 918 | 1426 | 1885 | 2245 | 2109 |
| 20 | -111 | -12 | -86 | 86 | 173 | 284 | 432 | 518 | 296 | 790 | 1086 | 1345 | 1370 |

611

## S.9  G2A-West

Table S.9  Raw Concrete Surface Strains Data for Development Length Test G2A-West

| Step | 1 | 2 | 3 | 4 | 5 | 6 | 7 | 8 | 9 | 10 | 11 | 12 |
|------|---|---|---|---|---|---|---|---|---|----|----|----|
| Load (Kips) | 80 | 110 | 140 | 170 | 200 | 230 | 254 | 275 | 288 | 293 | 297 | 297 |

| Gage | North Side CSS - microstrains | | | | | | | | | | | |
|------|-----|-----|-----|-----|-----|-----|-----|-----|-----|-----|-----|-----|
| 1 | 19 | 31 | 106 | 156 | 144 | 156 | 406 | 431 | 556 | 668 | 981 | 1043 |
| 2 | 125 | 125 | 162 | 237 | 325 | 362 | 462 | 600 | 650 | 737 | 1149 | 1249 |
| 3 | 131 | 169 | 169 | 194 | 306 | 306 | 431 | 518 | 581 | 606 | 1030 | 1105 |
| 4 | 200 | 250 | 300 | 350 | 375 | 275 | 499 | 562 | 475 | 712 | 1124 | 1236 |
| 5 | 163 | 150 | 150 | 200 | 250 | 325 | 363 | 463 | 450 | 475 | 588 | 725 |
| 6 | 131 | 131 | 169 | 169 | 244 | 319 | 381 | 431 | 431 | 469 | 406 | 494 |
| 7 | 82 | 82 | 94 | 132 | 182 | 257 | 358 | 332 | 332 | 420 | 420 | 408 |
| 8 | 88 | 100 | 175 | 175 | 213 | 251 | 389 | 338 | 363 | 389 | 338 | 351 |
| 9 | 101 | 113 | 113 | 163 | 239 | 251 | 302 | 327 | 339 | 339 | 339 | 365 |
| 10 | 88 | 75 | 138 | 126 | 214 | 251 | 289 | 289 | 314 | 314 | 302 | 314 |
| 11 | 81 | 119 | 131 | 144 | 219 | 293 | 256 | 256 | 356 | 293 | 231 | 281 |
| 12 | 44 | 44 | 81 | 69 | 156 | 156 | 231 | 219 | 244 | 257 | 219 | 369 |
| 13 | 37 | 50 | 75 | 87 | 187 | 187 | 262 | 249 | 311 | 311 | 311 | 299 |
| 14 | 25 | 37 | 62 | 100 | 162 | 175 | 225 | 262 | 374 | 424 | 437 | 437 |
| 15 | -31 | -56 | -94 | -19 | 44 | 69 | 106 | 156 | 269 | 406 | 381 | 344 |
| 16 | 44 | 44 | 81 | 81 | 131 | 144 | 169 | 194 | 319 | 382 | 382 | 382 |
| 17 | -19 | 81 | 56 | 94 | 156 | 156 | 281 | 494 | 644 | 731 | 819 | 806 |
| 18 | 87 | 137 | 150 | 162 | 374 | 511 | 649 | 786 | 886 | 936 | 936 | 936 |
| 19 | -12 | 125 | 87 | 150 | 312 | 387 | 561 | 699 | 798 | 811 | 798 | 786 |
| 20 | 25 | 62 | 62 | 112 | 262 | 399 | 511 | 623 | 711 | 773 | 760 | 760 |
| Gage | South Side CSS - microstrains | | | | | | | | | | | |
| 1 | 75 | 63 | 113 | 88 | 163 | 401 | 551 | 639 | 739 | 789 | 764 | 677 |
| 2 | 94 | 44 | 19 | 94 | 244 | 469 | 469 | 657 | 632 | 807 | 883 | 557 |
| 3 | 38 | -13 | 38 | 0 | 188 | 400 | 526 | 613 | 676 | 763 | 888 | 876 |
| 4 | 56 | 6 | 81 | -156 | 194 | 331 | 543 | 618 | 656 | 843 | 955 | 843 |
| 5 | 38 | 25 | 63 | 63 | 50 | 138 | 125 | 150 | 125 | 213 | 288 | 225 |
| 6 | -6 | -19 | -6 | 19 | 6 | 94 | 81 | 119 | -44 | 157 | 69 | 94 |
| 7 | 100 | 63 | 75 | 75 | 50 | 163 | 200 | 88 | 125 | 288 | 225 | 213 |
| 8 | 38 | 25 | 38 | 50 | 38 | 50 | 88 | 88 | 301 | 175 | 213 | 238 |
| 9 | 69 | 56 | 94 | 69 | 107 | 119 | 220 | 232 | 182 | 245 | 232 | 245 |
| 10 | 75 | 13 | 113 | 75 | 75 | 200 | 238 | 263 | 200 | 288 | 276 | 113 |
| 11 | 38 | 38 | 100 | 63 | 100 | 226 | 251 | 289 | 226 | 339 | 326 | 301 |
| 12 | 75 | 88 | 176 | 125 | 125 | 289 | 301 | 376 | 226 | 389 | 301 | 263 |
| 13 | 81 | 81 | 81 | 94 | 132 | 232 | 232 | 257 | 119 | 307 | 282 | 219 |
| 14 | 94 | 81 | 94 | 94 | 69 | 169 | 244 | 257 | 219 | 345 | 307 | 282 |
| 15 | 81 | 19 | 131 | 94 | 106 | 244 | 281 | 331 | 244 | 369 | 331 | 269 |
| 16 | 38 | 38 | -13 | 63 | 113 | -175 | 301 | 288 | 276 | 338 | 313 | 251 |
| 17 | 75 | 63 | 125 | 75 | 150 | 263 | 313 | 376 | 464 | 576 | 614 | 539 |
| 18 | 50 | 50 | -251 | 75 | 151 | 276 | 301 | 402 | 402 | 515 | 565 | 528 |
| 19 | 119 | 107 | 169 | 132 | 207 | 207 | 383 | 458 | 445 | 533 | 621 | 558 |
| 20 | 82 | 56 | 144 | 107 | 119 | 295 | 345 | 433 | 408 | 533 | 496 | 445 |

## S.10 G2B-East

Table S.10 Raw Concrete Surface Strains Data for Development Length Test G2B-East

| Step | 1 | 2 | 3 | 4 | 5 | 6 | 7 | 8 | 9 | 10 | 11 |
|---|---|---|---|---|---|---|---|---|---|---|---|
| Load (Kips) | 100 | 151 | 184 | 218 | 248 | 278 | 308 | 338 | 369 | 398 | 425 |

| Gage | North Side CSS - microstrains | | | | | | | | | | |
|---|---|---|---|---|---|---|---|---|---|---|---|
| 1 | 69 | 94 | 19 | 257 | 507 | 620 | 557 | 683 | 833 | 1058 | 1321 |
| 2 | 25 | 75 | 100 | 237 | 475 | 799 | 1336 | 1861 | 2423 | 2360 | 2548 |
| 3 | 88 | 138 | 113 | 200 | 213 | 338 | 851 | 1251 | 1726 | 1614 | 1651 |
| 4 | 19 | 94 | 144 | 131 | 169 | 356 | 868 | 1268 | 1880 | 3403 | 4477 |
| 5 | 62 | 125 | 162 | 187 | 175 | 437 | 912 | 1399 | 2049 | 3798 | 5072 |
| 6 | 69 | 132 | 144 | 182 | 232 | 257 | 69 | 307 | 546 | 2478 | 3707 |
| 7 | 94 | 144 | 182 | 194 | 232 | 320 | 345 | 320 | 683 | 2675 | 3840 |
| 8 | 81 | 194 | 244 | 207 | 257 | 370 | 357 | 420 | 533 | 946 | 1247 |
| 9 | 100 | 163 | 213 | 263 | 313 | 376 | 338 | 364 | 426 | 426 | 539 |
| 10 | 94 | 131 | 181 | 219 | 306 | 343 | 318 | 368 | 456 | 468 | 581 |
| 11 | 87 | 150 | 237 | 275 | 350 | 275 | 362 | 412 | 387 | 500 | 587 |
| 12 | 38 | 75 | 113 | 163 | 250 | 300 | 325 | 325 | 350 | 1213 | 1851 |
| 13 | 69 | 144 | 181 | 256 | 331 | 381 | 381 | 381 | 456 | 1307 | 1944 |
| 14 | 144 | 169 | 219 | 269 | 432 | 445 | 482 | 557 | 595 | 1384 | 2110 |
| 15 | 75 | 113 | 176 | 238 | 313 | 364 | 301 | 401 | 915 | 2019 | 2959 |
| 16 | 225 | 288 | 325 | 413 | 525 | 550 | 600 | 650 | 1126 | 1613 | 2051 |
| 17 | 138 | 213 | 225 | 263 | 400 | 400 | 413 | 438 | 1026 | 1501 | 2077 |
| 18 | 162 | 250 | 262 | 337 | 425 | 437 | 462 | 575 | 1624 | 2287 | 3111 |
| 19 | 119 | 181 | 218 | 306 | 418 | 468 | 530 | 692 | 1628 | 2177 | 3350 |
| 20 | 200 | 213 | 213 | 301 | 401 | 438 | 451 | 601 | 1466 | 2042 | 3132 |
| Gage | South Side CSS - microstrains | | | | | | | | | | |
| 1 | 150 | 225 | 287 | 362 | 449 | 499 | 537 | 849 | 1585 | 2147 | 2983 |
| 2 | 100 | 237 | 250 | 349 | 424 | 449 | 474 | 1011 | 2495 | 3818 | 5277 |
| 3 | 200 | 200 | 287 | 300 | 1000 | 437 | 450 | 537 | 1700 | 2450 | 3274 |
| 4 | 144 | 194 | 244 | 306 | 319 | 331 | 394 | 444 | 1481 | 2181 | 2843 |
| 5 | 156 | 231 | 293 | 318 | 356 | 406 | 406 | 480 | 1603 | 2202 | 2876 |
| 6 | 156 | 181 | 219 | 231 | 331 | 369 | 356 | 344 | 756 | 1581 | 2244 |
| 7 | 243 | 256 | 256 | 343 | 418 | 455 | 356 | 393 | 468 | 1403 | 1990 |
| 8 | 118 | 181 | 218 | 268 | 318 | 330 | 343 | 368 | 442 | 1377 | 1975 |
| 9 | 268 | 293 | 318 | 418 | 393 | 443 | 430 | 492 | 654 | 1602 | 2362 |
| 10 | 143 | 168 | 230 | 280 | 318 | 342 | 355 | 367 | 342 | 504 | 679 |
| 11 | 87 | 124 | 124 | 211 | 236 | 224 | 211 | 261 | 298 | 410 | 609 |
| 12 | 218 | 230 | 255 | 305 | 392 | 342 | 305 | 218 | 342 | 753 | 1275 |
| 13 | 131 | 231 | 218 | 255 | 305 | 555 | 1066 | 1290 | 1913 | 3134 | 3969 |
| 14 | 206 | 193 | 243 | 281 | 218 | 792 | 805 | 1241 | 1815 | 3137 | 3948 |
| 15 | 131 | 144 | 182 | 232 | 244 | 507 | 908 | 1208 | 2410 | 2985 | 3774 |
| 16 | 50 | 125 | 125 | 175 | 150 | 438 | 950 | 1388 | 1925 | 2763 | 3263 |
| 17 | 94 | 106 | 143 | 181 | 193 | 243 | 305 | 493 | 480 | 355 | 318 |
| 18 | 93 | 131 | 156 | 181 | 405 | 529 | -44 | 815 | 977 | 1077 | 1338 |
| 19 | 138 | 150 | 188 | 413 | 700 | 813 | 888 | 1126 | 1288 | 1388 | 1688 |
| 20 | 125 | 88 | 150 | 364 | 690 | 740 | 740 | 740 | 1041 | 1254 | 1505 |

613

## S.11 G2B-West

Table S.11 Raw Concrete Surface Strains Data for Development Length Test G2B-West

| Step | 1 | 2 | 3 | 4 | 5 | 6 | 7 | 8 | 9 | 10 | 11 | 12 |
|---|---|---|---|---|---|---|---|---|---|---|---|---|
| Load (Kips) | 100 | 150 | 180 | 210 | 240 | 270 | 300 | 322 | 334 | 341 | 342 | 328 |

| Gage | North Side CSS - microstrains | | | | | | | | | | | |
|---|---|---|---|---|---|---|---|---|---|---|---|---|
| 1 | 119 | 207 | 182 | 295 | 333 | 345 | 1174 | 1940 | 2417 | 2455 | 2505 | 2467 |
| 2 | 75 | 175 | 163 | 288 | 313 | 338 | 1215 | 1929 | 2392 | 2455 | 2429 | 2442 |
| 3 | 100 | 175 | 213 | 814 | 338 | 276 | 526 | 877 | 1140 | 1140 | 1178 | 1153 |
| 4 | 44 | 169 | 219 | 244 | 306 | 331 | 406 | 444 | 444 | 444 | 481 | 481 |
| 5 | 106 | 144 | 219 | 294 | 307 | 307 | 382 | 470 | 632 | 595 | 520 | 632 |
| 6 | 119 | 157 | 195 | 258 | 295 | 320 | 408 | 534 | 547 | 559 | 710 | 534 |
| 7 | 113 | 125 | 176 | 213 | 263 | 238 | 401 | 464 | 665 | 564 | 602 | 514 |
| 8 | 56 | 119 | 169 | 257 | 370 | 320 | 420 | 495 | 621 | 483 | 508 | 495 |
| 9 | 138 | 163 | 200 | 288 | 326 | 338 | 376 | 463 | 463 | 413 | 438 | 426 |
| 10 | 81 | 131 | 94 | 243 | 243 | 268 | 331 | 393 | 443 | 381 | 443 | 406 |
| 11 | 63 | 163 | 88 | 201 | 226 | 276 | 339 | 364 | 401 | 677 | 690 | 665 |
| 12 | 94 | 107 | 119 | 119 | 219 | 194 | 194 | 282 | 320 | 1085 | 1097 | 1110 |
| 13 | 94 | 132 | 132 | 169 | 232 | 232 | 307 | 383 | 408 | 1186 | 1161 | 1211 |
| 14 | 119 | 144 | 157 | 194 | 219 | 270 | 721 | 1097 | 1385 | 2063 | 2150 | 2000 |
| 15 | 106 | 106 | 106 | 156 | 193 | 306 | 717 | 1041 | 1303 | 1690 | 1653 | 1715 |
| 16 | 125 | 138 | 150 | 163 | 176 | 288 | 1154 | 1605 | 1931 | 1893 | 1806 | 1843 |
| 17 | 50 | 88 | 75 | 100 | 100 | 663 | 1402 | 1815 | 2065 | 2090 | 1977 | 1990 |
| 18 | 69 | 106 | 169 | 256 | 431 | 857 | 1257 | 1369 | 1294 | 1369 | 1219 | 1407 |
| 19 | 81 | 94 | 157 | 307 | 395 | 708 | 1122 | 1235 | 1322 | 1310 | 1285 | 1347 |
| 20 | 100 | 100 | 162 | 286 | 411 | 760 | 635 | 660 | 635 | 573 | 598 | 585 |
| Gage | South Side CSS - microstrains | | | | | | | | | | | |
| 1 | 50 | 125 | 113 | 301 | 401 | 840 | 966 | 1204 | 1442 | 1279 | 1204 | 1267 |
| 2 | -19 | 69 | 56 | 206 | 332 | 594 | 870 | 1070 | 1145 | 1245 | 1107 | 1258 |
| 3 | -50 | -12 | 12 | 150 | 287 | 574 | 860 | 1210 | 1447 | 1609 | 1496 | 1596 |
| 4 | 31 | 69 | 143 | 168 | 168 | 243 | 643 | 1029 | 1254 | 1366 | 1341 | 1404 |
| 5 | 81 | 181 | 194 | 181 | 181 | 294 | 319 | 519 | 731 | 856 | 819 | 906 |
| 6 | 181 | 256 | 294 | 306 | 344 | 406 | 469 | 682 | 907 | 1007 | 1032 | 1119 |
| 7 | 88 | 138 | 138 | 188 | 201 | 226 | 276 | 376 | 439 | 439 | 439 | 464 |
| 8 | 81 | 106 | 106 | 131 | 194 | 256 | 294 | 356 | 394 | 406 | 381 | 431 |
| 9 | 31 | 69 | 107 | 144 | 182 | 220 | 295 | 320 | 358 | 295 | 282 | 307 |
| 10 | 31 | 82 | 94 | 94 | 170 | 207 | 257 | 295 | 345 | 283 | 257 | 295 |
| 11 | 50 | 213 | 151 | 188 | 251 | 377 | 352 | 339 | 414 | 377 | 377 | 427 |
| 12 | 101 | 164 | 201 | 214 | 327 | 390 | 466 | 516 | 579 | 730 | 768 | 793 |
| 13 | 100 | 225 | 250 | 338 | 438 | 476 | 601 | 638 | 1077 | 1390 | 1390 | 1365 |
| 14 | 82 | 144 | 119 | 157 | 207 | 245 | 370 | 420 | 746 | 1160 | 1160 | 1160 |
| 15 | 113 | 225 | 263 | 275 | 413 | 413 | 588 | 588 | 938 | 1276 | 1326 | 1251 |
| 16 | 87 | 187 | 137 | 237 | 312 | 300 | 312 | 412 | 837 | 1000 | 987 | 975 |
| 17 | -50 | 50 | 150 | 62 | 212 | 299 | 399 | 998 | 1222 | 1272 | 1235 | 1247 |
| 18 | 87 | 236 | 199 | 274 | 398 | 485 | 559 | 957 | 1405 | 1417 | 1430 | 1442 |
| 19 | 162 | 249 | 237 | 299 | 336 | 423 | 1482 | 2416 | 2890 | 3039 | 2952 | 2989 |
| 20 | 149 | 274 | 274 | 348 | 485 | 485 | 1467 | 2437 | 2860 | 2909 | 2872 | 2897 |

## S.12 G2C-East

Table S.12  Raw Concrete Surface Strains Data for Development Length Test G2C-East

| Step | 1 | 2 | 3 | 4 | 5 | 6 | 7 | 8 | 9 | 10 | 11 | 12 |
|---|---|---|---|---|---|---|---|---|---|---|---|---|
| Load (Kips) | 100 | 150 | 180 | 210 | 241 | 270 | 300 | 330 | 353 | 364 | 367 | 358 |

| Gage | North Side CSS - microstrains | | | | | | | | | | | |
|---|---|---|---|---|---|---|---|---|---|---|---|---|
| 1 | -25 | -25 | -38 | 63 | 75 | 263 | 288 | 326 | 339 | 326 | 313 | 339 |
| 2 | 12 | 0 | 12 | 50 | 337 | 887 | 1349 | 1749 | 1986 | 2024 | 1924 | 1849 |
| 3 | -63 | -75 | -13 | -25 | 225 | 563 | 1126 | 1877 | 2415 | 2402 | 2628 | 2740 |
| 4 | 19 | 119 | 131 | 106 | 393 | 780 | 1342 | 2079 | 2778 | 3302 | 3814 | 3851 |
| 5 | -19 | 6 | 44 | 6 | 306 | 744 | 1357 | 2044 | 2794 | 3257 | 3870 | 3957 |
| 6 | 0 | 75 | 63 | 100 | 75 | 175 | 389 | 677 | 1191 | 1629 | 2356 | 2381 |
| 7 | -19 | 106 | 507 | 420 | 507 | 457 | 495 | 695 | 1033 | 1609 | 1935 | 2023 |
| 8 | 19 | -19 | 132 | 31 | 194 | 107 | 370 | 483 | 708 | 871 | 984 | 1034 |
| 9 | -13 | 100 | 63 | 125 | 175 | 225 | 238 | 438 | 726 | 864 | 989 | 876 |
| 10 | 56 | 94 | 144 | 156 | 219 | 256 | 306 | 519 | 1119 | 1444 | 1519 | 1482 |
| 11 | -6 | -344 | -244 | -6 | 31 | 131 | 131 | 331 | 631 | 656 | 781 | 756 |
| 12 | -37 | 112 | 50 | 125 | 187 | 287 | 237 | 625 | 1112 | 1387 | 1399 | 1474 |
| 13 | 50 | 100 | 113 | 200 | 263 | 325 | 363 | 688 | 1138 | 1425 | 1538 | 1525 |
| 14 | 113 | 113 | 163 | 238 | 338 | 413 | 451 | 689 | 1077 | 1340 | 1528 | 1528 |
| 15 | 44 | 144 | 144 | 219 | 282 | 320 | 395 | 746 | 1585 | 1936 | 2087 | 2036 |
| 16 | 131 | 156 | 181 | 244 | 307 | 1020 | 419 | 907 | 1583 | 1821 | 2009 | 1971 |
| 17 | 94 | 194 | 169 | 257 | 307 | 432 | 532 | 1584 | 2585 | 2998 | 3161 | 3136 |
| 18 | 25 | 150 | 137 | 262 | 350 | 387 | 487 | 1425 | 2312 | 2650 | 2687 | 2675 |
| 19 | 94 | 194 | 181 | 319 | 419 | 469 | 569 | 1419 | 1920 | 2257 | 2320 | 2320 |
| 20 | 138 | 163 | 200 | 401 | 451 | 576 | 1352 | 2691 | 3267 | 3543 | 3693 | 3618 |
| Gage | South Side CSS - microstrains | | | | | | | | | | | |
| 1 | 212 | 299 | 312 | 362 | 412 | 512 | 711 | 1772 | 2895 | 3406 | 3681 | 3805 |
| 2 | 175 | 200 | 287 | 324 | 337 | 387 | 474 | 1297 | 2358 | 2857 | 3194 | 3281 |
| 3 | 150 | 213 | 288 | 338 | 375 | 450 | 513 | 1326 | 2377 | 2865 | 3165 | 3228 |
| 4 | 144 | 206 | 256 | 294 | 331 | 381 | 444 | 719 | 1031 | 1119 | 1194 | 1156 |
| 5 | 150 | 175 | 225 | 275 | 288 | 350 | 438 | 688 | 988 | 1113 | 1188 | 1163 |
| 6 | 112 | 125 | 200 | 250 | 262 | 325 | 425 | 612 | 887 | 999 | 1124 | 1187 |
| 7 | 175 | 175 | 237 | 300 | 325 | 362 | 462 | 924 | 1585 | 1835 | 2122 | 2122 |
| 8 | 131 | 168 | 193 | 255 | 255 | 293 | 330 | 579 | 916 | 1140 | 1265 | 1227 |
| 9 | 56 | 168 | 193 | 218 | 255 | 330 | 380 | 741 | 1451 | 1799 | 1949 | 1924 |
| 10 | 187 | 212 | 249 | 287 | 299 | 349 | 337 | 798 | 1471 | 1820 | 1970 | 1870 |
| 11 | 124 | 124 | 137 | 237 | 249 | 249 | 361 | 610 | 921 | 934 | 996 | 1008 |
| 12 | 99 | 99 | 124 | 162 | 211 | 211 | 311 | 559 | 821 | 945 | 995 | 982 |
| 13 | 125 | 149 | 174 | 262 | 249 | 237 | 672 | 1445 | 2192 | 2553 | 2727 | 2727 |
| 14 | 87 | 87 | 100 | 175 | 125 | 437 | 1673 | 2784 | 3708 | 4232 | 4606 | 4631 |
| 15 | 6 | 44 | 94 | 106 | 106 | 644 | 1469 | 2406 | 3256 | 3744 | 4069 | 4119 |
| 16 | 94 | 194 | 219 | 256 | 269 | 744 | 1632 | 2583 | 3433 | 3934 | 4271 | 4322 |
| 17 | 168 | 131 | 131 | 81 | 243 | 792 | 1154 | 1366 | 1466 | 1616 | 1803 | 1753 |
| 18 | 100 | 124 | 274 | 585 | 710 | 1145 | 884 | 959 | 1033 | 909 | 1145 | 1083 |
| 19 | 188 | 225 | 263 | 626 | 714 | 852 | 989 | 1127 | 1240 | 1302 | 1378 | 1353 |
| 20 | -50 | 0 | 88 | 364 | 451 | 602 | 727 | 865 | 978 | 1053 | 1116 | 1040 |

615

## S.13 G2C-West

Table S.13 Raw Concrete Surface Strains Data for Development Length Test G2C-West

| Step | 1 | 2 | 3 | 4 | 5 | 6 | 7 | 8 | 9 | 10 |
|---|---|---|---|---|---|---|---|---|---|---|
| Load (Kips) | 100 | 150 | 158 | 188 | 218 | 244 | 262 | 277 | 287 | 291 |

| Gage | North Side CSS - microstrains | | | | | | | | | |
|---|---|---|---|---|---|---|---|---|---|---|
| 1 | 157 | -220 | -144 | 69 | 19 | 94 | 144 | 1186 | 1838 | 1788 |
| 2 | 25 | 63 | 50 | 188 | 238 | 326 | 388 | 1504 | 2055 | 2018 |
| 3 | 81 | 94 | 219 | 244 | 307 | 395 | 395 | 1046 | 1410 | 1798 |
| 4 | 38 | 100 | 213 | 250 | 313 | 401 | 401 | 488 | 501 | 914 |
| 5 | 82 | 107 | 320 | 157 | 245 | 282 | 270 | 408 | 445 | 821 |
| 6 | 44 | 132 | -44 | 82 | 182 | 257 | 195 | 282 | 395 | 697 |
| 7 | -113 | 25 | -25 | 50 | 125 | 163 | 301 | 326 | 376 | 313 |
| 8 | 13 | 100 | 125 | 75 | 251 | 238 | 188 | 225 | 463 | 576 |
| 9 | 0 | 75 | 38 | 163 | 150 | 275 | 150 | 225 | 350 | 275 |
| 10 | 25 | 125 | 187 | 237 | 299 | 299 | 312 | 412 | 449 | 462 |
| 11 | -157 | -69 | -19 | -56 | 6 | -220 | -82 | 31 | 220 | 94 |
| 12 | 628 | 703 | 653 | 778 | 828 | 916 | 929 | 941 | 954 | 1105 |
| 13 | -38 | 163 | 489 | 188 | 339 | 238 | 389 | 301 | 564 | 502 |
| 14 | -295 | 56 | 56 | 69 | 94 | 144 | 784 | 1097 | 846 | 1022 |
| 15 | 31 | 156 | 119 | 256 | 293 | 331 | 879 | 1254 | 1541 | 1690 |
| 16 | -501 | -38 | -238 | -50 | 125 | 225 | 476 | 914 | 1215 | 1352 |
| 17 | -401 | -263 | -213 | -226 | 150 | -25 | 150 | 677 | 777 | 902 |
| 18 | 6 | 69 | 19 | 294 | 369 | 620 | 507 | 1058 | 1221 | 1334 |
| 19 | -6 | -31 | -119 | 294 | 382 | 607 | 282 | 545 | 532 | 557 |
| 20 | 212 | -12 | -149 | 324 | 448 | 660 | 436 | 511 | 398 | 374 |
| Gage | South Side CSS - microstrains | | | | | | | | | |
| 1 | 44 | 44 | 56 | 257 | 433 | 596 | 496 | 534 | 559 | 571 |
| 2 | 75 | 25 | 75 | 275 | 463 | 613 | 525 | 550 | 538 | 563 |
| 3 | 69 | 81 | 94 | 330 | 518 | 692 | 667 | 705 | 692 | 667 |
| 4 | 13 | -25 | 25 | 125 | 50 | 125 | 963 | 1263 | 1363 | 1413 |
| 5 | 56 | 44 | 56 | 94 | 144 | 206 | 1155 | 1455 | 1630 | 1792 |
| 6 | 31 | 44 | 56 | 94 | 119 | 132 | 1134 | 1523 | 1836 | 2024 |
| 7 | 38 | 63 | 75 | 113 | 138 | 188 | 1089 | 1453 | 1778 | 2004 |
| 8 | 75 | 87 | 87 | 100 | 162 | 225 | 275 | 362 | 550 | 675 |
| 9 | 31 | 69 | 56 | 94 | 132 | 169 | 194 | 220 | 358 | 470 |
| 10 | 50 | 75 | 125 | 151 | 163 | 238 | 238 | 238 | 326 | 339 |
| 11 | 50 | 63 | 63 | 113 | 138 | 201 | 213 | 201 | 264 | 289 |
| 12 | 101 | 38 | 88 | 227 | 227 | 252 | 365 | 328 | 403 | 416 |
| 13 | -6 | 19 | 19 | 131 | 94 | 169 | 206 | 194 | 307 | 307 |
| 14 | 44 | 69 | 69 | 144 | 169 | 219 | 269 | 257 | 307 | 219 |
| 15 | 38 | 100 | 113 | 200 | 263 | 313 | 388 | 413 | 550 | 900 |
| 16 | 19 | 19 | 19 | 69 | 156 | 206 | 281 | 319 | 419 | 743 |
| 17 | 87 | 112 | 125 | 150 | 225 | 249 | 324 | 387 | 499 | 836 |
| 18 | 75 | 124 | 112 | 149 | 199 | 249 | 261 | 286 | 460 | 236 |
| 19 | 62 | 75 | 137 | 174 | 162 | 249 | 299 | 1331 | 1941 | 2103 |
| 20 | 62 | 112 | 149 | 199 | 211 | 273 | 336 | 1293 | 1926 | 2138 |

616

# VITA

Lieutenant Colonel (LTC) Karl F. Meyer was born in San Diego, California on January 14, 1962. In 1984 he received a Bachelor of Science degree from the U.S. Military Academy at West Point and was commissioned a Second Lieutenant in the United States Army. He served as a platoon leader, company executive officer and battalion civil engineer in the 864th Engineer Battalion at Fort Lewis, Washington. While serving as a company commander in the 92nd Engineer Battalion at Fort Stewart, Georgia, LTC Meyer was deployed to the Persian Gulf region for Operations Desert Shield and Desert Storm where he was awarded the Bronze Star Medal. In 1993, he earned a Master of Science degree in Civil Engineering from the Georgia Institute of Technology. From 1993 through 1996, he served as an instructor and assistant professor in the Department of Civil and Mechanical Engineering at the U.S. Military Academy. In 1997, LTC Meyer graduated from the U.S. Army Command and General Staff College and was assigned to the 130th Engineer Brigade in Hanau, Germany where he served as the Brigade Executive Officer and Brigade S-3. In 1999, LTC Meyer was selected to be a permanent faculty member in the Department of Civil and Mechanical Engineering at the U.S. Military Academy and returned to the Georgia Institute of Technology to pursue a Doctor of Philosophy degree in civil engineering. LTC Meyer was awarded a Doctor of Philosophy in Civil Engineering in 2002. LTC Meyer holds a Professional Engineer license in the state of Virginia. He is married to the former Robin Carlene Heath of Stone Mountain, Georgia and has two children, Abigail and John.